

Report to
NATIONAL SCIENCE FOUNDATION

***EFFECTS OF TRANSVERSE REINFORCEMENT
ON SEISMIC PERFORMANCE OF COLUMNS - A
PARTIAL PARAMETRIC INVESTIGATION***

REPRODUCED BY
U.S. DEPARTMENT OF COMMERCE
NATIONAL TECHNICAL INFORMATION SERVICE
SPRINGFIELD, VA. 22161

September 1988

construction technology laboratories, inc.

Report to

NATIONAL SCIENCE FOUNDATION
Washington, D.C.
Grant No. PFR-7902611

EFFECTS OF TRANSVERSE REINFORCEMENT ON
SEISMIC PERFORMANCE OF COLUMNS - A
PARTIAL PARAMETRIC INVESTIGATION

by

Atorod Azizinamini
Lakhpal S. Johal
Norman W. Hanson
Donald W. Musser
William G. Corley

Submitted by

CONSTRUCTION TECHNOLOGY LABORATORIES, INC.
5420 Old Orchard Road
Skokie, Illinois 60077

September 1988

Project No. CR-9617

Report Nos. 2644D
2645D
2649D
2650D
2651D

Any opinions, findings, conclusions
or recommendations expressed in this
publication are those of the author(s)
and do not necessarily reflect the views
of the National Science Foundation.





PROJECT TEAM

RESEARCH EXECUTED BY: Construction Technology Laboratories, Inc.,
Structural Development Section
Structural Engineering Department

RESPONSIBLE EXECUTIVE: Walter E. Kunze
President
Construction Technology Laboratories, Inc.

PROJECT MANAGEMENT: Dr. W. Gene Corley
Vice President
Engineering and Planning

Donald M. Schultz
Manager
Structural Development Section

PRINCIPAL INVESTIGATOR: Dr. W. Gene Corley
Vice President
Engineering and Planning

CO-PRINCIPAL INVESTIGATOR: Donald W. Musser
Manager
Structural Engineering Department
Portland Cement Association

CO-INVESTIGATORS: Dr. Atorod Azizinamini
Engineer
Structural Development Section

Lakhpal S. Johal
Former Senior Engineer
Structural Development Section

Norman W. Hanson
Principal Engineer
Structural Development Section

TABLE OF CONTENTS

	<u>Page</u>
LIST OF FIGURES	v
LIST OF TABLES	xvii
ACKNOWLEDGMENTS	xviii
SUMMARY AND CONCLUSION	xix
1.0 INTRODUCTION	1-1
2.0 GENERAL BACKGROUND	2-1
3.0 OBJECTIVE AND SCOPE	3-1
4.0 EXPERIMENTAL PROGRAM	4-1
4.1 Test Specimens	4-1
4.2 Reinforcement Details and Materials	4-1
4.3 Specimen Fabrication	4-7
4.4 Material Properties	4-11
4.5 Test Set-Up	4-11
4.6 Instrumentation	4-16
4.7 Data Acquisition	4-22
4.8 Test Procedures	4-22
5.0 SUMMARY OF TEST RESULTS	5-1
5.1 General Behavior of Specimens	5-1
5.2 Horizontal Load-Displacement Characteristics	5-12
5.3 Moment-Curvature Characteristics	5-15
5.4 Effect of Variables	5-37
6.0 ANALYSIS OF RESULTS	6-1
6.1 Concrete Core Compression Strain	6-1
6.2 Moment-Curvature Analysis	6-7
7.0 REFERENCES	7-1



TABLE OF CONTENTS

Continued

	<u>Page</u>
APPENDIX	A-1
Specimen NC-1	A-8
Specimen NC-2	A-12
Specimen NC-3	A-46
Specimen NC-4	A-78
Specimen NC-5	A-111
Specimen NC-6	A-143
Specimen NC-7	A-157
Specimen NC-8	A-174
Specimen NC-9	A-200
Specimen NC-10	A-221
Specimen NC-11	A-240
Specimen NC-12	A-256

LIST OF FIGURES

		<u>Page</u>
4-1	OVERALL VIEW OF TEST SPECIMEN	4-2
4-2	DETAILS OF TRANSVERSE REINFORCEMENT	4-4
4-3	REINFORCEMENT DETAILS FOR SQUARE COLUMNS	4-5
4-4	REPRESENTATIVE DETAILS FOR CIRCULAR COLUMN	4-8
4-5	REPRESENTATIVE REINFORCING CAGE	4-9
4-6	SPECIMEN MOLD	4-9
4-7	PLACEMENT OF CONCRETE	4-10
4-8	LOADING ARRANGEMENT	4-14
4-9	TEST SETUP	4-15
4-10	EXTERNAL INSTRUMENTATION	4-17
4-11	STRAIN GAGE LOCATIONS FOR SPECIMENS NC-1, NC-2, NC-3, NC-4 AND NC-5	4-18
4-12	STRAIN GAGE LOCATIONS FOR SPECIMENS NC-6 AND NC-7	4-19
4-13	CURVATURE AND STRAIN DETERMINATION	4-21
4-14	EXPERIMENTAL DEFINITION OF FIRST YIELD DISPLACEMENT	4-24
4-15	LOADING SCHEDULE	4-25
5-1	SKETCH OF THE CORNER LONGITUDINAL BARS, BEFORE AND AFTER TESTING, SPECIMEN NC-2	5-2
5-2	TEST SPECIMEN NC-1 AFTER TEST CONCLUSION	5-4
5-3	TEST SPECIMEN NC-2 AFTER TEST CONCLUSION	5-4
5-4	TEST SPECIMEN NC-3 AFTER TEST CONCLUSION	5-5
5-5	TEST SPECIMEN NC-4 AFTER TEST CONCLUSION	5-5
5-6	TEST SPECIMEN NC-5 AFTER TEST CONCLUSION	5-6
5-7	TEST SPECIMEN NC-6 AFTER TEST CONCLUSION	5-6
5-8	TEST SPECIMEN NC-7 AFTER TEST CONCLUSION	5-7
5-9	TEST SPECIMEN NC-8 AFTER TEST CONCLUSION	5-7
5-10	TEST SPECIMEN NC-9 AFTER TEST CONCLUSION	5-8
5-11	TEST SPECIMEN NC-10 AFTER TEST CONCLUSION	5-8
5-12	TEST SPECIMEN NC-11 AFTER TEST CONCLUSION	5-9
5-13	TEST SPECIMEN NC-12 AFTER TEST CONCLUSION	5-9
5-14	HORIZONTAL LOAD VERSUS DISPLACEMENT, SPECIMEN NC-2	5-13

LIST OF FIGURES

Continued

		<u>Page</u>
5-15	HORIZONTAL LOAD VERSUS DISPLACEMENT, SPECIMEN NC-3	5-14
5-16	ENERGY VERSUS DISPLACEMENT DUCTILITY RATIO FOR ALL SPECIMENS	5-18
5-17	CURVATURE DISTRIBUTION ALONG UPPER COLUMN, SPECIMEN NC-2 . .	5-19
5-18	CURVATURE DISTRIBUTION ALONG UPPER COLUMN, SPECIMEN NC-5 . .	5-20
5-19	CURVATURE DISTRIBUTION ALONG UPPER COLUMN, SPECIMEN NC-8 . .	5-21
5-20	CURVATURE DISTRIBUTION ALONG UPPER COLUMN, SPECIMEN NC-12 . .	5-22
5-21	CURVATURE DISTRIBUTION ALONG UPPER COLUMN, SPECIMEN NC-11 . .	5-25
5-22	MOMENT VERSUS CURVATURE FOR SPECIMEN NC-2	5-26
5-23	MOMENT VERSUS CURVATURE FOR SPECIMEN NC-5	5-27
5-24	MOMENT VERSUS CURVATURE FOR SPECIMEN NC-8	5-28
5-25	MOMENT VERSUS CURVATURE FOR SPECIMEN NC-12	5-29
5-26	MOMENT VERSUS CURVATURE FOR SPECIMEN NC-12 AT THE UPPER COLUMN STUB LEVEL	5-33
5-27	MOMENT VERSUS CURVATURE FOR SPECIMEN NC-12 AT 6 IN. ABOVE THE STUB	5-34
5-28	MOMENT VERSUS CURVATURE FOR SPECIMEN NC-6	5-35
5-29	MOMENT VERSUS CURVATURE FOR SPECIMEN NC-11	5-36
6-1	CORE STRAIN VERSUS DISPLACEMENT DUCTILITY RATIO, ALL SPECIMENS	6-3
6-2	CORE STRAIN VERSUS DISPLACEMENT DUCTILITY RATIO, SPECIMEN NC-9	6-4
6-3	CORE STRAIN VERSUS DISPLACEMENT DUCTILITY RATIO, SPECIMEN NC-10	6-5
6-4	CORE STRAIN VERSUS DISPLACEMENT DUCTILITY RATIO, SPECIMEN NC-12	6-6
6-5	STRESS-STRAIN CURVE FOR LONGITUDINAL STEEL	6-8
6-6	MODIFIED KENT AND PARK MODEL FOR STRESS-STRAIN BEHAVIOR OF COMPRESSED CONCRETE CONFINED BY RECTANGULAR HOOPS (36) . .	6-8

LIST OF FIGURES

Continued

		<u>Page</u>
6-7	SHEIKH AND UZUMERI MODEL FOR STRESS-STRAIN BEHAVIOR OF COMPRESSED CONCRETE CONFINED BY RECTANGULAR HOOPS	6-10
6-8	CROSS-SECTION OF SQUARE COLUMN WITH PERIPHERAL AND CROSSTIE .	6-10
6-9	MOMENT VERSUS CURVATURE FOR SPECIMEN NC-2	6-14
6-10	MOMENT VERSUS CURVATURE FOR SPECIMEN NC-3	6-15
6-11	MOMENT VERSUS CURVATURE FOR SPECIMEN NC-4	6-16
6-12	MOMENT VERSUS CURVATURE FOR SPECIMEN NC-5	6-17
6-13	MOMENT VERSUS CURVATURE FOR SPECIMEN NC-6	6-18
6-14	MOMENT VERSUS CURVATURE FOR SPECIMEN NC-7	6-19
6-15	MOMENT VERSUS CURVATURE FOR SPECIMEN NC-8	6-20
6-16	MOMENT VERSUS CURVATURE FOR SPECIMEN NC-9	6-21
6-17	MOMENT VERSUS CURVATURE FOR SPECIMEN NC-10	6-22
6-18	MOMENT VERSUS CURVATURE FOR SPECIMEN NC-12	6-23
A-1	SPECIMEN ORIENTATION	A-2
A-2	HORIZONTAL LOAD VERSUS DISPLACEMENT, SPECIMEN NC-5	A-5
A-3	CURVATURE DISTRIBUTION, SPECIMEN NC-5	A-6
A-4	MOMENT VERSUS CURVATURE, SPECIMEN NC-5	A-7
A-5	LOADING SCHEDULE, SPECIMEN NC-1	A-9
A-6	SPECIMEN NC-1 AFTER CYCLE #8	A-10
A-7	SPECIMEN NC-1 AT THE TEST CONCLUSION	A-10
A-8	HORIZONTAL LOAD VERSUS DISPLACEMENT, SPECIMEN NC-1	A-11
A-9	LOADING SCHEDULE, SPECIMEN NC-2	A-13
A-10	TEST SPECIMEN NC-2 AFTER CYCLE #9	A-14
A-11	TEST SPECIMEN NC-2 AFTER CYCLE #13	A-14
A-12	TEST SPECIMEN NC-2 AFTER CYCLE #17	A-15
A-13	TEST SPECIMEN NC-2 AFTER TEST CONCLUSION	A-15
A-14	SKETCH OF THE CORNER LONGITUDINAL BARS, BEFORE AND AFTER TESTING, SPECIMEN NC-2	A-17
A-15	HORIZONTAL LOAD VERSUS DISPLACEMENT, SPECIMEN NC-2	A-18

LIST OF FIGURES

Continued

	<u>Page</u>
A-16	MOMENT VERSUS CURVATURE FOR SPECIMEN NC-2 A-19
A-17	CURVATURE DISTRIBUTION ALONG UPPER COLUMN, SPECIMEN NC-2 A-21
A-18	MEASURED STRAIN, GAGE #13, SPECIMEN NC-2 A-22
A-19	MEASURED STRAIN, GAGE #14, SPECIMEN NC-2 A-23
A-20	MEASURED STRAIN, GAGE #15, SPECIMEN NC-2 A-24
A-21	MEASURED STRAIN, GAGE #16, SPECIMEN NC-2 A-25
A-22	MEASURED STRAIN, GAGE #17, SPECIMEN NC-2 A-26
A-23	MEASURED STRAIN, GAGE #18, SPECIMEN NC-2 A-27
A-24	MEASURED STRAIN, GAGE #19, SPECIMEN NC-2 A-28
A-25	MEASURED STRAIN, GAGE #20, SPECIMEN NC-2 A-29
A-26	MEASURED STRAIN, GAGE #21, SPECIMEN NC-2 A-30
A-27	MEASURED STRAIN, GAGE #22, SPECIMEN NC-2 A-31
A-28	MEASURED STRAIN, GAGE #23, SPECIMEN NC-2 A-32
A-29	MEASURED STRAIN, GAGE #24, SPECIMEN NC-2 A-33
A-30	MEASURED STRAIN, GAGE #25, SPECIMEN NC-2 A-34
A-31	MEASURED STRAIN, GAGE #26, SPECIMEN NC-2 A-35
A-32	MEASURED STRAIN, GAGE #27, SPECIMEN NC-2 A-36
A-33	MEASURED STRAIN, GAGE #28, SPECIMEN NC-2 A-37
A-34	MEASURED STRAIN, GAGE #29, SPECIMEN NC-2 A-38
A-35	MEASURED STRAIN, GAGE #30, SPECIMEN NC-2 A-39
A-36	MEASURED STRAIN, GAGE #31, SPECIMEN NC-2 A-40
A-37	MEASURED STRAIN, GAGE #32, SPECIMEN NC-2 A-41
A-38	MEASURED STRAIN, GAGE #33, SPECIMEN NC-2 A-42
A-39	MEASURED STRAIN, GAGE #34, SPECIMEN NC-2 A-43
A-40	MEASURED STRAIN, GAGE #35, SPECIMEN NC-2 A-44
A-41	MEASURED STRAIN, GAGE #36, SPECIMEN NC-2 A-45
A-42	LOADING SCHEDULE, SPECIMEN NC-3 A-47
A-43	TEST SPECIMEN NC-3 AFTER CYCLE #6 A-48
A-44	TEST SPECIMEN NC-3 AFTER CYCLE #8 A-48

LIST OF FIGURES

Continued

	<u>Page</u>
A-45 TEST SPECIMEN NC-3 AFTER CYCLE #12	A-49
A-46 TEST SPECIMEN NC-3 AFTER CYCLE #13	A-49
A-47 TEST SPECIMEN NC-3 AFTER CYCLE #14	A-51
A-48 TEST SPECIMEN NC-3 AFTER TEST CONCLUSION	A-51
A-49 HORIZONTAL LOAD VERSUS DISPLACEMENT, SPECIMEN NC-3	A-52
A-50 CURVATURE DISTRIBUTION ALONG UPPER COLUMN SPECIMEN NC-3	A-53
A-51 MOMENT VERSUS CURVATURE FOR SPECIMEN NC-3	A-54
A-52 MEASURED STRAIN, GAGE #13, SPECIMEN NC-3	A-56
A-53 MEASURED STRAIN, GAGE #14, SPECIMEN NC-3	A-57
A-54 MEASURED STRAIN, GAGE #15, SPECIMEN NC-3	A-58
A-55 MEASURED STRAIN, GAGE #16, SPECIMEN NC-3	A-59
A-56 MEASURED STRAIN, GAGE #17, SPECIMEN NC-3	A-60
A-57 MEASURED STRAIN, GAGE #19, SPECIMEN NC-3	A-61
A-58 MEASURED STRAIN, GAGE #20, SPECIMEN NC-3	A-62
A-59 MEASURED STRAIN, GAGE #22, SPECIMEN NC-3	A-63
A-60 MEASURED STRAIN, GAGE #23, SPECIMEN NC-3	A-64
A-61 MEASURED STRAIN, GAGE #24, SPECIMEN NC-3	A-65
A-62 MEASURED STRAIN, GAGE #25, SPECIMEN NC-3	A-66
A-63 MEASURED STRAIN, GAGE #26, SPECIMEN NC-3	A-67
A-64 MEASURED STRAIN, GAGE #27, SPECIMEN NC-3	A-68
A-65 MEASURED STRAIN, GAGE #28, SPECIMEN NC-3	A-69
A-66 MEASURED STRAIN, GAGE #29, SPECIMEN NC-3	A-70
A-67 MEASURED STRAIN, GAGE #30, SPECIMEN NC-3	A-71
A-68 MEASURED STRAIN, GAGE #31, SPECIMEN NC-3	A-72
A-69 MEASURED STRAIN, GAGE #32, SPECIMEN NC-3	A-73
A-70 MEASURED STRAIN, GAGE #33, SPECIMEN NC-3	A-74
A-71 MEASURED STRAIN, GAGE #34, SPECIMEN NC-3	A-75
A-72 MEASURED STRAIN, GAGE #35, SPECIMEN NC-3	A-76
A-73 MEASURED STRAIN, GAGE #36, SPECIMEN NC-3	A-77

LIST OF FIGURES

Continued

		<u>Page</u>
A-74	LOADING SCHEDULE, SPECIMEN NC-4	A-79
A-75	TEST SPECIMEN NC-4 AFTER CYCLE #3	A-80
A-76	TEST SPECIMEN NC-4 AFTER CYCLE #5	A-80
A-77	TEST SPECIMEN NC-4 AFTER CYCLE #7	A-81
A-78	TEST SPECIMEN NC-4 AFTER CYCLE #9	A-81
A-79	TEST SPECIMEN NC-5 AFTER CYCLE #11	A-83
A-80	TEST SPECIMEN NC-4 AFTER TEST CONCLUSION	A-83
A-81	HORIZONTAL LOAD VERSUS DISPLACEMENT, SPECIMEN NC-4	A-84
A-82	CURVATURE DISTRIBUTION ALONG UPPER COLUMN, SPECIMEN NC-4	A-85
A-83	MOMENT VERSUS CURVATURE FOR SPECIMEN NC-4	A-86
A-84	MEASURED STRAIN, GAGE #13, SPECIMEN NC-4	A-88
A-85	MEASURED STRAIN, GAGE #14, SPECIMEN NC-4	A-89
A-86	MEASURED STRAIN, GAGE #15, SPECIMEN NC-4	A-90
A-87	MEASURED STRAIN, GAGE #16, SPECIMEN NC-4	A-91
A-88	MEASURED STRAIN, GAGE #17, SPECIMEN NC-4	A-92
A-89	MEASURED STRAIN, GAGE #18, SPECIMEN NC-4	A-93
A-90	MEASURED STRAIN, GAGE #19, SPECIMEN NC-4	A-94
A-91	MEASURED STRAIN, GAGE #20, SPECIMEN NC-4	A-95
A-92	MEASURED STRAIN, GAGE #21, SPECIMEN NC-4	A-96
A-93	MEASURED STRAIN, GAGE #22, SPECIMEN NC-4	A-97
A-94	MEASURED STRAIN, GAGE #23, SPECIMEN NC-4	A-98
A-95	MEASURED STRAIN, GAGE #24, SPECIMEN NC-4	A-99
A-96	MEASURED STRAIN, GAGE #25, SPECIMEN NC-4	A-100
A-97	MEASURED STRAIN, GAGE #26, SPECIMEN NC-4	A-101
A-98	MEASURED STRAIN, GAGE #27, SPECIMEN NC-4	A-102
A-99	MEASURED STRAIN, GAGE #28, SPECIMEN NC-4	A-103
A-100	MEASURED STRAIN, GAGE #29, SPECIMEN NC-4	A-104
A-101	MEASURED STRAIN, GAGE #30, SPECIMEN NC-4	A-105
A-102	MEASURED STRAIN, GAGE #31, SPECIMEN NC-4	A-106

LIST OF FIGURES

Continued

	<u>Page</u>
A-103 MEASURED STRAIN, GAGE #32, SPECIMEN NC-4	A-107
A-104 MEASURED STRAIN, GAGE #33, SPECIMEN NC-4	A-108
A-105 MEASURED STRAIN, GAGE #35, SPECIMEN NC-4	A-109
A-106 MEASURED STRAIN, GAGE #36, SPECIMEN NC-4	A-110
A-107 LOADING SCHEDULE, SPECIMEN NC-5	A-112
A-108 TEST SPECIMEN NC-5 AFTER CYCLE #6	A-113
A-109 TEST SPECIMEN NC-5 AFTER CYCLE #8	A-113
A-110 TEST SPECIMEN NC-5 AFTER CYCLE #12	A-115
A-111 TEST SPECIMEN NC-5 AFTER CYCLE #14	A-115
A-112 TEST SPECIMEN NC-5 AFTER CYCLE #16	A-116
A-113 TEST SPECIMEN NC-5 AFTER TEST CONCLUSION	A-116
A-114 HORIZONTAL LOAD VERSUS DISPLACEMENT, SPECIMEN NC-5	A-117
A-115 MOMENT VERSUS CURVATURE FOR SPECIMEN NC-5	A-118
A-116 CURVATURE DISTRIBUTION ALONG UPPER COLUMN, SPECIMEN NC-5	A-119
A-117 MEASURED STRAIN, GAGE #13, SPECIMEN NC-5	A-121
A-118 MEASURED STRAIN, GAGE #14, SPECIMEN NC-5	A-122
A-119 MEASURED STRAIN, GAGE #15, SPECIMEN NC-5	A-123
A-120 MEASURED STRAIN, GAGE #16, SPECIMEN NC-5	A-124
A-121 MEASURED STRAIN, GAGE #17, SPECIMEN NC-5	A-125
A-122 MEASURED STRAIN, GAGE #18, SPECIMEN NC-5	A-126
A-123 MEASURED STRAIN, GAGE #19, SPECIMEN NC-5	A-127
A-124 MEASURED STRAIN, GAGE #20, SPECIMEN NC-5	A-128
A-125 MEASURED STRAIN, GAGE #21, SPECIMEN NC-5	A-129
A-126 MEASURED STRAIN, GAGE #22, SPECIMEN NC-5	A-130
A-127 MEASURED STRAIN, GAGE #23, SPECIMEN NC-5	A-131
A-128 MEASURED STRAIN, GAGE #24, SPECIMEN NC-5	A-132
A-129 MEASURED STRAIN, GAGE #25, SPECIMEN NC-5	A-133
A-130 MEASURED STRAIN, GAGE #26, SPECIMEN NC-5	A-134
A-131 MEASURED STRAIN, GAGE #27, SPECIMEN NC-5	A-135

LIST OF FIGURES

Continued

	<u>Page</u>
A-132 MEASURED STRAIN, GAGE #28, SPECIMEN NC-5	A-136
A-133 MEASURED STRAIN, GAGE #29, SPECIMEN NC-5	A-137
A-134 MEASURED STRAIN, GAGE #31, SPECIMEN NC-5	A-138
A-135 MEASURED STRAIN, GAGE #32, SPECIMEN NC-5	A-139
A-136 MEASURED STRAIN, GAGE #33, SPECIMEN NC-5	A-140
A-137 MEASURED STRAIN, GAGE #35, SPECIMEN NC-5	A-141
A-138 MEASURED STRAIN, GAGE #36, SPECIMEN NC-5	A-142
A-139 LOADING SCHEDULE, SPECIMEN NC-6	A-144
A-140 TEST SPECIMEN NC-6 AFTER CYCLE #2	A-146
A-141 TEST SPECIMEN NC-6 AFTER CYCLE #3	A-146
A-142 TEST SPECIMEN NC-6 AFTER CYCLE #5	A-147
A-143 TEST SPECIMEN NC-6 AFTER CYCLE #7	A-147
A-144 TEST SPECIMEN NC-6 AFTER CYCLE #9	A-148
A-145 TEST SPECIMEN NC-6 AFTER TEST CONCLUSION	A-148
A-146 HORIZONTAL LOAD VERSUS DISPLACEMENT, SPECIMEN NC-6	A-149
A-147 MOMENT VERSUS CURVATURE FOR SPECIMEN NC-6	A-151
A-148 CURVATURE DISTRIBUTION ALONG UPPER COLUMN SPECIMEN NC-6	A-152
A-149 MEASURED STRAIN, GAGE #15, SPECIMEN NC-6	A-153
A-150 MEASURED STRAIN, GAGE #16, SPECIMEN NC-6	A-154
A-151 MEASURED STRAIN, GAGE #17, SPECIMEN NC-6	A-155
A-152 MEASURED STRAIN, GAGE #20, SPECIMEN NC-6	A-156
A-153 LOADING SCHEDULE, SPECIMEN NC-7	A-158
A-154 TEST SPECIMEN NC-7 AFTER CYCLE #2	A-159
A-155 TEST SPECIMEN NC-7 AFTER CYCLE #5	A-159
A-156 TEST SPECIMEN NC-7 AFTER CYCLE #7	A-160
A-157 TEST SPECIMEN NC-7 AFTER CYCLE #9	A-160
A-158 TEST SPECIMEN NC-7 COMPLETING FORWARD LOADING CYCLE #11	A-162
A-159 TEST SPECIMEN NC-7 AFTER TEST CONCLUSION	A-162
A-160 HORIZONTAL LOAD VERSUS DISPLACEMENT, SPECIMEN NC-7	A-163

LIST OF FIGURES

Continued

	<u>Page</u>
A-161 CURVATURE DISTRIBUTION ALONG UPPER COLUMN, SPECIMEN NC-7 . . .	A-164
A-162 MOMENT VERSUS CURVATURE FOR SPECIMEN NC-7	A-165
A-163 MEASURED STRAIN, GAGE #13, SPECIMEN NC-7	A-167
A-164 MEASURED STRAIN, GAGE #15, SPECIMEN NC-7	A-168
A-165 MEASURED STRAIN, GAGE #16, SPECIMEN NC-7	A-169
A-166 MEASURED STRAIN, GAGE #17, SPECIMEN NC-7	A-170
A-167 MEASURED STRAIN, GAGE #18, SPECIMEN NC-7	A-171
A-168 MEASURED STRAIN, GAGE #19, SPECIMEN NC-7	A-172
A-169 MEASURED STRAIN, GAGE #20, SPECIMEN NC-7	A-173
A-170 LOADING SCHEDULE, SPECIMEN NC-8	A-175
A-171 TEST SPECIMEN NC-8 AFTER CYCLE #6	A-177
A-172 TEST SPECIMEN NC-8 AFTER CYCLE #8	A-177
A-173 TEST SPECIMEN NC-8 AFTER CYCLE #10	A-178
A-174 TEST SPECIMEN NC-8 AFTER CYCLE #12	A-178
A-175 TEST SPECIMEN NC-8 AFTER CYCLE #14	A-179
A-176 TEST SPECIMEN NC-8 AFTER TEST CONCLUSION	A-179
A-177 HORIZONTAL LOAD VERSUS DISPLACEMENT, SPECIMEN NC-8	A-180
A-178 CURVATURE DISTRIBUTION ALONG UPPER COLUMN, SPECIMEN NC-8 . . .	A-182
A-179 MOMENT VERSUS CURVATURE FOR SPECIMEN NC-8	A-183
A-180 MEASURED STRAIN, GAGE #13, SPECIMEN NC-8	A-184
A-181 MEASURED STRAIN, GAGE #15, SPECIMEN NC-8	A-185
A-182 MEASURED STRAIN, GAGE #16, SPECIMEN NC-8	A-186
A-183 MEASURED STRAIN, GAGE #17, SPECIMEN NC-8	A-187
A-184 MEASURED STRAIN, GAGE #18, SPECIMEN NC-8	A-188
A-185 MEASURED STRAIN, GAGE #21, SPECIMEN NC-8	A-189
A-186 MEASURED STRAIN, GAGE #22, SPECIMEN NC-8	A-190
A-187 MEASURED STRAIN, GAGE #23, SPECIMEN NC-8	A-191
A-188 MEASURED STRAIN, GAGE #24, SPECIMEN NC-8	A-192
A-189 MEASURED STRAIN, GAGE #25, SPECIMEN NC-8	A-193

LIST OF FIGURES

Continued

	<u>Page</u>
A-190 MEASURED STRAIN, GAGE #27, SPECIMEN NC-8	A-194
A-191 MEASURED STRAIN, GAGE #29, SPECIMEN NC-8	A-195
A-192 MEASURED STRAIN, GAGE #32, SPECIMEN NC-8	A-196
A-193 MEASURED STRAIN, GAGE #33, SPECIMEN NC-8	A-197
A-194 MEASURED STRAIN, GAGE #34, SPECIMEN NC-8	A-198
A-195 MEASURED STRAIN, GAGE #35, SPECIMEN NC-8	A-199
A-196 LOADING SCHEDULE, SPECIMEN NC-9	A-201
A-197 TEST SPECIMEN NC-9 AFTER CYCLE #7	A-202
A-198 TEST SPECIMEN NC-9 AFTER CYCLE #9	A-202
A-199 TEST SPECIMEN NC-9 AFTER CYCLE #11	A-204
A-200 TEST SPECIMEN NC-9 AFTER CYCLE #13	A-204
A-201 TEST SPECIMEN NC-9 AFTER TEST CONCLUSION	A-205
A-202 HORIZONTAL LOAD VERSUS DISPLACEMENT, SPECIMEN NC-9	A-206
A-203 CURVATURE DISTRIBUTION ALONG UPPER COLUMN SPECIMEN NC-9	A-207
A-204 MOMENT VERSUS CURVATURE FOR SPECIMEN NC-9	A-208
A-205 MEASURED STRAIN, GAGE #13, SPECIMEN NC-9	A-210
A-206 MEASURED STRAIN, GAGE #14, SPECIMEN NC-9	A-211
A-207 MEASURED STRAIN, GAGE #15, SPECIMEN NC-9	A-212
A-208 MEASURED STRAIN, GAGE #16, SPECIMEN NC-9	A-213
A-209 MEASURED STRAIN, GAGE #17, SPECIMEN NC-9	A-214
A-210 MEASURED STRAIN, GAGE #18, SPECIMEN NC-9	A-215
A-211 MEASURED STRAIN, GAGE #20, SPECIMEN NC-9	A-216
A-212 MEASURED STRAIN, GAGE #21, SPECIMEN NC-9	A-217
A-213 MEASURED STRAIN, GAGE #22, SPECIMEN NC-9	A-218
A-214 MEASURED STRAIN, GAGE #23, SPECIMEN NC-9	A-219
A-215 MEASURED STRAIN, GAGE #24, SPECIMEN NC-9	A-220
A-216 LOADING SCHEDULE, SPECIMEN NC-10	A-222
A-217 TEST SPECIMEN NC-10 AFTER CYCLE #8	A-223
A-218 TEST SPECIMEN NC-10 AFTER CYCLE #10	A-223

LIST OF FIGURES

Continued

	<u>Page</u>
A-219 TEST SPECIMEN NC-10 AFTER CYCLE #12	A-225
A-220 TEST SPECIMEN NC-10 AFTER CYCLE #13	A-225
A-221 TEST SPECIMEN NC-10 AFTER TEST CONCLUSION	A-226
A-222 HORIZONTAL LOAD VERSUS DISPLACEMENT, SPECIMEN NC-10	A-227
A-223 CURVATURE DISTRIBUTION ALONG UPPER COLUMN SPECIMEN NC-10	A-228
A-224 MOMENT VERSUS CURVATURE FOR SPECIMEN NC-10	A-229
A-225 MEASURED STRAIN, GAGE #13, SPECIMEN NC-10	A-231
A-226 MEASURED STRAIN, GAGE #14, SPECIMEN NC-10	A-232
A-227 MEASURED STRAIN, GAGE #15, SPECIMEN NC-10	A-233
A-228 MEASURED STRAIN, GAGE #16, SPECIMEN NC-10	A-234
A-229 MEASURED STRAIN, GAGE #17, SPECIMEN NC-10	A-235
A-230 MEASURED STRAIN, GAGE #18, SPECIMEN NC-10	A-236
A-231 MEASURED STRAIN, GAGE #20, SPECIMEN NC-10	A-237
A-232 MEASURED STRAIN, GAGE #21, SPECIMEN NC-10	A-238
A-233 MEASURED STRAIN, GAGE #22, SPECIMEN NC-10	A-239
A-234 LOADING SCHEDULE, SPECIMEN NC-11	A-241
A-235 TEST SPECIMEN NC-11 AFTER CYCLE #6	A-242
A-236 TEST SPECIMEN NC-11 AFTER CYCLE #8	A-242
A-237 TEST SPECIMEN NC-11 AFTER CYCLE #10	A-244
A-238 TEST SPECIMEN NC-11 AFTER CYCLE #12	A-244
A-239 TEST SPECIMEN NC-11 AFTER TEST CONCLUSION	A-245
A-240 HORIZONTAL LOAD VERSUS DISPLACEMENT, SPECIMEN NC-11	A-246
A-241 CURVATURE DISTRIBUTION ALONG UPPER COLUMN SPECIMEN NC-11	A-247
A-242 MOMENT VERSUS CURVATURE FOR SPECIMEN NC-11	A-249
A-243 MEASURED STRAIN, GAGE #13, SPECIMEN NC-11	A-250
A-244 MEASURED STRAIN, GAGE #14, SPECIMEN NC-11	A-251
A-245 MEASURED STRAIN, GAGE #15, SPECIMEN NC-11	A-252
A-246 MEASURED STRAIN, GAGE #16, SPECIMEN NC-11	A-253
A-247 MEASURED STRAIN, GAGE #17, SPECIMEN NC-11	A-254

LIST OF FIGURES

Continued

	<u>Page</u>
A-248 MEASURED STRAIN, GAGE #18, SPECIMEN NC-11	A-255
A-249 TRANSVERSE REINFORCEMENT DETAIL USED WITHIN 22 IN. ABOVE THE STUB, SPECIMEN NC-12	A-257
A-250 LOADING SCHEDULE, SPECIMEN NC-12	A-258
A-251 TEST SPECIMEN NC-12 AFTER CYCLE #2	A-259
A-252 TEST SPECIMEN NC-12 DURING CYCLE #5	A-259
A-253 TEST SPECIMEN NC-12 DURING CYCLE #7	A-260
A-254 TEST SPECIMEN NC-12 DURING CYCLE #11	A-260
A-255 TEST SPECIMEN NC-12 AFTER TEST CONCLUSION	A-262
A-256 TEST SPECIMEN NC-12 AFTER TEST CONCLUSION	A-262
A-257 HORIZONTAL LOAD VERSUS DISPLACEMENT, SPECIMEN NC-12	A-263
A-258 CURVATURE DISTRIBUTION ALONG UPPER COLUMN SPECIMEN NC-12	A-264
A-259 MOMENT VERSUS CURVATURE FOR SPECIMEN NC-12	A-266
A-260 MOMENT VERSUS CURVATURE FOR SPECIMEN NC-12, 6 IN. ABOVE THE STUB	A-267
A-261 MEASURED STRAIN, GAGE #13, SPECIMEN NC-12	A-268
A-262 MEASURED STRAIN, GAGE #14, SPECIMEN NC-12	A-269
A-263 MEASURED STRAIN, GAGE #15, SPECIMEN NC-12	A-270
A-264 MEASURED STRAIN, GAGE #16, SPECIMEN NC-12	A-271
A-265 MEASURED STRAIN, GAGE #17, SPECIMEN NC-12	A-272
A-266 MEASURED STRAIN, GAGE #18, SPECIMEN NC-12	A-273
A-267 MEASURED STRAIN, GAGE #19, SPECIMEN NC-12	A-274
A-268 MEASURED STRAIN, GAGE #20, SPECIMEN NC-12	A-275
A-269 MEASURED STRAIN, GAGE #21, SPECIMEN NC-12	A-276
A-270 MEASURED STRAIN, GAGE #22, SPECIMEN NC-12	A-277
A-271 MEASURED STRAIN, GAGE #23, SPECIMEN NC-12	A-278
A-272 MEASURED STRAIN, GAGE #24, SPECIMEN NC-12	A-279

LIST OF TABLES

	<u>Page</u>
4.1 DETAILS OF TEST VARIABLES	4-3
4.2 MATERIAL PROPERTIES	4-12
4.3 CONCRETE MIX PROPORTIONS	4-12
4.4 MATERIAL PROPERTIES	4-13
5.1 FIRST YIELD DISPLACEMENT AND YIELD CURVATURE FOR TEST SPECIMENS	5-16
5.2 THEORETICAL AND MAXIMUM APPLIED HORIZONTAL LOAD FOR TEST SPECIMENS	5-17
5.3 TEST RESULTS	5-31
5.4 MAINTAINED FLEXCURAL STRENGTH	5-32
5.5 TRANSVERSE REINFORCEMENT AREA FOR SQUARE COLUMN TEST SPECIMENS	5-39
5.6 PARAMETERS USED IN CALCULATING ACI TRANSVERSE REINFORCEMENT REQUIREMENT	5-40
6.1 MAXIMUM CORE COMPRESSION STRAIN	6-2
6.2 PARAMETERS USED IN MODIFIED KENT AND PARK MODEL	6-12
6.2 PARAMETERS USED IN MODIFIED KENT SHIEKH AND UZUMERI MODEL	6-13
A.1 HORIZONTAL LOADING HISTORY	A-3

ACKNOWLEDGMENTS

Work reported in this paper was based on research jointly supported by the National Science Foundation under Grant No. CEE85-44164 and the Portland Cement Association. All tests were performed in the Structural Laboratory of the Construction Technology Laboratories, Inc. Any opinions, findings, and conclusions or recommendations are those of the authors and do not necessarily reflect the views of the National Science Foundation.

SUMMARY AND CONCLUSION

Columns in building frames are normally designed to prevent both hinging and crushing during an earthquake. However, columns in buildings subjected to severe earthquakes may sometimes be subjected to forces that cause hinging. The possibility of yielding occurring at column ends makes it important to ensure that columns are capable of behaving in a ductile manner.

Performance of concrete structures in recent earthquakes has clearly demonstrated the need for adequate information on behavior and design of columns. Inadequate transverse column reinforcement has resulted in severe damage to structures. Code provisions for confining steel are currently based on limited data. The amount of transverse reinforcement in potential plastic hinge regions recommended by the American Concrete Institute (ACI) and the Uniform Building Code (UBC) is based on preserving the axial load strength of a column after the concrete cover has spalled. The amount of rectangular hoops and ties specified assumes that because of their shape, they are less efficient than circular spirals in confining the concrete.

To determine the adequacy of present code requirements, correlation of measured data with ductility demands of U.S. codes and development of code language describing proposed methods to design transverse reinforcement, an experimental program was carried out at Construction Technology Laboratories, Inc. (CTL). As part of the experimental program, a total of twelve full scale square and circular test columns were subjected to lateral loads causing hinging. Each specimen represented a portion of a frame subjected to simulated seismic loading. Controlled variables included the level of axial load, the amount and type of transverse reinforcement, and details of transverse reinforcement. Design compressive strength of concrete and specified yield stress of reinforcement were 6000 psi (41.4 MPa) and 60 ksi (414 MPa), respectively.

Based on results of the experimental investigation the following conclusions are made:

1. For a constant amount of confinement, flexural capacity of a column increases with axial load, but ductility reduces substantially.
2. Reduction in the amount of transverse reinforcement results in lower ductility and lower flexural strength.
3. For axial loads of up to 40% of the column design strength, standard 90 degree hook on the inner hoop is sufficient.
4. The ten bar diameter extension as required by Section A.1 of the 1983 ACI Building Code is not needed. Use of six bar diameter extension used in all specimens produced displacement ductilities exceeding or equal to those generally assumed in design.
5. For square columns, use of continuous square helix transverse reinforcement is an efficient detail which provides displacement ductilities generally assumed in design.
6. The required area of transverse reinforcement for square columns in the form of continuous square helix could conservatively be calculated based on the requirements for column confinement in ACI-318-83.

1.0 INTRODUCTION

Columns in building frames are normally designed to prevent hinging, crushing, or otherwise losing their capacity to support the building. However, columns in buildings subjected to an earthquake may sometimes be subjected to forces that cause hinging. The bases of columns in multi-story buildings are also generally designed to form plastic hinges to increase the efficiency of the inelastic mechanism. Thus, the possibility of hinging occurring at column ends makes it important to ensure that columns are capable of behaving in a ductile manner under required deformations (1-5).

Inadequate transverse column reinforcement can result in severe damage to structures. Current code provisions (6-7) for lateral reinforcement of compression member are based on providing confinement to increase concrete strain capacity. However, confinement may not always be the governing criteria for columns. Transverse reinforcement is also needed to prevent premature buckling of vertical reinforcement and to provide shear resistance at the potential plastic hinge regions.

An experimental program was carried out at Construction Technology Laboratories, Inc. (CTL) in which square and circular columns having differing amounts and details of transverse reinforcement and varying levels of axial load were subjected to moment reversals at increasing inelastic deformations. Observed behavior of the columns is described and a summary of test results is presented. Experimental results are compared to analytical predictions. Finally, design recommendations are made based on test results.

2.0 GENERAL BACKGROUND

The usual seismic resistant design of reinforced concrete ductile frame buildings (6, 7) provides a relative condition of a strong column and weak beam at any junction. The intent is to encourage hinging in the beams to absorb extreme displacements forced on the frame by seismic forces. Selna, Martin, Park, and Wyllie (8) examined design aspects of columns in frames. They expressed concern that a greater multiplier in the relative strength of columns and beams is needed to encourage beam hinging. That is, the summation of column moment capacities at a joint must be greater than the summation of beam moment capacities. However, in "gravity load dominated frames," it is possible for hinging to occur in the column (9).

The possibility of column hinging, and the continuing evidence of damage in columns during earthquakes have prompted research of column hinging. Testing has been directed toward understanding the function of lateral ties as:

1. Confinement for the column core
2. A means of preventing buckling of main reinforcement
3. Reinforcement for shear

Sheikh and Uzumeri (10) subjected square columns to axial loading. One of their conclusions was "concrete, when confined with rectangular ties and well distributed longitudinal steel, exhibits a very significant strength gain as well as increased ductility." In addition to confining the concrete, the ties also controlled buckling of the longitudinal bars. Spacings of ties for confinement were sufficient for buckling control.

Tests involving shear reversals in columns were reported by Wight and Sozen (11). They examined procedures for design of transverse reinforcement. Shear and confinement functions were identified for the transverse reinforcement. When insufficient transverse reinforcement was used, data indicated a progressive decrease in strength and stiffness under repeated reversals of hinging. However, when there was sufficient transverse reinforcement to confine the concrete and also carry the total shear, the columns maintained strength and stiffness. Axial compressive load in the

column specimens reduced the strength reduction effect of repeated cycles of hinging.

Many other investigators have also indicated the usefulness of hoops for confinement and to delay buckling of vertical reinforcement (12 through 29). A general finding of most reported experimental studies is that both concrete stress and strain capacity are enhanced by:

1. An increase in total amount of transverse reinforcement
2. A decrease in spacing of transverse reinforcement
3. An increase in the number of longitudinal bars located around the column perimeter and tied in the corner of a hoop bar

Hanson and Rabbat (30) reported that supplementary crossties with 135 degree hook on one end and 90 degree hook on the other perform satisfactorily when alternated end-for-end along the column longitudinal steel.

Moehle and Cavanagh (31) tested concrete columns under concentric monotonic compression with various transverse reinforcement. They concluded that the use of crossties with 90 degree and 135 degree hooks perform satisfactorily. They also found that crossties engaging only the perimeter hoops and not the vertical bars induced stress concentrations in the hoops, resulting in fracture of the perimeter hoops at the crossties.

Tanaka, et al (32) tested the effectiveness of different types of transverse reinforcement under axial compressive loading and cyclic flexure. They concluded the use of perimeter hoops composed of two U-shaped bars lapped in the cover concrete was satisfactory to only a limited extent. The limited study was carried out in investigating spliced crossties.

Ozcebe and Saatciogly (33) investigated the effect of confinement in concrete columns subjected to simulated seismic forces. They concluded that although the ACI-318-83 requirement for the amount of confinement is adequate to insure ductile behavior of columns, detailing requirements are not adequate for columns with unsupported longitudinal bars. The results of their tests showed the use of crossties in square columns increases the column's performance significantly, and the use of crossties with a 135 degree hook at one end and a 90 degree hook at the other end performs as

satisfactorily as those with 135 degree hooks at both ends.

Yeh and Sheikh (34) investigated flexural behavior of concrete columns subjected to high axial loads. Variables included detailing of longitudinal and lateral steel, spacing, and amount of lateral steel. They concluded that:

1. The detailing of longitudinal bars and ties is an important factor in performance of confined concrete columns subjected to combined axial and lateral loads;
2. Closer spacing of ties without increasing the total amount of confining reinforcements resulted in higher moment-capacity and ductility.
3. Crossties with 90 degree hooks at one end and 180 degree hooks at the other end are effective in confining concrete at small deformations; however, at large deformations the hooks tend to open resulting in a rapid loss of strength particularly under high axial loads.

In general, little research has been conducted to evaluate effects of hoop arrangements, length of hoop leg extensions, and angle of hoop leg bends. One of the most important factors that must be considered with regard to bend and hook length requirements for rectangular hoops and crossties is their contribution to reinforcement congestion and subsequent construction problems.

3.0 OBJECTIVE AND SCOPE

3.1 Objectives

The overall objective of this investigation is to recommend design criteria for transverse reinforcement in reinforced concrete columns for seismic resistant buildings. Specific objectives are:

1. To determine the adequacy of present code requirements.
2. To provide data on effects of transverse reinforcement on column behavior based on results of parametric load test investigation.
3. To correlate results of measured inelastic deformations with implied ductility demands of U.S. codes in determining reinforcement requirements.
4. To develop practical recommendations for detailing transverse reinforcement to facilitate constructibility of reinforcement and placement of concrete.

3.2 Scope of Investigation

Twelve full-scale column specimens with square and circular cross-sections were tested. Each test specimen consisted of a column with short stubs representing joining beams. Each specimen was subjected to a combination of constant axial load and cyclic horizontal loading.

Test variables included level of axial load, type of transverse reinforcement, and amount and spacing of transverse reinforcement. The effect of each variable on energy dissipation capabilities of the columns was investigated. Detailed test observations are described. Test results are compared with analytical models.

4.0 EXPERIMENTAL PROGRAM

This section gives a description of the test specimens and test procedures. A total of 12 specimens were tested. Eleven specimens had a square cross-section and one specimen (NC-11) had a circular cross-section.

4.1 Test Specimens

4.1.1 Specimens with Square Cross-Sections

Eleven full-scale column specimens with square cross-sections were tested. Figure 4-1 shows the overall dimensions. The complete column had a cross-section of 18x18 in. and a height of 11 ft 6 in. The distance between the beam-column stub interface and the pivot point support in the lower and upper columns represents the portion of a column in a building extending from the beam-column connection to approximately the points of inflection. The beam portion was simulated by a short stub as shown in Fig. 4-1. The beam stub also provided a point for application of lateral load and confinement of the joint region so that any hinging occurred in the column. The height of the upper column was greater than the height of the lower column to force hinging into the upper column. Except in Specimen NC-1, moment capacity of the lower column was increased by providing additional vertical reinforcement.

4.1.2 Specimen with Circular Cross-Section

One full-scale specimen (NC-11) with a circular cross-section was tested. This specimen was identical to the other specimens except that the upper column's cross-section was circular with a radius of 9 in.

4.2 Reinforcement Details and Materials

4.2.1 Specimens with Square Cross-Sections

Details of vertical and transverse reinforcement are listed in Table 4.1 and transverse reinforcement details are shown in Fig. 4-2. Vertical column steel consisted of eight No. 8 bars spaced symmetrically as shown in Fig. 4-3. The lower column was reinforced with six additional No. 6 bars in

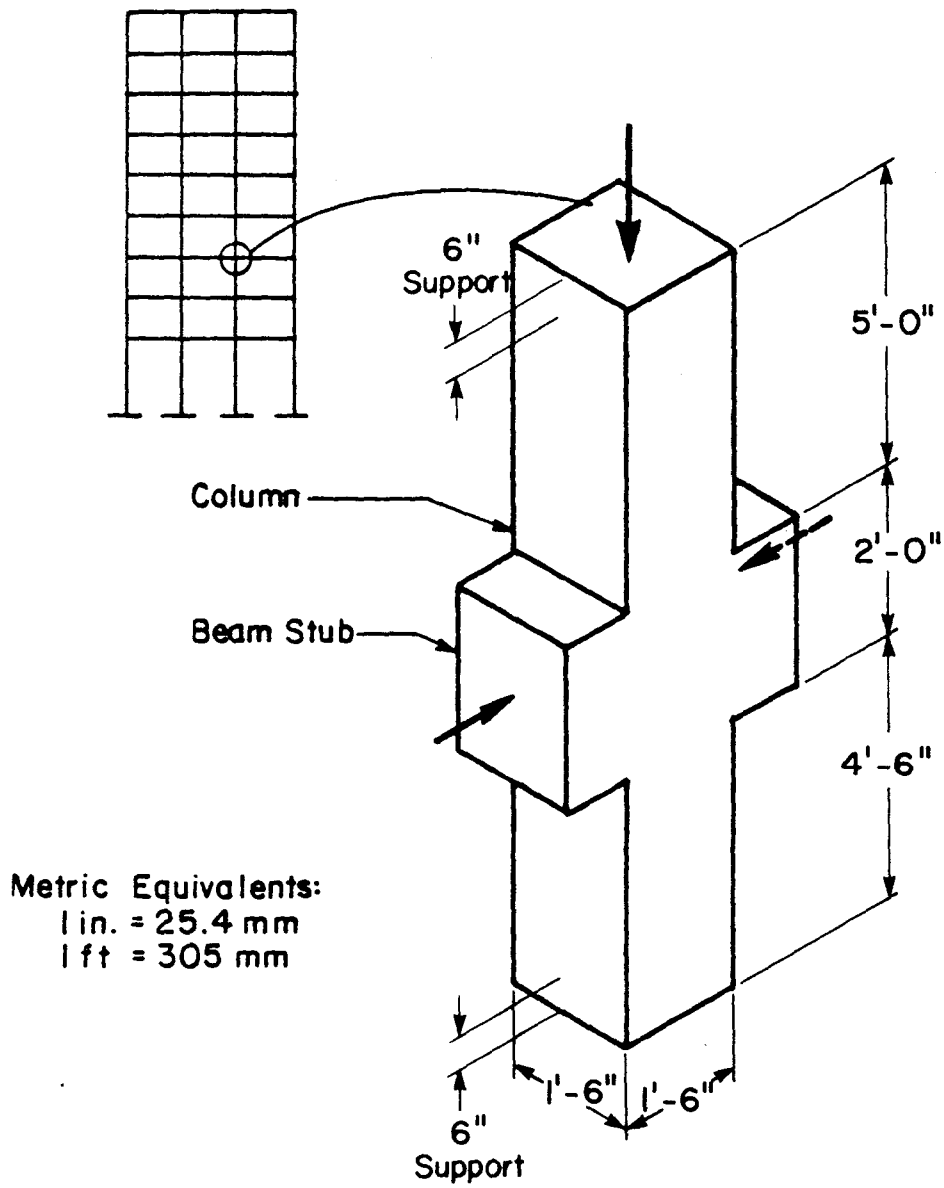


FIG. 4-1 OVERALL VIEW OF TEST SPECIMEN

Table 4.1 Details of Test Variables

Specimen Designation	Vertical Load.		Vertical Reinforcement		Transverse Reinforcement			Confined Length of column(in)	
	P_v/P_o^{***}	Kips	Bars	Percent	++ Detail	Bar Size	A_{sh} (sq. in.)		Percent
NC-1	0.30	570	8 No. 8	1.95	A	No. 4	0.68	2.19	22
NC-2	0.20	380	8 No. 8	1.95	B	No. 4	0.68	2.19	22
NC-3	0.40	780	8 No. 8	1.95	B	No. 4	0.68	2.19	22
NC-4	0.30	580	8 No. 8	1.95	B	No. 3	0.38	1.26	22
NC-5	0.30	575	8 No. 8	1.95	C	No. 4	0.68	2.19	22
NC-6	0.30	520	8 No. 8	1.95	D	No. 4	0.40	1.29	22
NC-7	0.30	540	8 No. 8	1.95	E	No. 4	0.40	1.29	22
NC-8	0.30	560	8 No. 8	1.95	B*	No. 4	0.68	2.19	22
NC-9	0.30	530	8 No. 8	1.95	F**	No. 4	0.40	1.29	22
NC-10	0.30	550	8 No. 8	1.95	F#	No. 3	0.22	1.29	22
NC-12	0.30	554	8 No. 8	1.95	F	No. 3	0.30	1.29	22

*Detail B modified by staggering inner and peripheral hoops.

**Detail F with no cross tie and No. 4 continuous square helix at 4-in. (100-mm) pitch.

#Detail F with no cross tie and No. 3 continuous square helix at 2-1/4in. (57-mm) pitch.

Metric Equivalents:

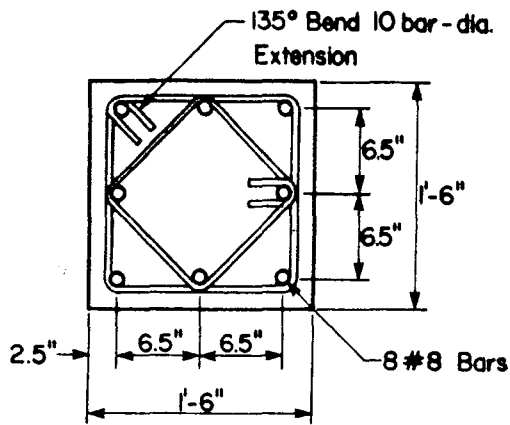
1 kip = 4.45 kN

1 kip = 25.4 mm

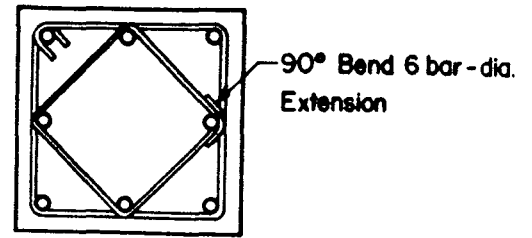
++Details of transverse reinforcements shown in figure 4-2

*** $P_o = 0.85 f_c(A_g - A_{st}) + A_{st} + f_y$

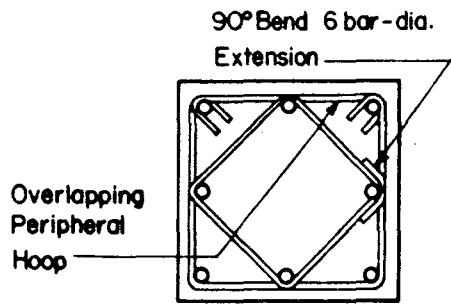
P_v = VERTICAL COLUMN LOAD



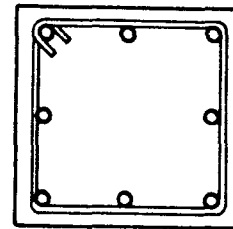
(a) Detail A



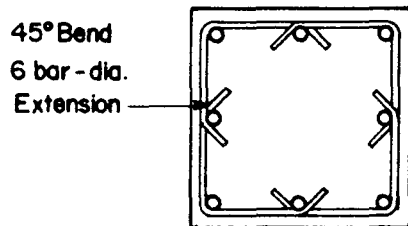
(b) Detail B



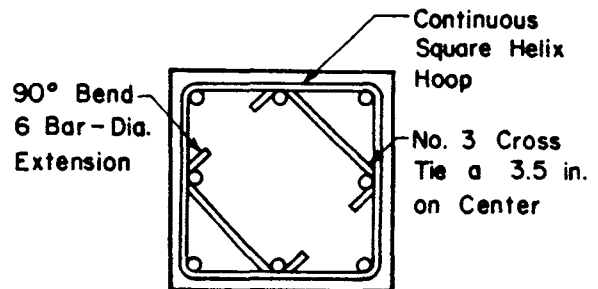
(c) Detail C



(d) Detail D



(e) Detail E

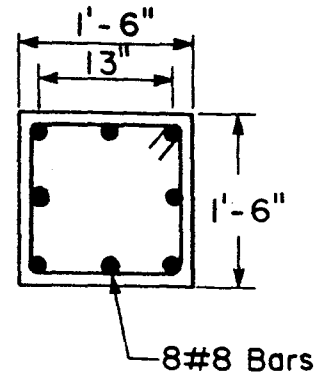
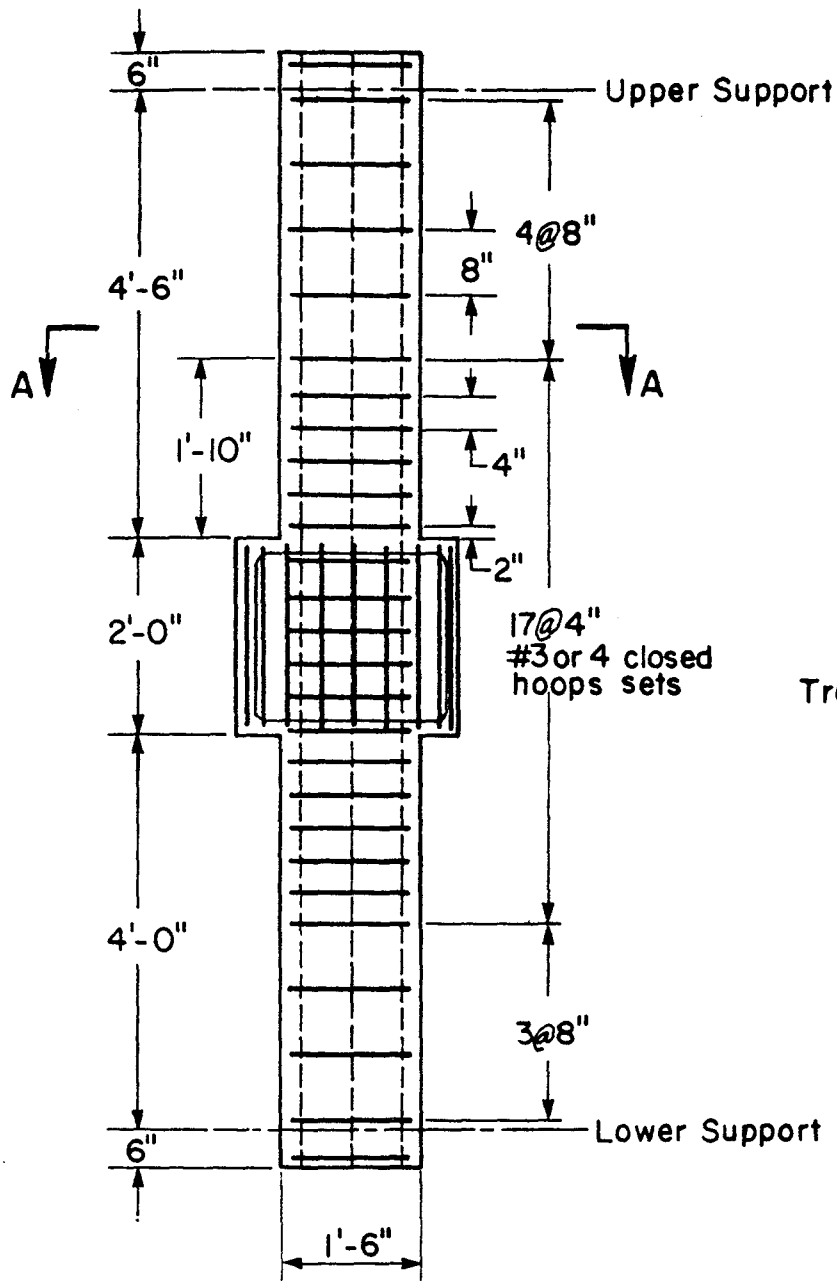


(f) Detail F

Clear Concrete Cover = 1.5"
Hoop Spacing = 4"

Metric Equivalents:
1 in. = 25.4 mm
1 ft = 305 mm

FIG. 4-2 DETAILS OF TRANSVERSE REINFORCEMENT



Section A-A

Transverse Reinforcement
Details Vary

Note: Lower column had
additional vertical
reinforcement not
shown in this Fig.

Metric Equivalents:
1 in. = 25.4 mm
1 ft = 305 mm

Elevation

FIG. 4-3 REINFORCEMENT DETAILS FOR SQUARE COLUMNS

the direction of lateral horizontal loads. This additional reinforcement was provided to increase flexural capacity of the lower column. This allowed the instrumentation to be provided in the plastic hinging region of the upper column only. Specimen NC-1 did not have additional reinforcement in the lower column. Transverse reinforcement for test Specimen NC-1, as shown in Fig. 4-2, was designed in accordance with provisions of Section A.4.4 of the 1983 ACI Building Code. This required 135 degree hook bends with ten bar-diameter extensions for both inner and peripheral confining hoops. For all other specimens, hook extensions were reduced to six bar-diameter lengths. In addition, in Specimens NC-2, NC-3, NC-4, NC-5, and NC-8, hook bends for inner hoops were reduced to 90 degrees as shown in Fig. 4-2. Peripheral hoops for Specimen NC-5 consisted of two overlapping pieces as shown in Fig. 4-2(c). The end anchorage for each piece consisted of 135 degree bend and six bar diameter extension. Specimen NC-6 used single peripheral hoops with 135 degree hook bends and six bar-diameter extensions as shown in Fig. 4-2(d).

Transverse reinforcement for Specimen NC-7 consisted of single peripheral hoops. Each of these hoops was formed with four identical ties as shown in Fig. 4-2(e). Specimen NC-8 used an arrangement as shown in Fig. 4-2(b) except that the inner and peripheral hoops were staggered vertically to provide a 2-in. (50 mm) center-to-center spacing between them.

Transverse reinforcement for Specimen NC-9 consisted of a No. 4 continuous square helix at 4-in. (100-mm) pitch. Specimen NC-10 used a No. 3 continuous square helix at 2-1/4 in. (57-mm) pitch. Specimen NC-12 used a No. 3 continuous square helix at 3-1/2-in. (89-mm) pitch with No. 3 crossties at 3-1/2-in. (89-mm) on center as shown in Fig. 4-2(h).

The length of column confined by transverse reinforcement was kept constant at 22 in. (0.56 m) above and below the beam stub. Except for Specimens NC-8, NC-9, NC-10, and NC-12 hoops were spaced 4 in. (100 mm) on center in the confined region. Transverse reinforcement in the unconfined region of the column was designed to carry maximum shear stress. This required a single No. 4 peripheral hoop spaced 8 in. (203 mm) on center.

Clear concrete cover over vertical reinforcement was maintained at 2.0 in. (51 mm) in upper and lower columns.

4.2.2 Specimen with Circular Cross-Section

Detail of vertical transverse reinforcement for Specimen NC-11 is shown in Fig. 4-4. It consisted of eight No. 8 bars placed symmetrically. The lower column was reinforced with six additional No. 6 bars as shown in Fig. 4-4. Transverse reinforcement within the confined region of the upper column consisted of 3/8 in. diameter spiral reinforcement at 2.25 in. pitch. Spiral reinforcement was continuous from approximately 2 ft 2 in. from the bottom of the specimen to 2 ft 2 in. from the top of the specimen. To prevent buckling of the additional corner bars in the lower column, #4 peripheral hoops were provided in the lower column only. To prevent crushing of the column near top and bottom supports, additional transverse reinforcement was provided within approximately 20 in. of the top and bottom ends of the specimen.

4.3 Specimen Fabrication

The column reinforcing cage was assembled first. The vertical bars were welded to the lower end bearing plate. Transverse hoops were dropped from the top and tied to vertical bars at designated locations and the upper load bearing plate was welded to the upper ends of vertical bars. Strain gages were attached to vertical and transverse reinforcement in the potential plastic hinge region. Fig. 4-5 shows a representative reinforcing cage.

The assembled cage was placed horizontally in the specimen form. Anchors, pipes, and tubes were positioned for later attachment of loading plates and external instrumentation, and to provide openings for loading rods. An assembled form with reinforcing cage is shown just prior to casting concrete in Fig. 4-6.

Casting of all specimens except NC-11 was completed within about two hours. The concrete was placed starting at one end and ending at the other and was consolidated with a spud vibrator. Placement of concrete is shown in Fig. 4-7. Test specimen and control cylinders were initially cured in the forms and molds and under polyethylene sheets. After three days, forms and molds were stripped and specimens were cured at approximately 72°F (22°C).

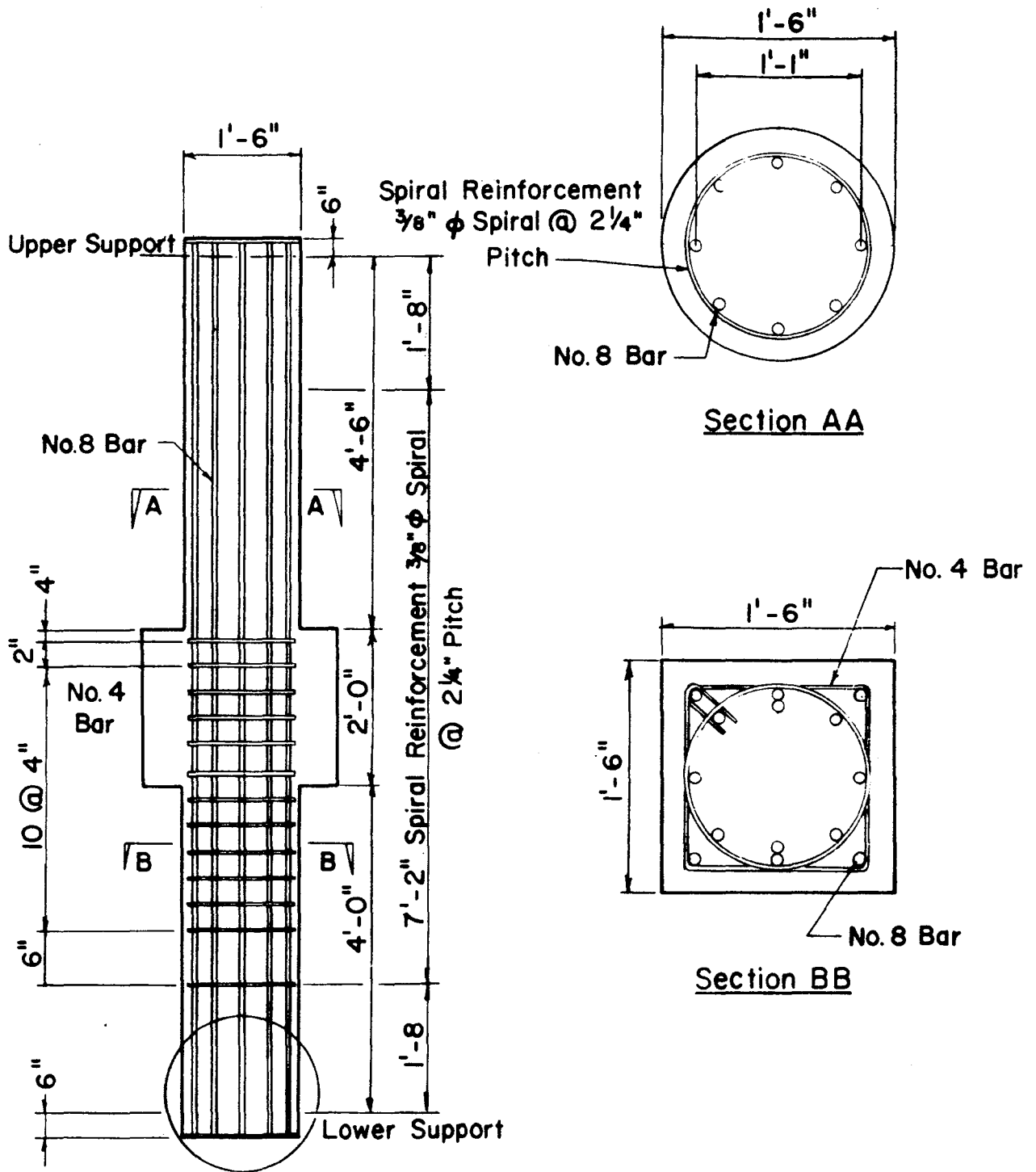


FIG. 4-4 REPRESENTATIVE DETAILS FOR CIRCULAR COLUMN

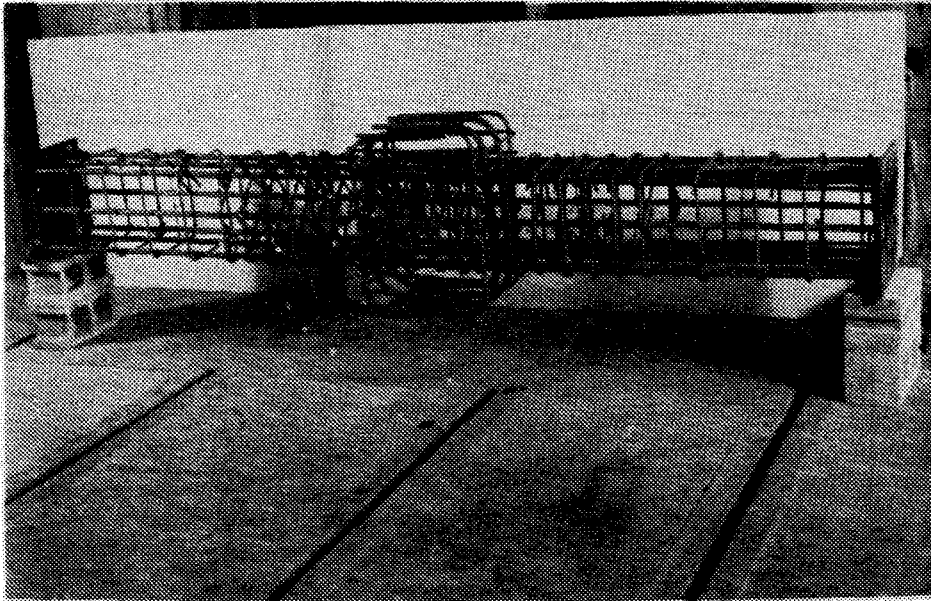


FIG. 4-5 REPRESENTATIVE REINFORCING GAGE

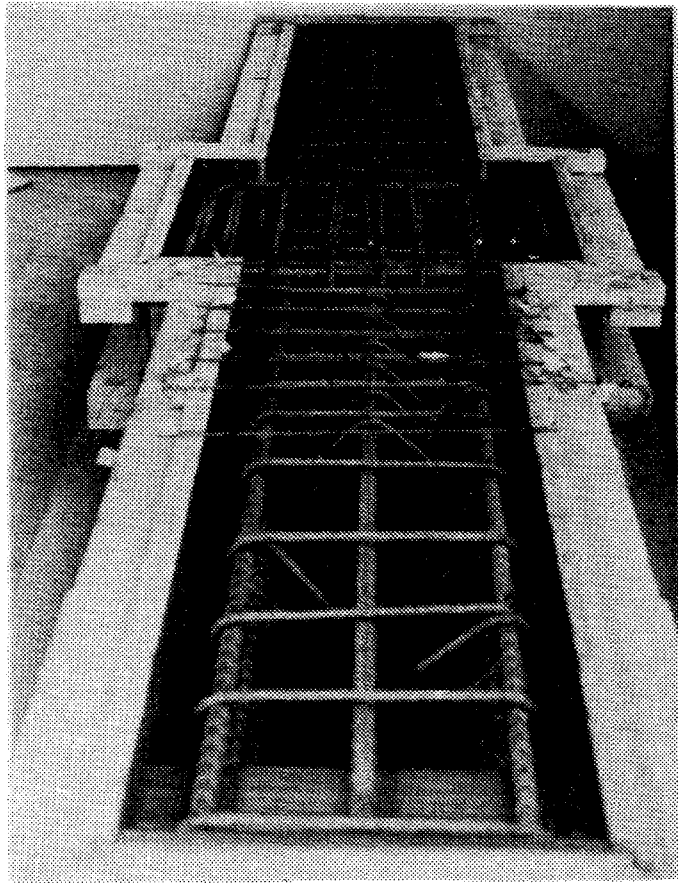


FIG. 4-6 SPECIMEN MOLD

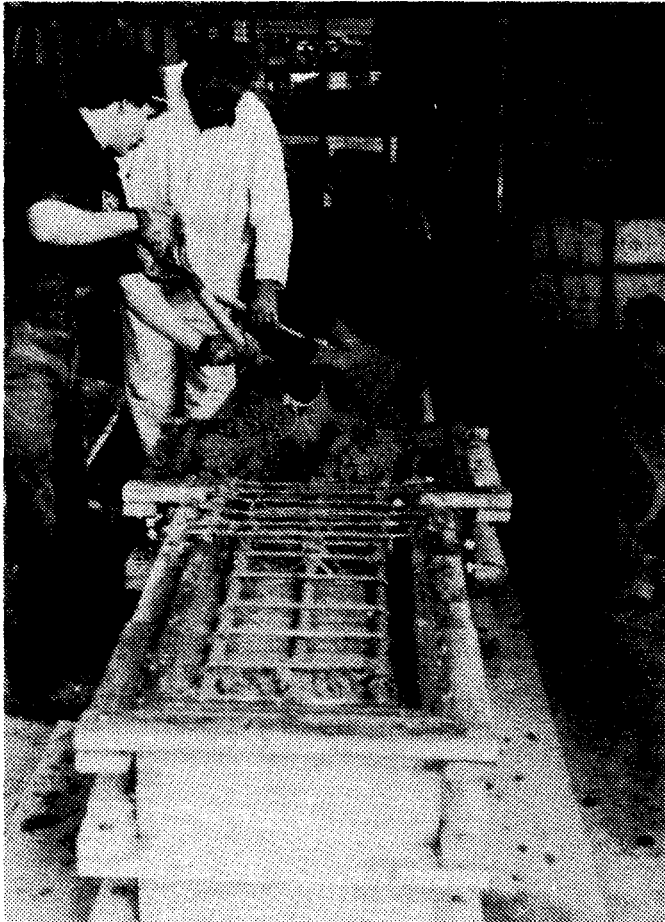


FIG. 4-7 PLACEMENT OF CONCRETE

Casting of Specimen NC-11 (circular cross-section) was similar to other specimens except that the lower column and beam stub were cast first. After approximately three days the specimen was raised to a vertical position and the upper column was cast.

4.4 Material Properties

Average material properties of transverse reinforcement and vertical reinforcement are given in Table 4.2. The reinforcement conformed to requirements of ASTM Designation A615 Grade 60 (35). All concrete mixes were prepared at Construction Technology Laboratories except for Specimen NC-12 which was cast using ready mix concrete. Mix proportions per cubic yard are listed in Table 4.3.

At least six 6x12-in. (152x305-mm) control cylinders were taken from the batches placed in and around the test region of upper column. Three cylinders were tested for compressive strength and three for splitting tensile strength. Age of concrete on the day of each column test, and average compressive and splitting tensile strengths are listed in Table 4.4.

4.5 Test Setup

Test set-up and loading arrangements are shown schematically in Fig. 4-8 and a photo of the test setup is shown in Fig. 4-9. The specimen was centered in a one-million-lb (4448 kN) capacity testing machine that was used to apply vertical compressive load. The lower end of the test column rested on a pin pivot. The upper end was centered below the spherically seated loading head of the movable platten of the testing machine. Uniform contact at the top of the column was ensured by using a thin layer of high strength plaster.

The lower column end was similarly bedded with plaster to the upper plate of the pin pivot. The pivot assembly consisted of two grooved 4-in. thick (102-mm) steel plates separated by a 4-in. diameter (102-mm) high-strength steel roller acting as the pivot.

The lateral loading system consisted of hydraulic rams and a pair of reaction frames as shown in Fig. 4-8. Each reaction frame consisted of a large wide-flange designed to withstand maximum expected lateral load

Table 4.2 Material Properties

Transverse Reinforcements				Vertical Reinforcement			
No. 3 Bar		No. 4 Bar		No. 8 Bar			
f_y (ksi)	f_{su} (ksi)	% Elongation	f_y (ksi)	f_{su} (ksi)	% Elongation	f_y (ksi)	% Elongation
89.4	101.3	8.5	65.8	100.9	15.4	63.7	13.1
						f_{su} (ksi)	106.7

f_y = YIELD STRESS
 f_{su} = TENSILE STRENGTH

Table 4.3 Concrete mix proportions

Ingredients	Quantity
Cement, Type I	565 lb
Elgin sand	1325 lb
1/4-in. to 3/8-in. gravel	859 lb
3/8-in. to 3/4-in. gravel	859 lb
Air Entrainment Agent	0.81 liter
Water	290 lb

Metric Equivalents:

1 lb = 4.448 N

1 in. = 25.4 mm

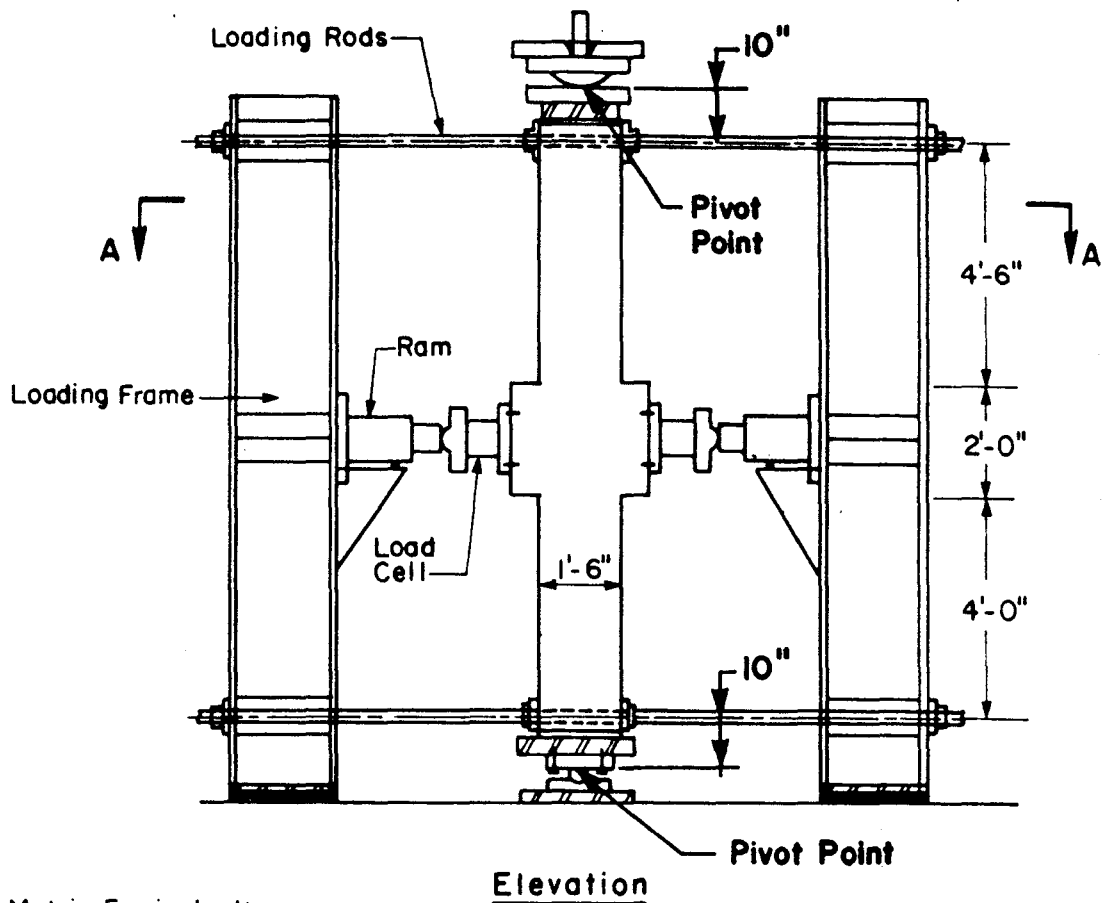
Table 4.4 Material properties

Specimen Designations	Strength* (psi)		Age at Test days
	f'_c	f_{ct}	
NC-1	5640	470	35
NC-2	5700	520	35
NC-3	5830	500	34
NC-4	5780	490	35
NC-5	5710	530	30
NC-6	5040	500	33
NC-7	5280	530	28
NC-8	5510	525	30
NC-9	5020	460	30
NC-10	5290	475	29
NC-11	5500	545	33
NC-12	5325	530	12

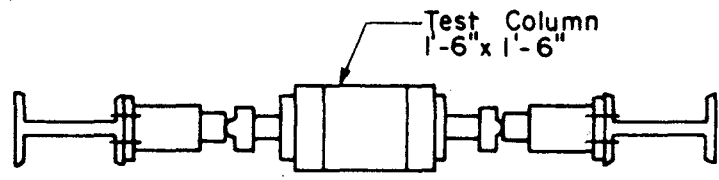
*Average concrete compressive and tensile strength determined from 6x12-in. (152x305-mm) cylinders on the day of the test.

f'_c = Concrete Compressive Strength

f_{ct} = Splitting Tensile Strength



Metric Equivalents:
 1 in. = 25.4 mm
 1 ft = 305 mm



Section A-A

FIG. 4-8 LOADING ARRANGEMENT

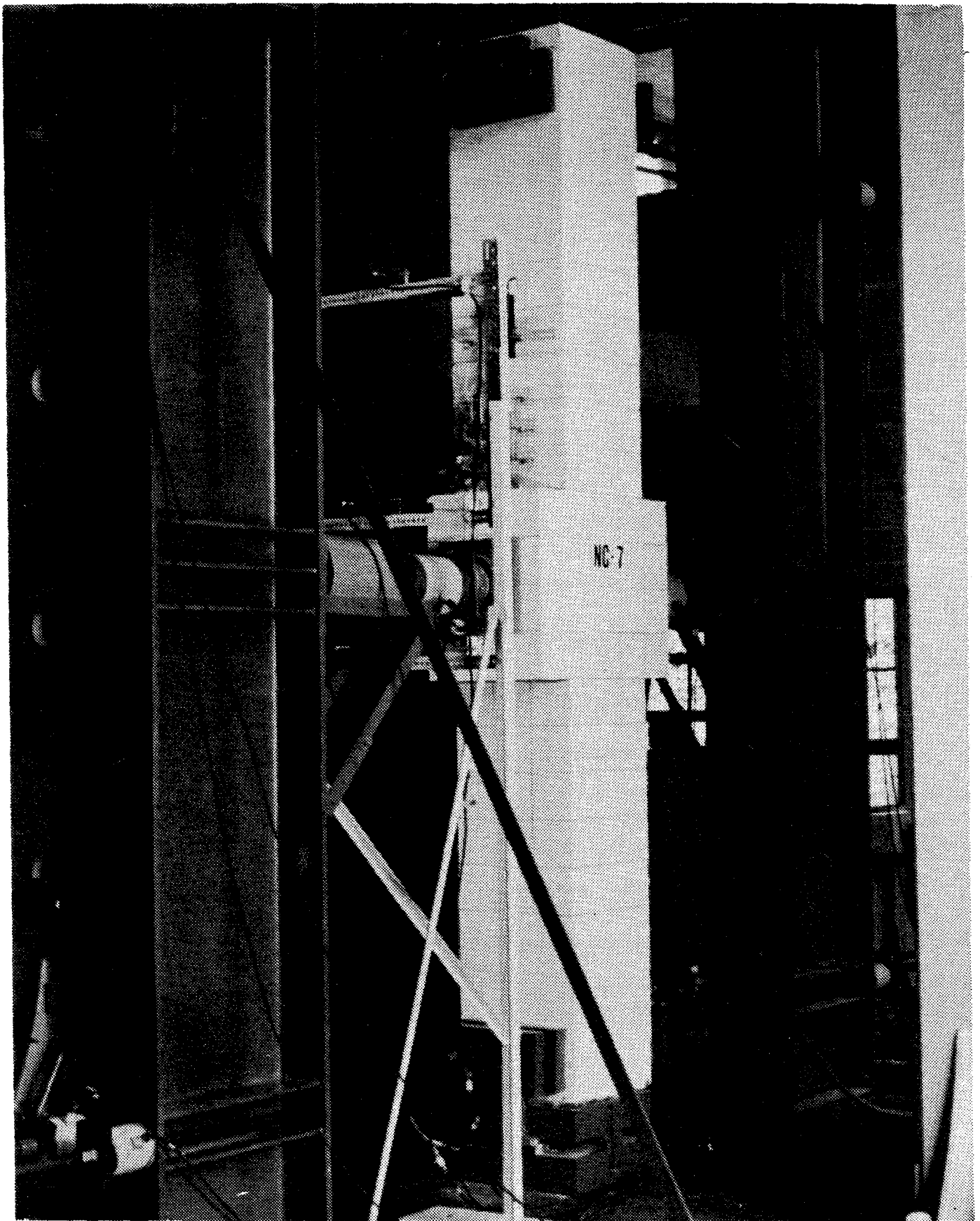


FIG. 4-9 TEST SETUP

with little deflection. These beams were strengthened by welding web stiffening plates at the horizontal load points. Lateral load was applied at beam stub centers of the specimen with a 200-ton (1779-kN) hydraulic ram on each side. The hydraulic ram and the load cell assembly were supported on a bracket attached to a flange of each reaction beam. The load was transferred to the specimen through a spherical bearing and a flat loading plate assembly. This allowed rotation of the beam stub at load point. The reaction frames were connected to the specimen by four 1-in. diameter (25.4-mm) threaded bars, two each at top and bottom as shown schematically in Fig. 4-8. Vertical and lateral loads were controlled by two independent loading systems.

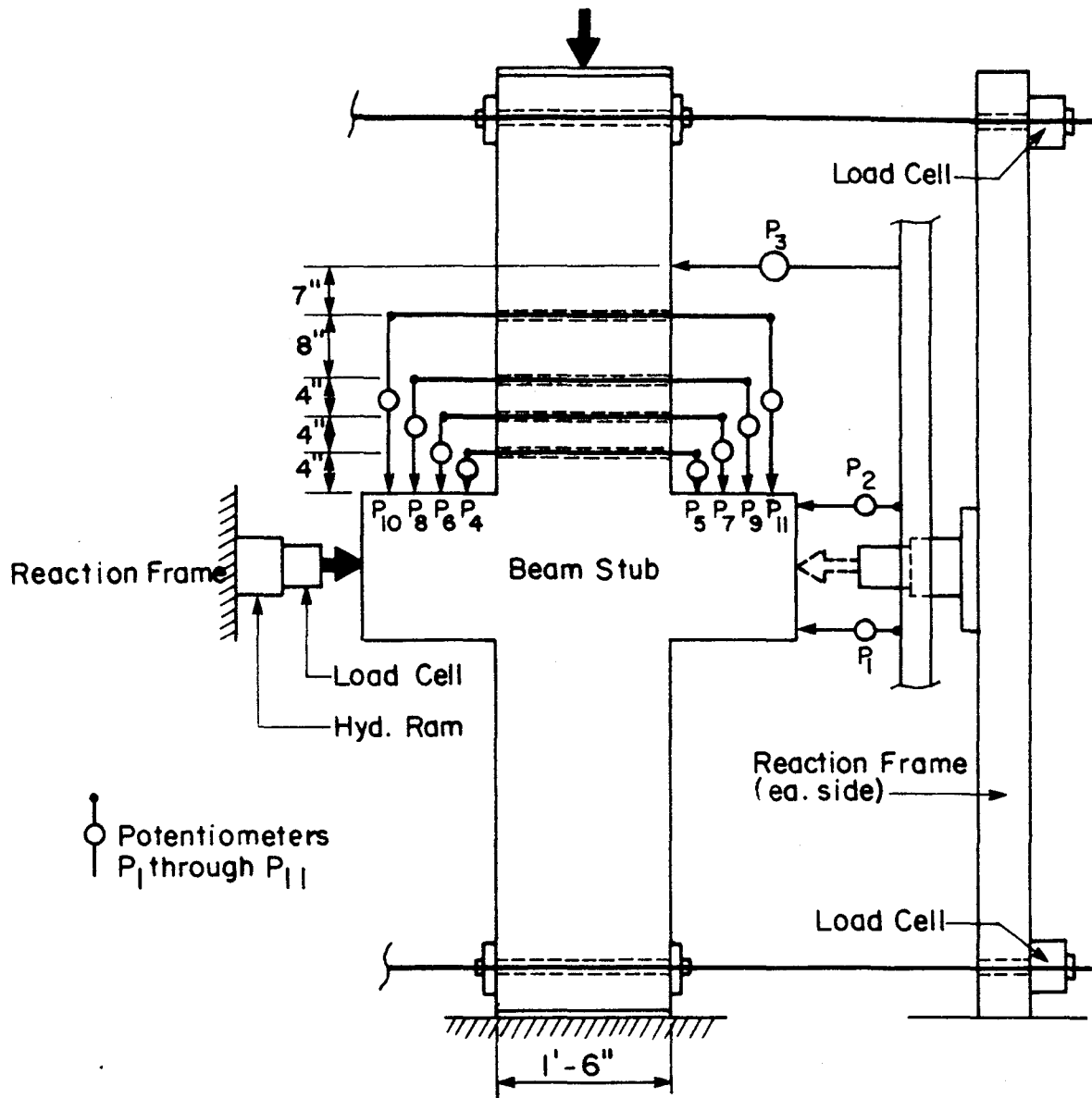
4.6 Instrumentation

Several types of instruments were required to obtain load-displacement, moment-curvature, vertical bar strain profiles, confining hoop strains, plastic hinge lengths, and maximum concrete compressive strains. External measurements were used to determine column axial and lateral loads, horizontal column displacements, column rotations, vertical reinforcement strains, and concrete strains. Internal measurements included strain on the vertical and transverse column reinforcement in the potential plastic hinge region.

Layout of external instrumentation, including load cells and potentiometers, is shown in Fig. 4-10. Locations of strain gages for transverse reinforcement for Specimens NC-1, NC-2, NC-3, NC-4, and NC-5 are shown in Fig. 4-11 and for Specimens NC-6 and NC-7 in Fig. 4-12. Locations of strain gages for Specimen NC-8 through NC-12 are described in Appendix A.

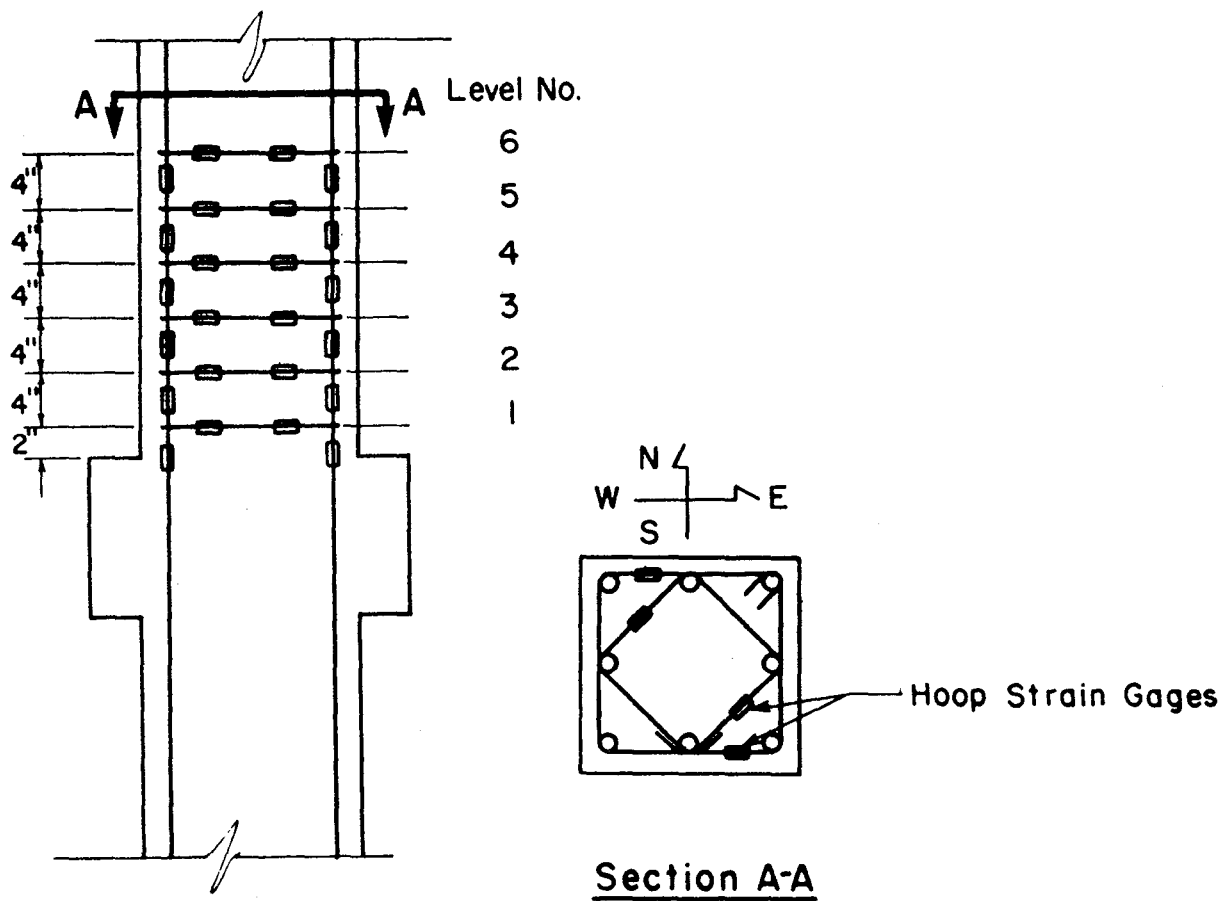
4.6.1 Forces

Column axial load was determined from the load measuring capsule of the testing machine. The load was controlled manually on the dial of the machine console. Lateral applied loads were measured by independent load cells on each side of the beam stub as shown in Fig. 4-10.



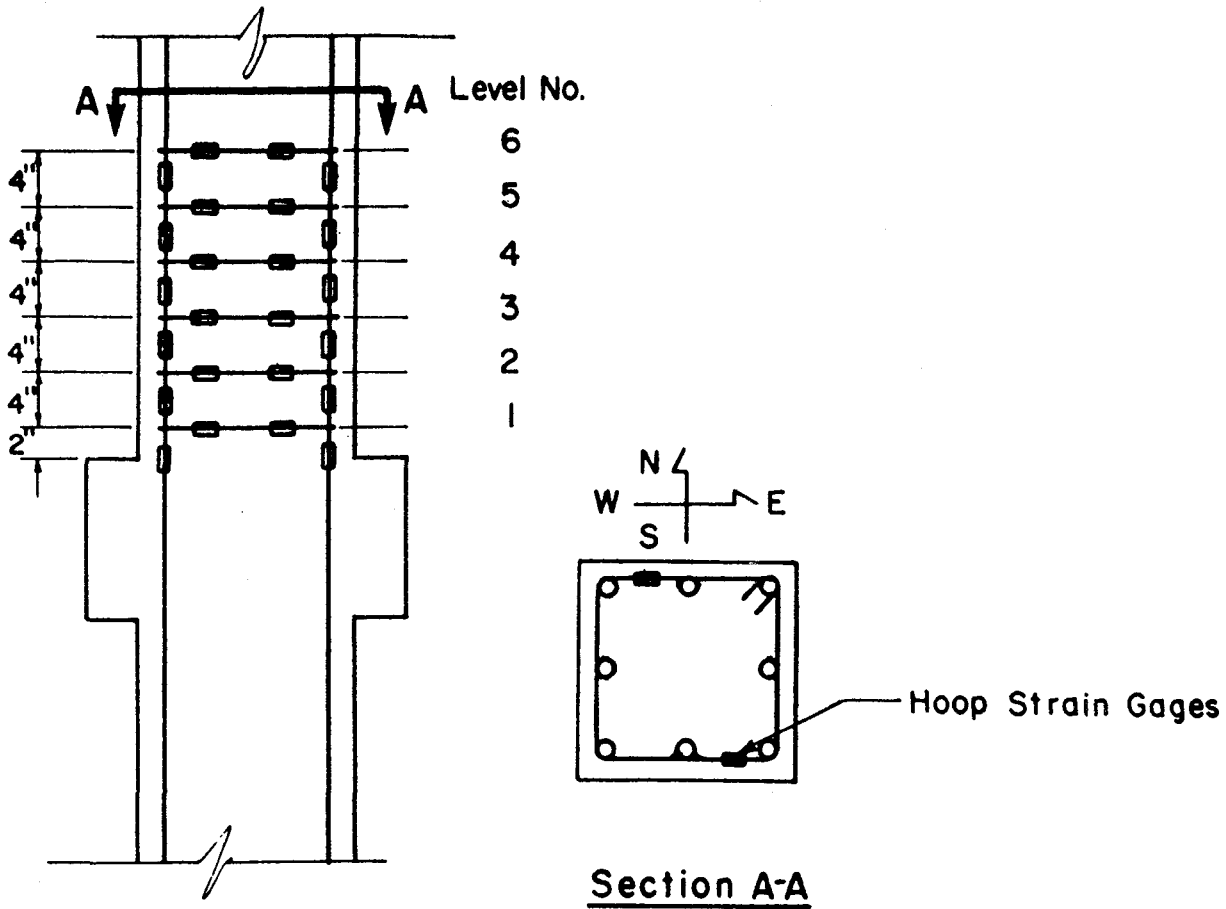
Metric Equivalents:
1 in. = 25.4 mm
1 ft = 305 mm

FIG. 4-10 EXTERNAL INSTRUMENTATION



Level Number	Gages attached to peripheral hoops		Gages attached to cross ties	
	South Side	North Side	East Side	West Side
1	# 13	# 25	# 19	# 31
2	# 14	# 26	# 20	# 32
3	# 15	# 27	# 21	# 33
4	# 16	# 28	# 22	# 34
5	# 17	# 29	# 23	# 35
6	# 18	# 30	# 24	# 36

FIG. 4-11 STRAIN GAGE LOCATIONS FOR SPECIMENS NC-1, NC-2, NC-3, NC-4 AND NC-5



Level Number	Gages attached to peripheral hoops	
	South Side	North Side
1	#13	#19
2	#14	#20
3	#15	#21
4	#16	#22
5	#17	#23
6	#18	#24

FIG. 4-12 STRAIN GAGE LOCATIONS FOR SPECIMENS NC-6 AND NC-7

4.6.2 Horizontal Displacements

Horizontal displacement was measured at three locations along the height of the test specimen. Displacement sensors P_1 , P_2 , and P_3 were 6-in. linear potentiometers connected between the specimen and an independent stand as shown in Fig. 4-10. Sensors P_1 and P_2 measured horizontal displacement at the bottom and top of beam stub, respectively, and P_3 measured horizontal displacement at midheight of the upper column. The measurement made by P_2 at the top of the beam stub was considered representative of displacement at the base of the upper column. A continuous plot of horizontal load versus displacement at each of these locations was obtained during each test.

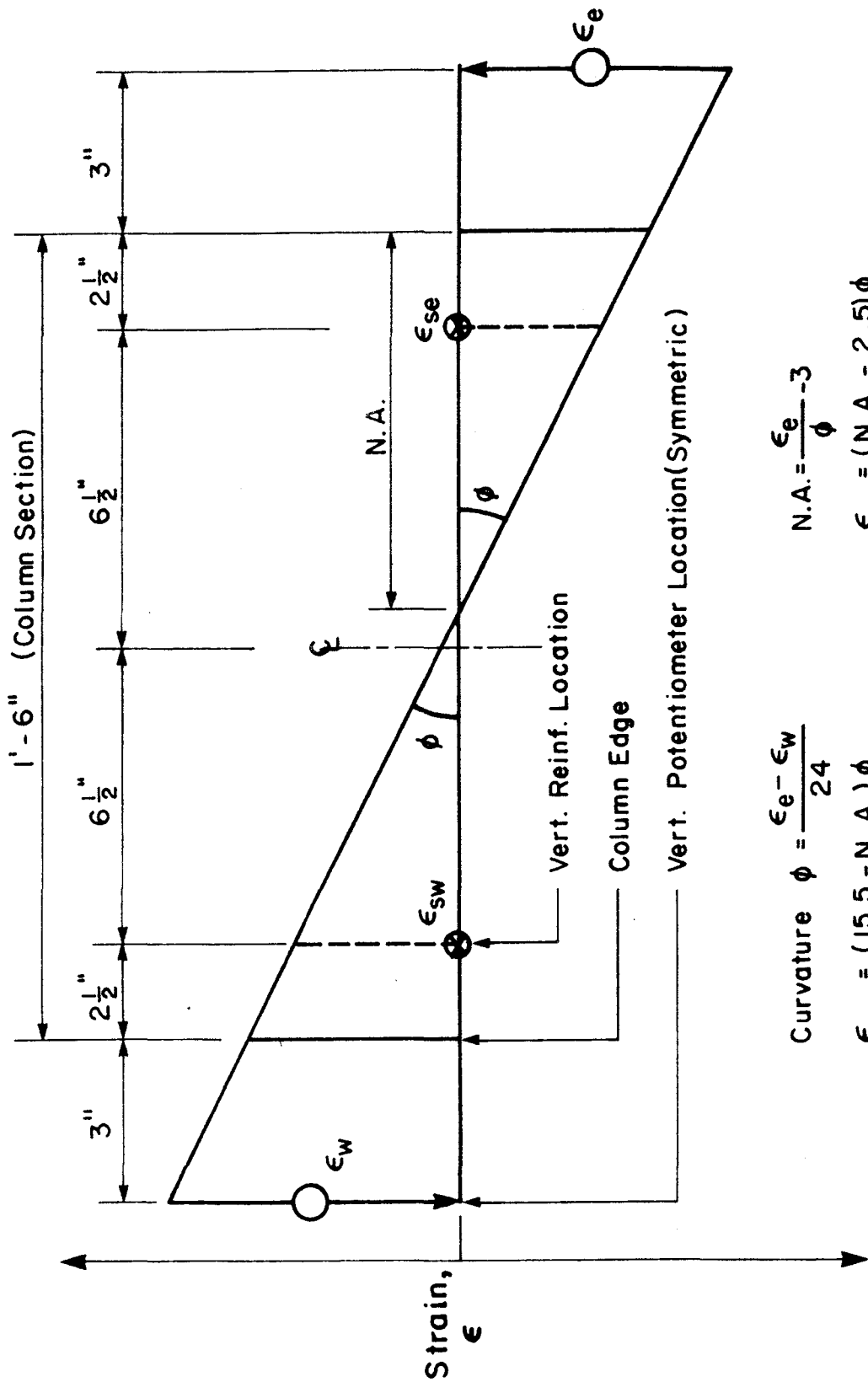
4.6.3 Strains and Curvatures

A series of linear potentiometers designated P_4 through P_{11} were used to sense displacement needed to determine rotations of the column above the beam stub. The location of these potentiometers as used in most specimens is shown in Fig. 4-10.

In Specimens NC-1 and NC-2, these measurements were made at column heights of 4, 8, and 12 in. (102, 203, and 305 mm), and 4, 8, 12, and 27 in. (102, 203, 305, and 686 mm), respectively, above the beam stub. In all other specimens, these measurements were made at heights of 4, 8, 12, and 20 in. (102, 203, 305, and 508 mm) above the stub. These potentiometers were attached to brackets on both sides of the specimen. Brackets were secured by a pair of 1/4-in. diameter (6-mm) threaded rods inserted through small conduits placed during construction of the specimen.

A strain distribution across the column section was obtained from a pair of potentiometers measuring longitudinal displacement over the same height on each side of the column.

Interpretation of this distribution gives concrete face and core strain as well as column curvature as shown in Fig. 4-13. This method assumes strain compatibility at the concrete-steel interface and that plane-sections remain plane.



$$\text{Curvature } \phi = \frac{\epsilon_e - \epsilon_w}{24}$$

$$\text{N.A.} = \frac{\epsilon_e}{\phi} - 3$$

$$\epsilon_{sw} = (15.5 - \text{N.A.}) \phi$$

$$\epsilon_{se} = (\text{N.A.} - 2.5) \phi$$

Metric Equivalents:
 1 in. = 25.4 mm
 1 ft = 305 mm

FIG. 4-13 CURVATURE AND STRAIN DETERMINATION

4.7 Data Acquisition

Loads, deformations, and strains were recorded at selected points during load cycling by a Digital Data Acquisition System (DDAS). A desk computer was interfaced with the DDAS to simultaneously store printed data. The on-line computer provided a tabulation of reduced data within seconds, and provided a display of selected information on the screen. A continuous plot of horizontal load versus displacement at the base of the upper column was obtained by an X-Y plotter.

4.8 Test Procedures

After placing the specimen in the test frame and attaching all instrumentation, the test was started by applying vertical load to the column. This vertical load was kept constant at a predetermined level during a test. Horizontal load was applied in a series of increments alternately first in the forward direction (east to west) and then in the reverse direction (west to east). One complete cycle hereafter is defined as consisting of one forward and one reverse horizontal loading. The specimen was loaded to initial yielding, to be defined in Section 4.8.2, in about three increments of horizontal force. Subsequent to initial yielding, loading was controlled by deflection increments. The columns above and below the beam stub were then subjected to a constant axial load and to moment reversals at increasing inelastic deformations.

4.8.1 Vertical Load

The vertical load applied to each column represented a fraction of the column axial load capacity as listed in Table 4-1. Column axial load capacity, P_o , was determined as follows:

$$P_o = 0.85 f'_c (A_g - A_{st}) + A_{st} F_y$$

where: A_g = gross area of column cross-section

A_{st} = area of vertical reinforcement

f'_c = compressive strength of concrete at the time of test

f_y = minimum specified yield strength of vertical reinforcement

4.8.2 Horizontal Loads

Maintaining the axial load constant, each specimen was subjected to a number of cycles of horizontal loading. In general, the first cycle of horizontal loading was in the "elastic" range. The horizontal load in the second cycle was that load corresponding to 75% of the theoretical moment capacity of the column cross-section. The first yield displacement, Δ_y , was found by extrapolating a straight line from the origin through the horizontal load-displacement point at $0.75 P_h$ to P_h , and calculating Δ_{y1} and Δ_{y2} as shown in Fig. 4-14, the average of Δ_{y1} and Δ_{y2} established the first yield displacement. In calculating the moment capacity, the provisions of the ACI 318-83 Building Code were used. Capacity reduction factor, ϕ , was taken as 1.0. Concrete compressive strength was determined from control test cylinders prior to test. Yield stress of reinforcing steel was assumed to be 60 ksi (419 MPa).

Horizontal displacement determined at first yield was used to control all subsequent cycles. Multiples of the yield displacement were imposed on the column to produce displacement ductilities as shown in the loading schedule of Fig. 4-15. Displacement ductility at each cycle was defined as the ratio of peak horizontal displacement to the first yield displacement.

The first yield curvature and curvature ductility were defined in a similar manner.

While column axial load was kept constant, the basic loading cycles were generally applied as follows: two cycles before displacement ductility 1, one cycle at displacement ductility 1, one cycle at displacement ductility between 1 and 2, two cycles each at displacement ductility 2, and subsequent ductilities. This pattern of ever increasing deformation in each cycle is not intended to represent any specific earthquake. Testing was stopped at a stage when the specimen could not sustain the vertical load under increasing lateral displacement.

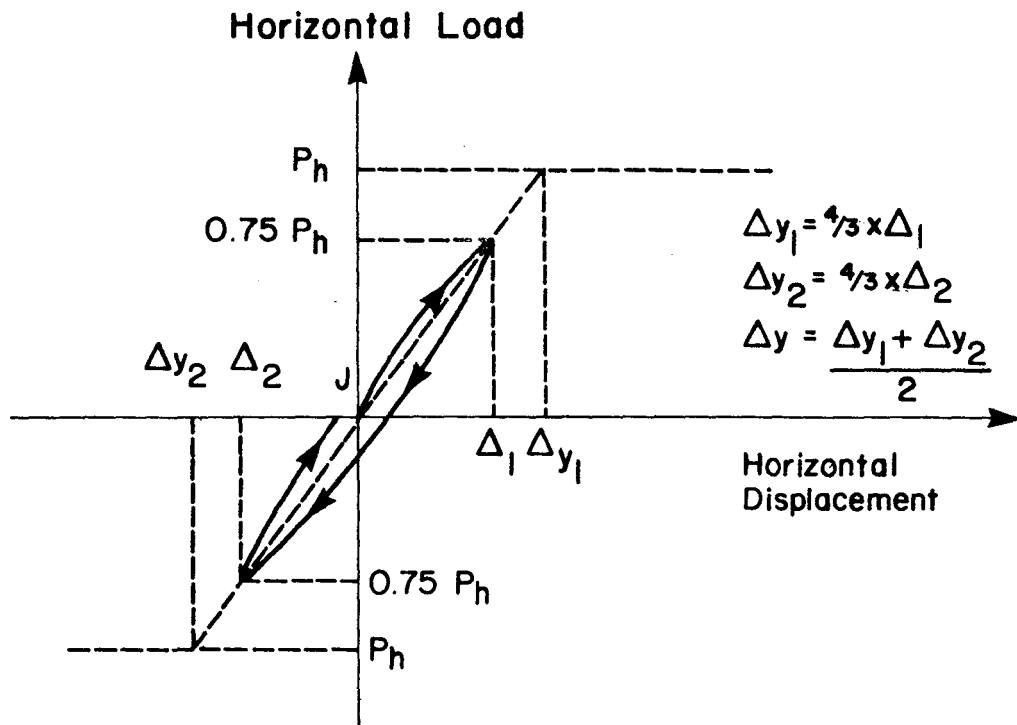


FIG. 4-14 EXPERIMENTAL DEFINITION OF FIRST YIELD DISPLACEMENT

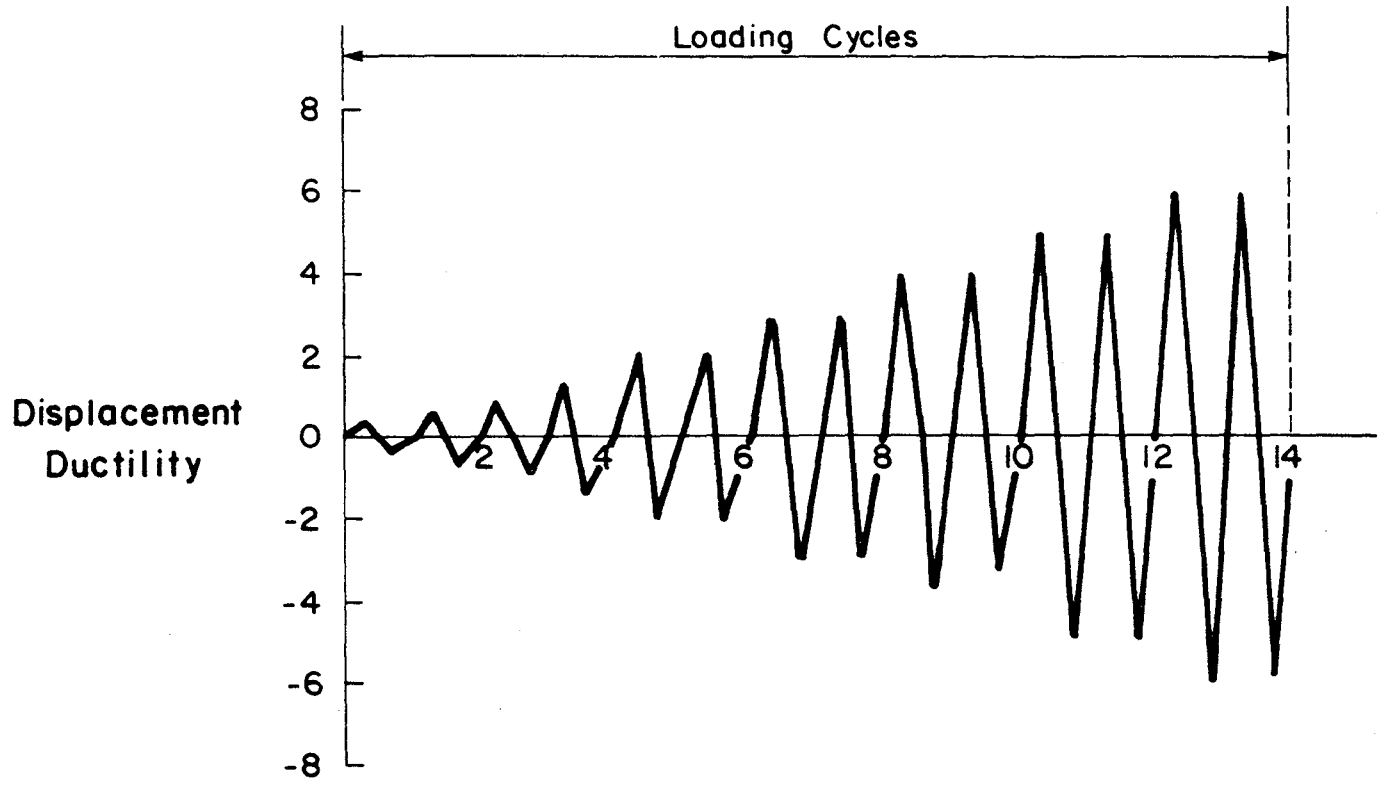


FIG. 4-15 LOADING SCHEDULE

5.0 SUMMARY OF TEST RESULTS

5.1 General Behavior of Specimens

The general behavior of test specimens is separately described by the type of transverse reinforcement used within 22 in. above the stub. The specimens are divided into two categories, those utilizing discrete transverse reinforcement and those employing some form of continuous transverse reinforcement. A more detailed description of the test behavior of each specimen is given in Appendix A.

5.1.1 Discrete Transverse Reinforcement

Specimens NC-1 through NC-8 employed discrete transverse reinforcement. Table 4-1 and Fig. 4-2 show the detail of reinforcement for each specimen. In all specimens the plastic hinge formed in the upper column except for Specimen NC-1 where the plastic hinge formed in the bottom column. In general, first cracking was observed during cycle #2. These cracks generally formed at the interface of the stub and upper column. Crushing of the cover concrete was generally first observed at the stub level during the first cycle at the displacement ductility ratio of two. However, in Specimen NC-2, which had an axial load corresponding to 20% of the column's axial load capacity, crushing of cover concrete was observed during the first cycle at the displacement ductility ratio of 3. In general, the specimens showed good strength and energy dissipation capabilities up to the last loading cycle. All specimens failed by buckling of the longitudinal bars in compression which coincided with the loss of anchorage of the transverse reinforcement at one or more levels. Except for Specimen NC-8, the anchorages of the inner hoops did not sustain any visible anchorage loss. In Specimen NC-8, the inner hoop located 7 in. above the stub lost anchorage at the time of failure.

Loss of anchorage of peripheral hoops influenced buckling of longitudinal bars. For discussion, the sketch in Fig. 5-1 shows the first four layers of peripheral hoops and the corner bars for Specimen NC-2. Also shown in Fig. 5-1 are anchorage locations and their final shape at conclusion of testing. The location of the anchorage was alternated at each

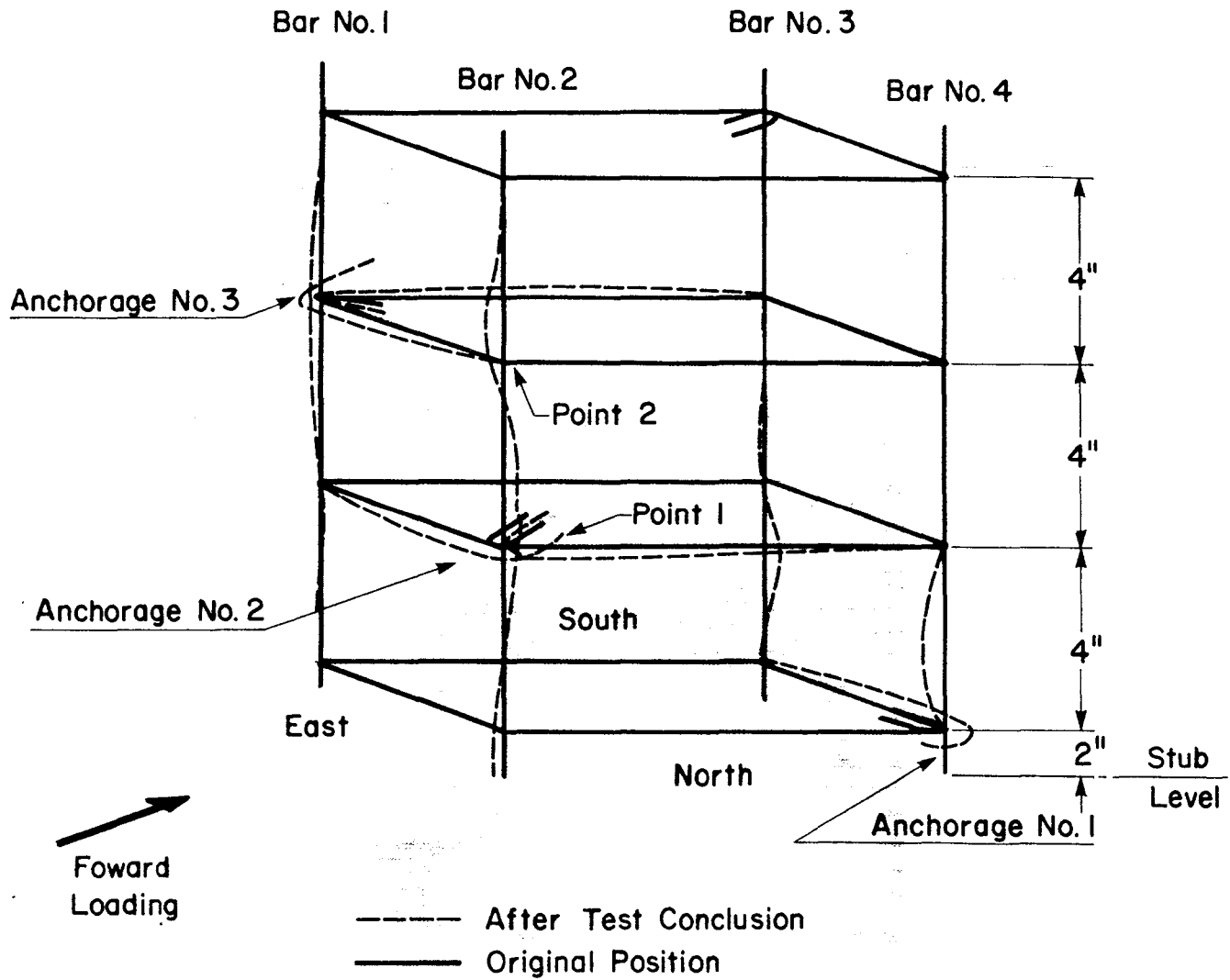


FIG. 5-1 SKETCH OF THE CORNER LONGITUDINAL BARS, BEFORE AND AFTER TESTING, SPECIMEN NC-2

level. The length of longitudinal bars engaged in buckling was influenced by the anchorage location as is evident from Fig. 5-1. As the anchorages for the peripheral hoops were lost, the laterally unbraced length of the longitudinal bars increased, thereby expediting buckling. The pattern of locating the anchorages for peripheral hoops also influenced the shape and length of the longitudinal bar engaged in buckling. As an example, referring to Fig. 5-1, as anchorage locations numbered 2 and 3 were lost, the longitudinal bar located at the northeast corner lost complete lateral support at point 1 and partial support at point 2 due to the loss of anchorage number 3.

In general, because of partial confinement, the concrete located between layers of transverse reinforcement spalled to a greater depth than concrete at the transverse reinforcement. This reduction of core cross-section is termed necking. Figures 5-2 through 5-13 show the hinging regions of Specimens NC-1 through NC-12 at test conclusion. Spalling of cover concrete in Specimens NC-2 through NC-8 extended approximately 18, 28, 27, 12, 48, 30 and 24 in. above the stub, respectively. For the same specimens, the location of maximum necking of the core at the plastic hinge was located at approximately 10, 8, 10, 6, 10, 6, and 9 in. above the stub, respectively.

5.1.2 Continuous Transverse Reinforcement

The upper column cross-section for Specimens NC-9, NC-10, and NC-12 was square. These specimens utilized continuous square helix transverse reinforcement. Specimen NC-11 was the only specimen with a circular upper column and it utilized continuous spiral transverse reinforcement.

Specimens NC-9, NC-10, and NC-12 showed good strength and energy dissipation capabilities. The major test behavior of these three specimens can be summarized as follows:

1. In general, first cracking was observed during cycle #2 at which time the maximum applied horizontal load corresponded to 75% of the upper column's theoretical moment-capacity calculated using the procedure outlined in Section 4.8.2.
2. First crushing of cover concrete was observed at the interface of the stub and upper column at the first cycle of displacement ductility ratio of two.

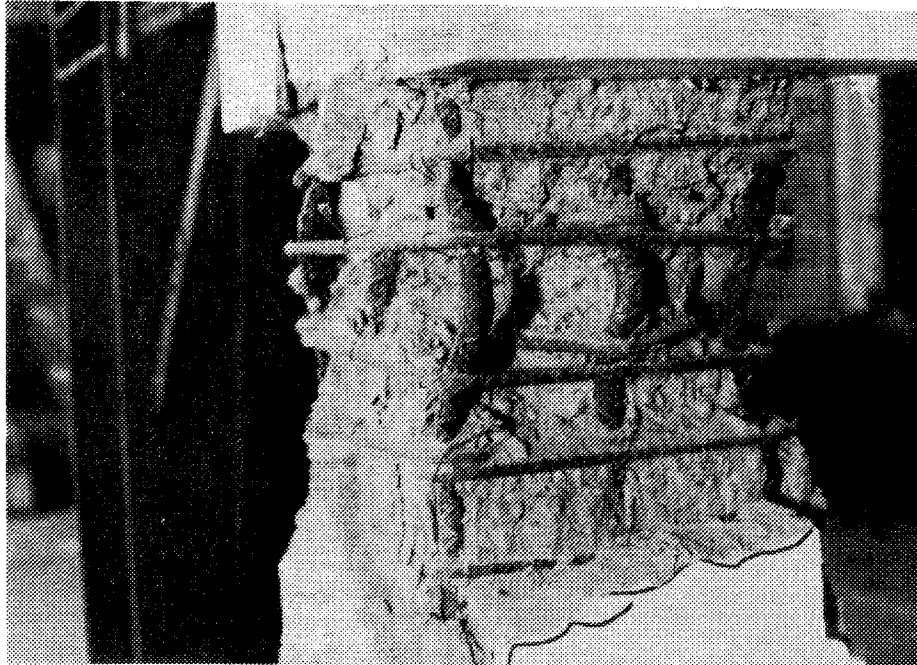


FIG. 5-2 TEST SPECIMEN NC-1 AFTER TEST CONCLUSION

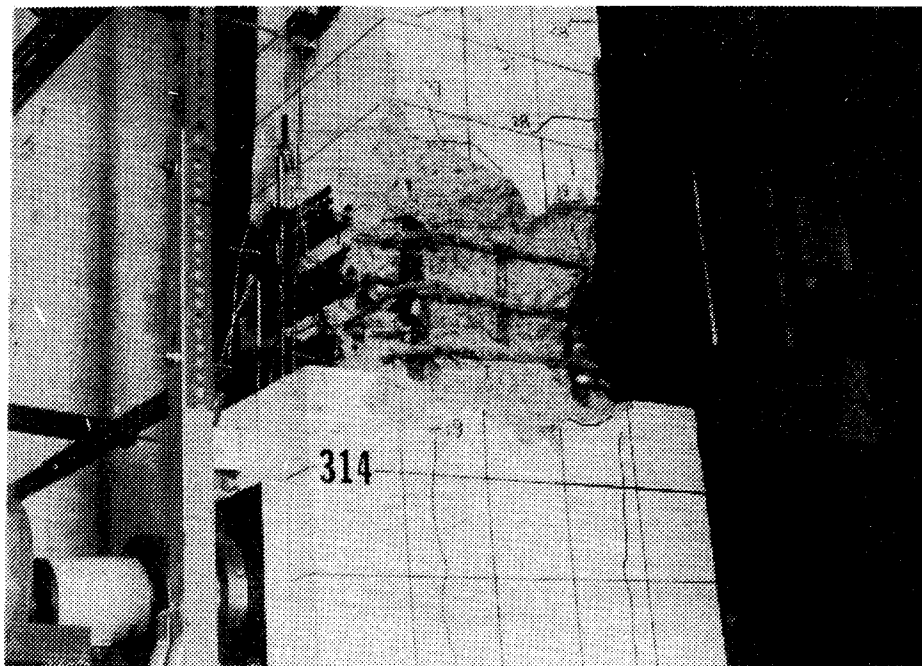


FIG. 5-3 TEST SPECIMEN NC-2 AFTER TEST CONCLUSION

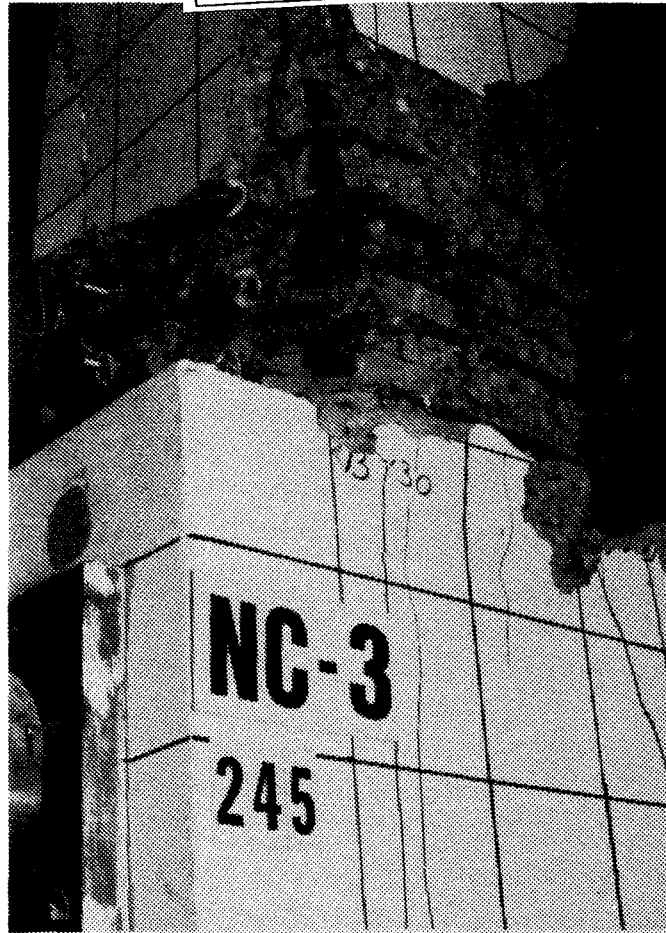


FIG. 5-4 TEST SPECIMEN NC-3 AFTER TEST CONCLUSION

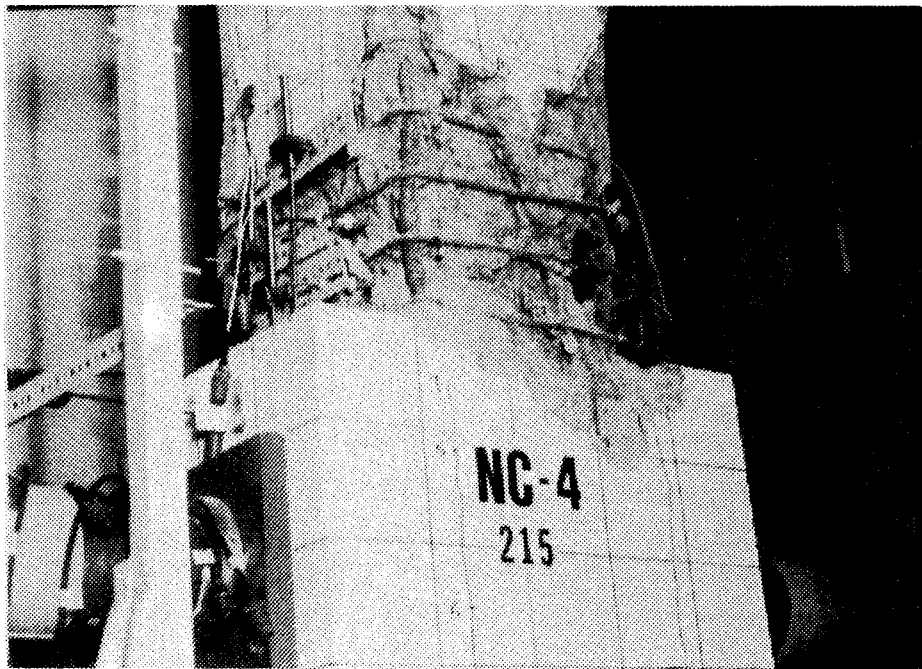


FIG. 5-5 TEST SPECIMEN NC-4 AFTER TEST CONCLUSION

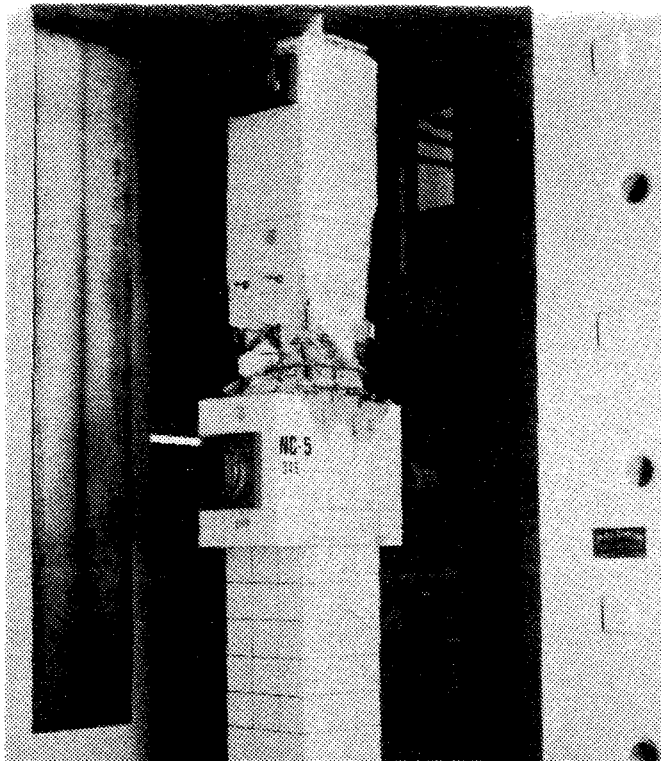


FIG. 5-6 TEST SPECIMEN NC-5 AFTER TEST CONCLUSION

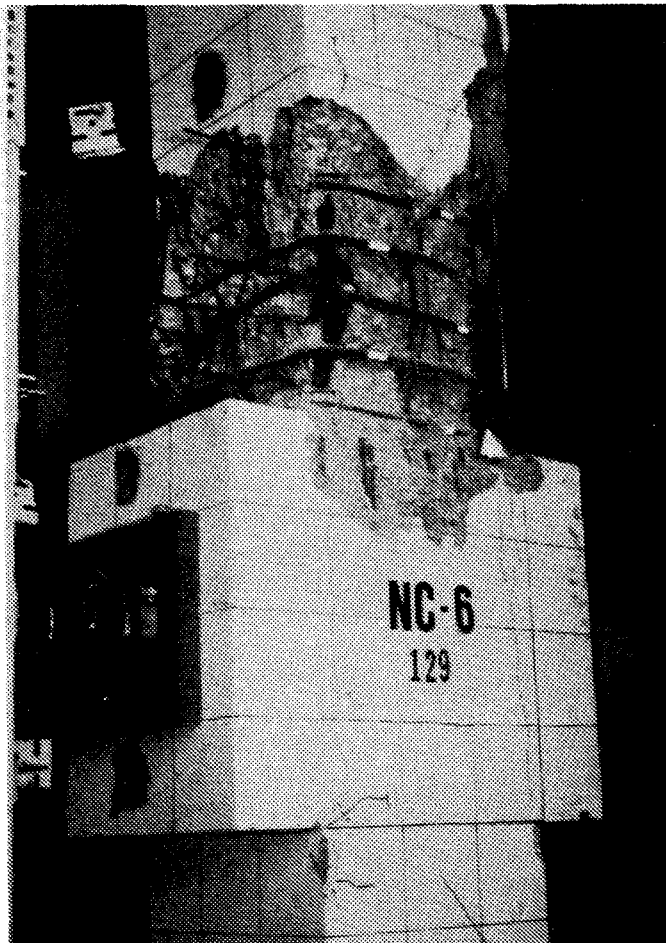


FIG. 5-7 TEST SPECIMEN NC-6 AFTER TEST CONCLUSION

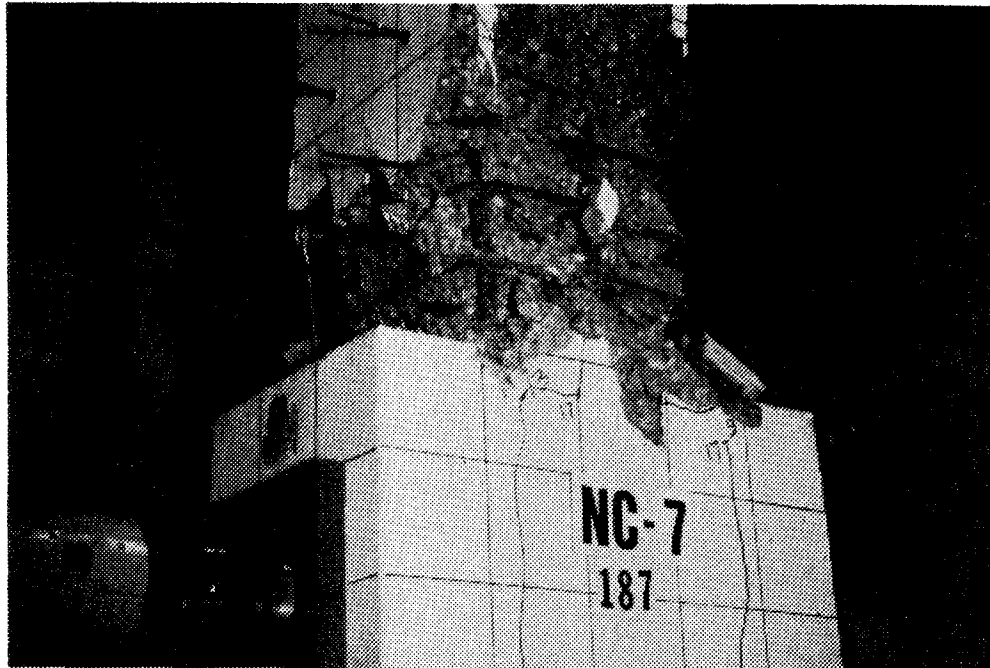


FIG. 5-8 TEST SPECIMEN NC-7 AFTER TEST CONCLUSION

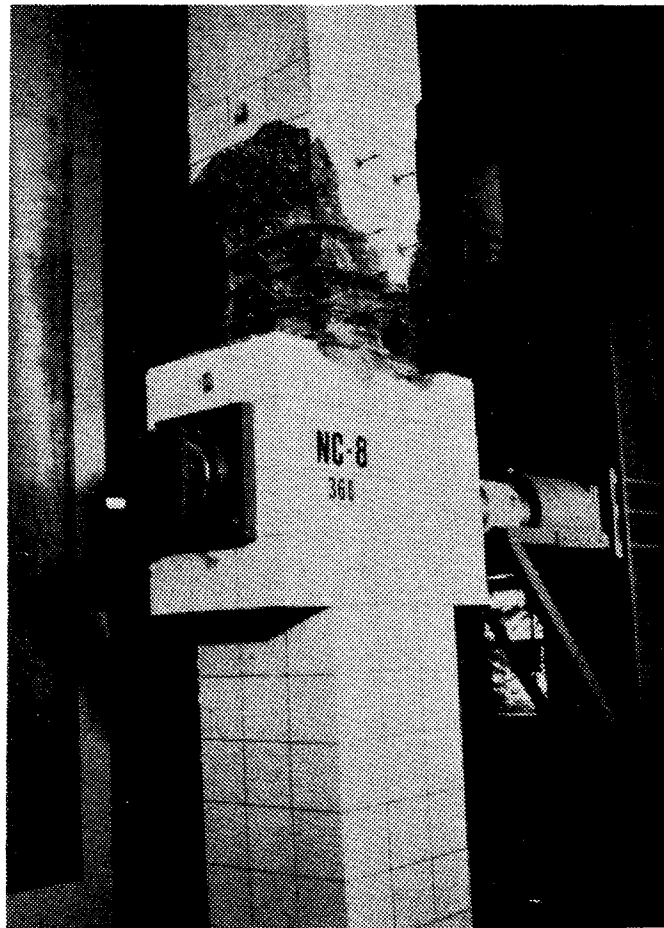


FIG. 5-9 TEST SPECIMEN NC-8 AFTER TEST CONCLUSION

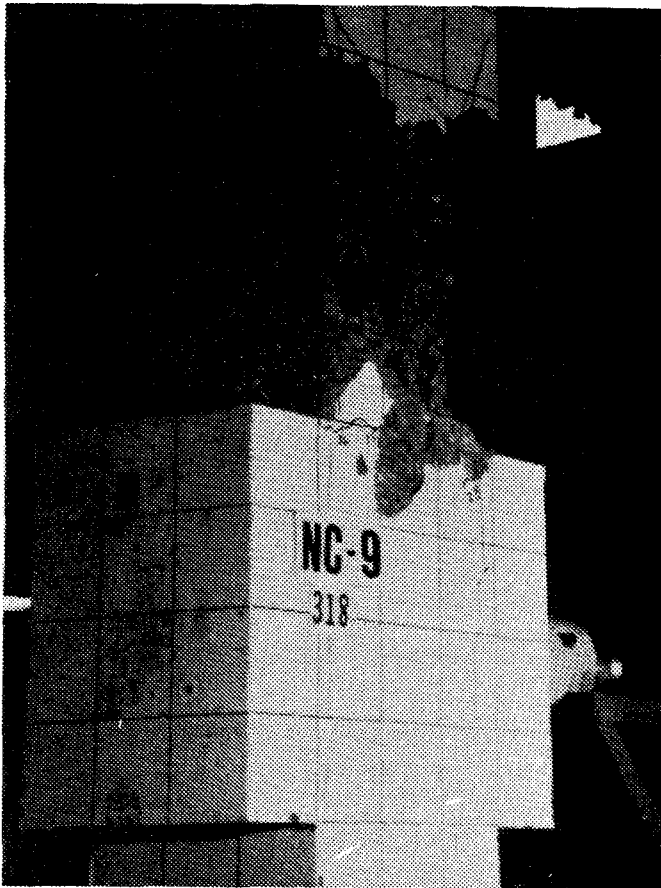


FIG. 5-10 TEST SPECIMEN NC-9 AFTER TEST CONCLUSION

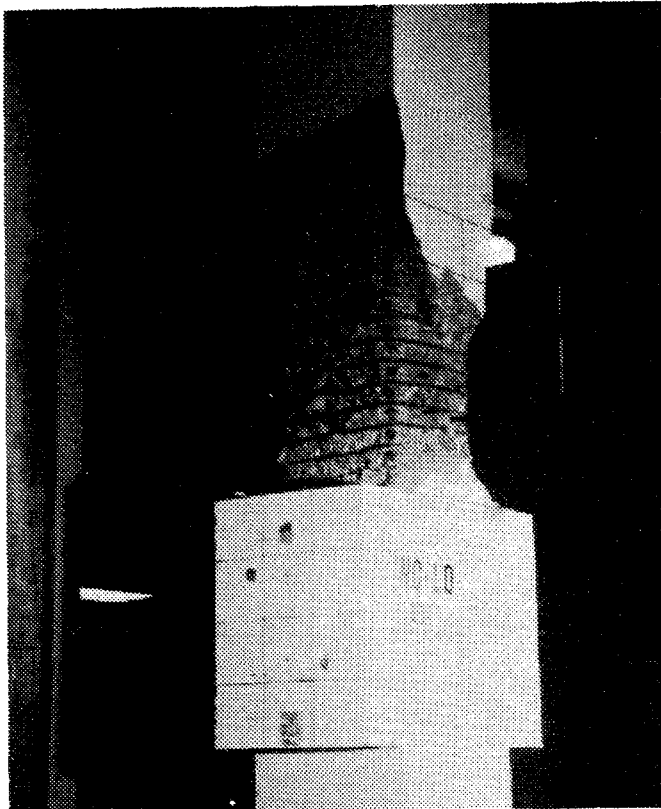


FIG. 5-11 TEST SPECIMEN NC-10 AFTER TEST CONCLUSION

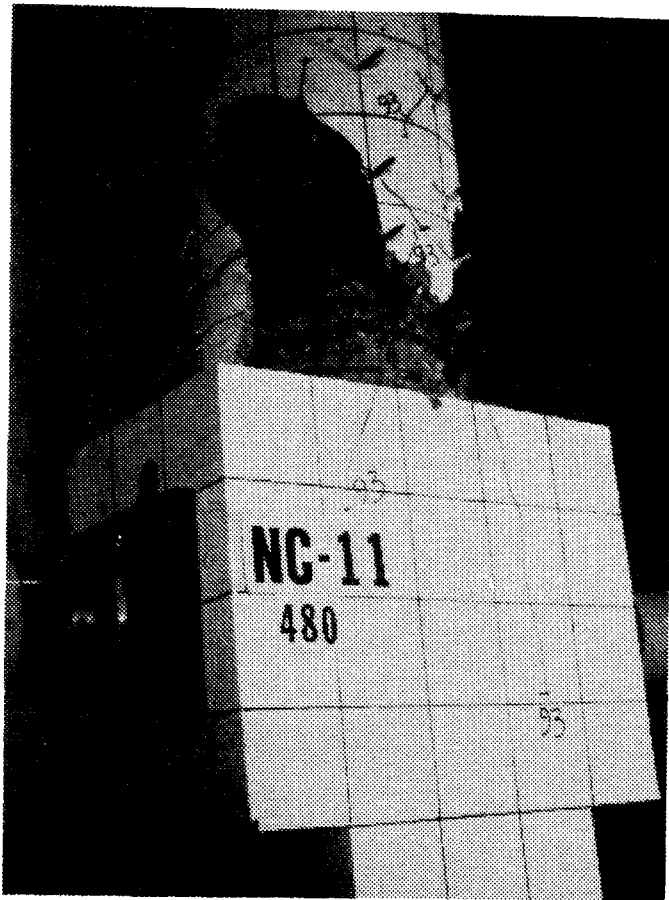


FIG. 5-12 TEST SPECIMEN NC-11 AFTER TEST CONCLUSION

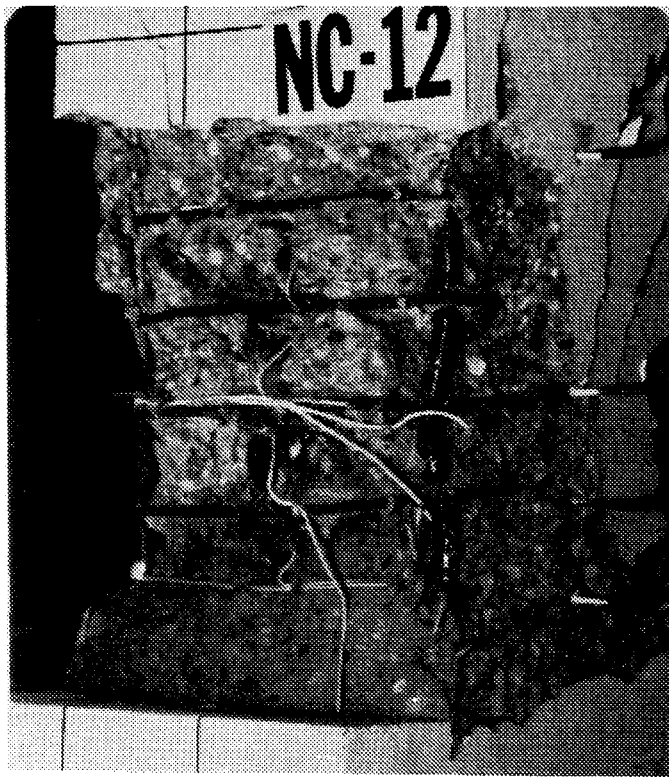


FIG. 5-13 TEST SPECIMEN NC-12 AFTER TEST CONCLUSION

3. The extent of spalling of cover concrete at displacement ductility ratio of three was larger than for specimens with discrete transverse reinforcement. In general, in comparison to specimens with discrete transverse reinforcements, spalling of the cover concrete occurred early and extended to higher distances above the stub at test conclusion.
4. In general, layers of transverse reinforcement located close to the stub were still embedded in concrete at test conclusion. This height above the stub was approximately 2, 3, and 4 in. for Specimen NC-9, NC-10, and NC-12, respectively.
5. Specimens NC-9 and NC-10 failed by buckling of the longitudinal bars located away from the corners. Addition of crossties in Specimen NC-12 resulted in simultaneous buckling of the middle and corner longitudinal bars.
6. The maximum lateral bending of the buckled bars occurred at approximately 10, 11, and 9 in. above the stub for Specimens NC-9, NC-10, and NC-12, respectively. In general, the necking portion of the plastic hinge occurred at the same locations.
7. The continuous nature of transverse reinforcement for these three specimens provided good confinement for core concrete, compared to specimens with discrete transverse reinforcement, and prevented spalling of core concrete, particularly at the location of maximum lateral bending of the buckled longitudinal bars.
8. Large elongations of the transverse reinforcement located at the level of maximum lateral bending of the buckled longitudinal bars were observed. However, this did not result in any visible cracking or fracture of transverse reinforcement at these levels.
9. Crossties in Specimen NC-12 were provided to prevent buckling of middle longitudinal bars as occurred in Specimens NC-9 and NC-10. This proved to be an appropriate way of achieving the goal as all three longitudinal bars on the compression face buckled simultaneously in Specimen NC-12. The 90° bend and six-bar diameter extension on these crossties proved to be sufficient.

10. Specimens NC-9 and NC-12 failed prior to completion of the first cycle at displacement ductility ratio of six, while Specimen NC-10 failed after one complete cycle of horizontal loading and before completing the reverse loading of the second cycle at displacement ductility ratio of six. All three specimens had the same amount of transverse reinforcement ($\rho = 1.29\%$), but used different size and spacing of transverse reinforcement.

These test observations show that using the same amount of transverse reinforcement with smaller spacing is most efficient with regard to displacement ductility. The pitch of the transverse reinforcement for Specimens NC-9, NC-10, and NC-12 was 4, 2.25, and 3.5 in., respectively.

Specimen NC-11 was the only specimen that had an upper column with a circular cross-section. The intent was to compare behavior of the circular and square columns with equal ultimate moment capacity. However, because of design limitations this was not possible. Thus, the results of Specimen NC-11 could not be directly compared to results of the other specimens. However, some comparisons in general behavior of Specimen NC-11 and those of NC-9, NC-10, and NC-12 can be made since they all utilized the same material, number and size of longitudinal reinforcing bars and some form of continuous transverse reinforcement. Following are some remarks and observations with regard to Specimen NC-11:

1. The volumetric ratio of transverse reinforcement provided was 1.29%, the same as that of Specimens NC-9, NC-10, and NC-12.
2. The first hair line cracks formed during cycle #2 at the interface of the upper column and stub. Some crushing of cover concrete was observed at the upper column-stub level during the first cycle at displacement ductility ratio of two.
3. The length of spalled cover concrete at displacement ductility ratio of three extended approximately 12 inches above the stub. This is less than for Specimens NC-9, NC-10, and NC-12 at the same displacement level.
4. Initiation of buckling of the longitudinal bars was first observed at displacement ductility ratio of eight, whereas for Specimens NC-9, NC-10, and NC-12 it was first observed at displacement ductility ratio of five.

5. The specimen failed prior to completion of the first cycle at displacement ductility ratio 10. This higher level of ductility can be attributed to the fact that the square spiral transverse reinforcement in Specimens NC-9, NC-10, and NC-12 was subjected to bending and axial tension while the circular spiral reinforcement of Specimen NC-11 was essentially subjected to tension. Therefore, spiral reinforcement was more efficient in confining core concrete and resulted in higher ductility. Fig. 5-12 shows the specimen at test conclusion. Cover concrete spalled off to 20 in. above the stub, much less than in Specimens NC-9, NC-10, and NC-12.
6. As in Specimens NC-9, NC-10, and NC-12, transverse reinforcement located at the level of maximum lateral bending of the buckled longitudinal bars experienced large elongations. However, no visible cracking or fracture of circular spiral reinforcement was observed.
7. In the cases of Specimens NC-9, NC-10, and NC-12 at least the first layer of transverse reinforcement was still embedded in concrete at test conclusion. This was not true for Specimen NC-11, however.

5.2 Horizontal Load-Displacement Characteristics

In this section, horizontal load-displacement behavior of the test specimens is described. A detailed description of each specimen is presented in Appendix A.

Figs. 5-14 and 5-15 show samples of horizontal load vs. horizontal displacement obtained for the test specimens. In these figures the solid line parallel to the horizontal axis represents the theoretical ultimate lateral load, calculated using ACI-318-83 Code provision, neglecting the P- Δ effect. However, if the P- Δ effect is included, the calculated maximum lateral load decreases as lateral displacement increases. The dashed lines represent the envelope of the points corresponding to maximum lateral loads at increasing lateral displacement levels. For each displacement level, the maximum lateral load was calculated using ACI-318-83 Code provision. Maximum horizontal displacement ranged from five to eight times yield displacement.

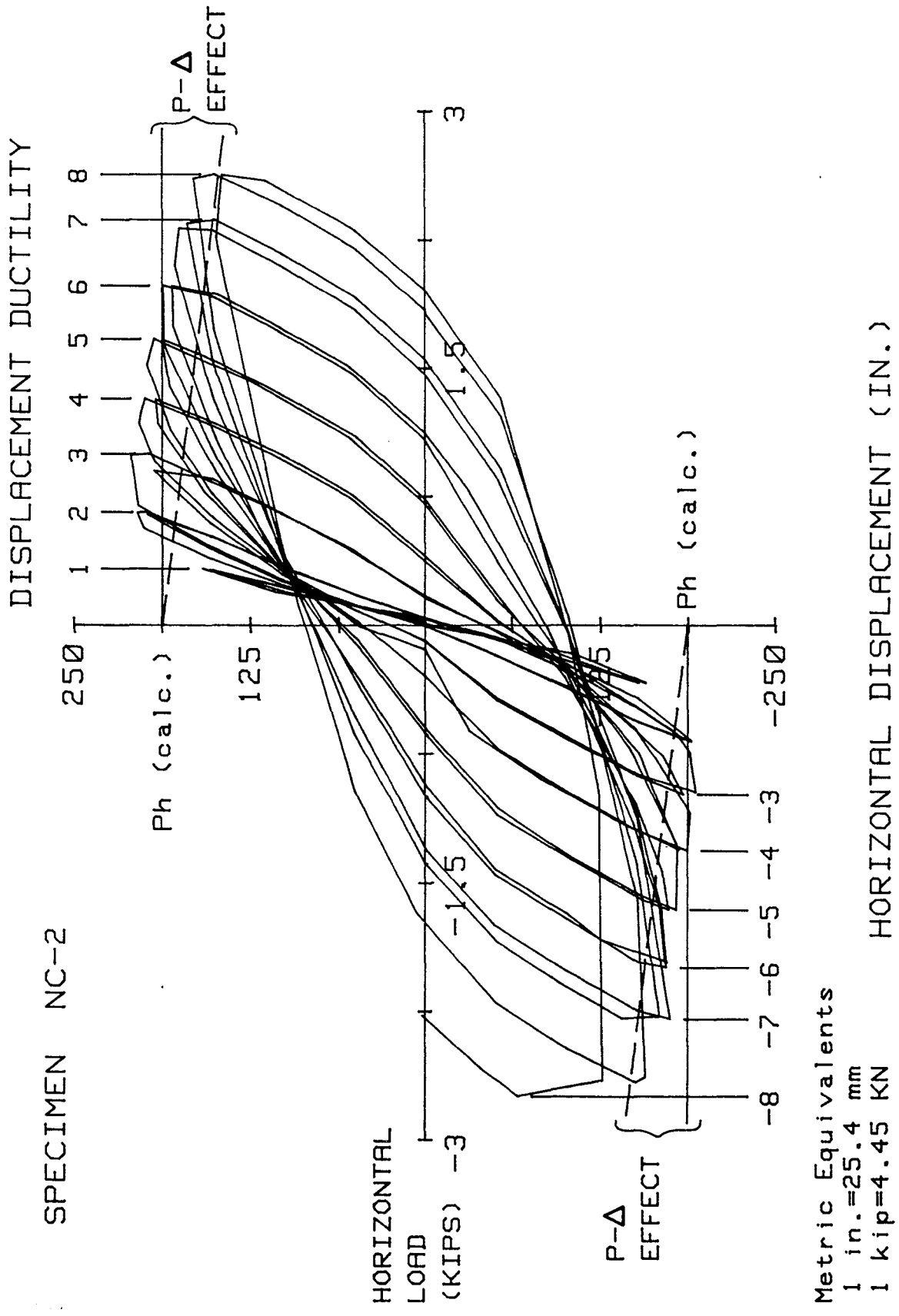
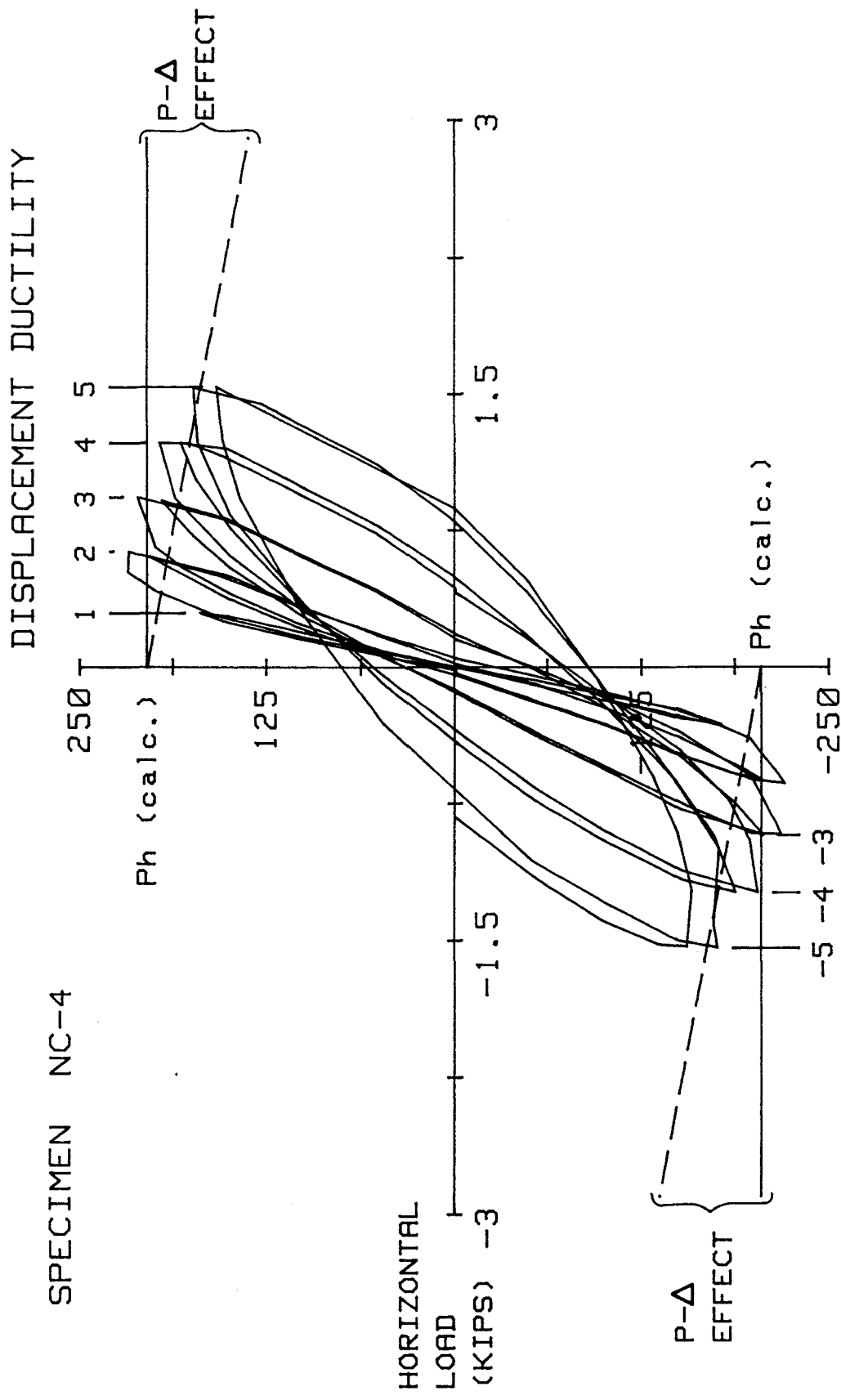


FIG. 5-14 HORIZONTAL LOAD VERSUS DISPLACEMENT, SPECIMEN NC-2



Metric Equivalents
 1 in.=25.4 mm
 1 kip=4.45 KN

HORIZONTAL DISPLACEMENT (IN.)

FIG. 5-15 HORIZONTAL LOAD VERSUS DISPLACEMENT, SPECIMEN NC-3

The first yield displacement was established using the procedure outlined in Section 4.8.2. Table 5.1 lists the first yield displacements for each specimen, which ranged from 0.28 to 0.33 in. In general, all specimens except Specimen NC-6 showed good strength and energy absorption capabilities.

In general, there was a drop in horizontal load carrying capacity of the specimens at the onset of cover concrete crushing. Table 5.2 lists the horizontal loads corresponding to ultimate moment capacity of the section and maximum applied horizontal load.

The area under each hysteresis loop is equal to the total dissipated energy in the specimen as a result of non-linear behavior. The predominant portion of this energy is dissipated as a result of plastic hinge formation. Consequently, the area under the hysteresis loops could be used as an index for relative performance of each transverse reinforcement detail utilized in the upper column as long as the hinge forms in the upper column. Figure 5-16 shows the energy per cycle versus the displacement ductility ratio at various displacement levels for all specimens. As is evident, a nearly linear relationship exists between the energy per cycle and the displacement ductility.

5.3 Moment-Curvature Characteristics

In this section the general moment-curvature and curvature distribution of the test specimens are described. A detailed discussion for each specimen can be found in Appendix A.

Representative plots of curvature distribution along the upper column are shown in Figs. 5-17 through 5-20. The curvature ductilities shown in these figures were calculated based on the procedure outlined in Section 4.8.2 and are based on the peak curvature observed during cycle #2 within a gage length including the first four inches above the stub. In these figures, each line at a particular displacement level is formed by joining four points, each point representing curvature at a given distance from the stub and at a particular loading stage. Curvatures measured over gage length within the first 4 in., 4 to 8 in., 8 to 12 in., and 12 to 20 in. from the stub are plotted along the vertical axis at the average gage

Table 5.1 First yield displacement and yield curvature for test specimens

Specimen# Designation	First yield Displacement (inches)	First yield Curvature ($\times 10^6$), in
NC-1	0.28	340
NC-2	0.33	394
NC-3	0.30	303
NC-4	0.30	158
NC-5	0.28	423
NC-6	0.30	535
NC-7	0.30	472
NC-8	0.28	665
NC-9	0.28	354
NC-10	0.28	395
NC-11	0.28	623
NC-12	0.28	117

Table 5.2 Theoretical and maximum applied horizontal load for test specimens

Specimen Designation	Theoretical Max horizontal load	Max applied horizontal load
NC-2	185	210
NC-3	190	235
NC-4	198	225
NC-5	196	230
NC-6	180	140
NC-7	187	215
NC-8	192	200
NC-9	181	215
NC-10	187	210
NC-11	150	165
NC-12	188	195

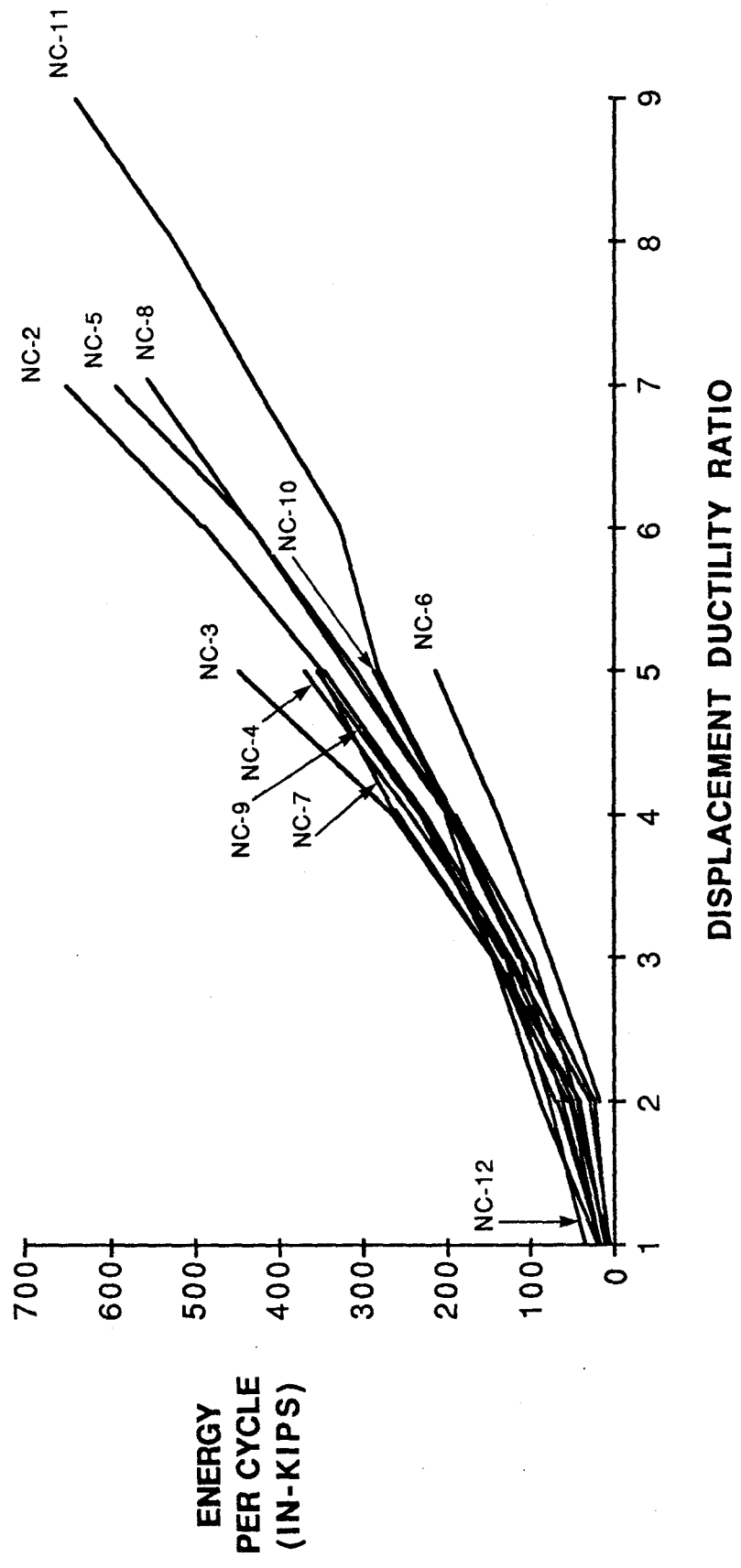


FIG. 5-16 ENERGY VERSUS DISPLACEMENT DUCTILITY RATIO FOR ALL SPECIMENS

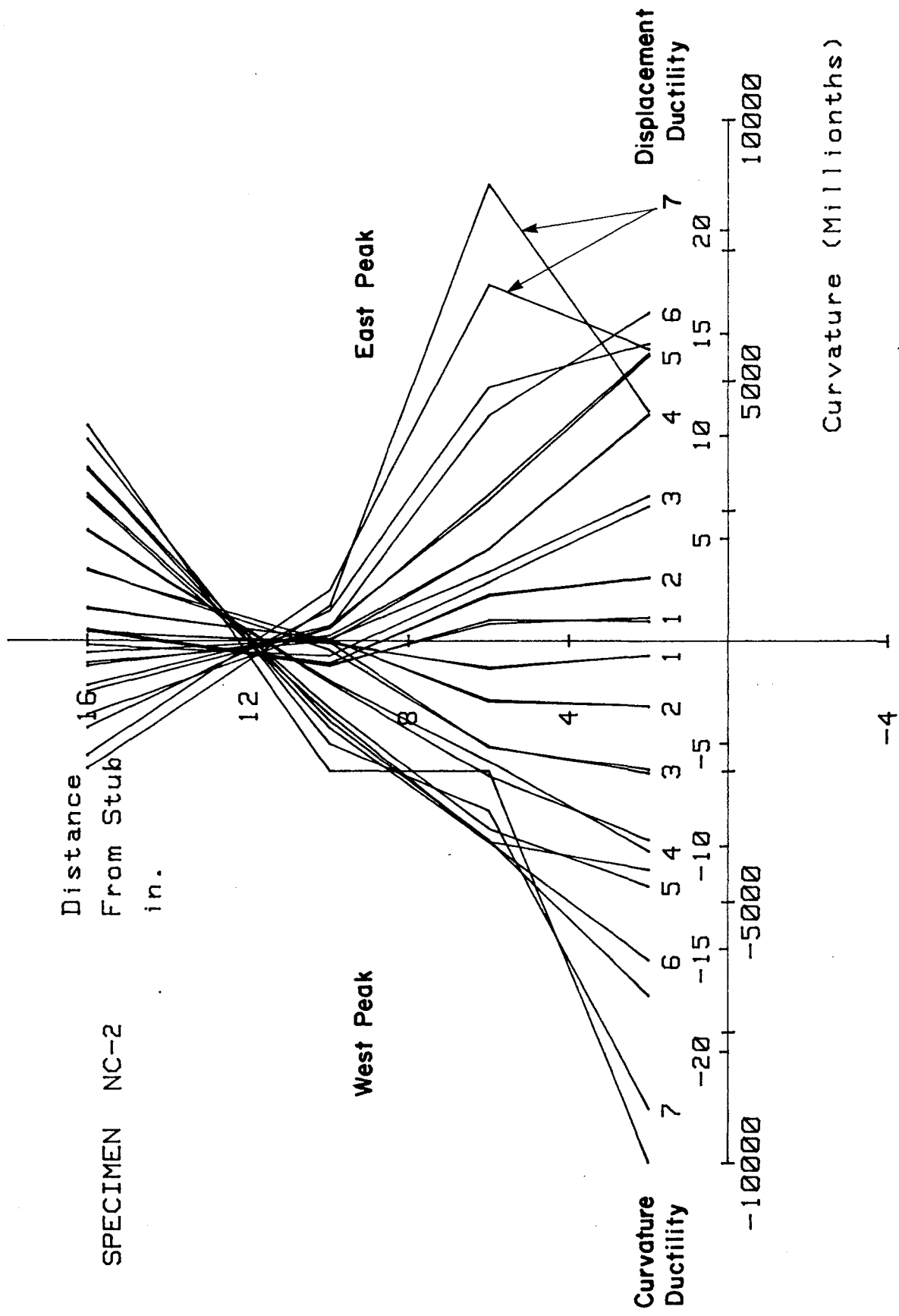


FIG. 5-17 CURVATURE DISTRIBUTION ALONG UPPER COLUMN, SPECIMEN NC-2

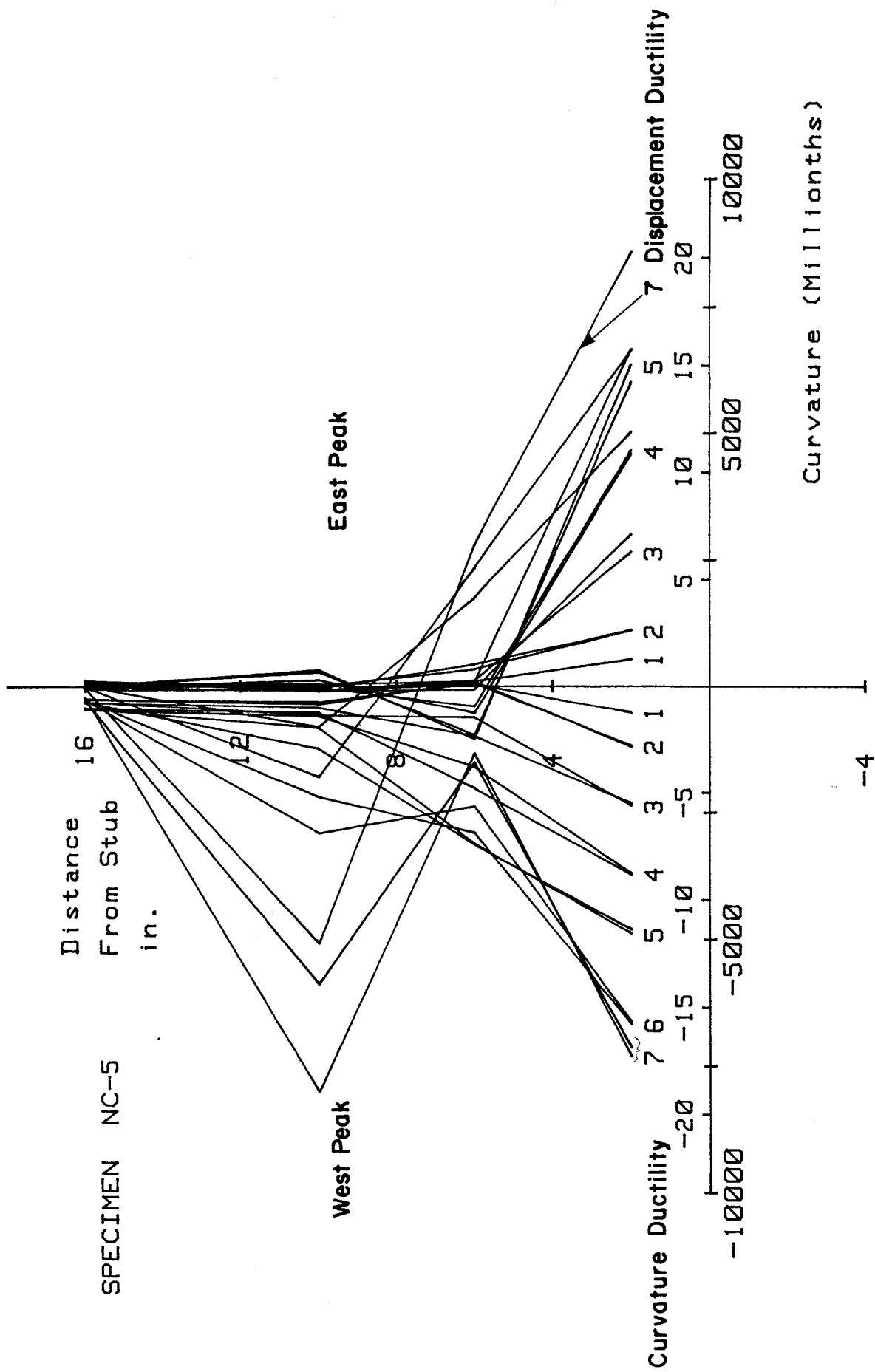


FIG. 5-18 CURVATURE DISTRIBUTION ALONG UPPER COLUMN, SPECIMEN NC-5

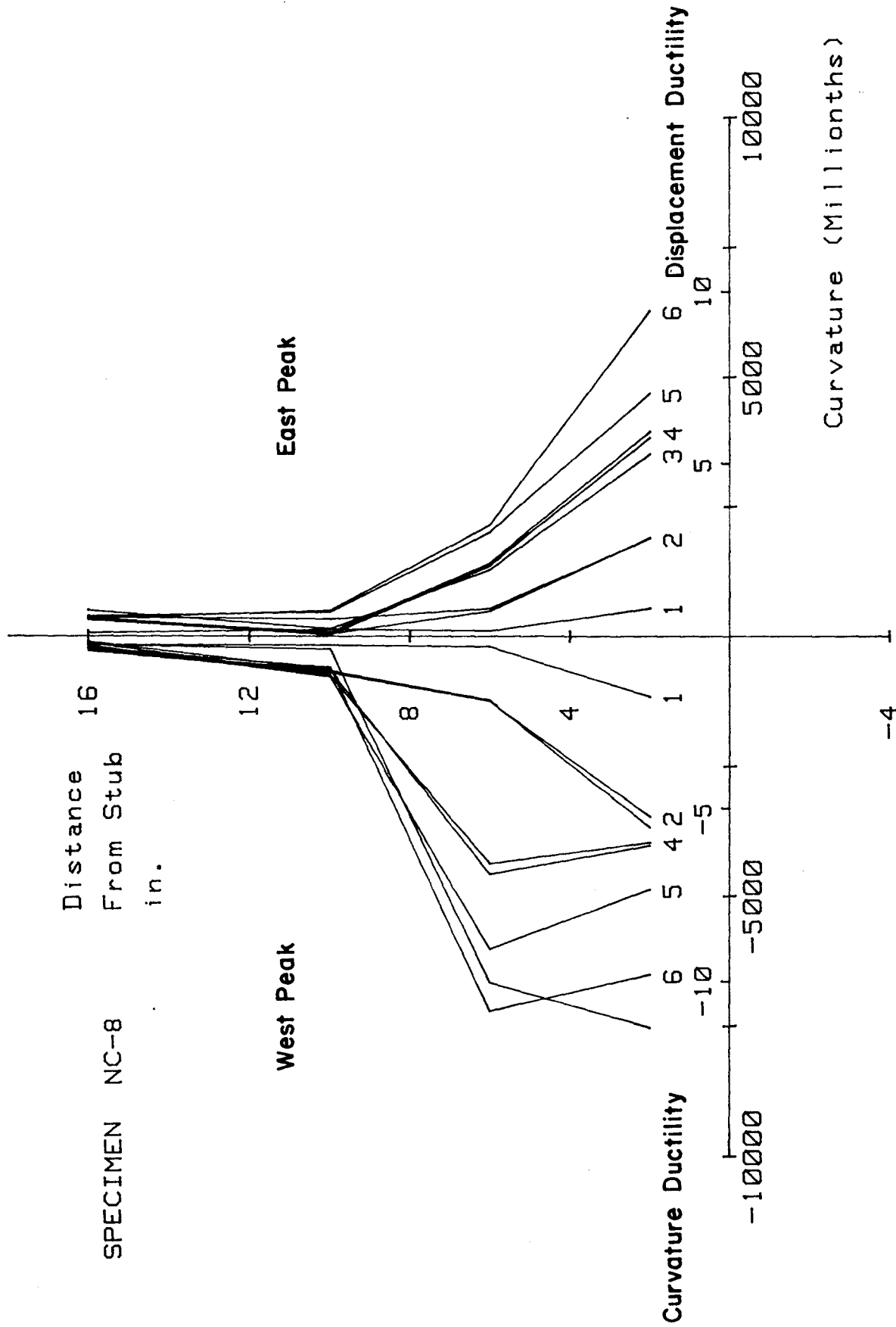


FIG. 5-19 CURVATURE DISTRIBUTION ALONG UPPER COLUMN, SPECIMEN NC-8

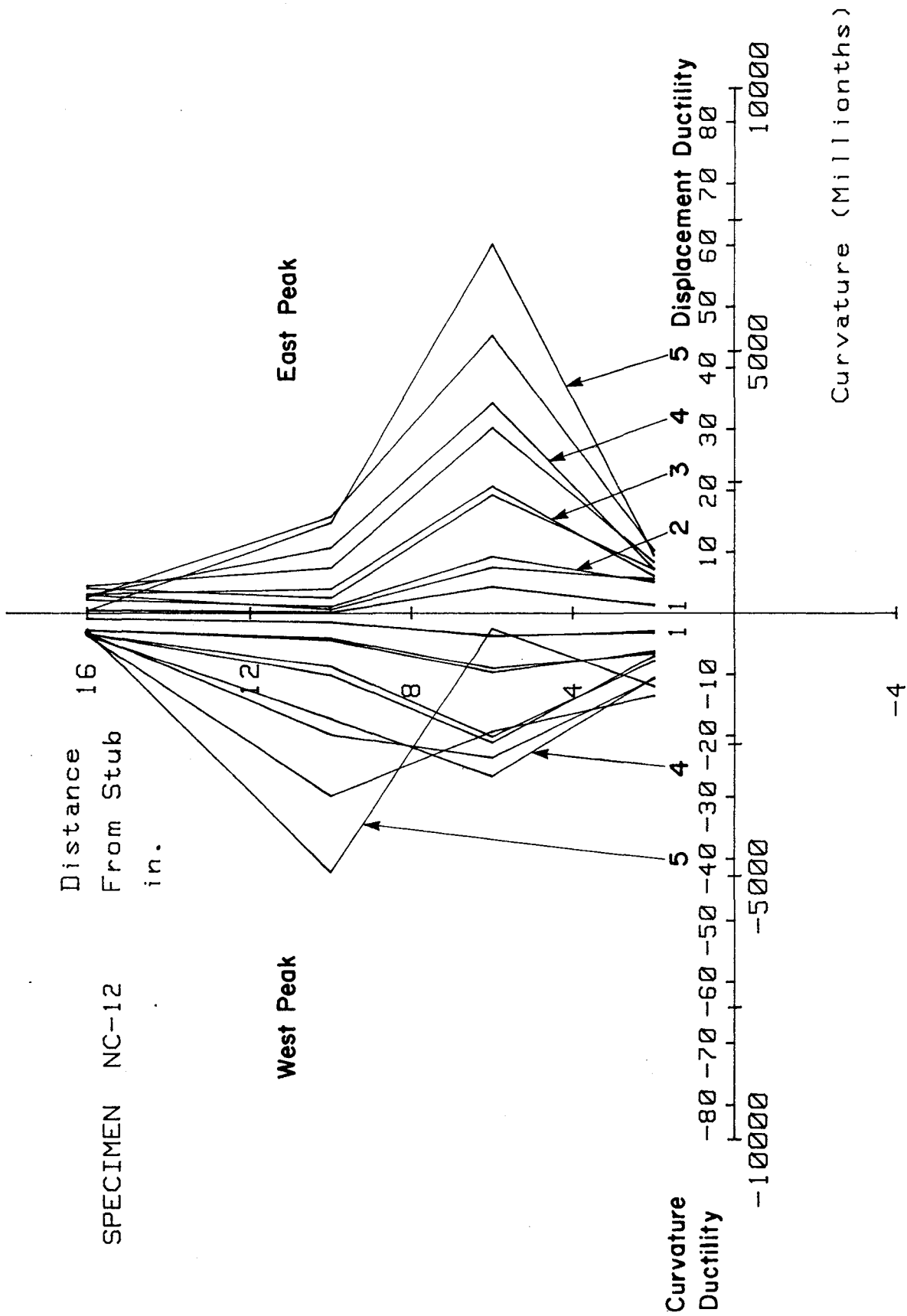


FIG. 5-20 CURVATURE DISTRIBUTION ALONG UPPER COLUMN, SPECIMEN NC-12

length distances of 2, 6, 10, and 16 in., respectively. Lines to the right and left of the vertical axis represents curvature distributions during the forward and reverse loading at each loading cycle, respectively.

Curvature distribution during the forward and reverse loading were generally symmetrical during early loading stages ($\mu \leq 2$).

Three distinct curvature distributions were observed. Figure 5-18 represents an example of the first category for which maximum curvature occurred at the first gage length above the stub throughout loading.

Figure 5-17 shows an example of the second category of curvature distribution for which maximum curvature at later stages of loading shifted from the first gage length to a higher distance above the stub. As shown in Fig. 5-17 for Specimen NC-2 the location of the largest curvature remained at the first gage length above the stub up to a displacement ductility ratio of six. However, at the next displacement level ($\mu=7$), at the peak of the forward loading cycles, the location of the highest curvature shifted to the second gage length above the stub while at the peak of the reverse loading cycle it remained at the first gage length above the stub. The distribution of the curvatures at displacement ductility of seven could, in part, be attributed to bending characteristics of the longitudinal bars.

Referring to Fig. 5-1 which shows a sketch of the transverse reinforcement and the final buckled shape of the corner longitudinal bars at the conclusion of testing for Specimen NC-2 ($\mu=8$). According to column theories, compression members with initial out-of-straightness displace laterally prior to reaching their buckling load. Considering the longitudinal bars as such compression members and referring to their final buckled shape (see Fig. 5-1), it could be concluded that bars numbered 1 and 2 would have displaced laterally the greatest amount in the region extending from 6 to 10 in. above the stub while for bars numbered 3 and 4 this displacement region would be located at a distance between 2 and 6 in. above the stub. Thus, as a result of the lateral displacement pattern of the bars numbered 1 through 4, it would be expected that the higher curvature would be at the second gage length and at the first gage length of the stub at the peak of the forward and reverse loading cycles (at displacement ductility ratio of seven), respectively.

The third type of curvature distribution was in specimens for which maximum curvature at all displacement levels occurred at locations other than the first gage length above the stub. Figure 5-20 shows curvature distribution for Specimen NC-12 as an example. For Specimen NC-12 this behavior can be attributed to the fact that transverse reinforcement within 4 in. of the stub was still covered by concrete at the test conclusion, thereby providing good confinement in this region. Consequently, the plastic hinge and the region of high curvature was forced upward.

Figure 5-20 shows that maximum curvature ductility at displacement ductility ratio of five is approximately 60 within the second gage length above the stub. However, it should be noted that reported curvature ductility ratios are relative to the first yield curvature within the gage length directly above the stub. For Specimen NC-12, that reference curvature was surprisingly small, so the calculated ductility ratio values are inflated. A recalculation of curvature ductility ratios relative to the measured curvature at first yield within the second gage length reduces the maximum ratio from 60 to 16.8. This reduced value is a better representation of the available curvature ductility of Specimen NC-12.

In all tests the ratio of curvature ductility to displacement ductility at the peaks of each loading cycle was variable and greater than one at various loading stages.

Figure 5-21 shows curvature distribution for Specimen NC-11 which had a circular cross-section and spiral reinforcement in the upper column. The maximum curvature ductility ratio for this specimen was achieved during the forward loading of cycle #20 ($\mu=9$) and was approximately 26. The curvature ductility is not equal to displacement ductility at all displacement levels. The maximum ratio of curvature ductility to displacement ductility at displacement ductility ratios of 1 through 9 were 1, 1.2, 1.5, 1.7, 1.8, 2.0, 2.2, 2.8, and 2.9, respectively.

Representative plots of moment vs. curvature for Specimens NC-2, NC-5, NC-8, and NC-12 are shown in Figs. 5-22 through 5-25. These plots include total moment at the upper column-stub beam interface. The calculated moment capacity, M_u , indicated in these figures, was determined using provisions of the 1983 ACI Building Code. Capacity reduction factor, ϕ , was taken

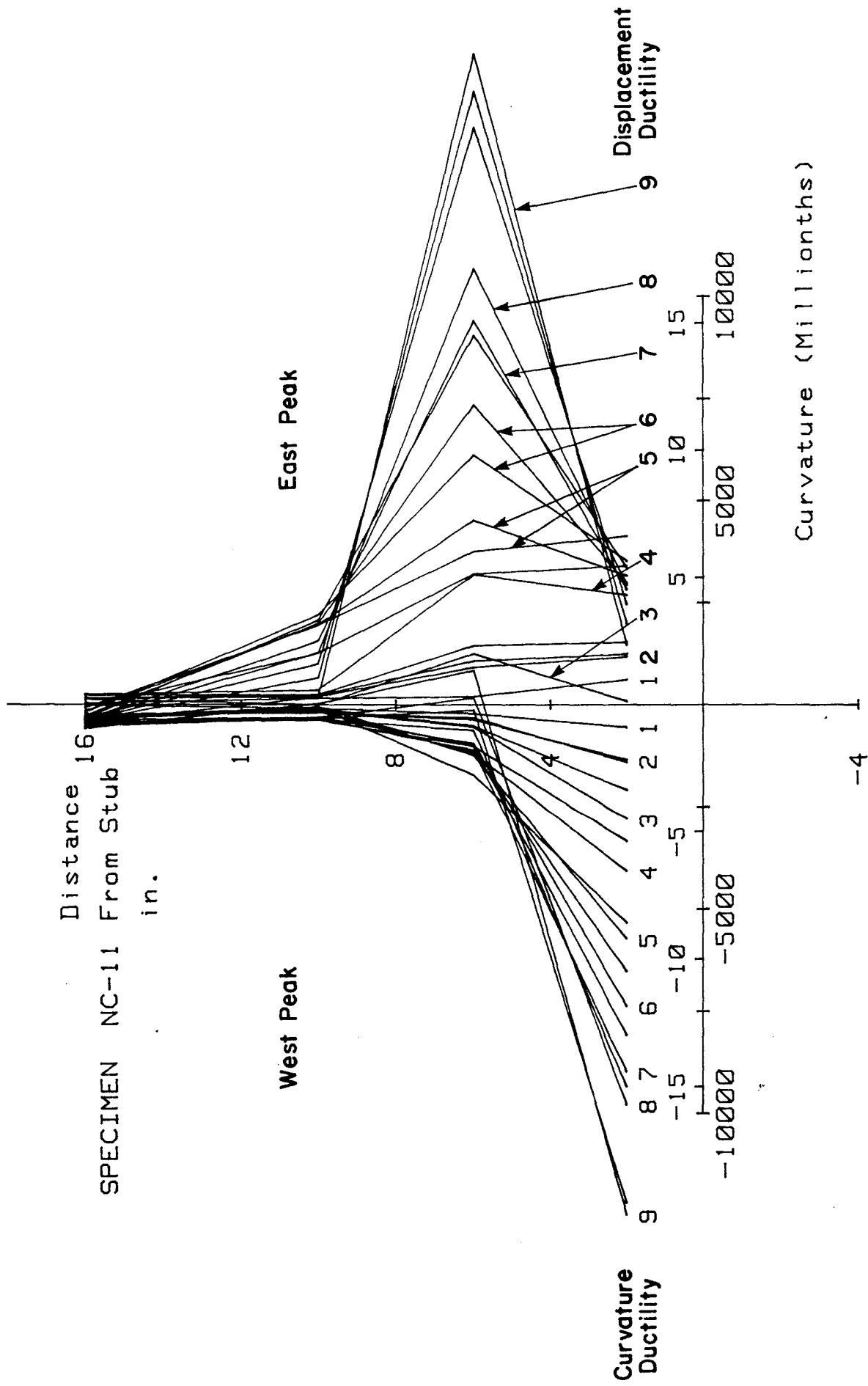


FIG. 5-21 CURVATURE DISTRIBUTION ALONG UPPER COLUMN, SPECIMEN NC-11

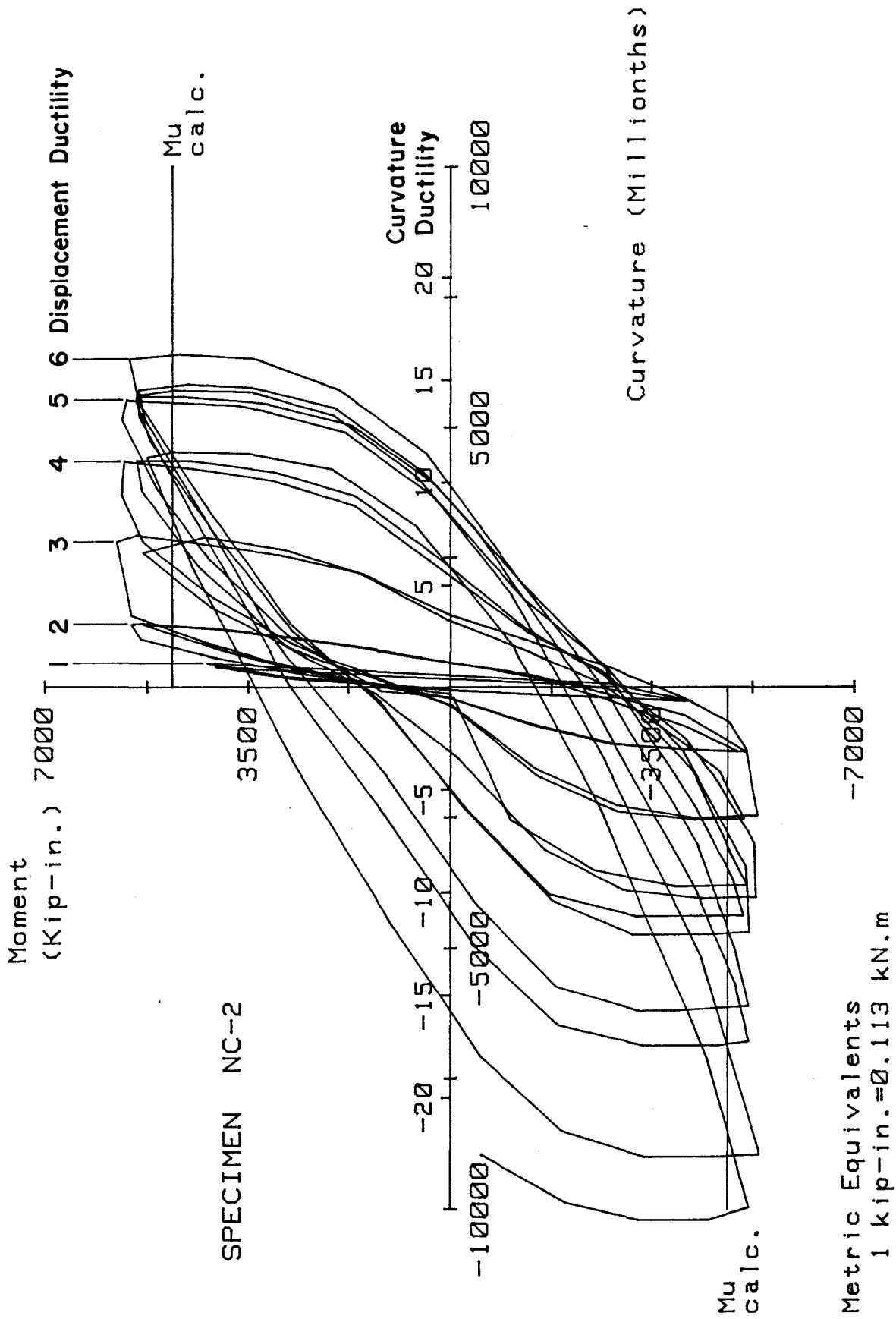


FIG. 5-22 MOMENT VERSUS CURVATURE FOR SPECIMEN NC-2

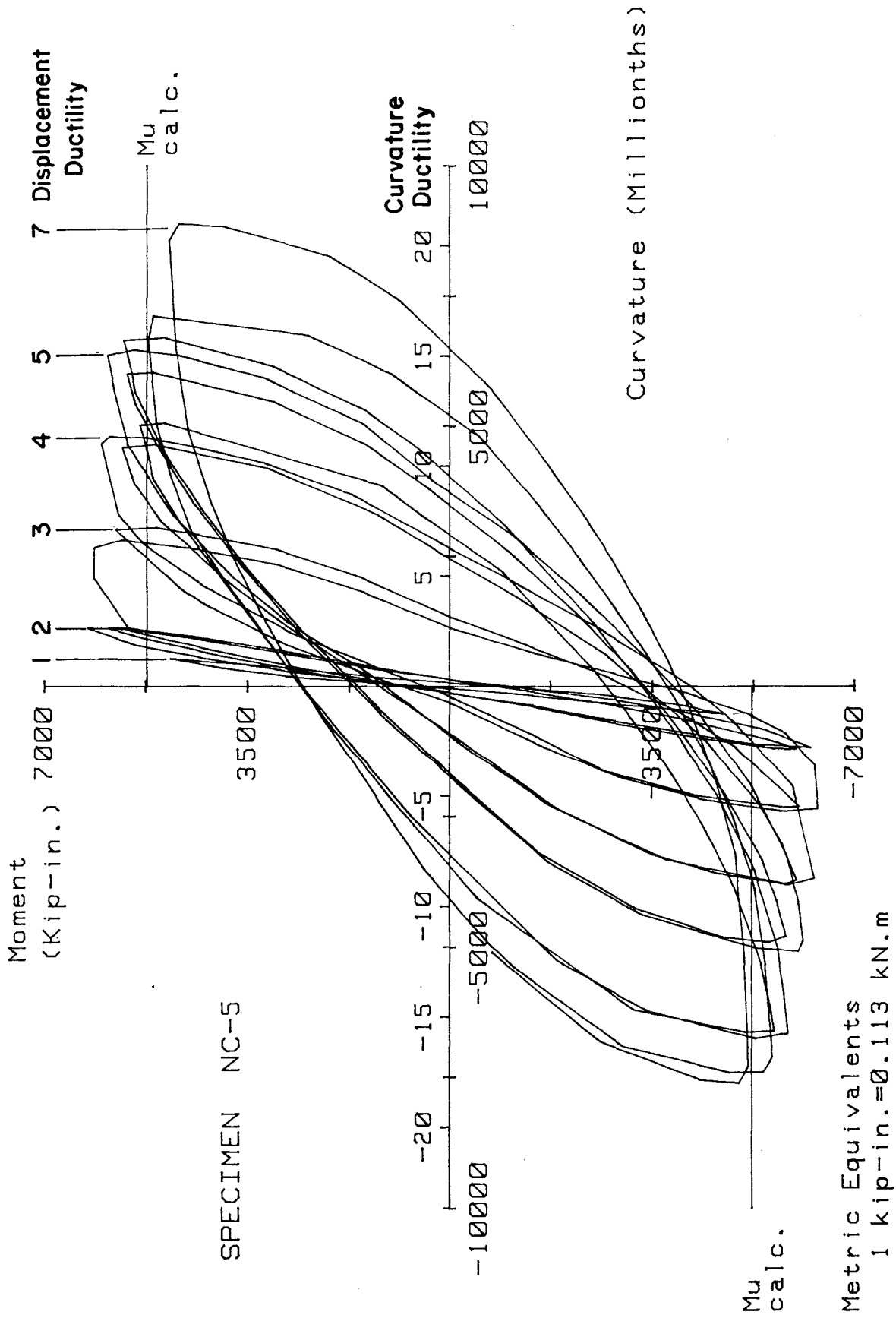


FIG. 5-23 MOMENT VERSUS CURVATURE FOR SPECIMEN NC-5

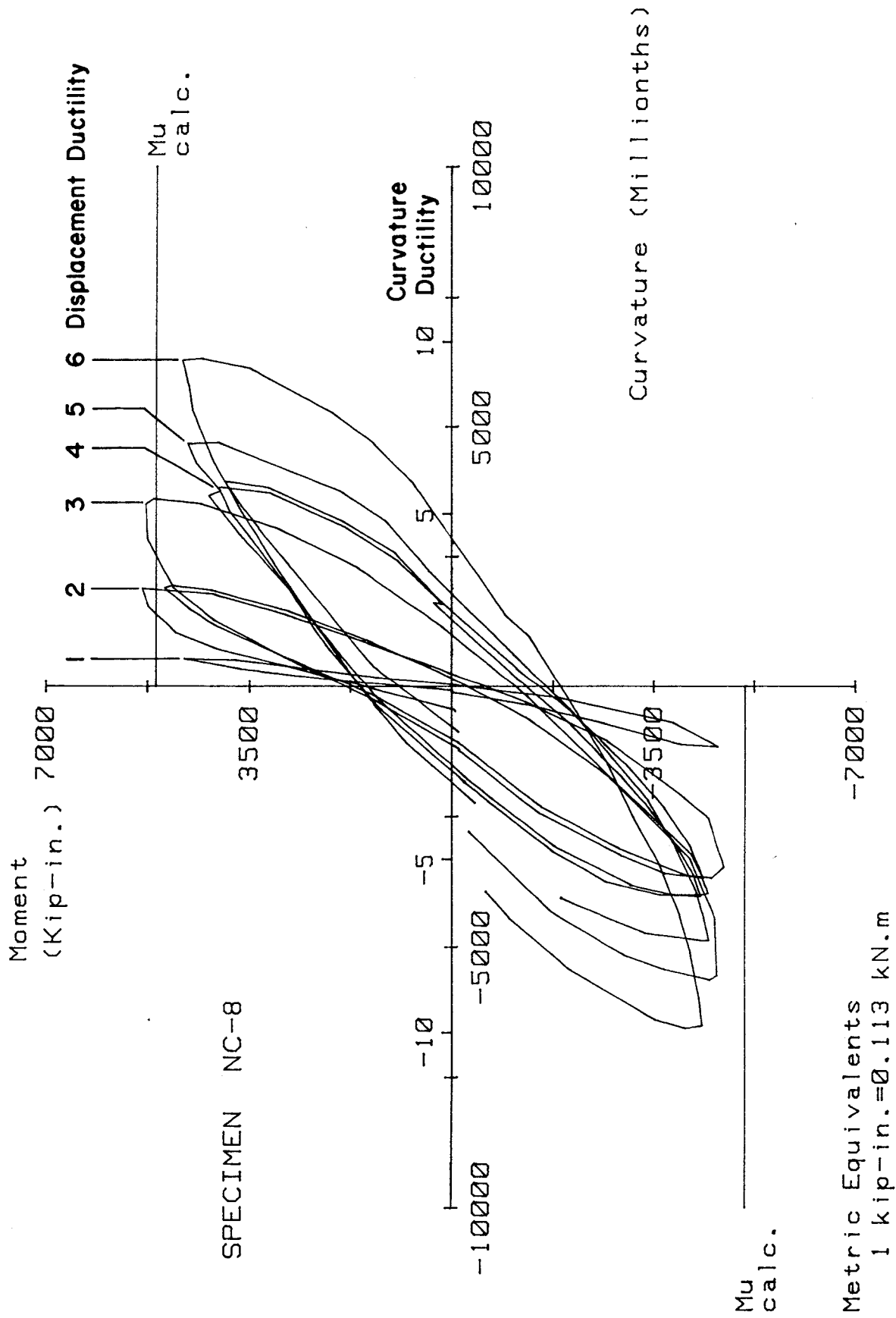


FIG. 5-24 MOMENT VERSUS CURVATURE FOR SPECIMEN NC-8

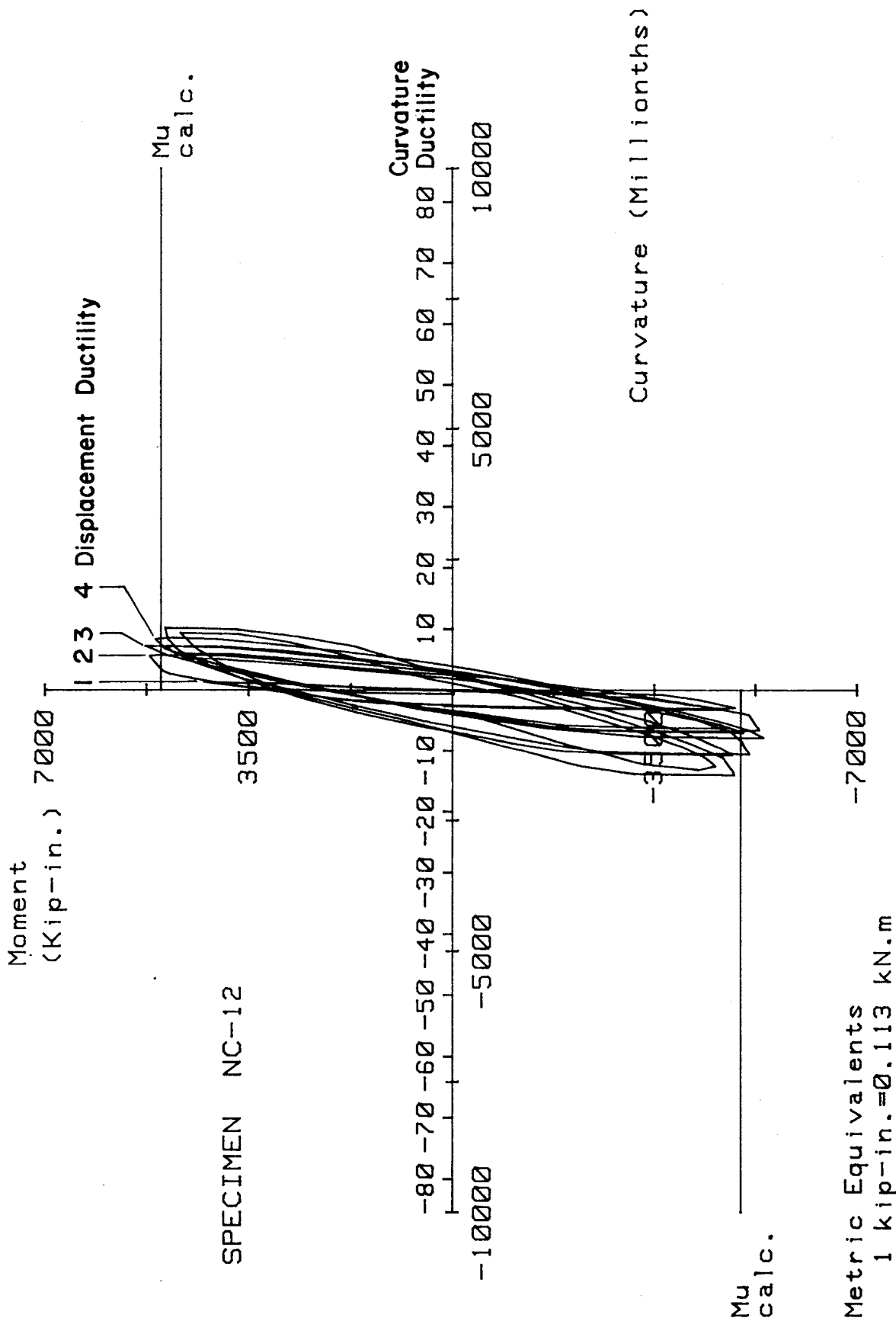


FIG. 5-25 MOMENT VERSUS CURVATURE FOR SPECIMEN NC-12

as 1.0. The curvatures in these plots are those obtained for the gage length within the first 4 in. above the stub. Measured displacement ductility, calculated flexural strength, and measured flexural strength values for all specimens are listed in Table 5.3.

The enhanced moment capacities can be partially attributed to confinement of the core concrete by transverse reinforcement. Of the specimens having axial loads equivalent to 30% of the column's axial load capacity, this enhanced moment capacity was largest for Specimen NC-5. The only specimen for which the ratio of maximum applied moment to calculated moment, M_u , was less than one was Specimen NC-6.

Table 5.4 shows the ratio of peak moment at the second cycle to peak moment at the first cycle at various displacement levels for all specimens. In general, small degradations in moment capacity was observed during the second cycle at each displacement level.

Figure 5-26 shows the moment-curvature characteristic of Specimen NC-12 at the first gage length above the stub. The small area under each hysteresis loop is the consequence of the different curvature distribution for this specimen (see Fig. 5-20). As discussed earlier, the maximum curvatures at various displacement levels for Specimen NC-12 occurred in the gage length from 4 to 8 in. above the stub. A plot of moment-curvature behavior at that gage length is shown in Fig. 5-27. This moment-curvature behavior is attributed to the good confinement of the upper column within the first 4 in. above the stub which caused a shift of the hinge region away from the stub.

Figure 5-28 shows the moment-curvature characteristic of Specimen NC-6 at the interface of the upper column-stub level. Several unexplained disturbances affecting the moment and curvature are discussed in the Appendix.

Figure 5-29 shows the moment-curvature behavior of Specimen NC-11 which had a circular upper column cross-section and spiral reinforcement. In general, the moment capacities of this specimen exceeded the calculated moment capacity, M_u , at all displacement levels.

Table 5.3 Test Results

Specimen Designation	Measured Displacement Ductility	Flexural Strength, kip-in.		Measured / Calculated
		Calculated	Measured	
NC-1	6	5184	6102	1.18
NC-2	8	4814	5773	1.20
NC-3	5	5198	6514	1.25
NC-4	5	5268	6152	1.17
NC-5	7	5226	6365	1.22
NC-6	5	4800	3651	0.76
NC-7	5	4950	5873	1.19
NC-8	6	5100	5351	1.05
NC-9	5	4810	5591	1.16
NC-10	5	4970	5379	1.08
NC-11	9	4000	4543	1.14
NC-12	5	5000	5389	1.08

Metric Equivalent:

1 kip-in. = 0.113 kNm

Table 5.4 Maintained Flexural Strength

Specimen I.D.	Displacement Ductility Ratio																	
	1		2		3		4		5		6		7		8		9	
	East Peak	West Peak	East Peak	West Peak	East Peak	West Peak	East Peak	West Peak	East Peak	West Peak	East Peak	West Peak	East Peak	West Peak	East Peak	West Peak	East Peak	West Peak
NC-1	-	0.98	0.96	0.94	0.97	1.01	0.94	0.97	0.94	0.97	0.96	0.94	-	-	-	-	-	-
NC-2	0.97	1.00	0.92	0.96	0.96	0.97	0.97	0.98	0.97	0.97	1.00	0.97	0.97	0.97	-	-	-	-
NC-3	0.95	0.97	0.94	0.96	0.93	0.98	0.93	0.95	0.93	-	-	-	-	-	-	-	-	-
NC-4	-	0.94	0.93	0.95	0.94	0.94	0.94	0.90	0.92	-	-	-	-	-	-	-	-	-
NC-5	-	0.94	0.94	0.95	0.94	0.95	0.94	0.95	0.94	0.95	0.96	0.93	0.93	0.93	-	-	-	-
NC-6	-	0.94	0.94	0.94	0.94	0.94	0.93	0.94	0.91	0.90	-	-	-	-	-	-	-	-
NC-7	-	0.94	0.95	0.94	0.94	0.94	0.90	0.94	0.74	-	-	-	-	-	-	-	-	-
NC-8	-	0.93	0.90	0.91	1.03	1.10	0.99	0.96	0.99	0.97	0.95	-	-	-	-	-	-	-
NC-9	-	0.89	0.92	0.94	0.95	0.96	0.90	0.86	0.90	-	-	-	-	-	-	-	-	-
NC-10	-	0.90	0.92	0.92	0.95	0.94	0.94	0.93	0.94	0.93	-	-	-	-	-	-	-	-
NC-11	-	0.96	-	0.96	0.94	0.99	0.89	0.96	0.89	0.99	0.98	0.99	0.96	0.99	1.01	0.95	0.92	0.91
NC-12	0.97	0.90	0.90	0.94	0.96	0.94	0.95	0.92	0.95	0.92	-	-	-	-	-	-	-	-

Note : Data not obtained or judged meaningless are replaced with a dash in the tabulation.

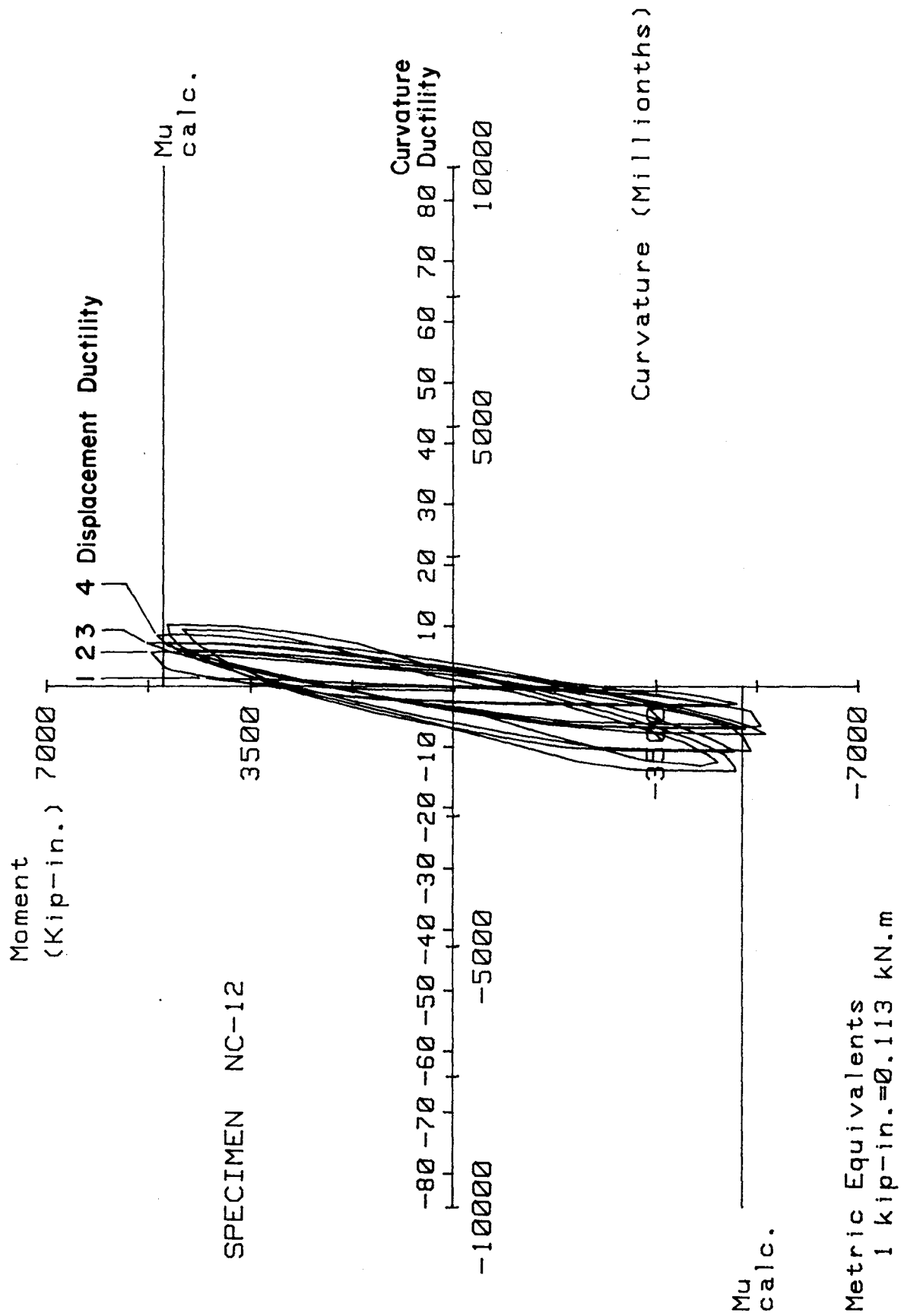


FIG. 5-26 MOMENT VERSUS CURVATURE FOR SPECIMEN NC-12 AT THE UPPER COLUMN STUB LEVEL

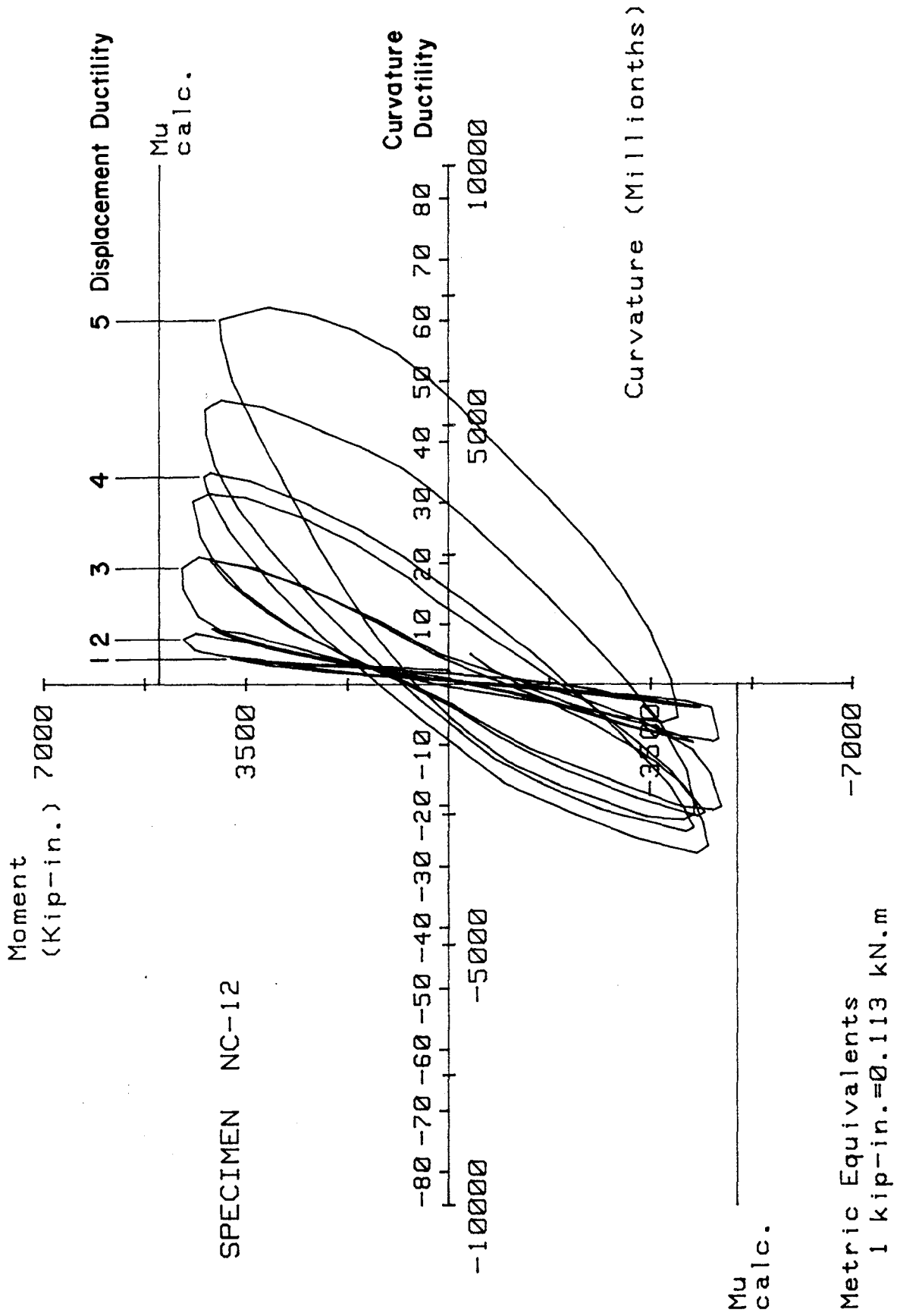


FIG. 5-27 MOMENT VERSUS CURVATURE FOR SPECIMEN NC-12 AT 6 IN. ABOVE THE STUB

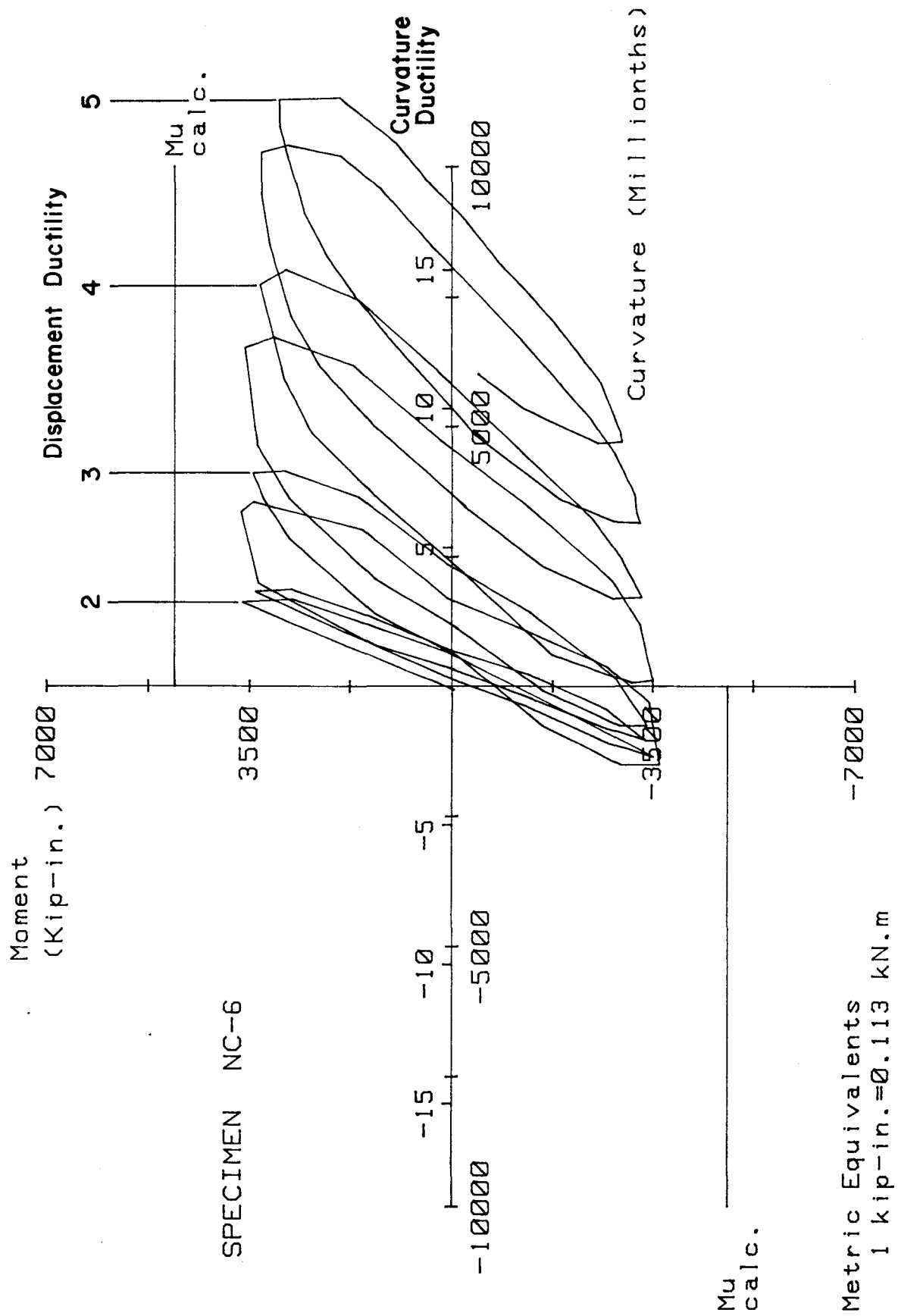
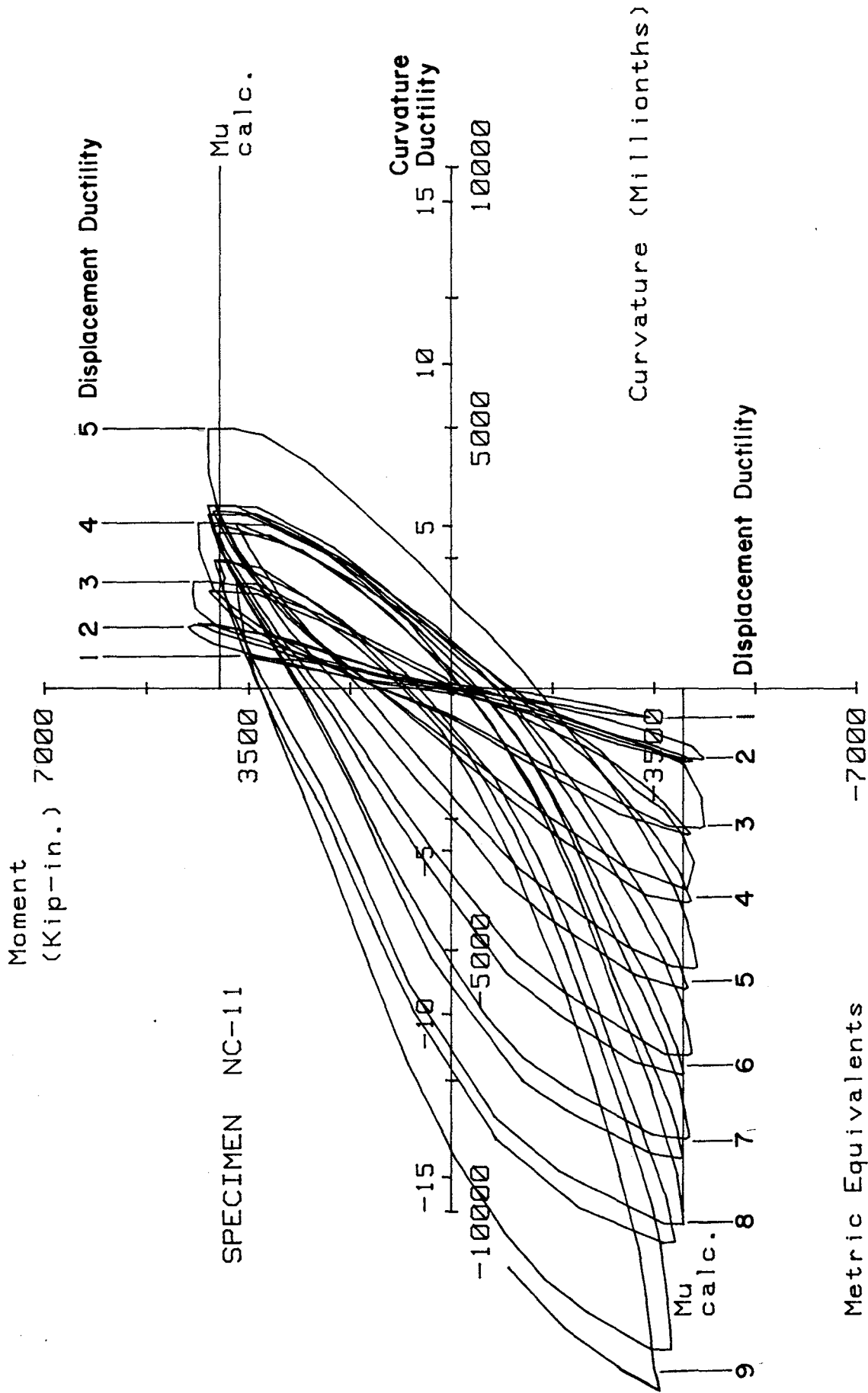


FIG. 5-28 MOMENT VERSUS CURVATURE FOR SPECIMEN NC-6



Metric Equivalents
 1 kip-in. = 0.113 kN.m

FIG. 5-29 MOMENT VERSUS CURVATURE FOR SPECIMEN NC-11

5.4 Effect of Variables

5.4.1 Axial Load

A comparison of results from Specimens NC-2 and NC-3 indicates that the flexural capacity of the column increased with axial load but ductility decreased substantially.

5.4.2 Details of Transverse Reinforcement

A comparison of test results from Specimens NC-1 and NC-5 indicates that flexural capacity and ductility of Specimen NC-5 were not reduced by the use of overlapping peripheral hoops.

Specimen NC-7 failed before completion of the second cycle at displacement ductility ratio of five. However, test results indicate special hoops used in Specimen NC-7 are capable of providing good strength and energy dissipation capabilities in the neighborhood of displacement ductility ratio of five.

Staggering the inner and peripheral hoops in Specimen NC-8 resulted in lower flexural capacity than in Specimen NC-1. However, Specimen NC-8 still provided displacement ductility ratio of six and failed before the completion of the second cycle at displacement ductility ratio of seven.

Specimens NC-9, NC-10, and NC-12 used continuous square helix transverse reinforcement. Specimens NC-9 and NC-10 failed by buckling of the middle longitudinal bars. Thus, in Specimen NC-12 crossties were added to provide additional support for middle longitudinal bars. As a result, Specimen NC-12 failed by simultaneous buckling of corner and middle longitudinal bars. All three specimens used the same volumetric ratio of transverse reinforcement. A comparison of test results from NC-9 and NC-10 indicates that for the same amount of transverse reinforcement, reducing the pitch results in a reduction in flexural capacity. However, it provides a slightly higher ductility. Considering that Specimens NC-9, NC-10, and NC-12 failed prior to completion of two cycles at the displacement ductility ratio of six, the continuous square helix transverse reinforcement is not as effective as the circular spiral reinforcement as indicated by qualitative comparison of test results from Specimen NC-11 with Specimens NC-9, NC-10, and NC-12. This can be attributed to the mechanism by which the circular

spiral and square helix transverse reinforcements provide confinement for core concrete. Circular spiral reinforcement is primarily subject to uniform tension, whereas square helix reinforcement is subjected to both bending and axial tension. Consequently, spiral reinforcement provides uniform confinement for core concrete whereas the square helix reinforcement provides only partial confinement.

A qualitative comparison of the behavior of Specimens NC-9, NC-10, and NC-12 with other specimens utilizing discrete type transverse reinforcement indicates continuous square helix reinforcement was able to enclose the core concrete more efficiently at test conclusion. In general, the use of square helix transverse reinforcement resulted in extensive cover concrete spalling.

5.4.3 Area of Transverse Reinforcement

The area of lateral reinforcement provided for the square columns ranged between 46 and 97 percent of the ACI-318-83 requirement. Table 5.5 gives the required area of lateral reinforcement for each square column along with the provided area. In calculating the required area the actual concrete compressive strength, f'_c , specified yield strength of the lateral reinforcement, f_y , the applied axial load, P , and the theoretical maximum shear at the upper column-beam stub interface were used. Table 5-6 lists the values of these parameters for all test specimens. The required area of lateral reinforcement in Table 5-5 was taken as the maximum ACI-318-83 requirement for maintaining axial strength after spalling of the cover concrete and shear requirements. The required volumetric ratio of spiral reinforcement by ACI-318-83 code for Specimen NC-11, the circular column, was 2.05%, while the provided volumetric ratio of the spiral reinforcement was 1.29%.

Although the area of provided lateral reinforcement for all test specimens was less than the ACI-318-83 requirement, resulting displacement ductilities exceed those implied by the code.

A comparison of results from Specimen NC-1 with those of NC-4 and NC-7 indicates the use of almost 50% less transverse reinforcement in these two specimens resulted in only slightly lower ductility. Maintained strength was also generally lower at all load stages.

Table 5.5 Transverse reinforcement area for square column test specimens

Specimen I.D.	Area Required by ACI, sq. in.	Area Provided, sq. in.	Area Provided / Area Required by ACI
NC-1	0.72	0.68	0.94
NC-2	0.73	0.68	0.93
NC-3	0.74	0.68	0.92
NC-4	0.81	0.38	0.47
NC-5	0.73	0.68	0.93
NC-6	0.64	0.40	0.63
NC-7	0.67	0.40	0.60
NC-8	0.70	0.68	0.97
NC-9	0.64	0.40	0.63
NC-10	0.42	0.20	0.52
NC-12	0.65	0.30	0.46

Table 5.6 Parameters used in Calculating ACI transverse reinforcement requirement

Specimen I.D.	f_c (ksi)	f_y (ksi)	N_u (kips)	V_u (kips)
NC-1	5.64	60	570	93
NC-2	5.70	60	380	88
NC-3	5.83	60	780	90
NC-4	5.78	60	580	94
NC-5	5.71	60	575	93
NC-6	5.04	60	520	86
NC-7	5.28	60	540	89
NC-8	5.51	60	560	91
NC-9	5.02	60	530	86
NC-10	5.29	60	550	89
NC-11	5.50	60	460	71
NC-12	5.32	60	534	90

5.4.4 Hook Bends of Inner Hoops

All specimens except NC-1 used 90 degree hook bends for inner hoops. All specimens using inner hoops behaved satisfactorily, except for Specimen NC-8. This indicates a standard 90 degree hook on the inner hoops is sufficient.

5.4.5 Hook Extensions

Test results indicate a ten bar-diameter extension as required by Section A.1 of the 1983 ACI Building Code is not needed. Six bar-diameter extensions used in all specimens produced displacement ductilities exceeding those generally assumed in design.

6.0 ANALYSIS OF RESULTS

6.1 Concrete Core Compression Strain

In general, crushing of the cover concrete occurred during the first cycle at displacement ductility ratio of two except for Specimens NC-2 and NC-8 for which partial crushing of cover concrete occurred at the first cycle at displacement ductility ratios of 3 and 1, respectively. In all specimens partial crushing occurred first at the interface of the upper column and the beam stub.

Table 6.1 shows the maximum core compressive strain achieved during testing for all specimens. Maximum core compressive strain for specimens NC-2, NC-3, NC-4, NC-5, NC-6 and NC-7 were approximated using the horizontal deflection of the stub and making the following assumptions: 1) plastic hinge was concentrated over a 10 in. length just above the stub column, and 2) depth of the neutral axis measured from the extreme compressive face at the ultimate load was 12 in. Maximum core compressive strain for Specimen NC-1 was approximated in a similar way, except that plastic hinge was assumed to be concentrated over a 10 in. length just below the stub column. For other specimens, maximum core compressive strain were calculated using the measured curvatures in the upper column. The maximum core strain varies between 0.036 and 0.134. Also shown in the table are the predicted maximum core compressive strains using Corley's (36) equation:

$$E_{cu} = 0.003 + 0.02 b/z + (p''f_y/20)^2$$

where: b = column width
 z = distance between the points of zero and maximum moment
 p'' = ratio of the volume of one layer of transverse reinforcement plus the compressive longitudinal bar over the volume of core concrete

f_y = yield strength of transverse reinforcement

Figure 6-1 shows the plot of maximum core compressive strain vs. ductility ratio for all specimens at 2 in. above the stub. As is evident, in the cases of Specimens NC-10, and NC-12 at this location strain is generally relatively small compared to other specimens at all displacement ductility ratios. Figures 6-2, 6-3, and 6-4 show plots of maximum core

Table 6.1 Maximum Core Compression Strain

Specimen I.D.	Maximum Core Compression Strain	Maximum Core Compression Strain by Corley's equation
NC-1	0.046	0.026
NC-2	0.063	0.026
NC-3	0.036	0.026
NC-4	0.036	0.020
NC-5	0.047	0.026
NC-6	0.036	0.020
NC-7	0.036	0.020
NC-8	0.085	0.026
NC-9	0.076	0.020
NC-10	0.065	0.021
NC-11	0.134	0.021
NC-12	0.074	0.021

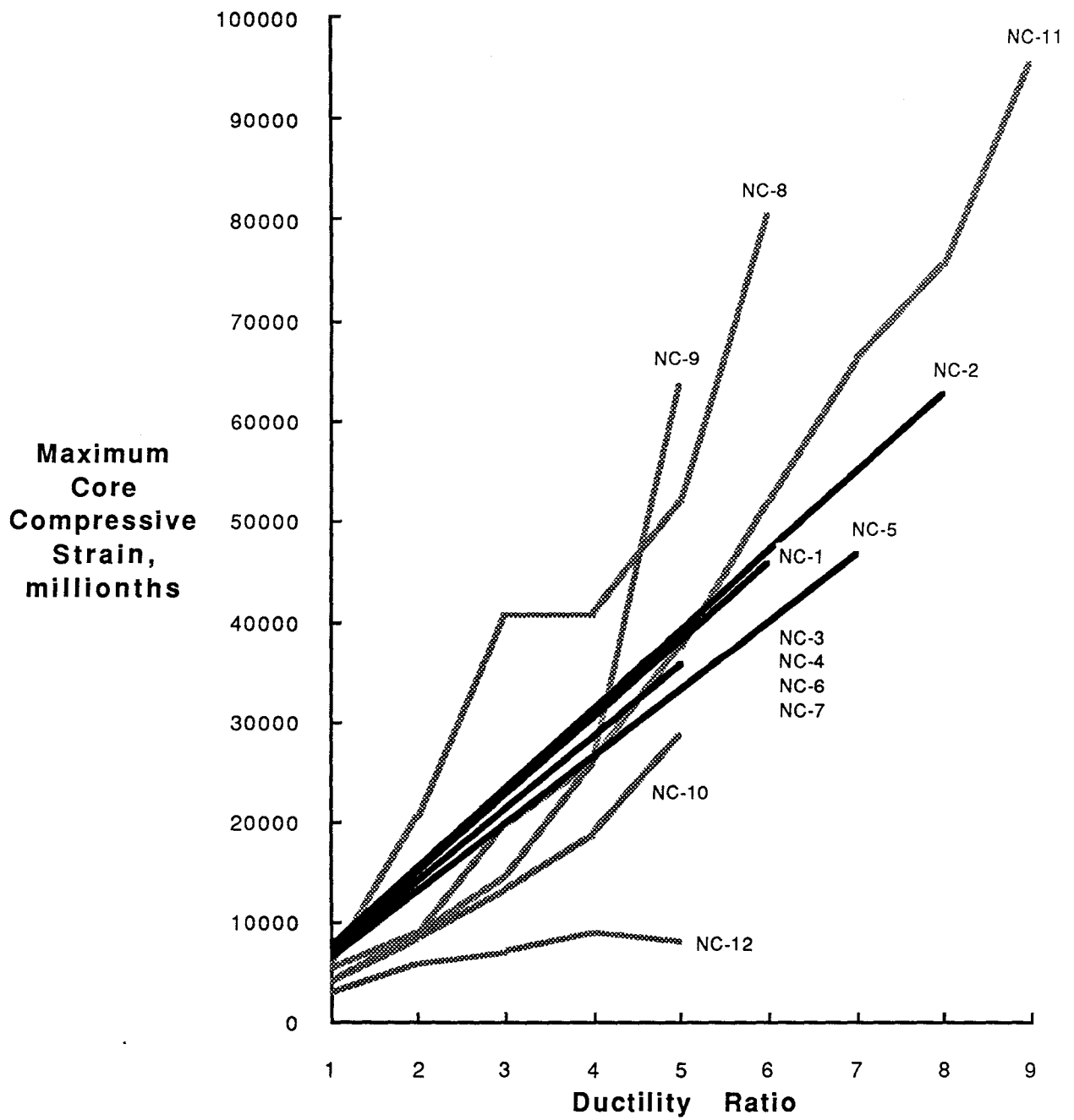


FIG. 6-1 CORE STRAIN VERSUS DISPLACEMENT DUCTILITY RATIO, ALL SPECIMENS

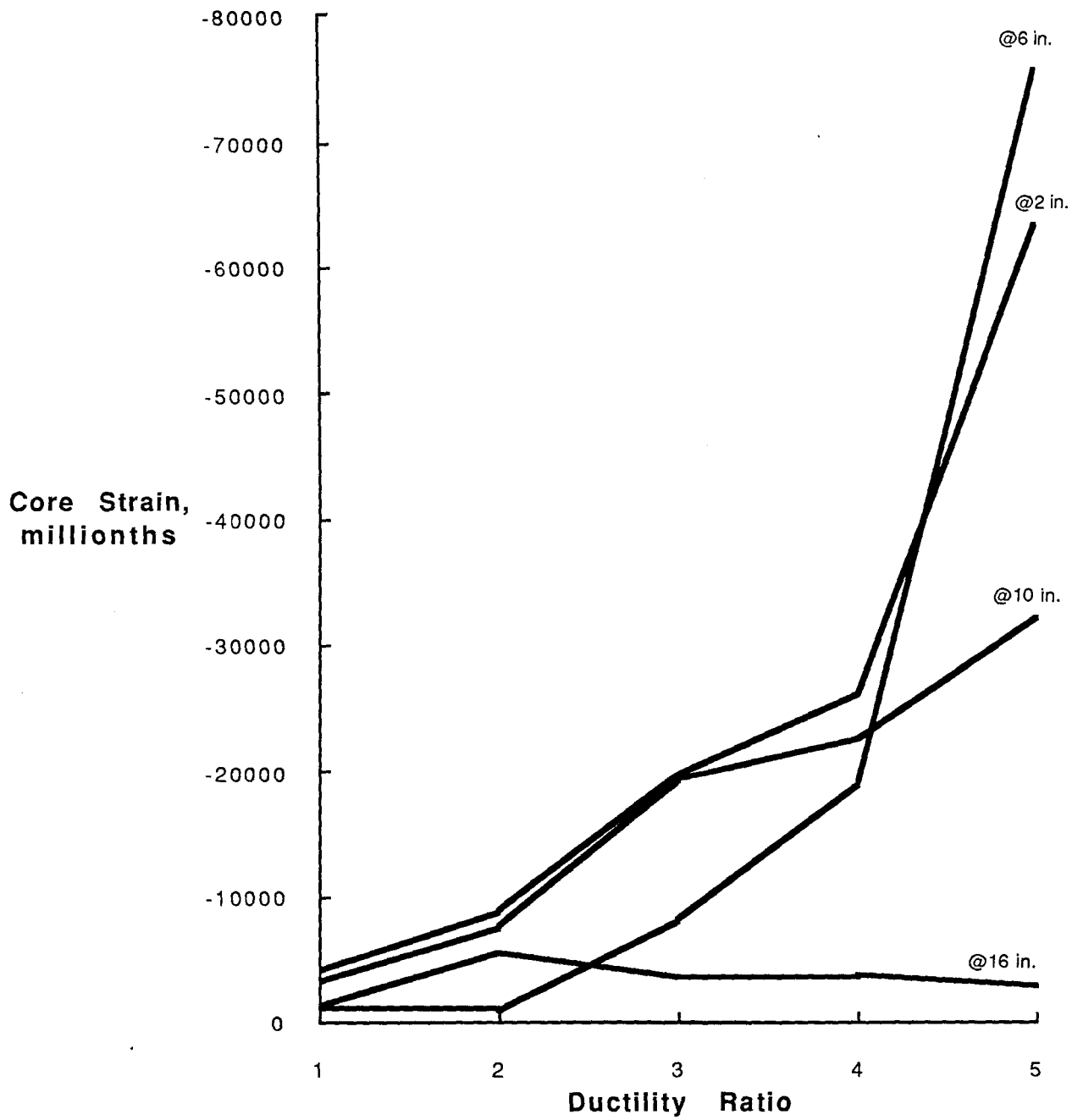


FIG. 6-2 CORE STRAIN VERSUS DISPLACEMENT DUCTILITY RATIO, SPECIMEN NC-9

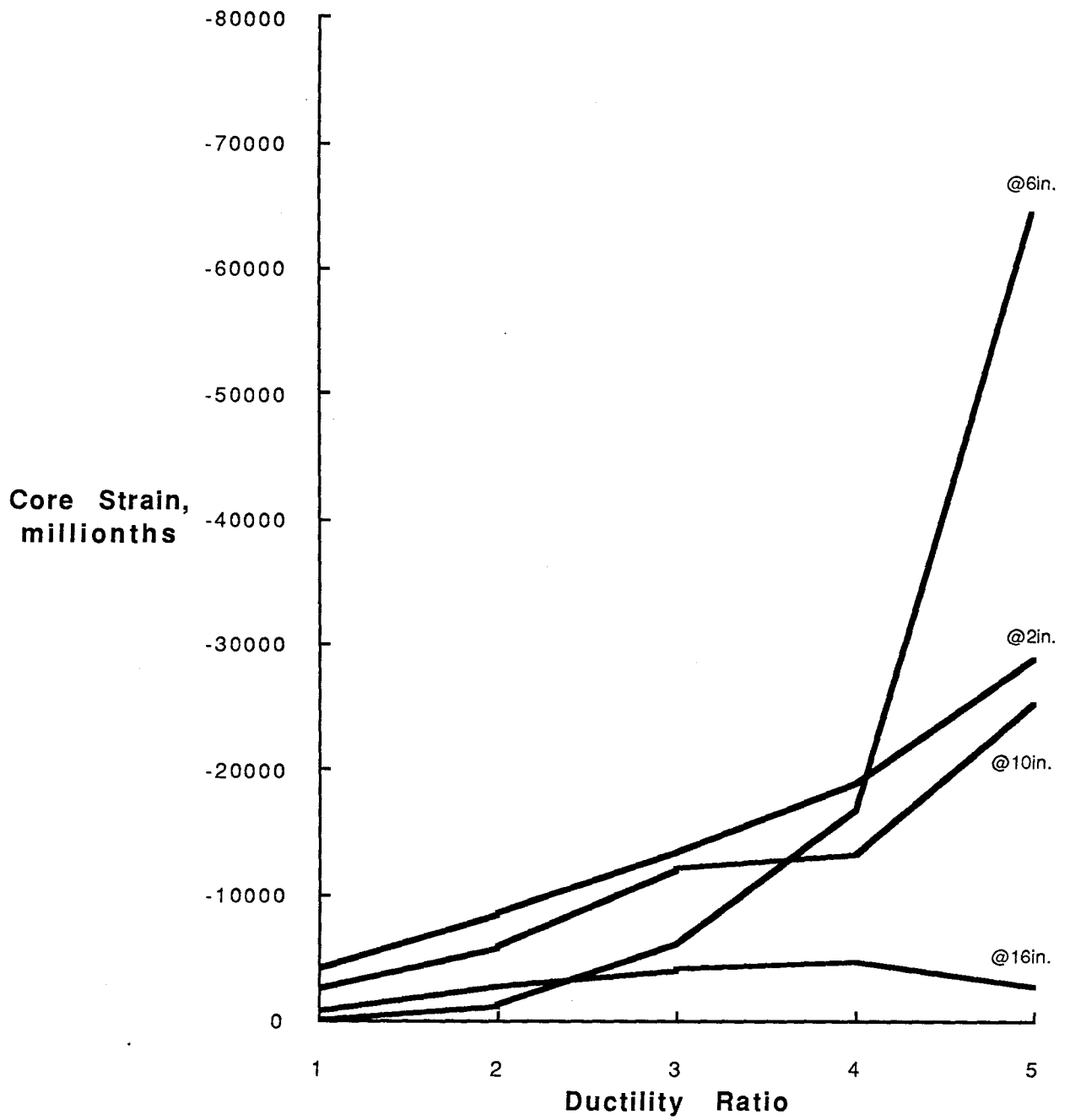


FIG. 6-3 CORE STRAIN VERSUS DISPLACEMENT DUCTILITY RATIO, SPECIMEN NC-10

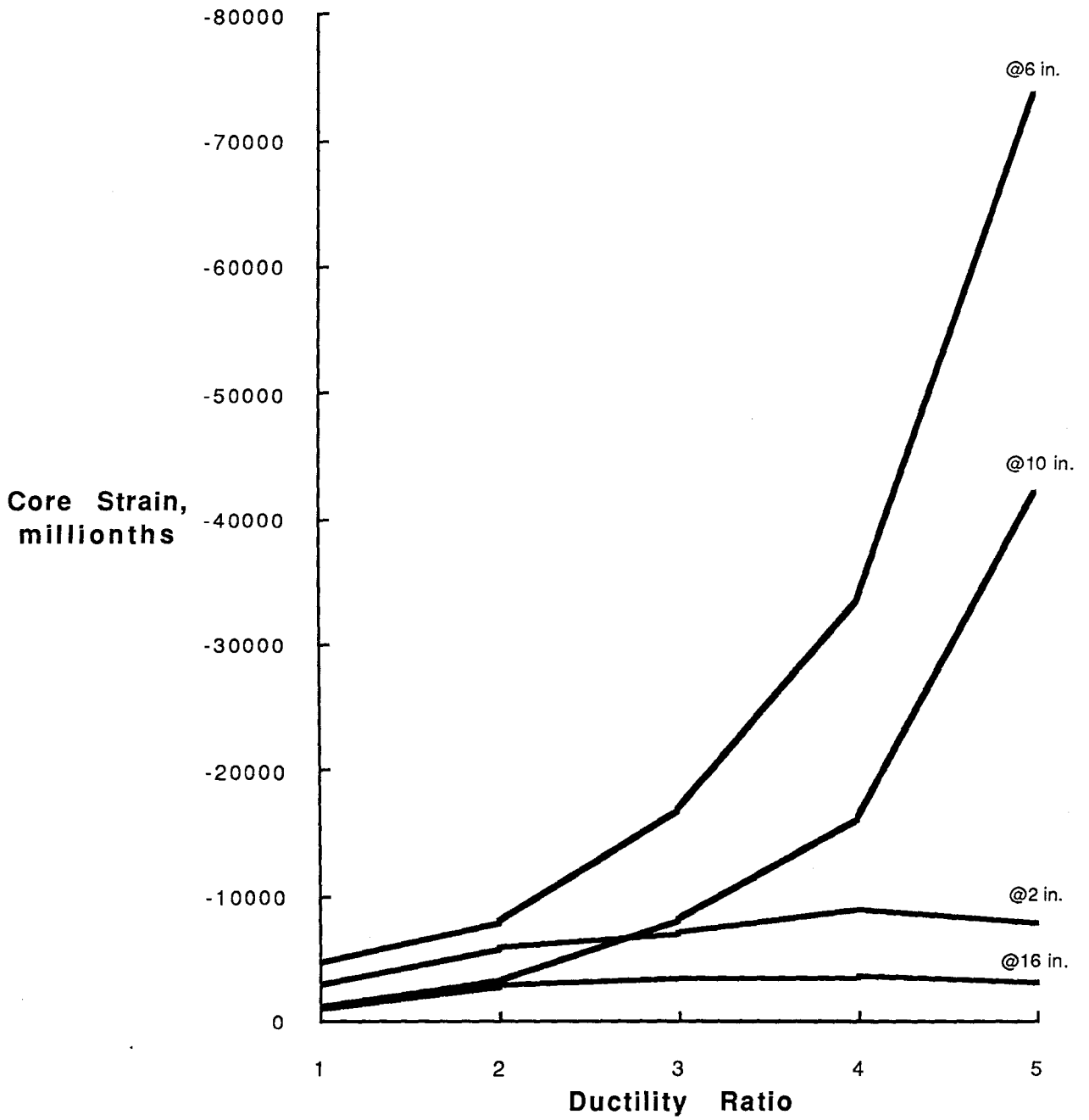


FIG. 6-4 CORE STRAIN VERSUS DISPLACEMENT DUCTILITY RATIO, SPECIMEN NC-12

compressive strain vs. displacement ductility ratio for Specimens NC-9, NC-10, and NC-12, respectively. Each plot shows the strain at 2, 6, 10, and 16 in. above the stub. As can be seen from these figures, maximum core compressive strains at all load stages were not necessarily located within the first 4 in. above the stub. This behavior is more pronounced in Specimen NC-12. This behavior of Specimens NC-9, NC-10, and NC-12 can be attributed in part to the fact that at test conclusion layers of transverse reinforcement within a few inches above the stub were still covered by concrete providing good confinement in this region. Consequently, the plastic hinge was forced upward and therefore, the region of high curvature as well as the region of high core compression strain for these specimens is generally located at some distance from the stub.

6.2 Moment-Curvature Analysis

Theoretical moment-curvature relationships for the test specimens were calculated based on equilibrium of forces and the following assumptions:

1. Stress-strain curve for longitudinal steel is as shown in Fig. 6-5.
2. Stress-strain curve for confined and unconfined concrete in compression is known.
3. A plane section before bending remains plane after bending.
4. Strain in concrete and longitudinal steel are compatible.

For the confined concrete, two different concrete compressive stress distributions were used. A brief description of each model follows:

1. Modified Kent and Park (37) model - according to this model, the stress-strain behavior of compressed concrete confined by rectangular steel hoops is as shown in Fig. 6-6. Referring to Fig. 6-6 for various regions, the stress is defined as follows:

For region AB ($\epsilon_c < 0.002 K$)

$$f_c = Kf'_c \left[\frac{2\epsilon_c}{.002K} - \left(\frac{\epsilon_c}{0.002K} \right)^2 \right]$$

For region BC ($\epsilon_c < 0.002 K$)

$$f_c = Kf'_c [1 - Z_m(\epsilon_c - 0.002K)]$$

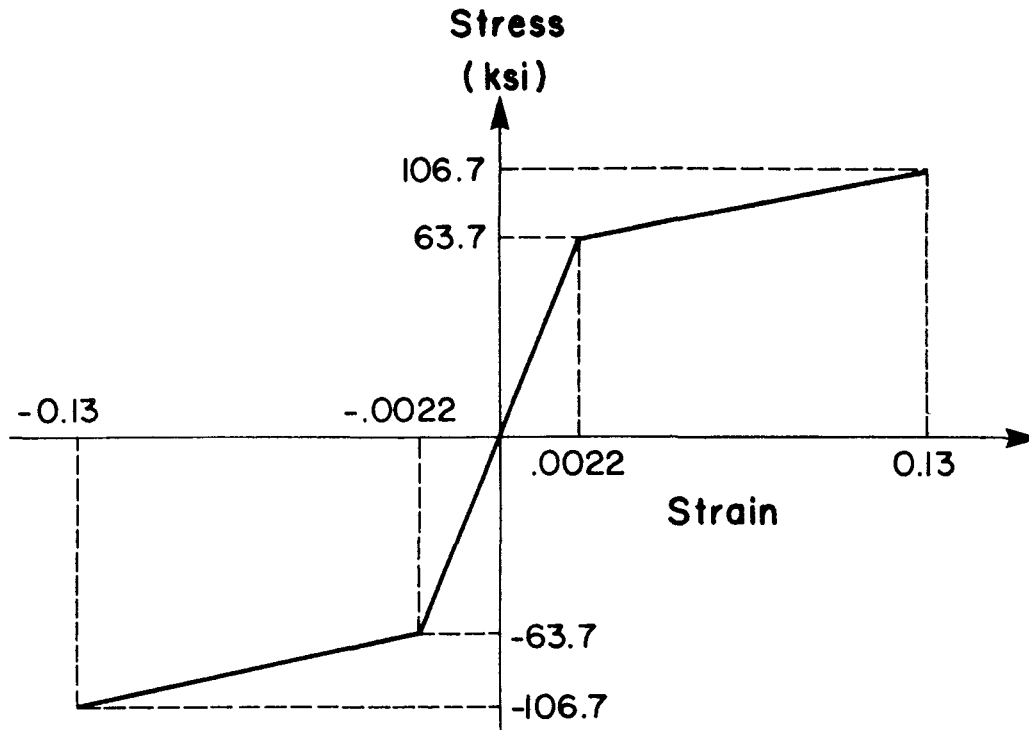


FIG. 6-5 STRESS-STRAIN CURVE FOR LONGITUDINAL STEEL

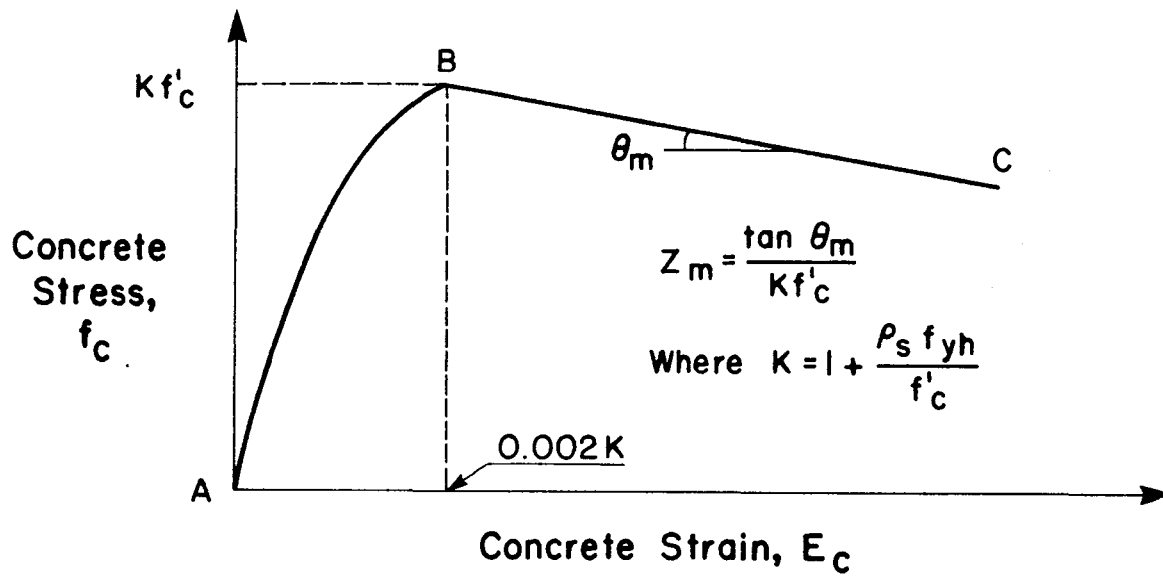


FIG. 6-6 MODIFIED KENT AND PARK MODEL FOR STRESS-STRAIN BEHAVIOR OF COMPRESSED CONCRETE CONFINED BY RECTANGULAR HOOPS (36)

but not less than $0.2 K f'_c$, in which

$$Z_m = \frac{0.5}{\frac{3 + 0.29 f'_c}{145 f'_c - 1000} + \frac{3}{4} \rho_s \sqrt{\frac{h^*}{S_h}} - 0.002K}$$

where: f'_c is in megapascals (1 MPa = 145 psi)

$$K = 1 + \frac{\rho_s f_{yh}}{f'_c}$$

h^* = width of the concrete core measured to the outside of the peripheral hoop

S_h = center-to-center spacing of hoop sets

ρ_s = ratio of volume of rectangular steel hoops to volume of concrete core measured to outside of the peripheral hoop

f_{yh} = yield strength of steel hoops

f'_c = concrete compressive cylinder strength

ϵ_c = concrete compressive strain

2. Sheikh and Uzumeri (38) model - according to this model the stress-strain curve for confined concrete is as shown in Fig. 6-7. The curve is defined completely by four parameters, K_s , ratio of the strength of the confined concrete to the strength of unconfined concrete, ϵ_{s1} and ϵ_{s2} , the minimum and maximum strains corresponding to the maximum stress in concrete and ϵ_{s85} , the strain corresponding to 85 percent of the maximum stress on the descending part of the curve.

The parameter K_s for square sections with uniformly distributed longitudinal steel is:

$$K_s = 1 + \frac{2.738^2}{\rho_{occ}} \left[\left(1 - \frac{nc^2}{5.58^2}\right) \left(1 - \frac{S}{2B}\right)^2 \right] \sqrt{\frac{\rho_s f'_s}{S}}$$

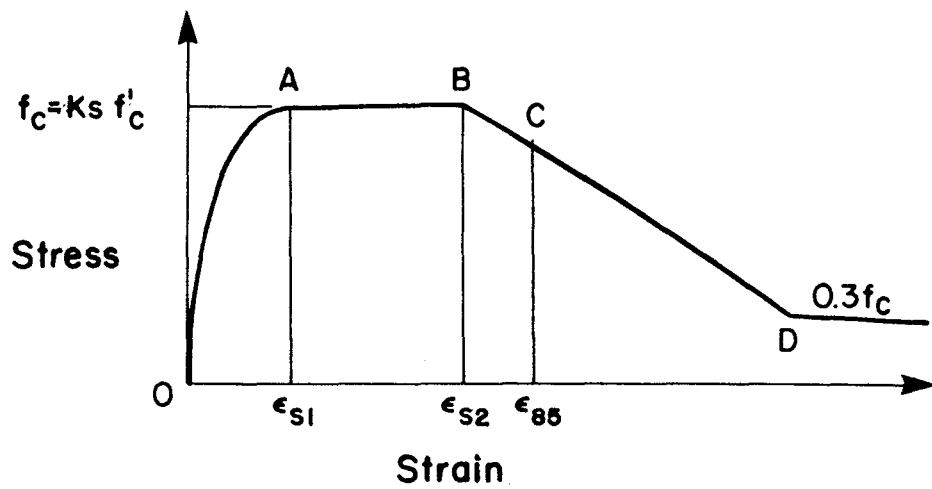


FIG. 6-7 SHEIKH AND UZUMERI MODEL FOR STRESS-STRAIN BEHAVIOR OF COMPRESSED CONCRETE CONFINED BY RECTANGULAR HOOPS

where: B = center-to-center distance of perimeter tie of rectangular core

$P_{occ} = 0.85 f'_c (A_{oc} - A_s)$ in kips

$A_{co} = \text{core area} = B^2$

$A_s = \text{total area of longitudinal bars}$

$f'_c = \text{specified concrete compressive strength}$

n = the number of arcs, as shown in Fig. 6-8

C = the center-to-center distance between longitudinal bars

S = tie spacing

$f'_s = \text{the stress in the lateral steel at the time of maximum resistance of confined concrete in kips per square inch}$

$\rho_s = \text{the ratio of the volume of total lateral reinforcement to the volume of core}$

The parameters ϵ_{s1} , ϵ_{s2} , and ϵ_{s85} are defined as follows:

$$\epsilon_{s1} = 0.55 K_S f'_c \times 10^{-6}$$

$$\epsilon_{s2} = \epsilon_{00} \left[1 + \frac{0.81}{C} \left(1 - 5 \left(\frac{S}{B} \right)^2 \right) \right] \frac{\rho_s f'_s}{\sqrt{f'_c}}$$

and

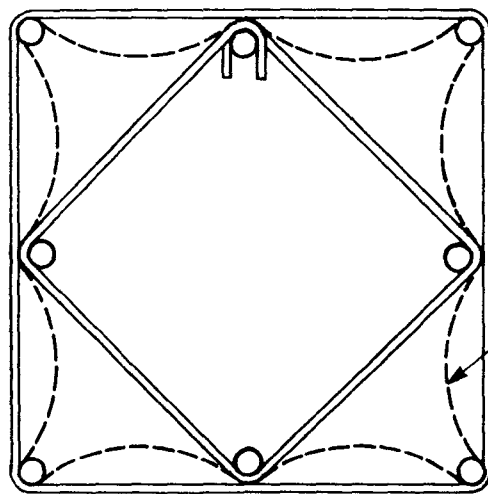
$$\epsilon_{s85} = 0.225 \rho_s \sqrt{\frac{B}{S}} + \epsilon_{s2}$$

where: $\epsilon_{00} = \text{strain corresponding to the maximum stress in plain concrete (0.0022 in the case of present tests).}$

Sheikh and Uzumeri do not provide an equation for the stress-strain curve between points O and A in Fig. 6-7. In this study, the following equation was used for the OA portion of the curve:

$$f_c = K_S f'_c \left[\frac{2\epsilon_c}{0.0022} - \left(\frac{\epsilon_c}{0.0022} \right)^2 \right]$$

Tables 6.2 and 6.3 give values of some of the parameters used to define the stress-strain curve for confined concrete using a modified Kent and Park, and Sheikh and Uzumeri models, respectively. In the Sheikh and Uzumeri model for Specimens NC-6 through NC-10, it was assumed that the middle



$N = \text{No. of Arcs} = 8$

Arc

FIG. 6-8 CROSS-SECTION OF SQUARE COLUMN
WITH PERIPHERAL AND CROSSTIE

Table 6.2 Parameters used in Modified Kent and Park model

Specimen I.D.	ρ_s (%)	S_h (in.)	f_{yh} (ksi)	f'_c (ksi)
NC-2	0.0211	4	65.8	5.7
NC-3	0.0211	4	65.8	5.83
NC-4	0.0119	4	89.4	5.78
NC-5	0.0211	4	65.8	5.71
NC-6	0.0129	4	65.8	5.04
NC-7	0.0129	4	65.8	5.28
NC-8	0.0211	4	65.8	5.51
NC-9	0.0129	4	65.8	5.02
NC-10	0.0129	2.25	89.4	5.29
NC-12	0.0110	3.5	89.4	5.33

Table 6.3 Parameters used in Shiekh and Uzumeri Model

Specimen I.D.	C (in.)	n	S (in.)	ρ_s (%)	f'_s (ksi)	f'_c (ksi)
NC-2	6.5	8	4	0.0225	65.8	5.70
NC-3	6.5	8	4	0.0225	65.8	5.83
NC-4	6.5	8	4	0.0125	89.4	5.78
NC-5	6.5	8	4	0.0225	65.8	5.71
NC-6	13	4	4	0.0138	65.8	5.04
NC-7	13	4	4	0.0138	65.8	5.28
NC-8	13	4	4	0.0225	65.8	5.51
NC-9	13	4	4	0.0138	65.8	5.02
NC-10	13	4	2.25	0.0136	89.4	5.29
NC-12	6.5	8	3.5	0.0115	89.4	5.31

longitudinal bars are not effective in confining the core concrete, and thus a value of four for n was used in predicting the stress-strain curves for confined concrete for these specimens.

The stress-strain curves for unconfined concrete were predicted using a modified Kent and Park model with ρ_s equal to zero.

Figures 6-9 through 6-18 show a comparison of the analytical and experimental moment curvature behavior of the test specimens. The analyses shows an early peak of bending moment capacity followed by decreasing moment for increasing curvatures. The analysis line should define the maximum point of moment versus curvature for each cycle of the repeated reversals of loading used in this study. Typically, the experimental data exceeds the capacity shown by the two analyses at increasing curvatures. The difference between the analytical and experimental results could be explained in part as follows:

1. The confined concrete stress-strain model of Sheikh and Uzumeri (38) were developed based on concrete column under concentric loading. Thus, the effect of strain gradient is not included in the model. Strain gradient may reduce the confinement demand and improve behavior.
2. The confined concrete stress-strain models of Kent and Park, and Sheikh and Uzumeri do not include the effect of cyclic loading. Cyclic loading may increase confinement demand and degrade behavior as compared to one-time loading.
3. The presence of a stub column provides additional confinement to the adjacent column cross-section. This additional confinement tends to increase the flexural capacity of the column cross-section at this location.
4. In the development of their confined model Sheikh and Uzumeri assumed that, from the onset of loading, the portion of the effectively confined concrete is some percentage of the core area. The percentage is a function of such parameters as arrangement and spacing of the lateral reinforcements. However, it is possible that in the early stages of loading, the full concrete area is effective, particularly before the first observed crushing of the

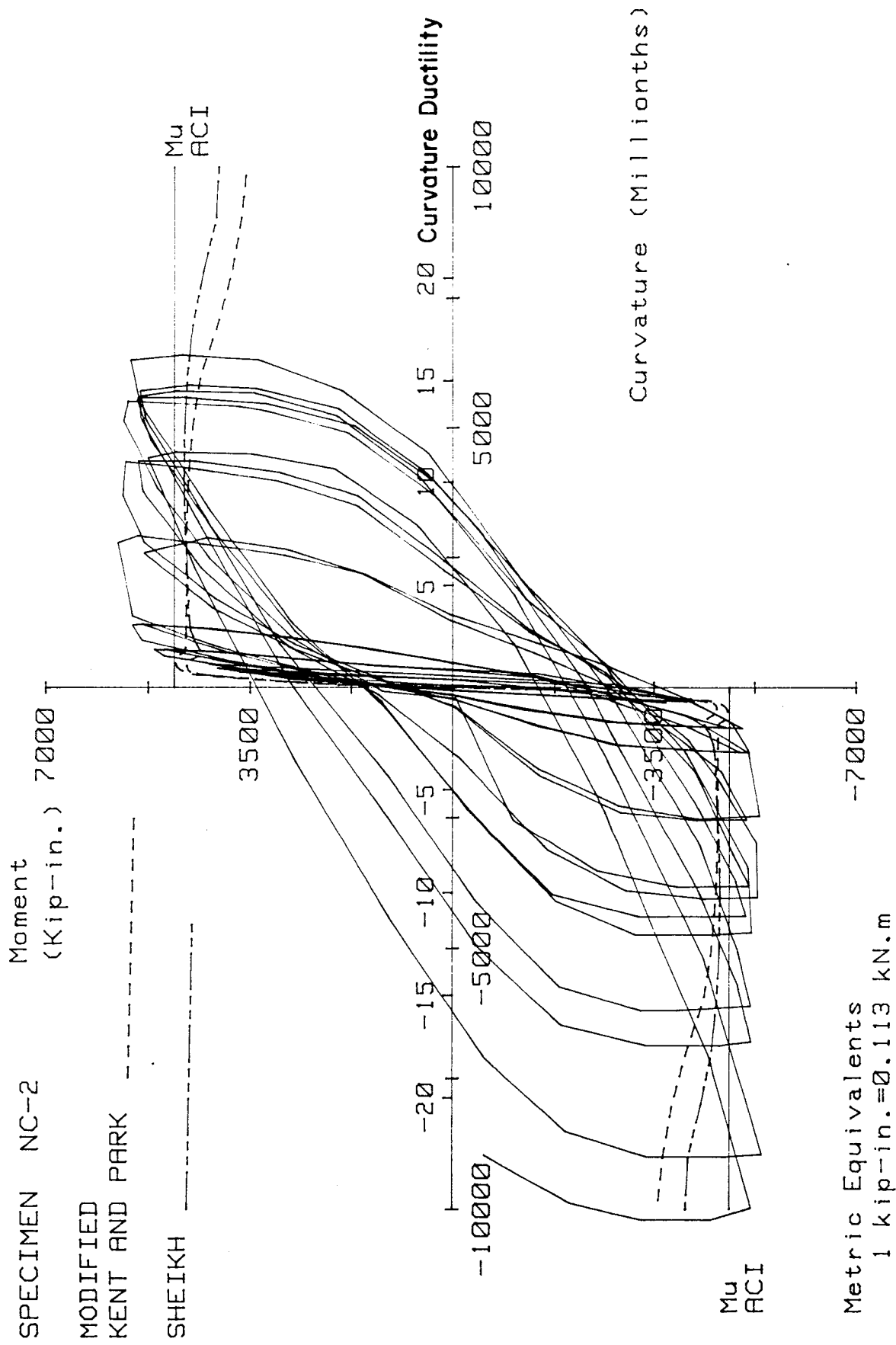


FIG. 6-9 MOMENT VERSUS CURVATURE FOR SPECIMEN NC-2

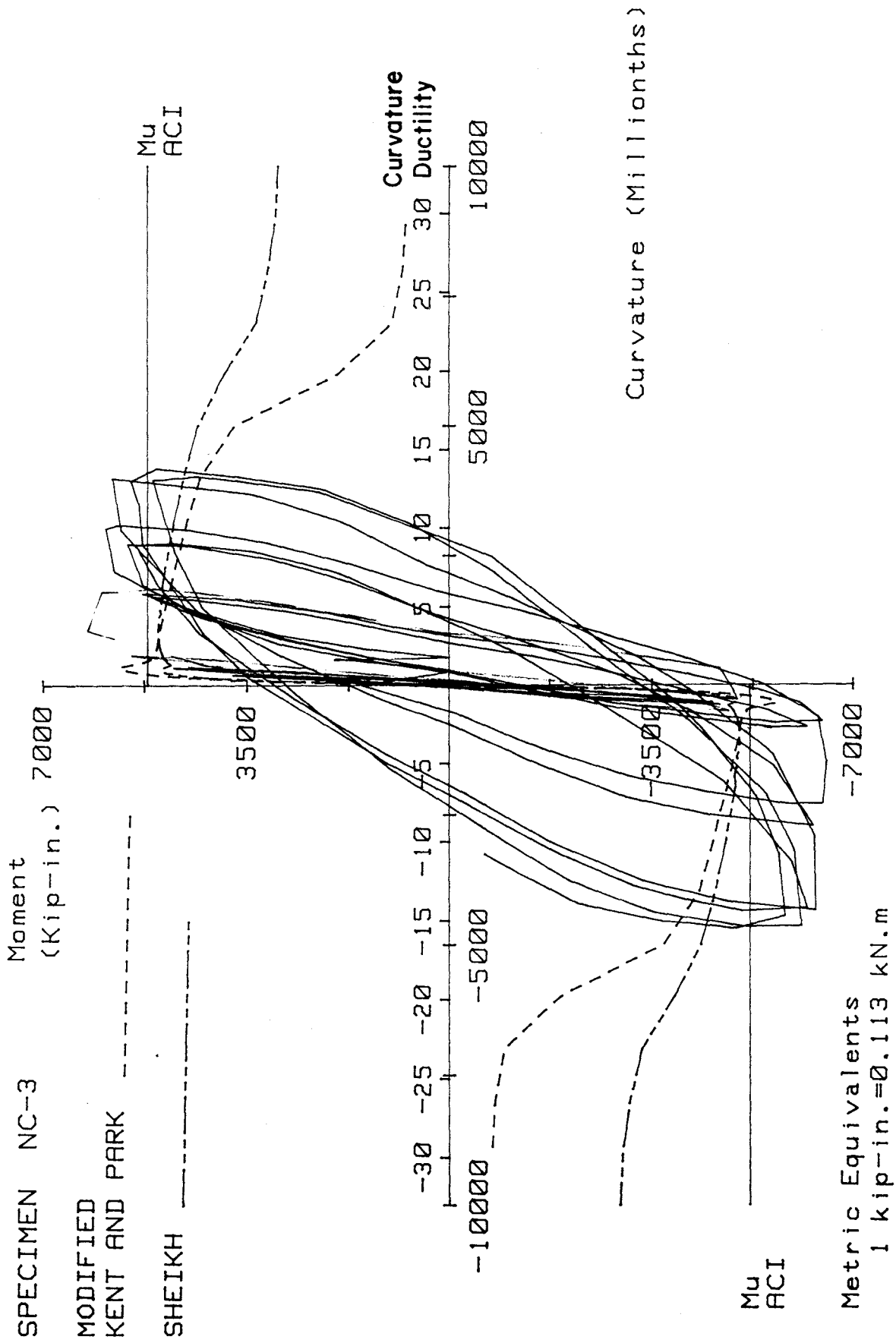


FIG. 6-10 MOMENT VERSUS CURVATURE FOR SPECIMEN NC-3

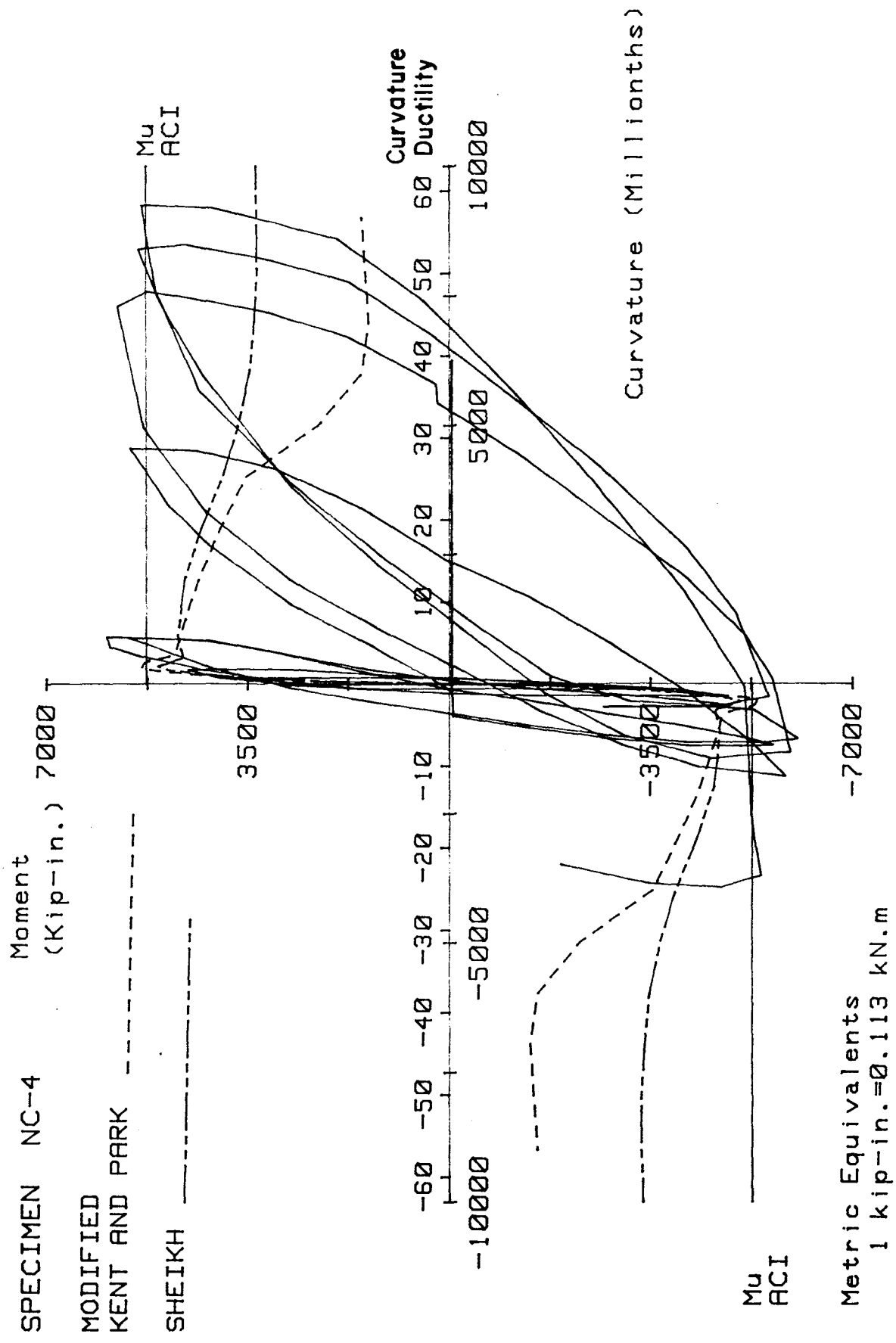


FIG. 6-11 MOMENT VERSUS CURVATURE FOR SPECIMEN NC-4

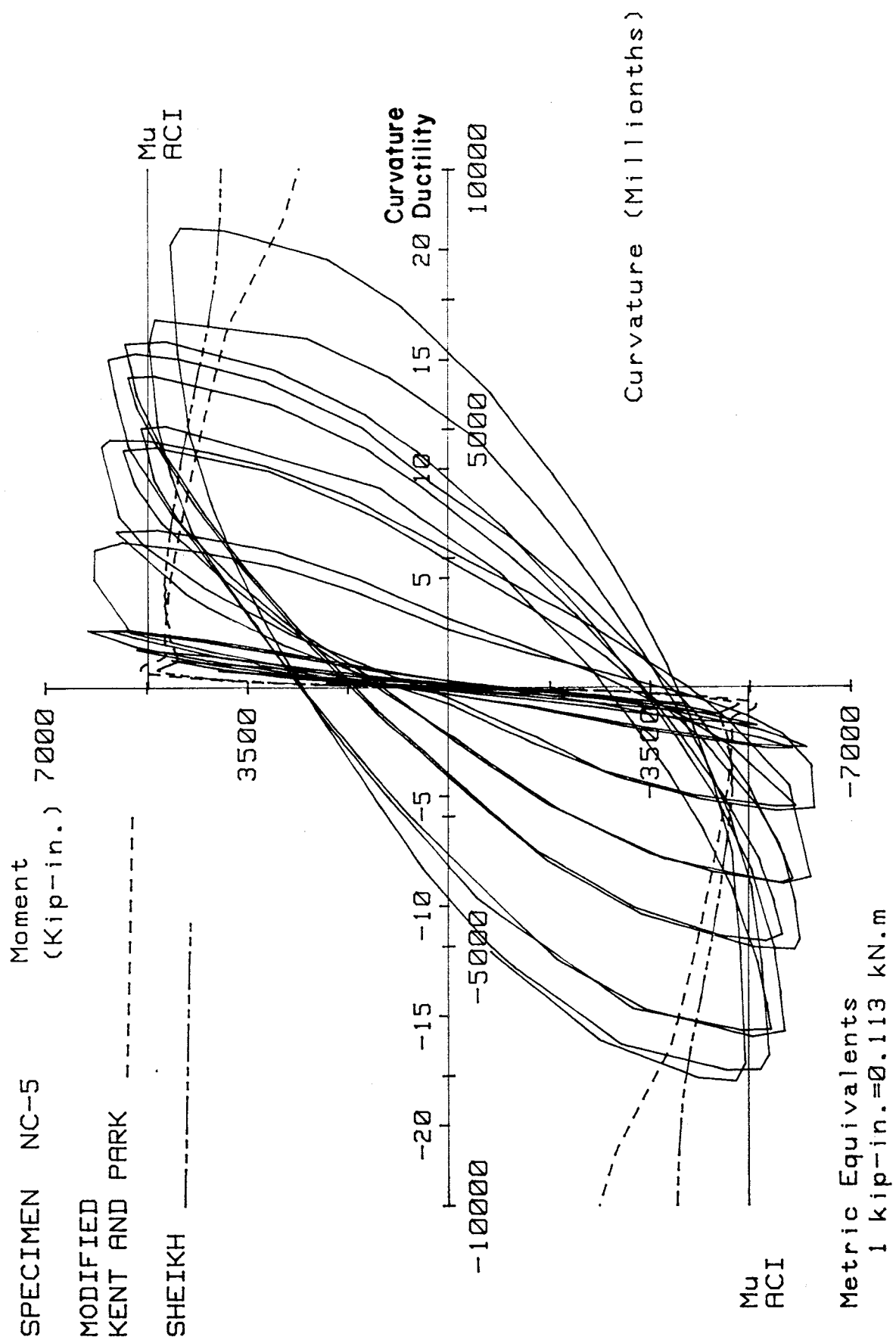


FIG. 6-12 MOMENT VERSUS CURVATURE FOR SPECIMEN NC-5

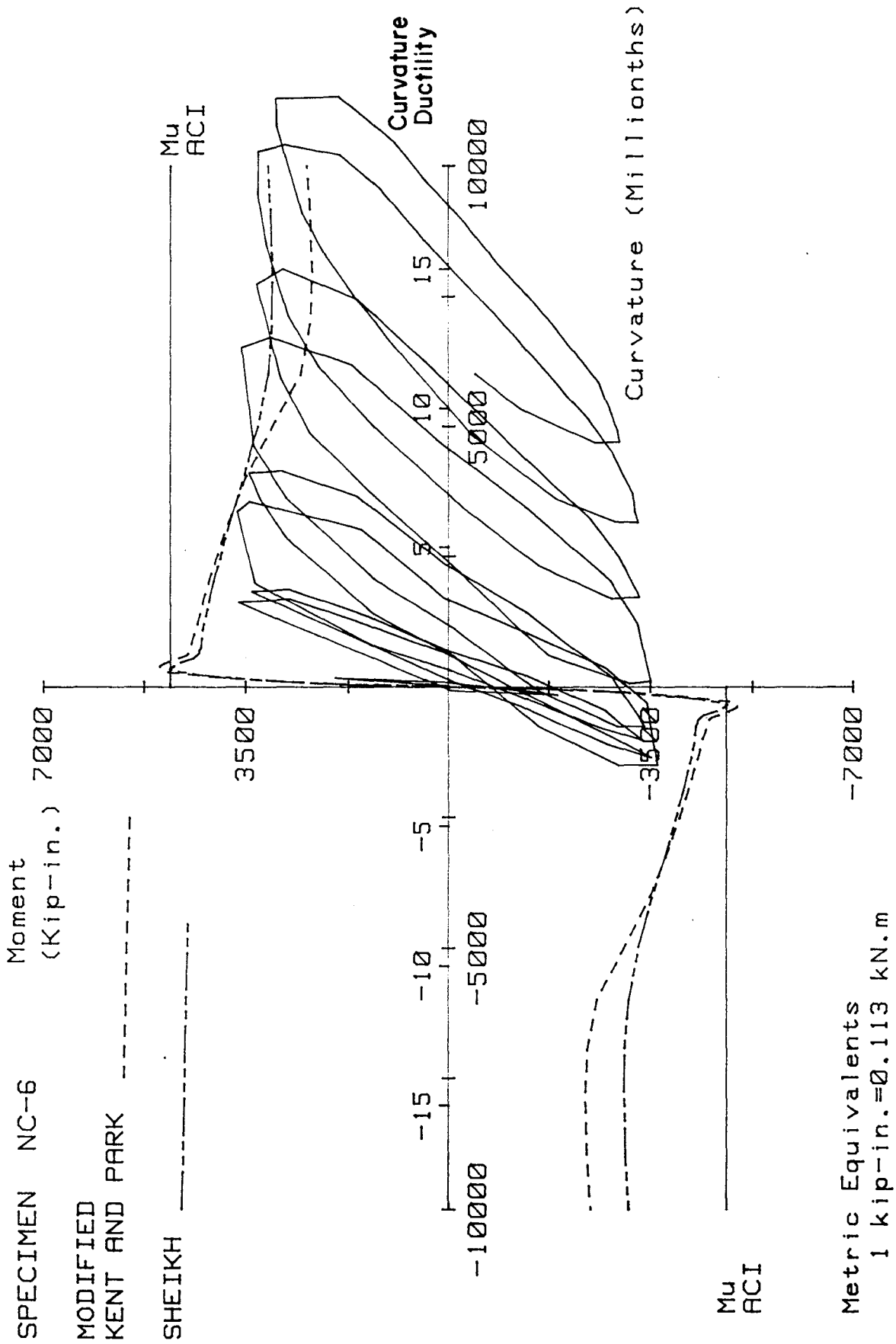


FIG. 6-13 MOMENT VERSUS CURVATURE FOR SPECIMEN NC-6

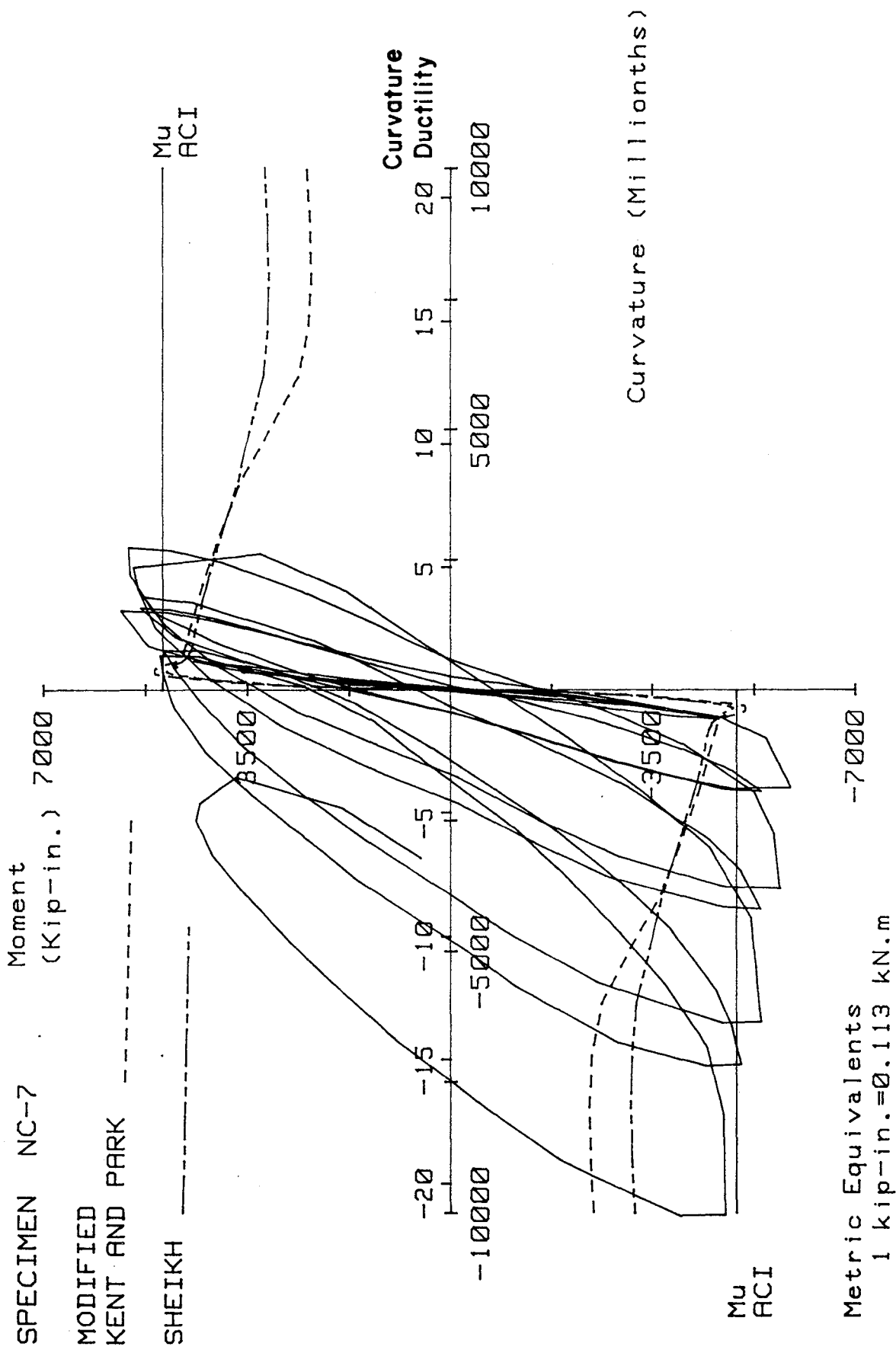


FIG. 6-14 MOMENT VERSUS CURVATURE FOR SPECIMEN NC-7

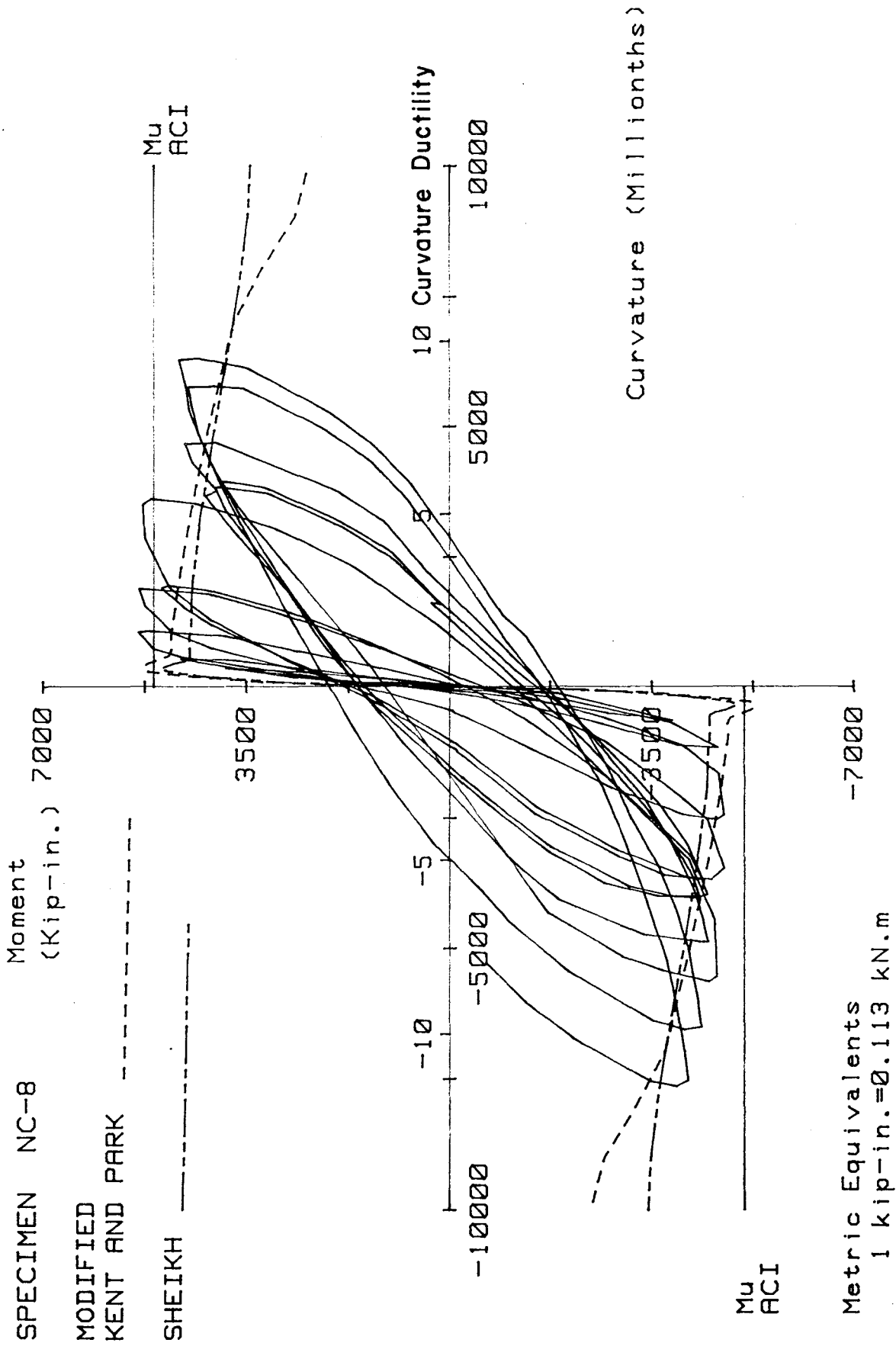


FIG. 6-15 MOMENT VERSUS CURVATURE FOR SPECIMEN NC-8

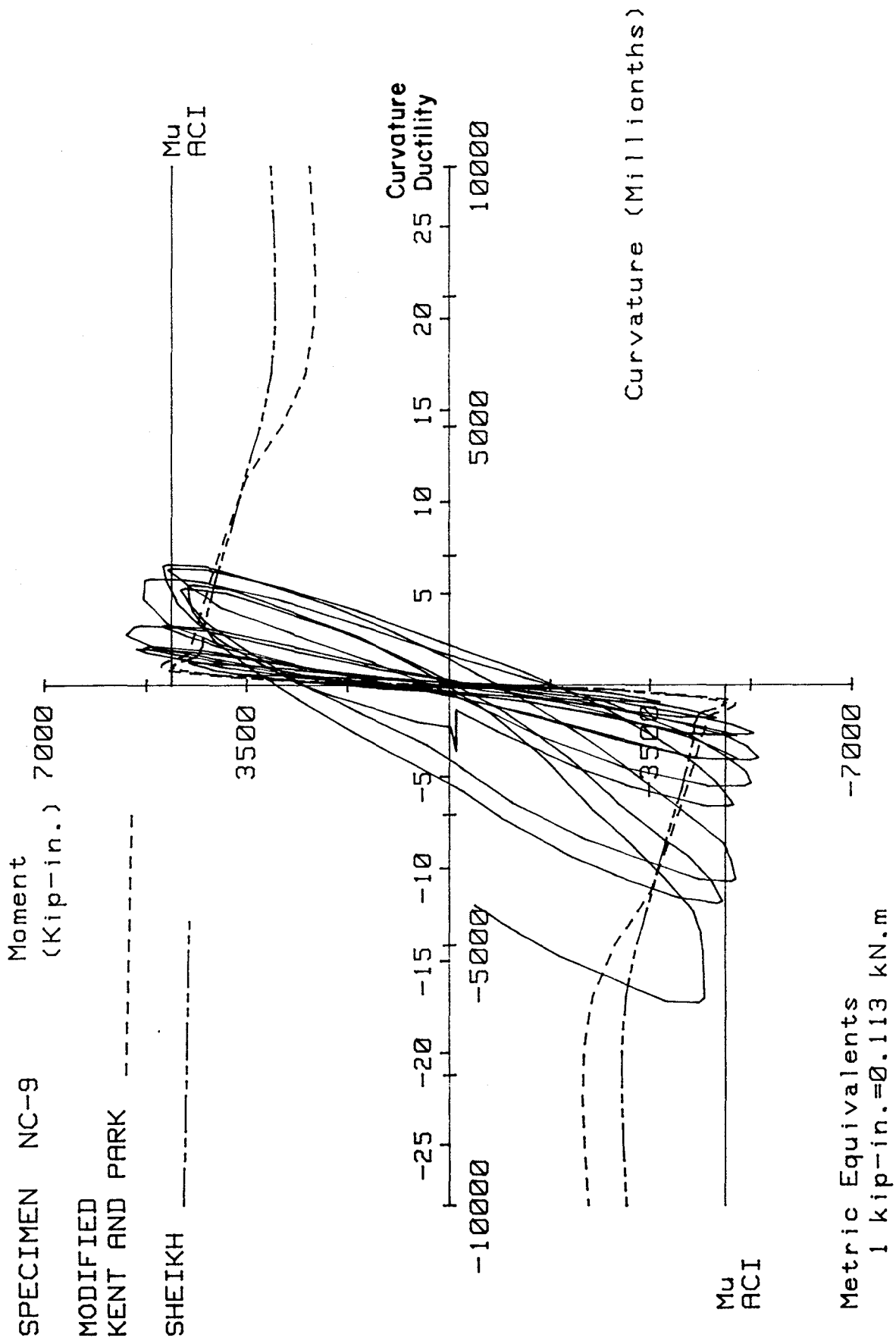


FIG. 6-16 MOMENT VERSUS CURVATURE FOR SPECIMEN NC-9

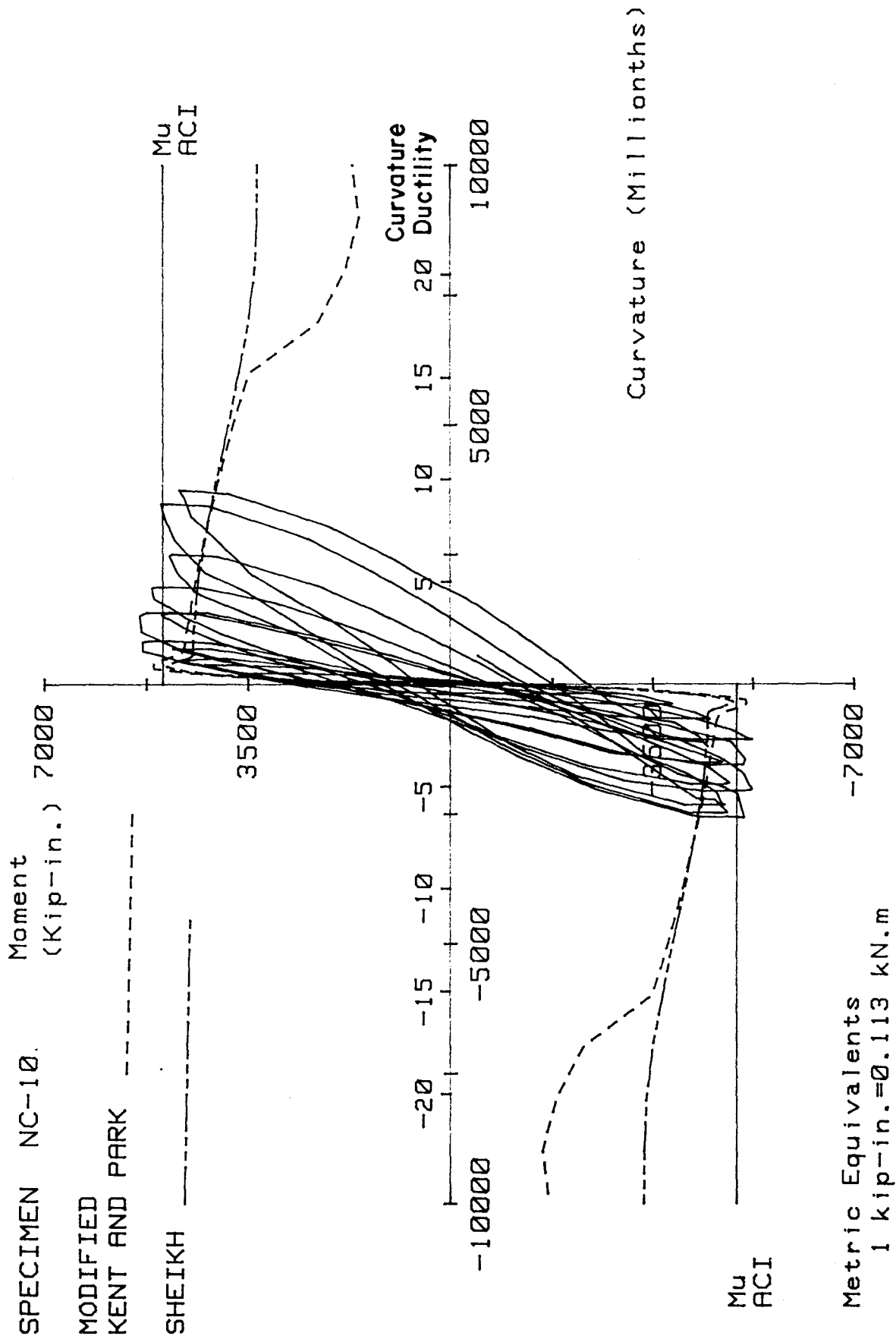


FIG. 6-17 MOMENT VERSUS CURVATURE FOR SPECIMEN NC-10

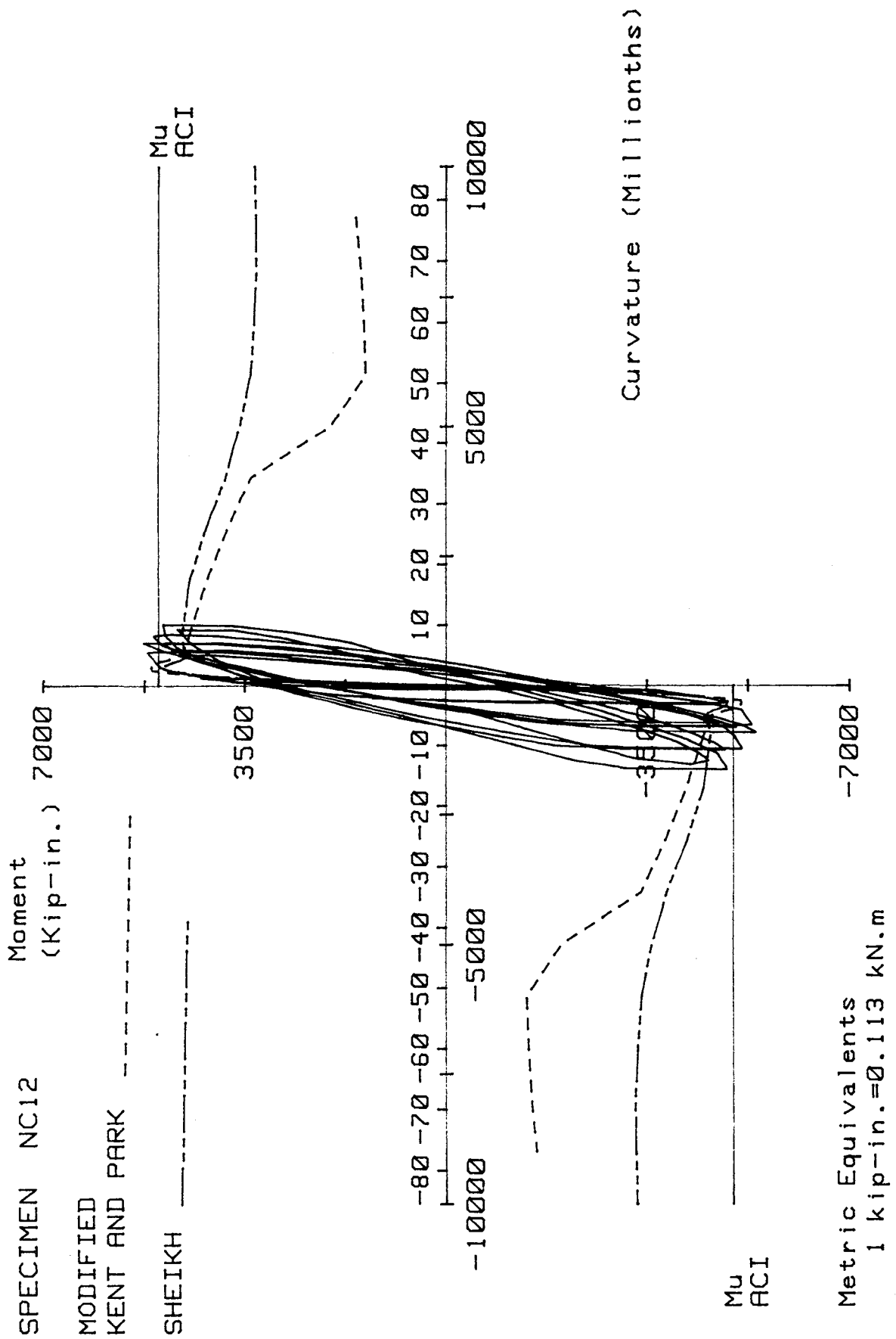


FIG. 6-18 MOMENT VERSUS CURVATURE FOR SPECIMEN NC-12

cover concrete. In this study the maximum moment for test specimens generally occurred during the first cycle at the displacement ductility ratio of two, during which time the first crushing of cover concrete was also observed. Even after first crushing, the longitudinal bars and the transverse reinforcement were completely covered by concrete. Only at displacement ductility ratios of four and higher had spalling of cover concrete extended to a stage where transverse reinforcement was visible. These experimental evidences suggest the shape of the effective concrete area is not the same from the onset of loading to point of failure, but rather, changes as the applied load increases.

7.0 REFERENCES

1. Ghosh, S.K., and Corley, W.G., "Behavior of Reinforced Concrete Framing System," Proceedings of the ASCE Conference on the 1985 Mexico City Earthquake, 1986.
2. Kreger, M.E., and Soren, M.A., "A Study of the Causes of Column Failures in the Imperial County Services Building During the 15 of October, 1979, Imperial Valley Earthquake," A Report to the National Science Foundation, University of Illinois, 1983.
3. Mitchell, D., Adams, J., Devall, R.H., Lo, R.E., and Weichert, D., "Lessons from the 1985 Mexico City Earthquake," Canadian Journal of Civil Engineering, 13, pp. 535-557.
4. Zeris, C.A., and Altman, R., "Implications of Damage to the Imperial County Services Building for Earthquake-Resistant Design," Proceedings of the Eighth World Conference on Earthquake Engineering, San Francisco, California, 1984, 4, pp. 823-830.
5. "Reconnaissance Report, Imperial County California Earthquake, October, 1979," Earthquake Engineering Research Institute, Berkeley, California, February 1980.
6. ACI Committee 318, Building Code Requirements for Reinforced Concrete (ACI 318-83), American Concrete Institute, Detroit, Michigan, 1983.
7. Uniform Building Code, International Conference of Building Officials, Whittier, California, 1985.
8. Selna, L., etal, "Strong and Tough Concrete Columns for Seismic Forces," Journal of the Structural Division, American Society of Civil Engineers, August 1980, pp. 1717-1734.

9. Paulay, T., "Developments in the Seismic Design of Reinforced Concrete Frames in New Zealand," Canadian Journal of Civil Engineering, Vol. 8, 1981, pp. 91-131.
10. Sheikh, S.A., and Uzumeri, S.M., "Strength Decay of RC Columns Under Shear Reversals," Journal of the Structural Division, American Society of Civil Engineers, May 1980, pp. 1079-1102.
11. Wight, J.K., and Sozen, M.A., "Strength Decay of RC Columns Under Shear Reversals," Journal of the Structural Division, American Society of Civil Engineers, May 1975, pp. 1053-1065.
12. Burdette, E.G., and Hilsdorf, H.K., "Behavior of Laterally Reinforced Concrete Columns," Journal of the Structural Division, ASCE, Vol. 97, No. ST 2, Proceedings Paper 7905, February 1971, pp. 587-602.
13. Chan, W.W.L., "The Ultimate Strength and Deformation of Plastic Hinges in Reinforced Concrete Frameworks," Magazine of Concrete Research, Vol. 7, No. 21, November 1955, pp. 121-132.
14. Hognestad, E., "A Study of Combined Bending and Axial Load in Reinforced Concrete Members," University of Illinois Engineering Experimental Station, Bulletin No. 399, 1951, p. 128.
15. King, J.W.H., "The Effect of Lateral Reinforcement in Concrete Columns," The Structural Engineer, Vol. 24, No. 7, July 1946.
16. King, J.W.H., et al "Discussion of Effect of Lateral Reinforcement in Reinforced Concrete Columns," The Structural Engineer, Vol. 25, No. 6, June 1947.
17. Roy, H.E.H., and Sozen, M.A., "Concrete Ductility, Flexural Mechanics of Reinforced Concrete," Proceedings of the International Symposium, Vol. 1, Miami, Florida, November 1964, Paper No. 7, 21 pp.

18. Soliman, M.T.M., and Yu, C.W., "The Flexural Stress-Strain Relationship of Concrete Confined by Rectangular Transverse Reinforcement," Magazine of Concrete Research, Vol. 19, No. 61, December 1967.
19. Stockl, S., "Research Concerning the Confining Effect of Stirrups on the Load-Carrying Behavior of Centrally Loaded Reinforced Concrete Columns," (in German), Report No. 51, Materials Testing Laboratory, Technical University of Munich, 1965.
20. Szulcynski, T., and Sozen, M.A., "Load-Deformation Characteristics of Concrete Prisms with Rectilinear Transverse Reinforcement," Structural Research Series No. 224, University of Illinois Civil Engineering Studies, September 1961, 55 pp.
21. Weigler, H., and Henzel, J., "Investigations Concerning the Load-Carrying Capacity of Concrete Columns Reinforced with Horizontal Welded Wire Fabric," (in German), German Committee for Reinforced Concrete, No. 174, 1965.
22. Yamashiro, R., and Siess, C.P., "Moment-Rotation Characteristics of Reinforced Concrete Members Subjected to Bending, Shear, and Axial Load," Civil Engineering Studies, Structural Research Series No. 260, University of Illinois, December 1962.
23. Some, N.F., "Compression Tests on Hoop-Reinforced Concrete," Journal of the Structural Division, American Society of Civil Engineers, Vol. 96, No. ST7, July 1970, pp. 1495-1509.
24. Bertero, V.V., and Vallenias, J., "Confined Concrete: Research and Development Needs," Workshop on Earthquake-Resistant Reinforced Concrete Building Construction, University of California, Berkeley, July 1977, pp. 594-610.

25. Kaar, P.H., etal, "Limiting Strains of Concrete Confined by Rectangular Hoops," PCA Research and Development Bulletin RD53, Portland Cement Association, Skokie, Illinois, 1978, 12 pp.
26. Gill, W., "Ductility of Rectangular Reinforced Concrete Columns with Axial Load," Research Report 70-1, Department of Civil Engineering, University of Canterbury, Christchurch, New Zealand, February 1979, 136 pp.
27. Potangaroa, R.T., "Ductility of Spirally Reinforced Concrete Columns Under Seismic Loading," Research Report, Canterbury, Christchurch, New Zealand, February 1979, 116 pp.
28. Moehle, J.P., and Cavanagh, T., "Confinement Effectiveness of Crossties in Reinforced Concrete," a report based on the experimental work undertaken in partial fulfillment of requirements for the Master of Science degree of the second author, 1984.
29. Sheikh, S.A., "A Comparative Study of Confinement Models," Journal of the American Concrete Institute, Vol. 79, July-August 1982, pp. 296-306.
30. Hanson, N.W., and Rabbat, B.G., "Tests of Ductile Behavior of Lightweight Concrete Columns for Seismic Design," Proceedings of the Eighth World Conference on Earthquake Engineering, Vol. 6, San Francisco, California, July 21-28, 1984, pp. 545-552.
31. Moehle, J.P., and Cavanagh, T., "Confinement Effectiveness of Crossties in RC," ASCE, Vol. 111, No. 10, October 1985.
32. Tanaka, H., Park, R., and McName, B., "Anchorage of Transverse Reinforcement in Rectangular Reinforced Concrete Columns in Seismic Design," Research Report, Department of Civil Engineering, University of Canterbury, Christchurch, New Zealand, October 1985.

33. Ozcebe, G., and Saatcioglu, M., "Confinement of Concrete Columns for Seismic Loading," ACI Structural Journal, Vol. 84, No. 4, July-August 1987.
34. Yeh, C.C., and Sheikh, S., "Flexural Behavior of Confined Columns Subjected to High Axial Loads," Proceeding of Fifth Canadian Conference on Earthquake Engineering, Ottawa, Canada, July 1987.
35. Standard Specifications for Deformed and Plain Billet-Steel Bars for Concrete Reinforcement, A615-76a, American Society for Testing and Materials, Philadelphia, Pennsylvania.
36. Corley, W.G., "Rotational Capacity of Reinforced Concrete Beams," Journal of the Structural Division, ASCE, Vol. 92, No. ST5, Proc. Paper 4939, October 1966, pp. 121-146.
37. Park, R., Priestly, M.J.N., and Gill, W.D., "Ductility of Square - Confined Columns," Proceedings, ASCE, Vol. 108, ST4, April 1982, pp. 929-950.
38. Sheikh, S.A., and Uzumeri, S.M., "Analytical Model for Concrete Confinement in Tied Columns," Proceedings, ASCE, Vol. 108, ST 12, December 1982, pp. 2703-2722.

APPENDIX A

Detailed behavior of each test specimen is given in this Appendix. The following items are discussed for each specimen except Specimen NC-1.

1. Transverse Reinforcement Detail - The transverse reinforcement used within 22 in. above the column is described.
2. Loading History - The applied loading history for each specimen is described in this section. The description of loading history uses the following terminology:
 - A. Cycle - One cycle consists of forward and reverse loading. Figure A-1 shows orientation of each specimen with respect to the direction of horizontal loading. To start a cycle of horizontal loading a specimen was loaded in the forward direction (east to west). Following unloading the specimen was then loaded in the reverse direction (west to east). Finally, the cycle was completed by unloading the horizontal load.
 - B. Displacement and Curvature Ductility - The displacement ductility ratio, μ , is defined as the ratio of maximum horizontal displacement at the peak of forward or reverse loading of each cycle to the first yield displacement. The first yield displacement and curvature ductility were established using the procedure outlined in Section 4.8.2. The curvature ductility ratio is defined in a similar manner. Table A.1 shows the cycles applied to each specimen and the corresponding nominal displacement ductility ratios.
3. Test Observations - The description of observed performance of each specimen includes the first observed cracking and crushing of cover concrete, the extent of cover spalling at various loading stages, plastic hinge length, initiation of longitudinal bar buckling and other unique observations for each test specimen.
4. Load-Deflection and Moment-Curvature Characteristics - This section contains the horizontal load-deflection characteristics of the

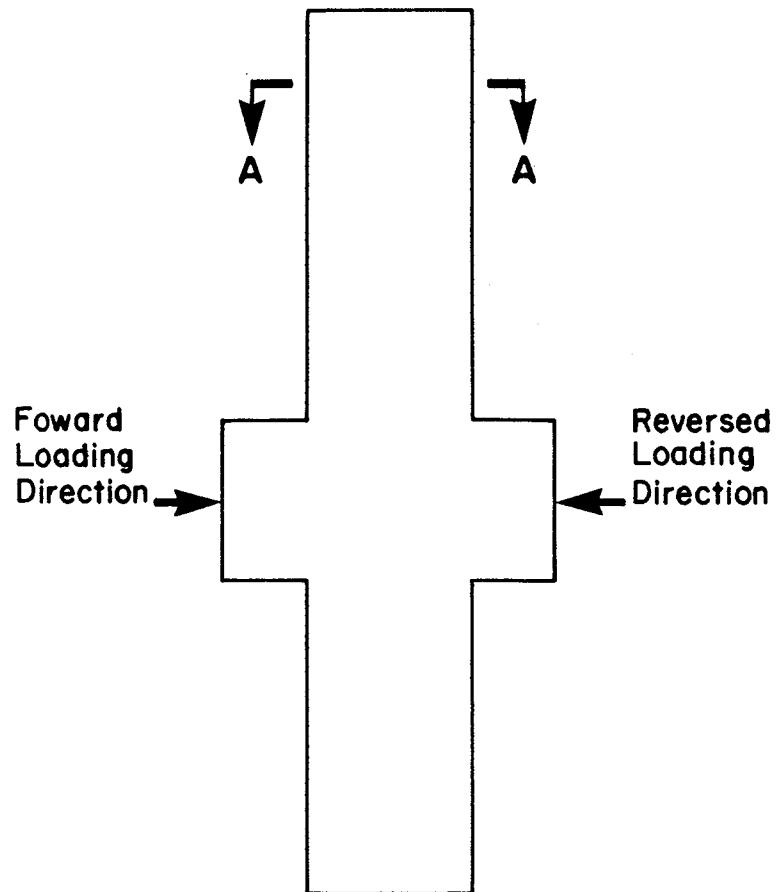
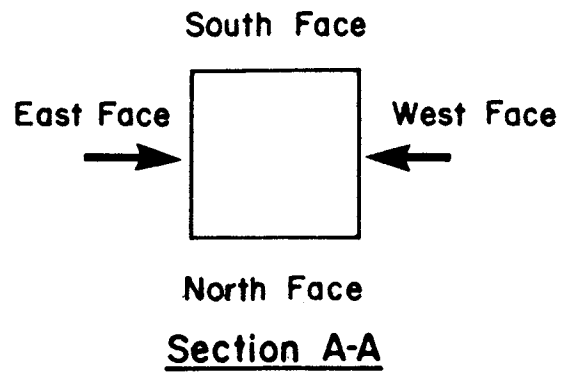


FIG. A-1 SPECIMEN ORIENTATION

Table A.1 Horizontal Loading History

Cycle Number	Displacement Ductility											
	Specimen NC-1	Specimen NC-2	Specimen NC-3	Specimen NC-4	Specimen NC-5	Specimen NC-6	Specimen NC-7	Specimen NC-8	Specimen NC-9	Specimen NC-10	Specimen NC-11	Specimen NC-12
1	-	-	-	-	-	-	-	-	-	-	-	-
2	-	-	-	-	-	2	-	-	-	-	-	-
3	1	1	1	1	1	2	1	1	1	1	1	1
4	1	1	1	2	1.4	3	2	1.5	1.5	1.5	1.5	1
5	2	1.5	1.5	2	2	3	2	2	1.5	2	2	2
6	2	1.5	2	3	2	4	3	2	2	2	2	2
7	3	2	2	3	3	4	3	2	2	3	3	3
8	3	2	3	4	3	5	4	3	3	3	3	3
9	4	3	3	4	4	5	4	4	3	4	4	4
10	4	3	4	5	4	-	5	4	4	4	4	4
11	5	4	4	5	5	-	5	4	4	5	5	5
12	5	4	5	-	5	-	-	5	5	5	5	5
13	6	5	5	-	6	-	-	6	5	-	6	-
14	6	5	6	-	6	-	-	6	5	-	6	-
15	-	6	-	-	7	-	-	7	-	-	7	-
16	-	6	-	-	7	-	-	-	-	-	7	-
17	-	7	-	-	-	-	-	-	-	-	8	-
18	-	7	-	-	-	-	-	-	-	-	8	-
19	-	8	-	-	-	-	-	-	-	-	9	-
20	-	8	-	-	-	-	-	-	-	-	9	-

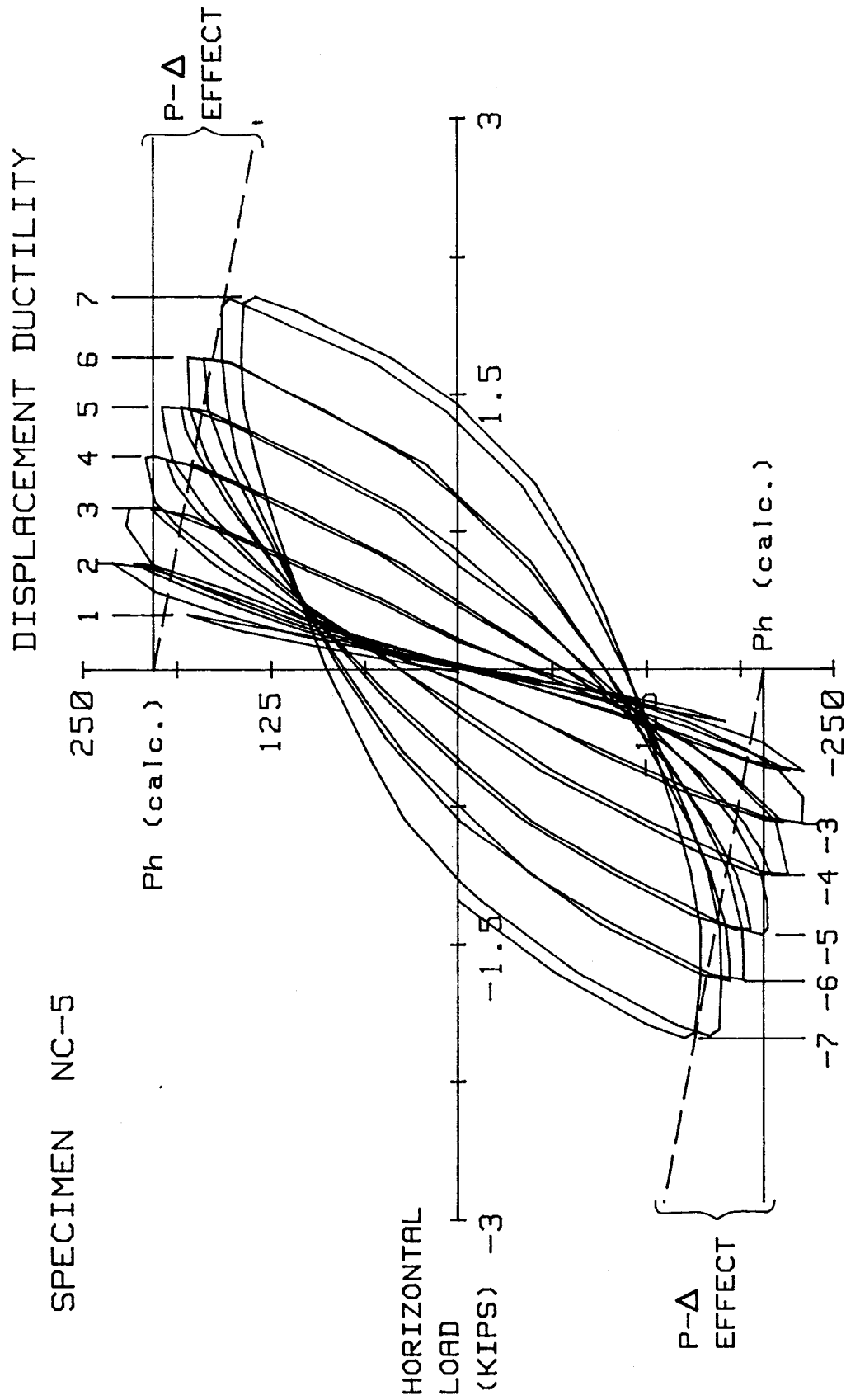
specimen. Figure A-2 shows a typical horizontal load-deflection plot. In this figure the solid line parallel to the horizontal axis represents the theoretical ultimate lateral load, calculated using ACI-318-83 Code provisions, neglecting the P- Δ effect. However, if the P- Δ effect is included, the calculated maximum lateral load decreases as lateral displacement increases. The dashed line in Fig. A-2 represents the envelope of the points corresponding to maximum lateral loads at increasing lateral displacement levels. For each displacement level, the maximum lateral load was calculated using ACI-318-83 Code provision. Also described in this section is the moment-curvature characteristic of each test specimen in terms of the curvature distribution along the upper column and measured moment-curvature response of specimens at the interface of the upper column and beam stub.

Figure A-3 shows an example of a curvature distribution plot. Section 4.8.2 describes the general procedure used to obtain curvature distribution.

Figure A-4 shows an example of the moment-curvature plot at the interface of the upper column and stub. This plot includes the total moment at the upper column-stub interface. The moment, M , is determined using the provision of the 1983 ACI Building Code. The capacity reduction factor, ϕ , was taken as 1.0.

The curvature ductility ratios reported in all moment-curvature plots are based on curvatures measured within the first 4 in. above the stub.

5. Transverse Reinforcement Strain - In this section data obtained from strain gages attached to transverse reinforcement within the critical region of the upper column (within 22 in. above the stub) is discussed. Plots of data obtained from strain gages up to the time when they ceased to function are presented.



Metric Equivalents
 1 in. = 25.4 mm
 1 kip = 4.45 kN

HORIZONTAL DISPLACEMENT (IN.)

FIG. A-2 HORIZONTAL LOAD VERSUS DISPLACEMENT, SPECIMEN NC-5

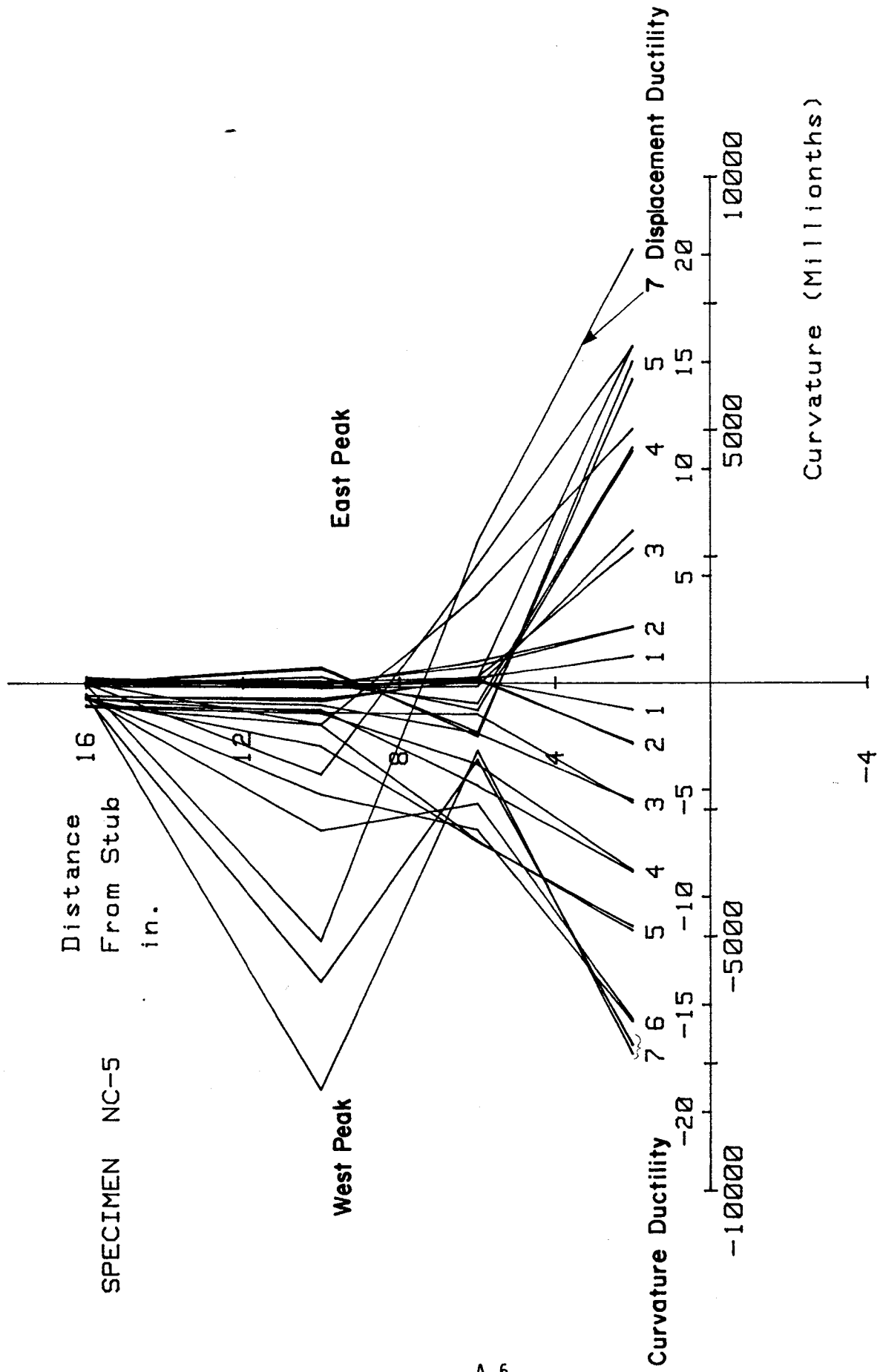


FIG. A-3 CURVATURE DISTRIBUTION, SPECIMEN NC-5

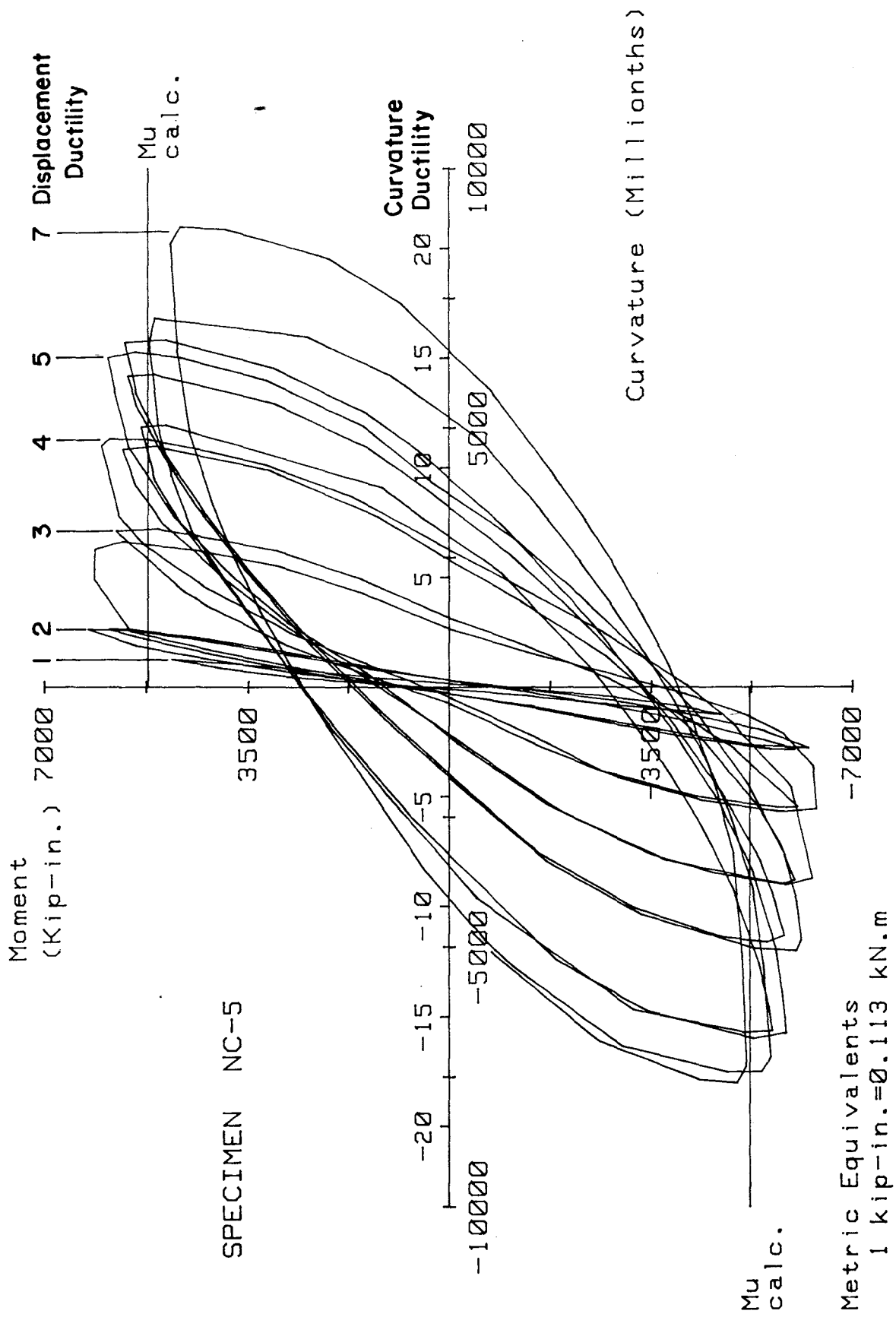


FIG. A-4 MOMENT VERSUS CURVATURE, SPECIMEN NC-5

SPECIMEN NC-1

Transverse reinforcement used in Specimen NC-1 was detailed in accordance with ACI-318-83 Building Code. Figure 4-2A shows the transverse reinforcement detail. End anchorage consisted of a 135° bend with 10-bar diameter extension for both peripheral hoops and crossties. The area of the transverse reinforcement provided was 94% of the area required by ACI-318-83 Code.

Testing of Specimen NC-1 began with the application of 570 kips of axial load, which corresponds to 30% of the column's axial load capacity. While maintaining the axial load constant, the specimen was subjected to a number of cyclic horizontal loadings. Figure A-5 shows the history of applied horizontal loading. The first yield displacement and curvature ductility were established during cycle #2 as 0.28 in. and 0.00034 in.⁻¹, respectively. Subsequently, horizontal loading consisted of displacement-controlled testing to a maximum displacement ductility ratio of six.

As discussed in Section 4.1.1, the intent was to force the formation of the hinge in the upper column by adjusting the length of the upper and lower column. However, for Specimen NC-1 the hinge formed in the lower column where no instrumentation was implanted. In subsequent specimens additional reinforcement was provided in the bottom column, assuring the formation of the hinge in the upper column.

Due to formation of the hinge in the bottom column of Specimen NC-1, only partial results were obtained. Figure A-6 shows the bottom column at the end of cycle #8 ($\mu=3$). After loading the specimen in the forward and reverse directions for two cycles at a displacement ductility of six, an attempt was made to increase the horizontal displacement to the next level ($\mu=7$). However, the corner and middle longitudinal bars of the lower column in compression buckled prior to completion of the first cycle at this displacement level. Figure A-7 shows the specimen at test conclusion. Figure A-8 shows the horizontal load vs. horizontal displacement of Specimen NC-1.

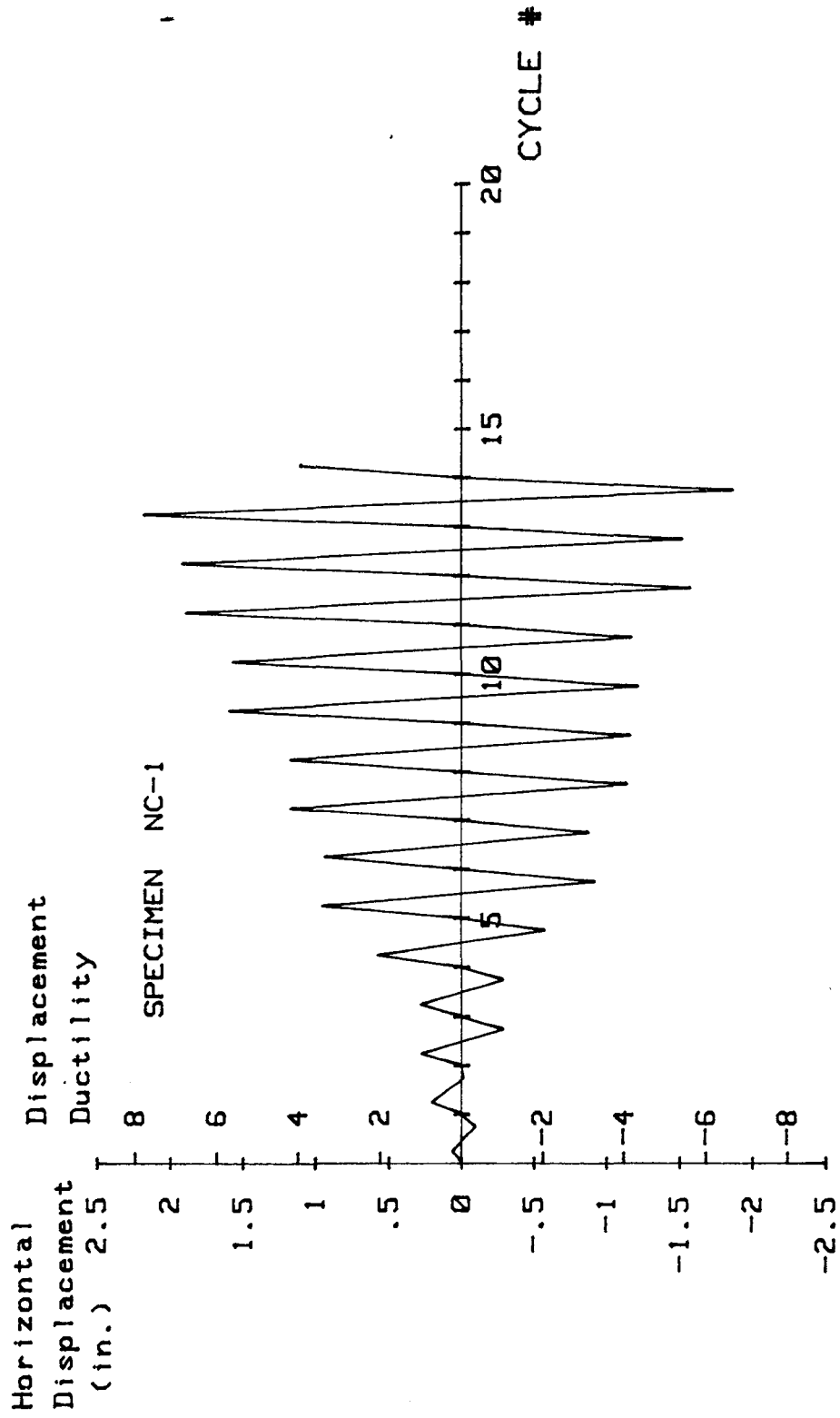


FIG. A-5 LOADING SCHEDULE, SPECIMEN NC-1



FIG. A-6 SPECIMEN NC-1 AFTER CYCLE #8

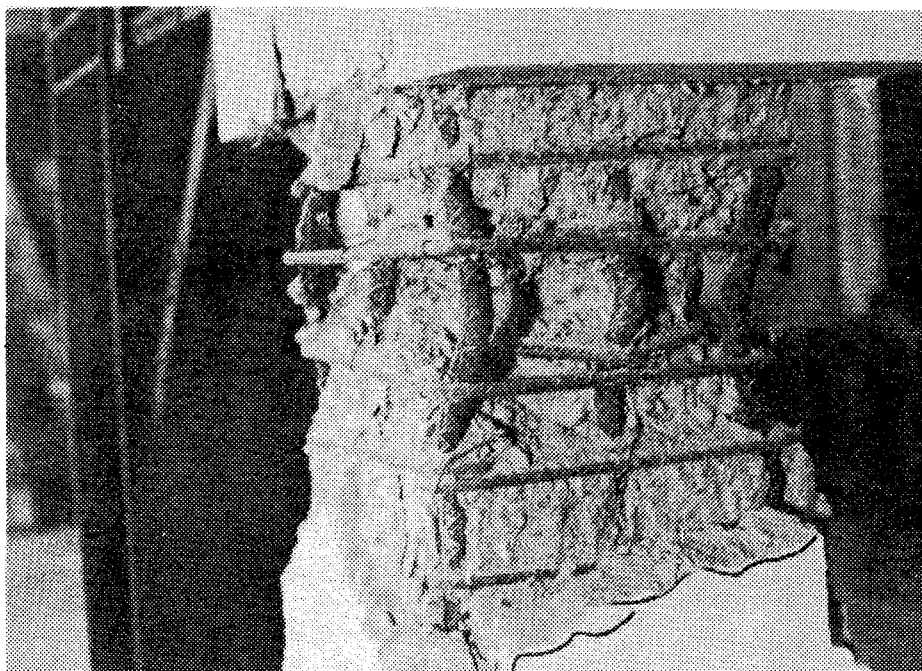
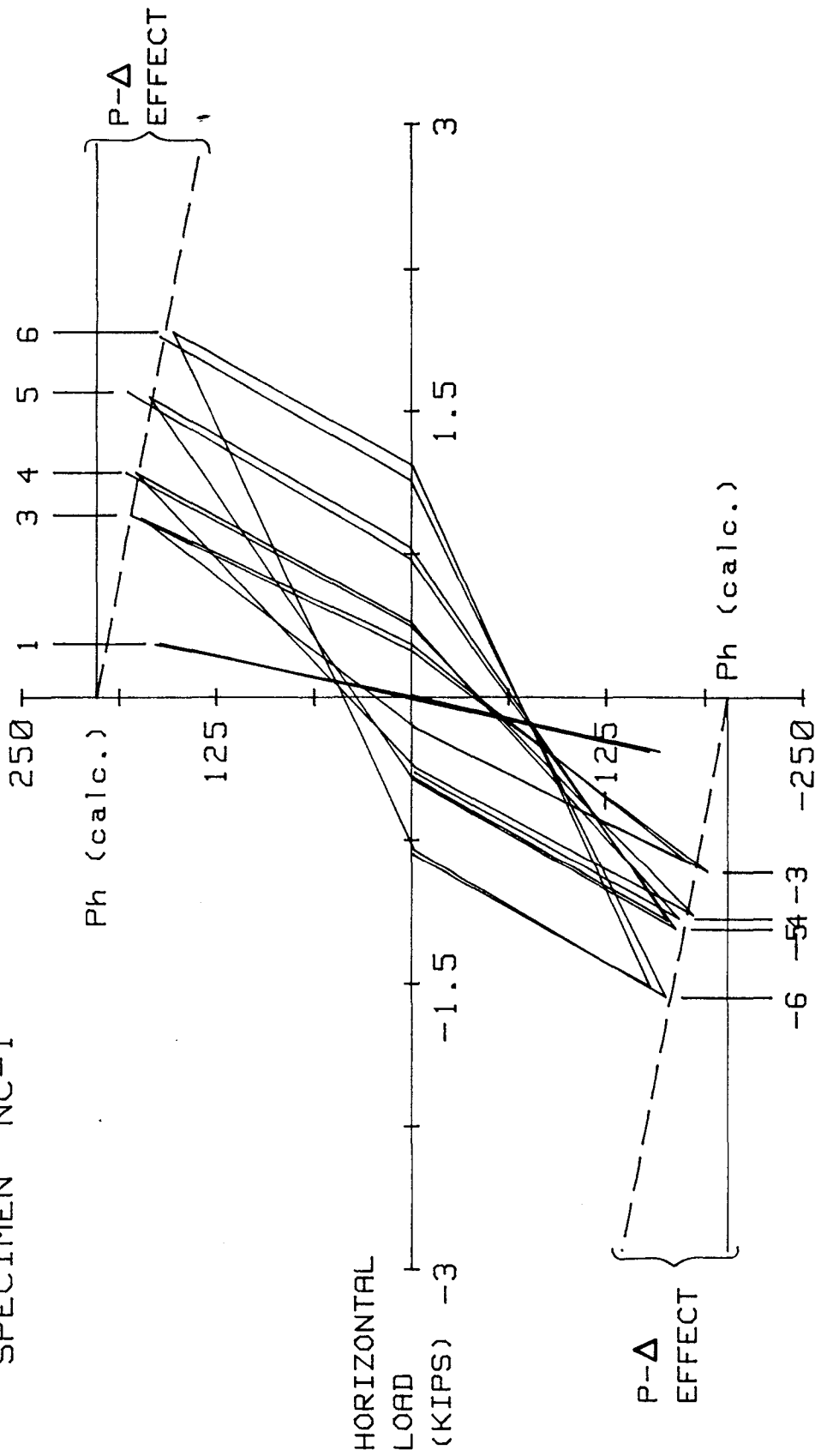


FIG. A-7 SPECIMEN NC-1 AT THE TEST CONCLUSION

SPECIMEN NC-1

DISPLACEMENT DUCTILITY



Metric Equivalents
1 in.=25.4 mm
1 kip=4.45 KN

HORIZONTAL DISPLACEMENT (IN.)

FIG. A-8 HORIZONTAL LOAD VERSUS DISPLACEMENT, SPECIMEN NC-1

Specimen NC-2

Transverse Reinforcement Detail

Figure 4-2b shows the transverse reinforcement in Specimen NC-2. End anchorage of the peripheral hoops consisted of a 135° bend with a 6-bar diameter extension. The interior hoop was anchored by a 90° bend with a 6-bar diameter extension. The area of transverse reinforcement A_{sh} was 0.68 in.², which corresponds to a volumetric reinforcement ratio, ρ , of 2.19%. The area of the transverse reinforcement provided was 93% of the area required by ACI-318-83 Code.

Loading History

Testing of the specimen began with application of 380 kips of axial load, which corresponds to 20% of the column's axial load capacity. The axial load was maintained constant while the specimen was subjected to a total of 20 complete cycles of horizontal loading. Using the procedure outlined in Section 4.8.2, the first yield displacement was established to be 0.33 in. The corresponding yield curvature was 394×10^{-6} radians/in.⁻¹.

Subsequently, horizontal cyclic loading consisted of displacement-controlled testing to a maximum displacement ductility ratio of eight. Figure A-9 show the history of applied horizontal load versus horizontal displacement.

Test Observations

Hairline cracks were first observed at cycle #4 ($\mu=1$). These cracks were observed at the junction of the stub and column and at approximately 5 in. and 13 in. above the stub. At cycle #9 ($\mu=3$), some crushing of the cover concrete in the vicinity of the stub was observed as shown in Fig. A-10. Figures A-11 and A-12 show the test portion of the specimen during cycle #13 ($\mu=5$) and 17 ($\mu=7$), respectively.

The loss of cover concrete was gradual. At cycle #17 ($\mu=7$) the cover concrete was partially spalled on both the east and west faces. However, the transverse reinforcement was still not visible. After completion of two cycles at a displacement ductility ratio of eight, an attempt was made to apply a cycle at the next higher displacement level ($\mu=9$). During that

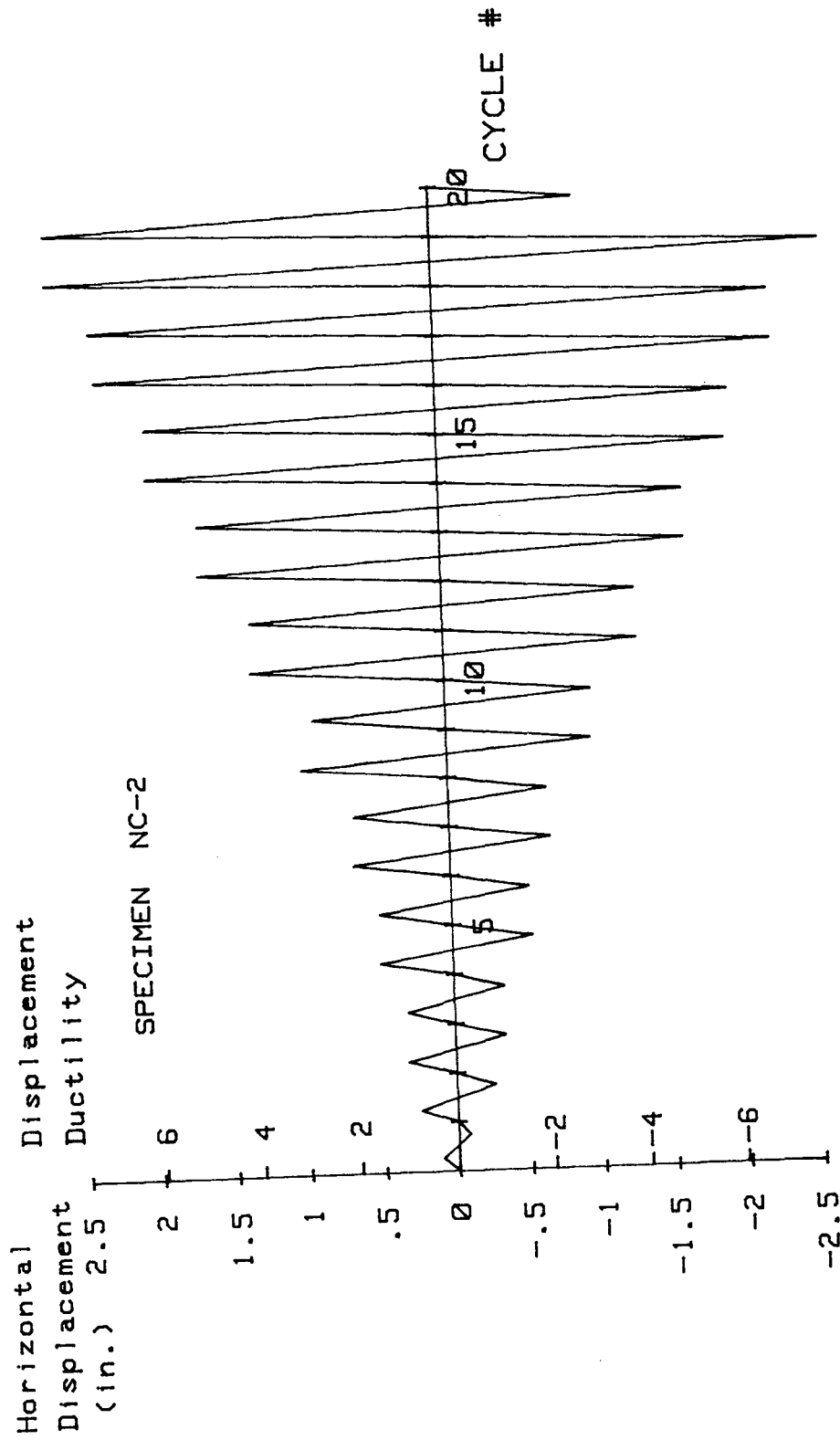


FIG. A-9 LOADING SCHEDULE, SPECIMEN NC-2

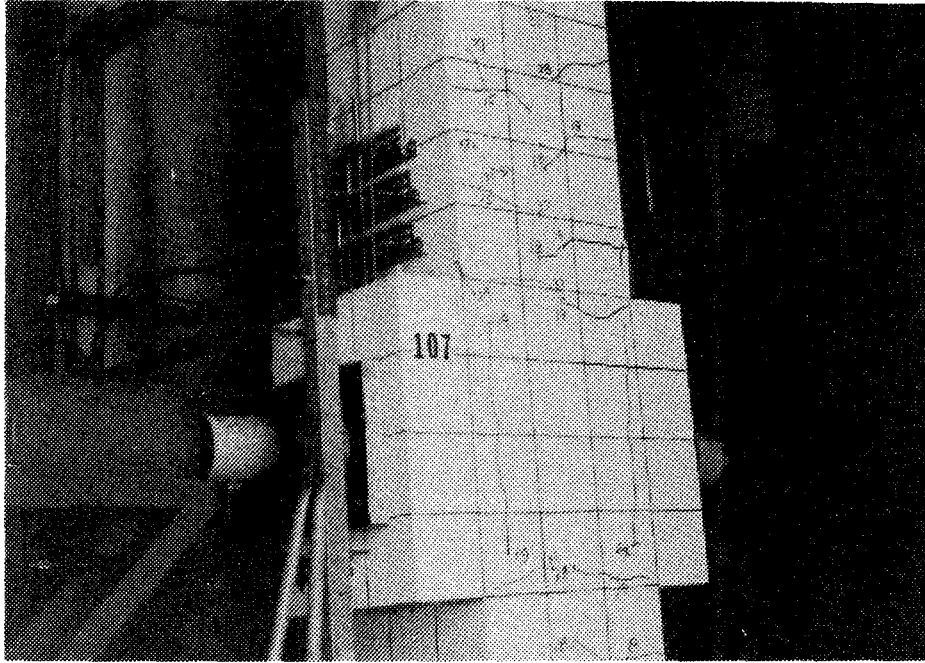


FIG. A-10 TEST SPECIMEN NC-2 AFTER CYCLE #9

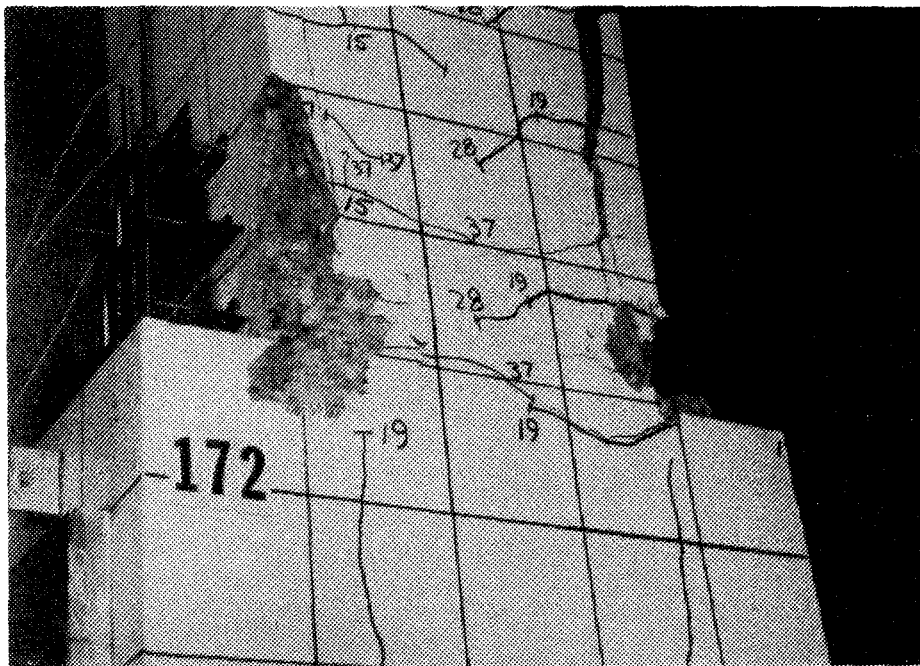


FIG. A-11 TEST SPECIMEN NC-2 AFTER CYCLE #13

attempt the transverse reinforcement located at distances of 2 and 6 in. from the stub lost end anchorage and the longitudinal bars buckled. No apparent damage was inflicted to the interior hoop which remained intact. Figure A-13 shows the specimen after the test. The plastic hinge region extended from approximately 2 to 12 in. above the stub.

The sketch in Fig. A-14 shows the upper column's first four layers of peripheral hoops and the corner bars. Also shown in Fig. A-14 are the anchorage locations and their final shape at conclusion of testing. The location of the anchorage was alternated at each level. Buckling of longitudinal bars was influenced by the anchorage location as is evident from Fig. A-14. As the anchorage for peripheral hoops was lost the laterally unbraced length of the longitudinal bar was increased, thereby expediting buckling. The pattern of locating the anchorage for the peripheral hoops also influenced buckling of the longitudinal bar. For instance, as anchorage locations numbered 2 and 3 were lost, the longitudinal bar located at the northeast corner lost complete lateral support at point 1 and partial support at point 2 due to the loss of anchorage numbered 3.

Load-Deflection and Moment-Curvature Characteristics

Horizontal load versus the horizontal displacement for Specimen NC-2 is shown in Fig. A-15. At all displacement ductilities the applied horizontal load was greater than the calculated horizontal load based on the capacity of the upper column cross-section using the procedure outlined in Section 4.8.2. In addition to good strength behavior, the specimen showed good energy absorption capabilities as shown in Fig. A-15. Figure A-16 shows the moment-curvature characteristics of the specimen at the column-stub level. The ultimate flexural capacity of the column using the procedure outlined in Section 4.8.2 was 4814 in-kips. The maximum applied moment was 5773 in-kips. The moment-carrying capacity of the column section just above the stub remained greater than the theoretical value at all displacement levels. Small degradations in flexural capacity were observed between the first and second cycle at each ductility level. The ratio of the moment at the peak of the second cycle to the peak moment at the first cycle ranged from .9 to 1.0 at all displacement levels except the last loading cycle at which time the ratio was 0.7.

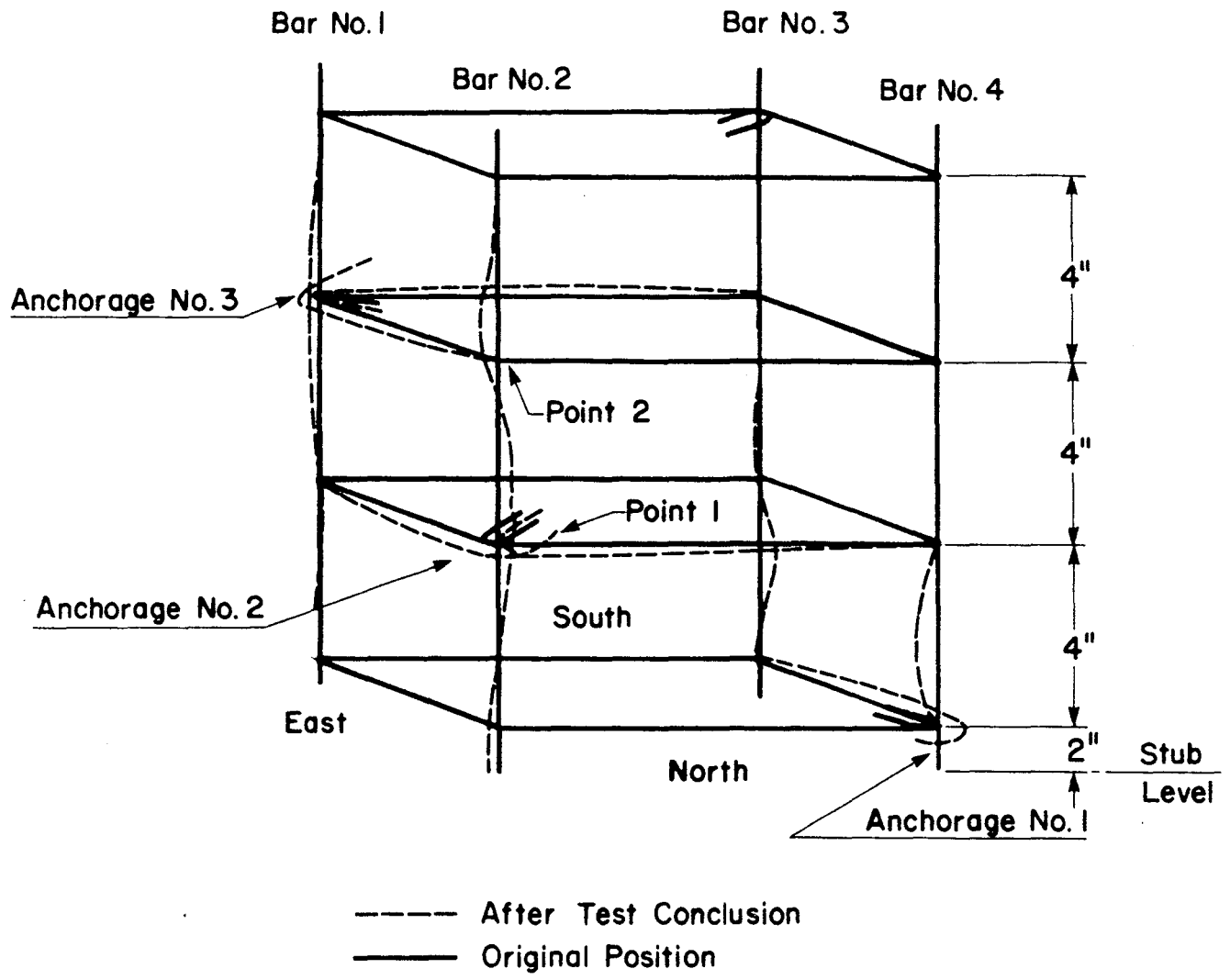


FIG. A-14 SKETCH OF THE CORNER LONGITUDINAL BARS, BEFORE AND AFTER TESTING, SPECIMEN NC-2

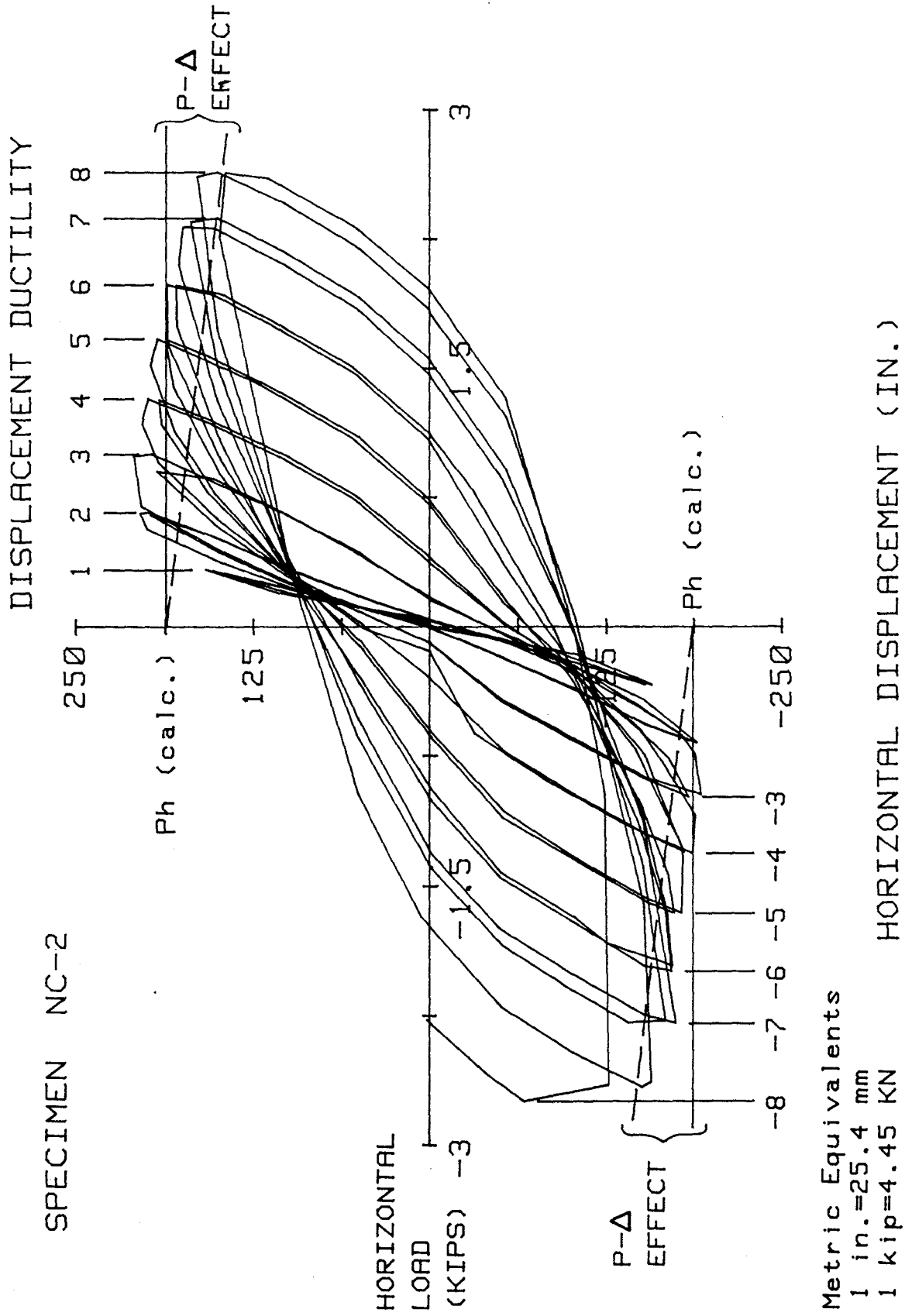
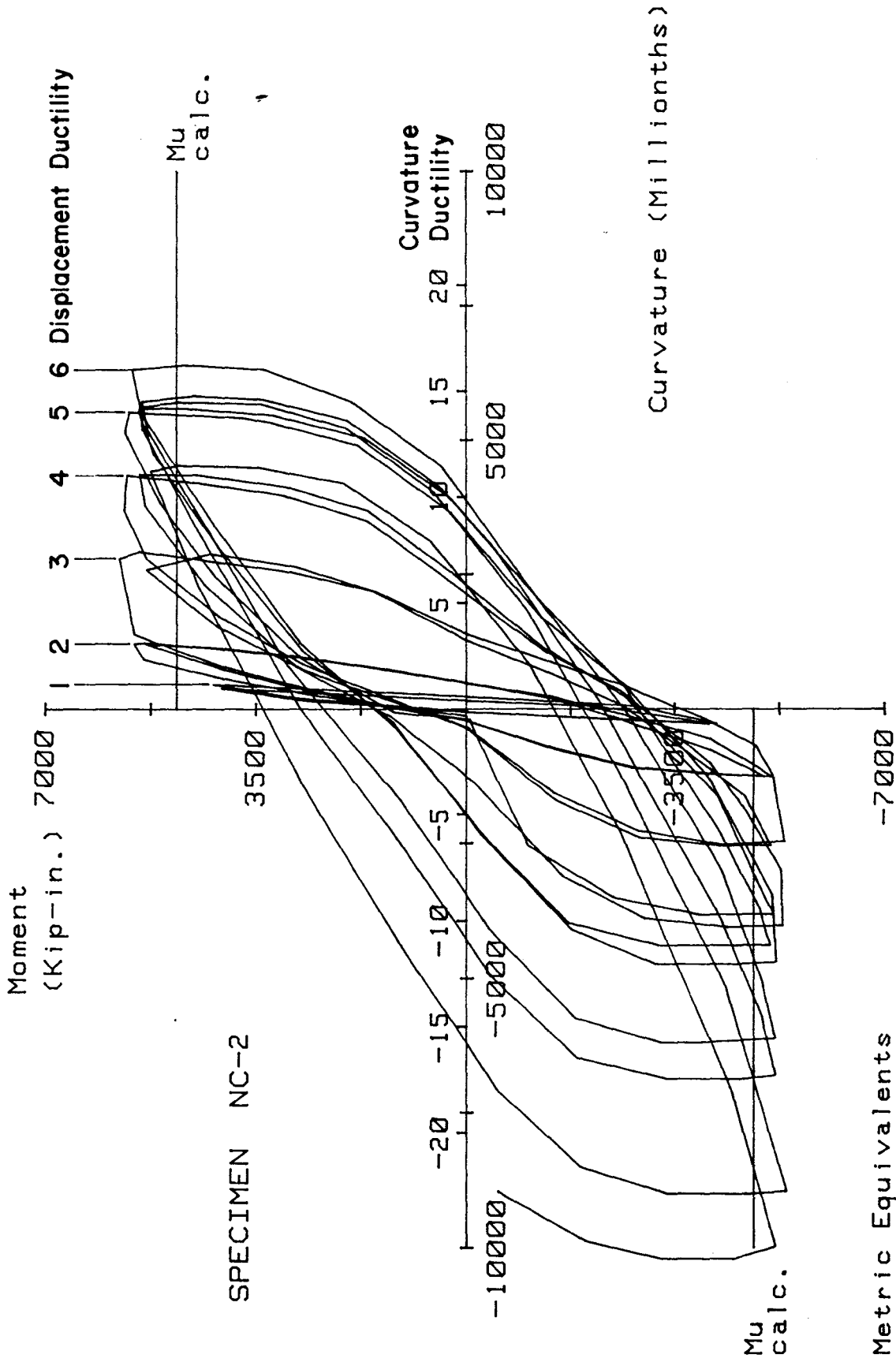


FIG. A-15 HORIZONTAL LOAD VERSUS DISPLACEMENT, SPECIMEN NC-2



Metric Equivalents
 1 kip-in. = 0.113 kN.m

FIG. A-16 MOMENT VERSUS CURVATURE FOR SPECIMEN NC-2

Figure A-17 shows the curvature distribution for the upper column. As shown in the figure, up to a displacement ductility ratio of six, the location of the largest curvature remained at a distance of 2 in. above the stub. However, at the next displacement level ($\mu=7$), at the peak of the forward loading cycles, the location of the highest curvature shifted to a distance 6 in. above the stub while at the peak of the reverse loading cycle it remained at a distance just 2 in. above the stub. The distribution of the curvatures at displacement ductility of seven could, in part, be attributed to bending characteristics of the longitudinal bars. Figure A-14 shows the final buckled shape of the corner bars at the conclusion of testing ($\mu=8$). According to column theories, the compression members with initial out-of-straightness displace laterally prior to reaching their buckling load. Considering the longitudinal bars as such compression members and referring to their final buckled shape (see Fig. A-14), it could be concluded that at a displacement ductility ratio of seven bending of bars #1 and #2 would be larger in the region extending from 6 to 10 in. above the stub while for bars #3 and #4 this region would be located at a distance between 2 and 6 in. above the stub. Thus, as a result of the bending pattern of bars #1 through #4 shown in Fig. 4, it would be expected to have the higher curvature at a distance 6 in. and 2 in. above the stub at the peak of the forward and reverse loading cycles (at displacement ductility of seven), respectively.

Transverse Reinforcement Strain

Figures A-18 through A-41 show strain data obtained from strain gages attached to transverse reinforcements. Figure 4-11 shows the location of the strain gages. Only one strain gage was attached at each location, therefore, it was impossible to separate the effect of possible bending that could take place in transverse reinforcements. Through cycle #10 ($\mu=3$) the measured strain on all transverse reinforcement remained less than half the specified yield strain. Some of the strain gages were lost beyond cycle #10. In general, strain on the peripheral and interior hoops located 2 in. above the stub was smaller than strain at corresponding locations on the next two levels during the early load stages. Strain on the interior hoops was generally smaller than strain on the peripheral hoops.

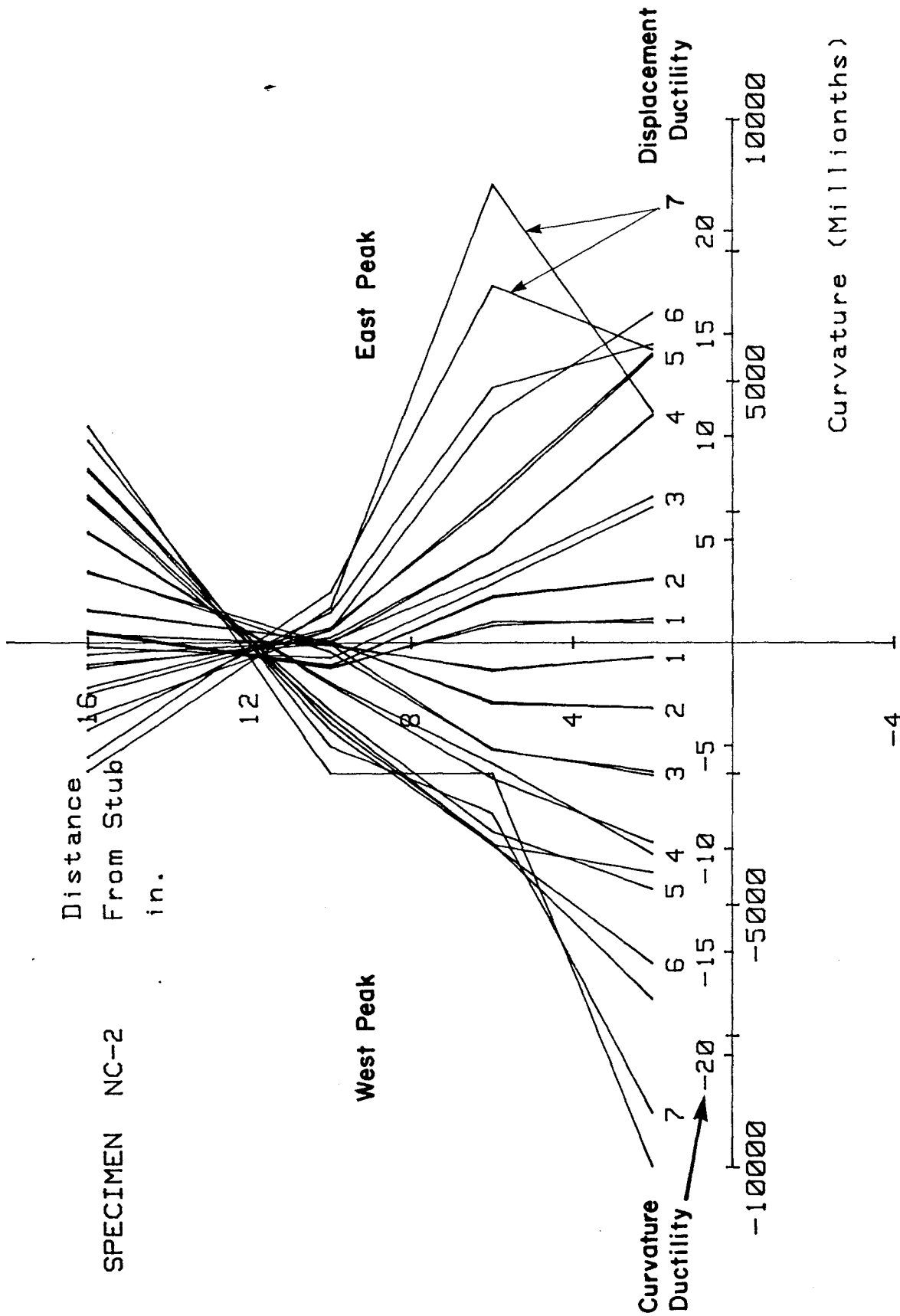


FIG. A-17 CURVATURE DISTRIBUTION ALONG UPPER COLUMN, SPECIMEN NC-2

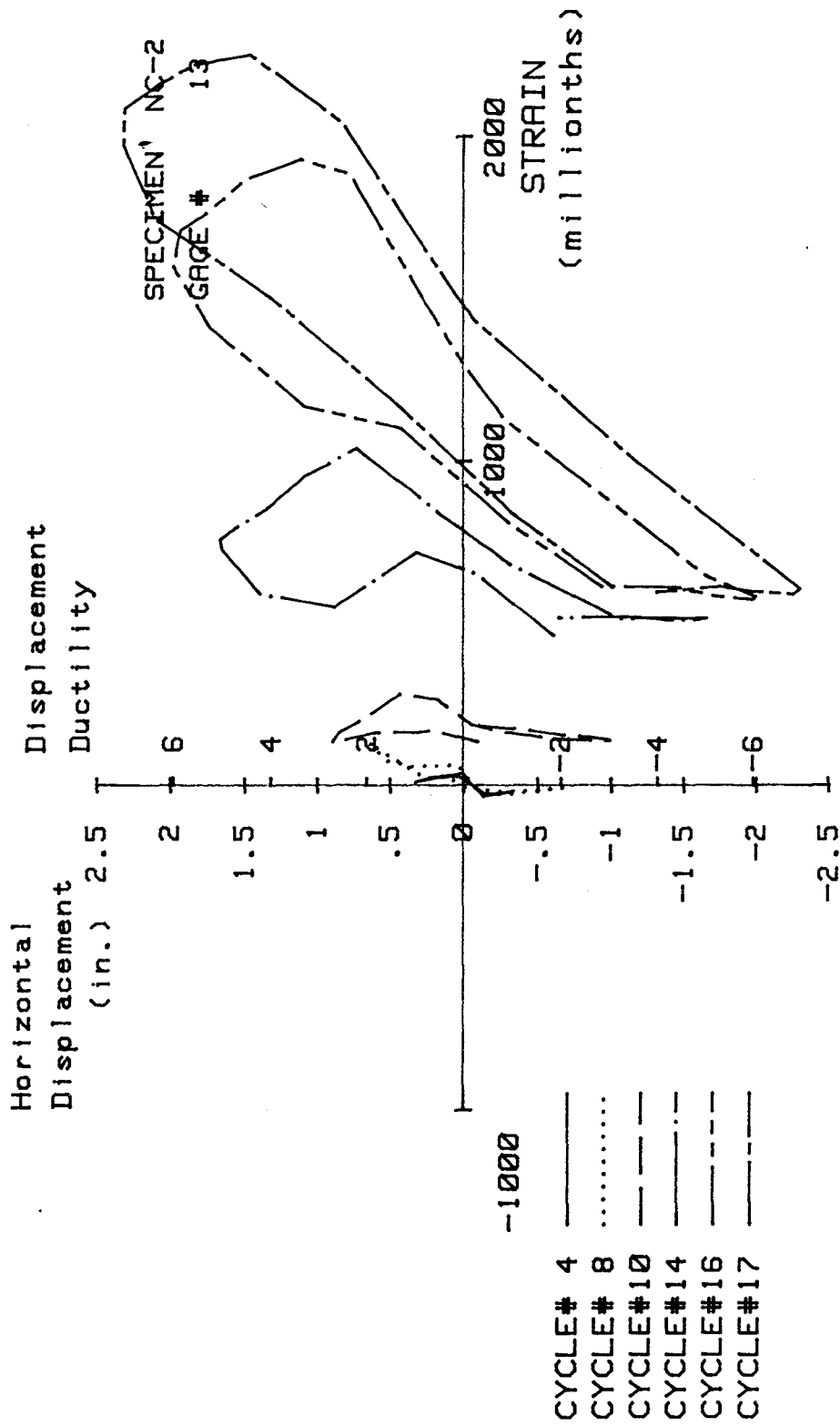


FIG. A-18 MEASURED STRAIN, GAGE #13, SPECIMEN NC-2

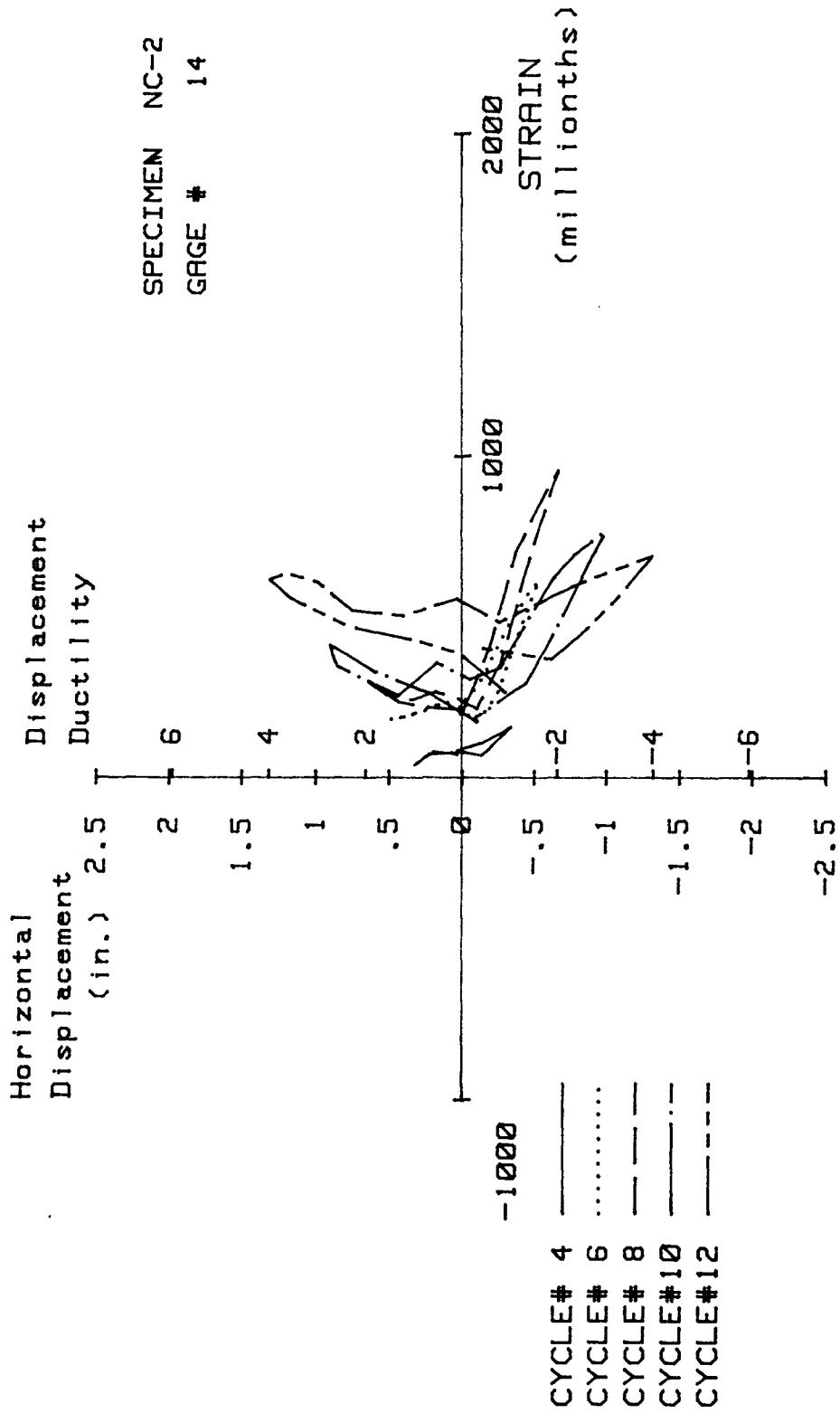


FIG. A-19 MEASURED STRAIN, GAGE #14, SPECIMEN NC-2

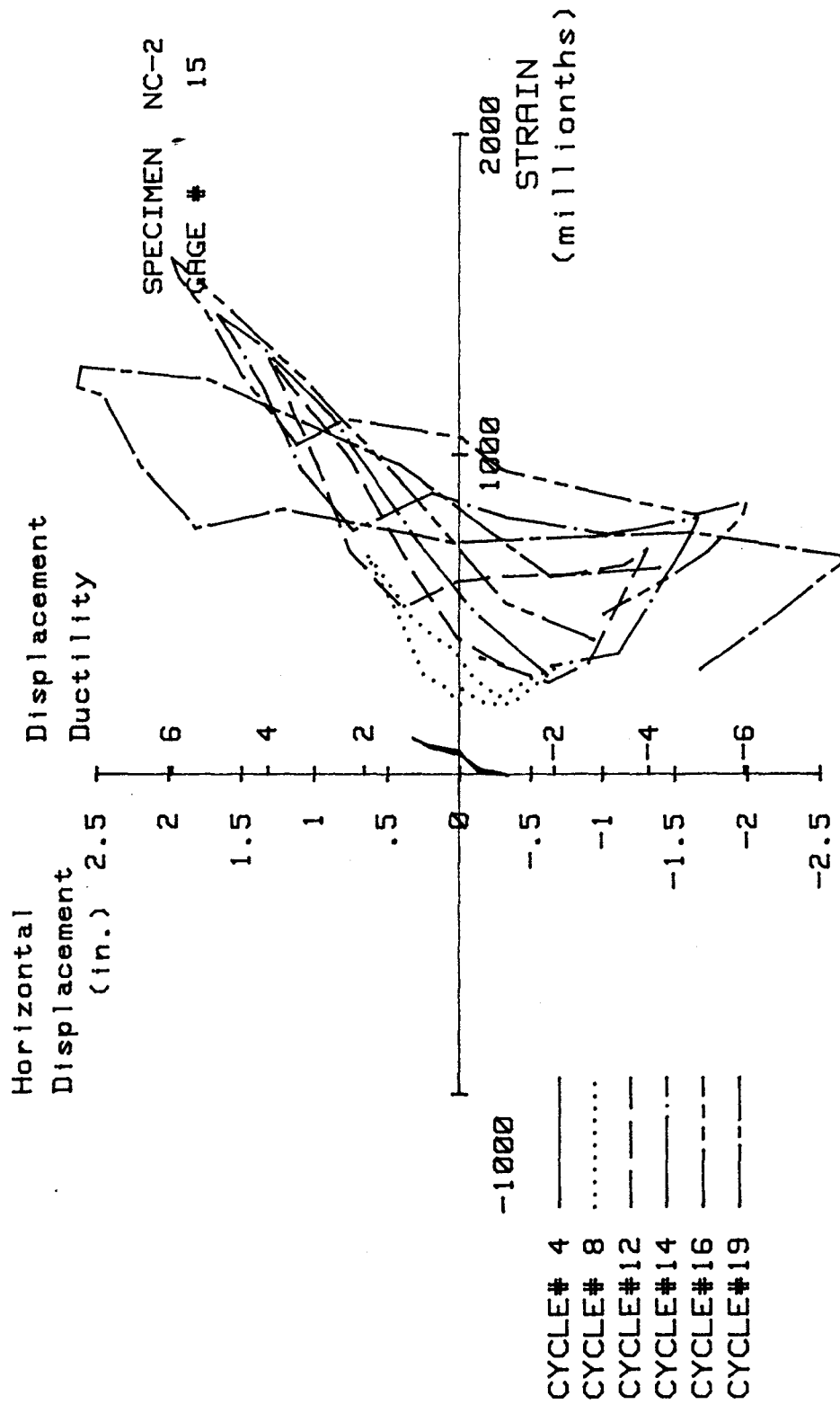


FIG. A-20 MEASURED STRAIN, GAGE #15, SPECIMEN NC-2

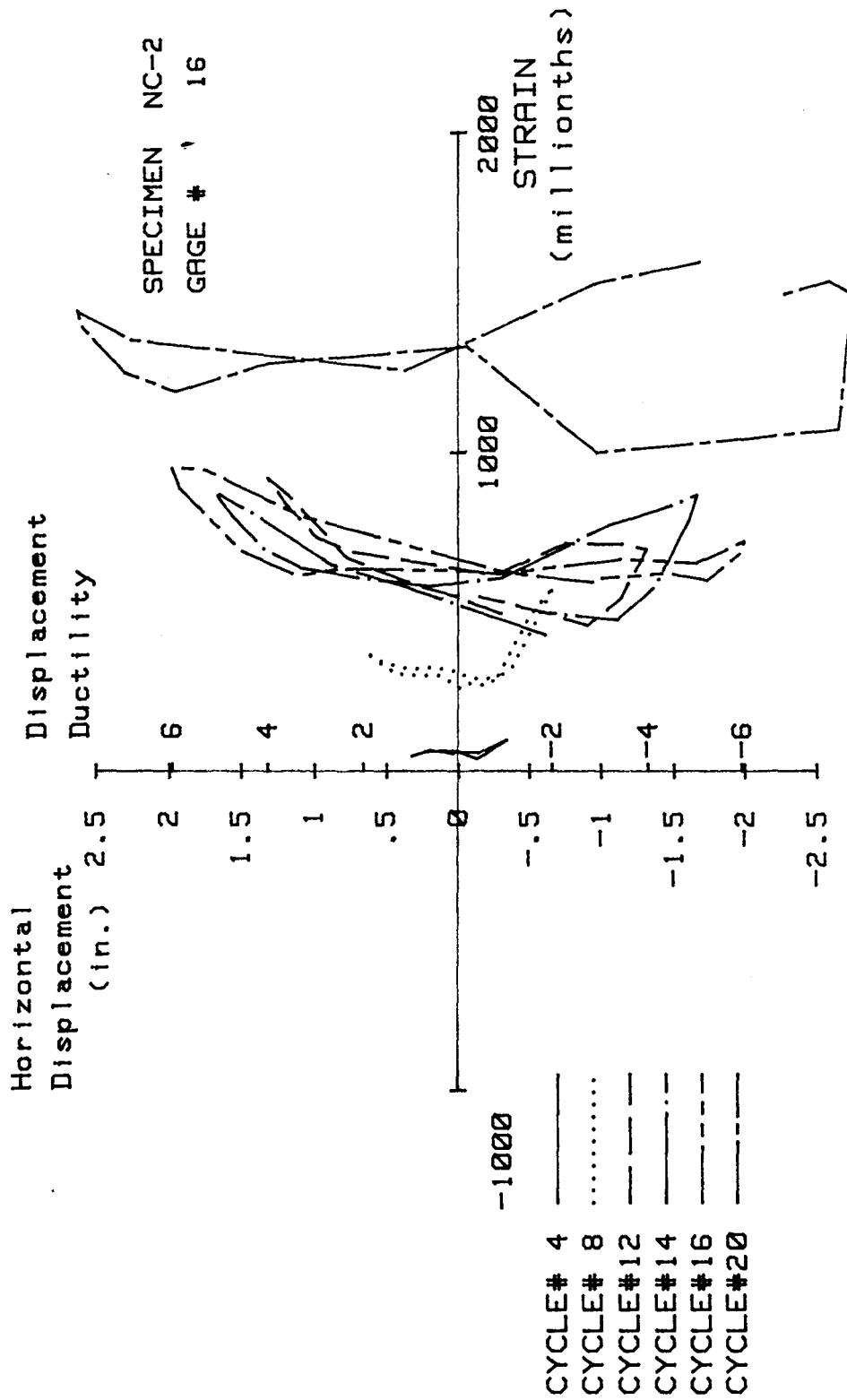


FIG. A-21 MEASURED STRAIN, GAGE #16, SPECIMEN NC-2

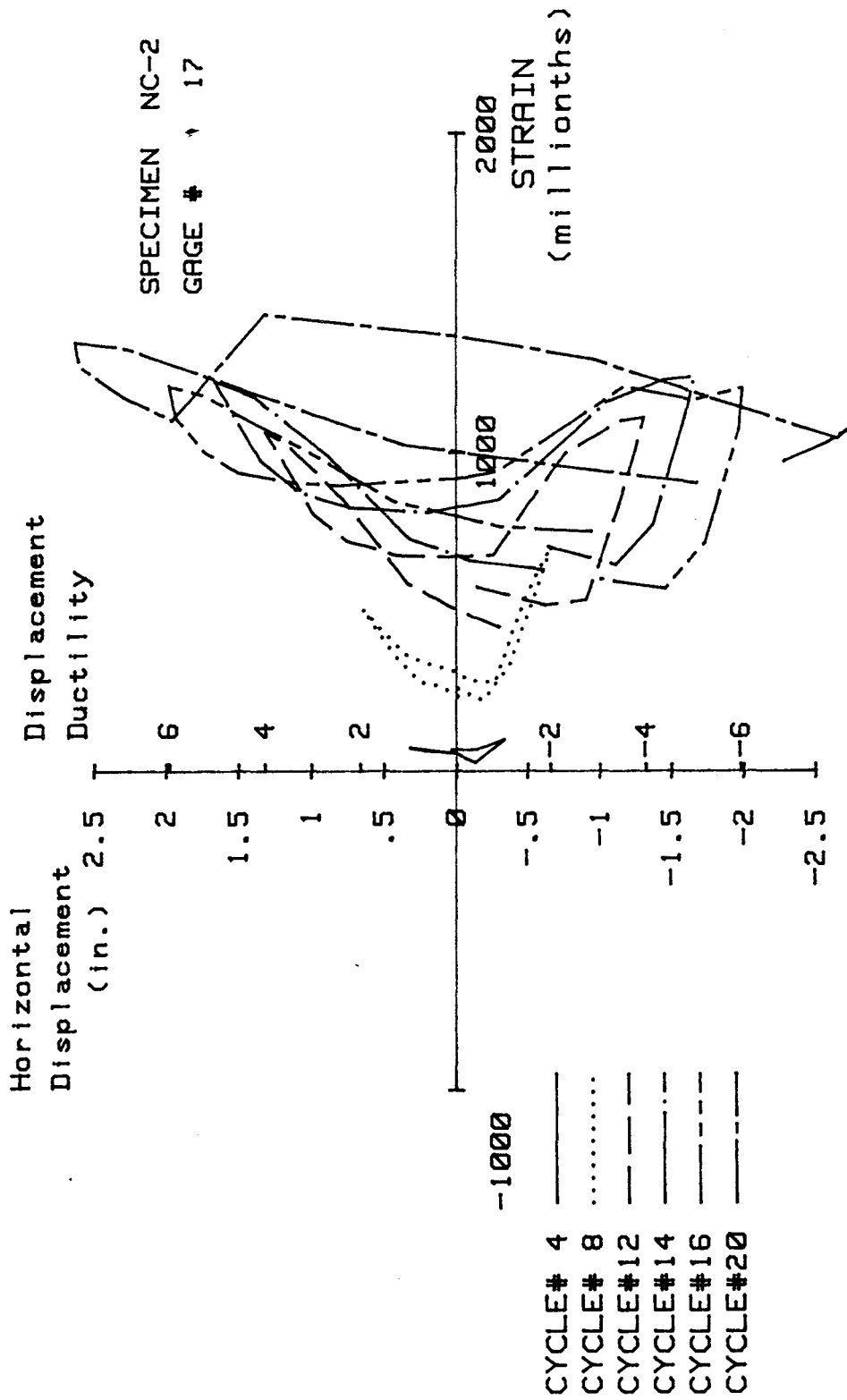


FIG. A-22 MEASURED STRAIN, GAGE #17, SPECIMEN NC-2

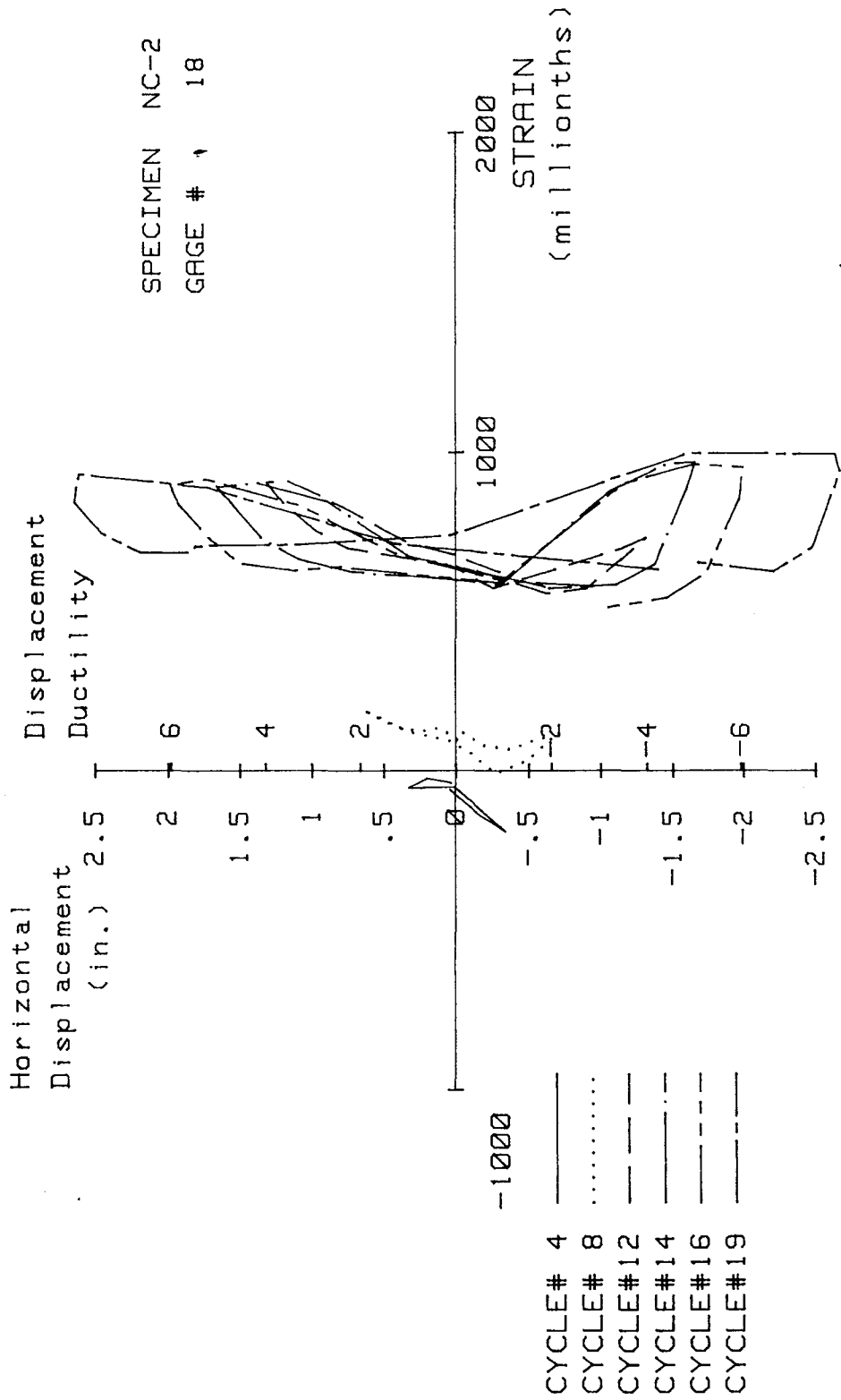


FIG. A-23 MEASURED STRAIN, GAGE #18, SPECIMEN NC-2

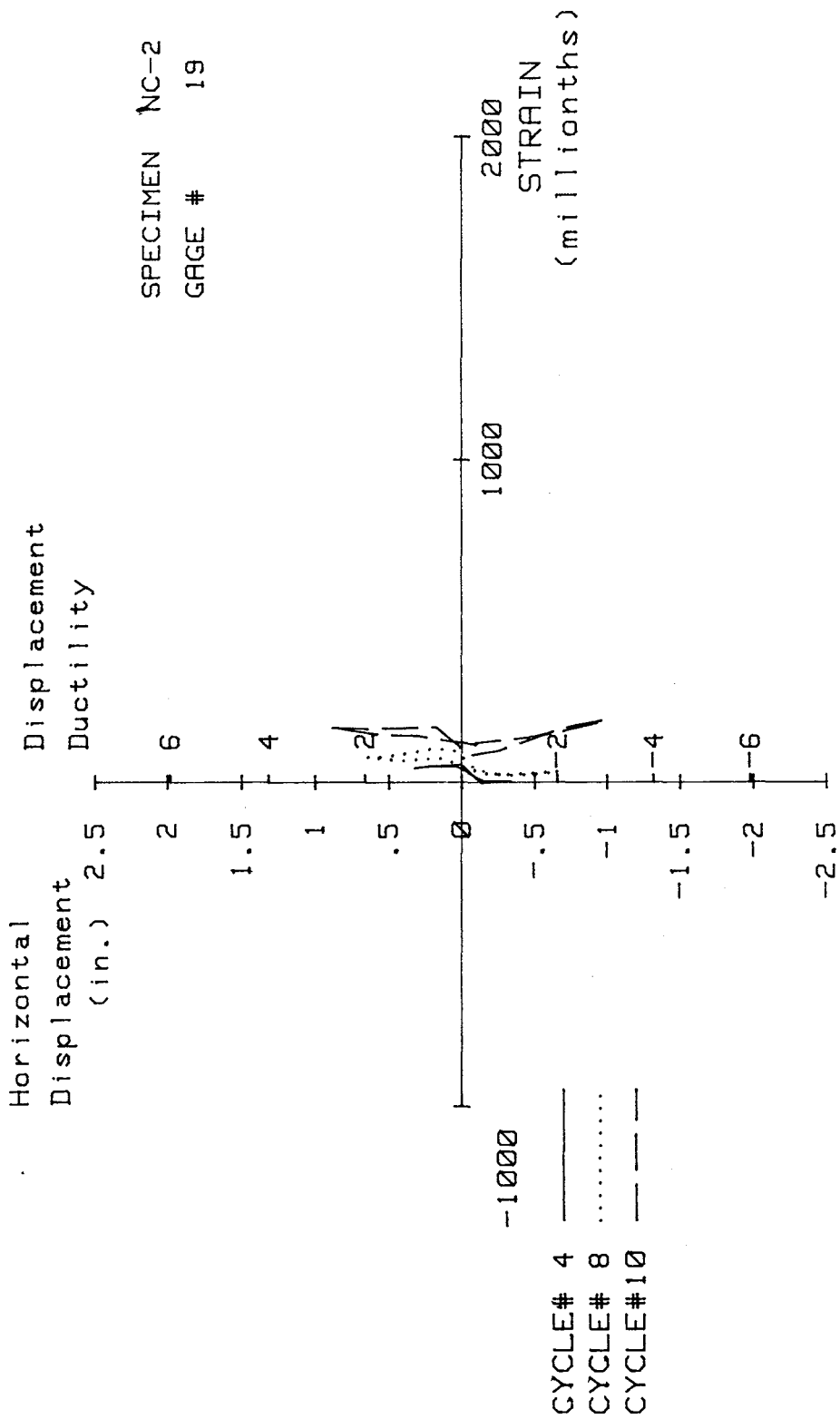


FIG. A-24 MEASURED STRAIN, GAGE #19, SPECIMEN NC-2

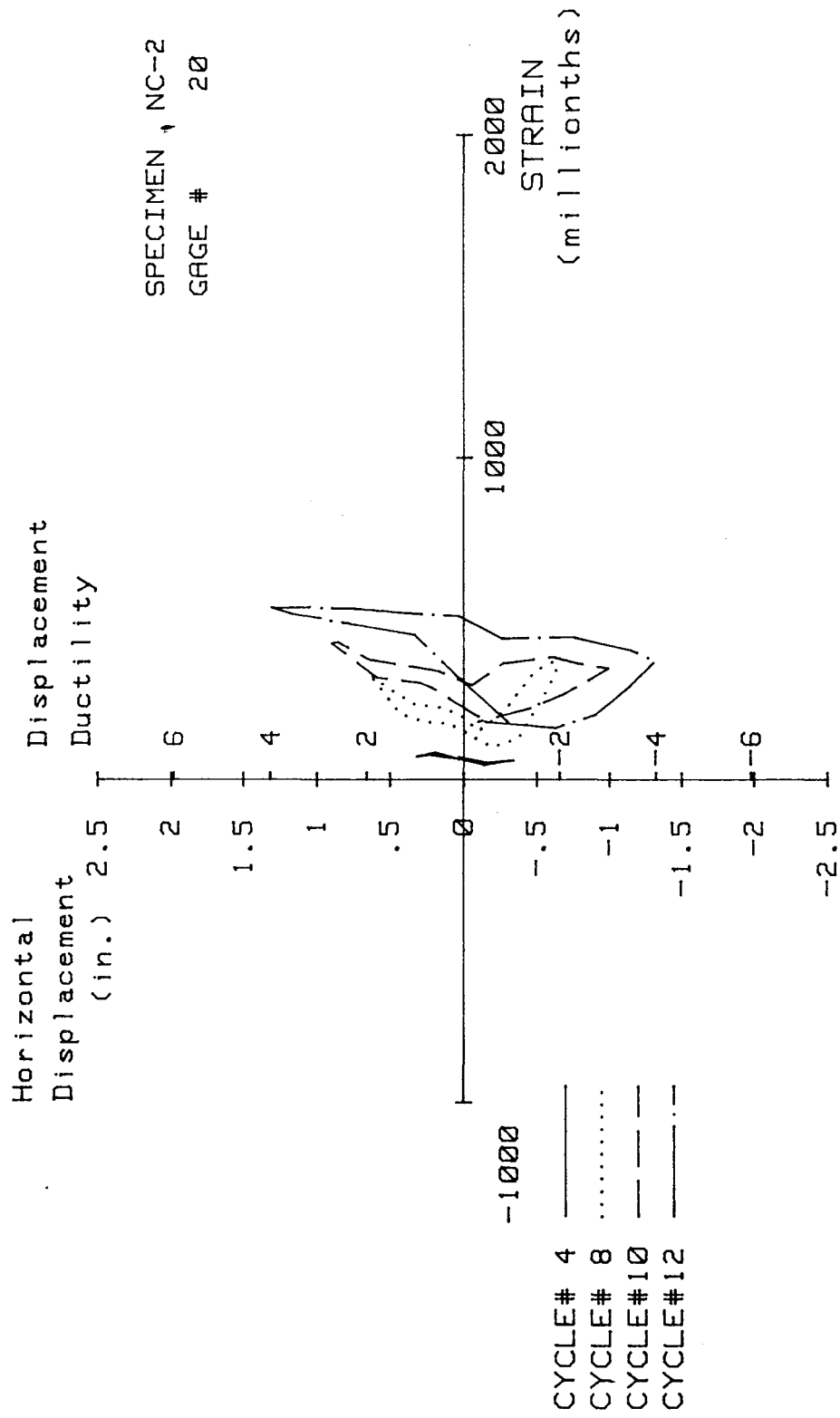


FIG. A-25 MEASURED STRAIN, GAGE #20, SPECIMEN NC-2

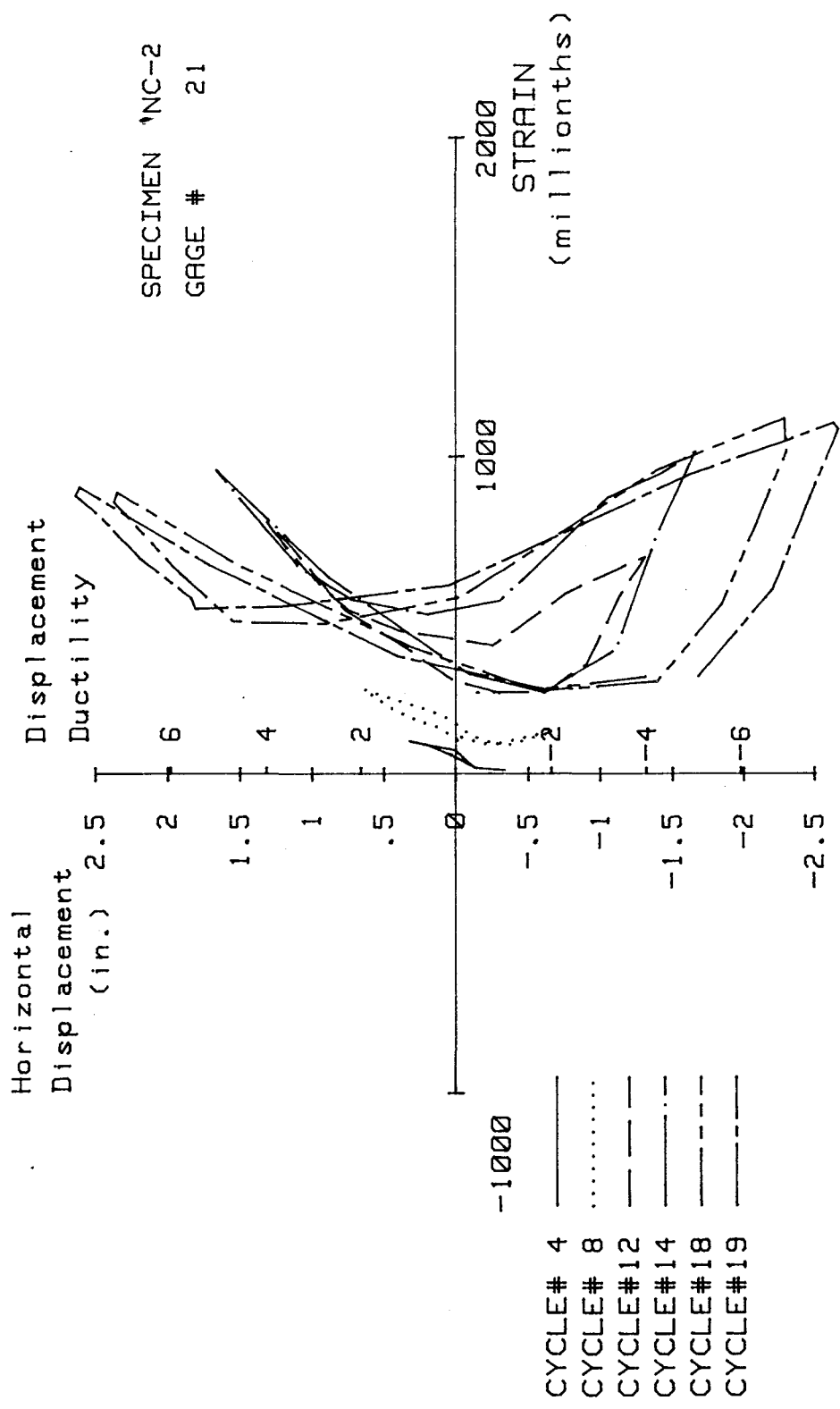


FIG. A-26 MEASURED STRAIN, GAGE #21, SPECIMEN NC-2

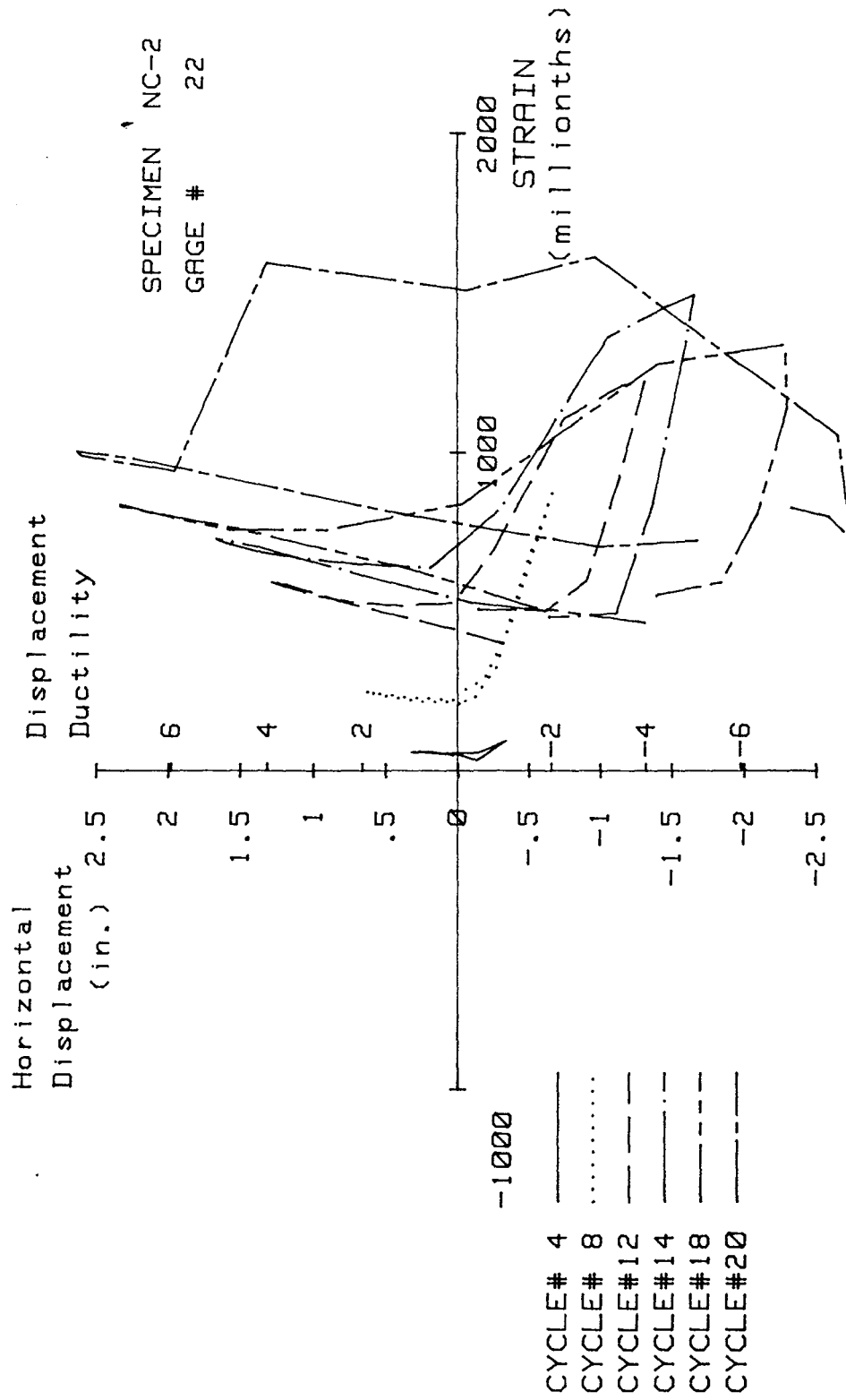


FIG. A-27 MEASURED STRAIN, GAGE #22, SPECIMEN NC-2

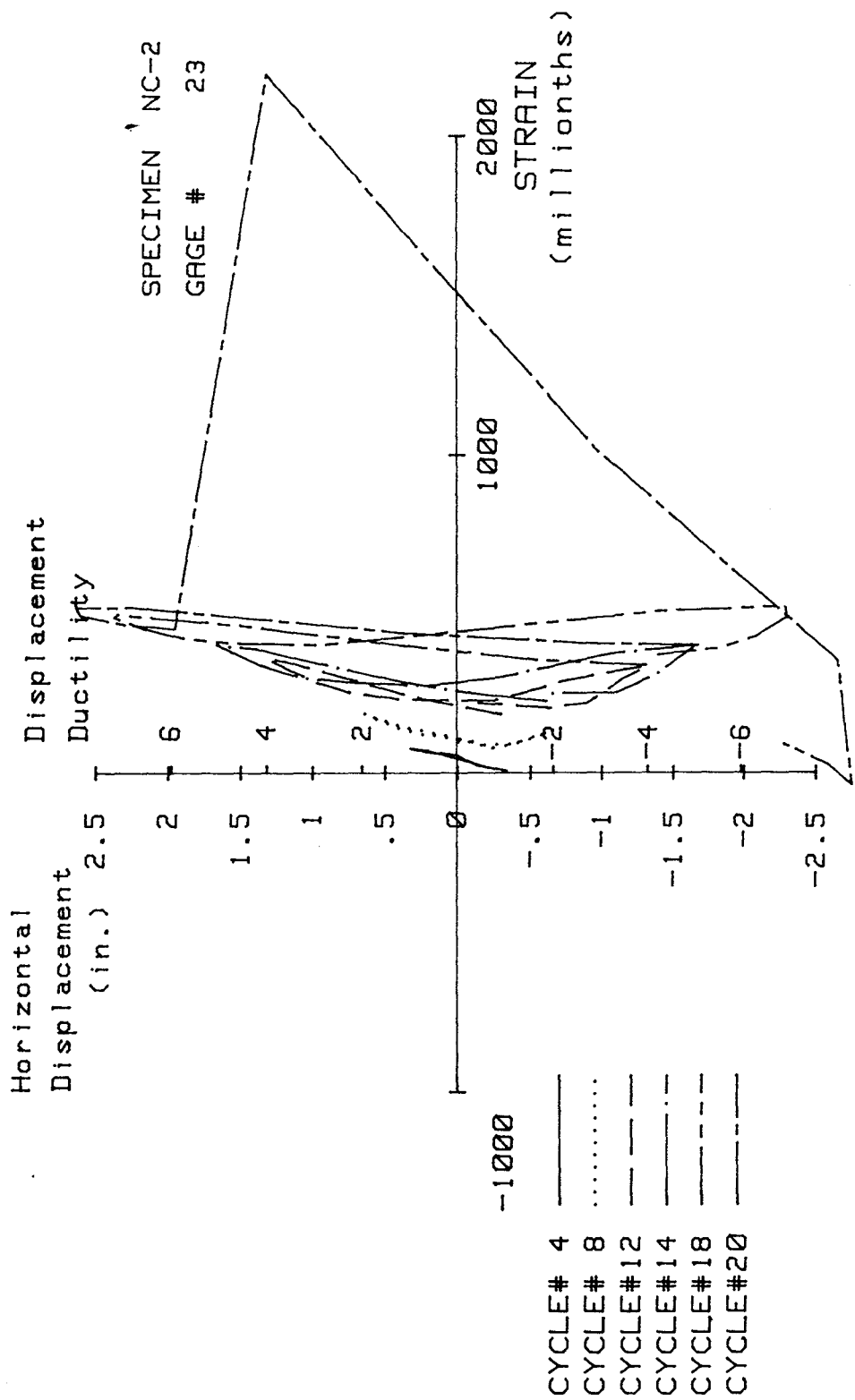


FIG. A-28 MEASURED STRAIN, GAGE #23, SPECIMEN NC-2

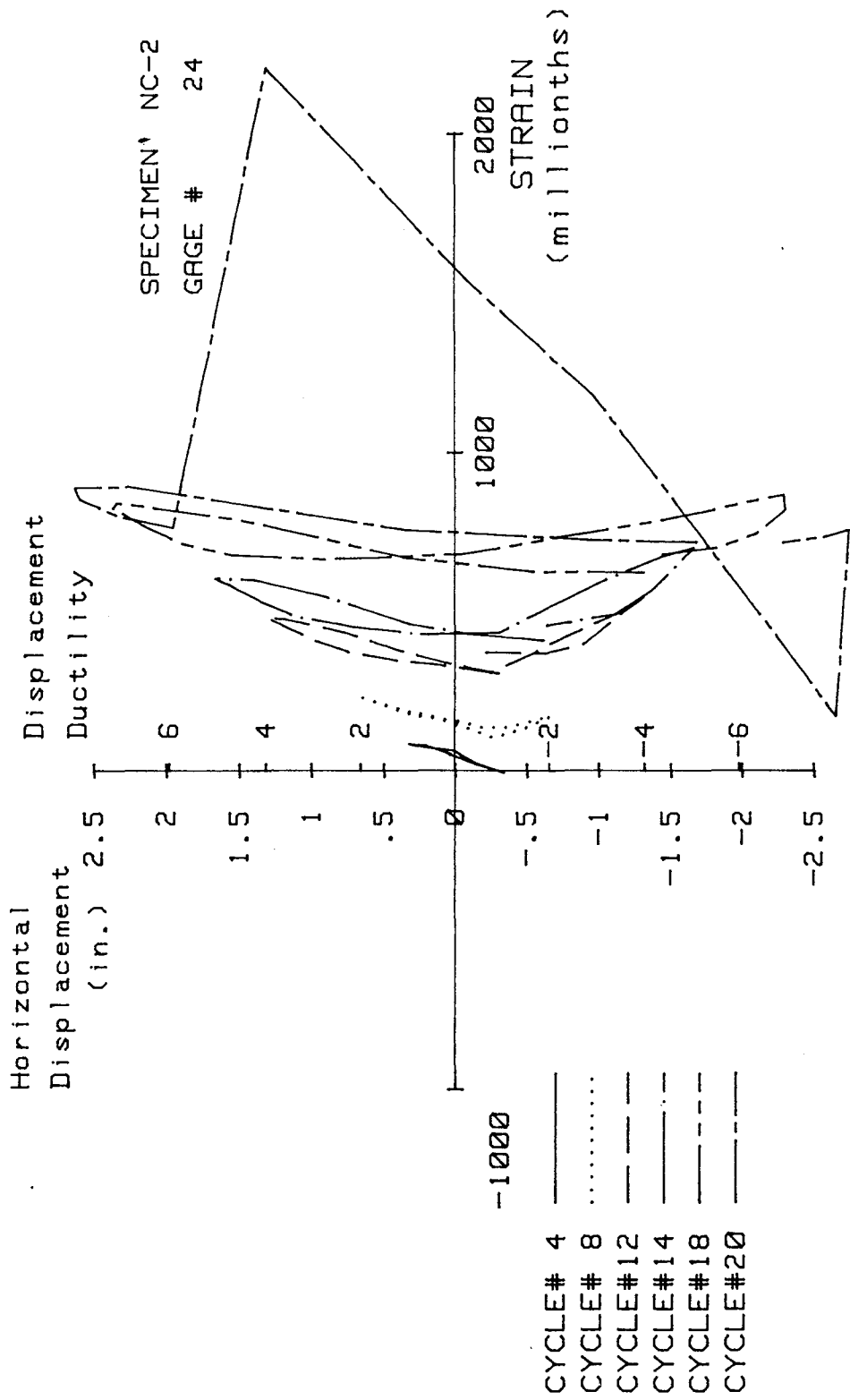


FIG. A-29 MEASURED STRAIN, GAGE #24, SPECIMEN NC-2

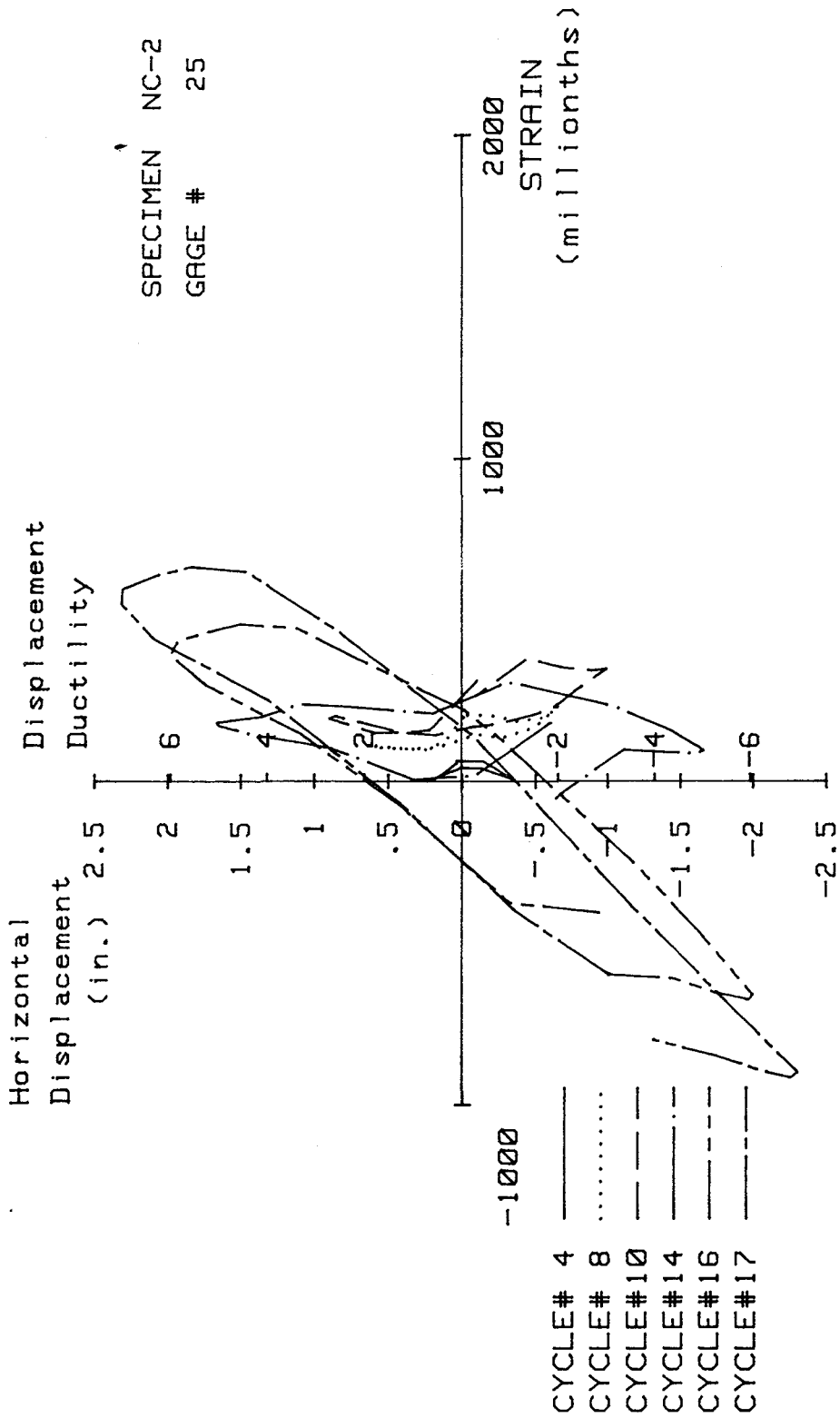


FIG. A-30 MEASURED STRAIN, GAGE #25, SPECIMEN NC-2

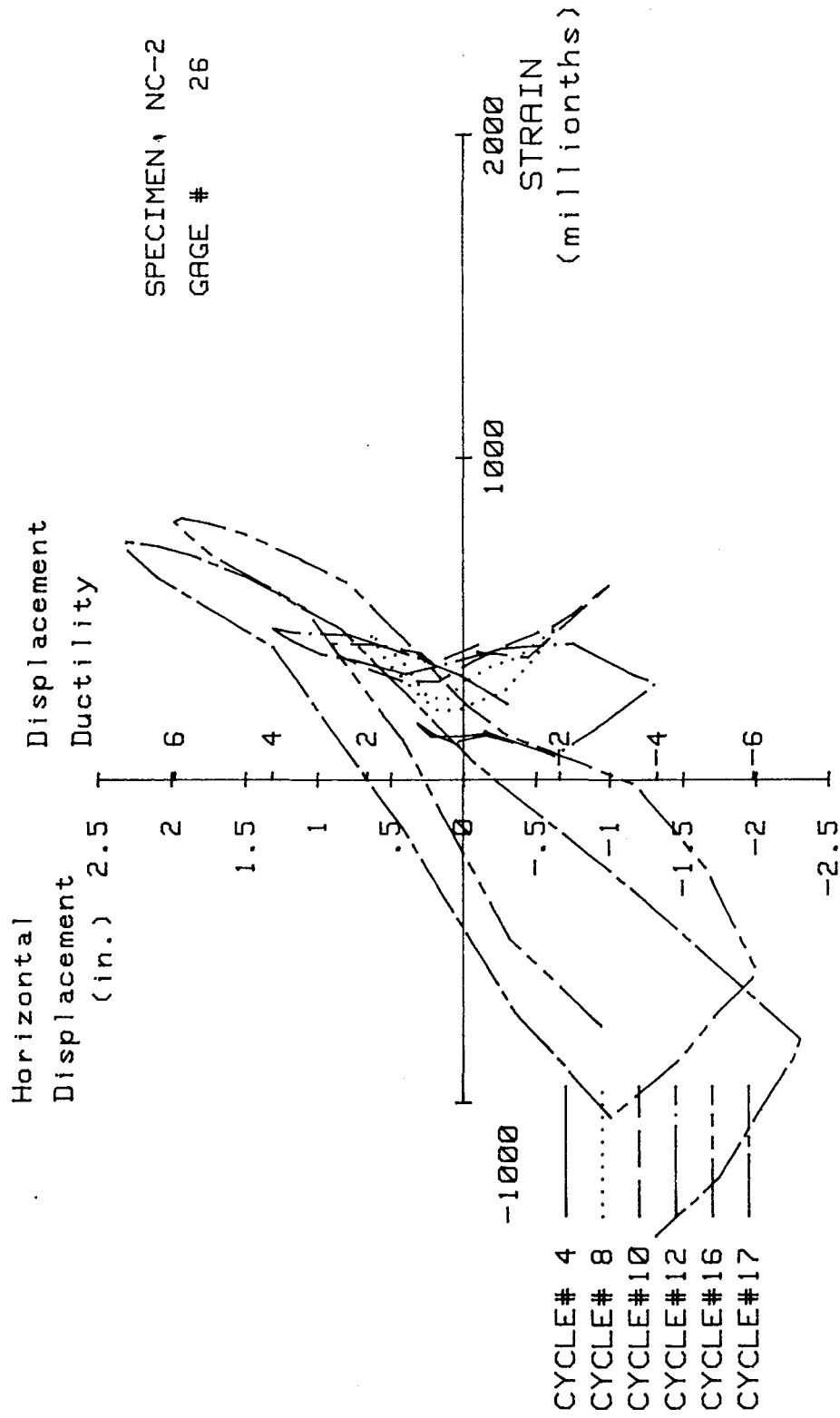


FIG. A-31 MEASURED STRAIN, GAGE #26, SPECIMEN NC-2

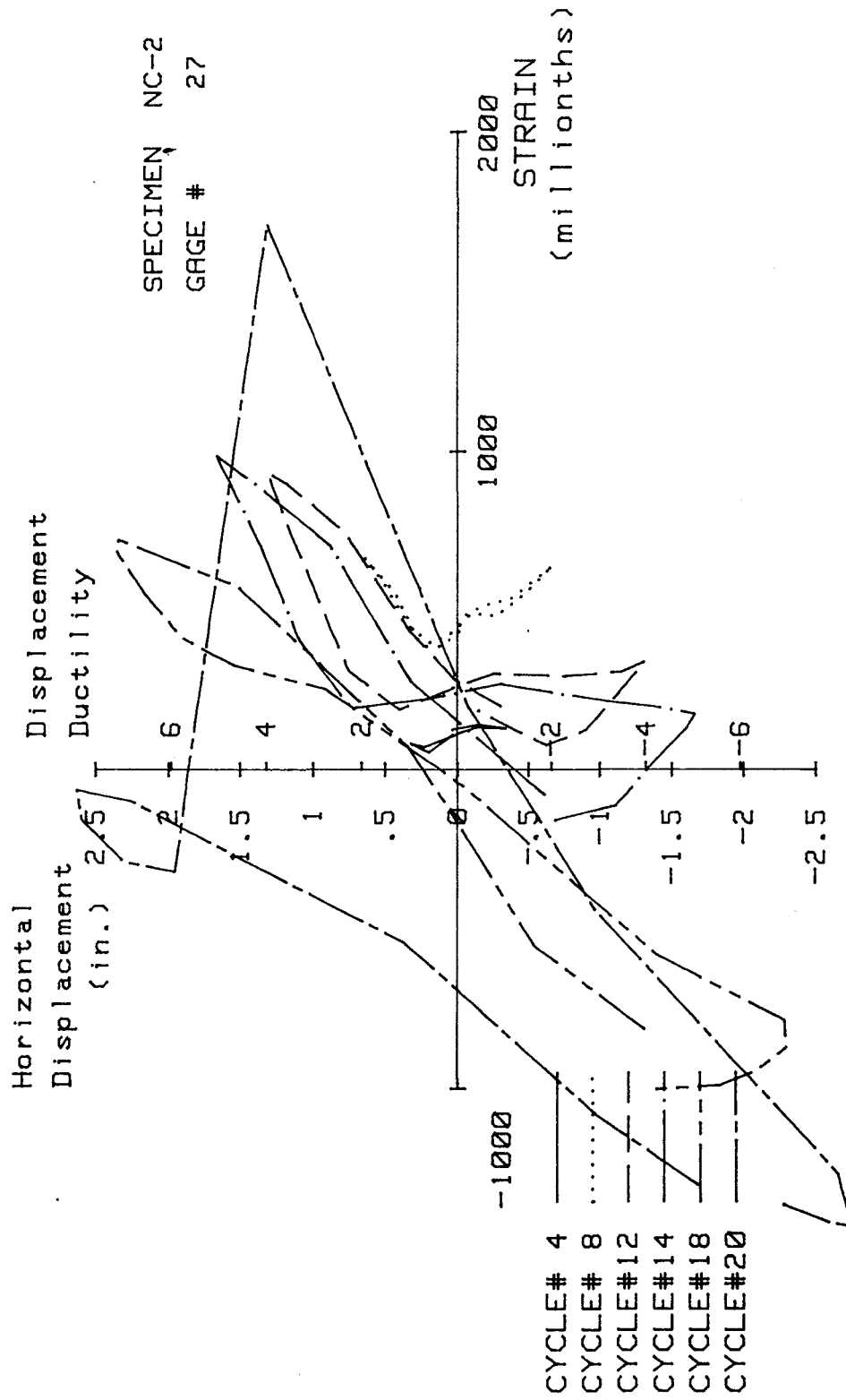


FIG. A-32 MEASURED STRAIN, GAGE #27, SPECIMEN NC-2

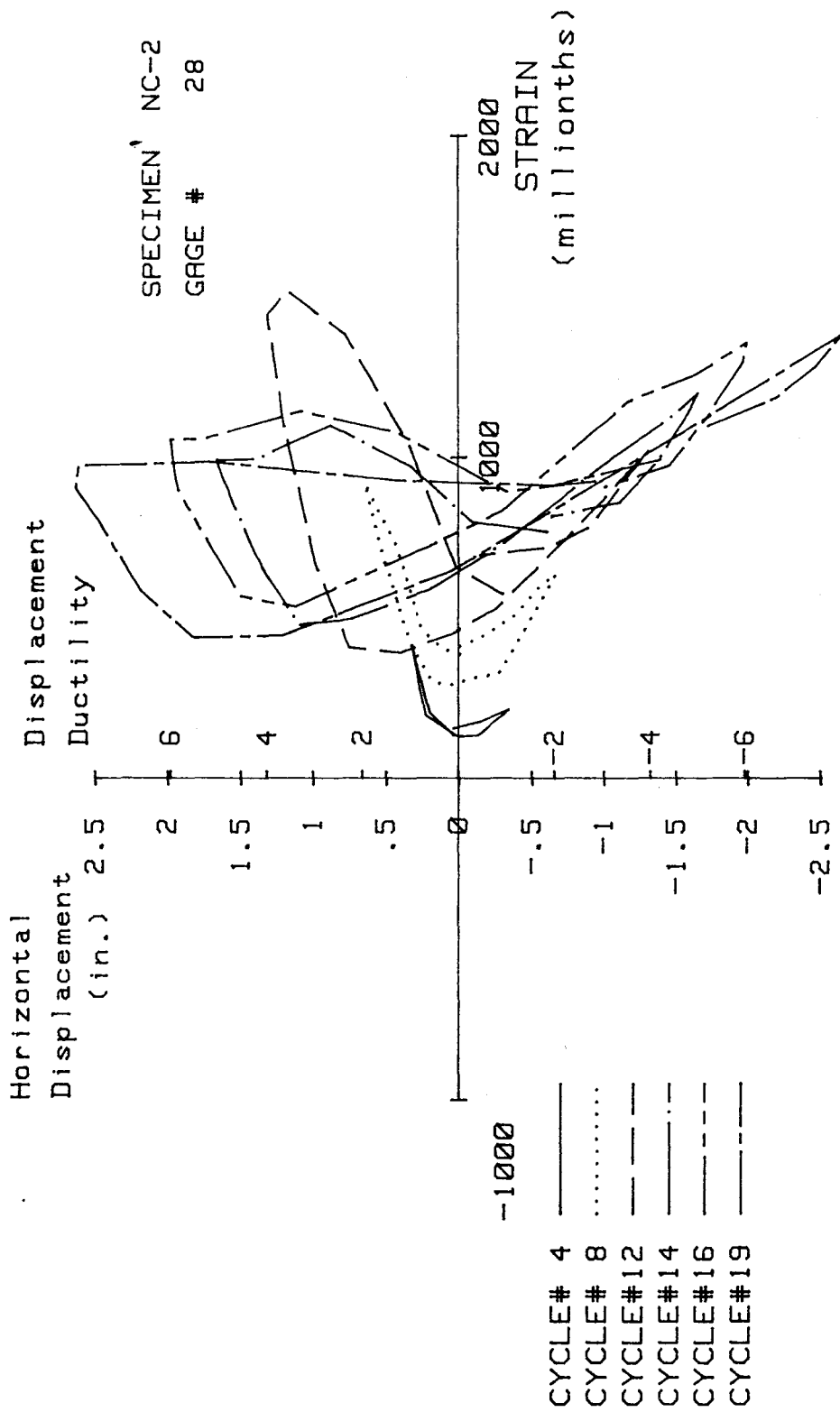


FIG. A-33 MEASURED STRAIN, GAGE #28, SPECIMEN NC-2

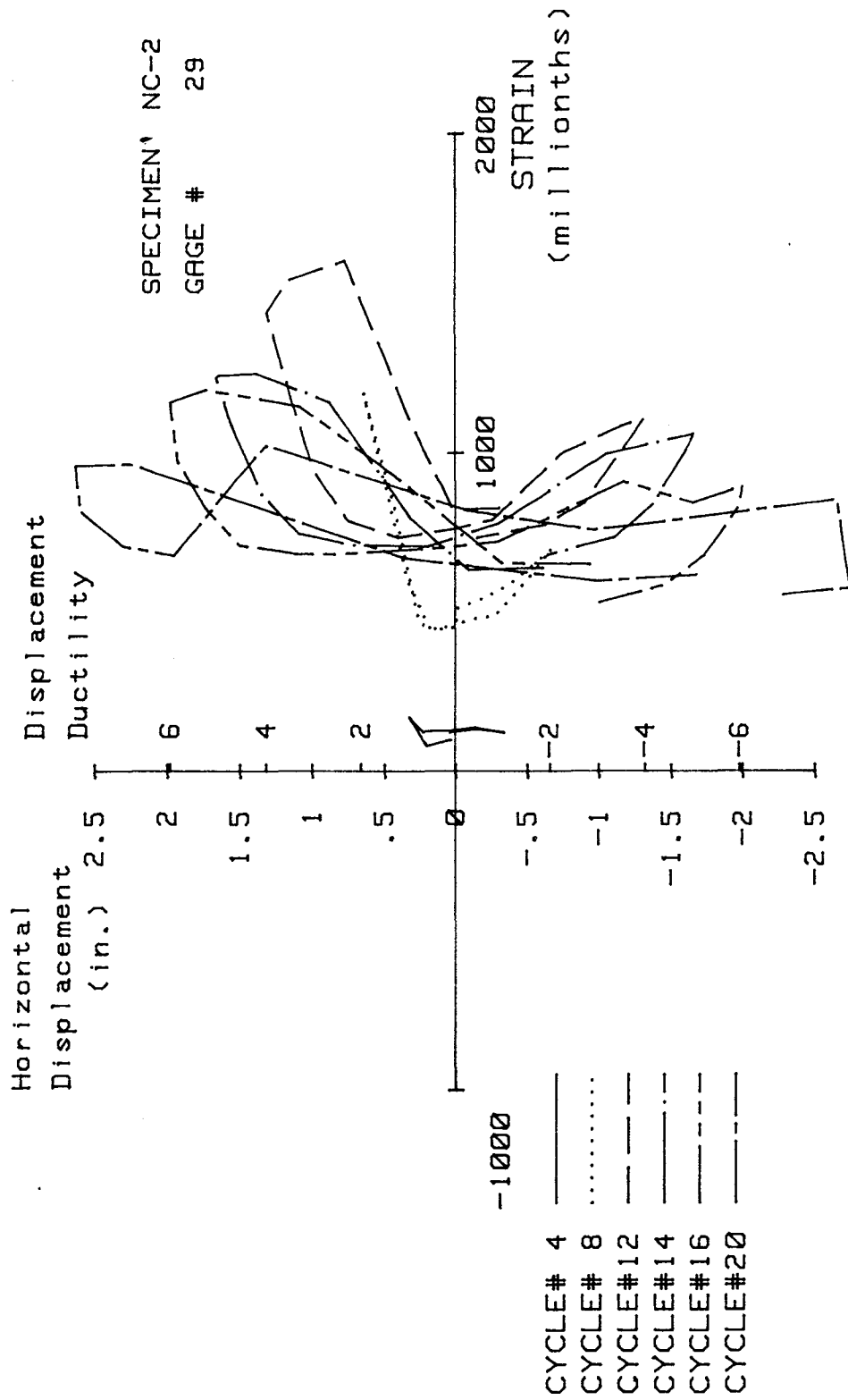


FIG. A-34 MEASURED STRAIN, GAGE #29, SPECIMEN NC-2

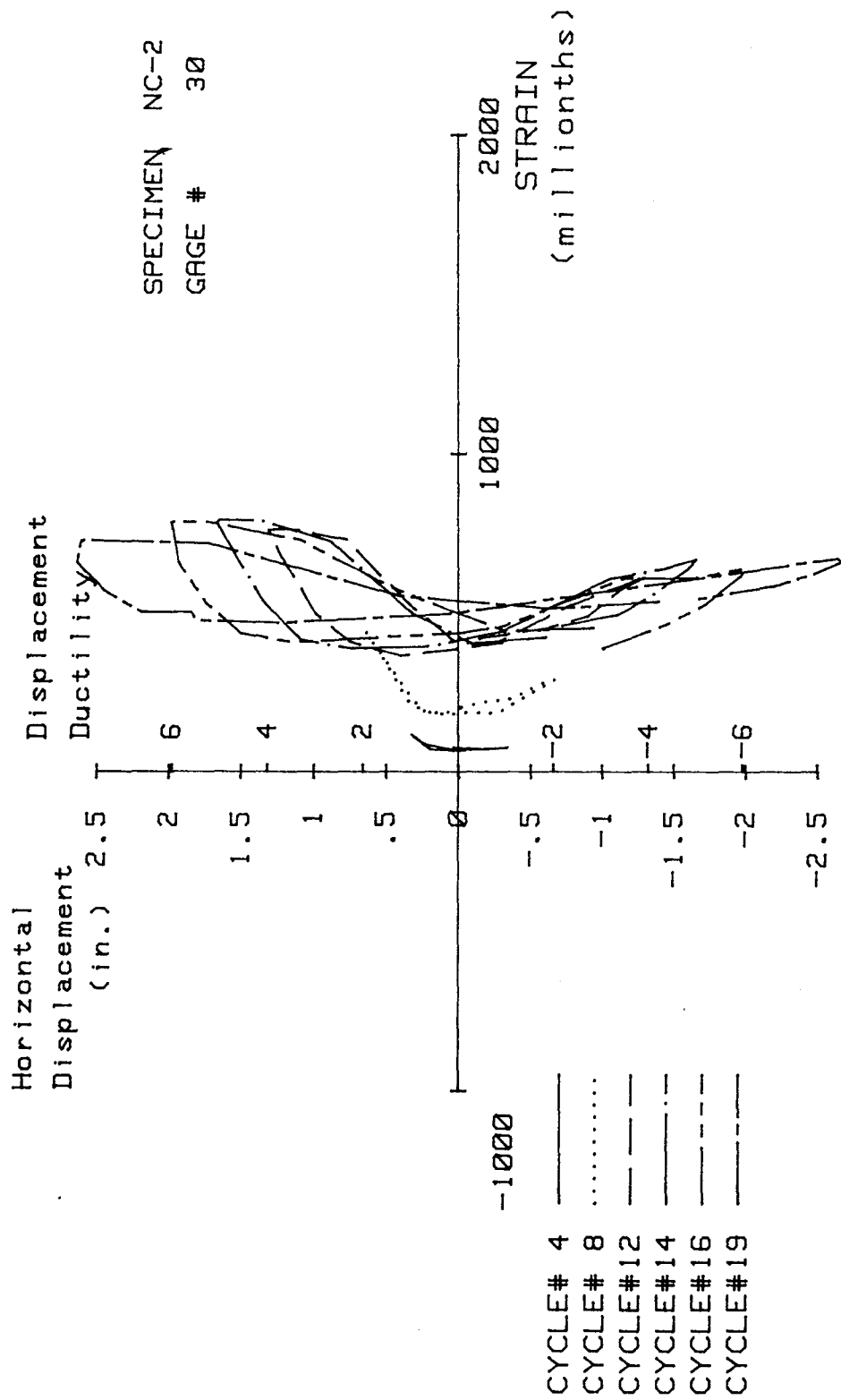


FIG. A-35 MEASURED STRAIN, GAGE #30, SPECIMEN NC-2

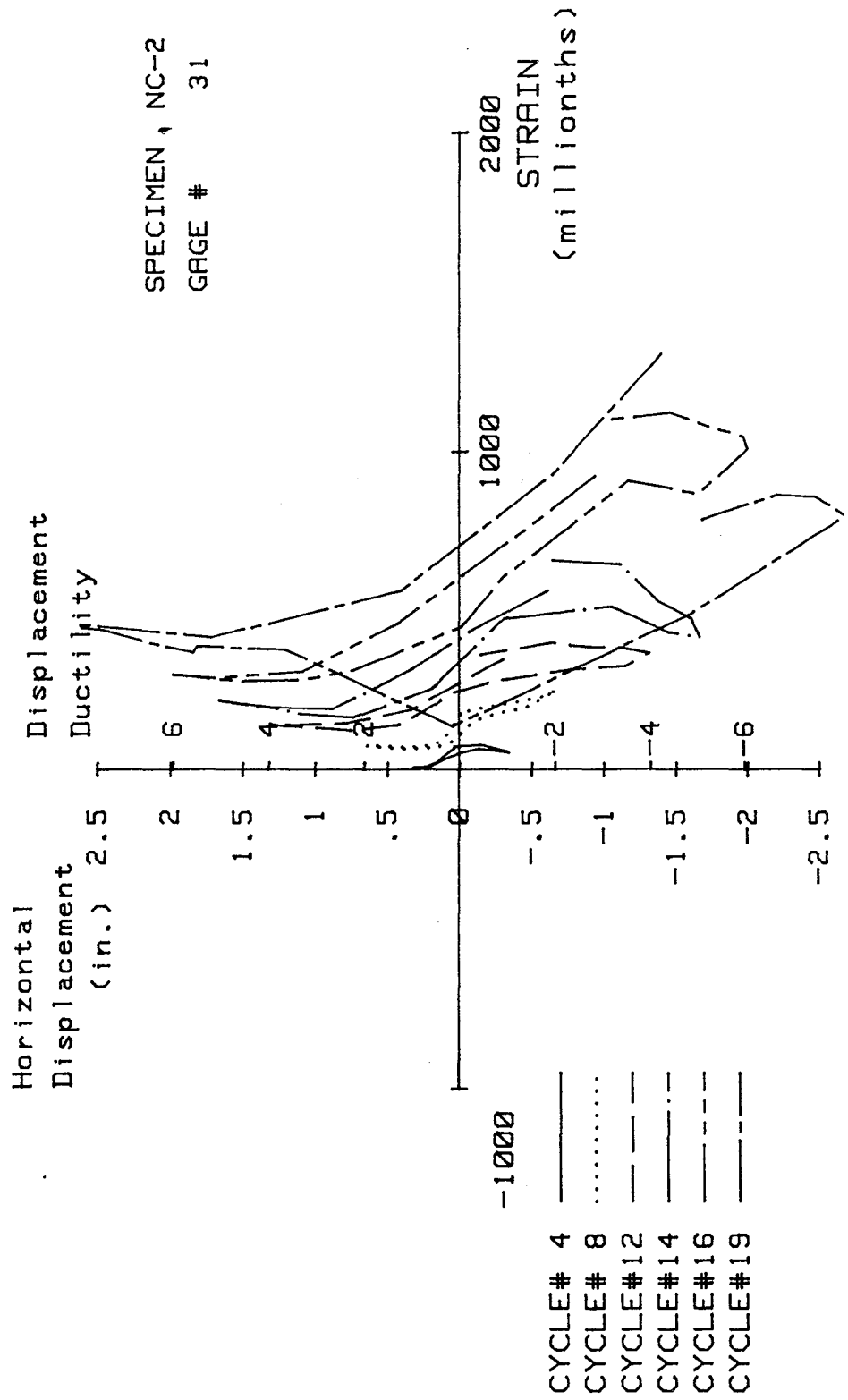


FIG. A-36 MEASURED STRAIN, GAGE #31, SPECIMEN NC-2

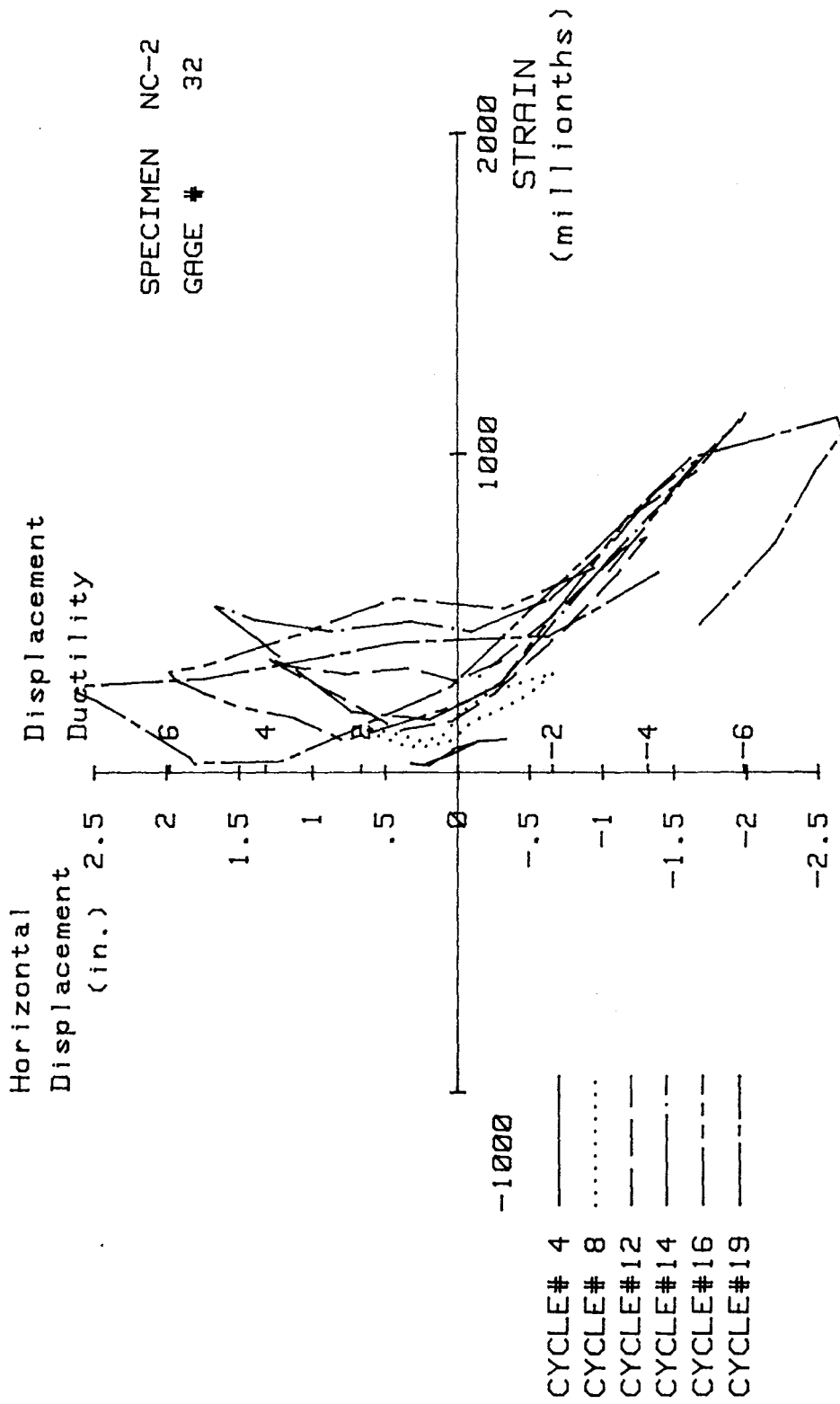


FIG. A-37 MEASURED STRAIN, GAGE #32, SPECIMEN NC-2

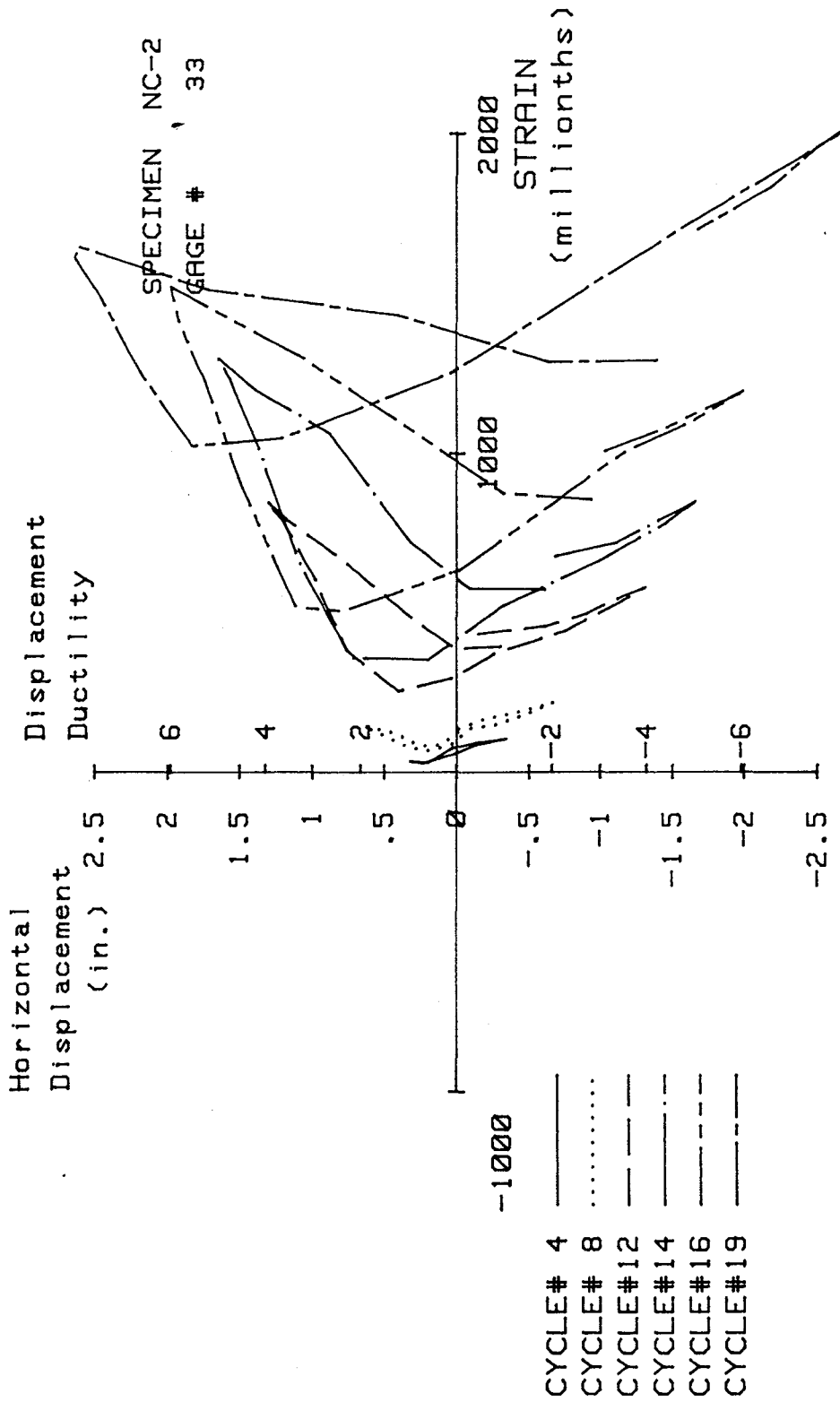


FIG. A-38 MEASURED STRAIN, GAGE #33, SPECIMEN NC-2

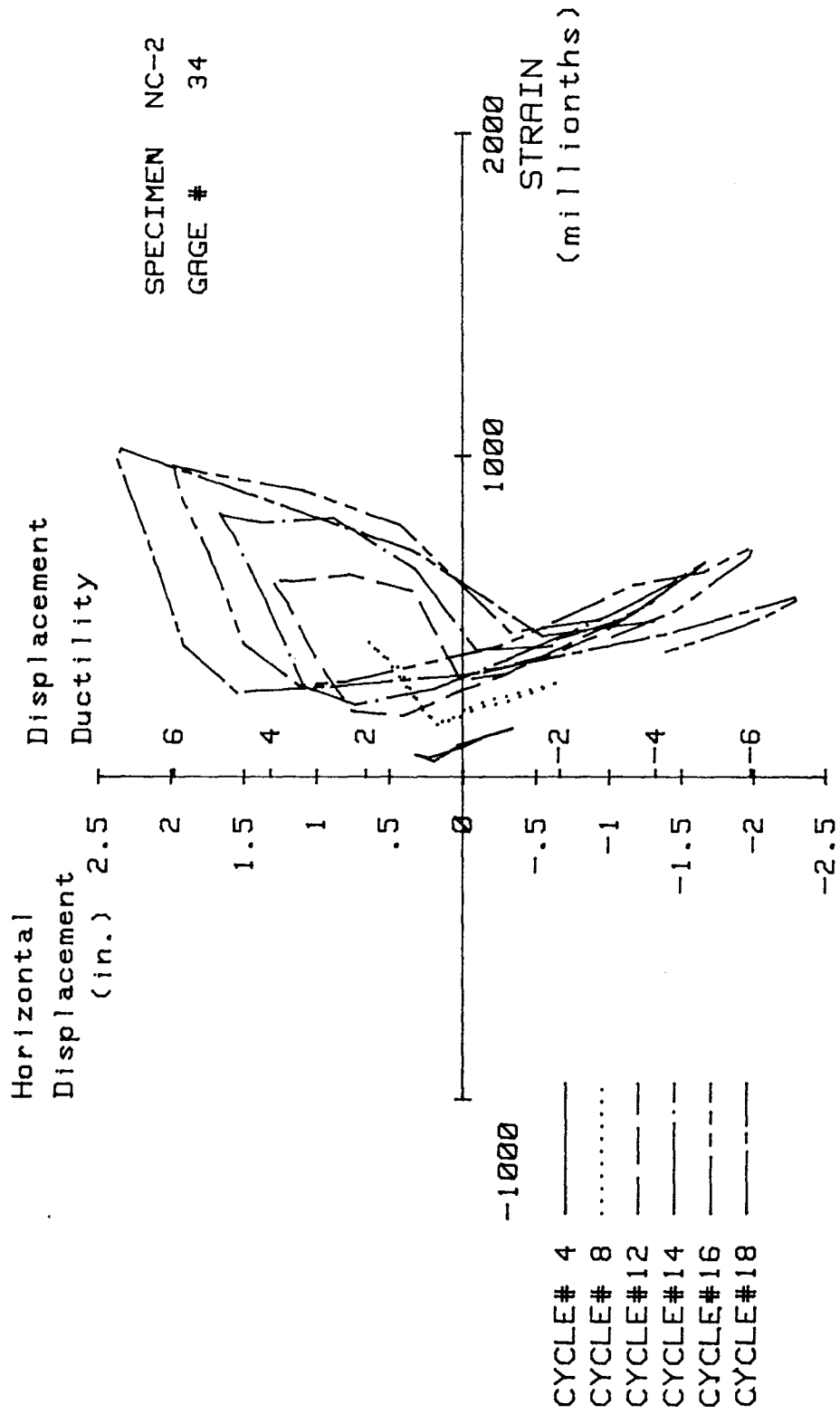


FIG. A-39 MEASURED STRAIN, GAGE #34, SPECIMEN NC-2

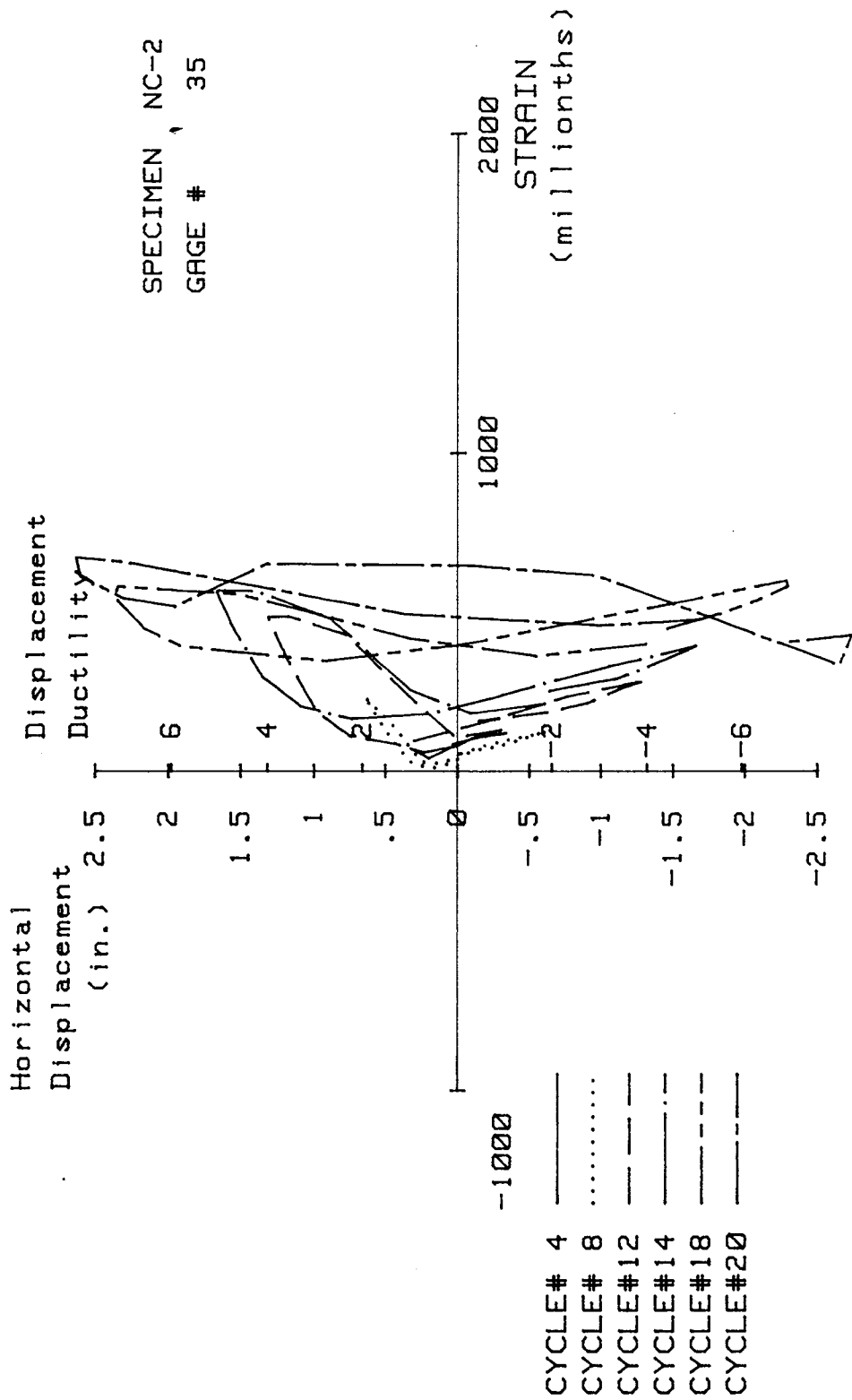


FIG. A-40 MEASURED STRAIN, GAGE #35, SPECIMEN NC-2

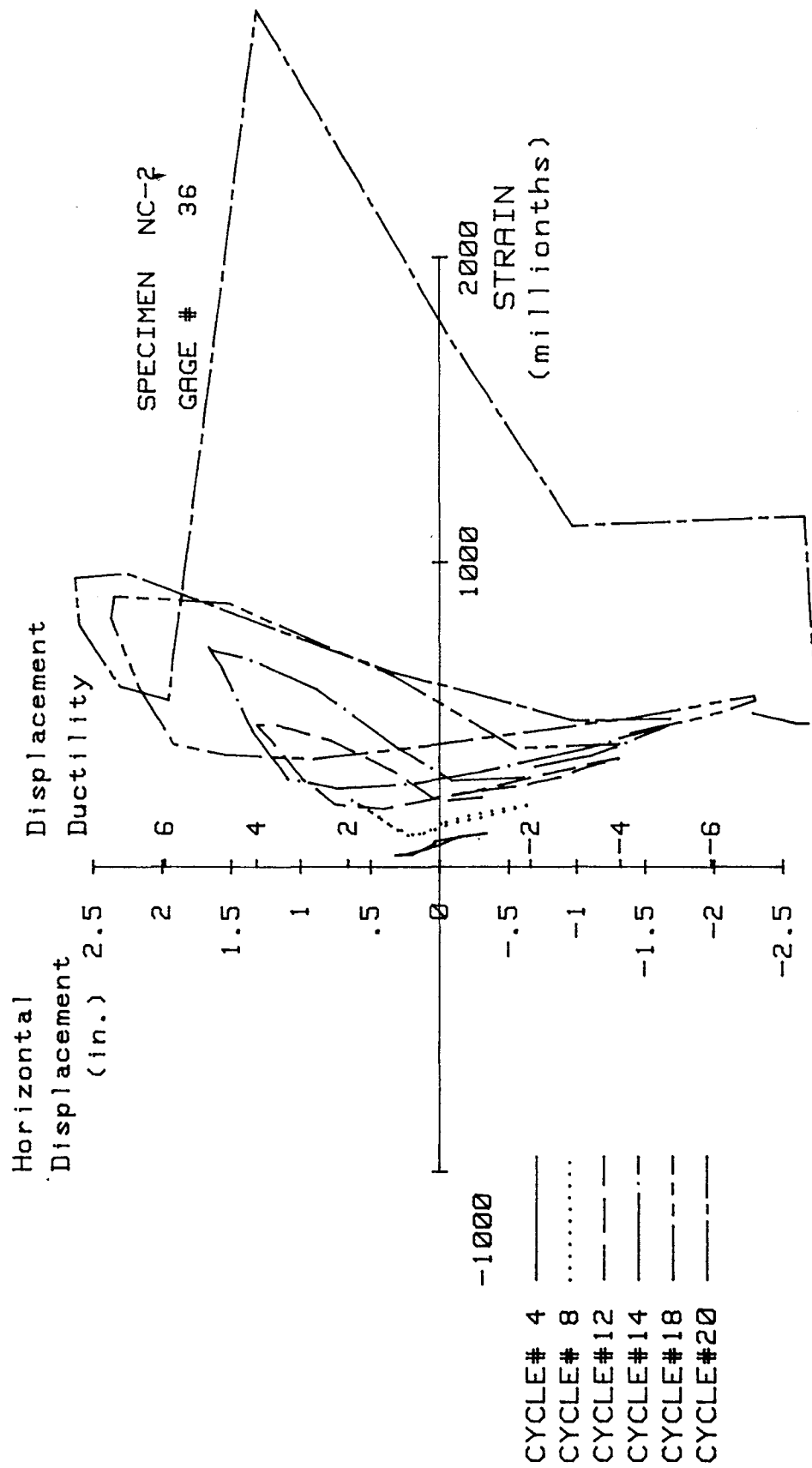


FIG. A-41 MEASURED STRAIN, GAGE #36, SPECIMEN NC-2

Specimen NC-3

Transverse Reinforcement Detail

The details of transverse reinforcement details used in Specimen NC-3 were identical to those used in Specimen NC-2 and are shown in Figure 4-2b. The area of the transverse reinforcement provided was 92% of the area required by ACI-318-83 Code.

Load History

The applied axial load was 780 kips which corresponds to 40% of the column axial load capacity. The applied axial load was maintained constant throughout the cyclic load test. Figure A-42 shows the history of the applied lateral load. The first yield displacement and the yield curvature obtained during cycle #2 were 0.3 in. and $303 \times 10^{-6} \text{ in.}^{-1}$, respectively. Subsequently, the horizontal cyclic loading consisted of displacement-controlled testing to a maximum displacement ductility ratio of six. One complete cycle at a displacement ductility ratio of six was applied. However, the specimen failed prior to the completion of the second cycle at this displacement level.

Test Observations

The first cracks were observed in the upper column at cycle #4 ($\mu=1$). These cracks formed approximately 5 and 10 in. above the stub. Some crushing of the concrete cover was visible at cycle #6 ($\mu=2$) at the junction of the upper column and the stub as shown in Fig. A-43. The cover concrete was partially spalled off at cycle #8 ($\mu=3$) as shown in Fig. A-44. The photograph in Fig. A-45 shows the test specimen at the end of cycle #12 ($\mu=5$). The plastic hinge length was relatively short and was confined predominantly to within 8 in. of the stub. Application of the second cycle at displacement ductility ratio of five (cycle #13) inflicted visible damage at a more rapid rate than previous cycles with the cover concrete on the corner spalling over a distance of approximately 20 in. from the stub (see Fig. A-46). However, at the end of cycle #13 ($\mu=5$), no disturbance to anchorage of the peripheral or interior hoops was observed.

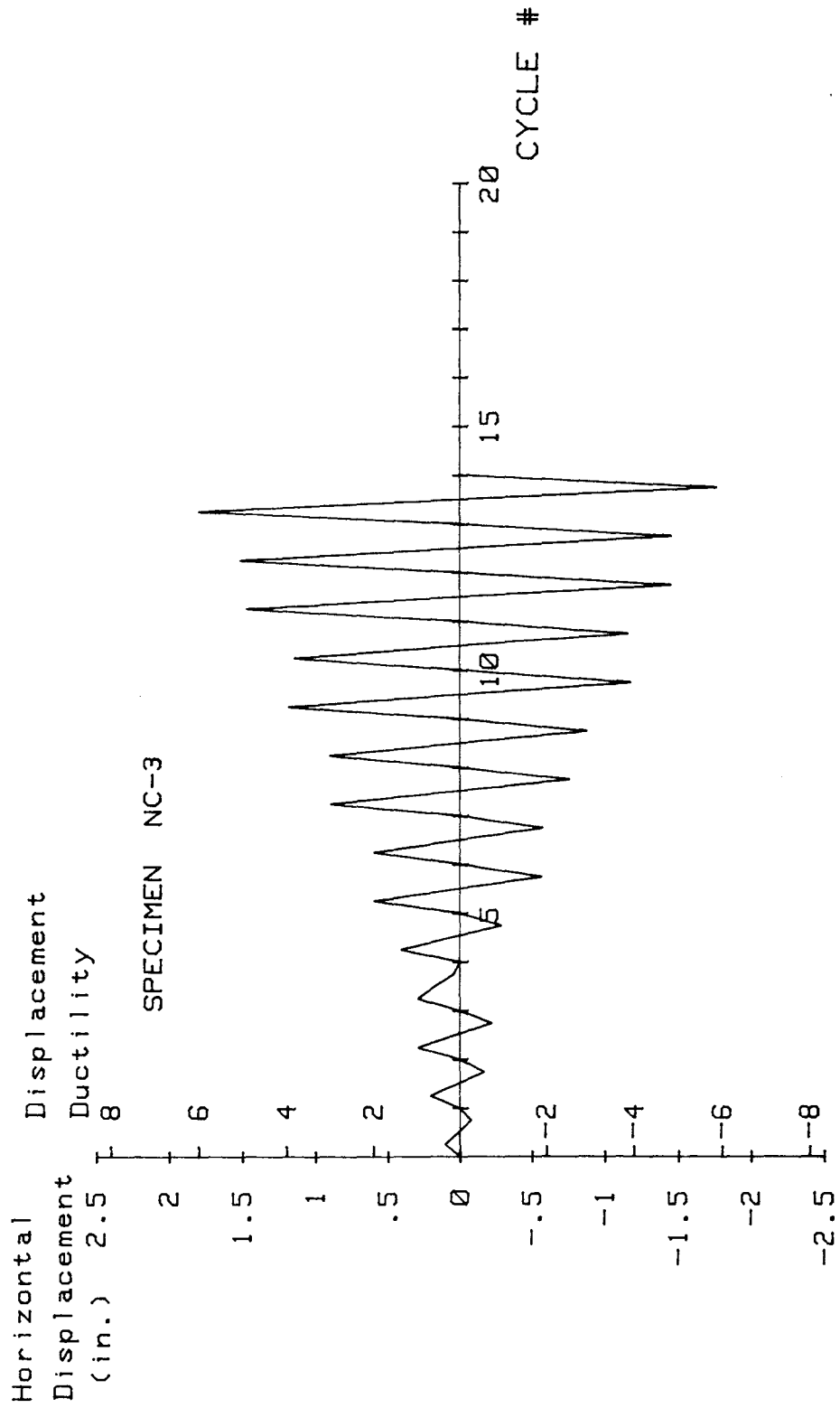


FIG. A-42 LOADING SCHEDULE, SPECIMEN NC-3

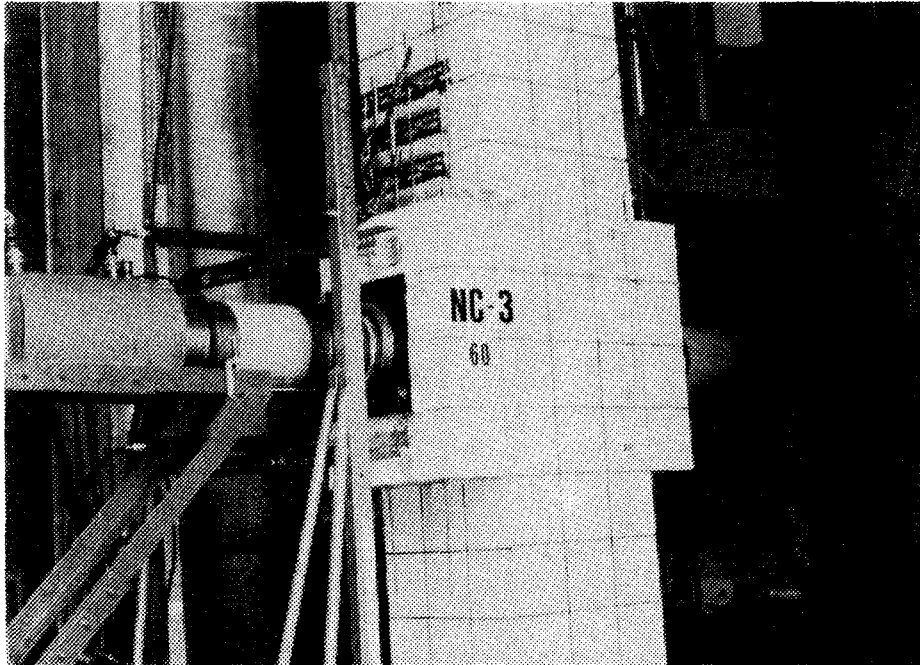


FIG. A-43 TEST SPECIMEN NC-3 AFTER CYCLE #6

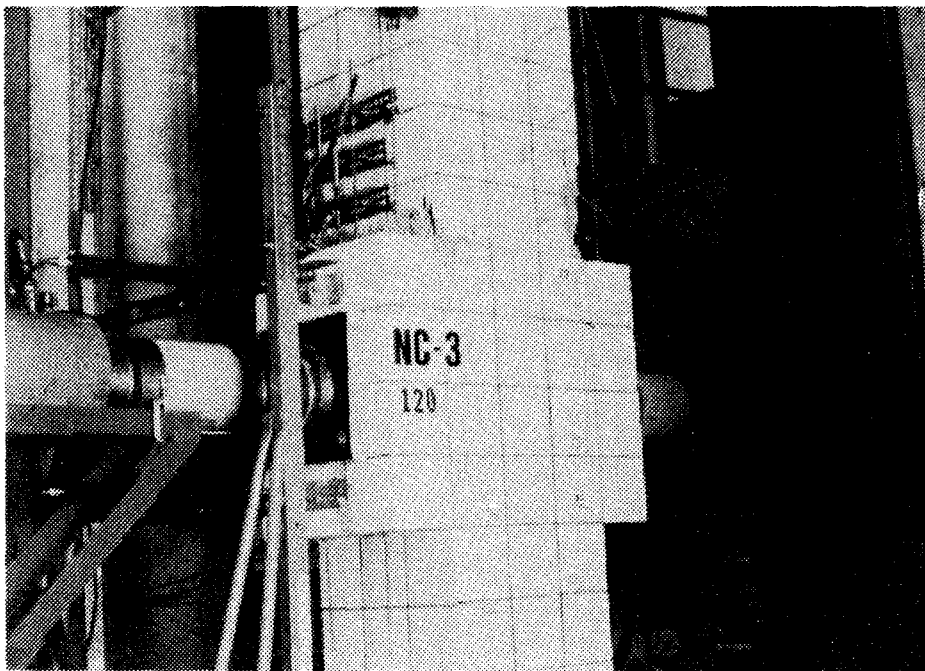


FIG. A-44 TEST SPECIMEN NC-3 AFTER CYCLE #8

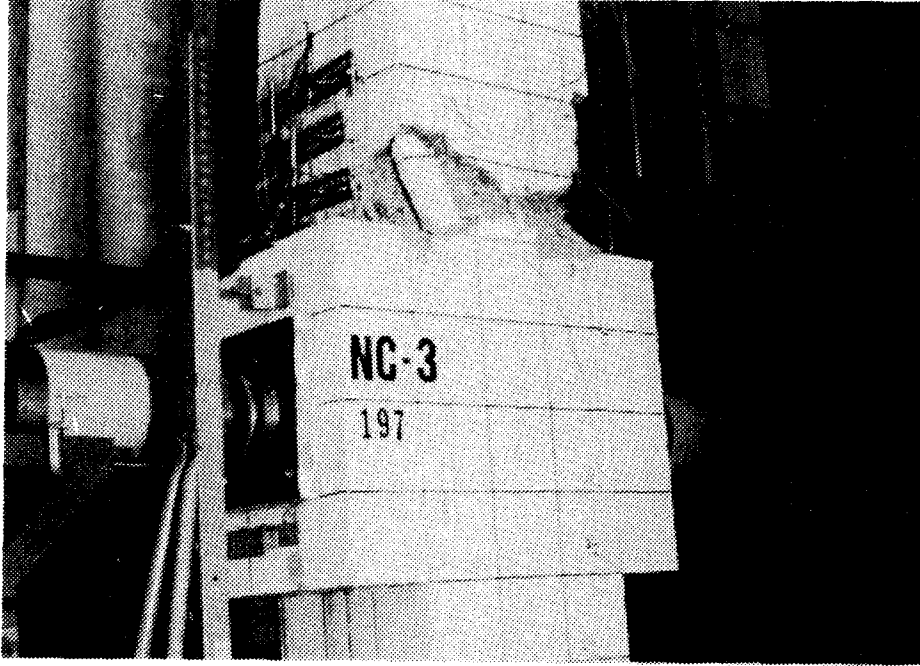


FIG. A-45 TEST SPECIMEN NC-3 AFTER CYCLE #12

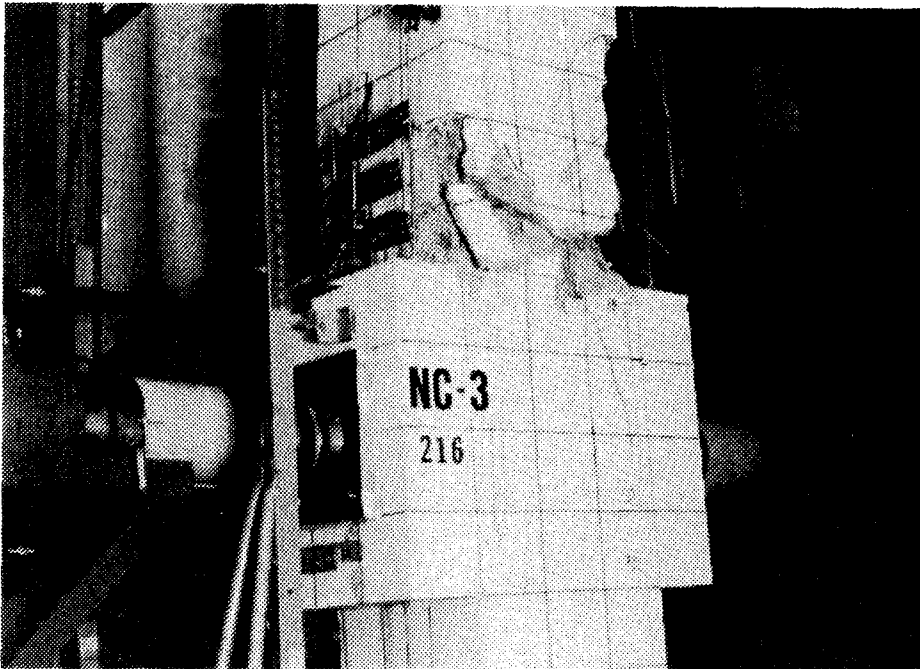


FIG. A-46 TEST SPECIMEN NC-3 AFTER CYCLE #13

An additional cycle at displacement ductility of six was applied. The maximum horizontal loads were 140 and 175 kips for forward and reverse loading, respectively. Figure A-47 shows the specimen at the end of cycle #14 ($\mu=6$). At this point some lateral bending of the corner bars was visible. The specimen failed when an attempt was made to apply an additional cycle at displacement ductility ratio of six, at which time the corner bars buckled and anchorage was lost on peripheral hoops at 6 and 10 in. from the stub (see Fig. A-48).

Load Deflection and Moment-Curvature Characteristics

Horizontal load displacement characteristics of the specimen are shown in Fig. A-49. The horizontal load-carrying capacity of the section at each displacement ductility ratio was more than the theoretical value. In addition to good strength behavior, the specimen showed good energy dissipation capability. A measure of energy dissipation is the area inside a load displacement loop. The area of the hysteresis loop at the displacement ductility ratio of five was higher than for any other specimen at this displacement level. Figure A-50 shows the curvature distribution along the test region of the specimen. As is evident from the figure, the maximum curvature remained within the first 4 in. above the stub until a displacement ductility ratio of four was reached. However, at the next two displacement levels ($\mu=5$ and 6) maximum curvature occurred between 4 and 8 in. above the stub. This behavior is in accordance with the final buckled shape of the longitudinal bars since the length of the longitudinal bars engaged in buckling was predominantly within 4 to 8 in. above the stub.

Figure A-51 shows the moment curvature characteristics of the specimen at the upper column-stub level. The theoretical moment capacity of the column section using the procedure outlined in Section 4.8.2 was 5198 in-kips. The maximum applied moment was 6514 in-kips (during the displacement ductility ratio of three) which is 25% more than the theoretical value. This enhanced moment capacity was larger than for all other specimens, which could be attributed to the relatively higher level of applied axial load (40% of the column axial load capacity compared to 20% and 30% for the other specimens). The ratio of the peak moment for the

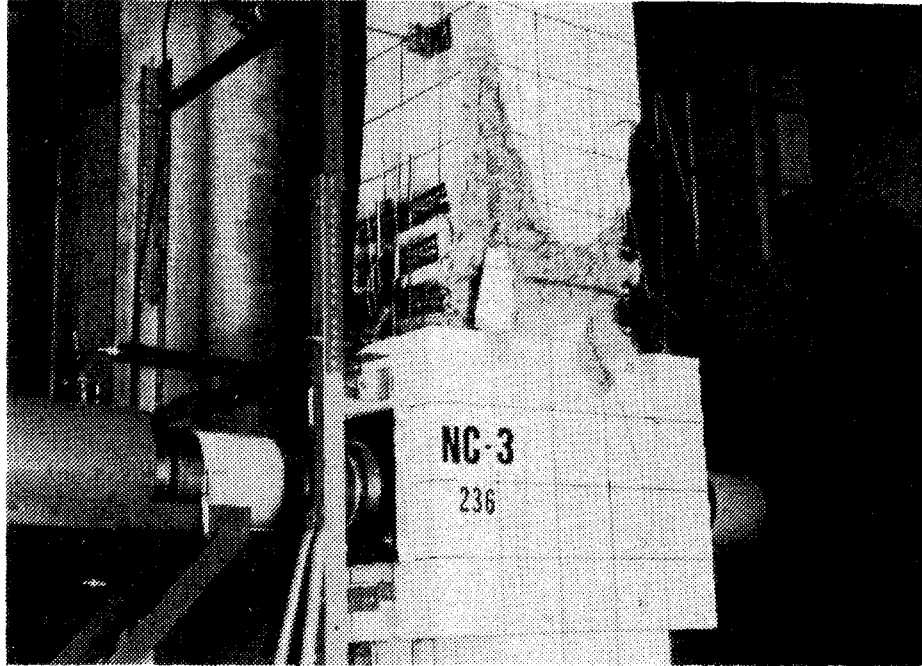


FIG. A-47 TEST SPECIMEN NC-3 AFTER CYCLE #14

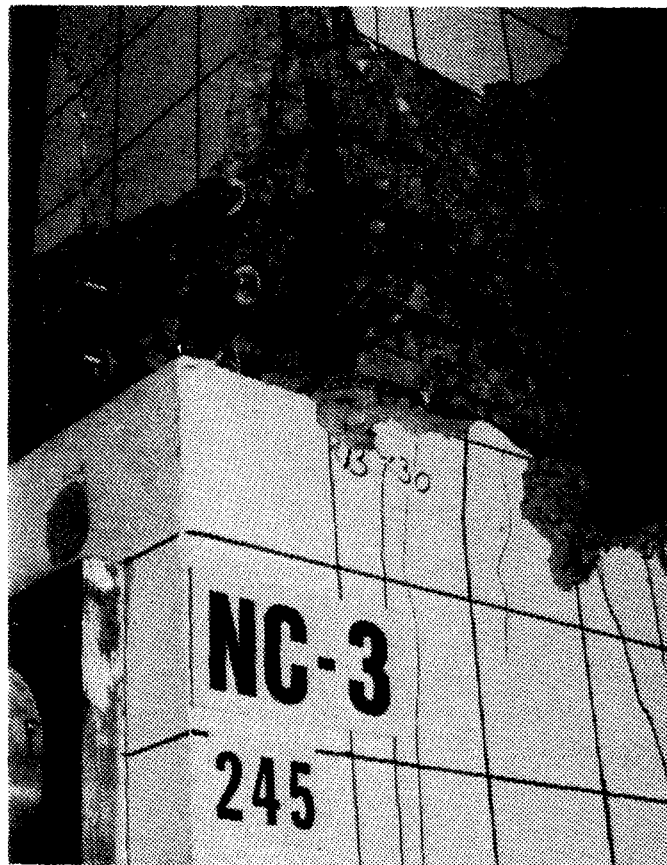
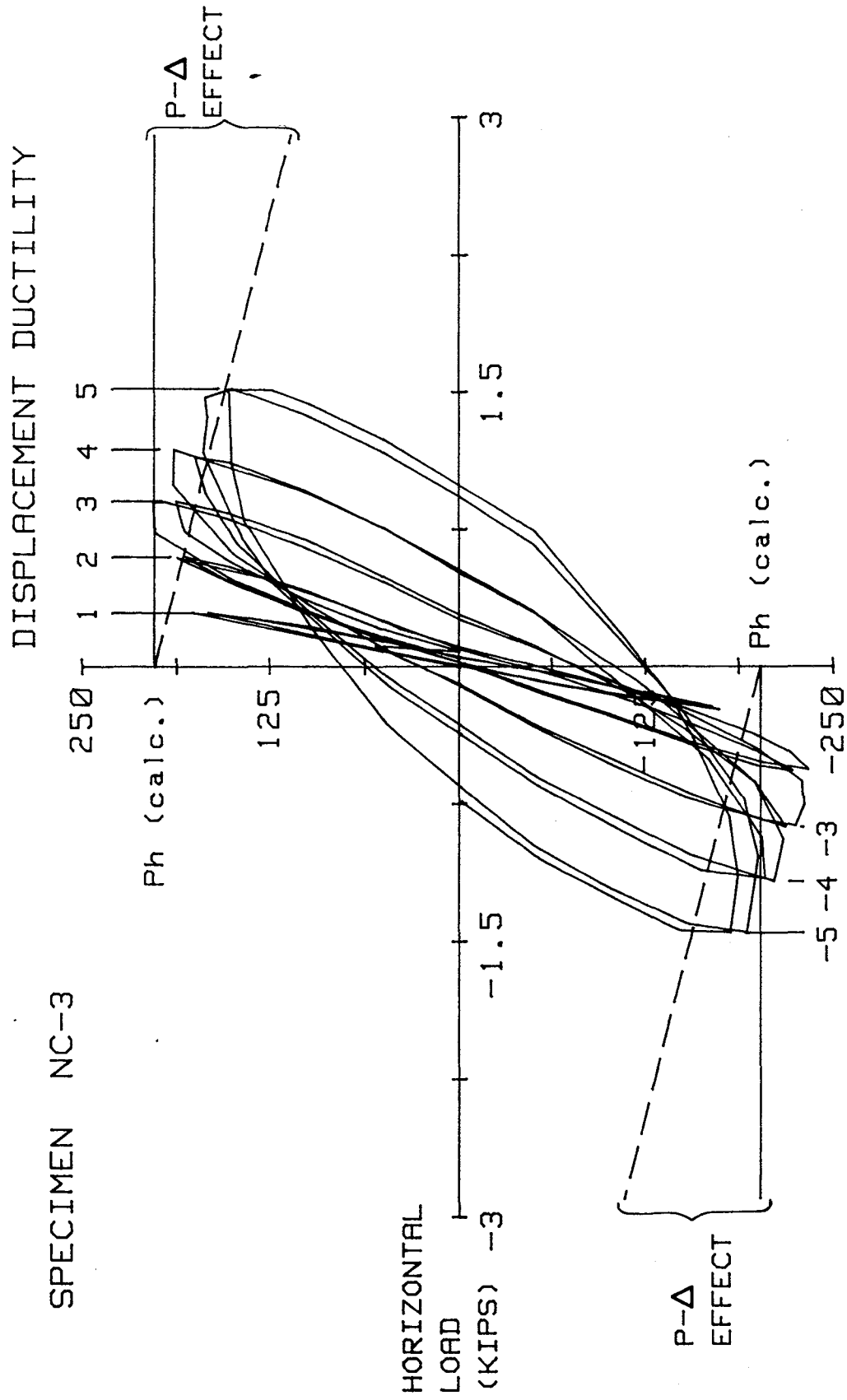


FIG. A-48 TEST SPECIMEN NC-3 AFTER TEST CONCLUSION



SPECIMEN NC-3

Metric Equivalents
 1 in. = 25.4 mm
 1 kip = 4.45 kN

HORIZONTAL DISPLACEMENT (IN.)

FIG. A-49 HORIZONTAL LOAD VERSUS DISPLACEMENT, SPECIMEN NC-3

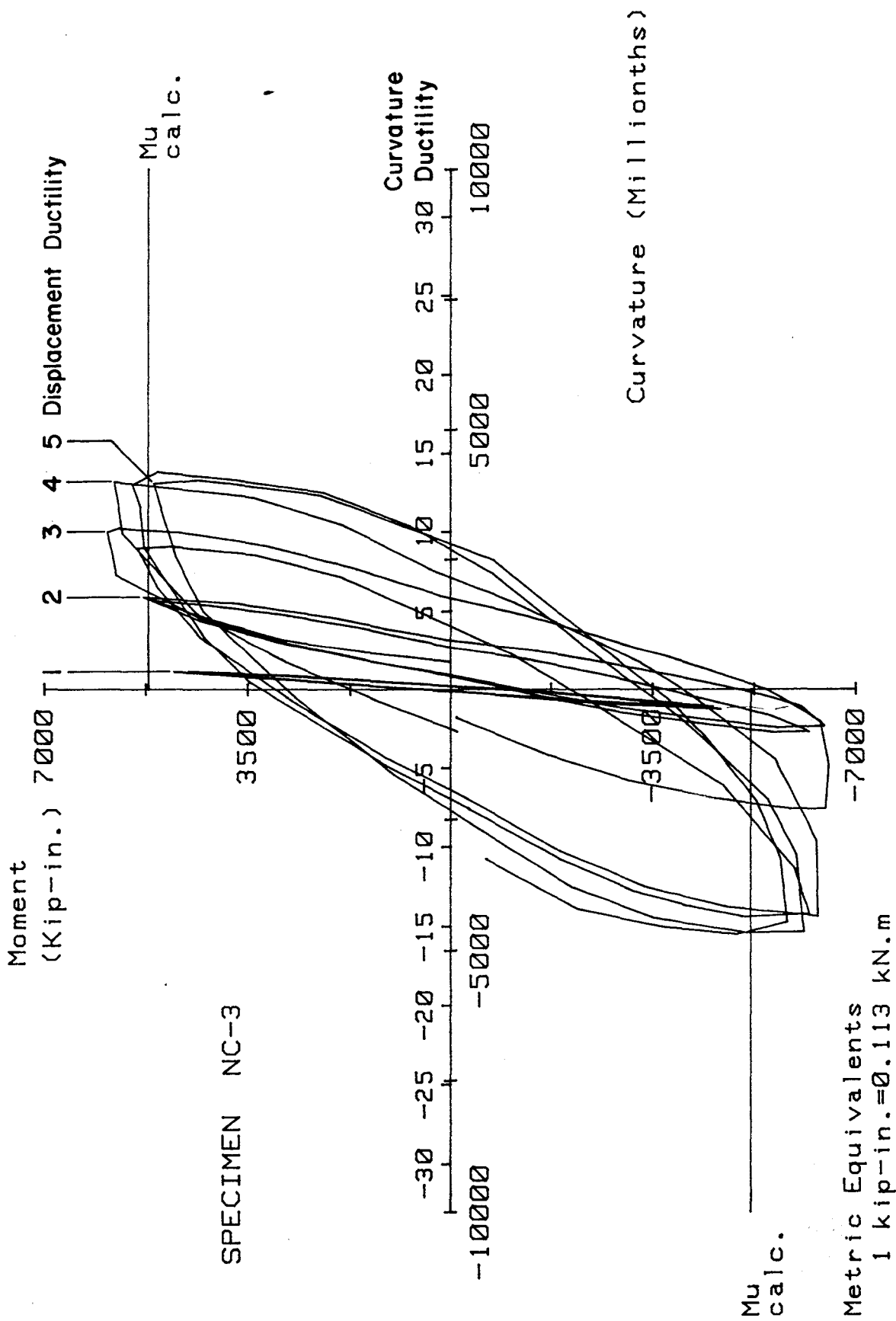


FIG. A-57 MOMENT VERSUS CURVATURE FOR SPECIMEN NC-3

second cycle to the peak moment at the first cycle at various displacement ductility ratios ranged from 0.93 to 0.98. The maximum curvature ductility ratio at the displacement ductility ratio of 5 was 20. This indicates the higher demand on curvature ductility in comparison to displacement ductility for earthquake design of buildings which rely on the post elastic behavior of the structure.

Transverse Reinforcement Strain

Figure 4-11 shows the locations of the strain gages attached to the transverse reinforcements. The results obtained from these strain gages are shown in Figs. A-52 through A-73.

The minimum specified yield strain of the transverse reinforcement was 2070 micro-strain (Grade 60). First yielding was observed on the transverse reinforcement located 6 in. above the stub during cycle #10 ($\mu=4$), at which time strain on the peripheral hoops and interior hoops was 3746 and 2173 micro-strain, respectively.

In general, at large displacement levels the strain on the peripheral hoops was larger than the strains on the interior hoops. For instance, at the peak of the reversal loading cycle #11 ($\mu=4$), maximum strain on the peripheral hoops and interior hoops located 6 in. above the stub was 8980 and 2790 micro-strain, respectively. The ratio of peripheral hoop strain to interior hoop strain was variable at different locations and displacement levels.

In general, strain on the peripheral and interior hoops located 2 in. above the stub was smaller than the strain on the transverse reinforcement located 6 and 10 in. above the stub.

Peripheral and interior hoops located 22 in. above the stub experienced the least strains.

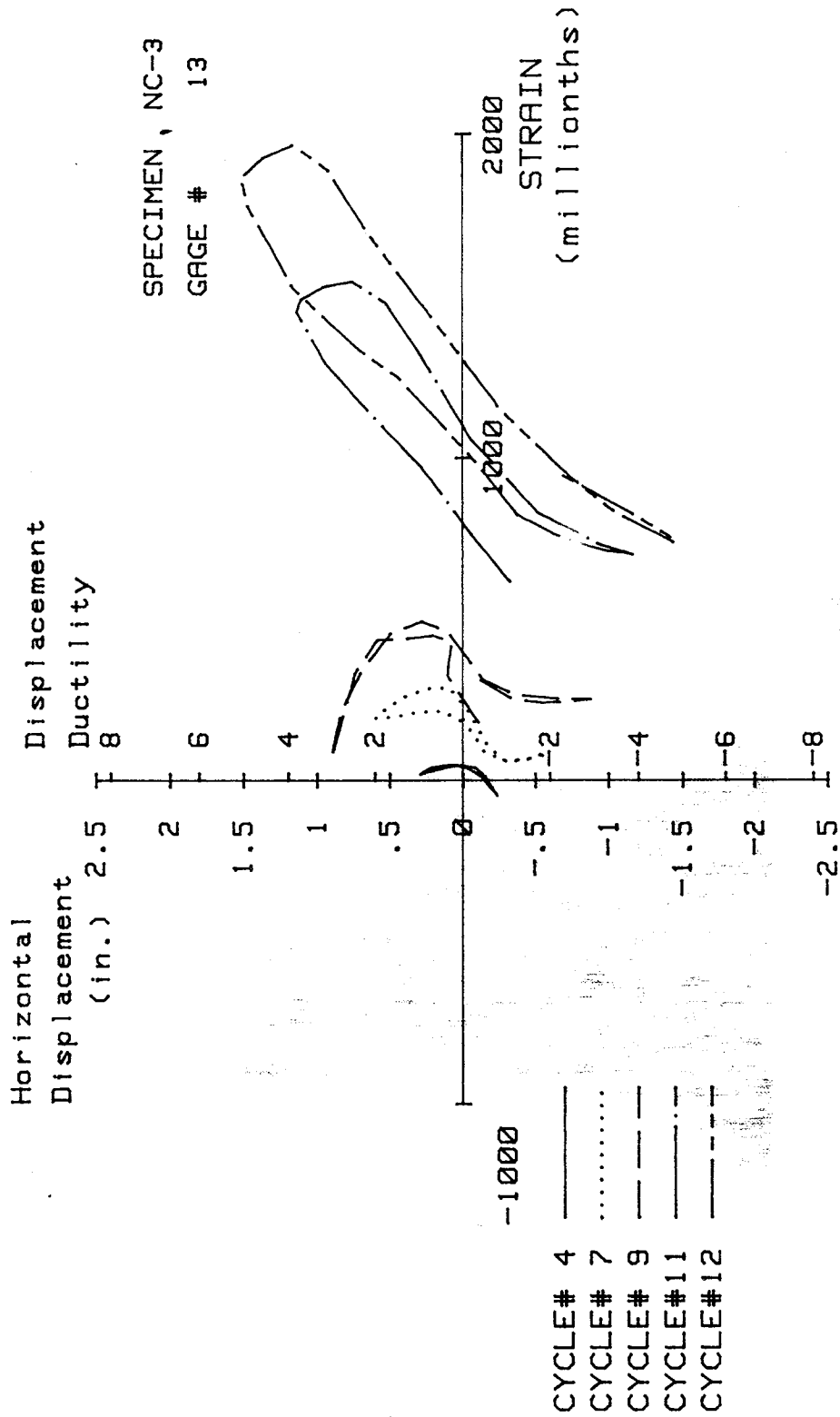


FIG. A-52 MEASURED STRAIN, GAGE #13, SPECIMEN NC-3

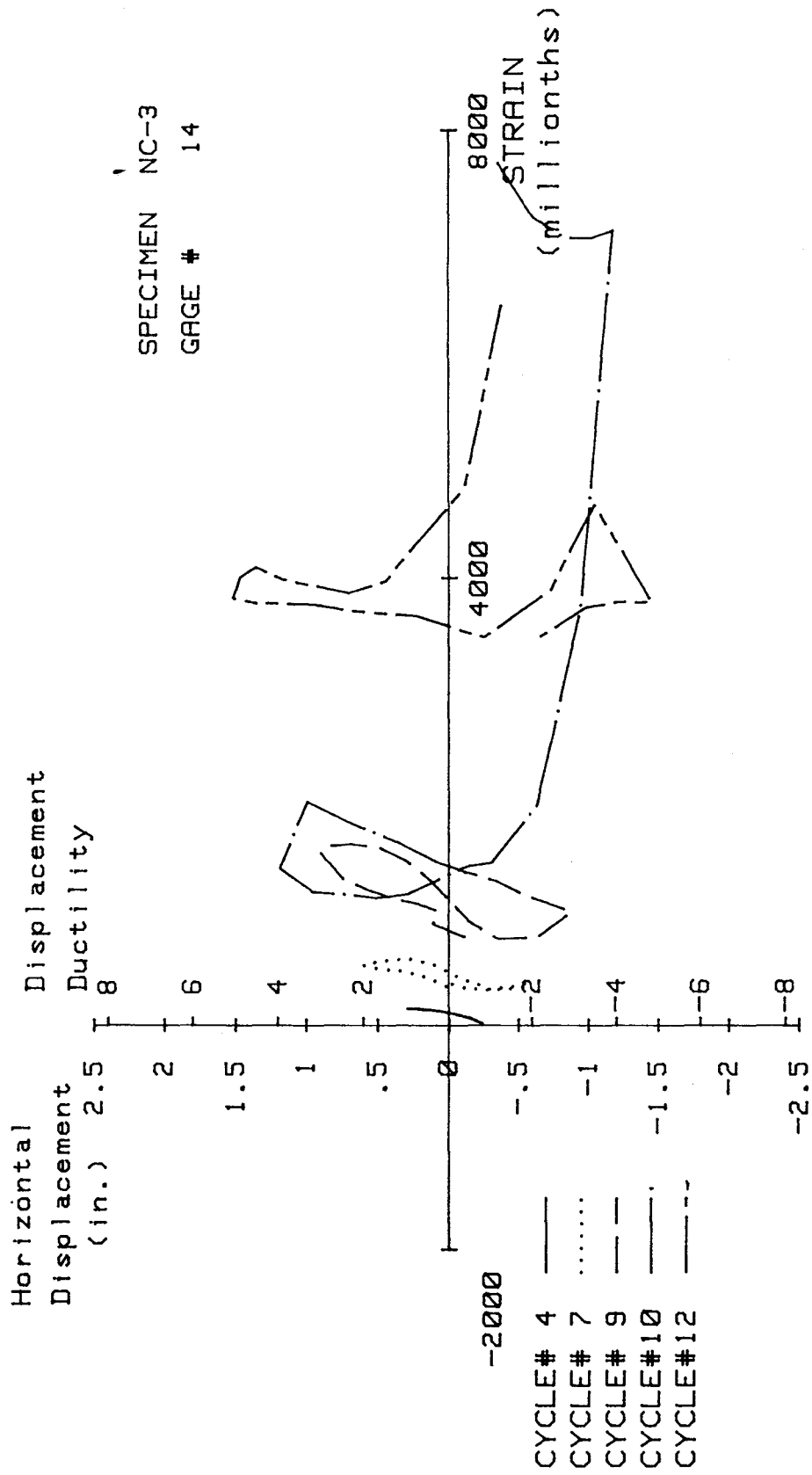


FIG. A-53 MEASURED STRAIN, GAGE #14, SPECIMEN NC-3

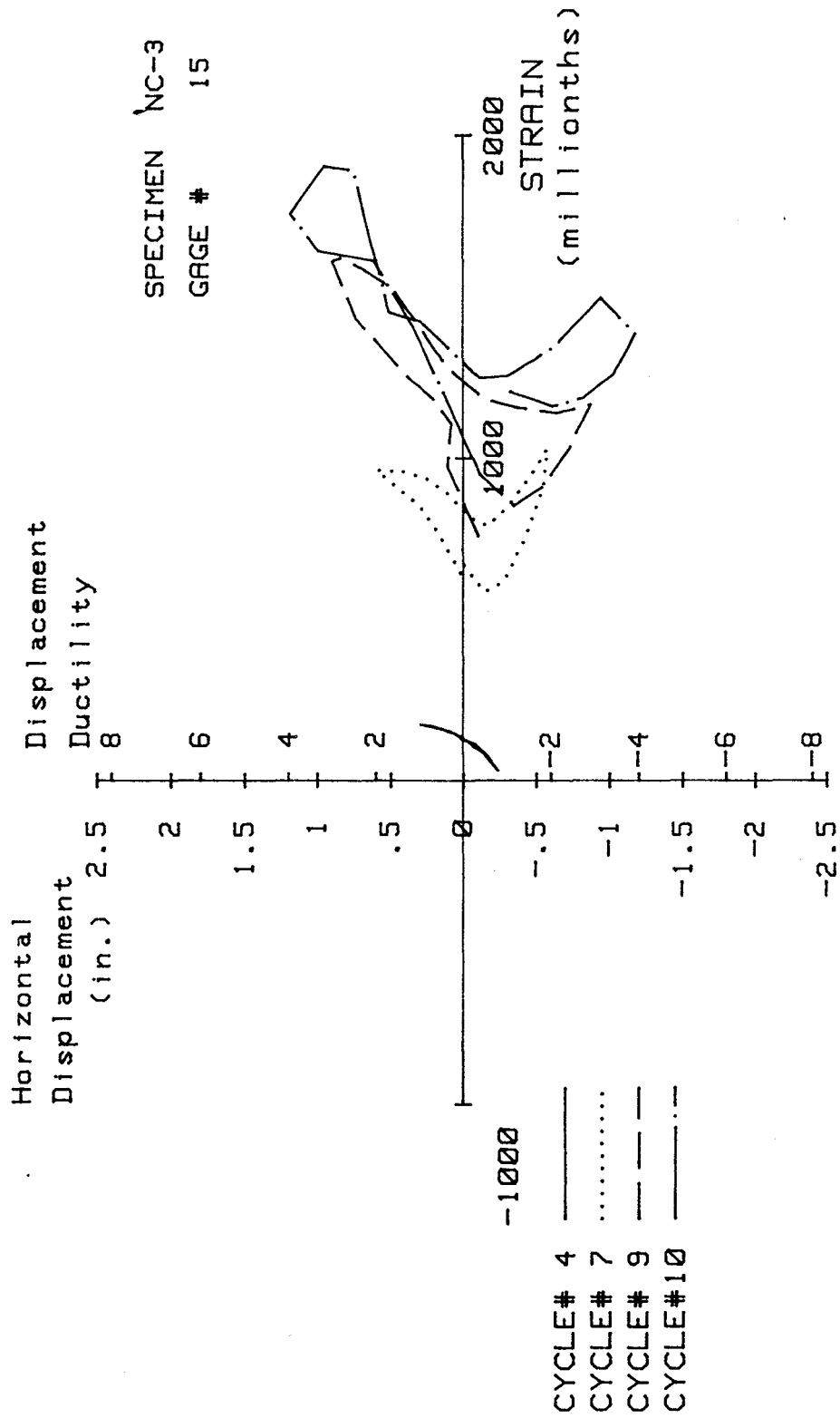


FIG. A-54 MEASURED STRAIN, GAGE #15, SPECIMEN NC-3

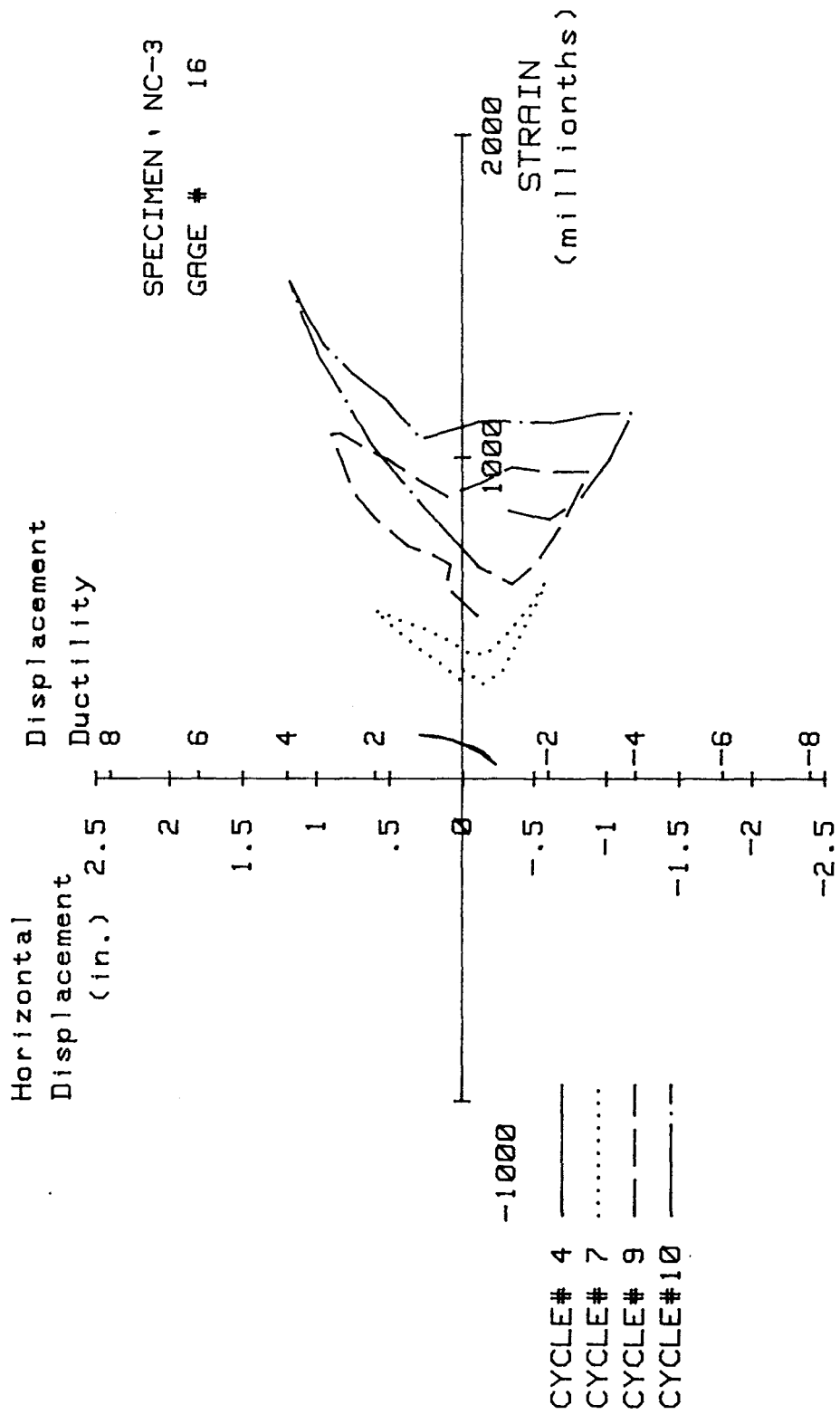


FIG. A-55 MEASURED STRAIN, GAGE #16, SPECIMEN NC-3

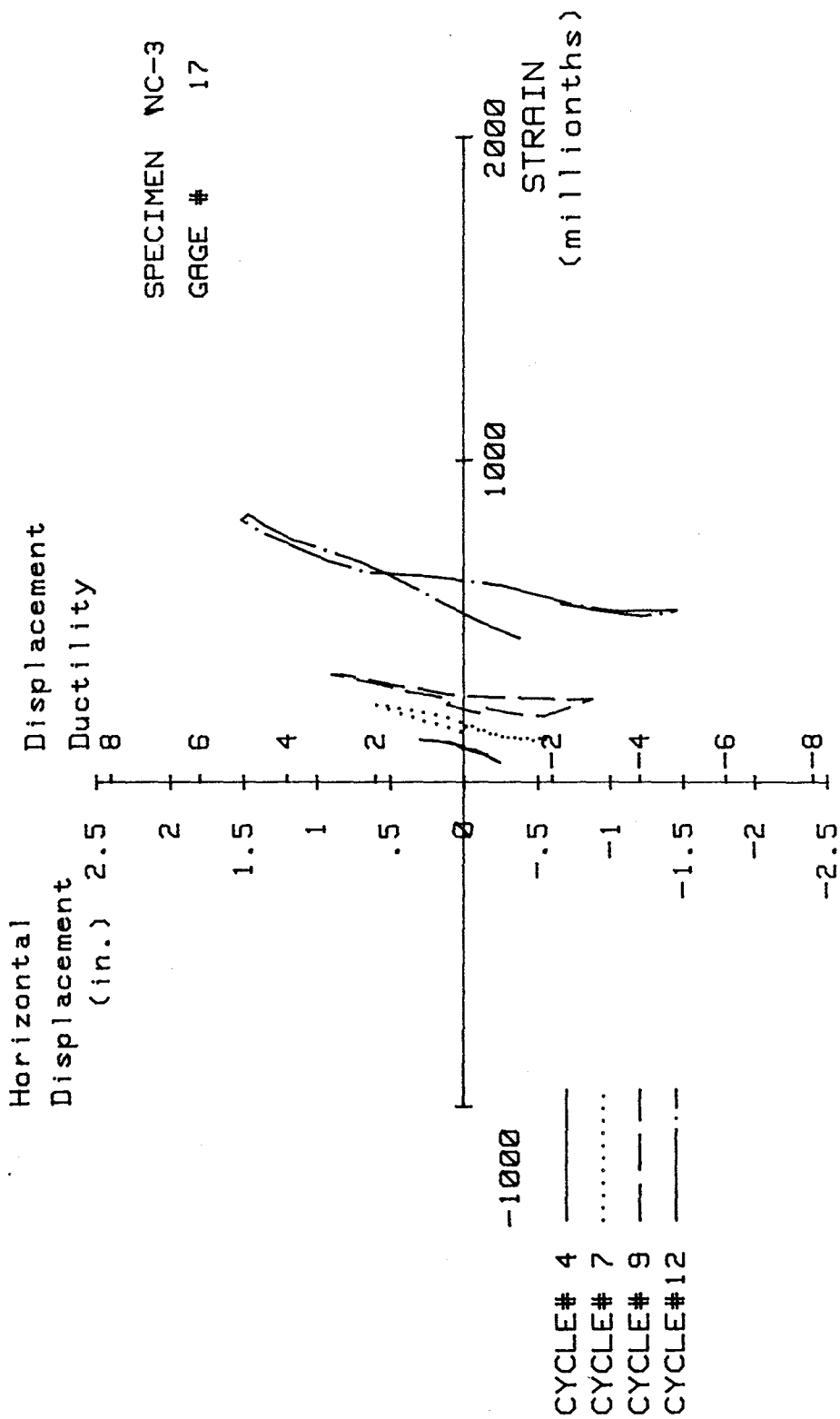


FIG. A-56 MEASURED STRAIN, GAGE #17, SPECIMEN NC-3

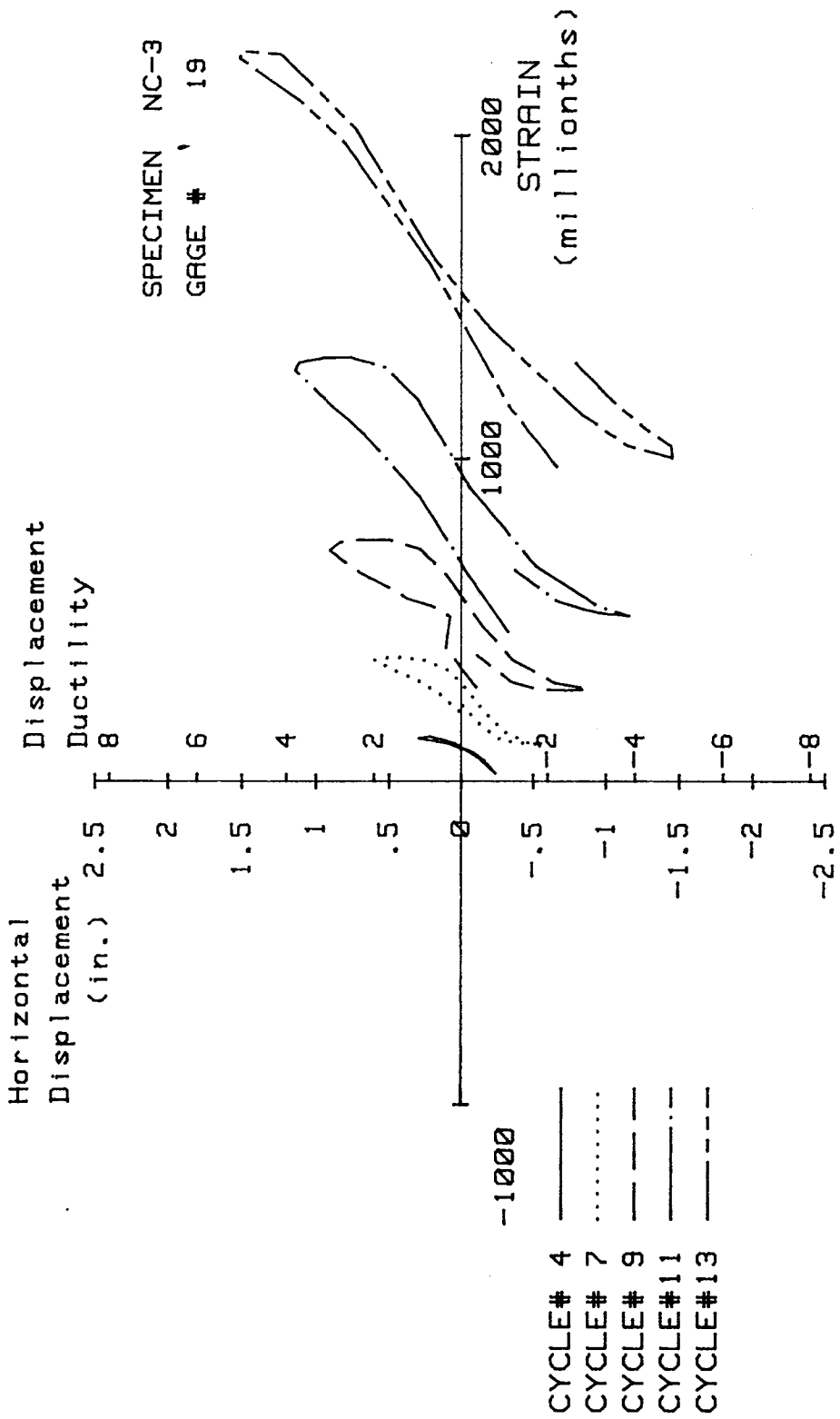


FIG. A-57 MEASURED STRAIN, GAGE #19, SPECIMEN NC-3

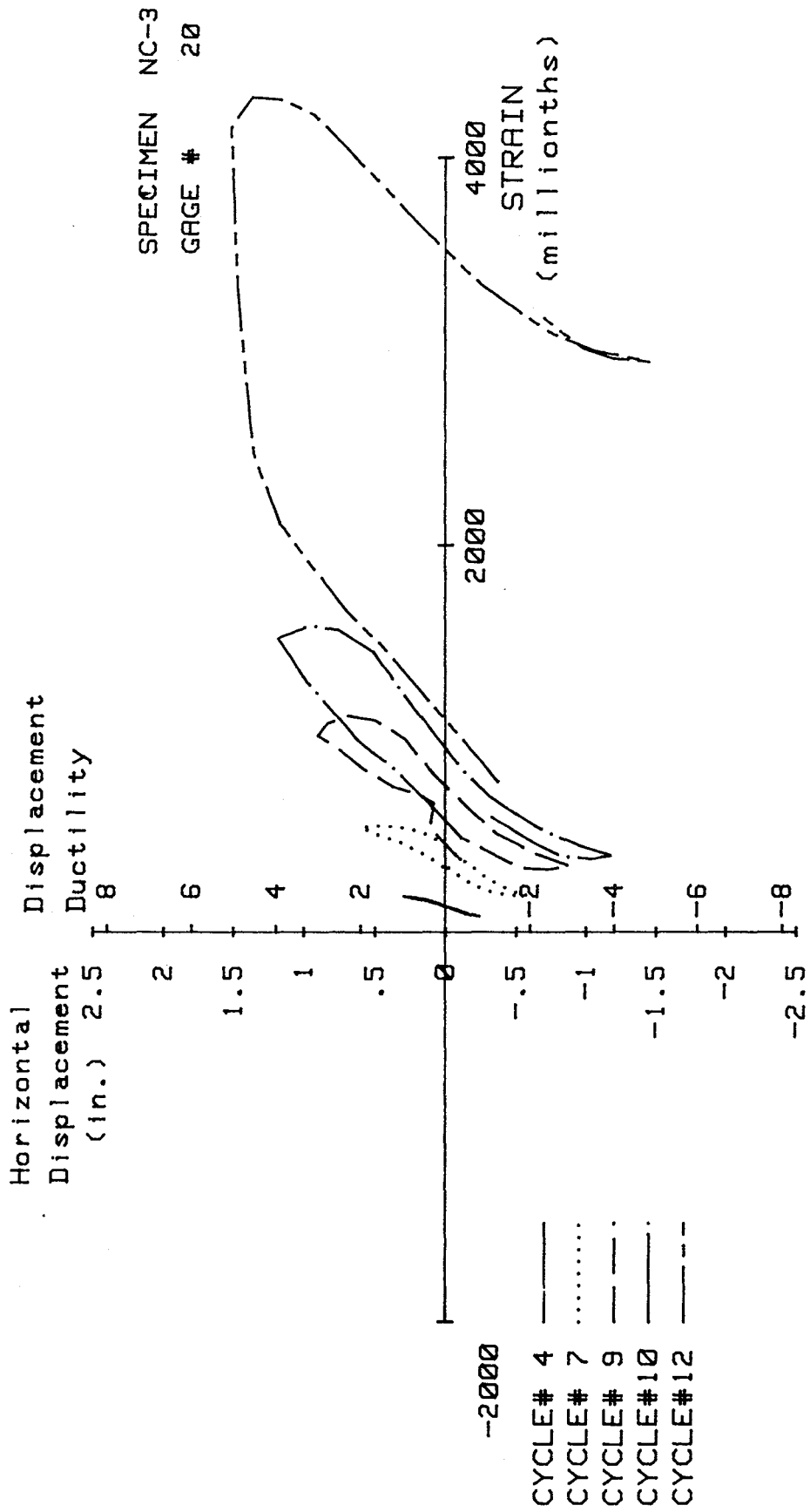


FIG. A-58 MEASURED STRAIN, GAGE #20, SPECIMEN NC-3

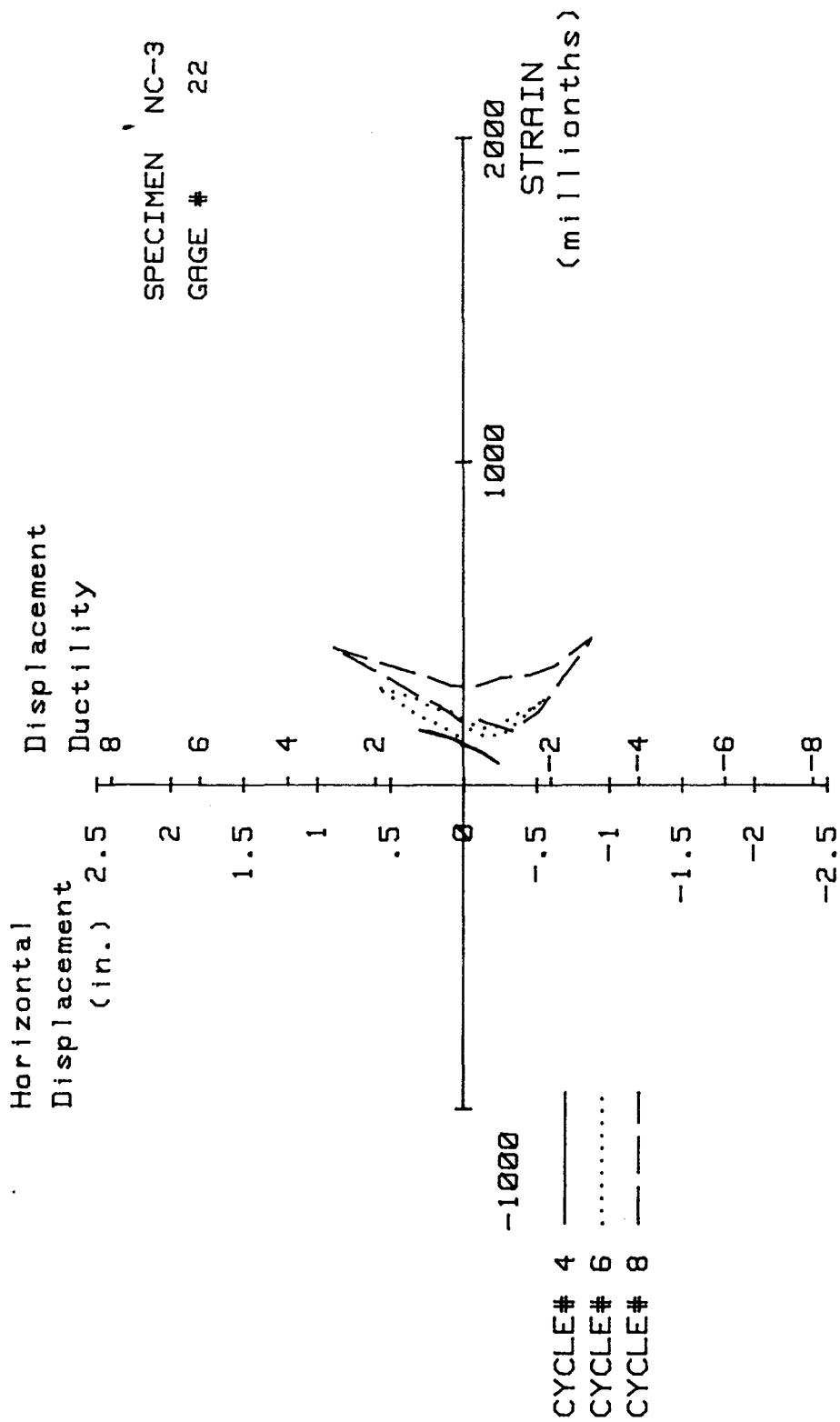


FIG. A-59 MEASURED STRAIN, GAGE #22, SPECIMEN NC-3

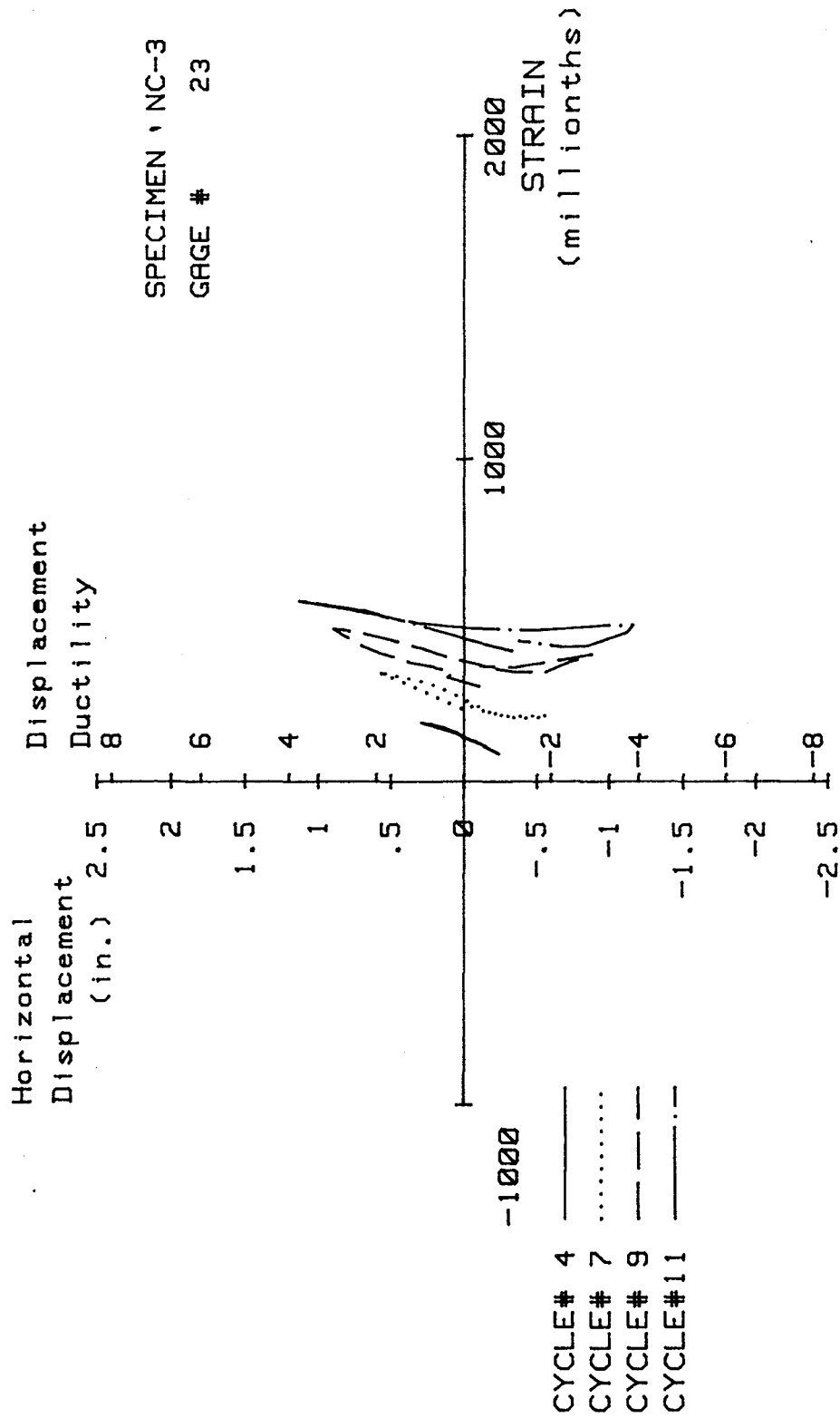


FIG. A-60 MEASURED STRAIN, GAGE #23, SPECIMEN NC-3

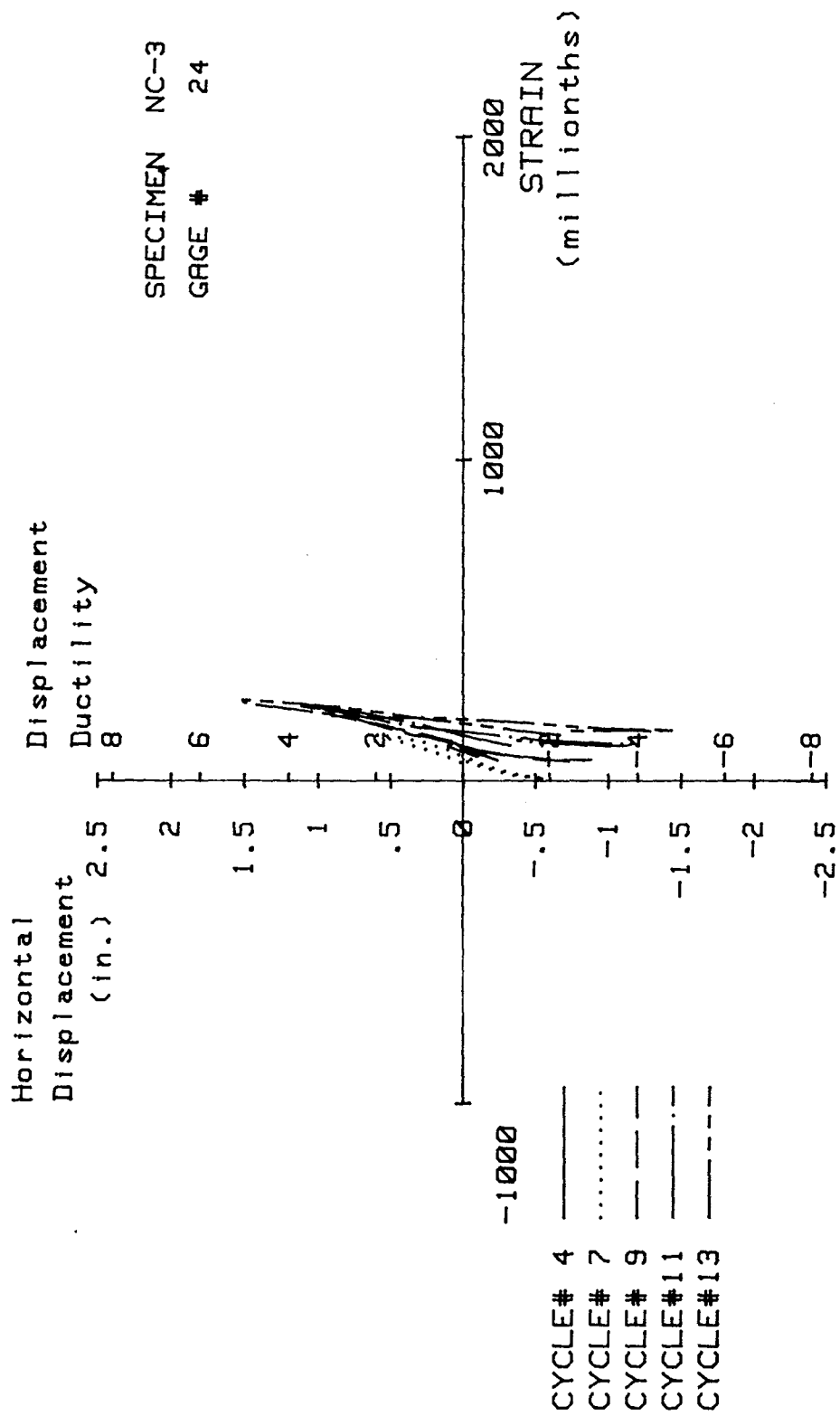


FIG. A-61 MEASURED STRAIN, GAGE #24, SPECIMEN NC-3

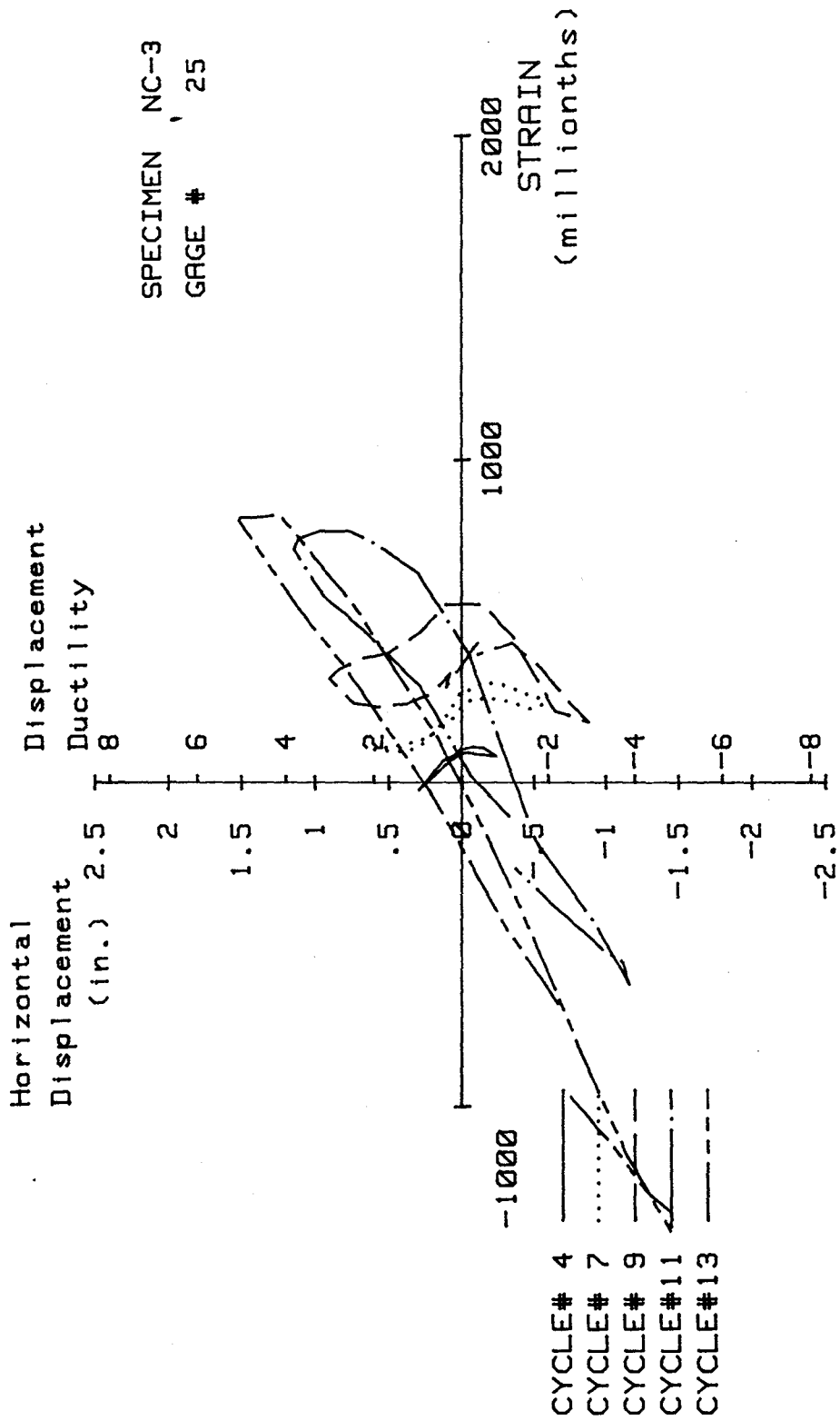


FIG. A-62 MEASURED STRAIN, GAGE #25, SPECIMEN NC-3

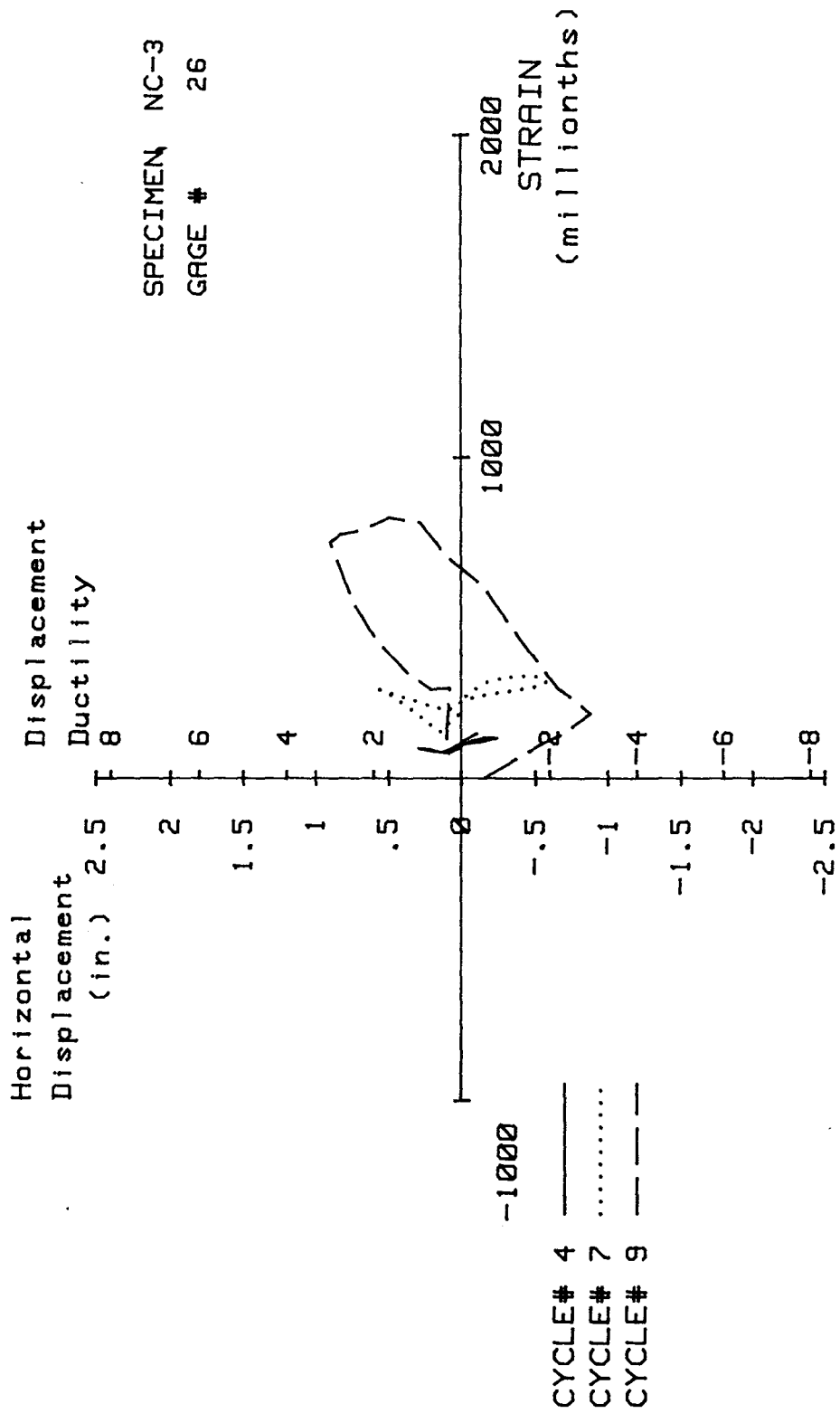


FIG. A-63 MEASURED STRAIN, GAGE #26, SPECIMEN NC-3

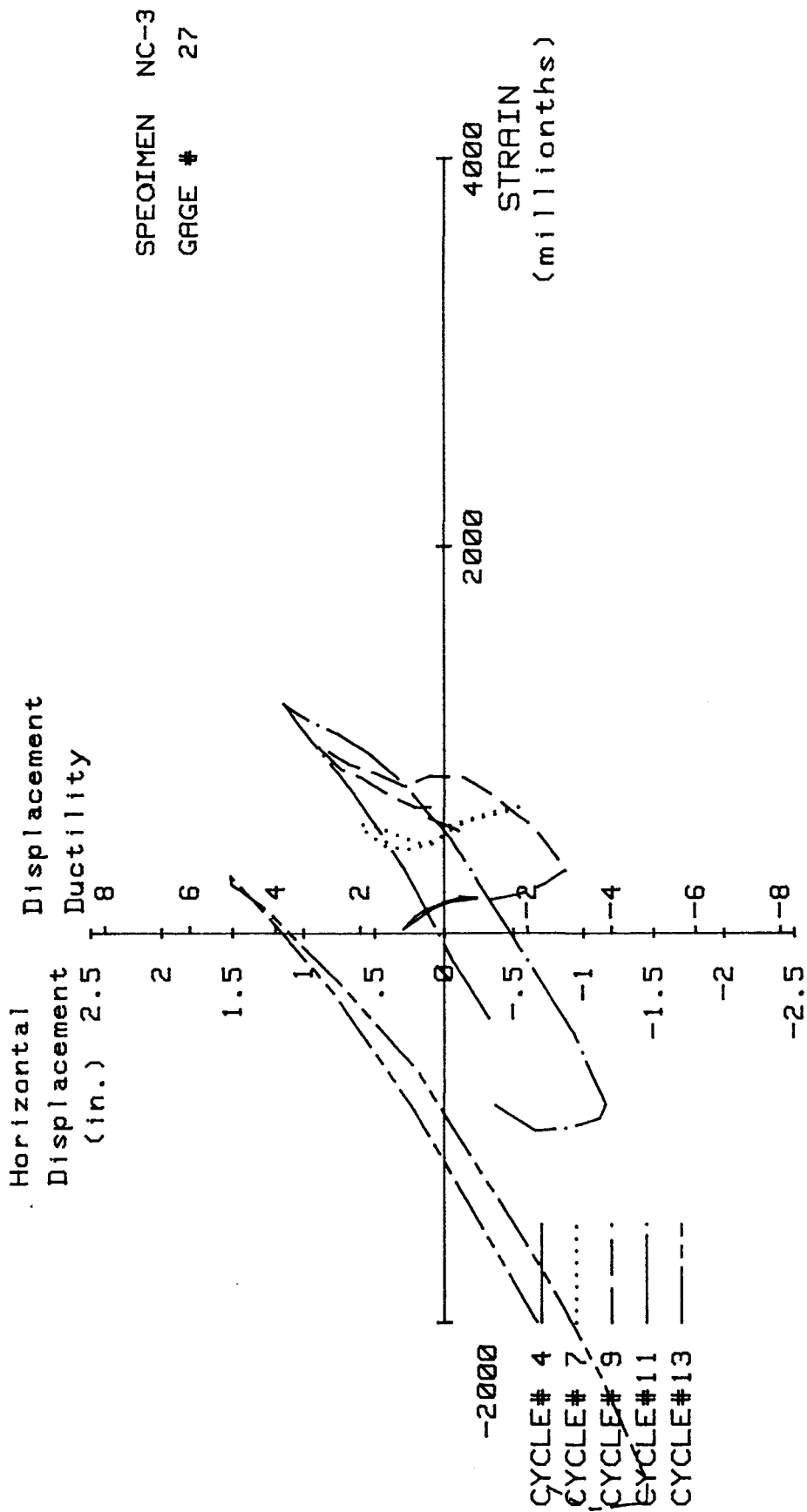


FIG. A-64 MEASURED STRAIN, GAGE #27, SPECIMEN NC-3

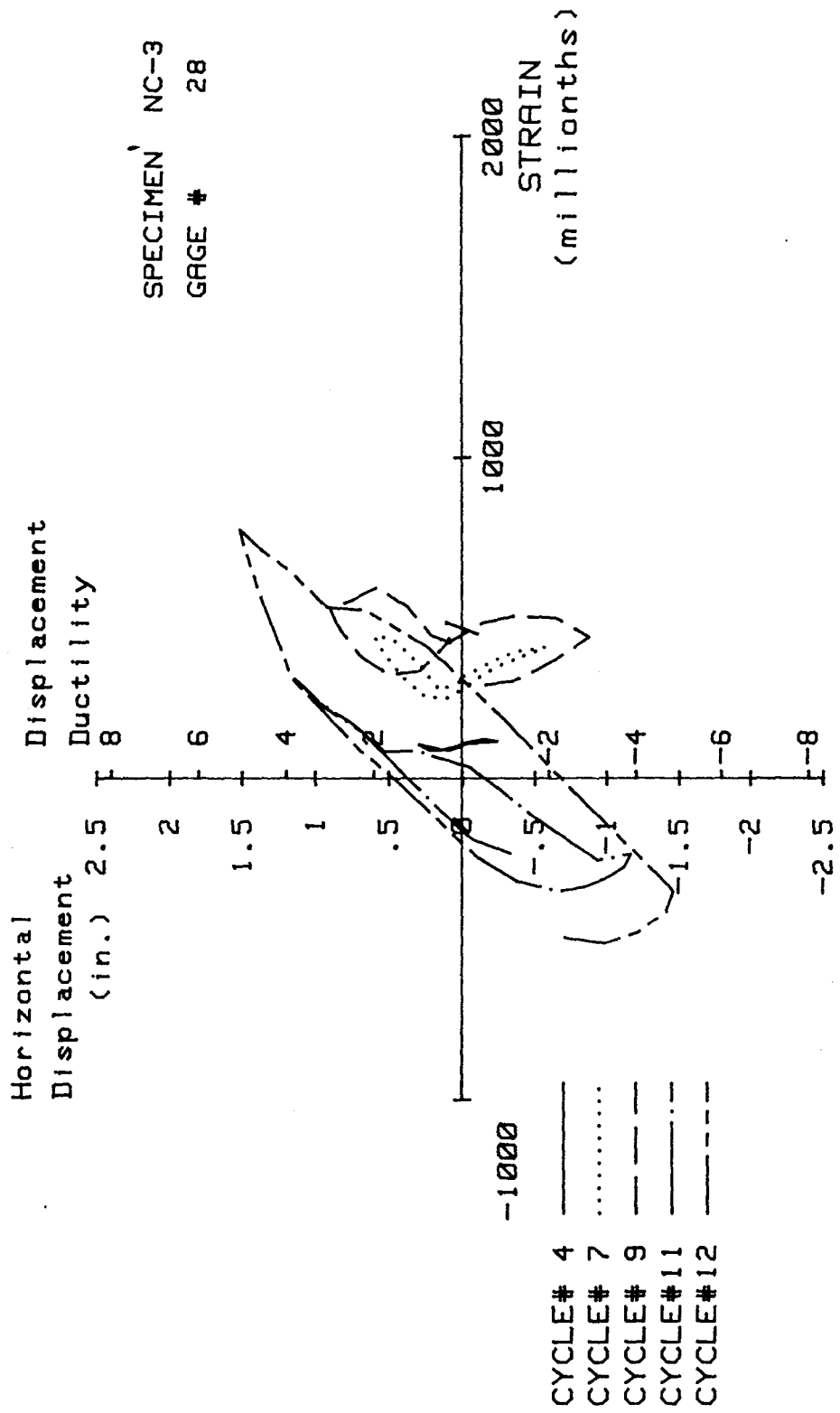


FIG. A-65 MEASURED STRAIN, GAGE #28, SPECIMEN NC-3

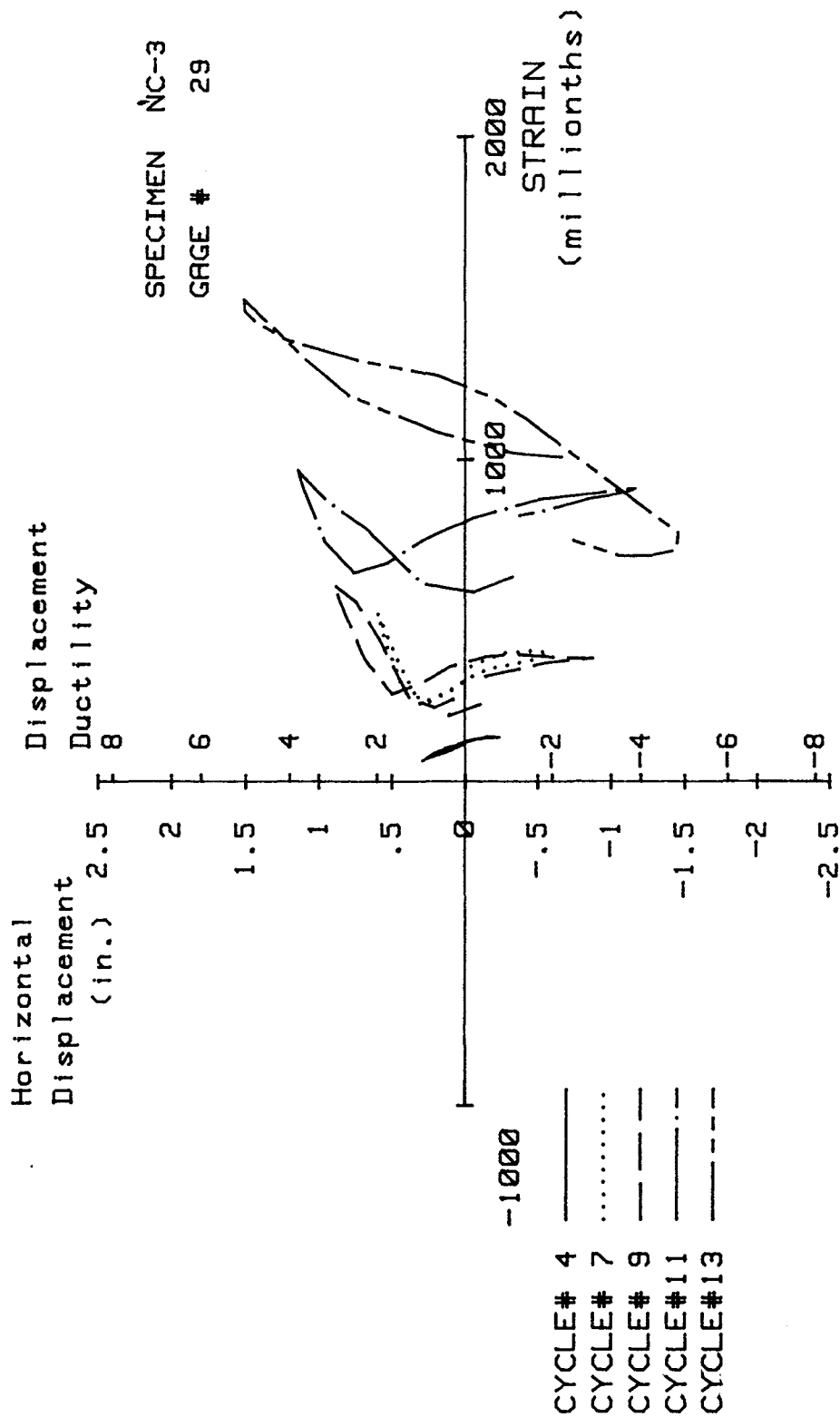


FIG. A-66 MEASURED STRAIN, GAGE #29, SPECIMEN NC-3

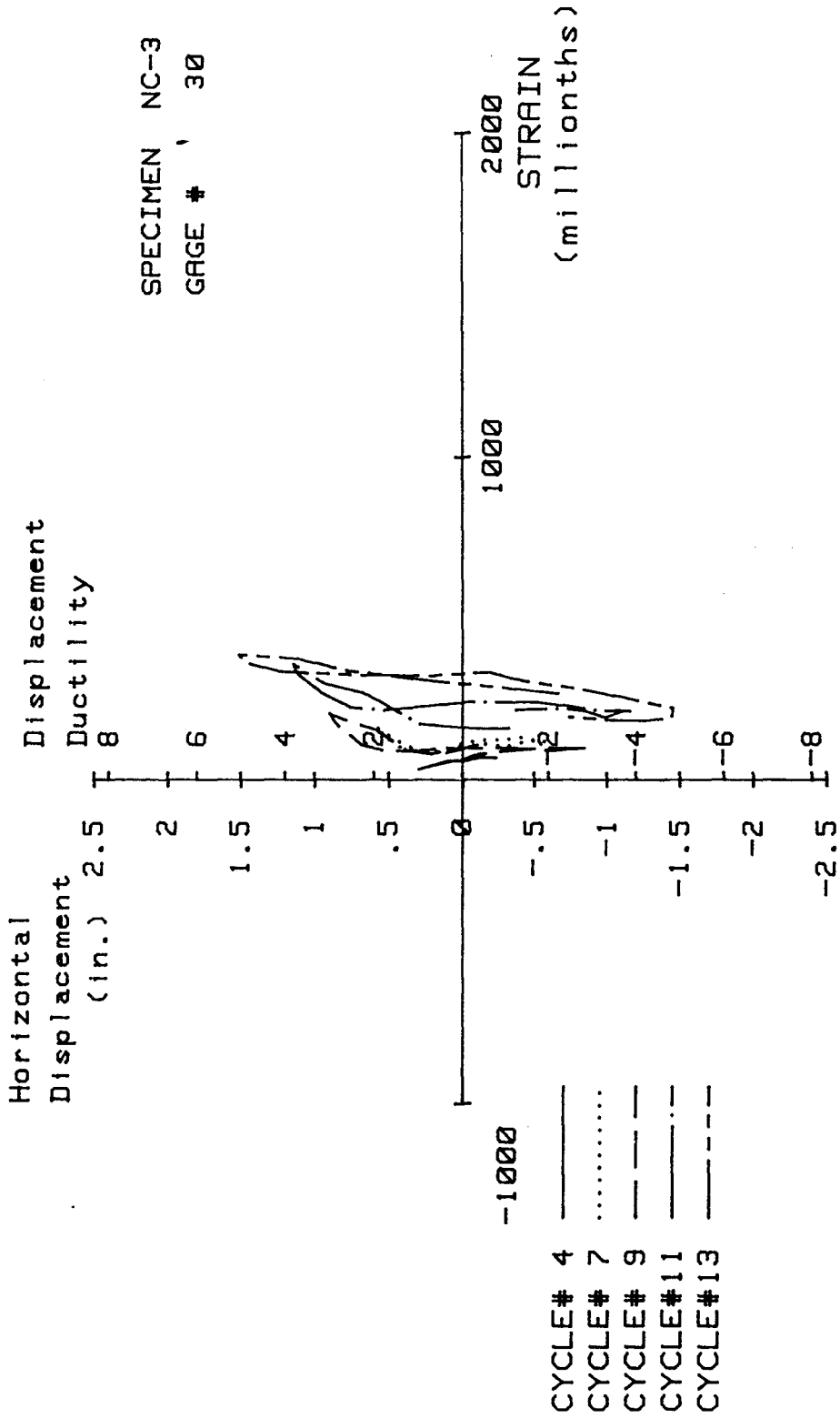


FIG. A-67 MEASURED STRAIN, GAGE #30, SPECIMEN NC-3

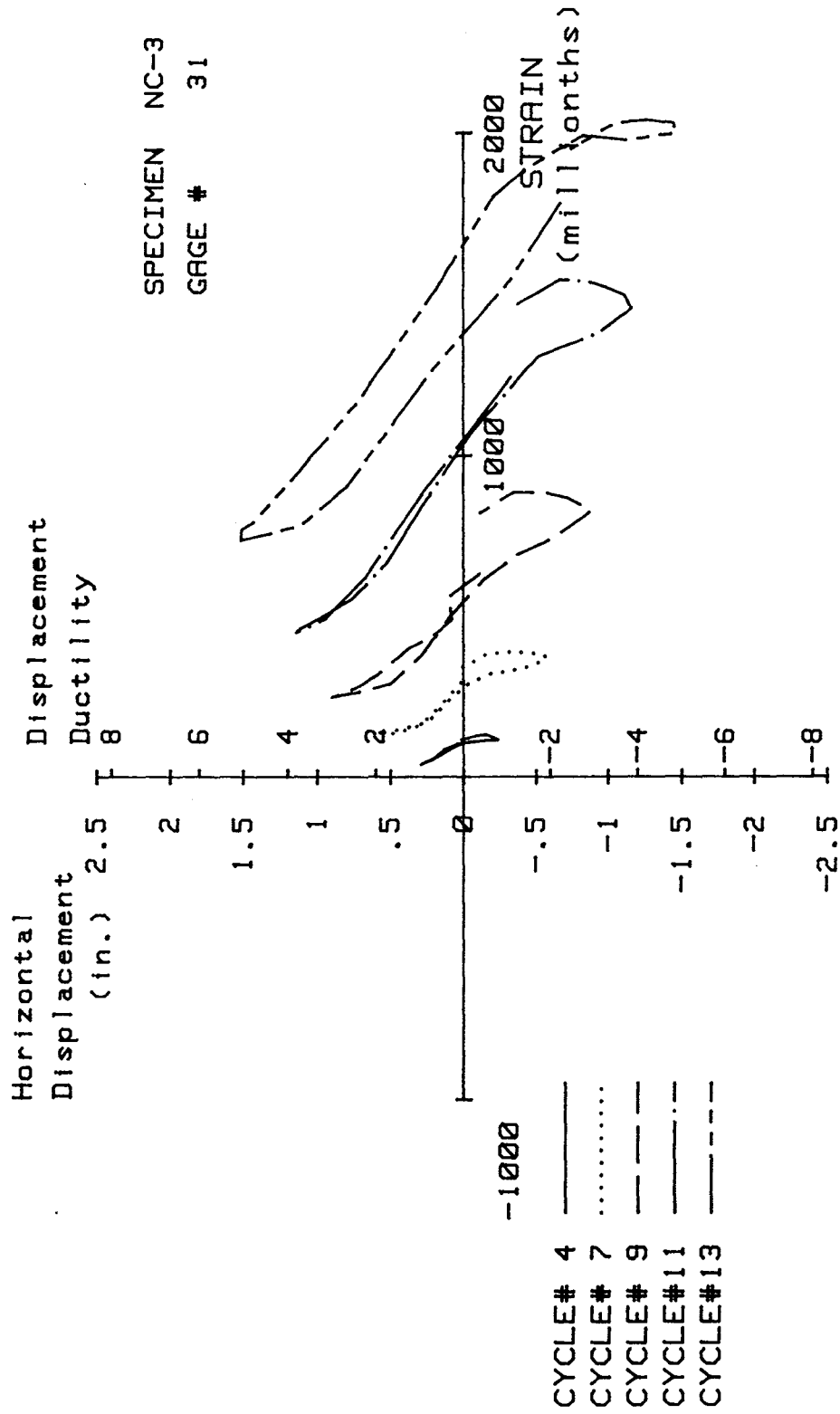


FIG. A-68 MEASURED STRAIN, GAGE #31, SPECIMEN NC-3

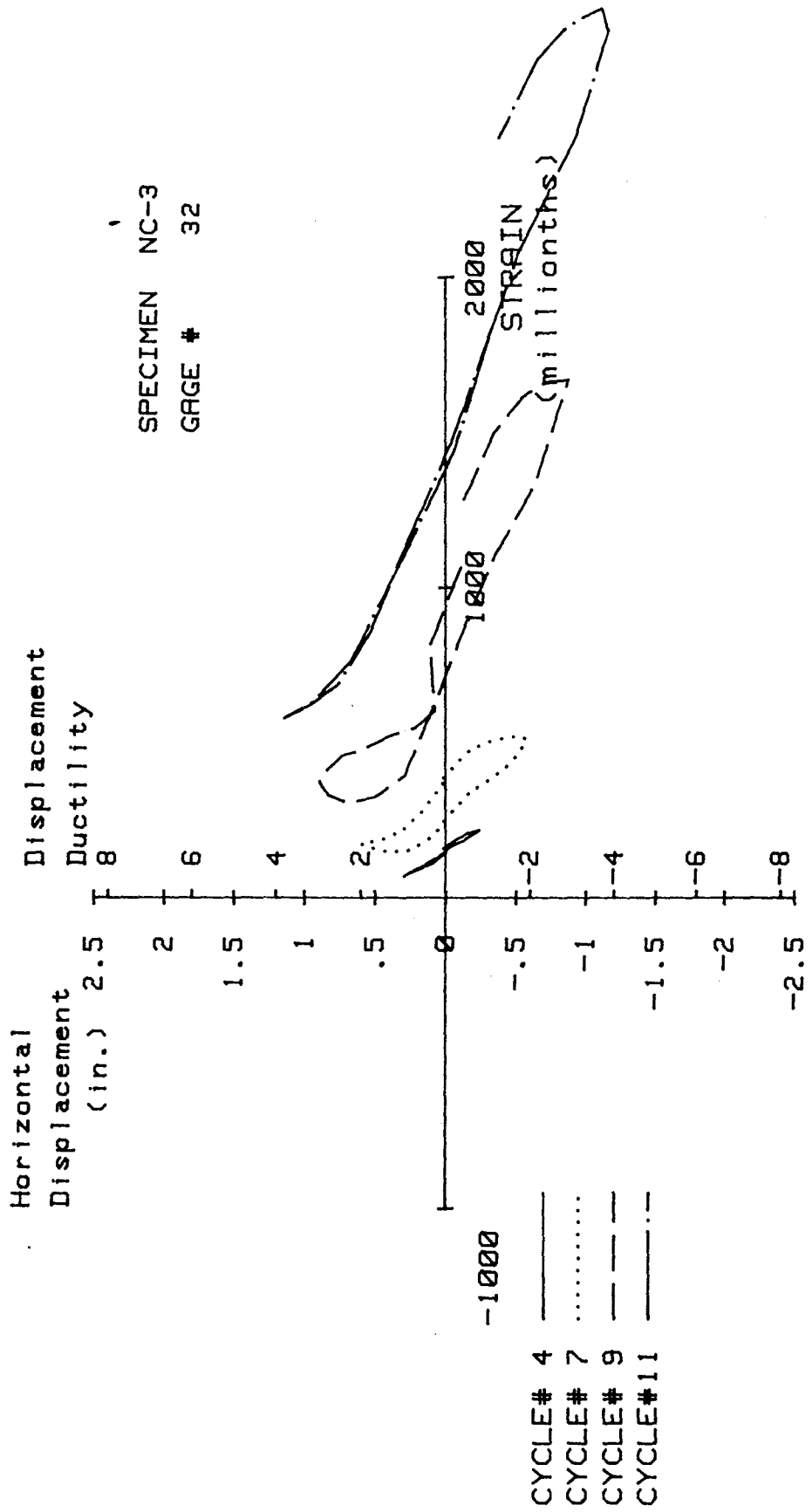


FIG. A-69 MEASURED STRAIN, GAGE #32, SPECIMEN NC-3

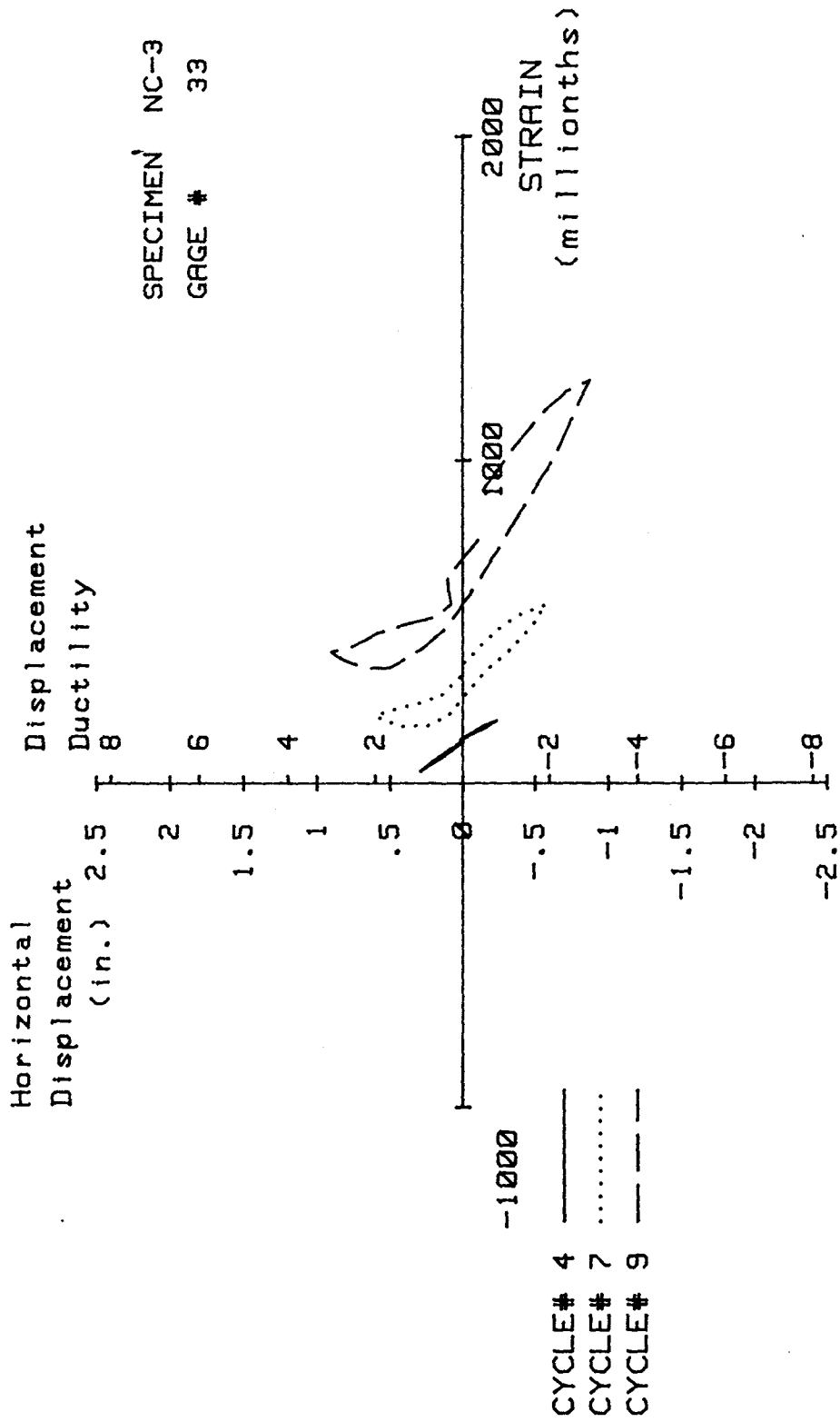


FIG. A-70 MEASURED STRAIN, GAGE #33, SPECIMEN NC-3

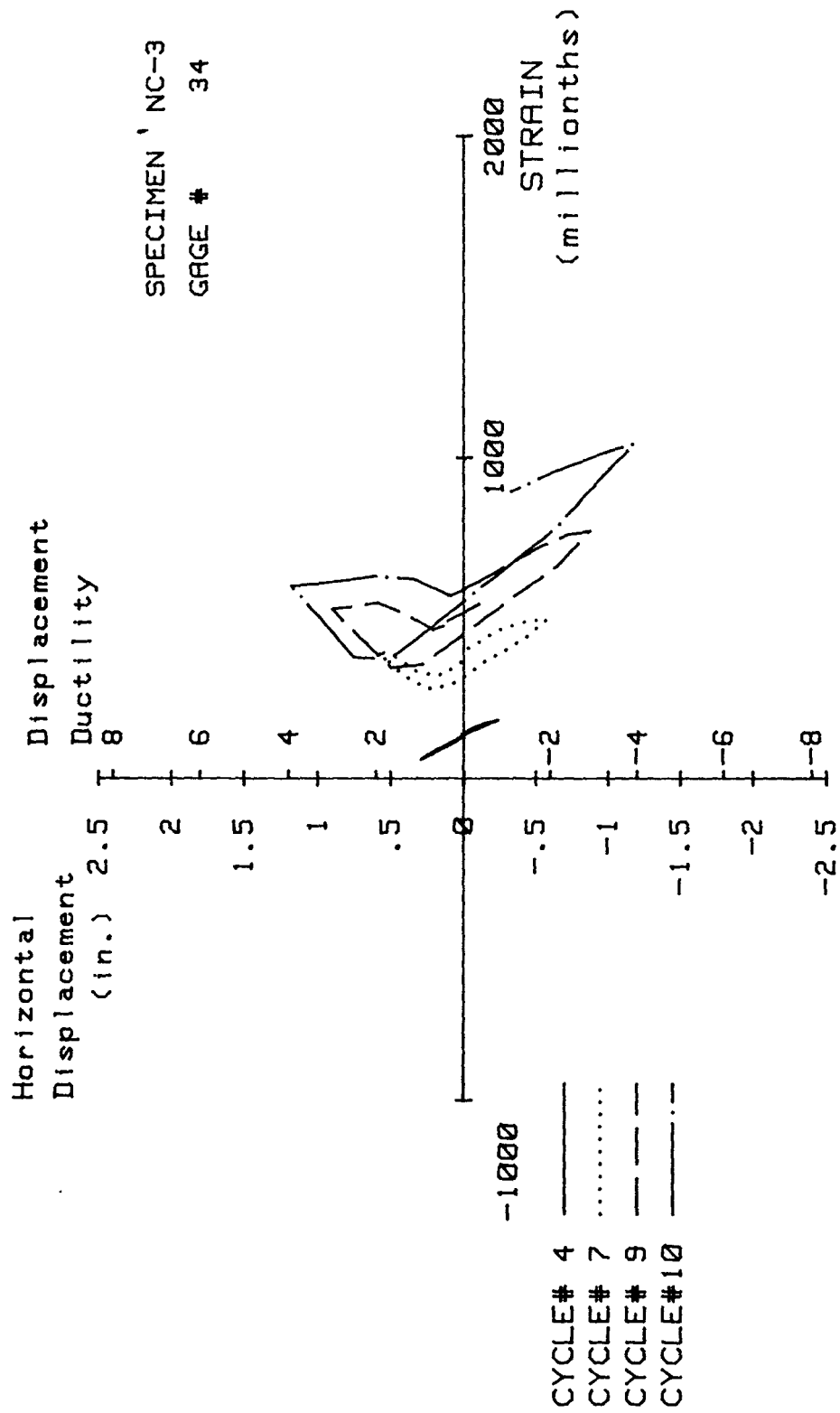


FIG. A-71 MEASURED STRAIN, GAGE #34, SPECIMEN NC-3

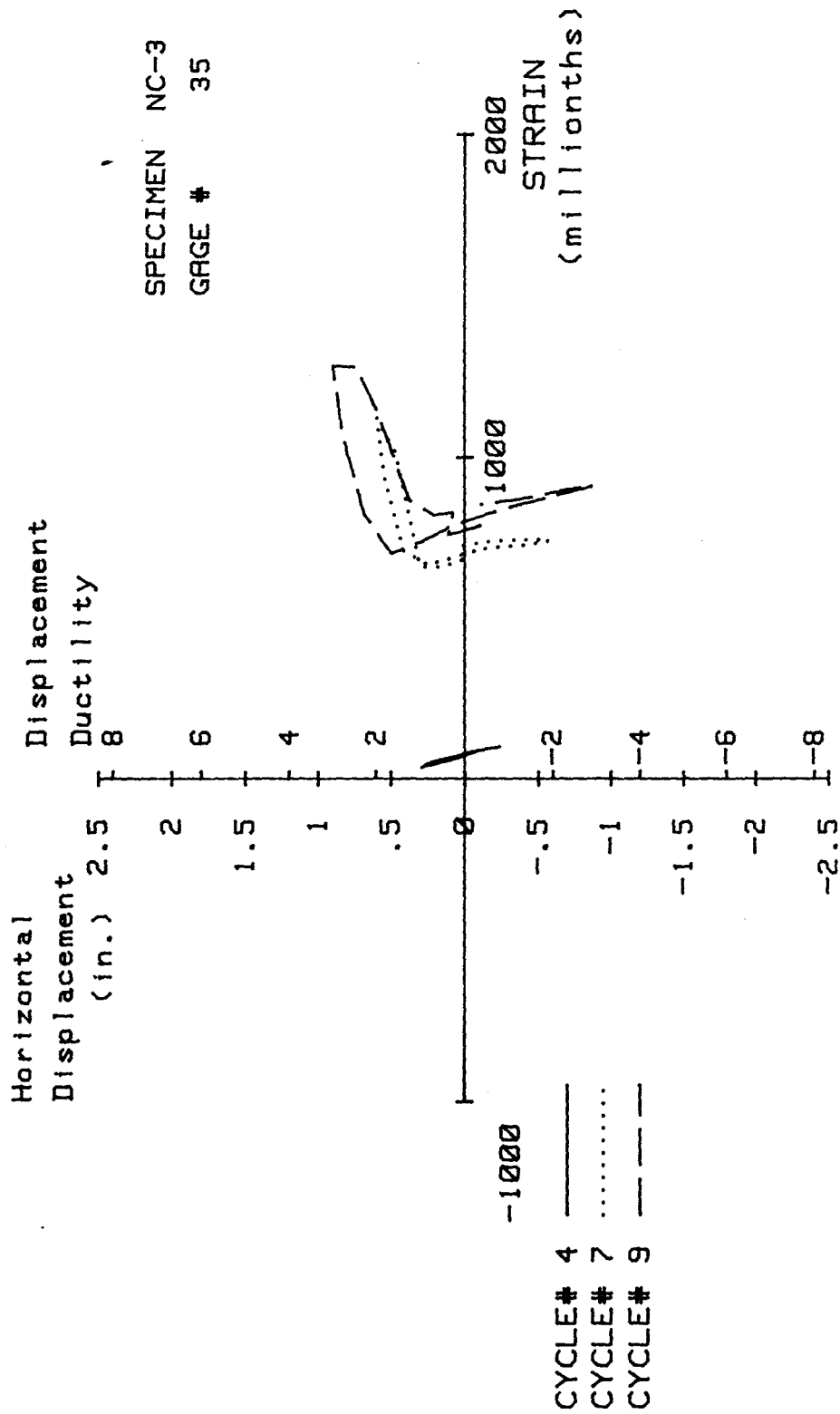


FIG. A-72 MEASURED STRAIN, GAGE #35, SPECIMEN NC-3

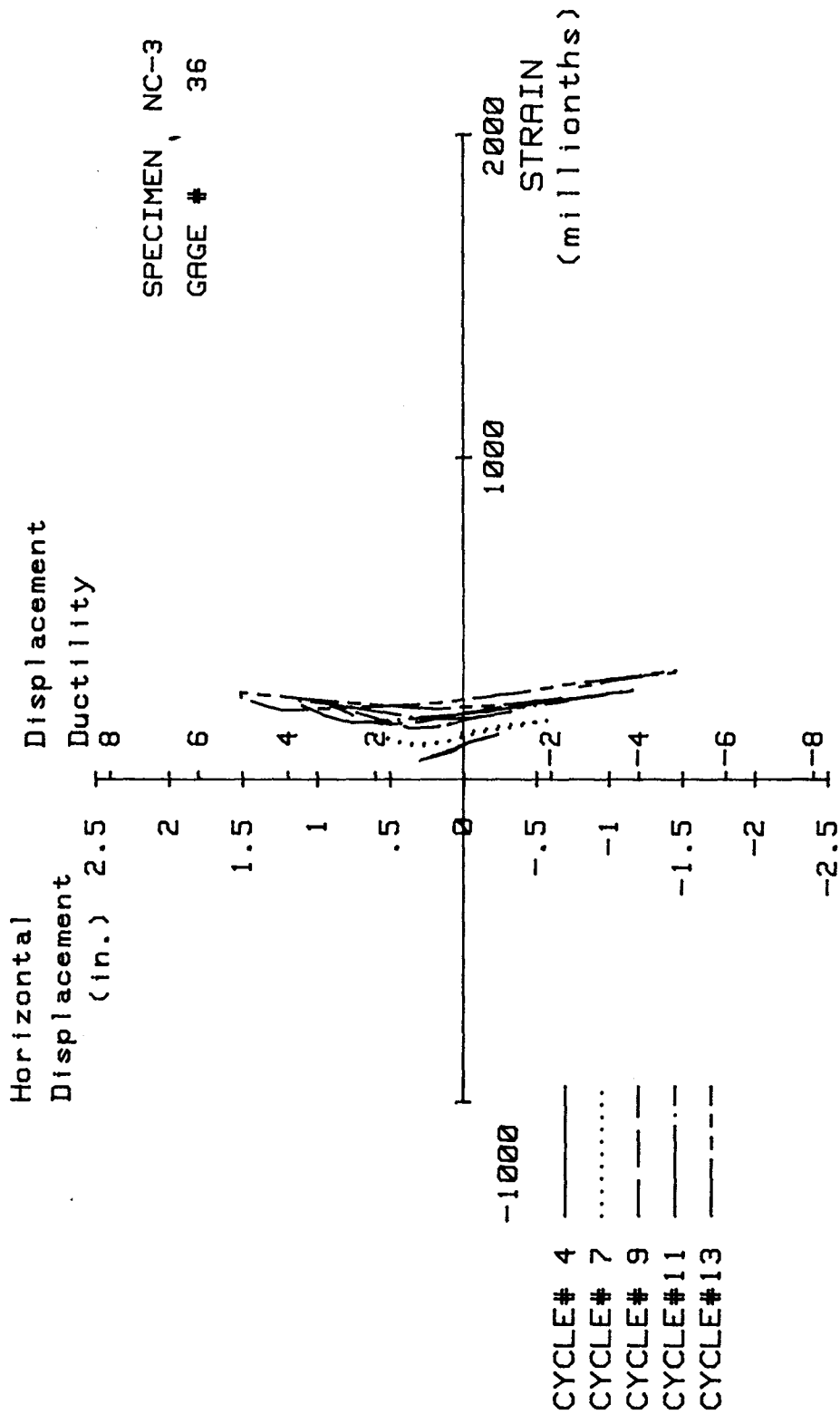


FIG. A-73 MEASURED STRAIN, GAGE #36, SPECIMEN NC-3

Specimen NC-4

Transverse Reinforcement Detail

Transverse reinforcement detail for Specimen NC-4 was similar to details used in Specimens NC-2 and NC-3 except that #3 bars were used for both the peripheral and interior hoops. Figure 4-2b shows the transverse reinforcement used in Specimen NC-4. The area of transverse reinforcement was 0.38 in.^2 , which corresponds to a volumetric ratio, ρ , of 1.26%. The area of the transverse reinforcement provided was 47% of the area required by ACI-318-83 Code.

Load History

The applied axial load was 580 kips, equivalent to 30% of the column axial load capacity. Figure A-74 shows the history of the applied horizontal load. A total of 11 complete cycles of horizontal loading was applied to the specimen before failure. The first yield displacement and the yield curvature were found to be 0.3 in. and $159 \times 10^{-6} \text{ in.}^{-1}$, respectively. The maximum displacement ductility ratio for Specimen NC-4 was five.

Test Observations

The first hairline cracks in the upper columns were observed during cycle #2. These cracks formed at the junction of the upper column and the stub and at 10 and 17 in. above the stub. Figure A-75 shows the specimen at cycle #3 ($\mu=1$). At the end of cycle #4 ($\mu=2$), hairline cracks had formed to a distance 30 in. above the stub. Some crushing of the cover concrete at the junction of the upper column and the stub was apparent at the end of cycle #5 ($\mu=2$) (see Fig. A-76).

Figure A-77 shows the specimen at the end of cycle #7 ($\mu=3$) where cover concrete had spalled to approximately 6 in. above the stub. However, no longitudinal or transverse reinforcement was visible at this point. Increasing the horizontal displacement ductility ratio to four resulted in more visible damage to the region just 6 in. above the stub as shown in Fig. A-78).

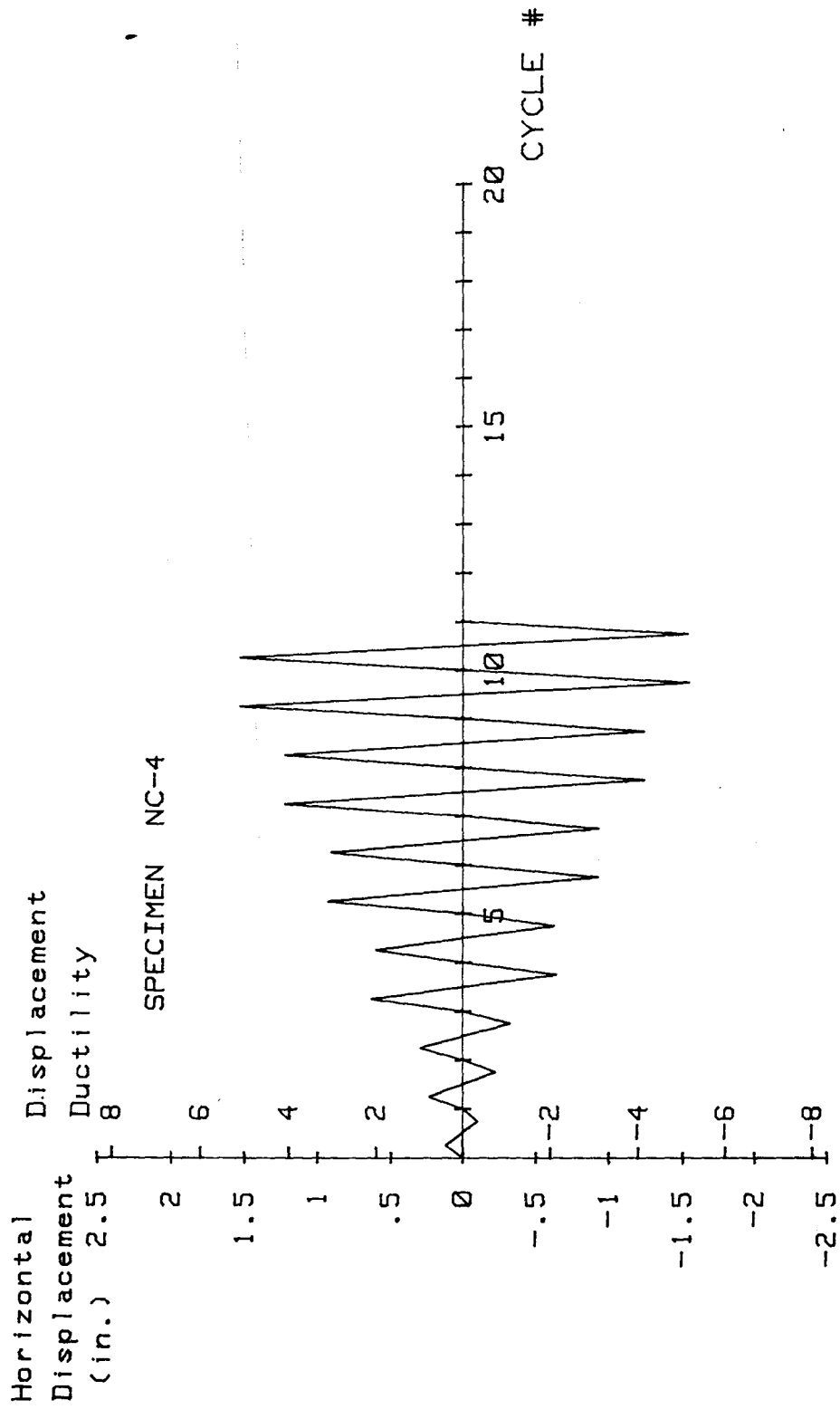


FIG. A-74 LOADING SCHEDULE, SPECIMEN NC-4

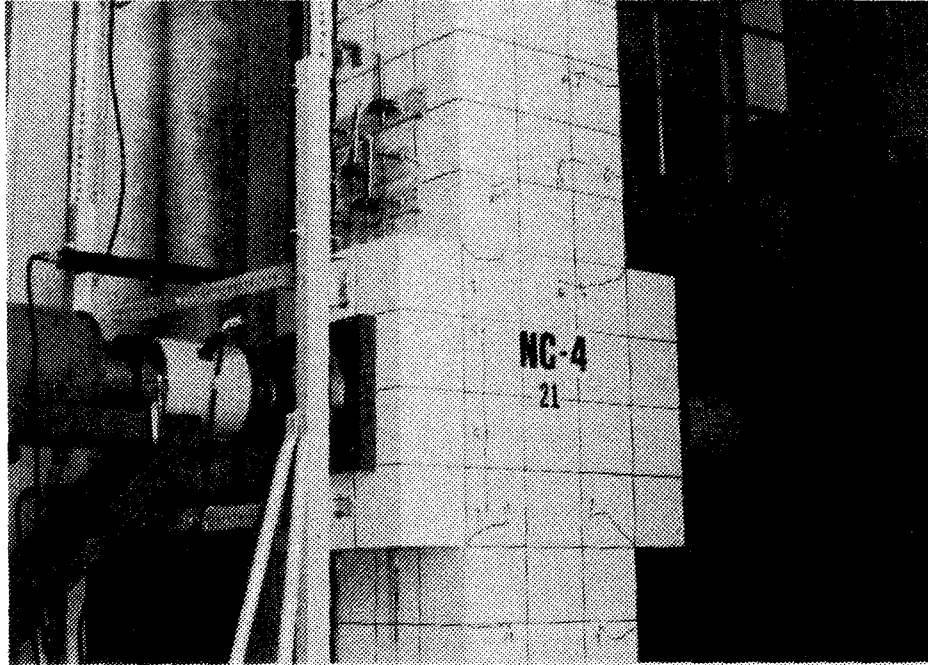


FIG. A-75 TEST SPECIMEN NC-4 AFTER CYCLE #3

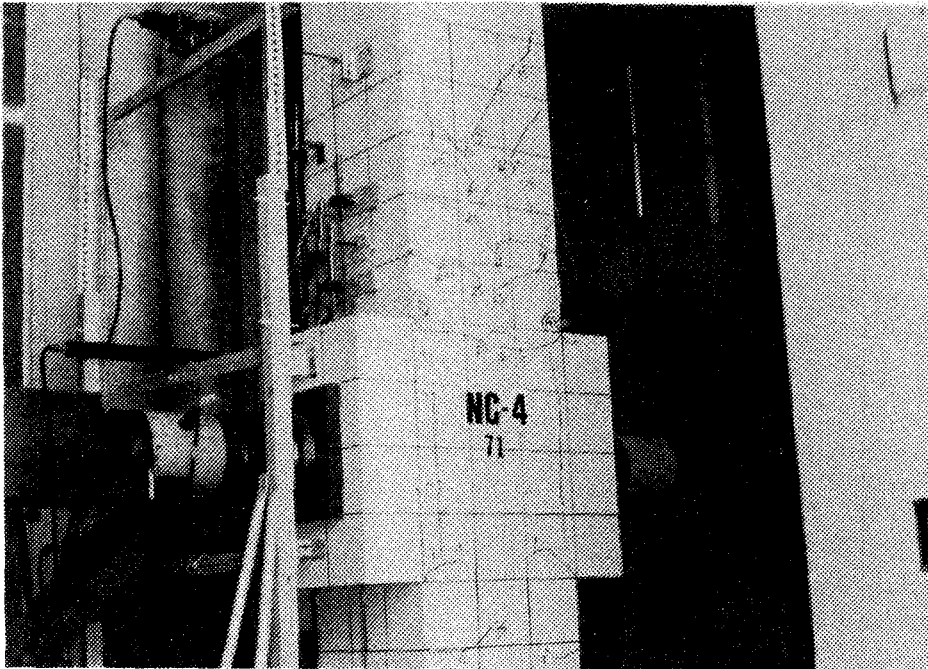


FIG. A-76 TEST SPECIMEN NC-4 AFTER CYCLE #5

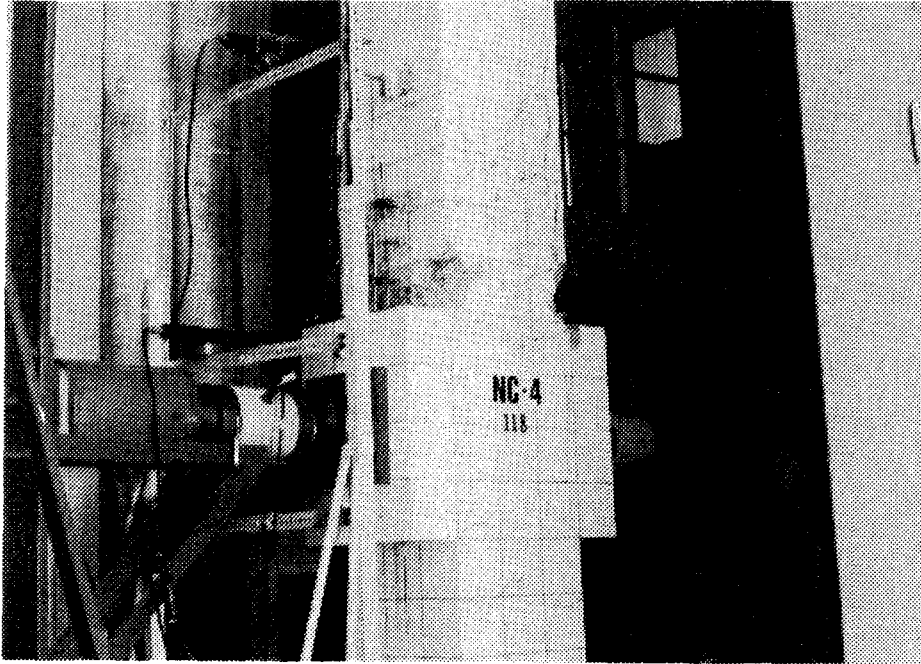


FIG. A-77 TEST SPECIMEN NC-4 AFTER CYCLE #7

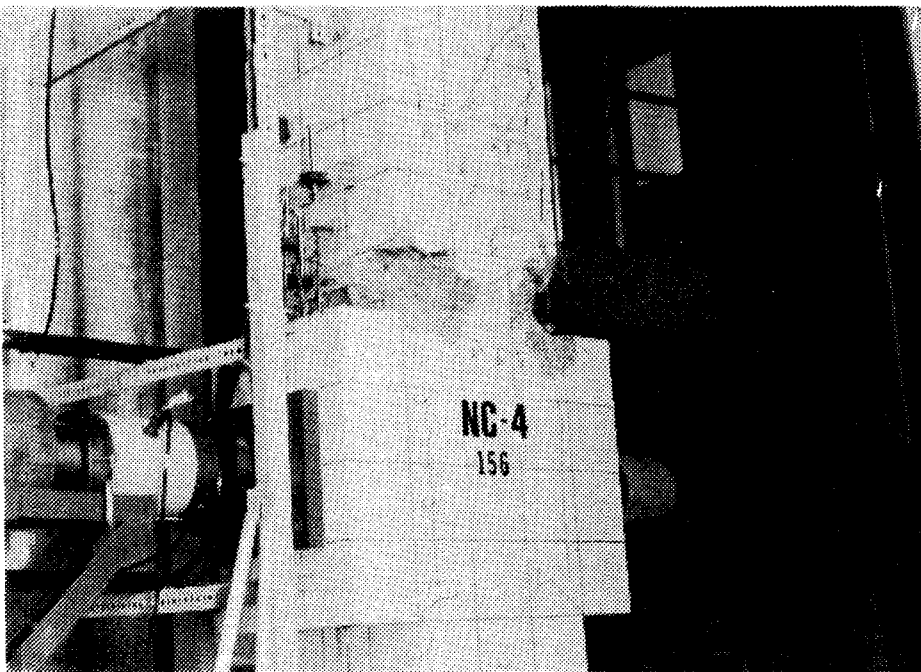


FIG. A-78 TEST SPECIMEN NC-4 AFTER CYCLE #9

Figure A-79 shows the specimen at the end of cycle #11 ($\mu=5$). Enough concrete had spalled at this point so that the the vertical and transverse reinforcement were visible within a distance of 18 in. above the stub. However, at the end of cycle #11 ($\mu=5$), no disturbance to the transverse or longitudinal reinforcement was observed.

Subsequent to application of cycle #11 ($\mu=5$), the specimen was subjected to a horizontal displacement of 1.8 in. to achieve a displacement ductility ratio of six. Before completing the first cycle at this displacement level, however, the anchorages of the peripheral hoops were lost at distances of 6, 10, and 14 in. from the stub and the corner vertical bars buckled. Some loss of anchorage of the interior hoops at 10 in. above the stub was visible. The length of the longitudinal bars engaged in buckling was relatively large in this specimen (approximately 12 in).

Figure A-80 shows the specimen at test conclusion.

The final length of the plastic hinge extended from approximately 2 to 12 in. above the stub.

Load Deflection and Moment-Curvature Characteristics

Figure A-81 shows the horizontal load displacement characteristics of the specimen. The horizontal load-carrying capacity of the column remained above the theoretical value shown by the dashed line in Fig. A-81 at all displacement levels, except at the second cycle of displacement ductility ratio of five.

Figure A-82 shows curvature distribution along the upper column. Beyond a displacement ductility ratio of three the distribution of curvature is very unsymmetric.

Figure A-83 shows the moment-curvature characteristic of the specimen at the upper column-stub level. The theoretical value of the moment capacity of the column section using the procedure outlined in Section 4.8.2 was found to be 5268 in-kips. The maximum applied moment was 6152 in-kips. Negligible degradation in moment capacity of the column cross-section was observed as the peak applied moments at various displacement levels remained above the theoretical value. The ratio of the peak moment at the second cycle to the peak moment at the first cycle ranged between 0.9 to 0.95 at various displacement levels.

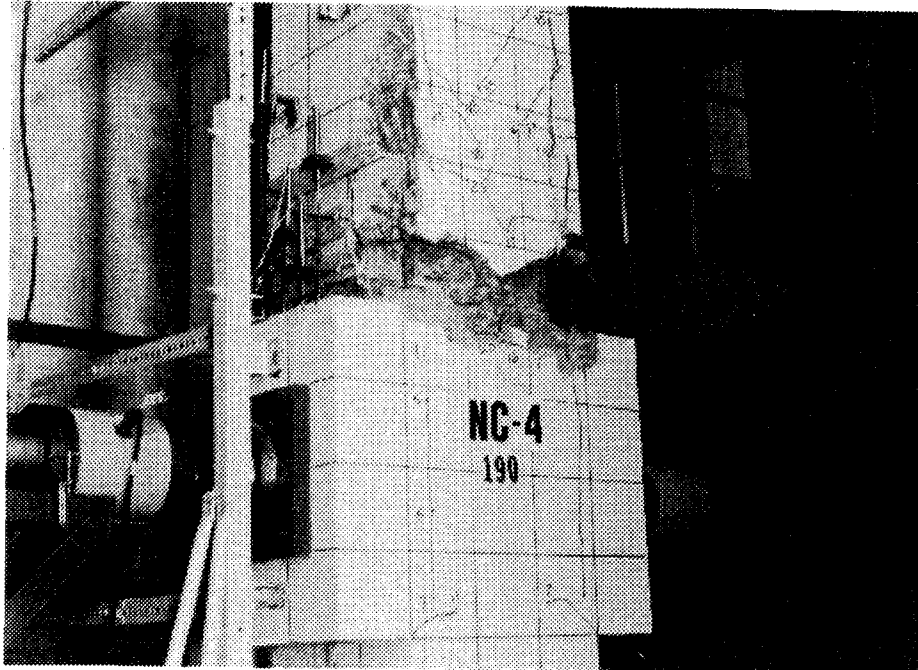


FIG. A-79 TEST SPECIMEN NC-5 AFTER CYCLE #11

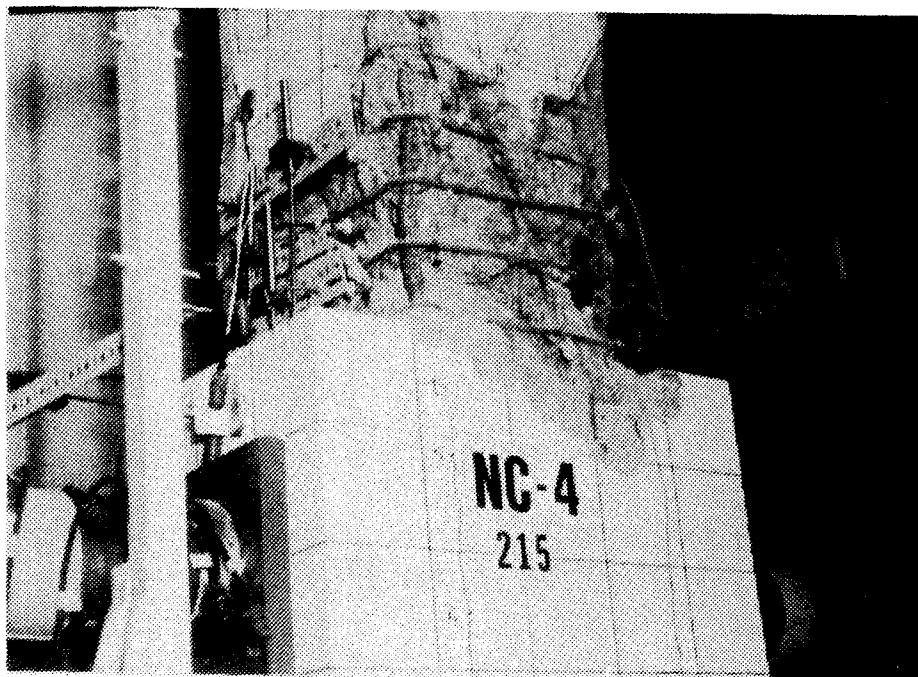
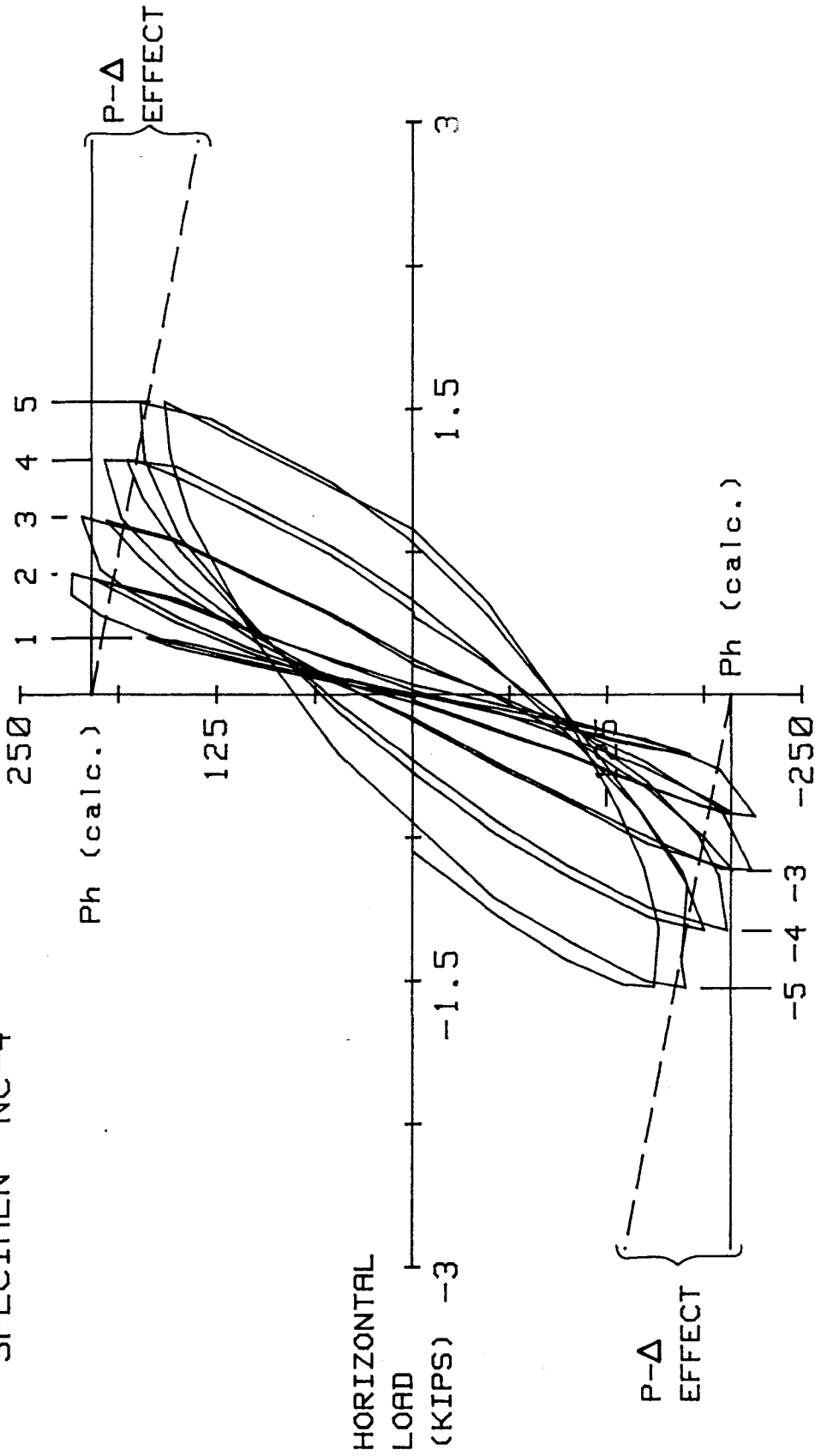


FIG. A-80 TEST SPECIMEN NC-4 AFTER TEST CONCLUSION

DISPLACEMENT DUCTILITY

SPECIMEN NC-4



Metric Equivalents
1 in. = 25.4 mm
1 kip = 4.45 KN

HORIZONTAL DISPLACEMENT (IN.)

FIG. A-81 HORIZONTAL LOAD VERSUS DISPLACEMENT, SPECIMEN NC-4

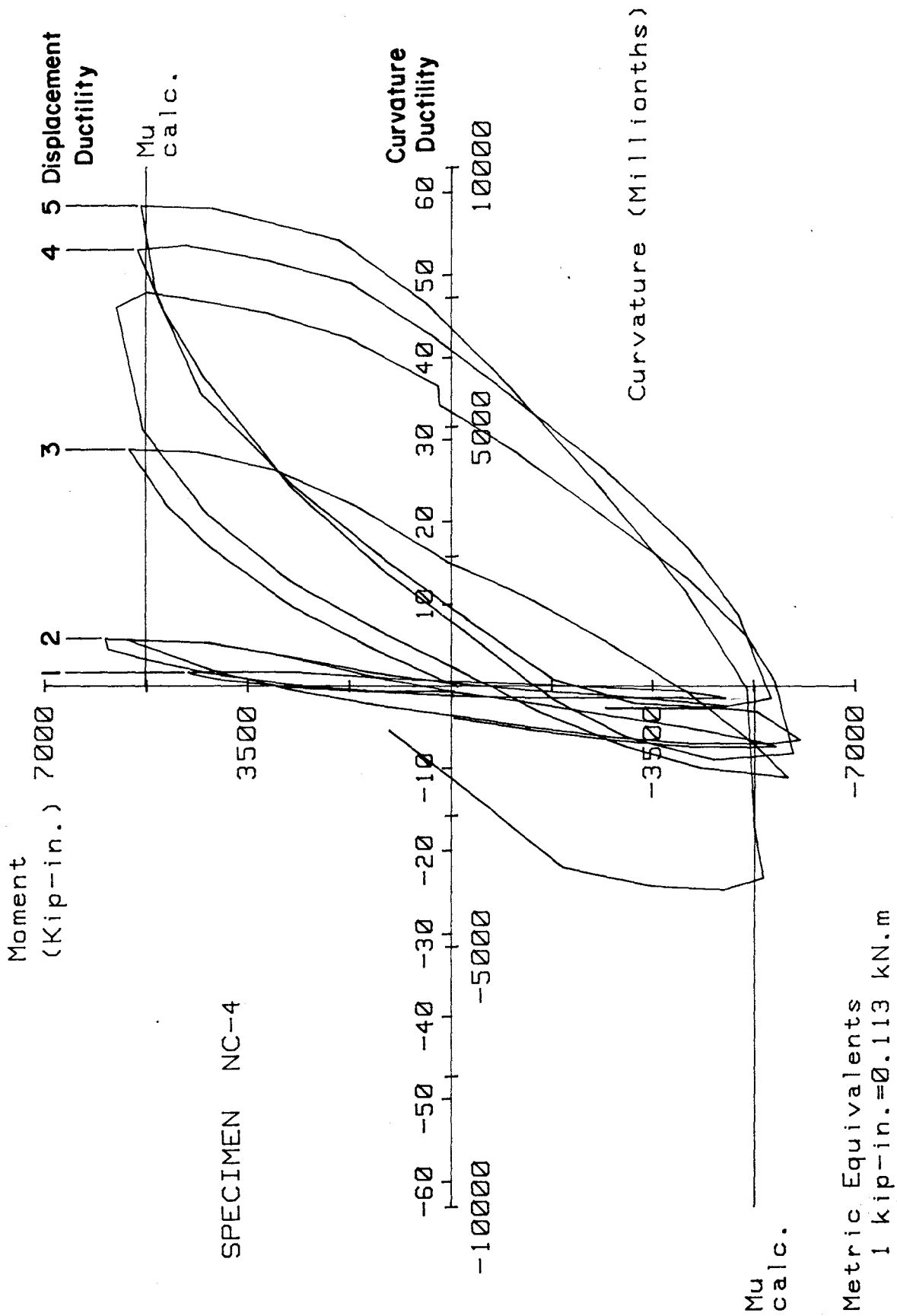


FIG. A-83 MOMENT VERSUS CURVATURE FOR SPECIMEN NC-4

Transverse Reinforcement Strain

Figure 4-11 shows the location of the strain gages attached to the transverse reinforcements. Figures A-84 through A-106 show data obtained from the strain gages.

The specified yield strain of the transverse reinforcement material was 2070 micro-strain. Yielding was first observed on the peripheral hoops located 18 in. above the stub during cycle #6 ($\mu=3$), at which time the maximum strain on the interior hoops at the same level was 1900 micro-strain.

In general, during the early stages of loading ($\mu=4$), the maximum strain occurred at the transverse reinforcements located 14 and 18 in. above the stub. The strain on the interior hoops was generally smaller than the strain on the peripheral hoops.

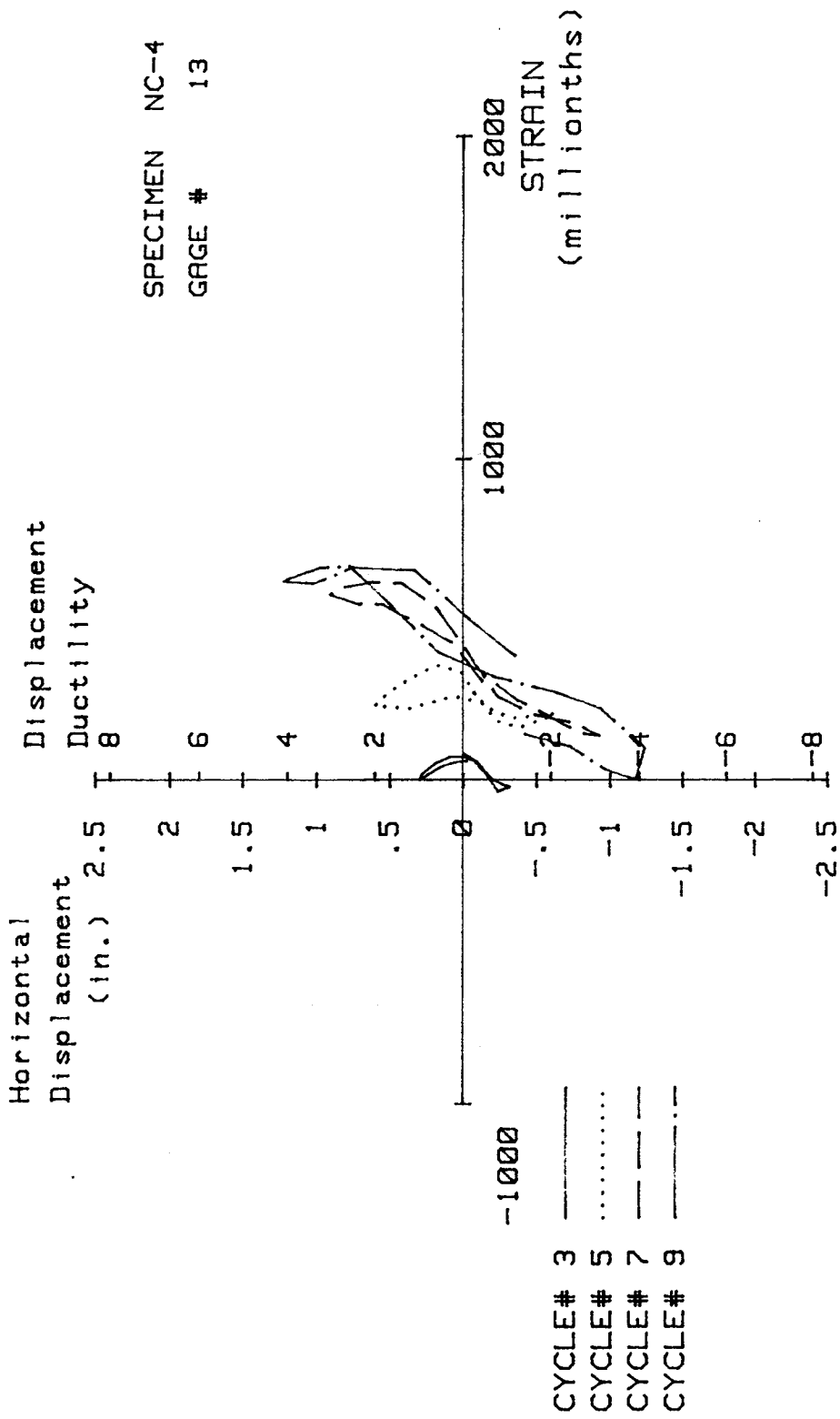


FIG. A-84 MEASURED STRAIN, GAGE #13, SPECIMEN NC-4

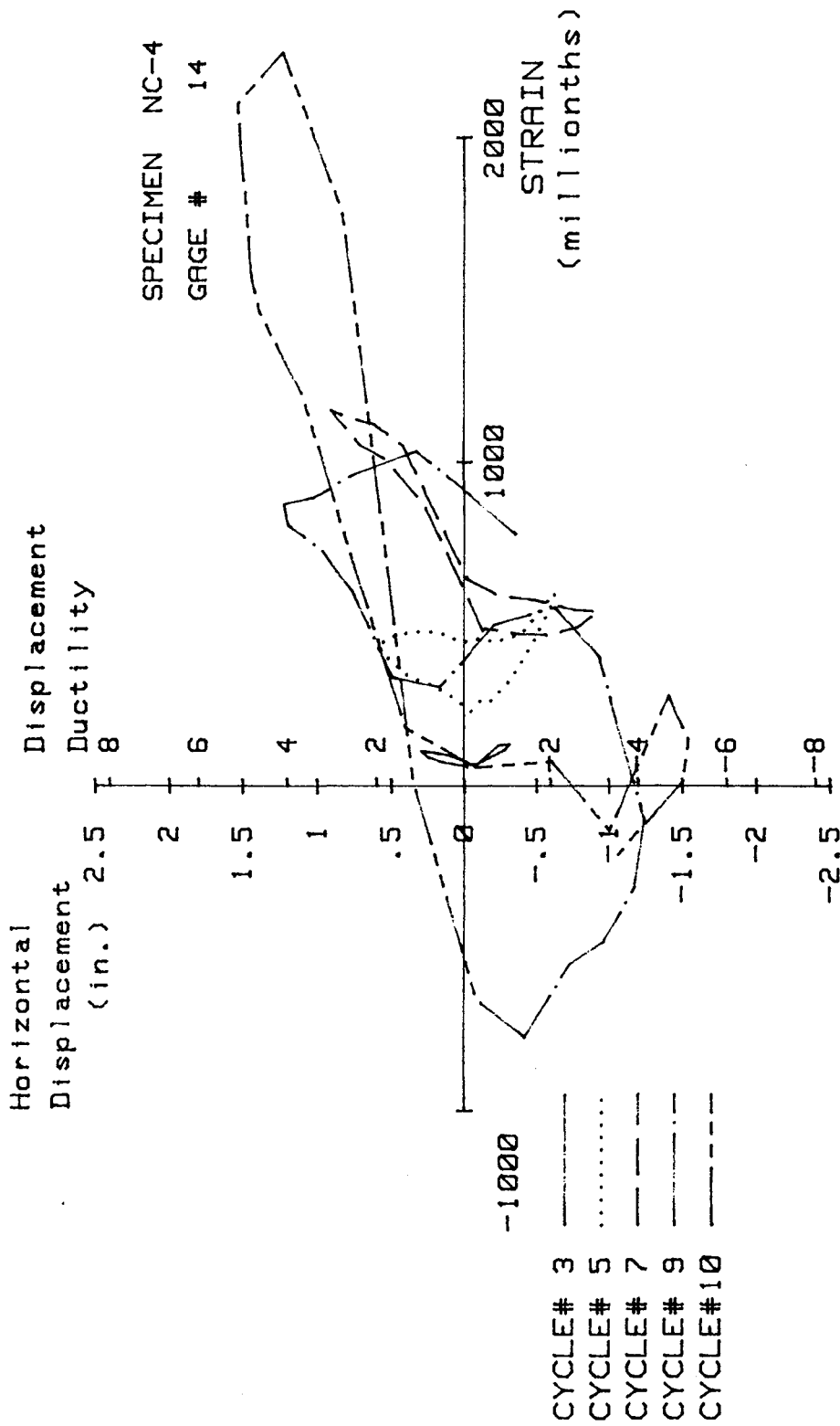


FIG. A-85 MEASURED STRAIN, GAGE #14, SPECIMEN NC-4

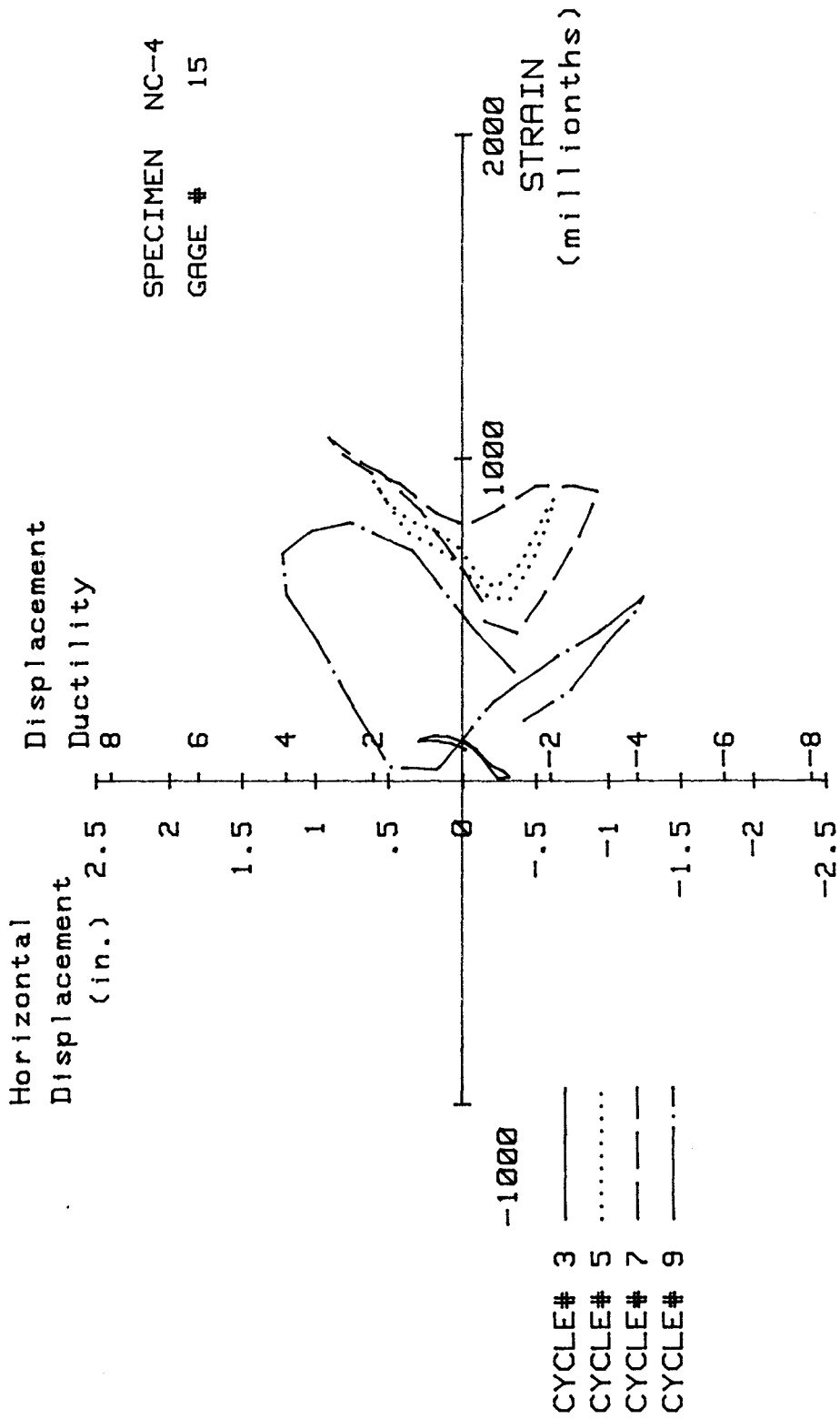


FIG. A-86 MEASURED STRAIN, GAGE #15, SPECIMEN NC-4

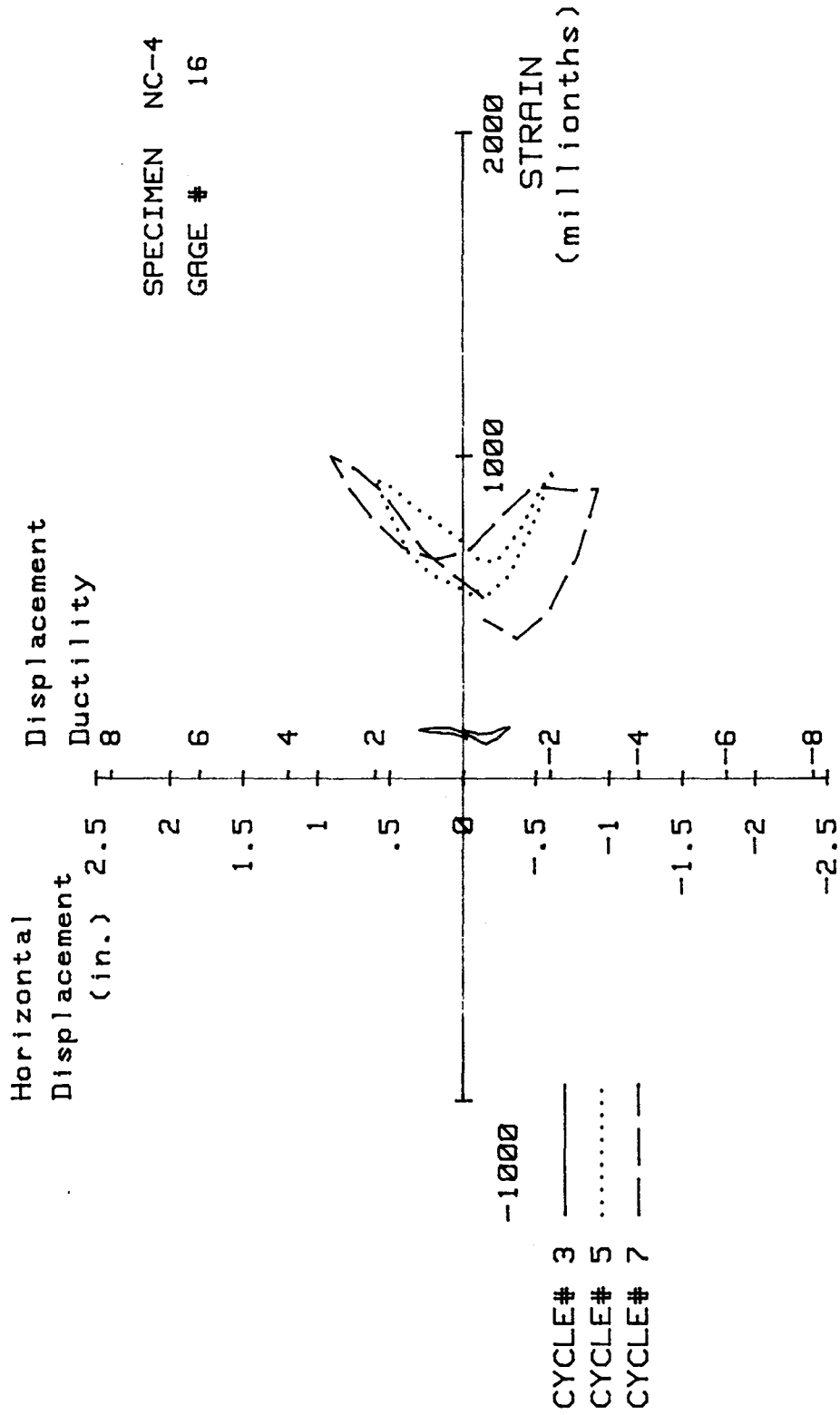


FIG. A-87 MEASURED STRAIN, GAGE #16, SPECIMEN NC-4

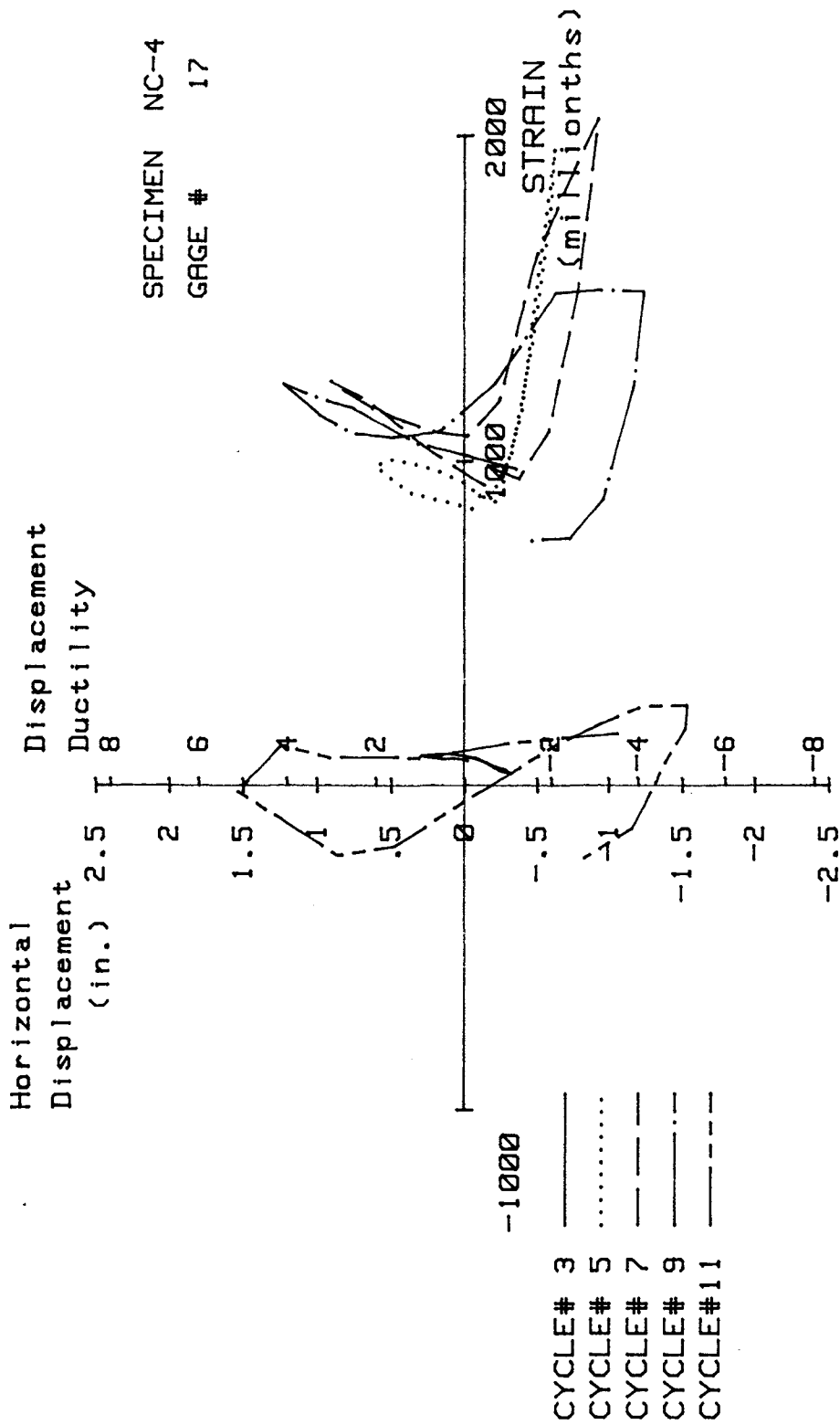


FIG. A-88 MEASURED STRAIN, GAGE #17, SPECIMEN NC-4

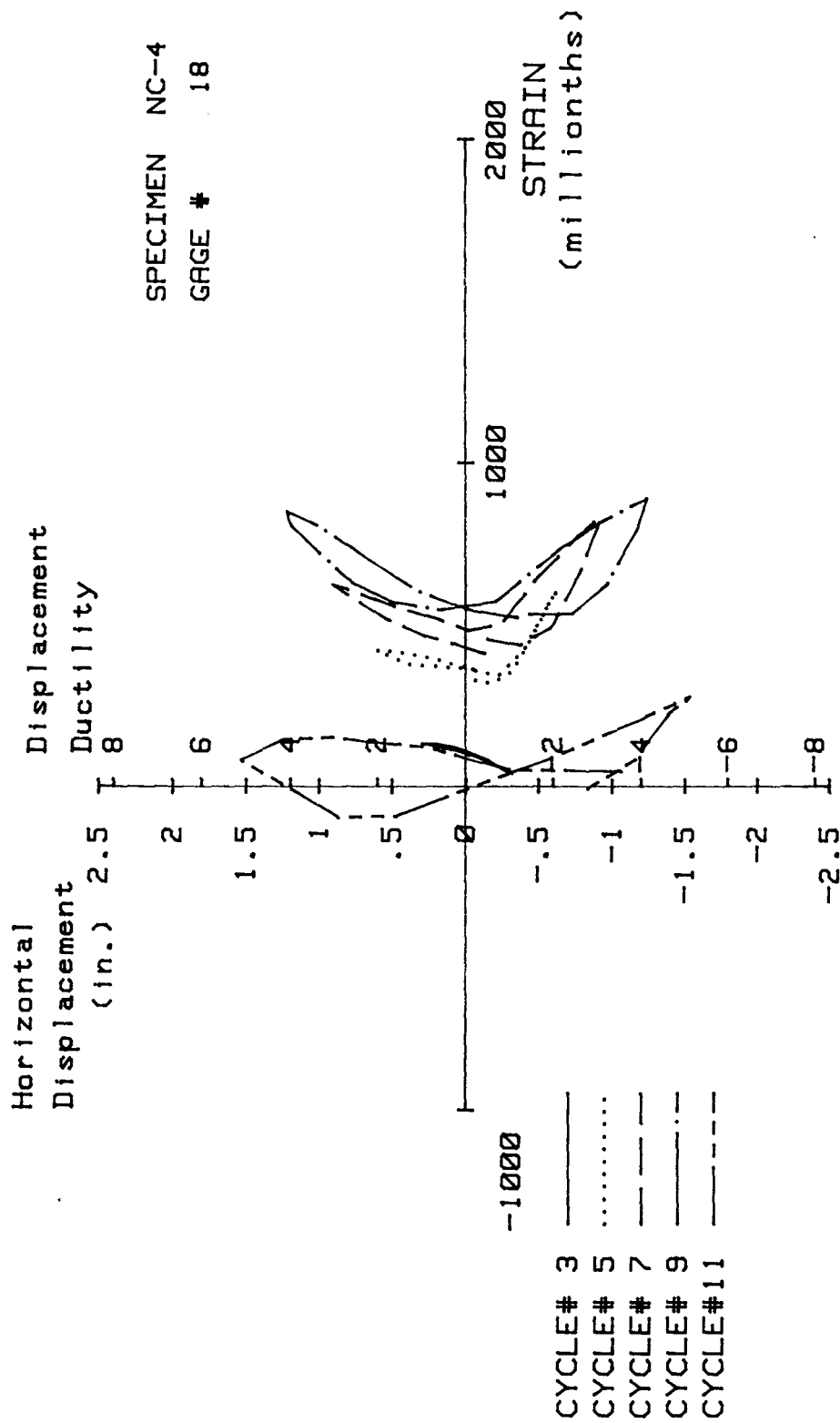


FIG. A-89 MEASURED STRAIN, GAGE #18, SPECIMEN NC-4

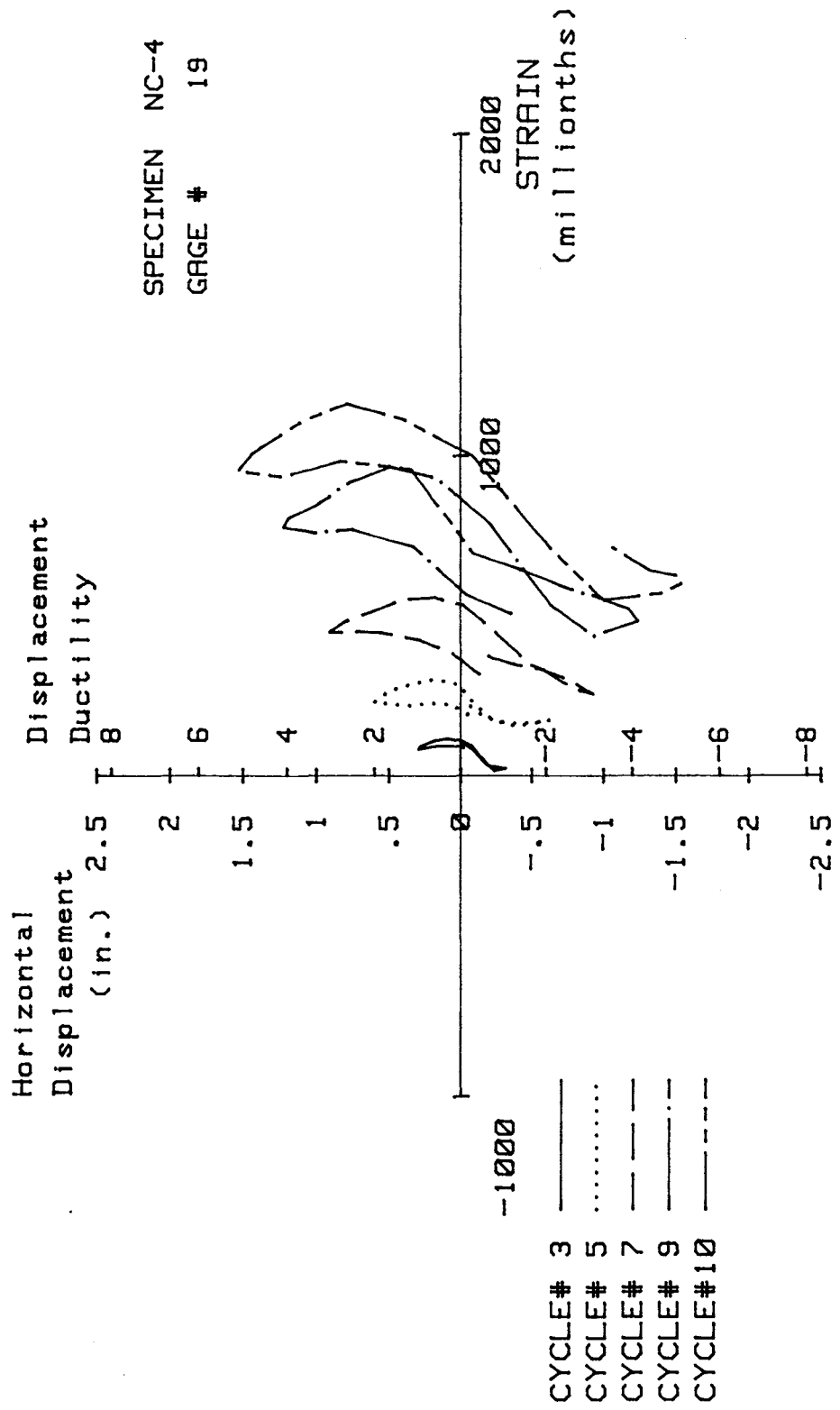


FIG. A-90 MEASURED STRAIN, GAGE #19, SPECIMEN NC-4

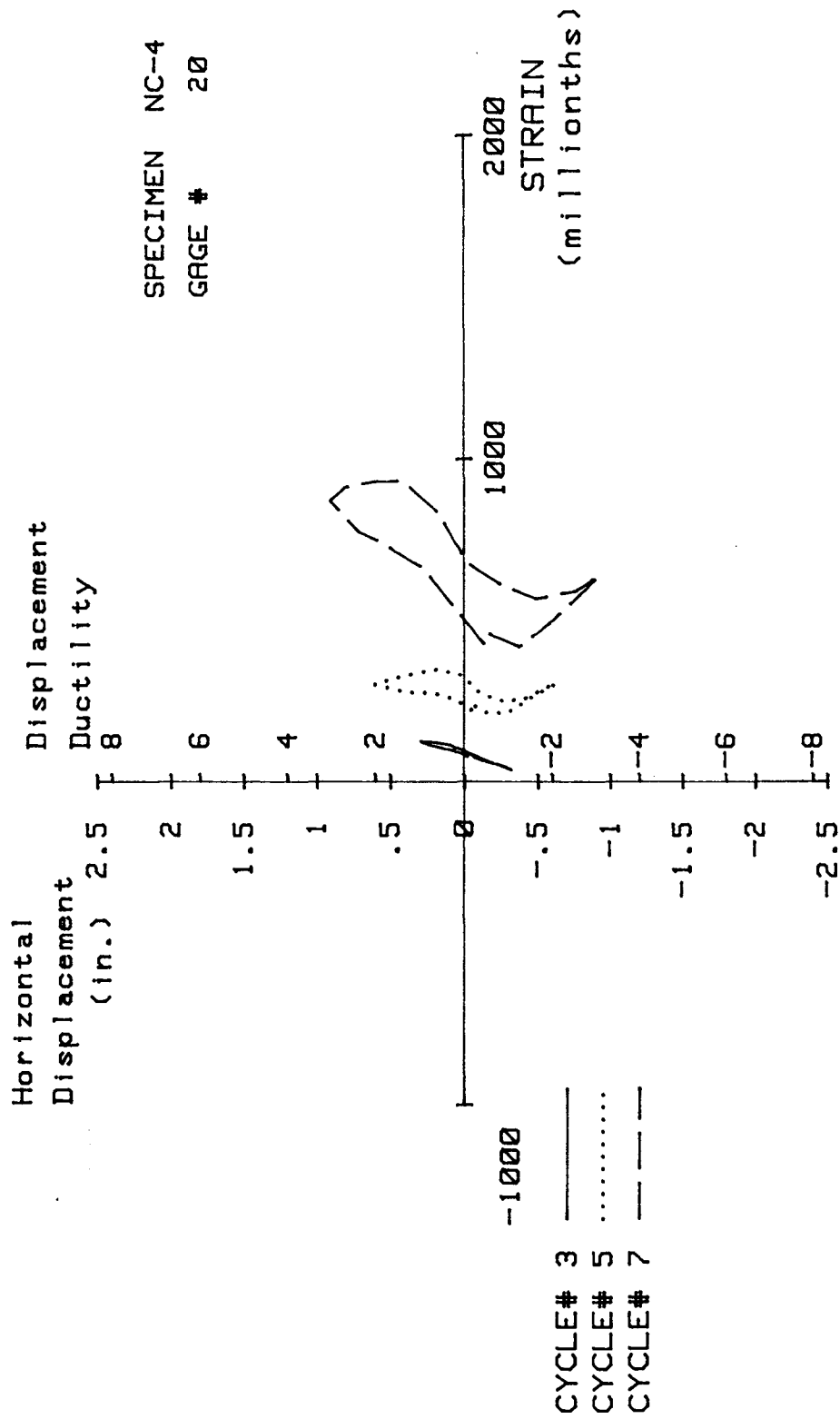


FIG. A-91 MEASURED STRAIN, GAGE #20, SPECIMEN NC-4

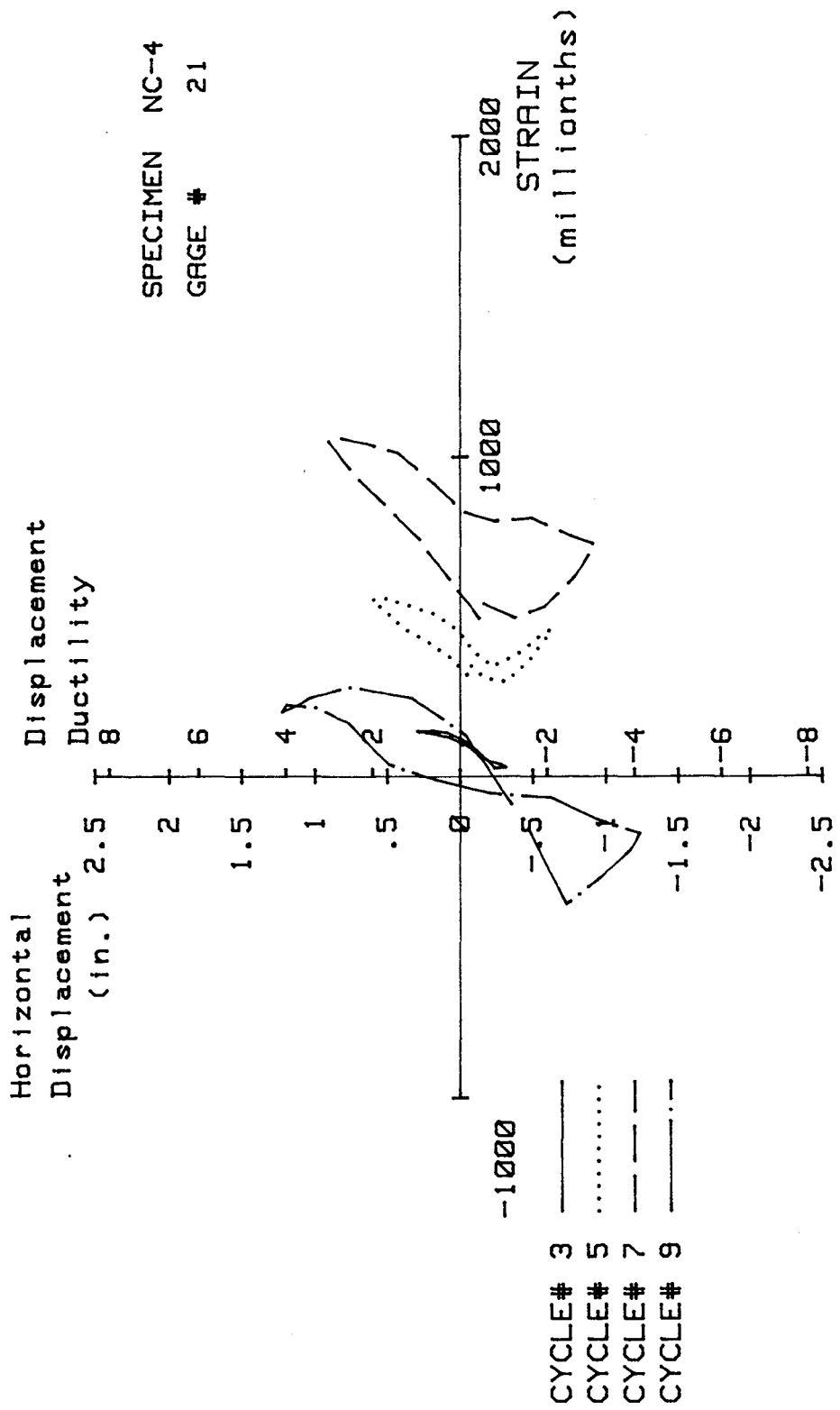


FIG. A-92 MEASURED STRAIN, GAGE #21, SPECIMEN NC-4

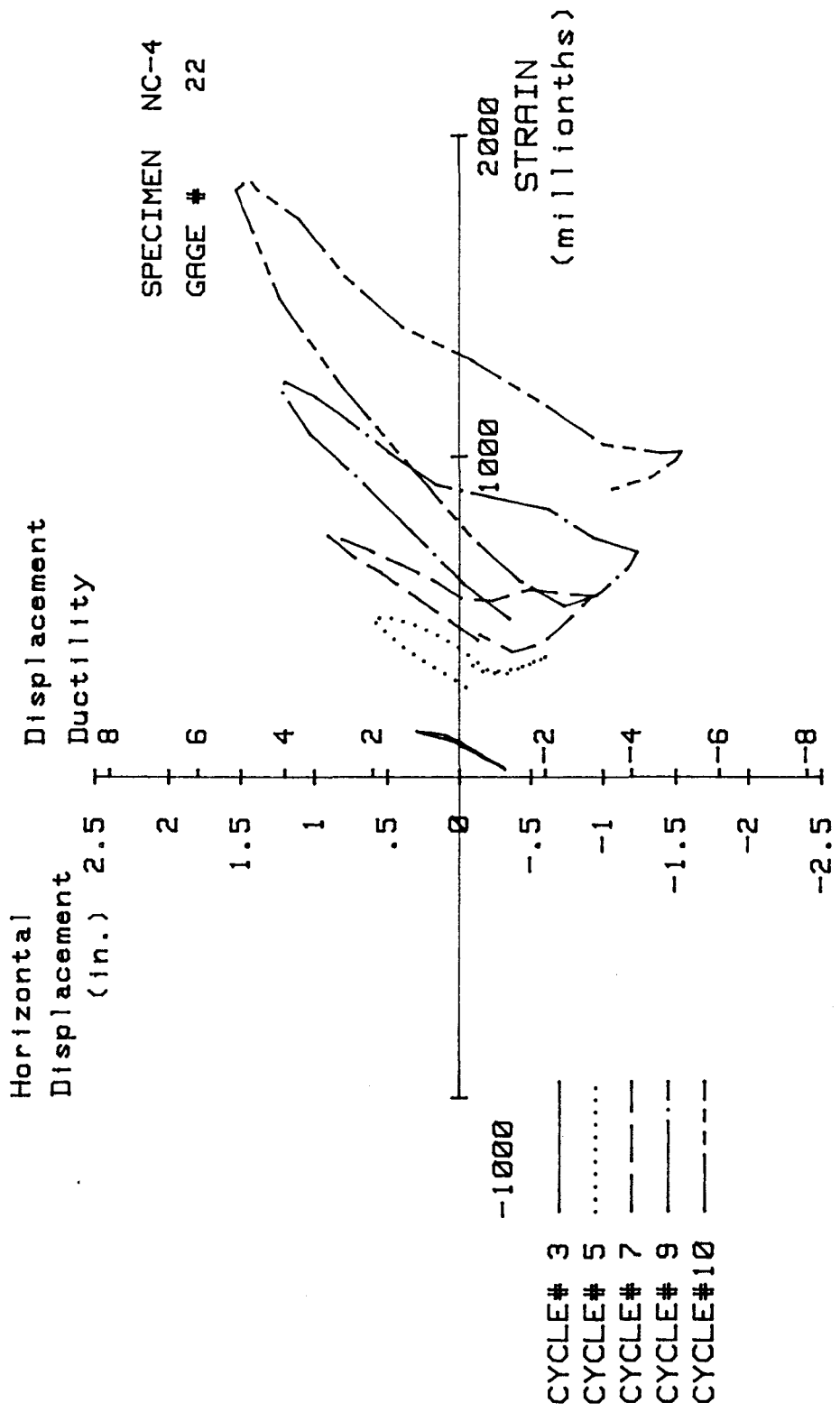


FIG. A-93 MEASURED STRAIN, GAGE #22, SPECIMEN NC-4

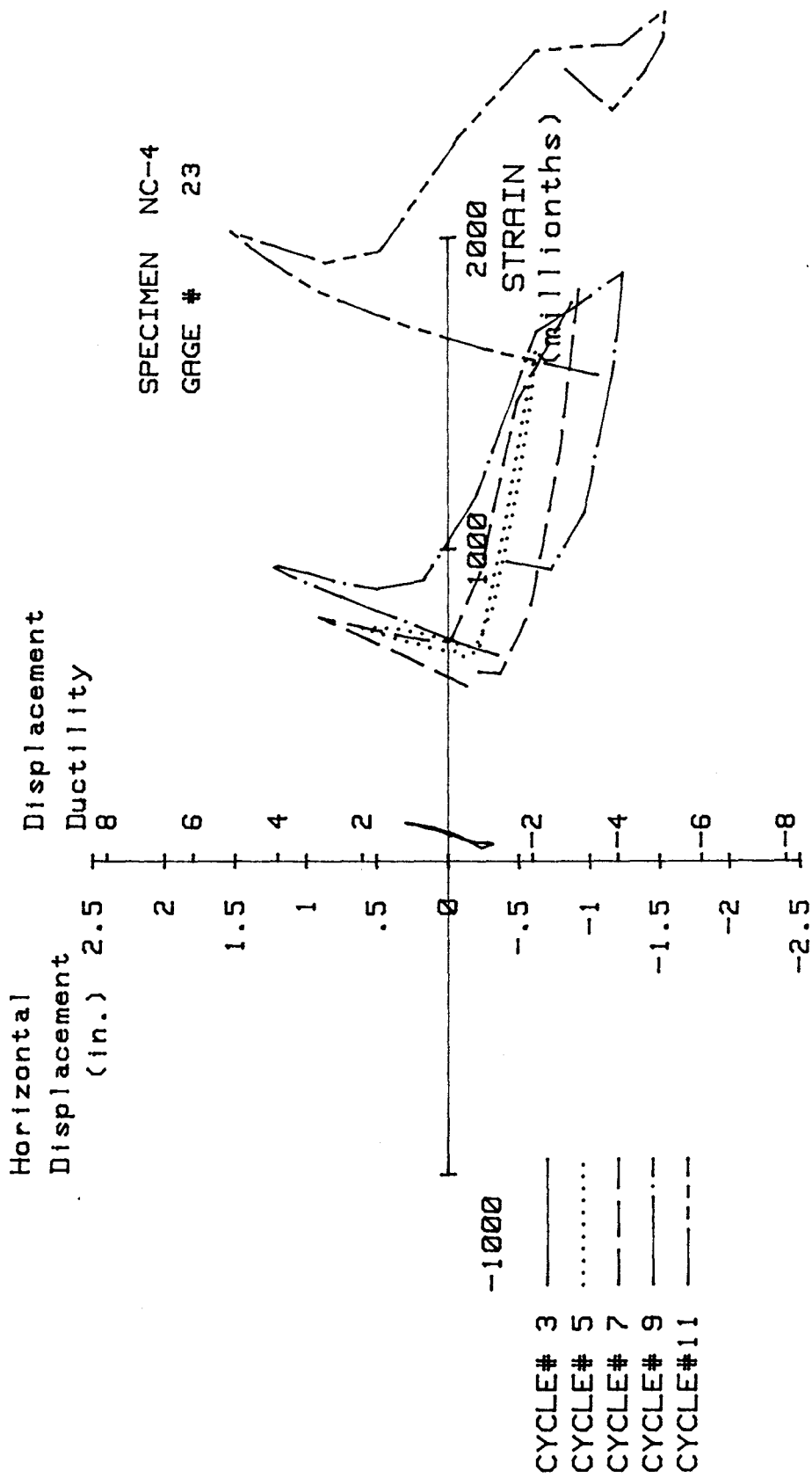


FIG. A-94 MEASURED STRAIN, GAGE #23, SPECIMEN NC-4

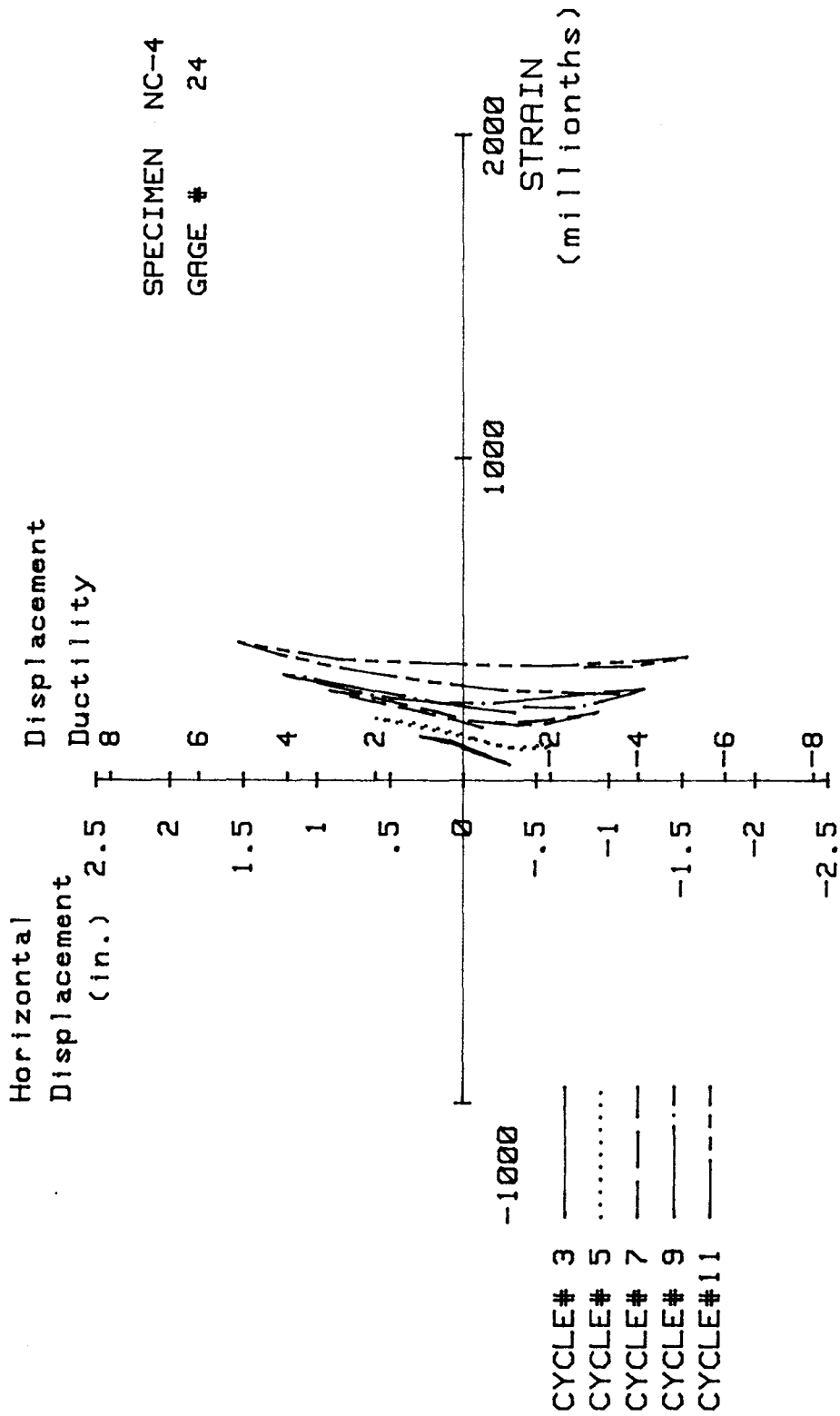


FIG. A-95 MEASURED STRAIN, GAGE #24, SPECIMEN NC-4

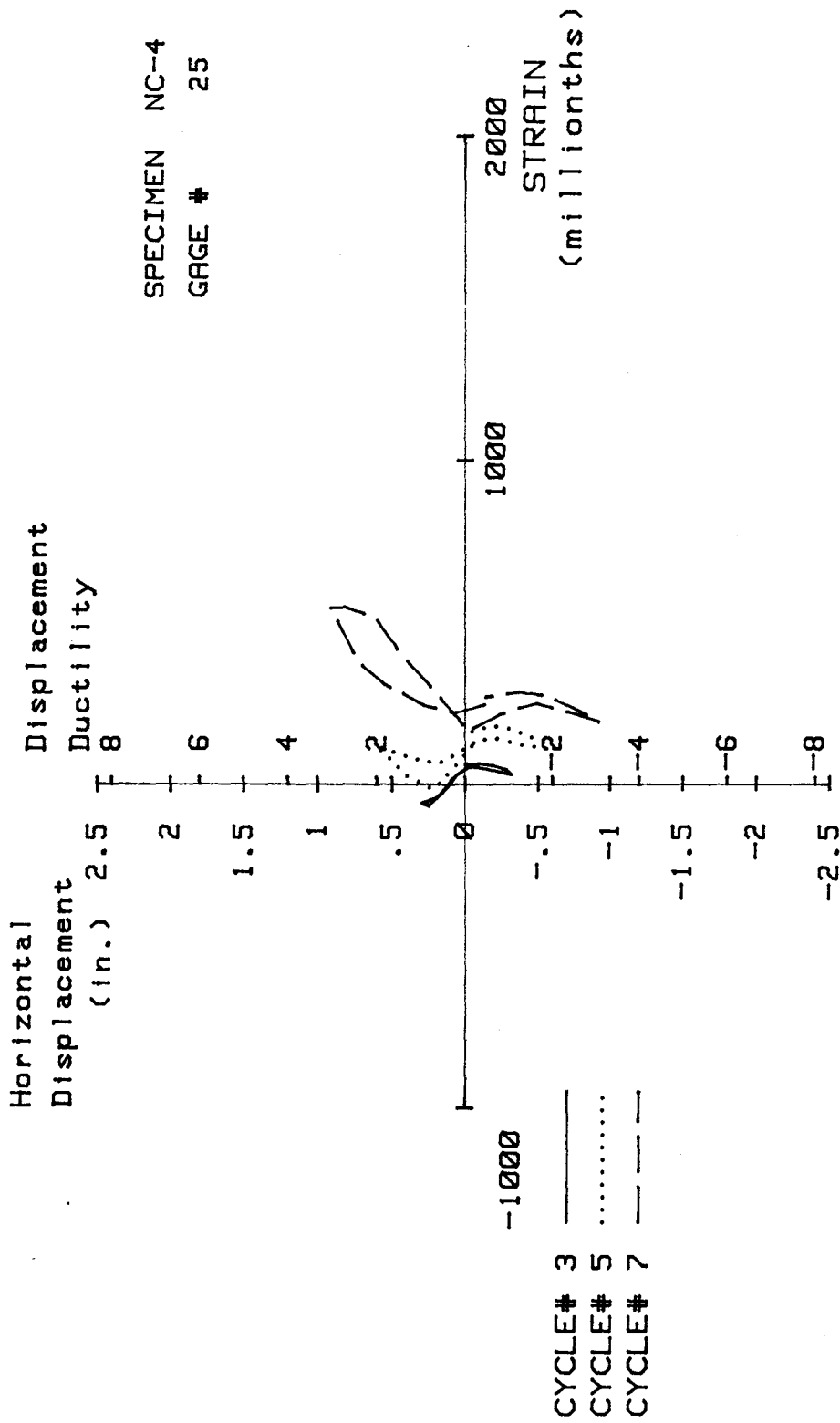


FIG. A-96 MEASURED STRAIN, GAGE #25, SPECIMEN NC-4

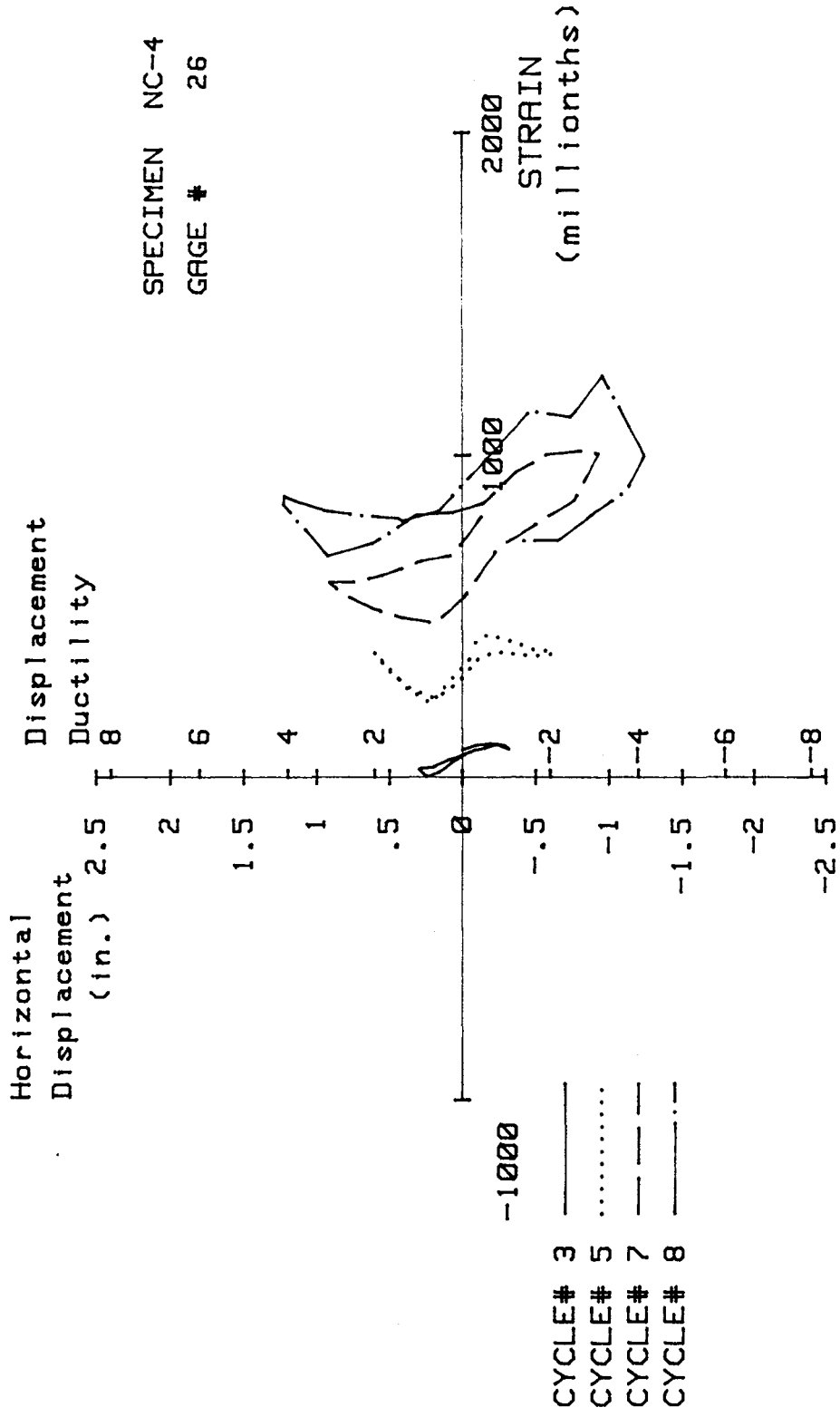


FIG. A-97 MEASURED STRAIN, GAGE #26, SPECIMEN NC-4

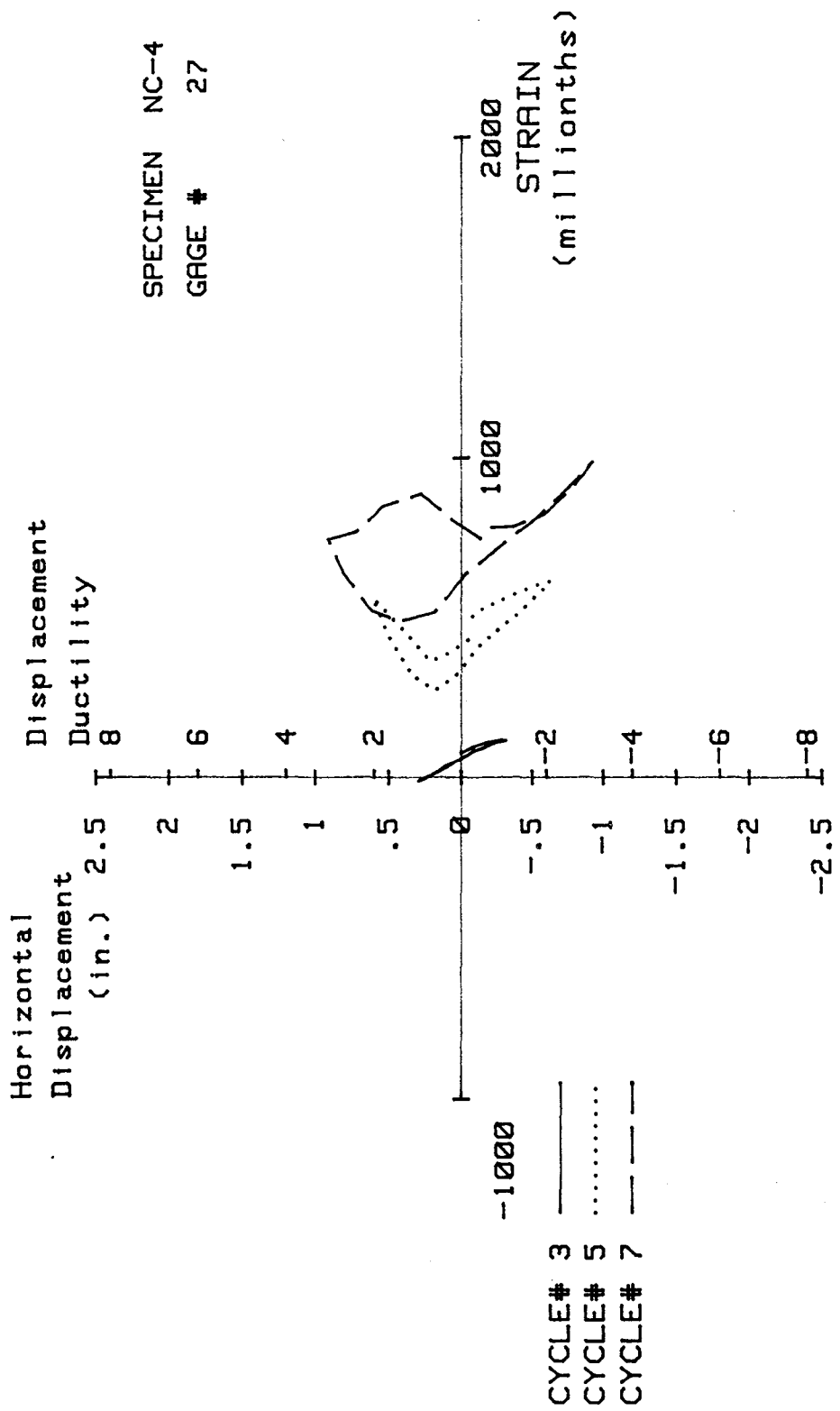


FIG. A-98 MEASURED STRAIN, GAGE #27, SPECIMEN NC-4

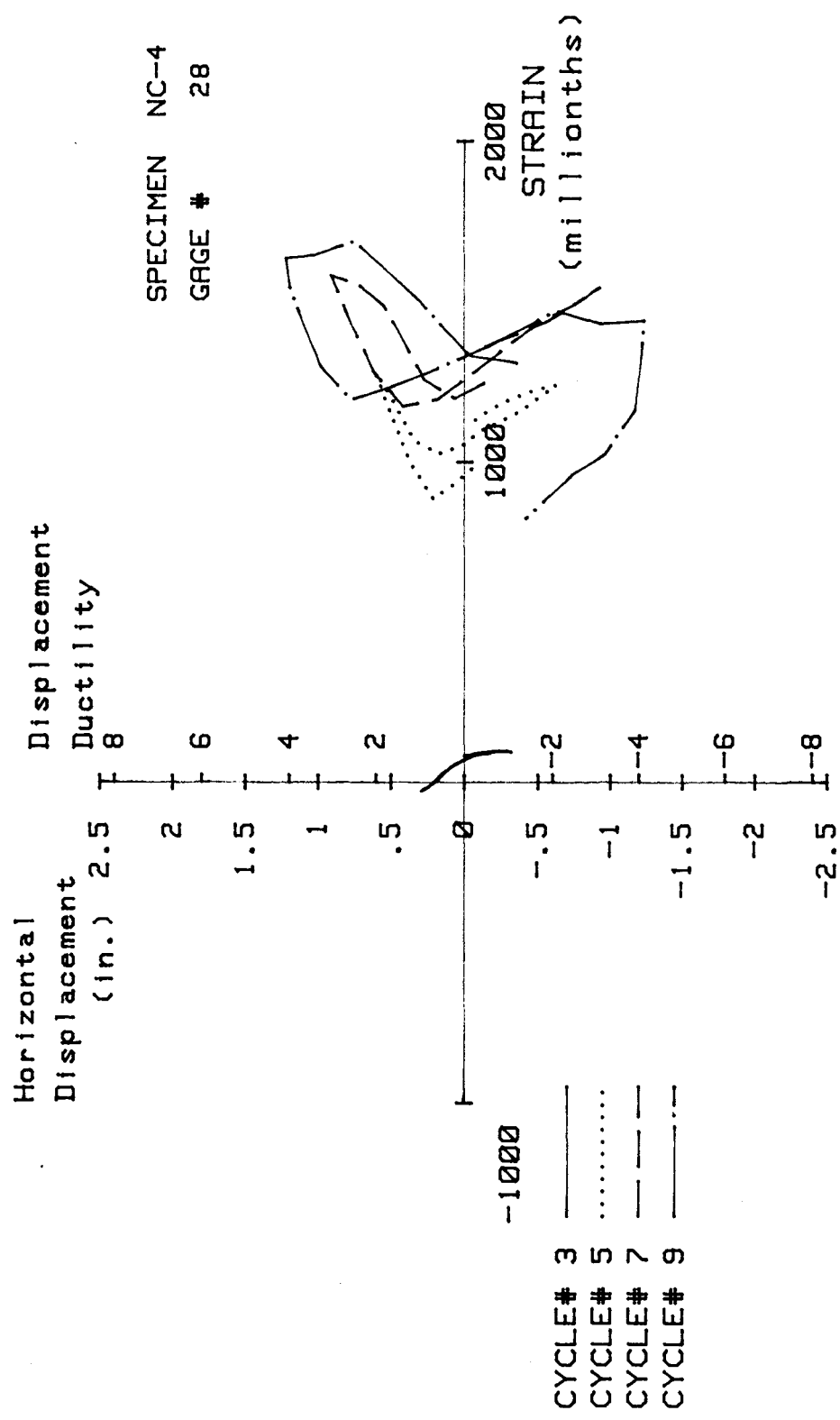


FIG. A-99 MEASURED STRAIN, GAGE #28, SPECIMEN NC-4

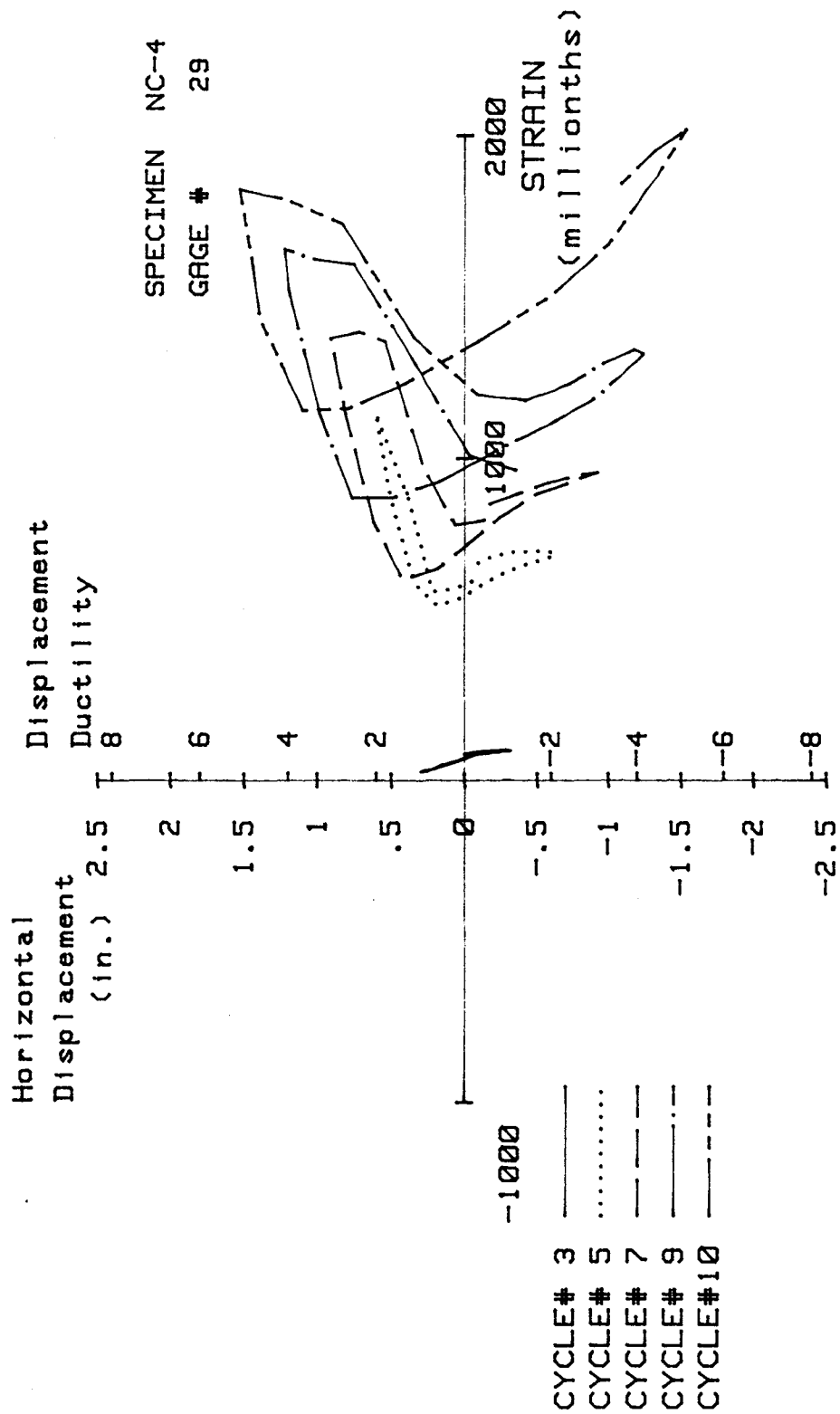


FIG. A-100 MEASURED STRAIN, GAGE #29, SPECIMEN NC-4

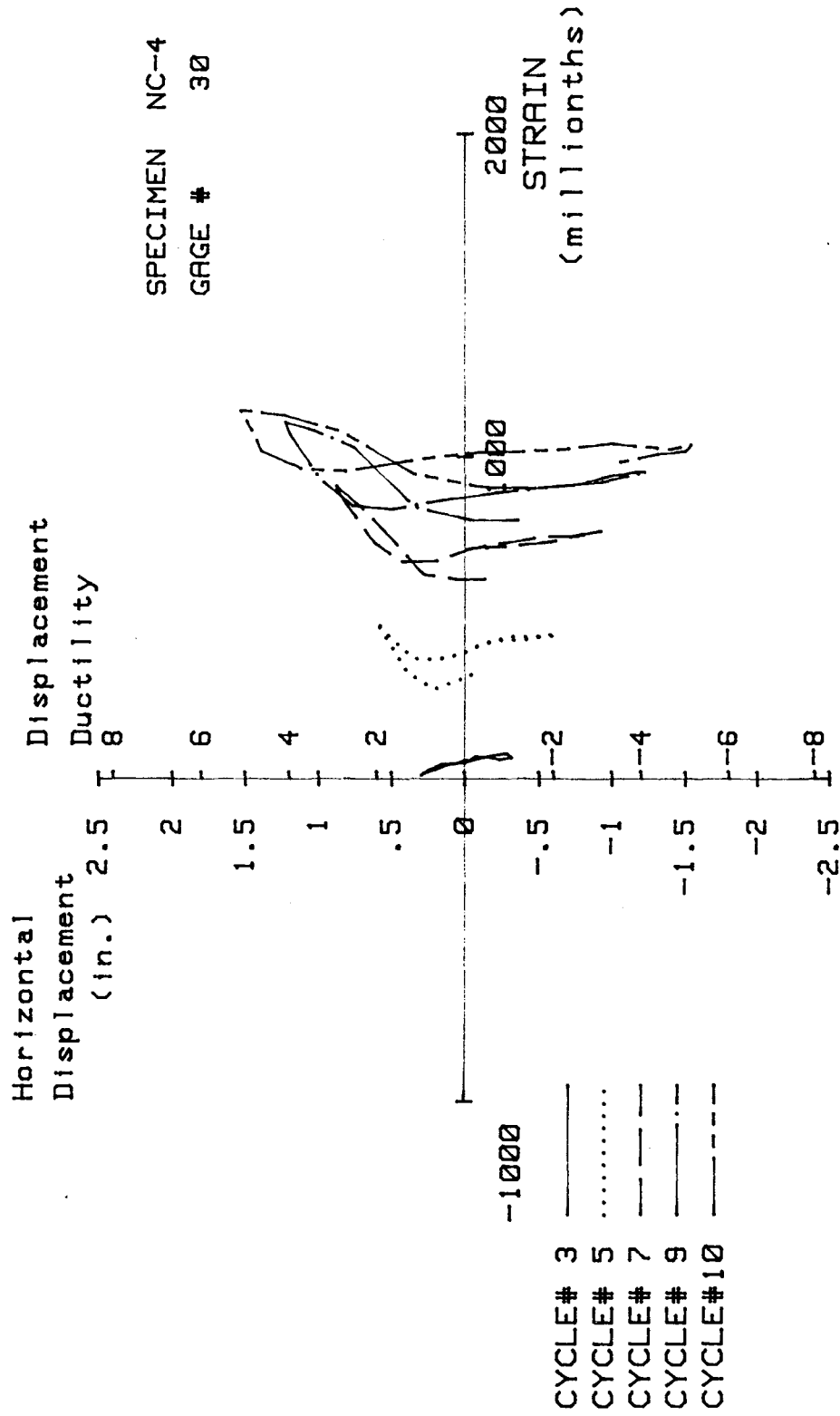


FIG. A-101 MEASURED STRAIN, GAGE #30, SPECIMEN NC-4

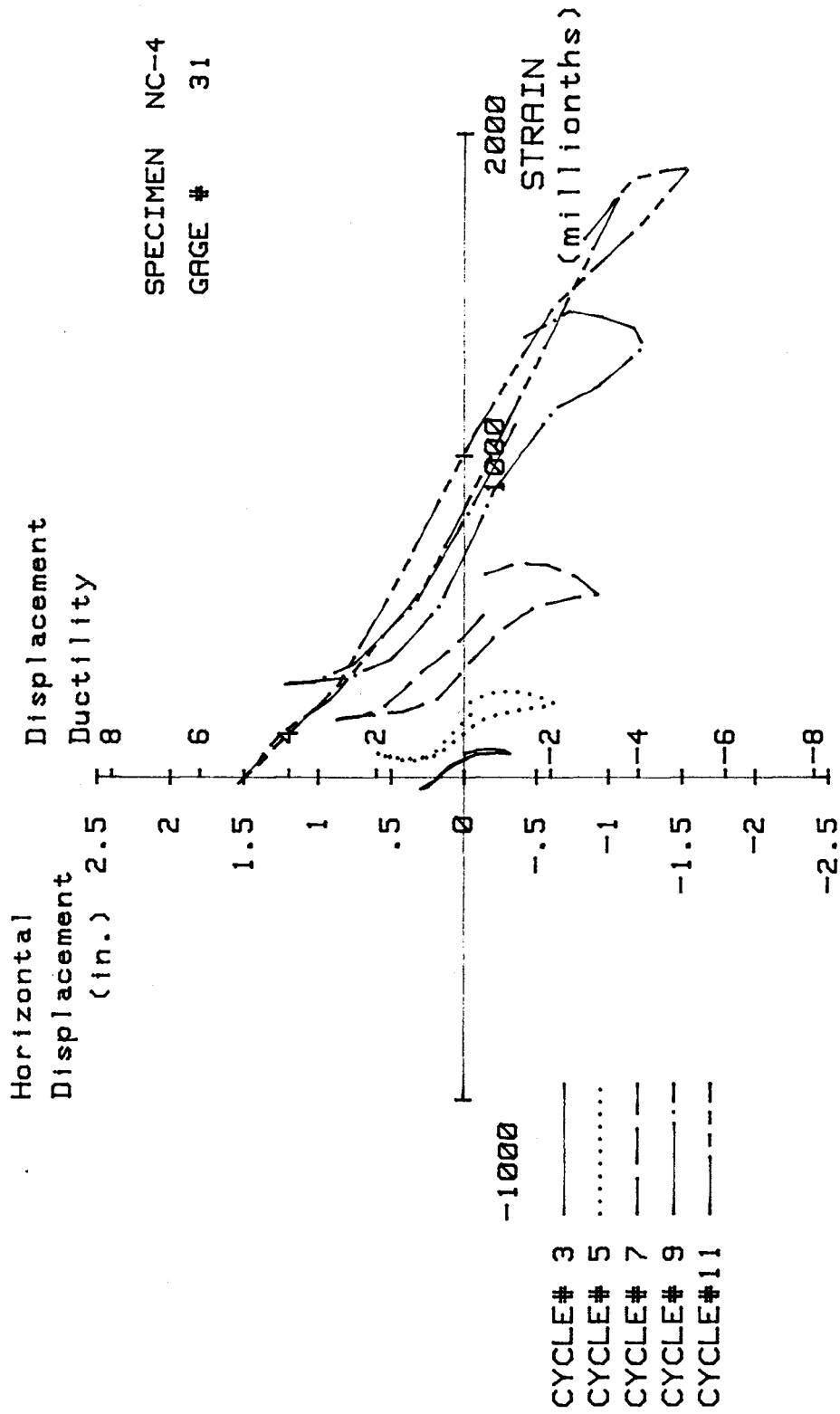


FIG. A-102 MEASURED STRAIN, GAGE #31, SPECIMEN NC-4

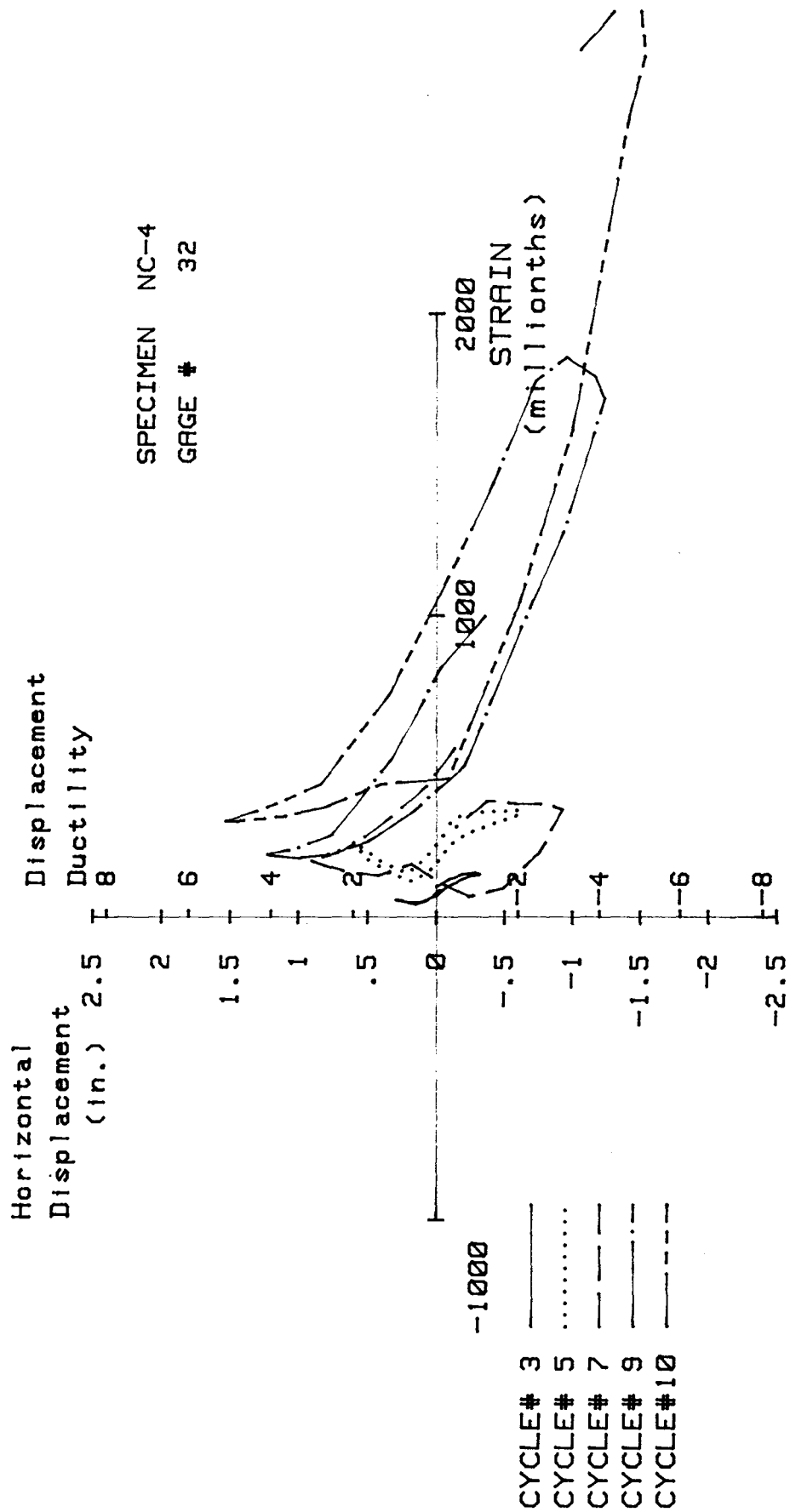


FIG. A-103 MEASURED STRAIN, GAGE #32, SPECIMEN NC-4

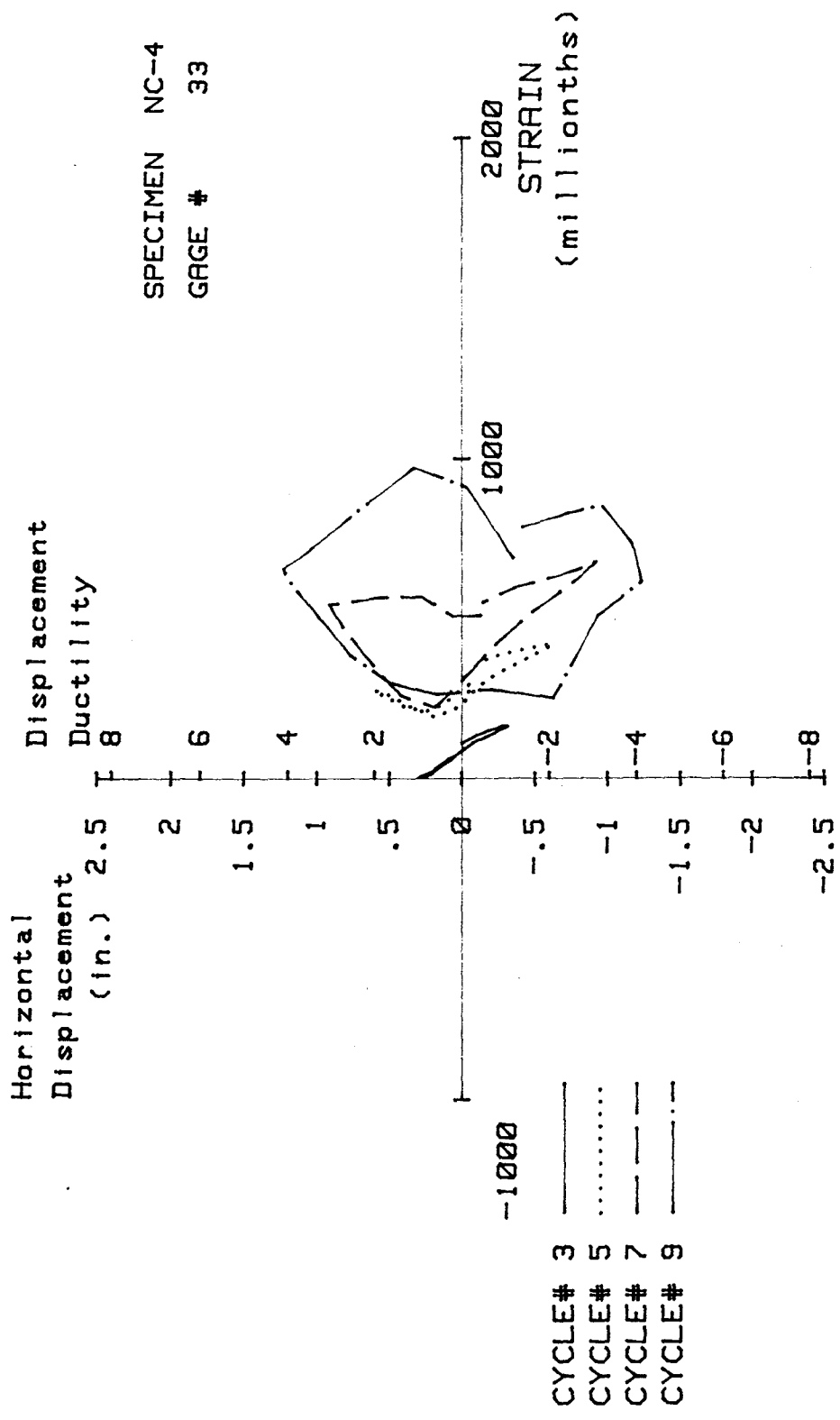


FIG. A-104 MEASURED STRAIN, GAGE #33, SPECIMEN NC-4

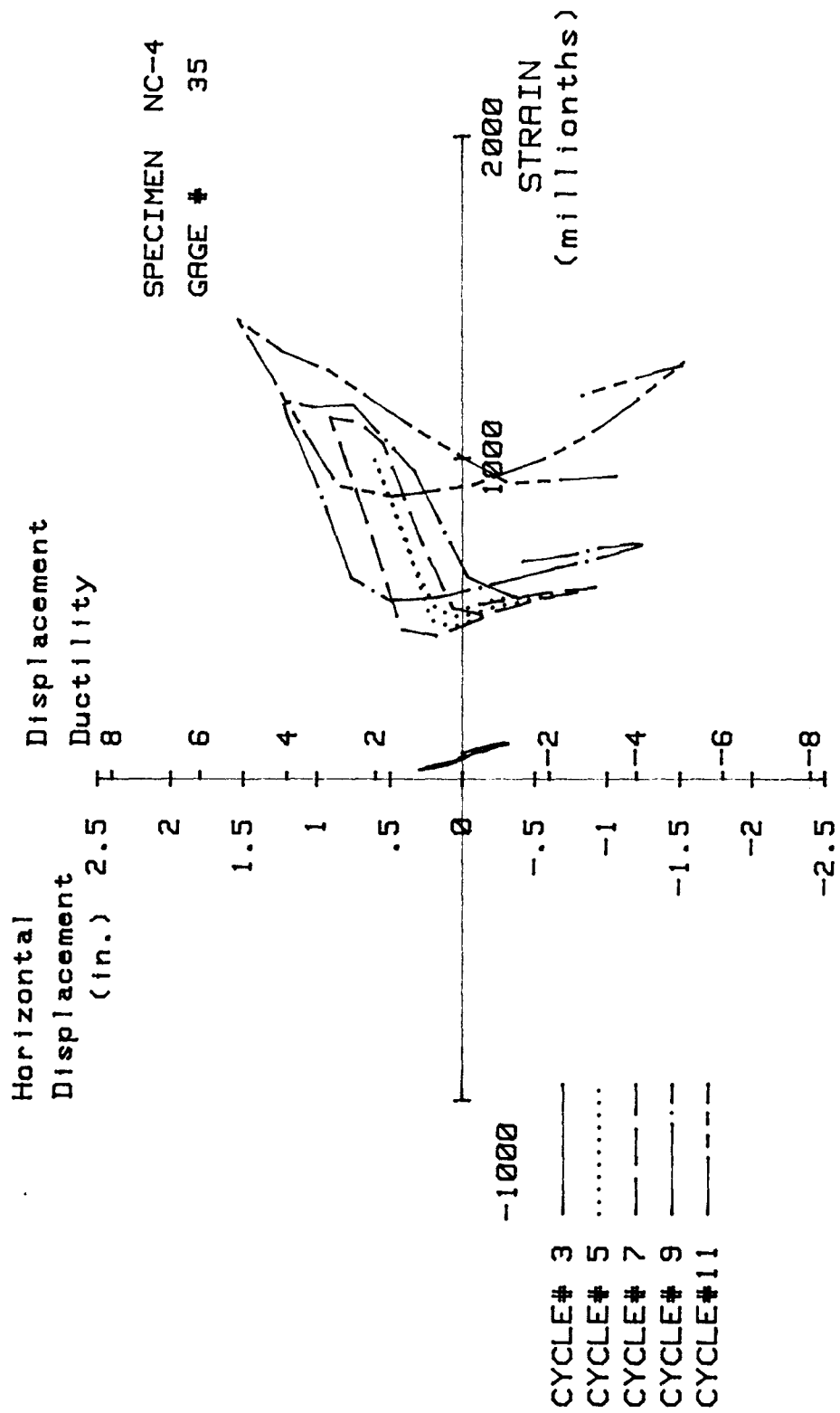


FIG. A-105 MEASURED STRAIN, GAGE #35, SPECIMEN NC-4

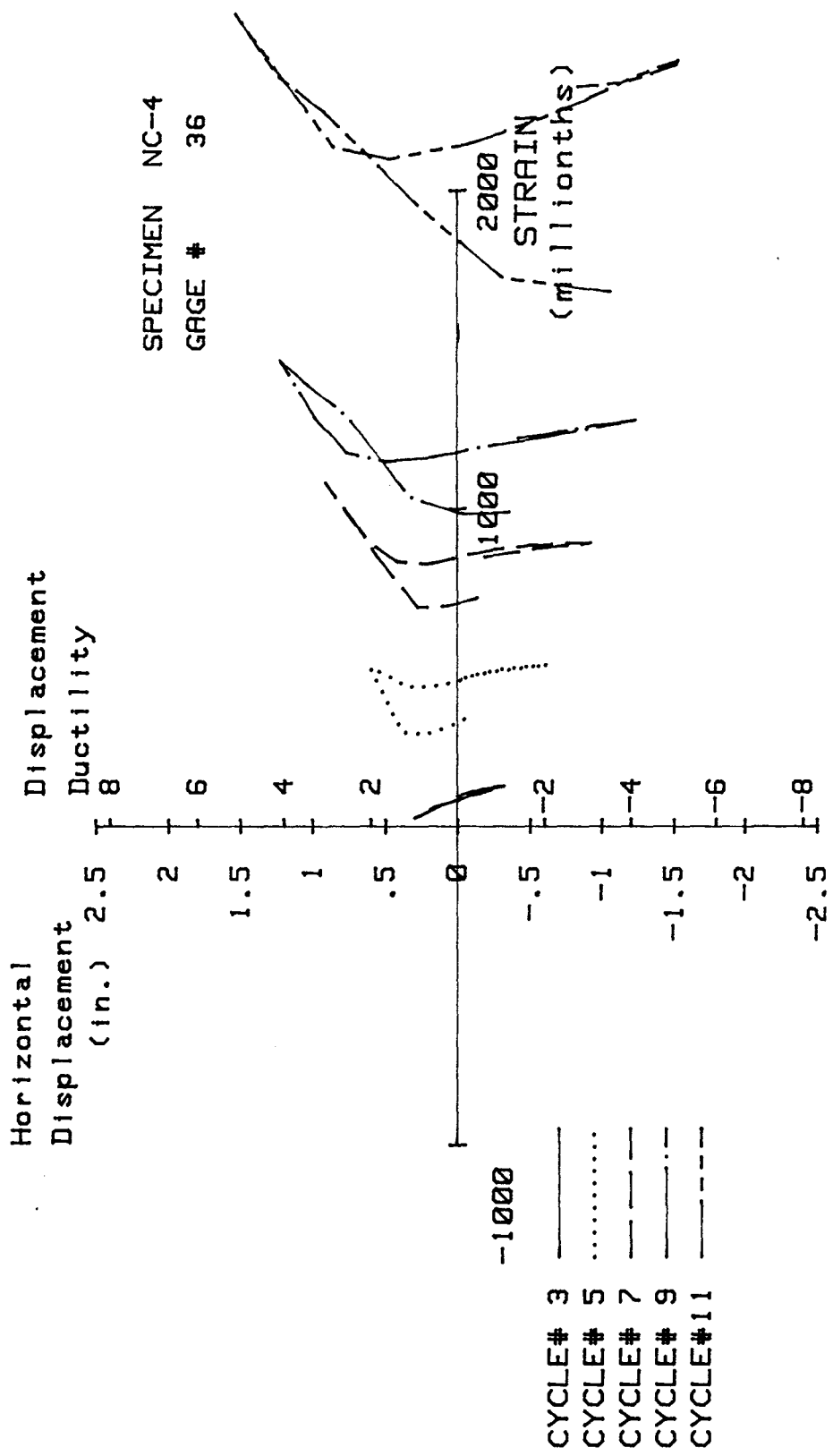


FIG. A-106 MEASURED STRAIN, GAGE #36, SPECIMEN NC-4

Specimen NC-5

Transverse Reinforcement Detail

Figure 4-2c shows the transverse reinforcement for Specimen NC-5. Number 4 bars were used in both the peripheral and interior hoops. The peripheral hoops consisted of a U-shaped and straight piece with hooks at the end. All hooks in the peripheral hoops had 135° bend and 6-bar diameter extensions. The interior hoops were identical to those used in Specimens NC-2 and NC-3. The total effective area of transverse reinforcement provided was 0.68 sq in. The area of the transverse reinforcement provided was 93% of the area required by ACI-318-83 Code.

Load History

The applied axial load was 575 kips, corresponding to 30% of the column axial load capacity.

Maintaining a constant axial load, the specimen was subjected to 16 complete cycles of horizontal loading. Figure A-107 shows the history of the applied horizontal displacement. First yield displacement and the yield curvature were determined to be 0.28 in. and $423 \times 10^{-6} \text{ in.}^{-1}$, respectively, using the procedure outlined in Section 4.8.2. Subsequent to establishing the first yield displacement, horizontal loading consisted of displacement-controlled testing to a maximum displacement ductility ratio of seven.

At the completion of cycle #16 ($\mu=7$) the horizontal displacement was increased to obtain a displacement ductility ratio of eight. However, the specimen failed prior to completion of the first cycle at $\mu=8$.

Test Observations

The first hairline cracks were observed at the peak of the forward loading at cycle #2. These cracks formed at the junction of the upper column and the stub and at distances 4 and 9 in. above the stub.

A small amount of crushing of the cover concrete was observed at cycle #5 ($\mu=2$), however, no spalling of the cover concrete had yet taken place.

Figure A-108 shows the specimen at the end of cycle #6 ($\mu=2$). Limited spalling of the cover concrete at the corners of the stub-upper column interface was visible. Increasing the horizontal displacement to a

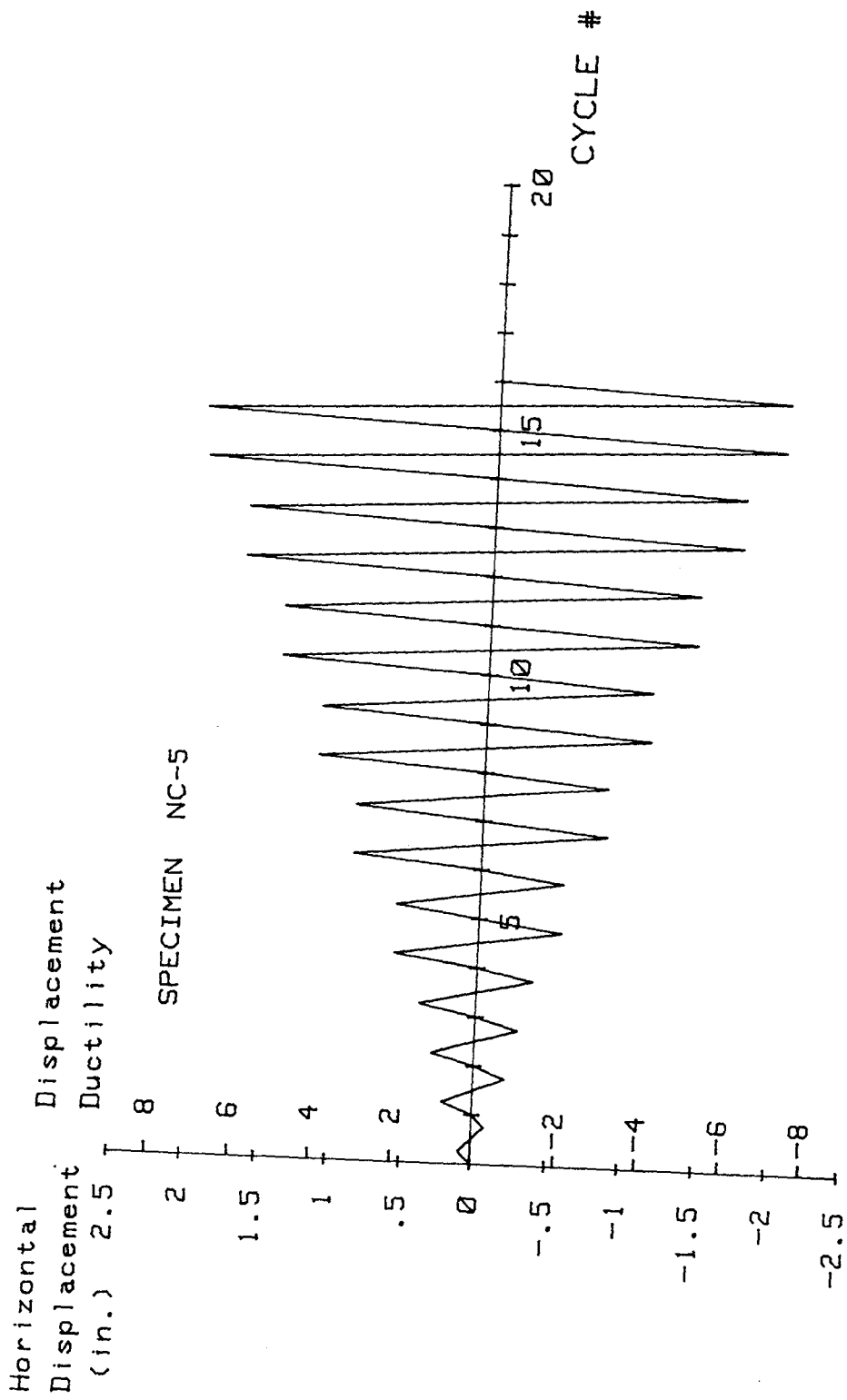


FIG. A-107 LOADING SCHEDULE, SPECIMEN NC-5

Reproduced from
best available copy.

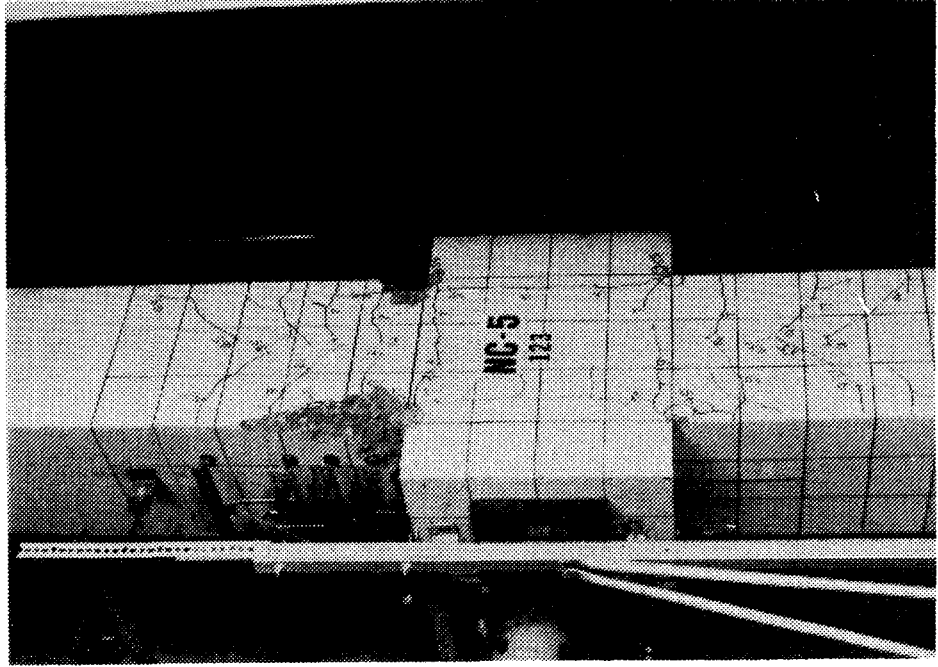


FIG. A-109 TEST SPECIMEN NC-5 AFTER CYCLE #8

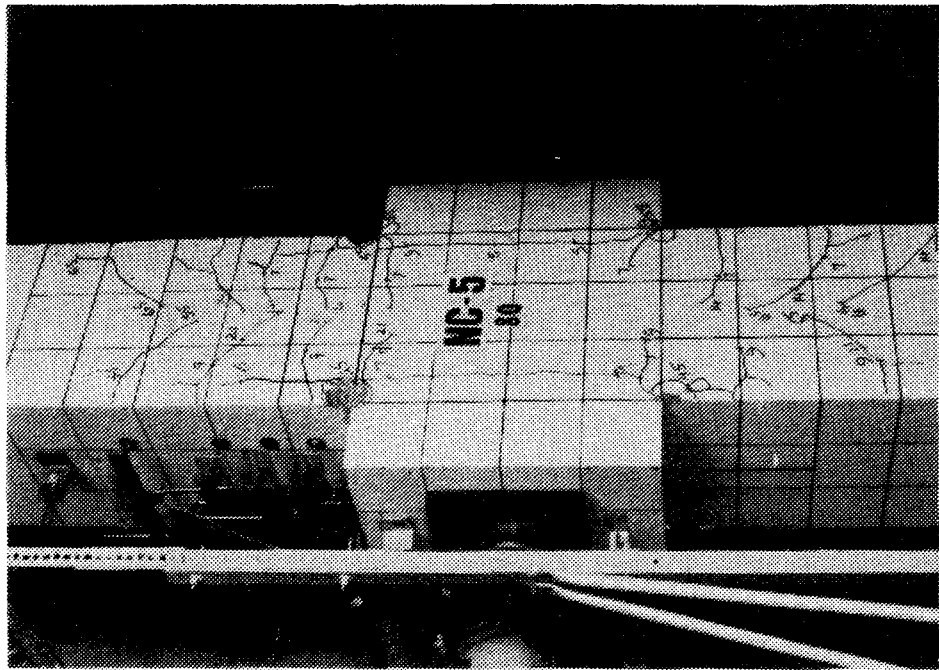


FIG. A-108 TEST SPECIMEN NC-5 AFTER CYCLE #6

displacement ductility ratio of three resulted in more spalling of the cover concrete (see Fig. A-109). The spalling was confined primarily to a region within 6 in. above the stub.

Figure A-110 shows the specimen at the end of cycle #12. The cover concrete had spalled off to such an extent that the corner longitudinal bars and some of the peripheral hoops were visible. Figure A-111 shows the specimen at the end of cycle #14 ($\mu=6$). The peripheral hoops and the corner longitudinal bars within 12 in. above the stub were visible, though no visible damage was observed in the transverse reinforcement or longitudinal bars.

Figure A-112 shows the specimen at the end of cycle #16 ($\mu=7$). At this load stage some lateral bending of the corner bars was visible. In addition, some cover concrete spalled off such that some crossties and the middle longitudinal bars were visible. However, the anchorages of the peripheral hoops were still embedded inside the core concrete and no apparent damage to the anchorages of the peripheral hoops was observed. The specimen failed by buckling at the corner longitudinal bars before completing the first cycle at a displacement ductility ratio of eight (see Fig. A-113). Buckling of the corner longitudinal bars coincided with loss of anchorage of the peripheral hoops at 2 and 6 in. above the stub.

Load Deflection and Moment-Curvature Characteristics

Figure A-114 shows the horizontal load-deflection behavior of the specimen. At all displacement levels (with the exception of the second cycle into displacement ductility ratio of seven), the applied horizontal load was greater than the theoretical value calculated using the procedure outlined in Section 4.8.2.

Figure A-115 shows curvature distribution along the upper column. The maximum curvature ductility at the displacement ductility ratio of 7 was 20, and was located within 4 in. above the column. Figure A-116 shows the moment curvature characteristics of the column at the upper column-stub level. The theoretical moment capacity of the column cross-section calculated using the procedure outlined in Section 4.8.2 was 5226 in-kips, while the maximum applied moment was 6365 in-kips, approximately 22% more than the calculated value. The ratio of the peak moment at the second cycle

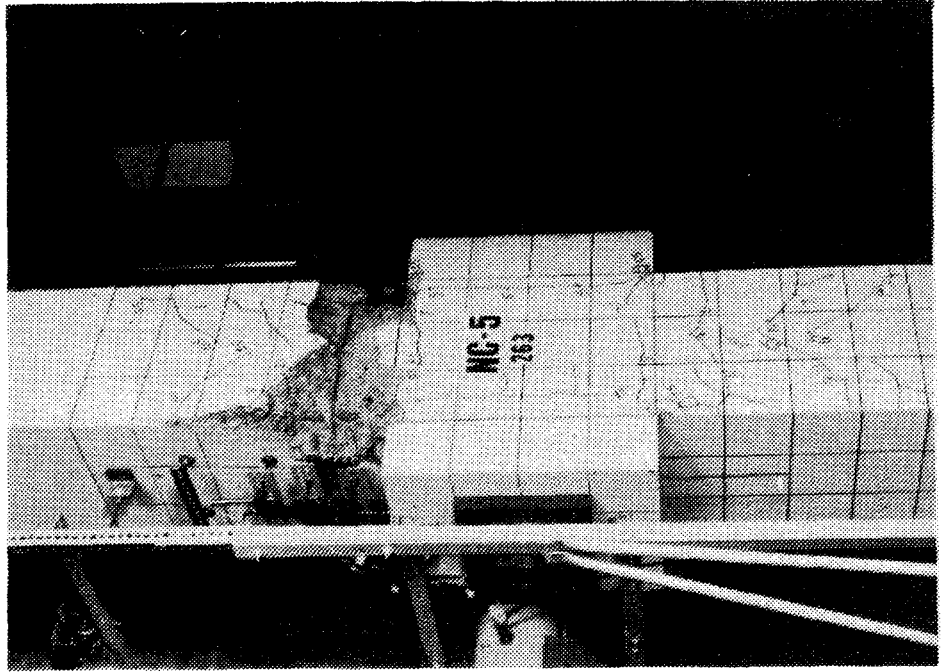


FIG. A-111 TEST SPECIMEN NC-5 AFTER CYCLE #14

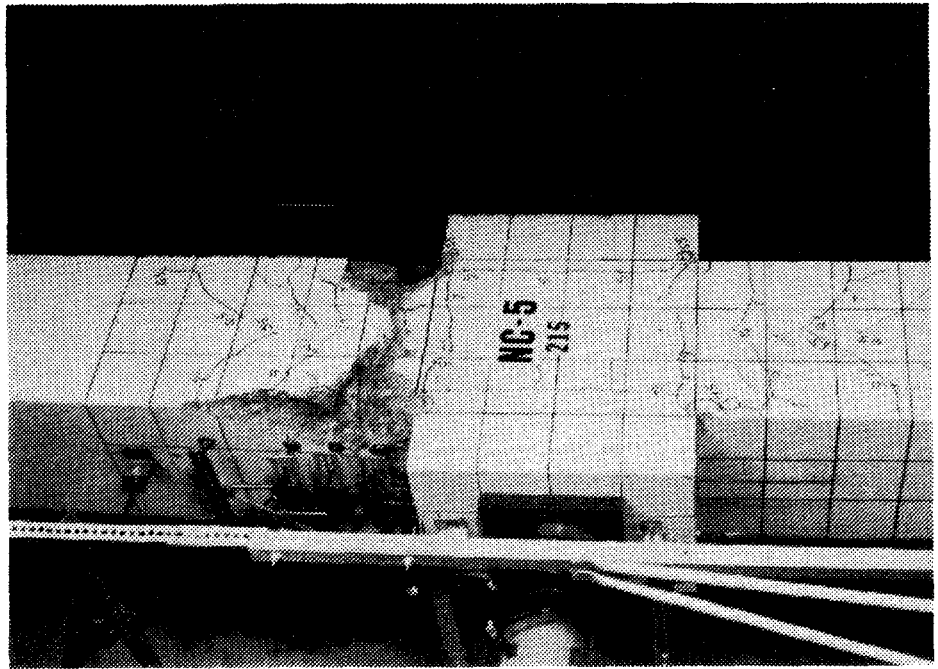


FIG. A-110 TEST SPECIMEN NC-5 AFTER CYCLE #12

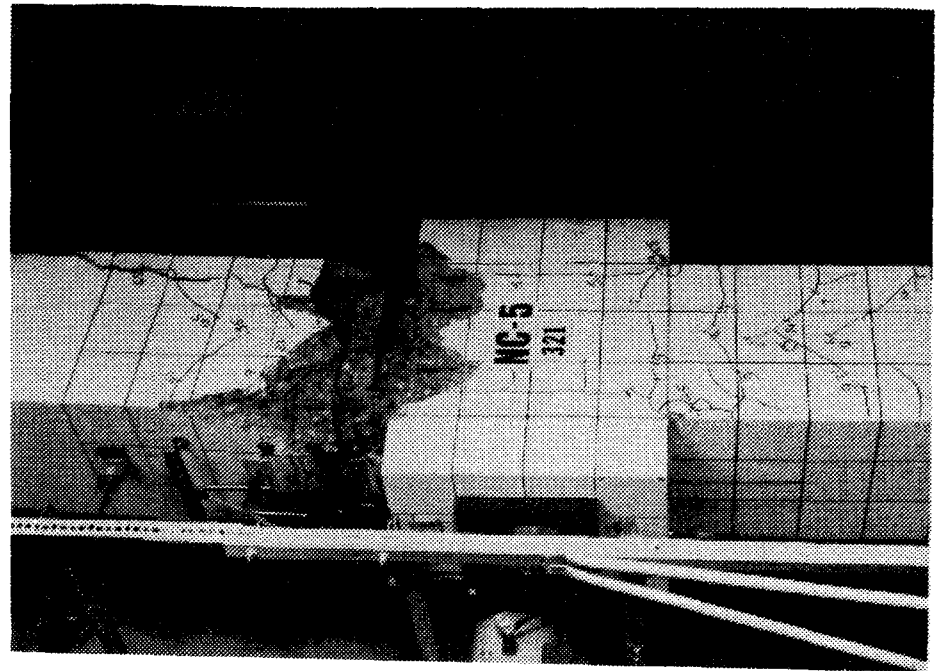


FIG. A-112 TEST SPECIMEN NC-5 AFTER CYCLE #16

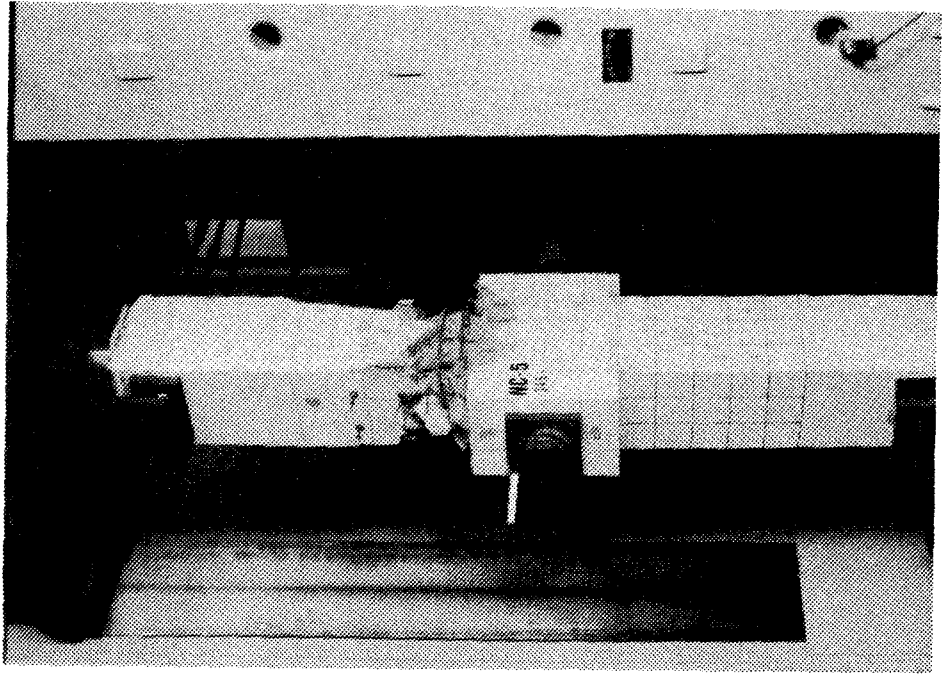
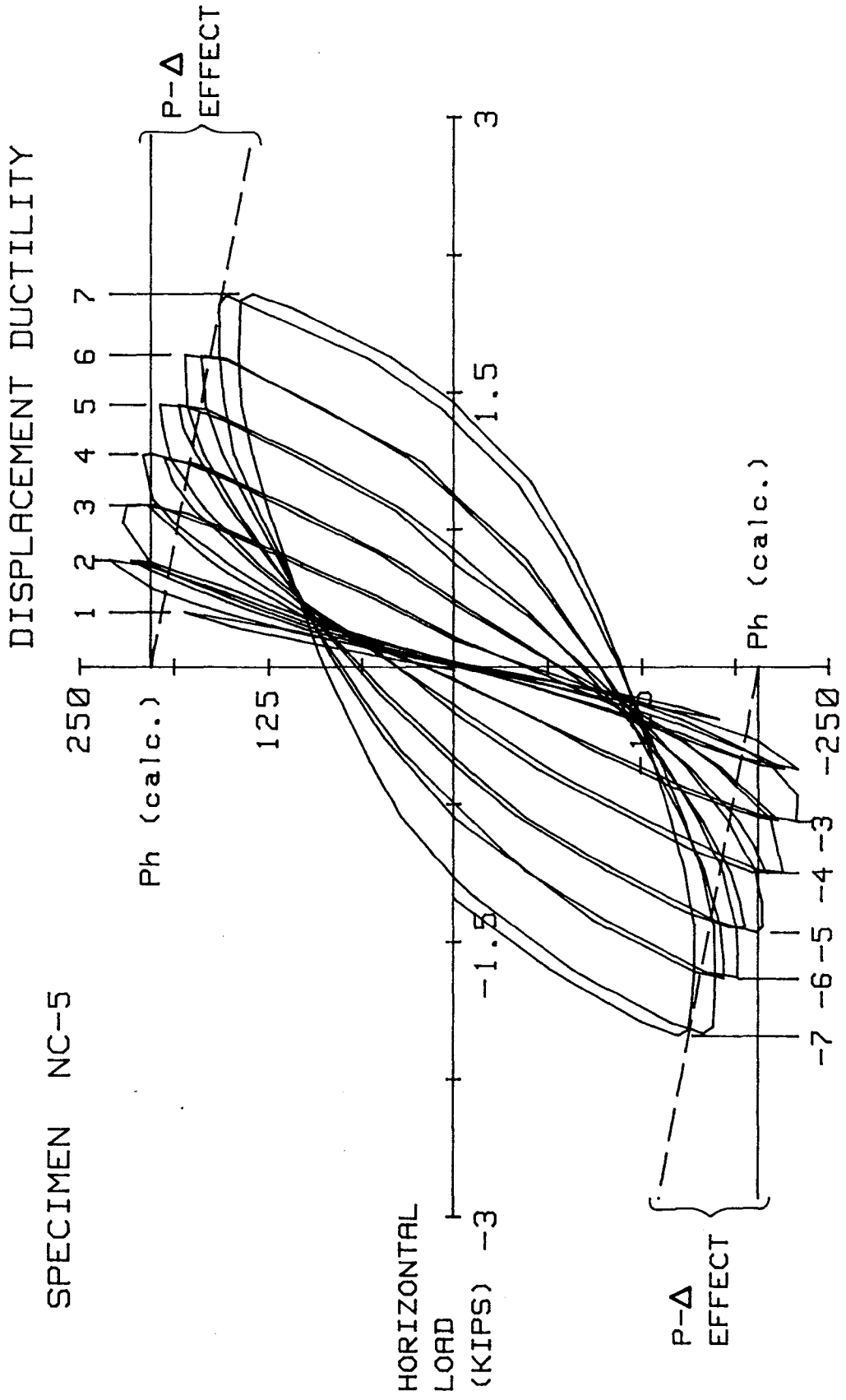


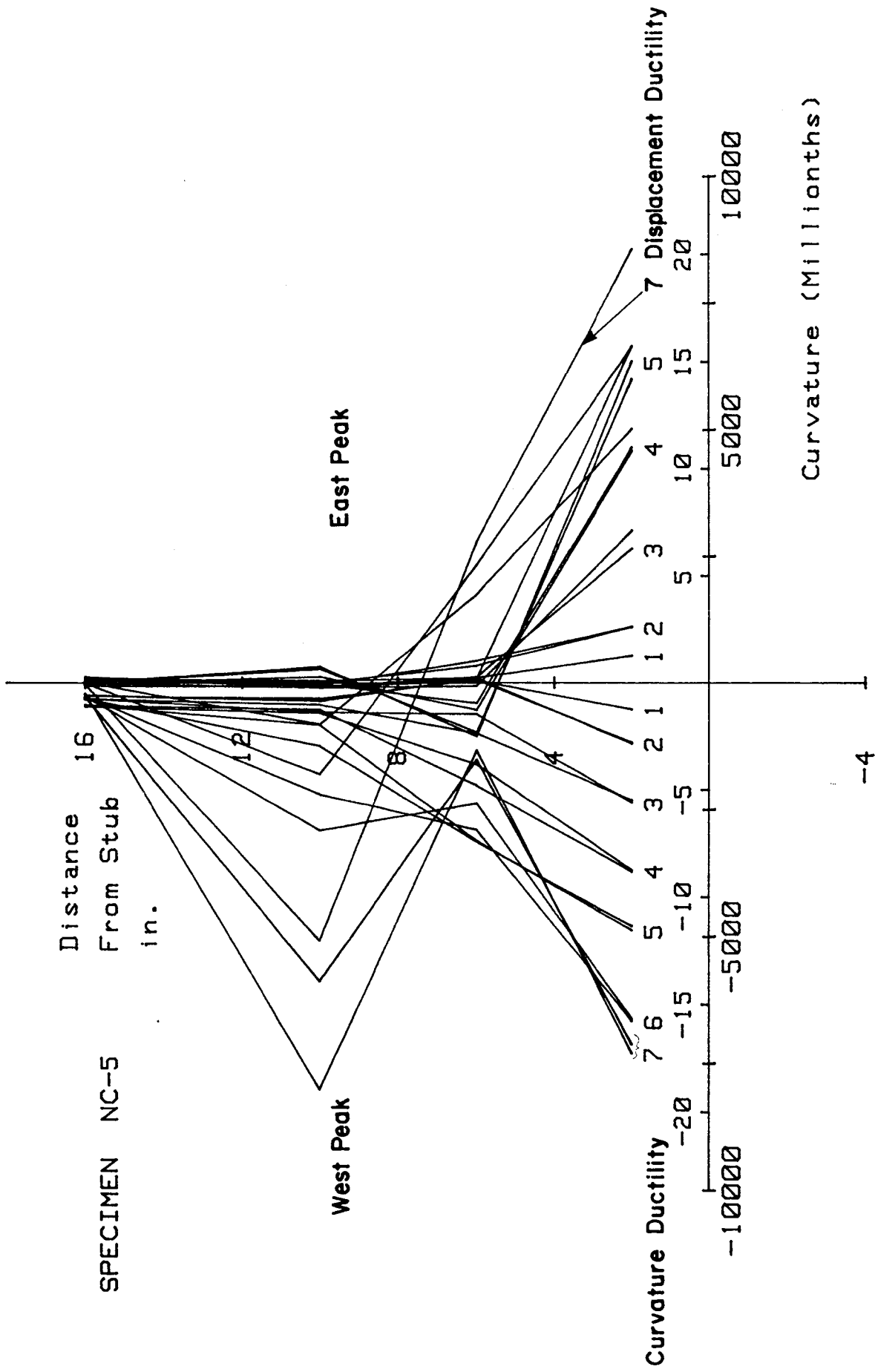
FIG. A-113 TEST SPECIMEN NC-5 AFTER TEST CONCLUSION



Metric Equivalents
 1 in.=25.4 mm
 1 kip=4.45 KN

HORIZONTAL DISPLACEMENT (IN.)

FIG. A-114 HORIZONTAL LOAD VERSUS DISPLACEMENT, SPECIMEN NC-5



SPECIMEN NC-5

FIG. A-116 CURVATURE DISTRIBUTION ALONG UPPER COLUMN, SPECIMEN NC-5

to the peak moment at the first cycle at various displacement levels varied between 0.93 and 0.95.

Transverse Reinforcement Strain

Figure 4-11 shows the locations of 24 strain gages attached to the transverse reinforcement. Figures A-117 through A-138 show the data obtained from these strain gages.

Beyond cycle #9 some of the strain gages were lost. The specified minimum yield strain of the transverse reinforcement was 2070 micro-strain. The first measured strain greater than yield strain was observed during cycle #15 ($\mu=7$) on the interior hoops located 10 in. from the stub at which time the strain on the peripheral hoop at the same level was 2030 micro-strain. It should be noted, however, that at this stage some of the strain gages were lost. Therefore, the first yielding could have occurred at some other location.

In general, strain on the interior hoops was smaller than strain on the peripheral hoops through cycle #7 ($\mu=3$). However, beyond this load stage, strain on the interior hoops exceeded that on the peripheral hoops in some cases.

During the early loading stages (through cycle #7), strain on the transverse reinforcements located 2 in. above the stub was the least.

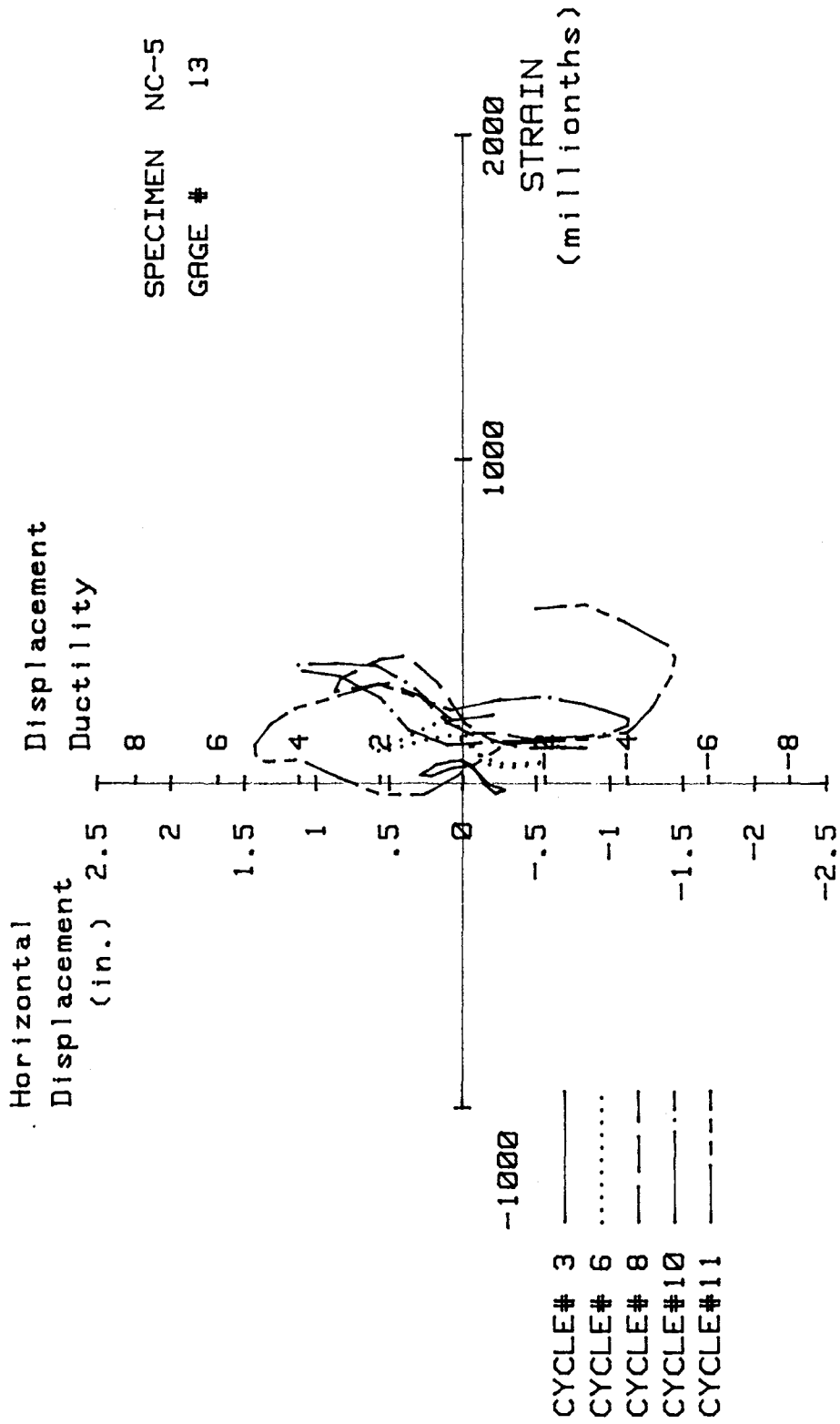


FIG. A-117 MEASURED STRAIN, GAGE #13, SPECIMEN NC-5

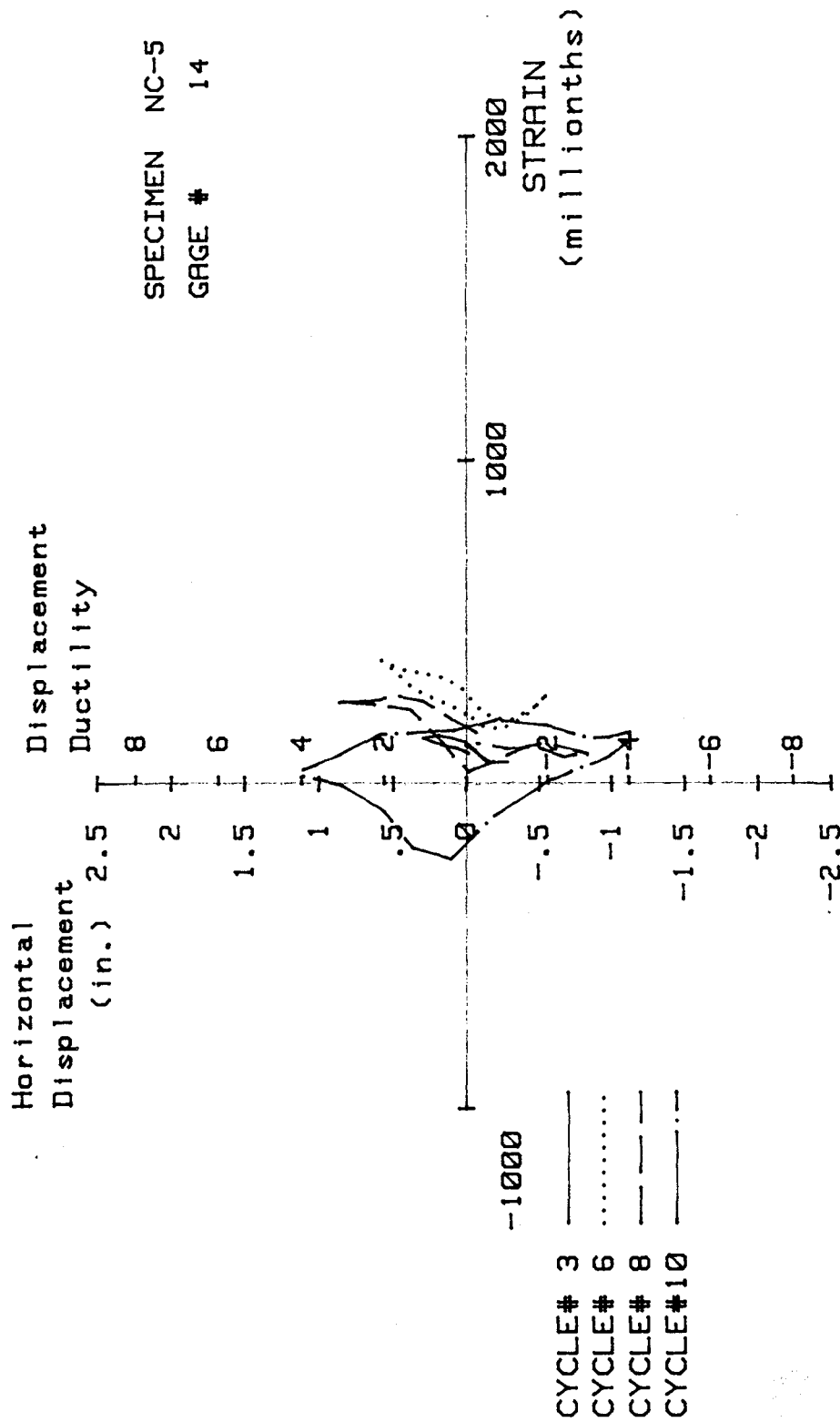


FIG. A-118 MEASURED STRAIN, GAGE #14, SPECIMEN NC-5

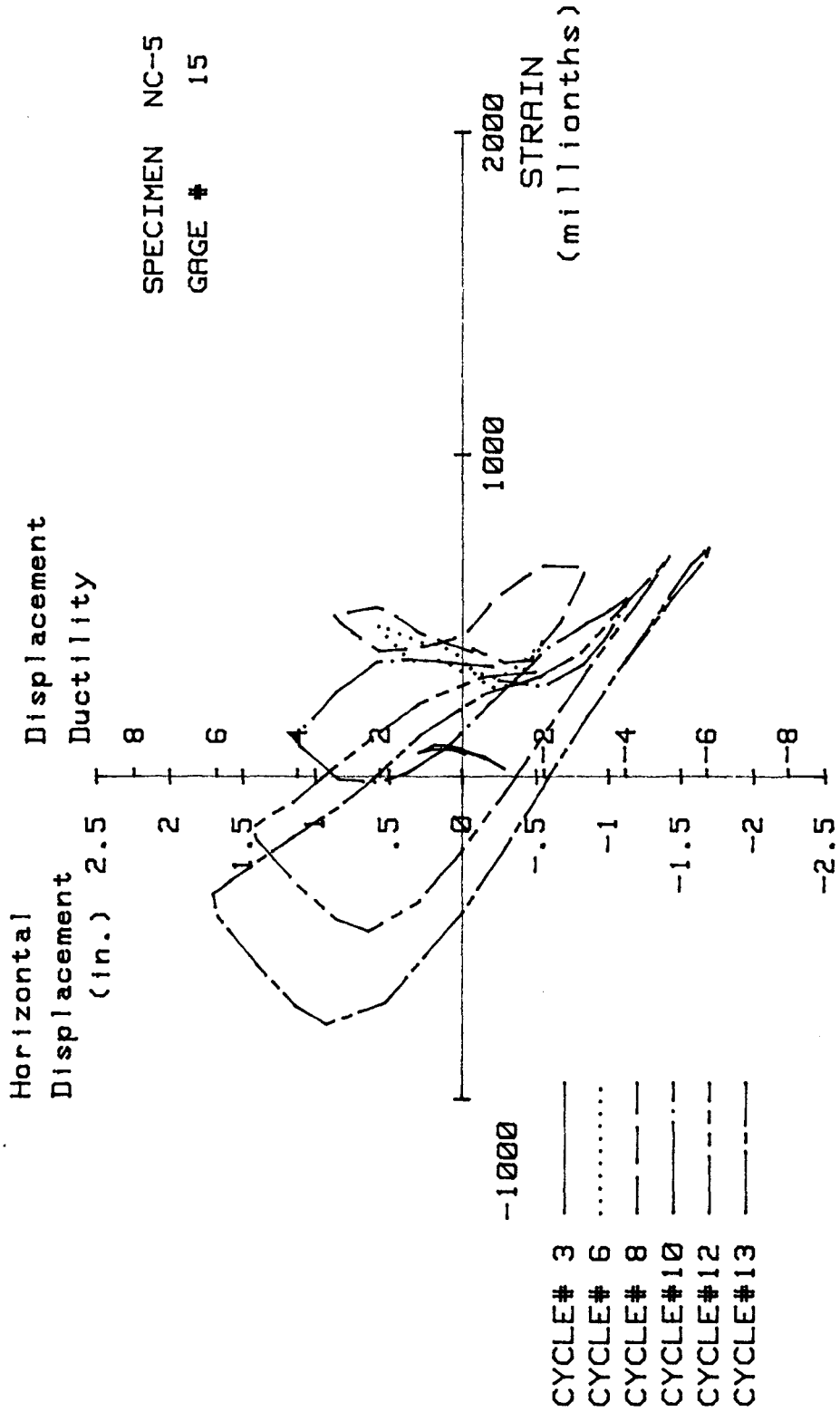


FIG. A-119 MEASURED STRAIN, GAGE #15, SPECIMEN NC-5

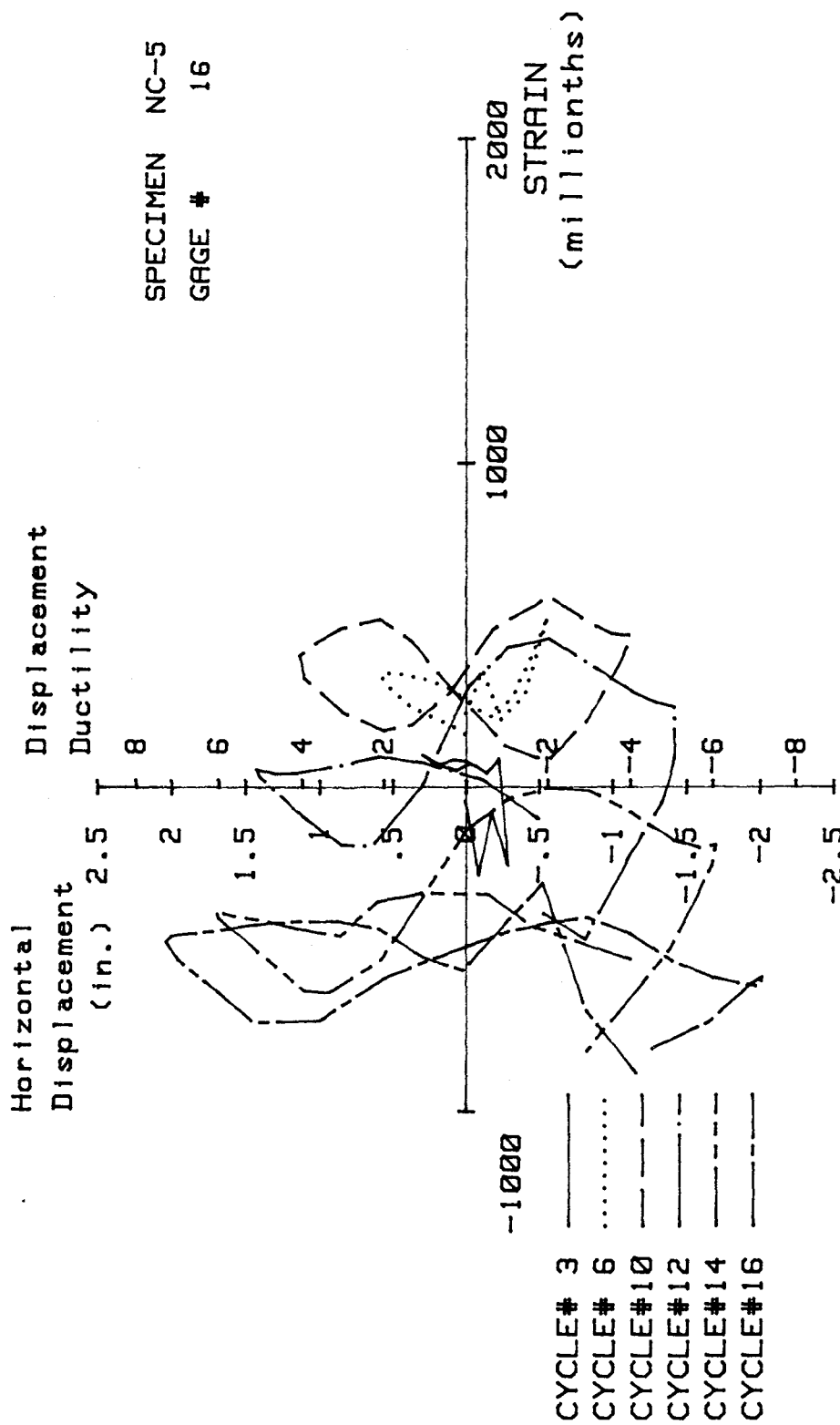


FIG. A-120 MEASURED STRAIN, GAGE #16, SPECIMEN NC-5

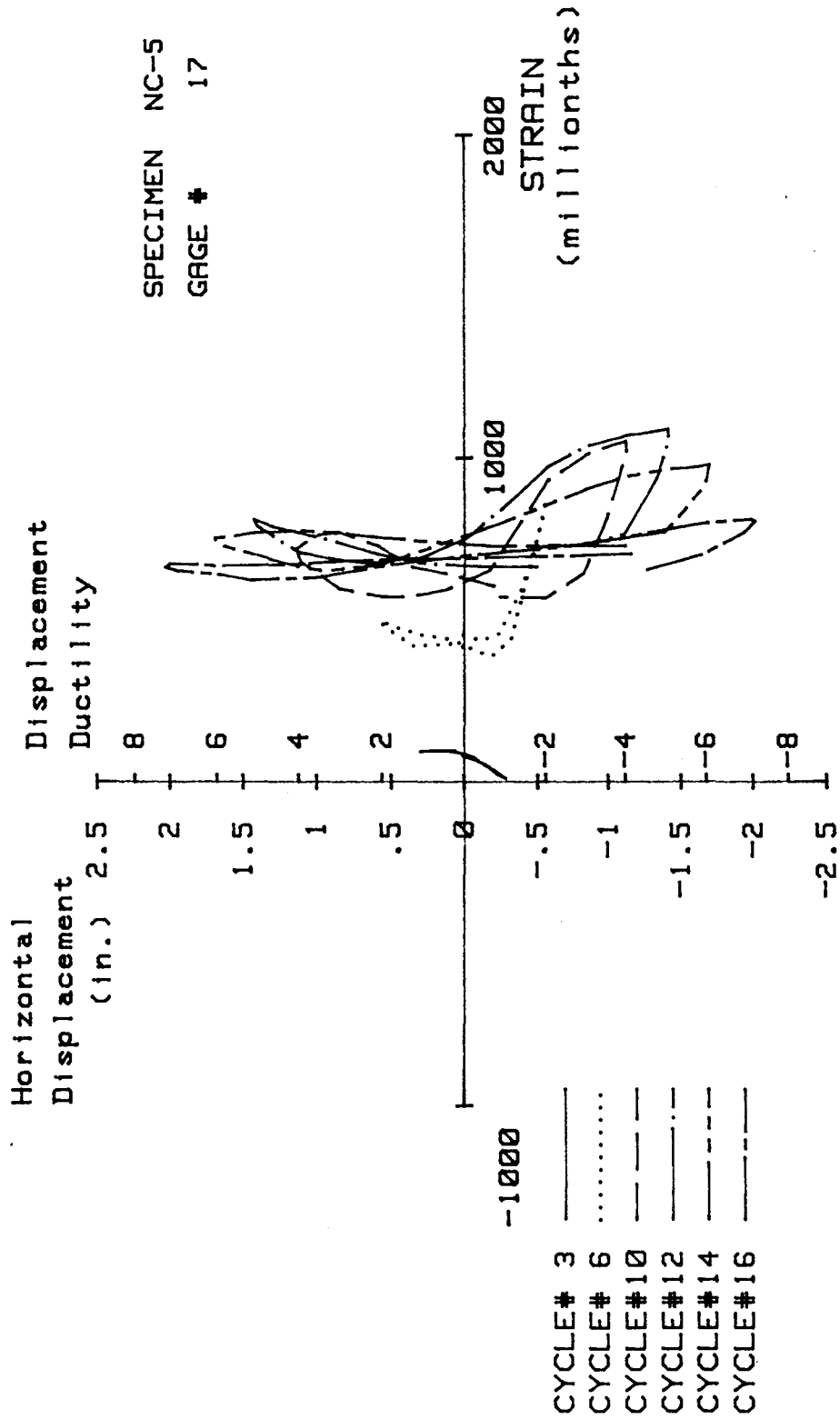


FIG. A-121 MEASURED STRAIN, GAGE #17, SPECIMEN NC-5

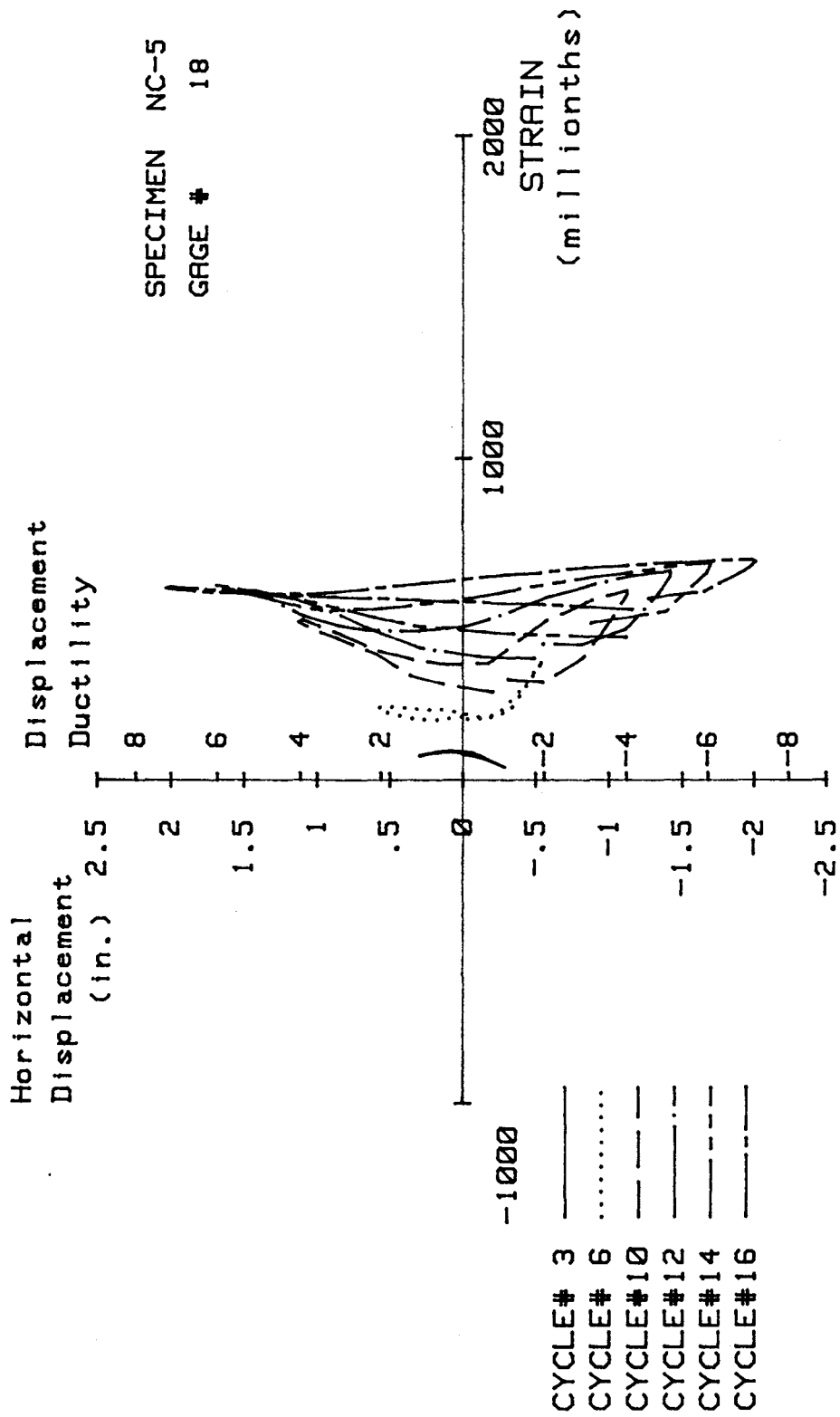


FIG. A-122 MEASURED STRAIN, GAGE #18, SPECIMEN NC-5

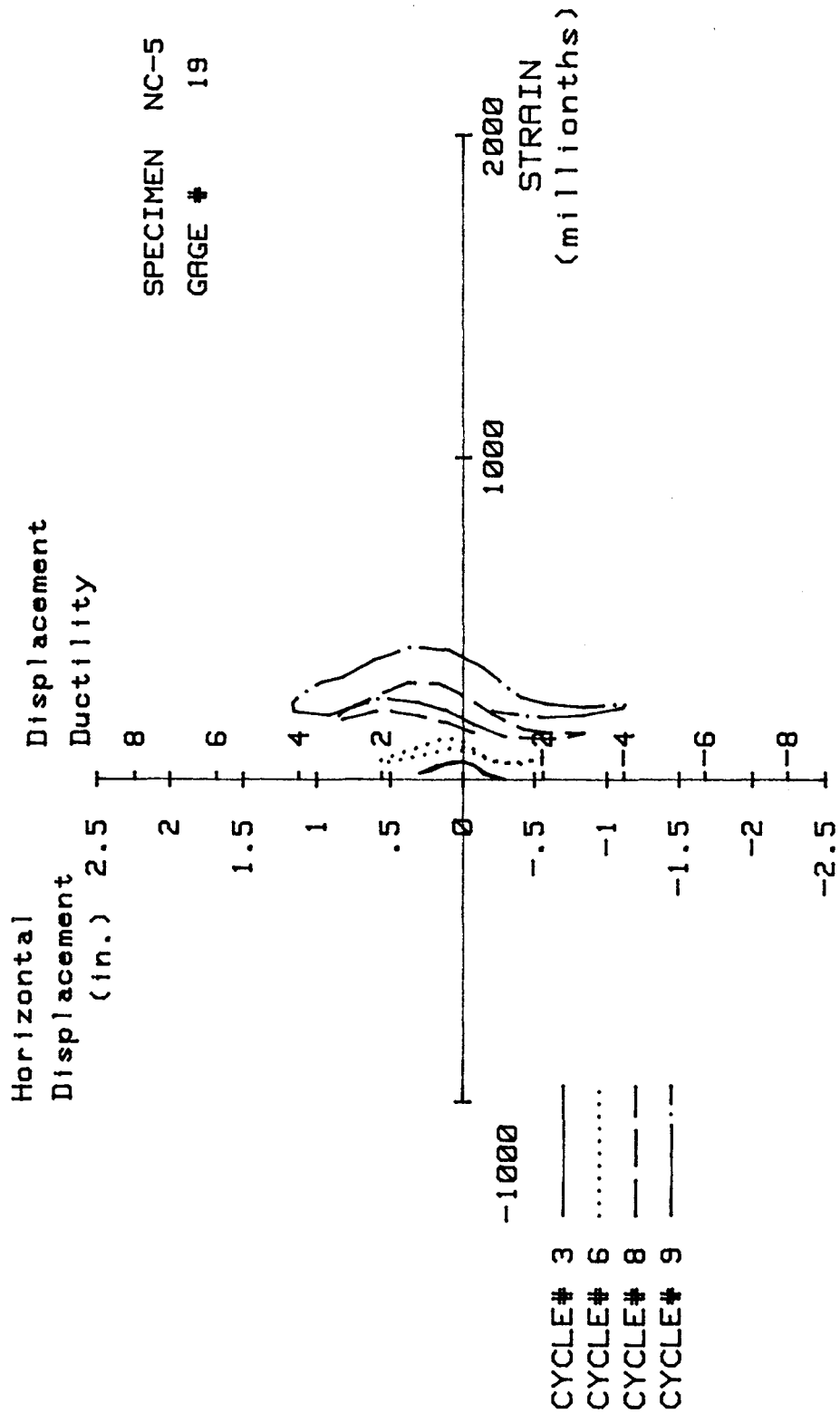


FIG. A-123 MEASURED STRAIN, GAGE #19, SPECIMEN NC-5

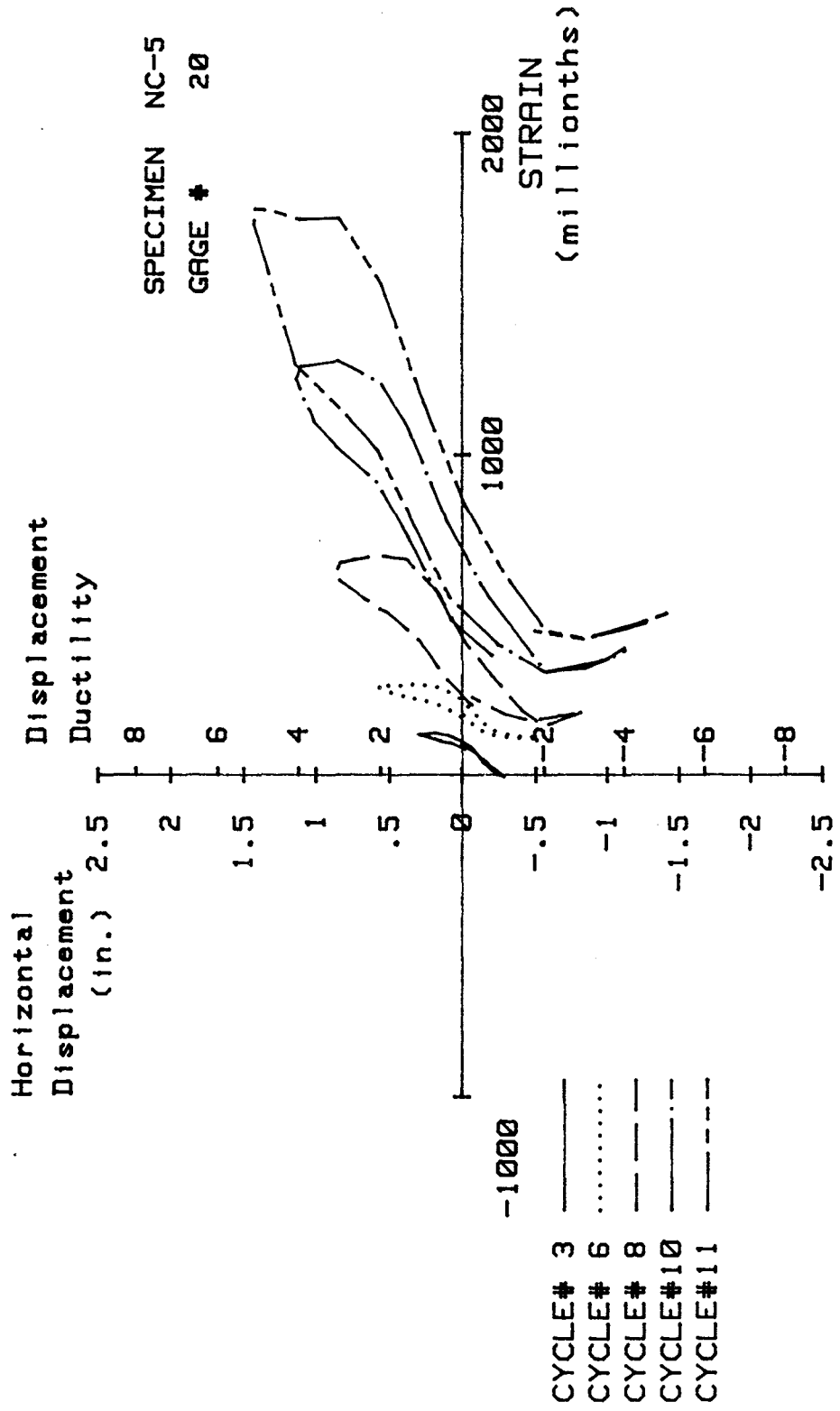


FIG. A-124 MEASURED STRAIN, GAGE #20, SPECIMEN NC-5

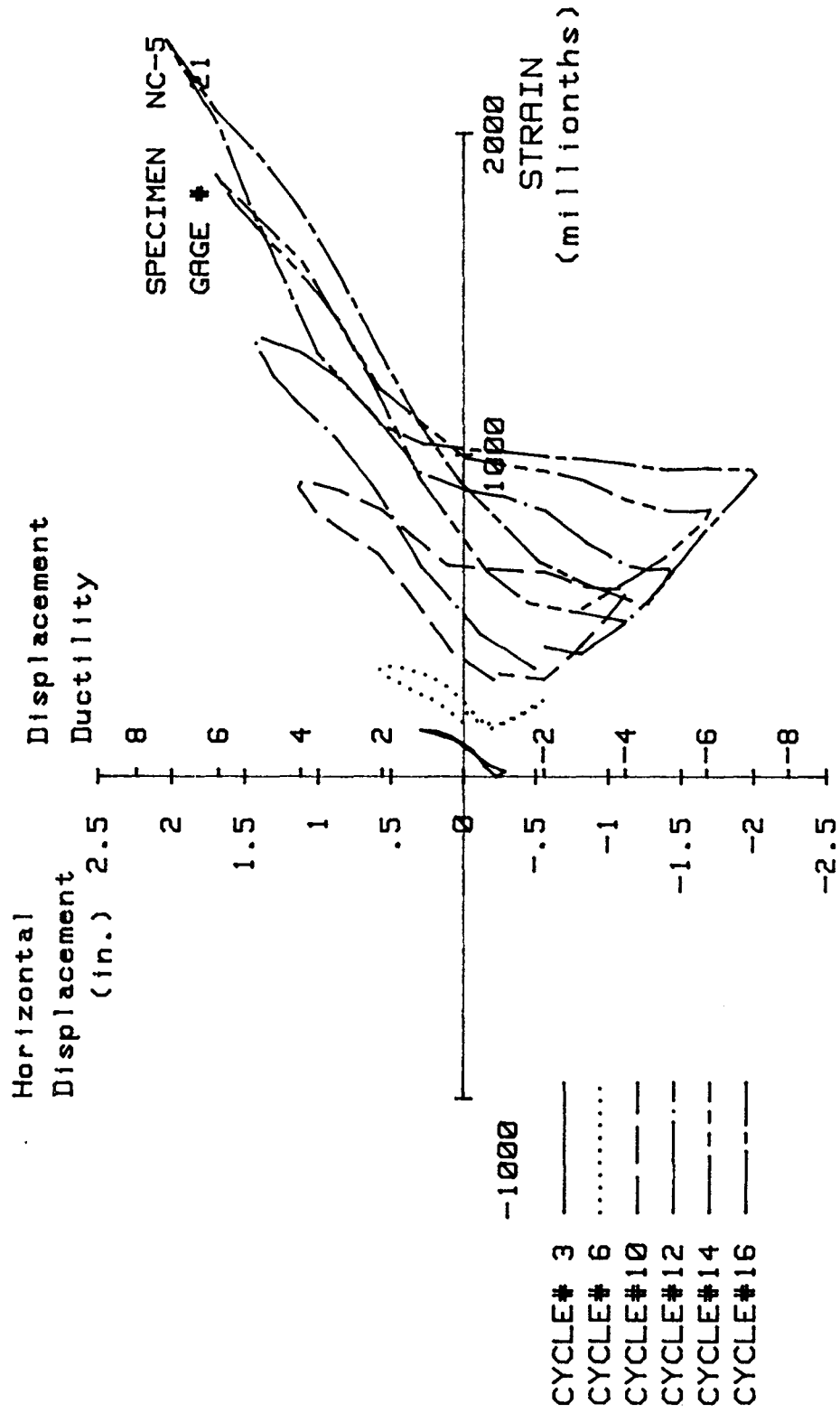


FIG. A-125 MEASURED STRAIN, GAGE #21, SPECIMEN NC-5

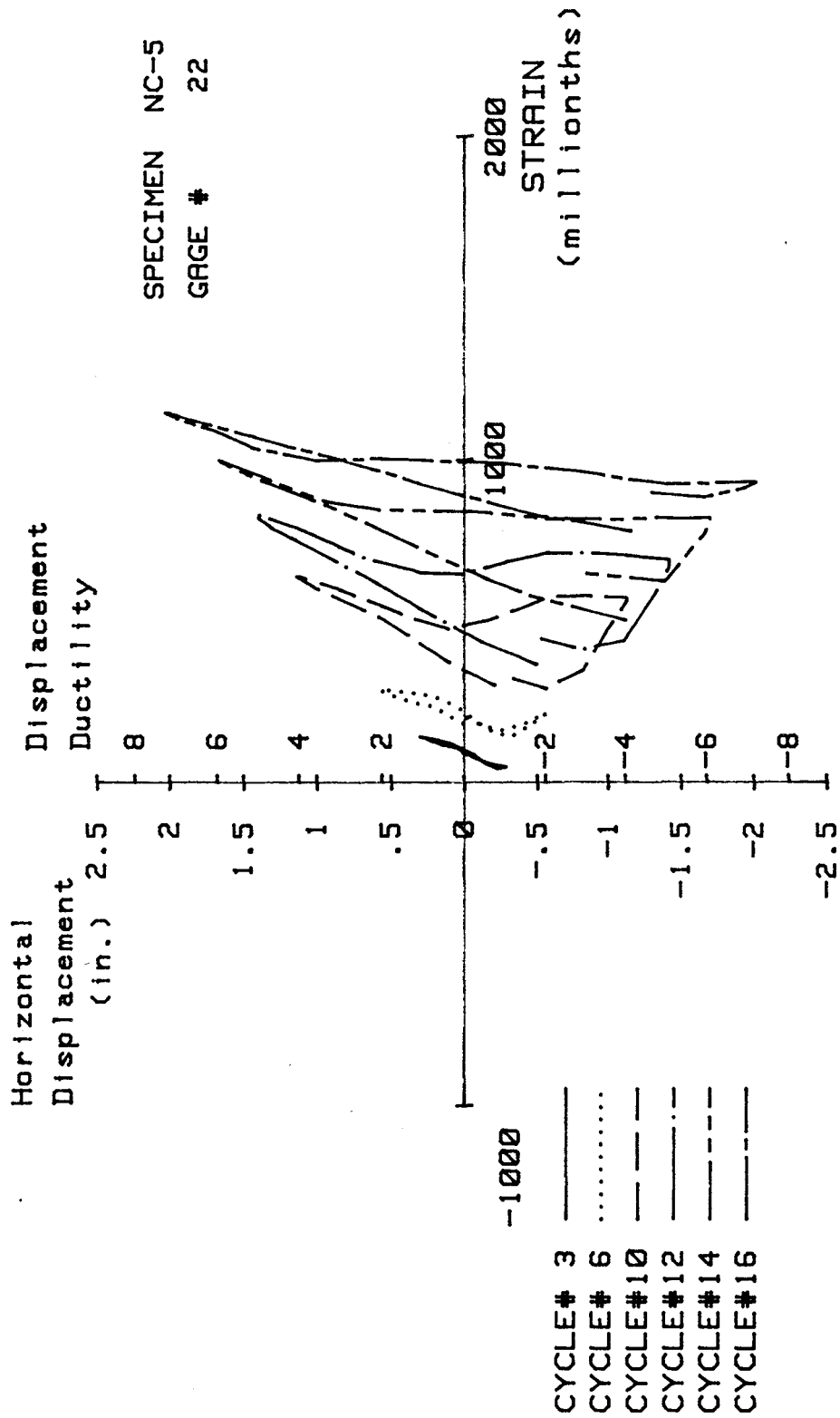


FIG. A-126 MEASURED STRAIN, GAGE #22, SPECIMEN NC-5

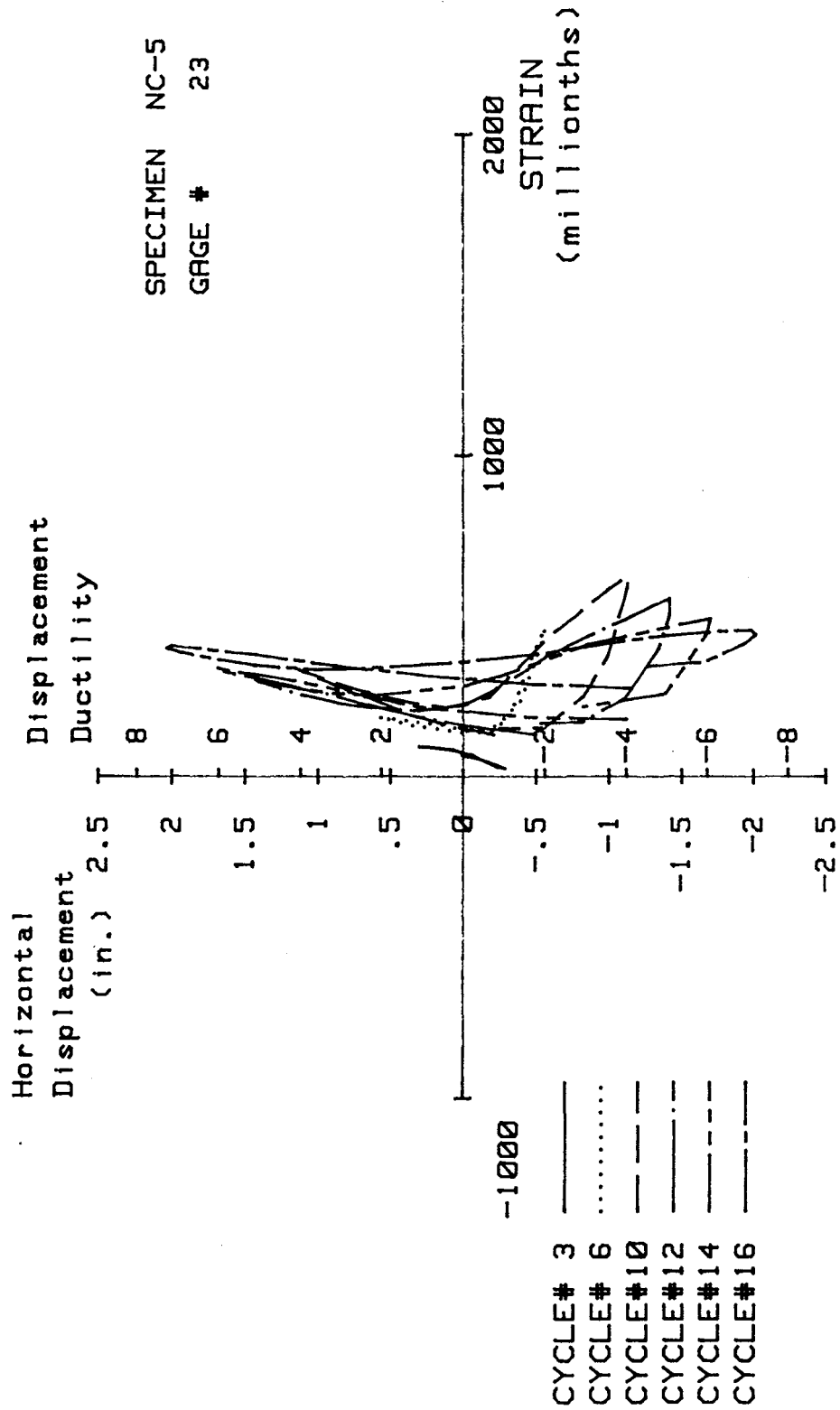


FIG. A-127 MEASURED STRAIN, GAGE #23, SPECIMEN NC-5

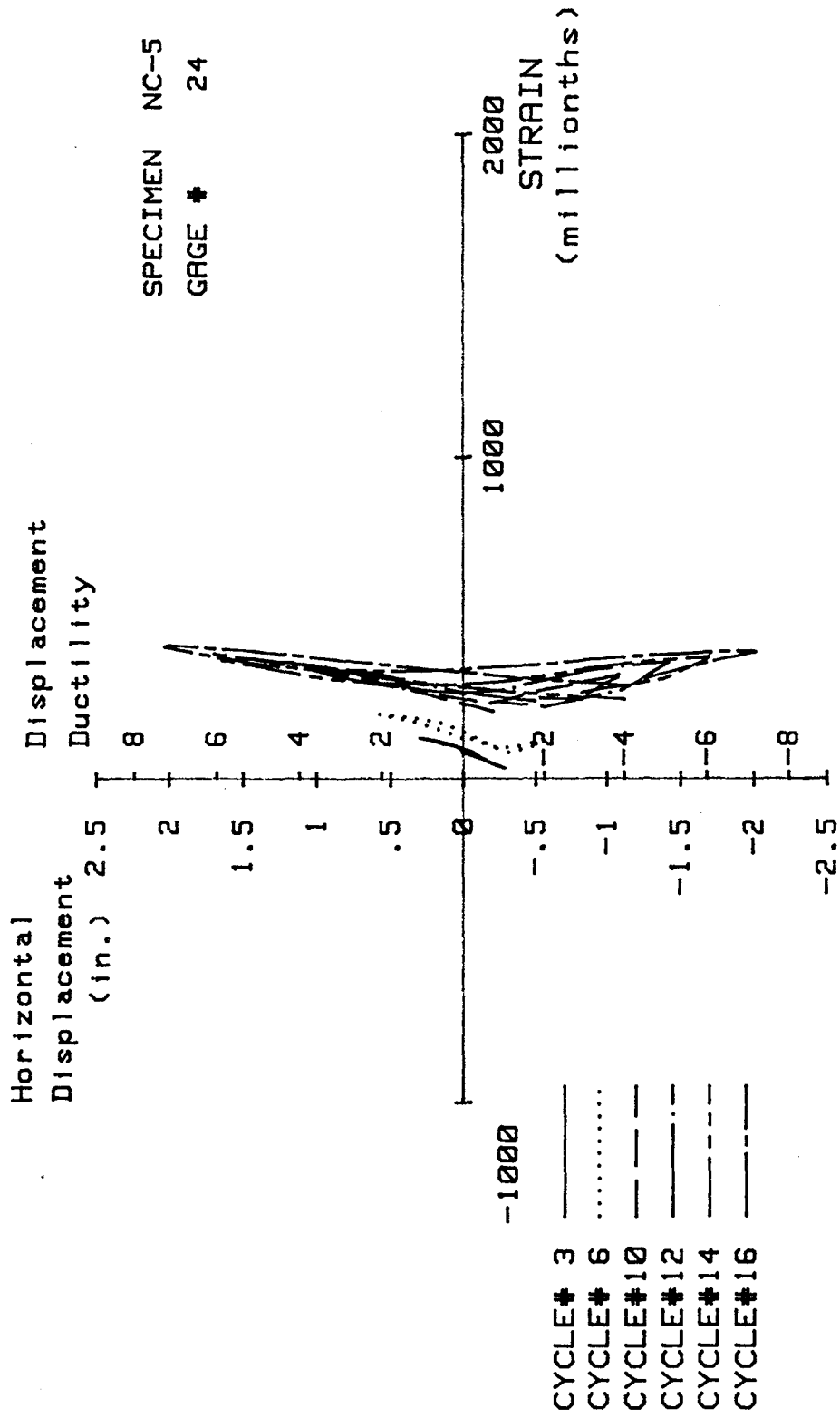


FIG. A-128 MEASURED STRAIN, GAGE #24, SPECIMEN NC-5

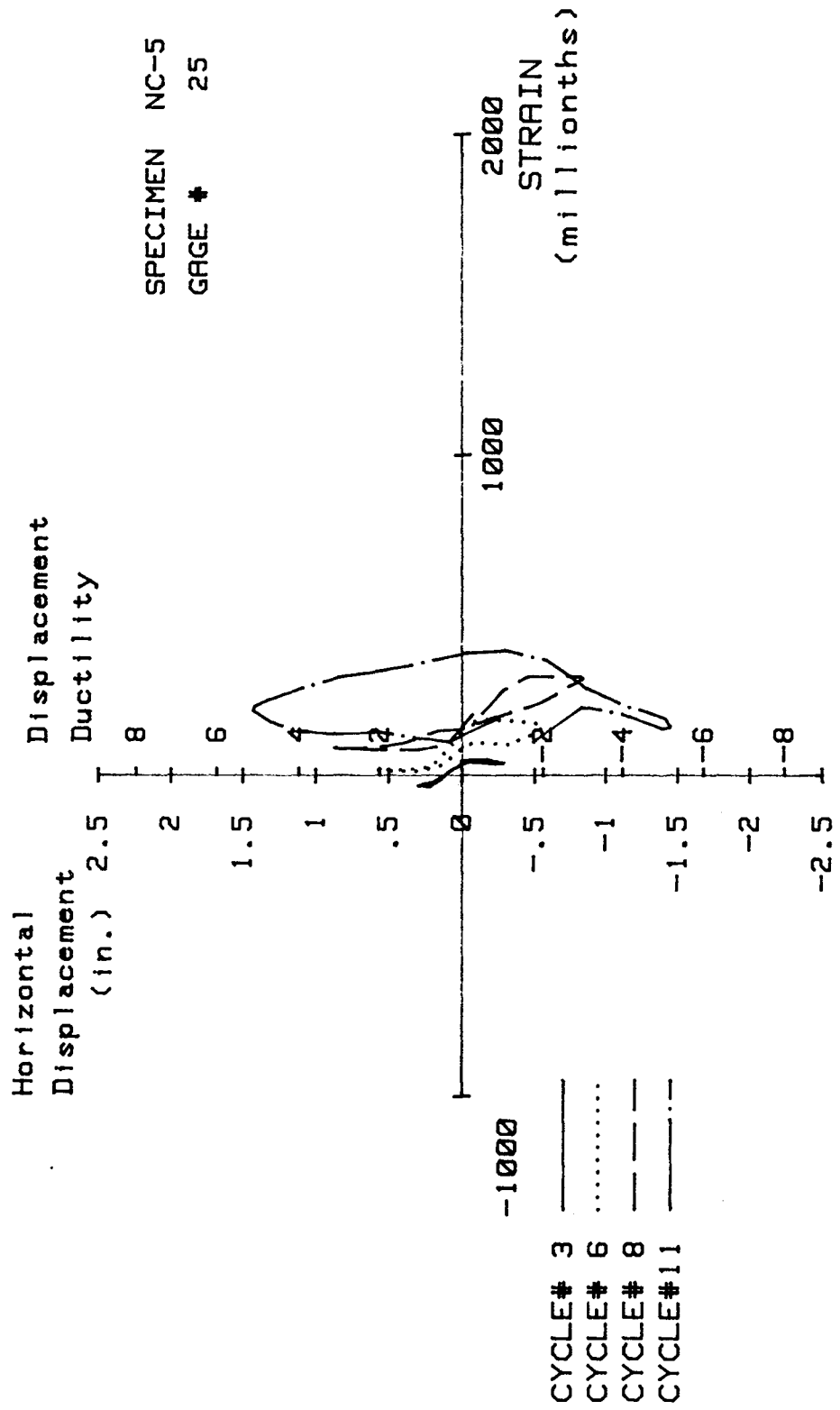


FIG. A-129 MEASURED STRAIN, GAGE #25, SPECIMEN NC-5

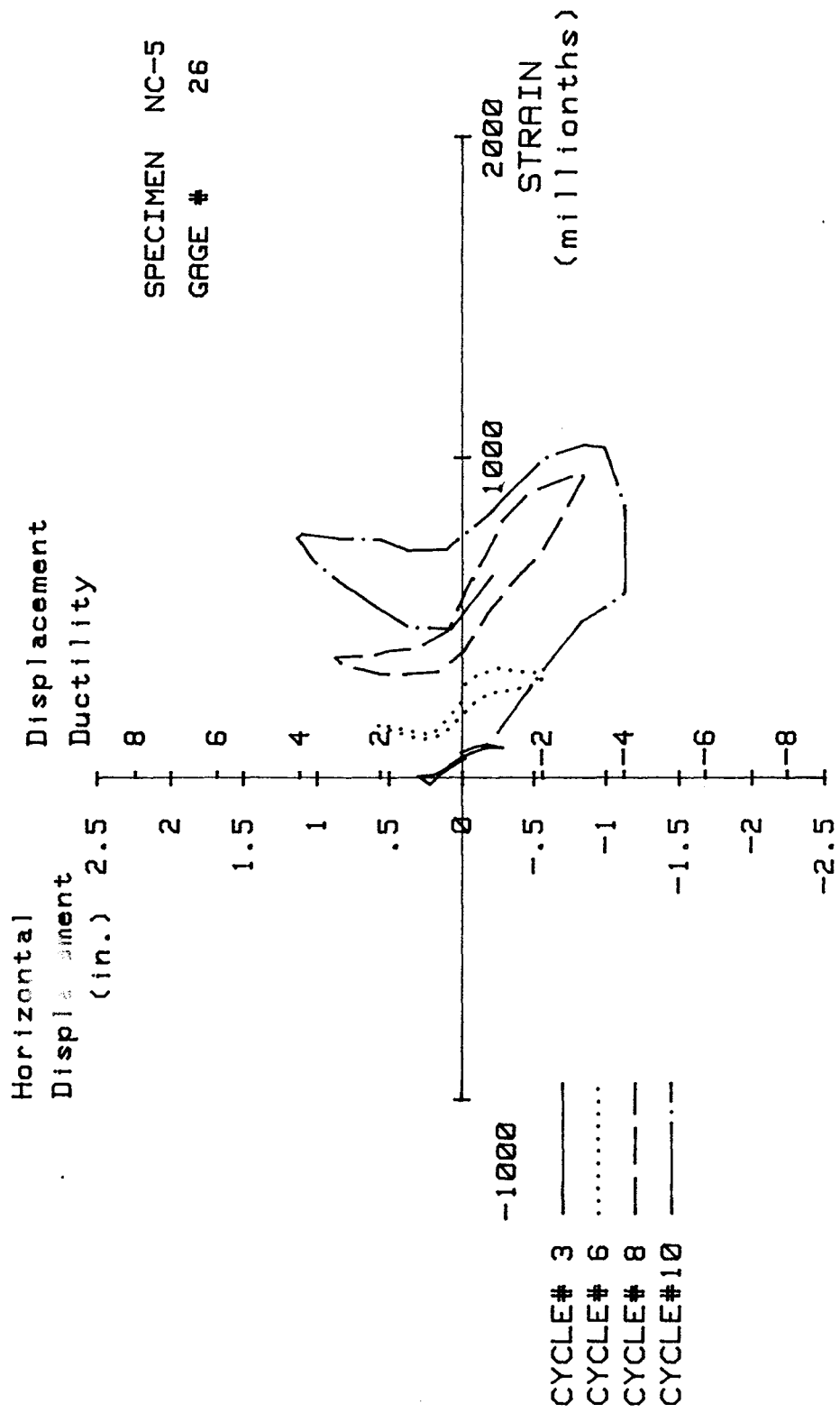


FIG. A-130 MEASURED STRAIN, GAGE #26, SPECIMEN NC-5

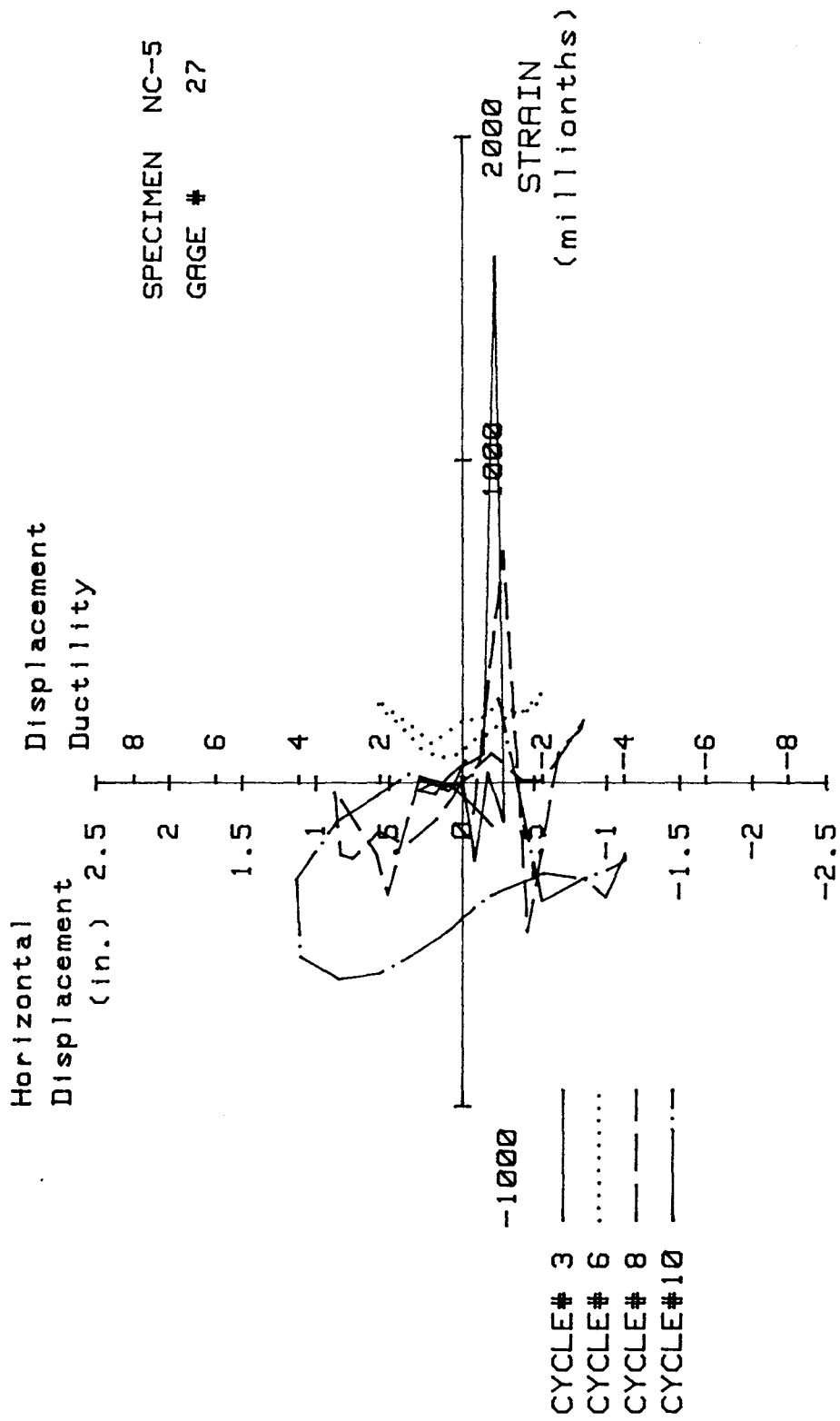


FIG. A-131 MEASURED STRAIN, GAGE #27, SPECIMEN NC-5

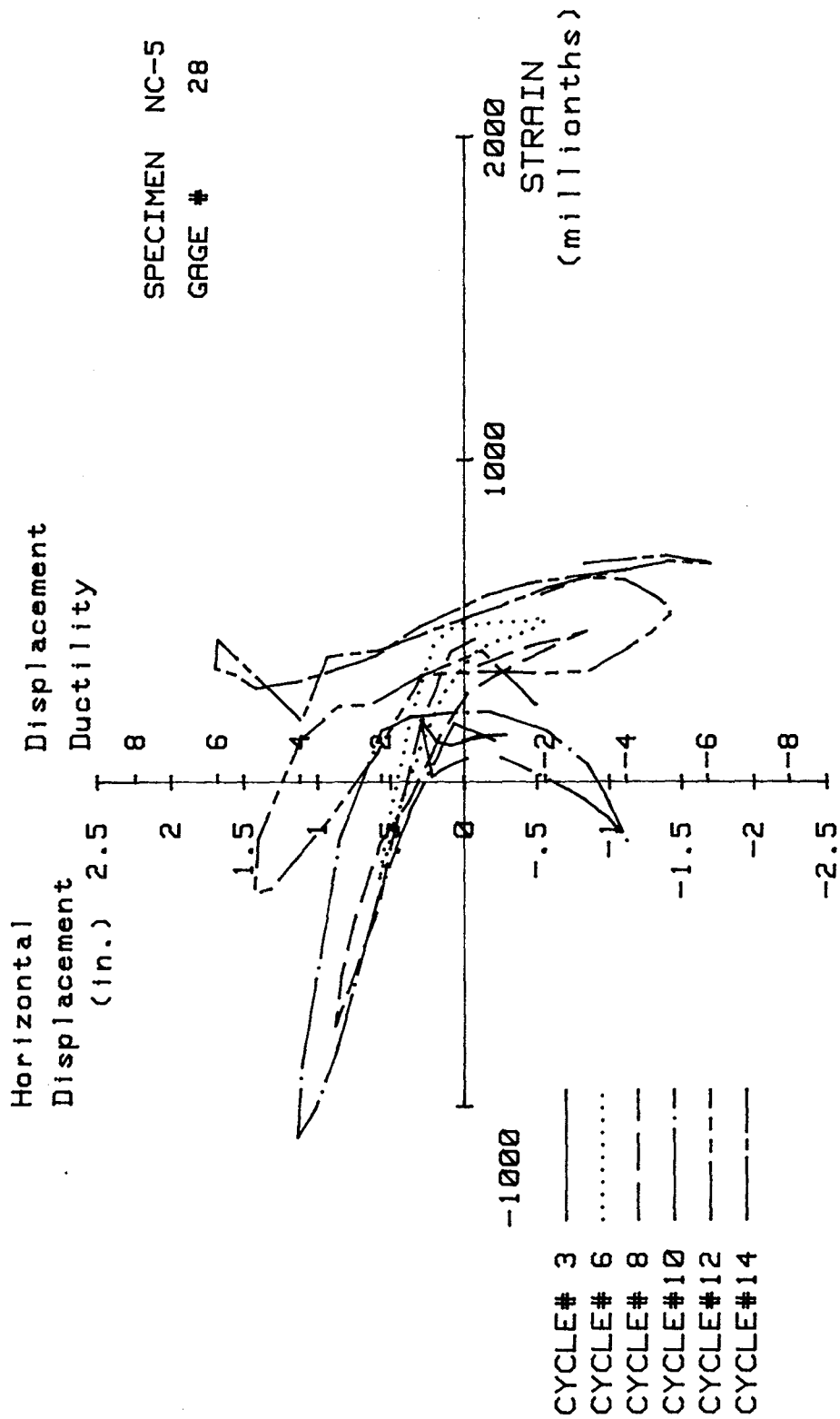


FIG. A-132 MEASURED STRAIN, GAGE #28, SPECIMEN NC-5

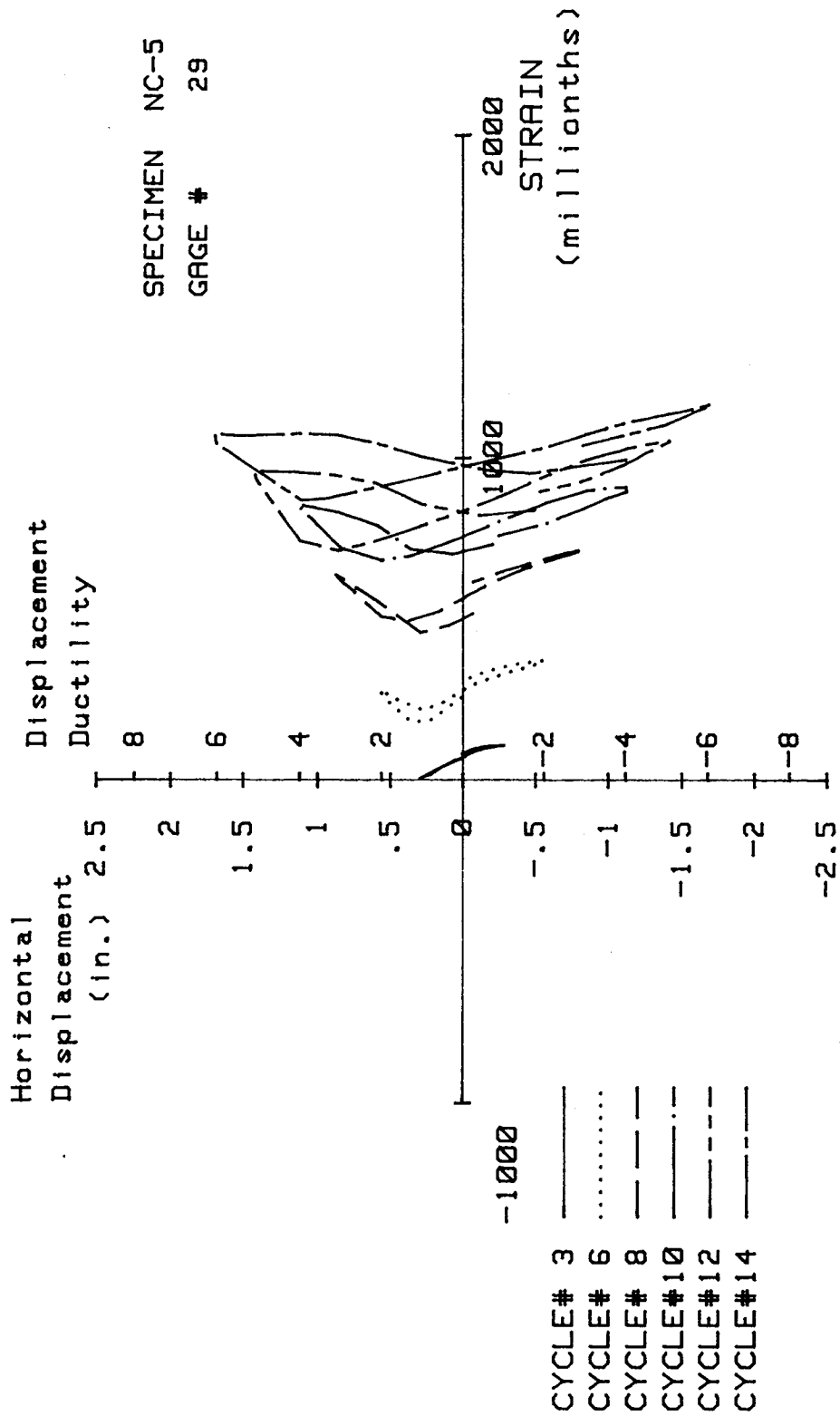


FIG. A-133 MEASURED STRAIN, GAGE #29, SPECIMEN NC-5

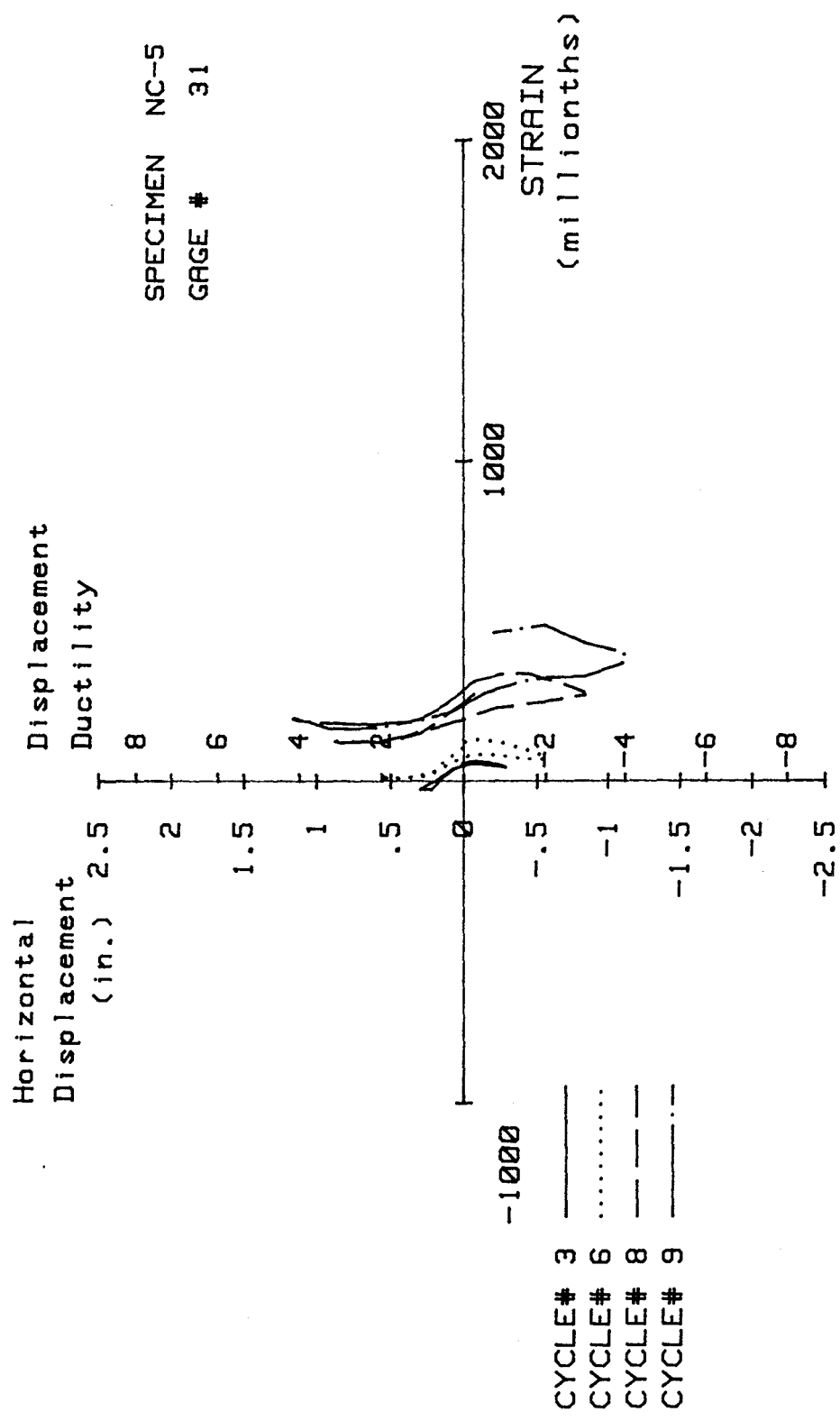


FIG. A-134 MEASURED STRAIN, GAGE #31, SPECIMEN NC-5

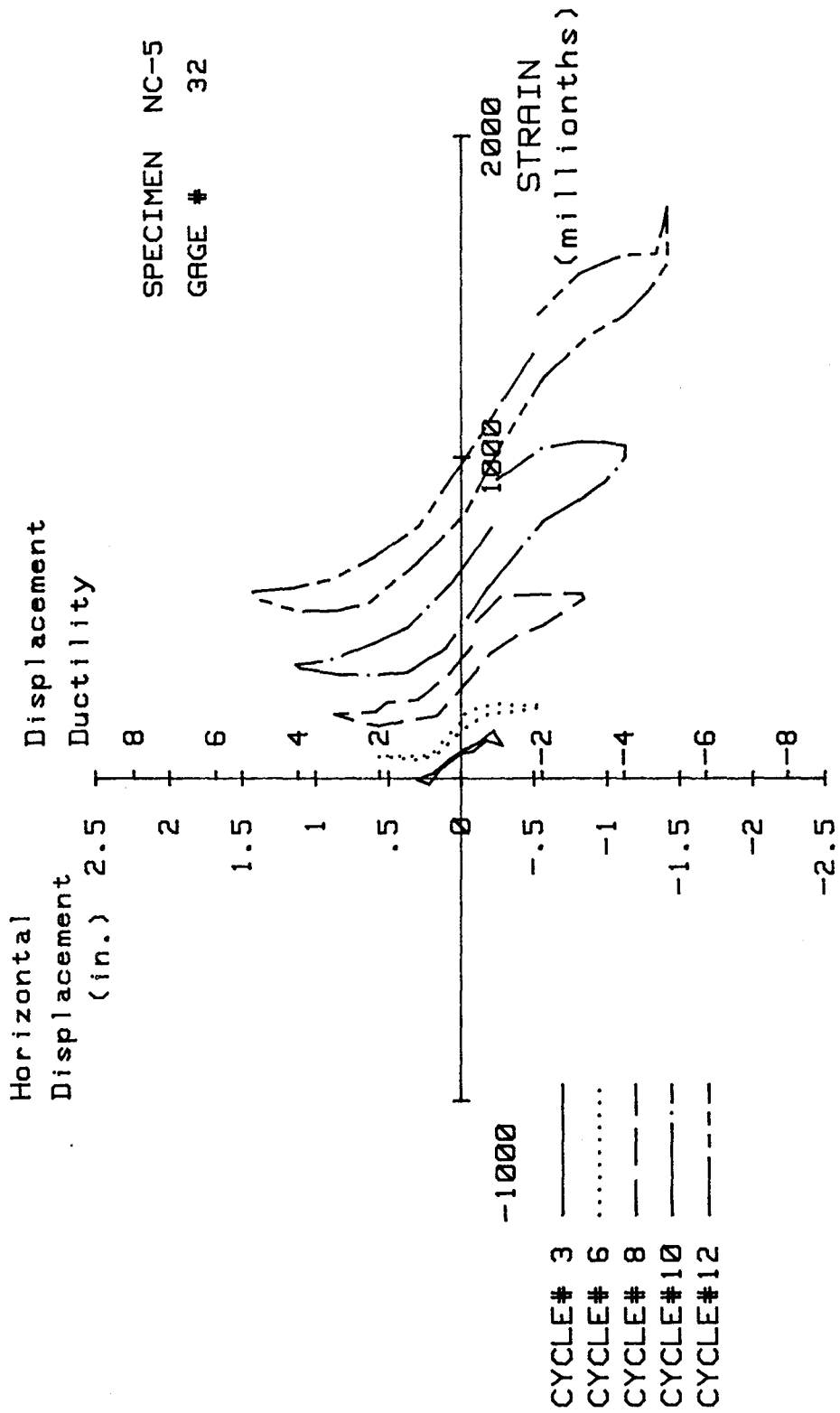


FIG. A-135 MEASURED STRAIN, GAGE #32, SPECIMEN NC-5

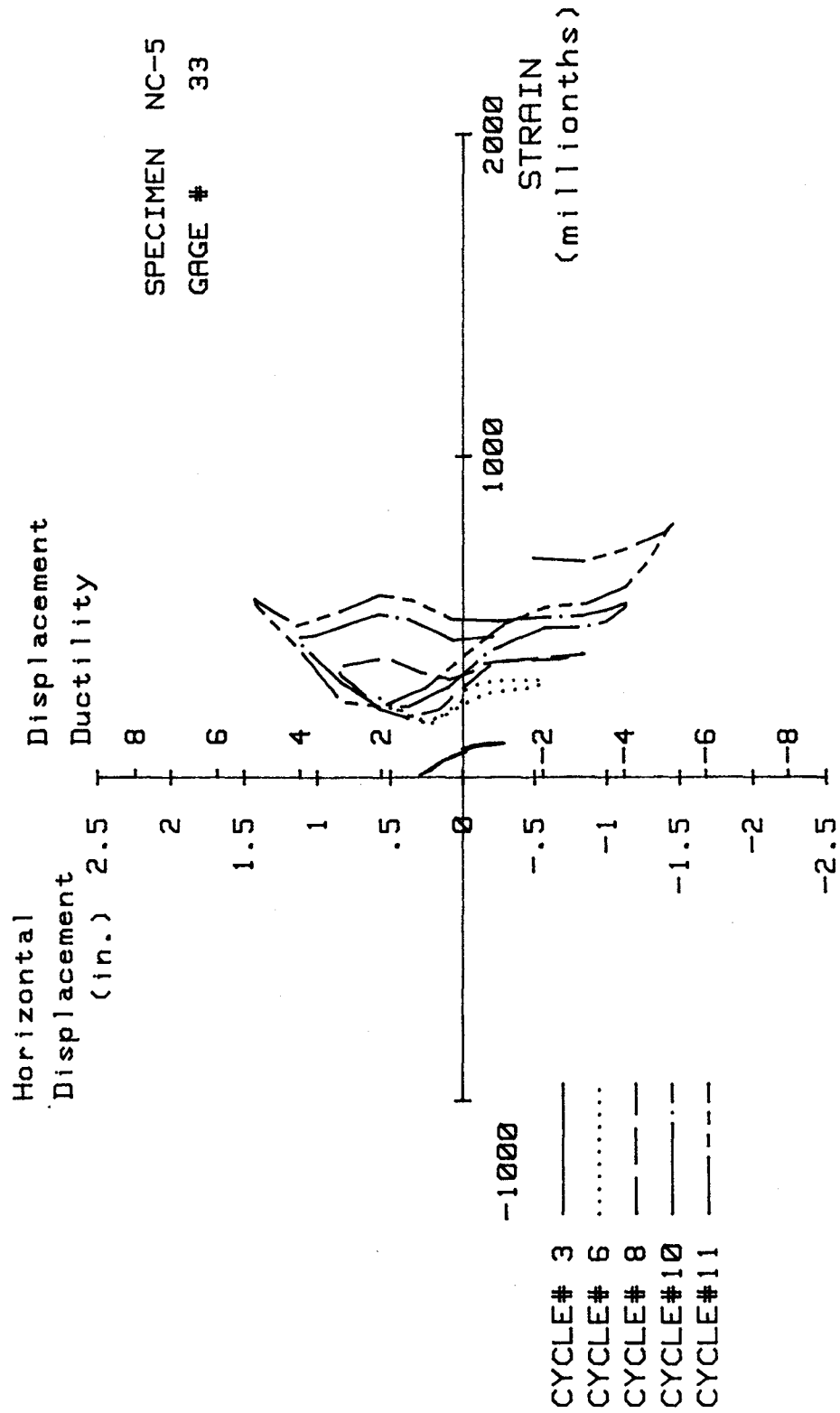


FIG. A-136 MEASURED STRAIN, GAGE #33, SPECIMEN NC-5

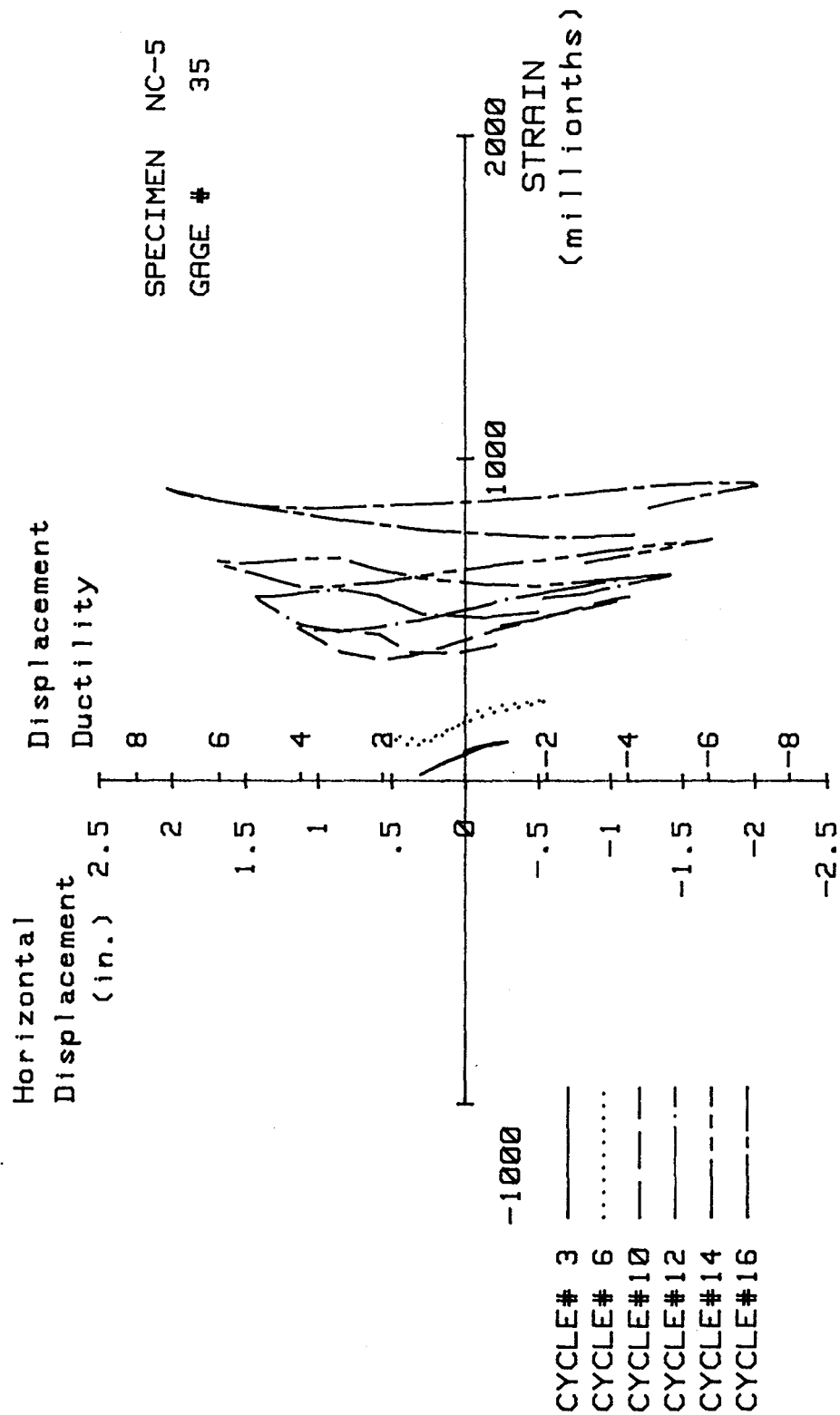


FIG. A-137 MEASURED STRAIN, GAGE #35, SPECIMEN NC-5

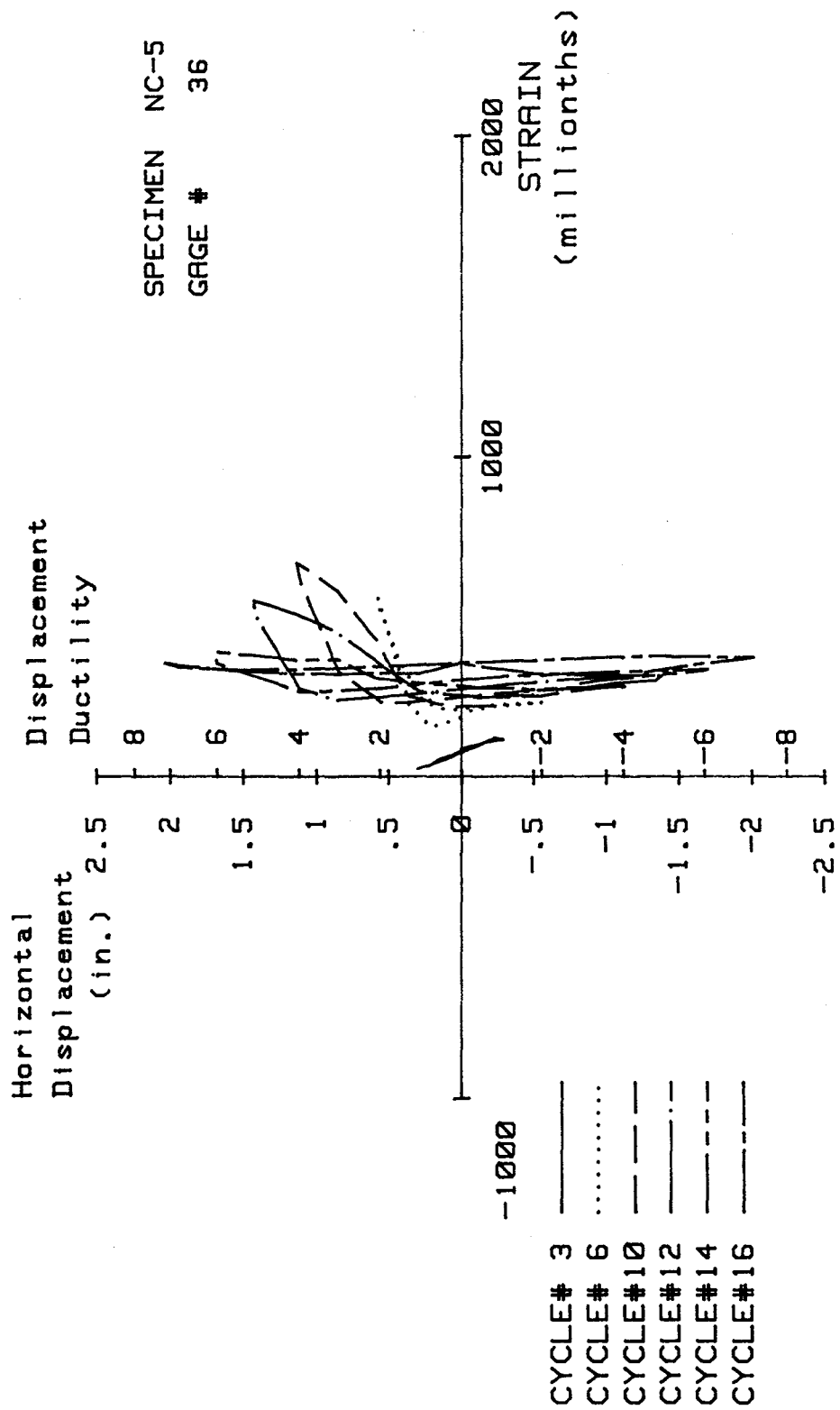


FIG. A-138 MEASURED STRAIN, GAGE #36, SPECIMEN NC-5

Specimen NC-6

Transverse Reinforcement Detail

Figure 4-2d shows the transverse reinforcement used for Specimen NC-6. It consisted of #4 peripheral hoops with 4-in. spacing. The area of transverse reinforcement was 0.4 in.², corresponding to a volumetric reinforcement ratio, ρ , of 1.29%. No crossties were used in this specimen. The area of the transverse reinforcement provided was 63% of the area required by ACI-318-83 Code.

Load History

Testing began by applying 520 kips of axial load, corresponding to 30% of the column axial load capacity. Maintaining the applied axial load constant, the specimen was next subjected to nine complete cyclic horizontal loadings. Based on the procedure outlined in Section 4.8.2, the horizontal load corresponding to the theoretical ultimate flexural capacity of the column section was calculated as 180 kips. The specimen was subjected to horizontal loads of approximately 128 and 125 kips in forward and reverse directions, respectively. The resulting horizontal displacements were 0.61 and 0.59 in. in the forward and reverse directions, respectively. Based on these results, the calculated first yield displacement would be 0.85 in. This was judged to be excessive when compared to previous tests. Using experimental information gained from previous tests, the decision was made to use 0.3 in. as the first yield displacement and 535×10^{-6} in.⁻¹ as the yield curvature. Consequently, horizontal displacement cycle #2 corresponded to a displacement ductility ratio of two. Subsequently, horizontal cyclic loading consisted of displacement-controlled testing to a maximum displacement ductility ratio of five. After completion of two cycles at the displacement ductility ratio of five, an attempt was made to subject the specimen to two additional cycles at the next displacement level ($\mu=6$); however, the specimen failed before completing the first cycle at this displacement level. Figure A-139 show the history of applied cyclic horizontal loading.

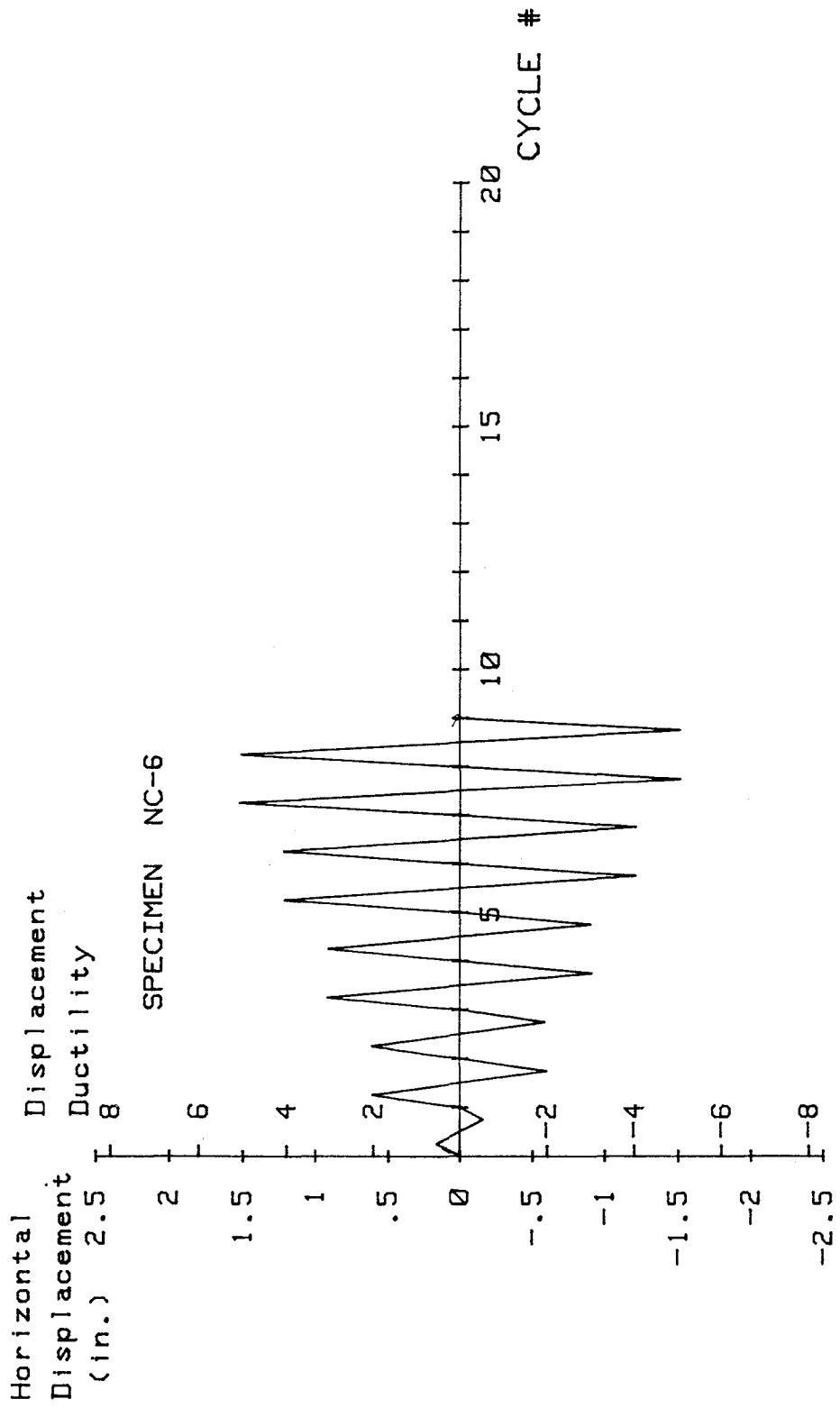


FIG. A-139 LOADING SCHEDULE, SPECIMEN NC-6

Test Observations

The first hairline cracks were observed during cycle #2 ($\mu=2$) at the junction of the stub and the upper column and at distances of approximately 5, 12, 15, 21, and 28 in. above the stub (see Fig. A-140). Some small crushing of the cover concrete was also observed at the end of cycle #2.

Figure A-141 shows the test specimen at the end of cycle #3 ($\mu=3$). Though spalling of the concrete cover was confined to a region within 6 in. above the stub, some large cracks developed which extended to 15 in. above the stub. Application of an additional cycle at the displacement ductility ratio of three (cycle #5) did not further extend the visible damage to the specimen (see Fig. A-142). As shown in Fig. A-143, increasing the horizontal displacement to that of $\mu=4$ did extend the region within which the concrete cover spalled off to a distance 21 in. above the stub.

Figure A-144 shows the specimen at the end of cycle #9 ($\mu=5$). The longitudinal bars and the anchorages of the peripheral hoop did not sustain any visible damage at this stage. The specimen failed before completing the first cycle at a displacement ductility ratio of six. As shown in Fig. A-145, the specimen failed by buckling of the corner and middle longitudinal bars. Buckling of the longitudinal bars coincided with the loss of the anchorage of the peripheral hoop located at a distance of 10 in. above the stub. At test conclusion no visible damage was sustained by the anchorages of the other peripheral hoops. The peripheral hoop located 2 in. above the stub was still covered by concrete to some extent at the end of testing.

Load Deflection and Moment-Curvature Characteristics

Figure A-146 shows the horizontal load displacement characteristics of the specimen. The horizontal load corresponding to the ultimate flexural capacity of the specimen was determined to be 181.5 kips using the procedure outlined in Section 4.8.2. However, the maximum applied horizontal load was only 135 kips. The applied horizontal load at all load stages was much less than the theoretical value indicated by the dashed line in Fig. A-146. No explanation of this understrength has been developed.

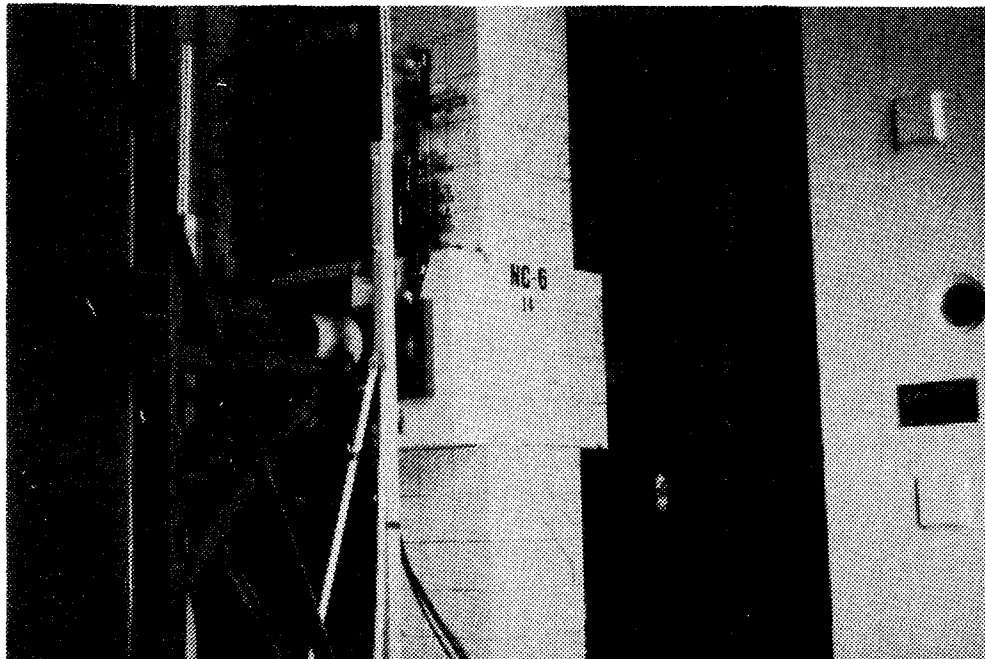


FIG. A-140 TEST SPECIMEN NC-6 AFTER CYCLE #2

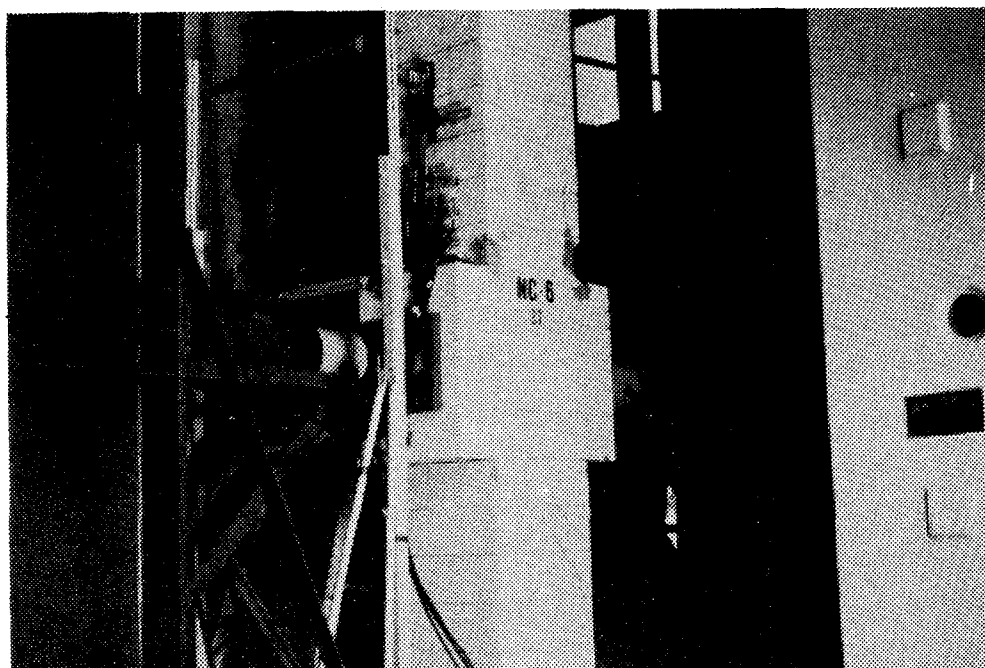


FIG. A-141 TEST SPECIMEN NC-6 AFTER CYCLE #3

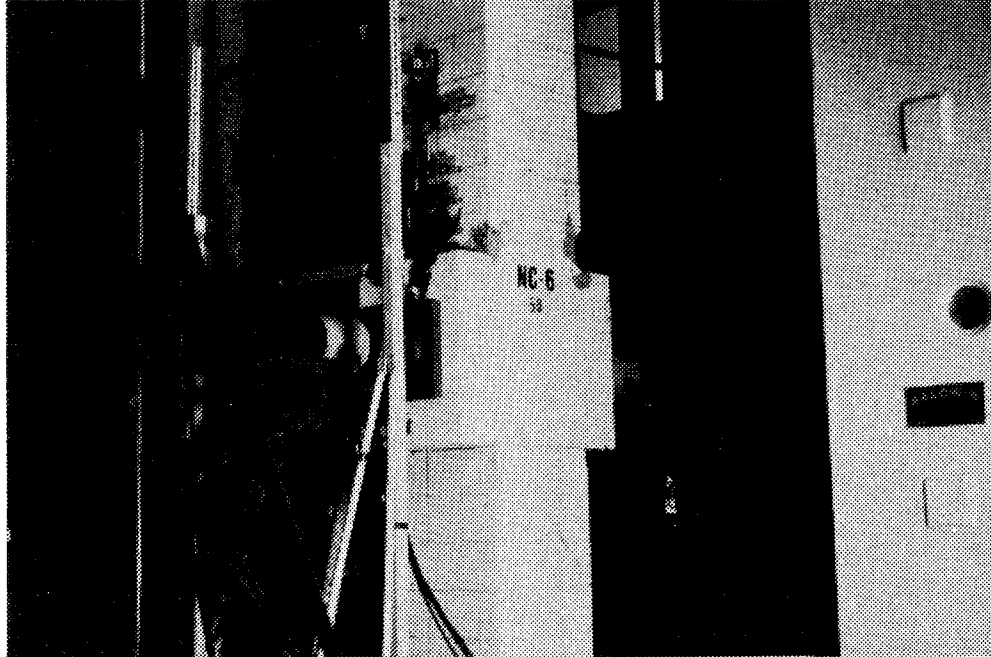


FIG. A-142 TEST SPECIMEN NC-6 AFTER CYCLE #5

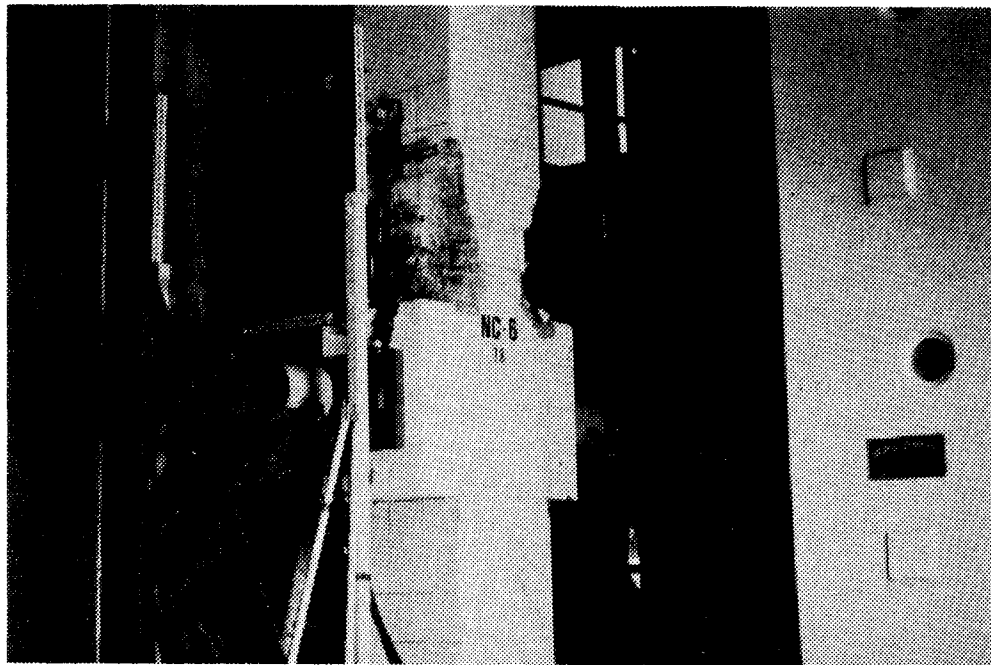


FIG. A-143 TEST SPECIMEN NC-6 AFTER CYCLE #7

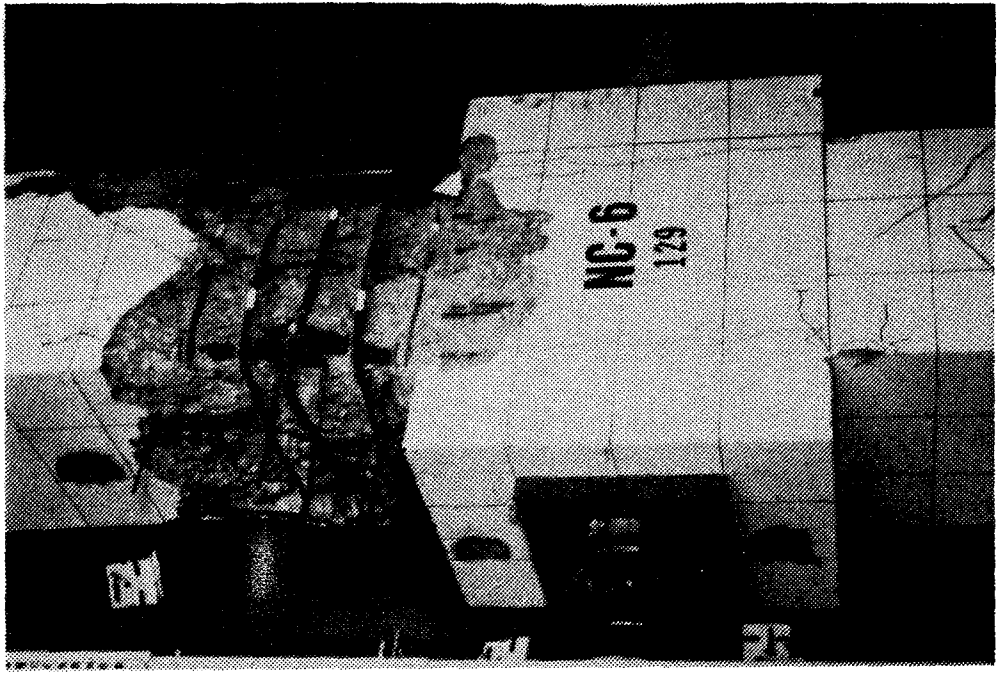


FIG. A-145 TEST SPECIMEN NC-6 AFTER TEST CONCLUSION

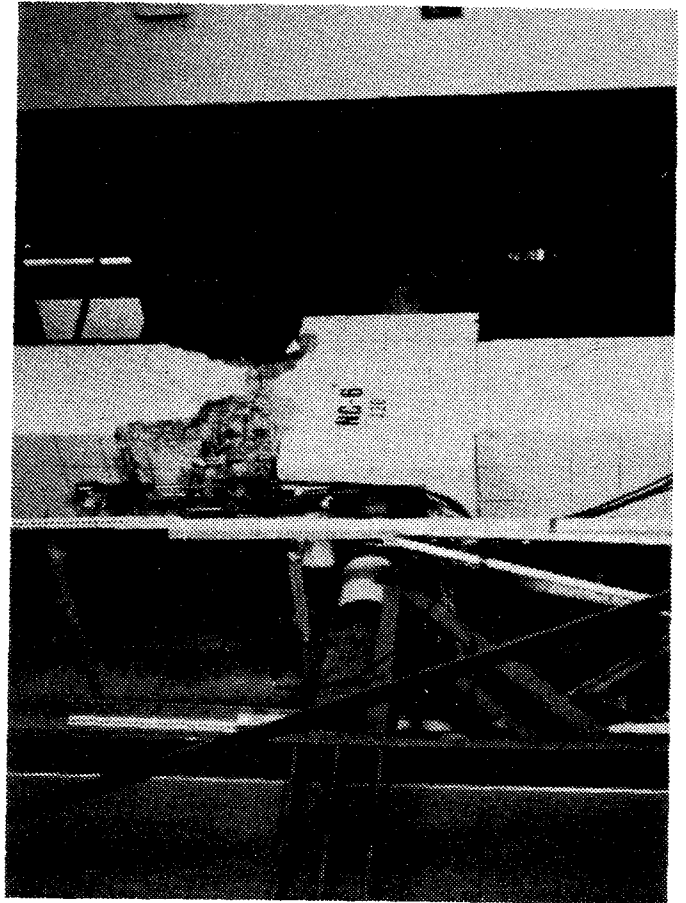
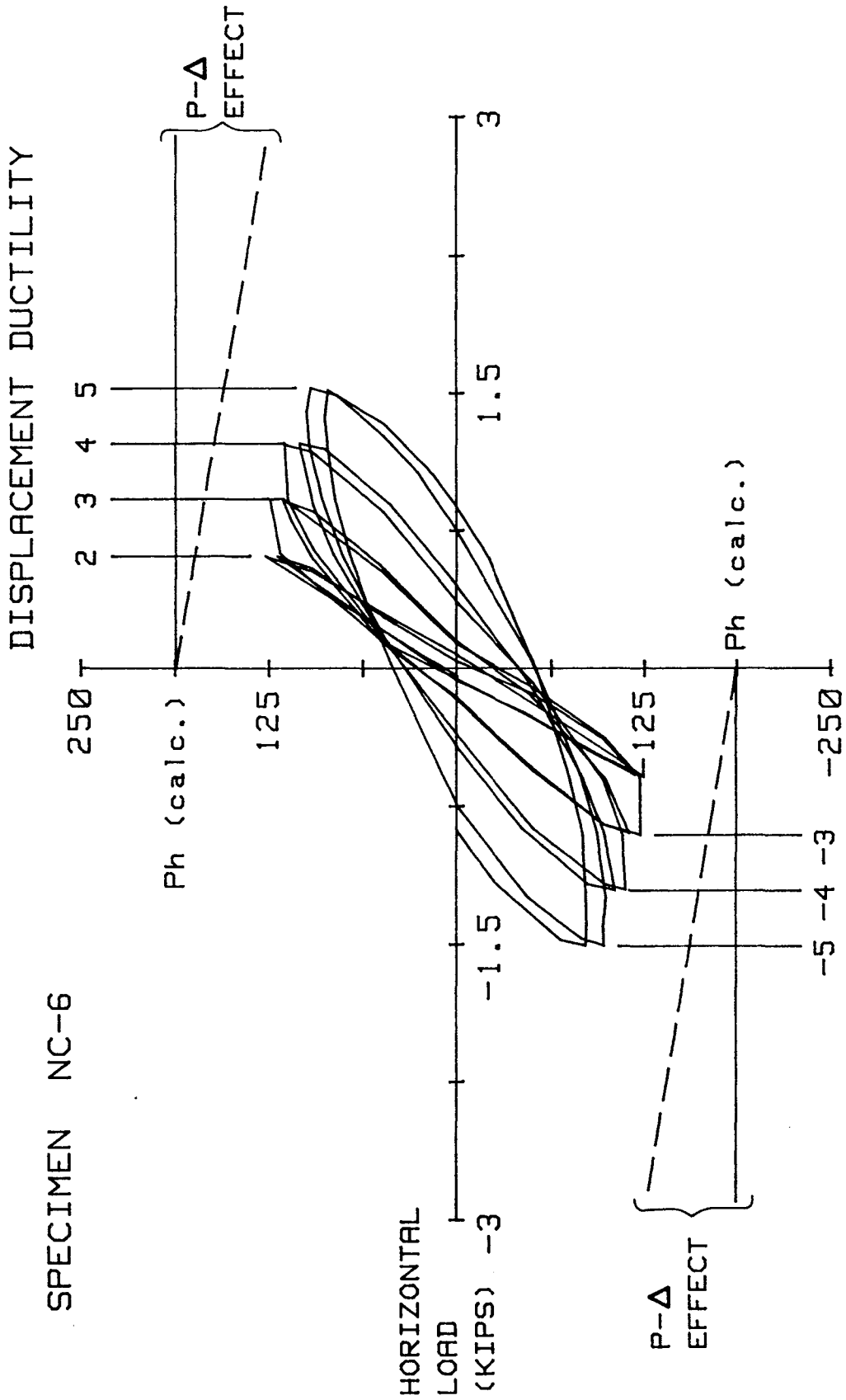


FIG. A-144 TEST SPECIMEN NC-6 AFTER CYCLE #9



Metric Equivalents
 1 in. = 25.4 mm
 1 kip = 4.45 kN

HORIZONTAL DISPLACEMENT (IN.)

FIG. A-146 HORIZONTAL LOAD VERSUS DISPLACEMENT, SPECIMEN NC-6

Figure A-147 shows the curvature distribution along the upper column. The maximum curvature ductility at the displacement ductility ratio of 5 was approximately 20.

Figure A-148 shows the moment curvature characteristic of the column cross-section at the upper column-stub level. As shown in Fig. A-148, the applied moment was smaller than the theoretical value at the displacement ductility ratios. Additionally, each hysteresis loop "shifted" at each displacement level. The extent of "shifting" was unique to Specimen NC-6 and was not observed in any other specimen. No explanation of the "shifted" curvature loops has been developed.

Transverse Reinforcement Strain

Twelve strain gages were attached to the transverse reinforcement. Figure 4-12 shows the location of each strain gage, and Figs. A-149 through A-152 show the data obtained from each strain gage.

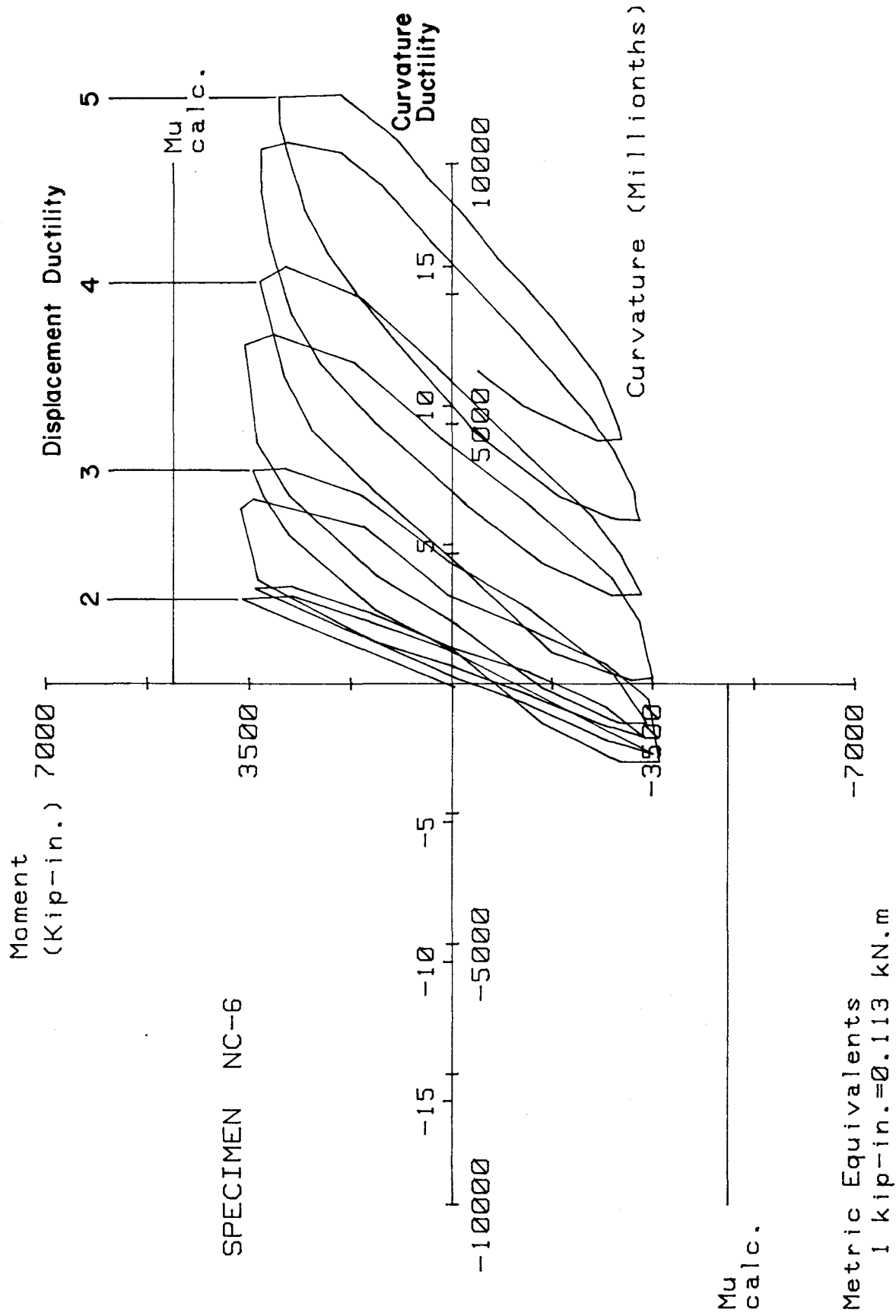


FIG. A-147 MOMENT VERSUS CURVATURE FOR SPECIMEN NC-6

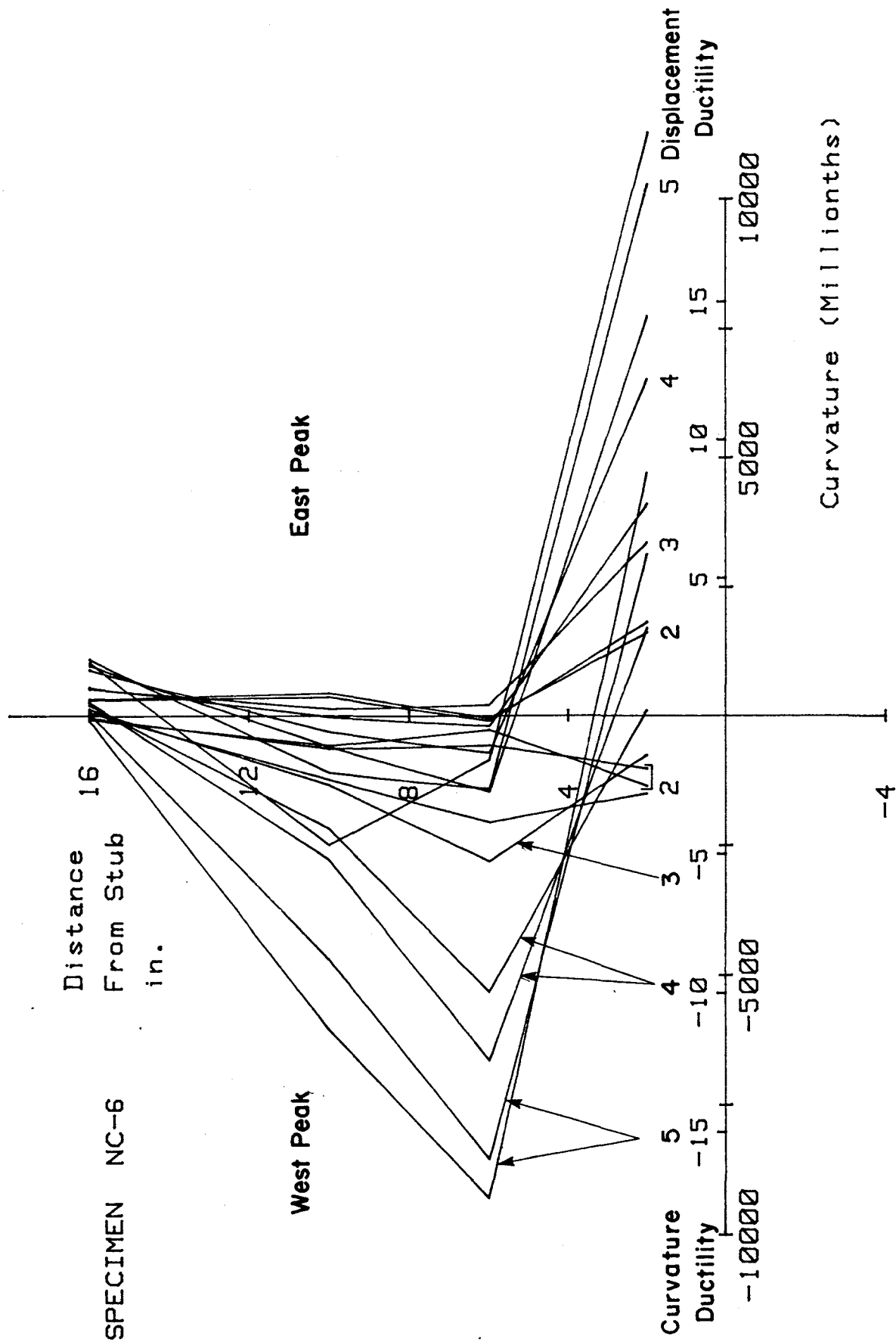


FIG. A-148 CURVATURE DISTRIBUTION ALONG UPPER COLUMN SPECIMEN NC-6

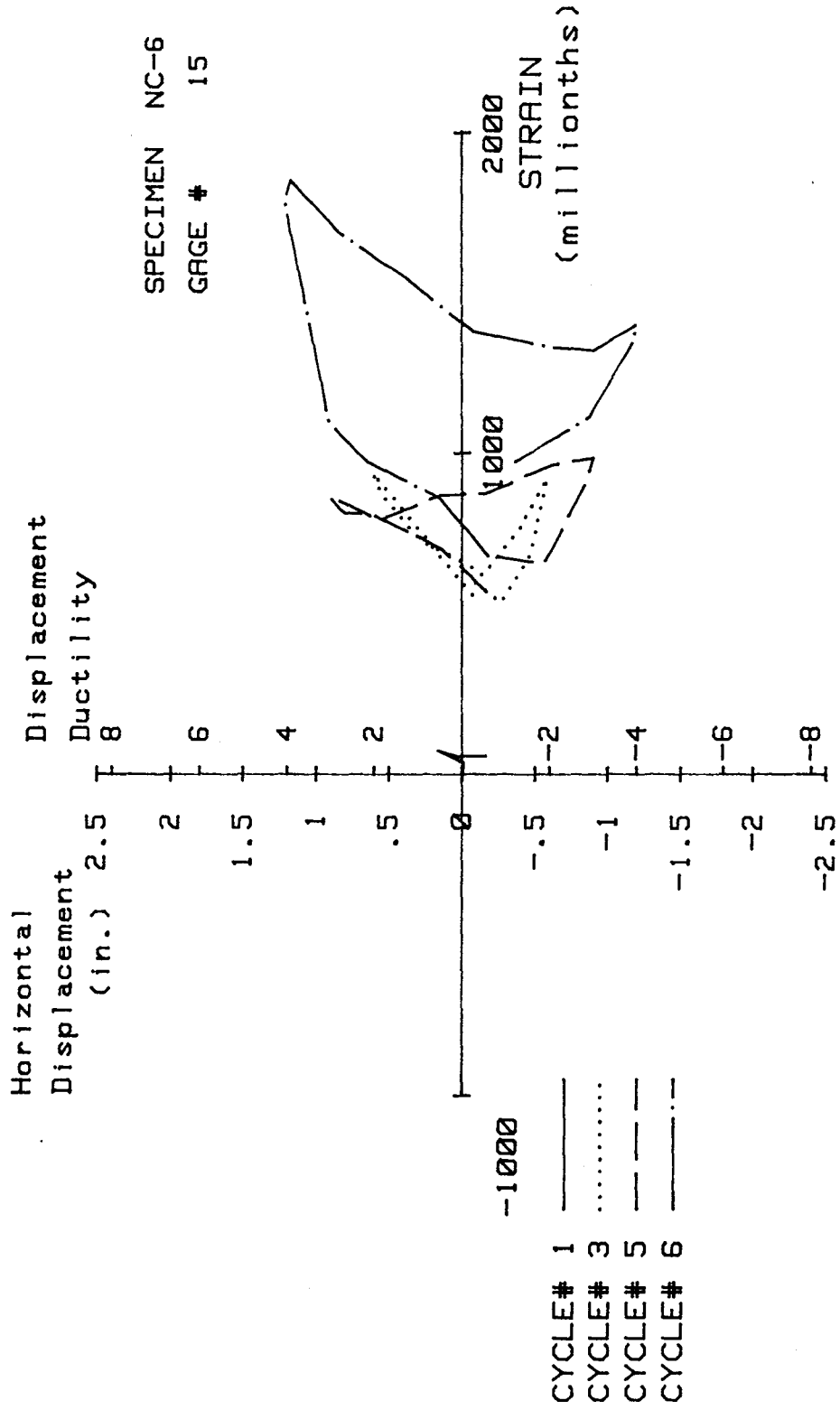


FIG. A-149 MEASURED STRAIN, GAGE #15, SPECIMEN NC-6

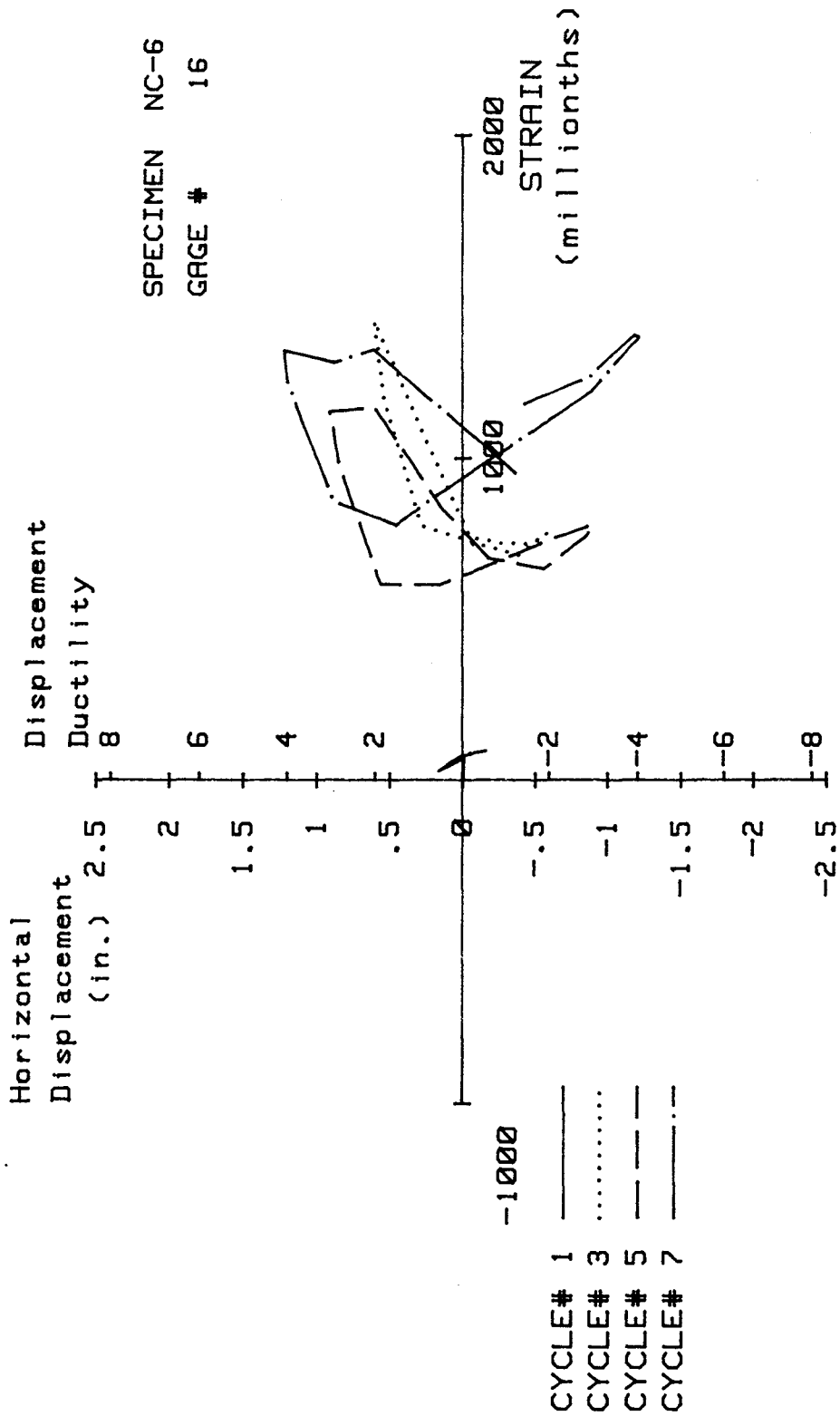


FIG. A-150 MEASURED STRAIN, GAGE #16, SPECIMEN NC-6

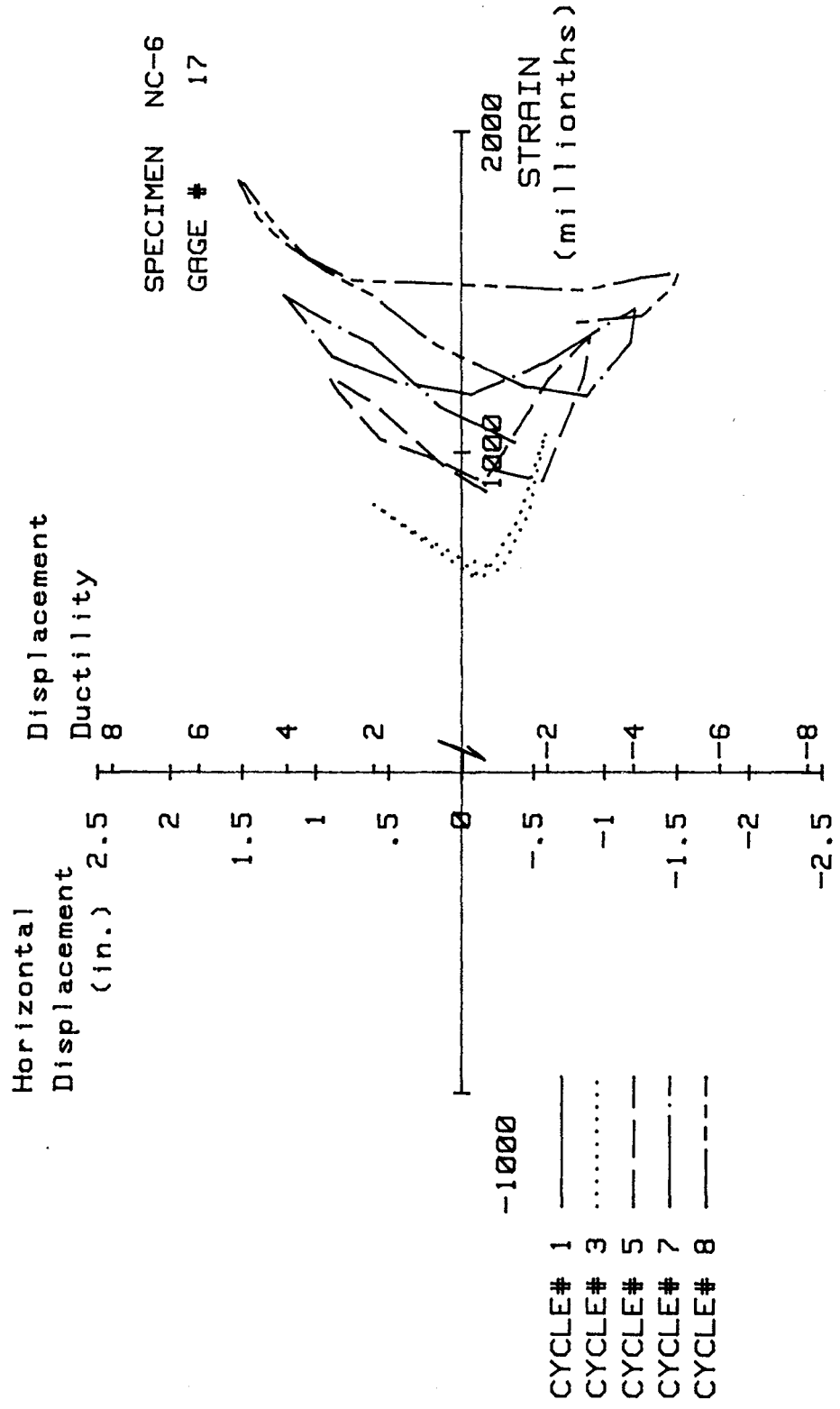


FIG. A-151 MEASURED STRAIN, GAGE #17, SPECIMEN NC-6

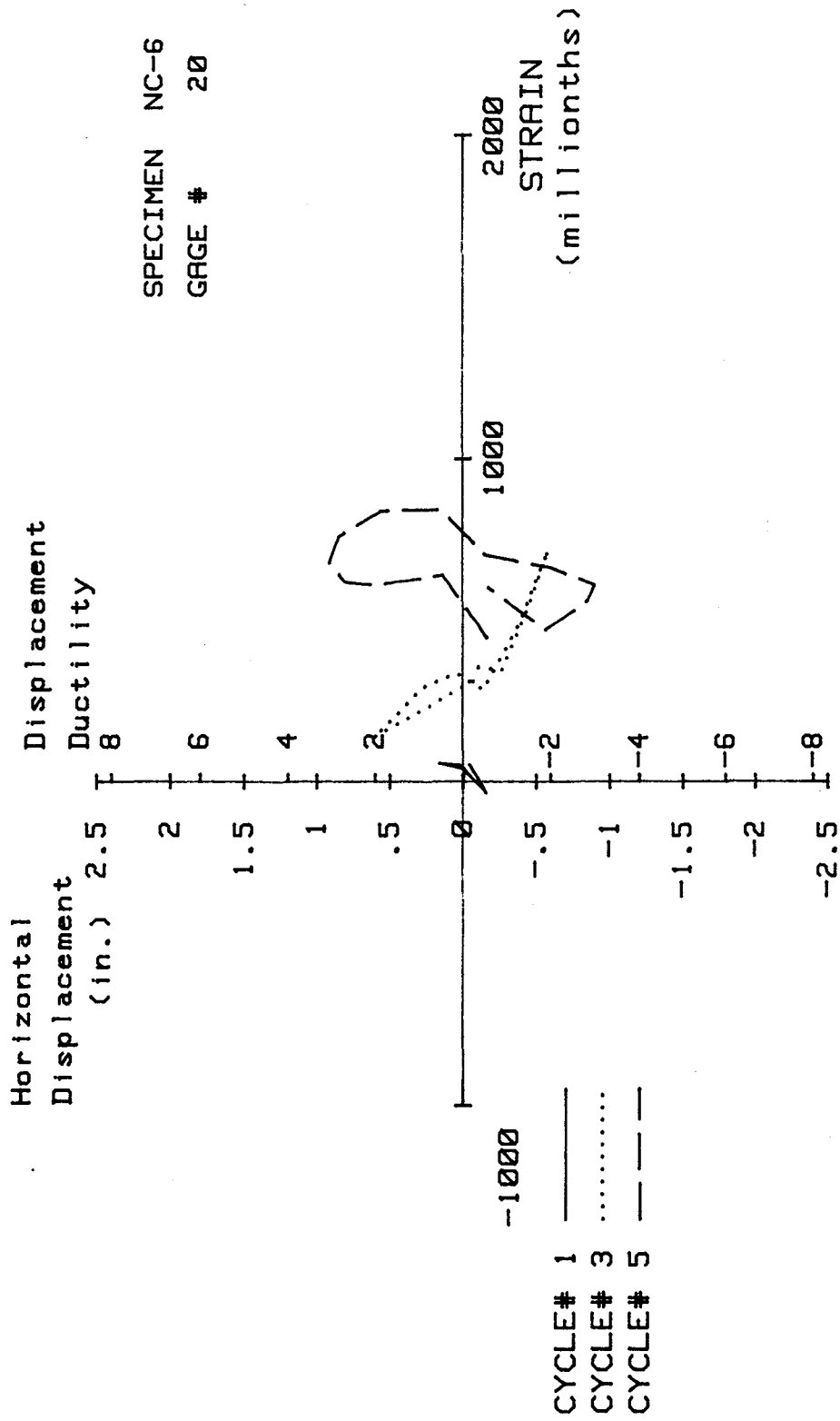


FIG. A-152 MEASURED STRAIN, GAGE #20, SPECIMEN NC-6

Specimen NC-7

Transverse Reinforcement Detail

Transverse reinforcement for Specimen NC-7 consisted of single peripheral hoops. Each hoop layer was formed with four identical pieces as shown in Fig. 4-2e. The ends of each piece were bent 45° and extended 6-bar diameters. Peripheral hoops were constructed at each level by placing four pieces from the sides and tying them to the longitudinal bars. The advantage of using this type of detail is the ease of construction, as it is not necessary to drop each peripheral hoop from the cage top. Every piece of the peripheral hoop was made of #4 bars. The area of transverse reinforcement provided was 0.4 sq in., corresponding to a volumetric reinforcement ratio of 1.29%. The area of the transverse reinforcement provided was 60% of the area required by ACI-318-83 Code.

Load History

Testing began with the application of 540 kips of axial load, which corresponds to 30% of the column's axial load capacity. While maintaining the axial load constant, the specimen was subjected to cyclic horizontal loading. Figure A-153 shows the history of the applied cyclic horizontal load. The first yield displacement and the yield curvature were calculated to be 0.3 in. and $472 \times 10^{-6} \text{ in.}^{-1}$, respectively, during cycle #2. Subsequently, horizontal cyclic loading consisted of displacement-controlled testing to a maximum displacement ductility ratio of five. The specimen failed before completing the second cycle at the displacement ductility ratio of five.

Test Observations

The first hairline cracks were observed during cycle #1 at the junction of the stub and the upper column. Further hairline cracks formed at distances of approximately 7, 15, and 26 in. from the stub during cycle #2 (see Fig. A-154).

Figure A-155 shows the specimen at the end of cycle #5 ($\mu=2$). Some crushing of cover concrete at the stub level and spalling of the cover concrete was evident. Figure A-156 shows the specimen at the end of cycle #7 ($\mu=3$). Cover spalling had extended to a distance 12 in. from the

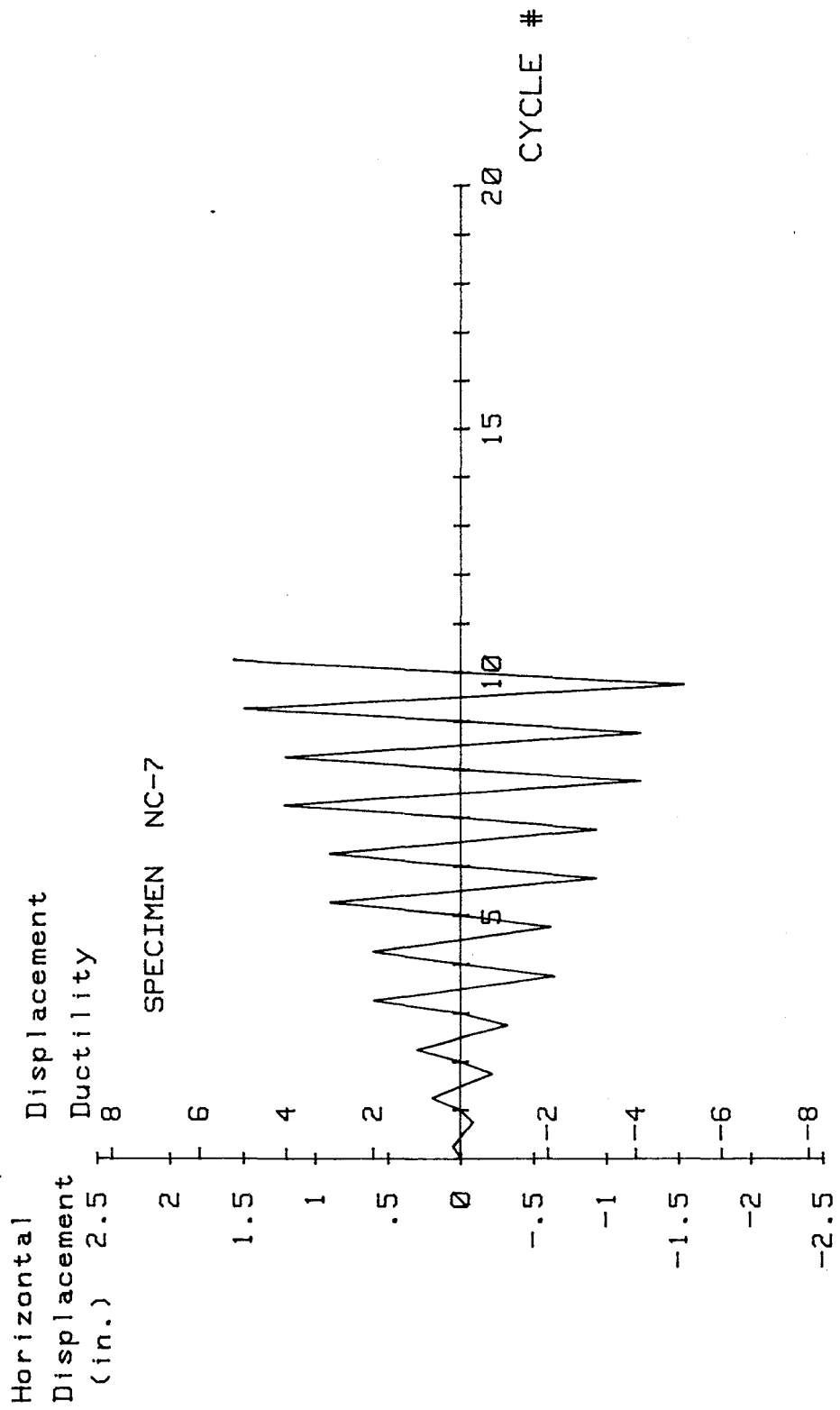


FIG. A-153 LOADING SCHEDULE, SPECIMEN NC-7

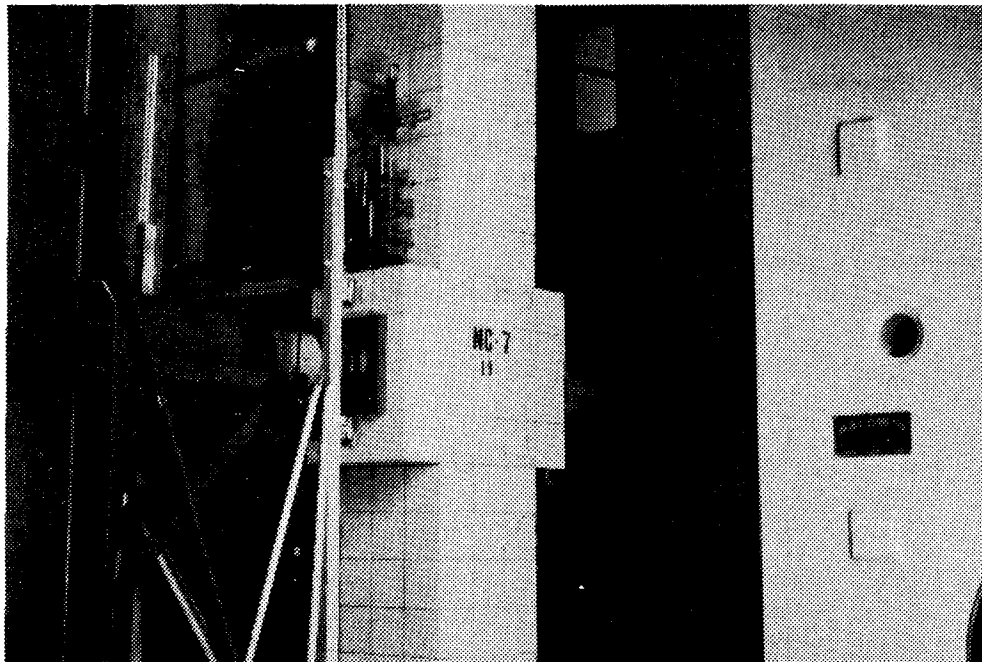


FIG. A-154 TEST SPECIMEN NC-7 AFTER CYCLE #2

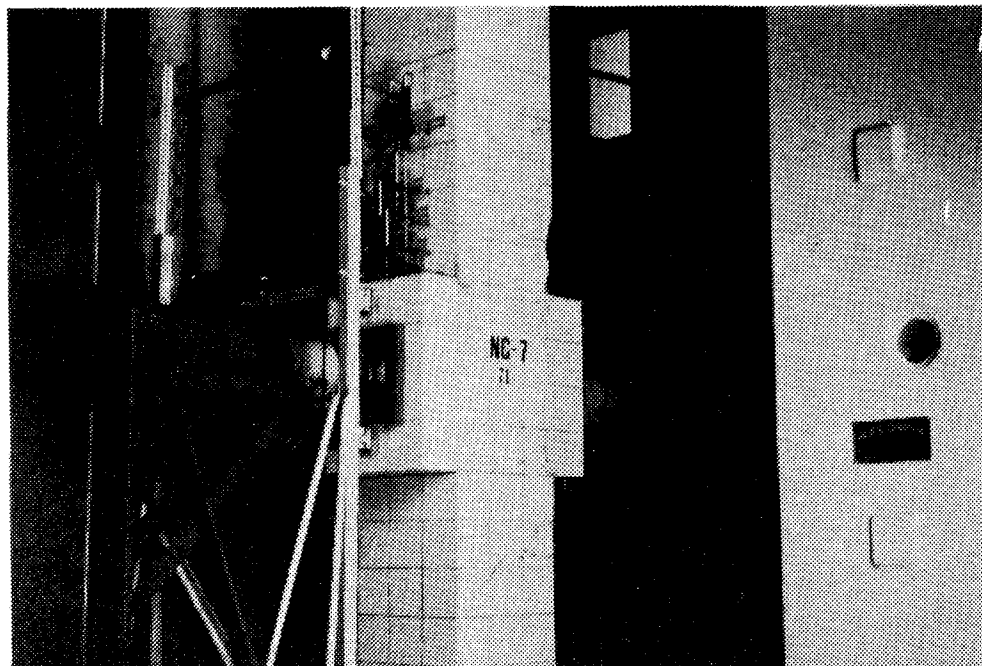


FIG. A-155 TEST SPECIMEN NC-7 AFTER CYCLE #5

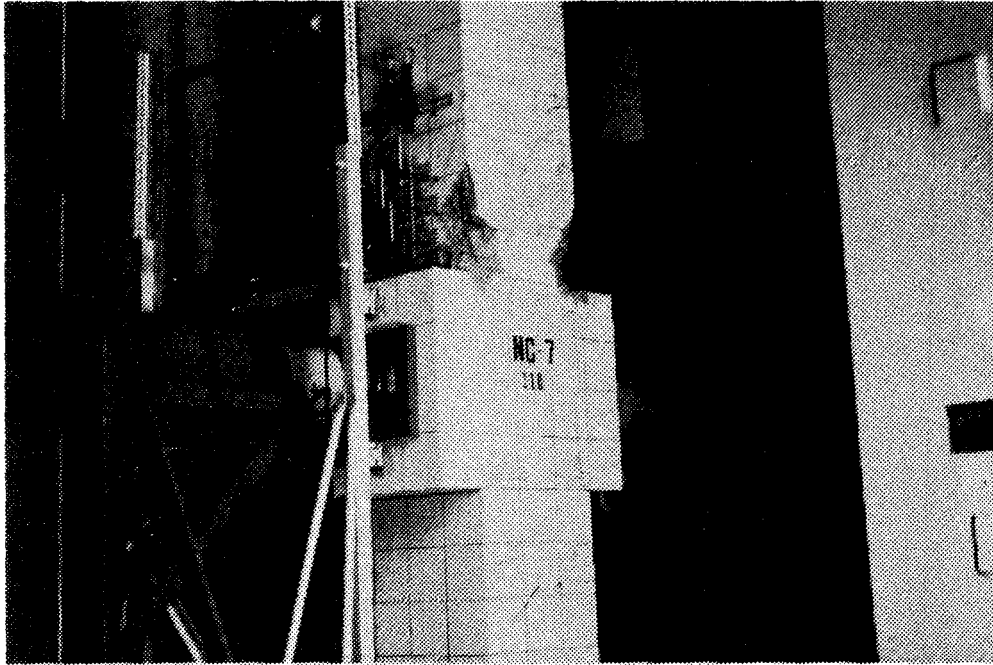


FIG. A-156 TEST SPECIMEN NC-7 AFTER CYCLE #7

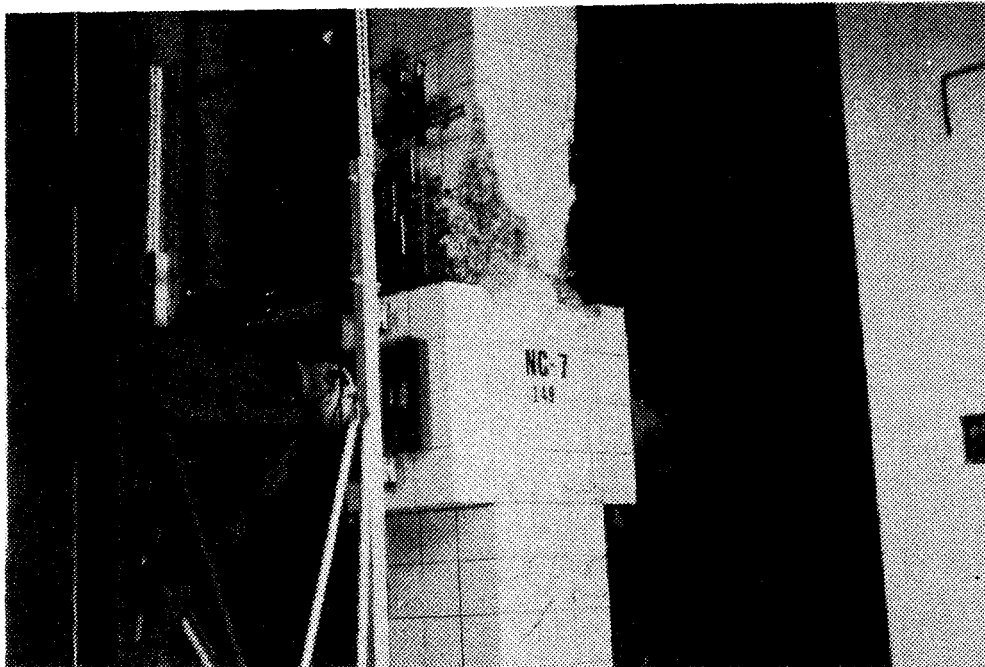


FIG. A-157 TEST SPECIMEN NC-7 AFTER CYCLE #9

stub. Increasing the horizontal displacement to achieve a displacement ductility ratio of four (cycle #9) extended the spalled region to a distance of 21 in. from the stub. Figure A-157 shows the specimen at the end of cycle #9. The specimen was then subjected to one cycle at a displacement ductility ratio of five. At this stage no visible damaged had been inflicted on the longitudinal bars or the anchorages of the peripheral hoops. Subsequently, an attempt was made to apply an additional cycle at the same displacement ductility ratio. Figure A-158 shows the specimen after completion of forward loading at the second cycle of displacement ductility ratio of five. As indicated in the figure, all peripheral hoops and longitudinal bars were intact. However, before completing the reverse loading cycle, the specimen failed by buckling of longitudinal bars on the compression side. Buckling of the longitudinal bars coincided with the loss of anchorage of the peripheral hoops at distances of 6 and 10 in. from the stub.

Figure A-159 shows the specimen at test conclusion. The peripheral hoops located 2 in. above the stub were still partially covered with concrete. No visible damage was inflicted to the anchorage of the peripheral hoops located 14 in. above the stub and beyond.

Load Deflection and Moment-Curvature Characteristics

Figure A-160 shows the horizontal load deflection response of the specimen up to the displacement ductility ratio of four. The maximum applied horizontal load was approximately 215 kips. Except for the second cycle at the displacement ductility ratio of four, the applied horizontal load exceeded the theoretical value shown by the dashed line in Fig. A-160.

Figure A-161 shows the curvature distribution along the upper column. The curvature ductility ratio at displacement ductility ratio of 4 was 15.

Figure A-162 shows the moment-curvature behavior of the column cross-section at the upper column-stub level. Maximum applied moment was 5873 in-kips, whereas the theoretical moment calculated using procedures outlined in Section 4.8.2 was 4950 in-kips. The maximum applied moment during the first cycle at a displacement ductility ratio of five was 5003 in-kips.



FIG. A-158 TEST SPECIMEN NC-7 COMPLETING FORWARD LOADING CYCLE #11

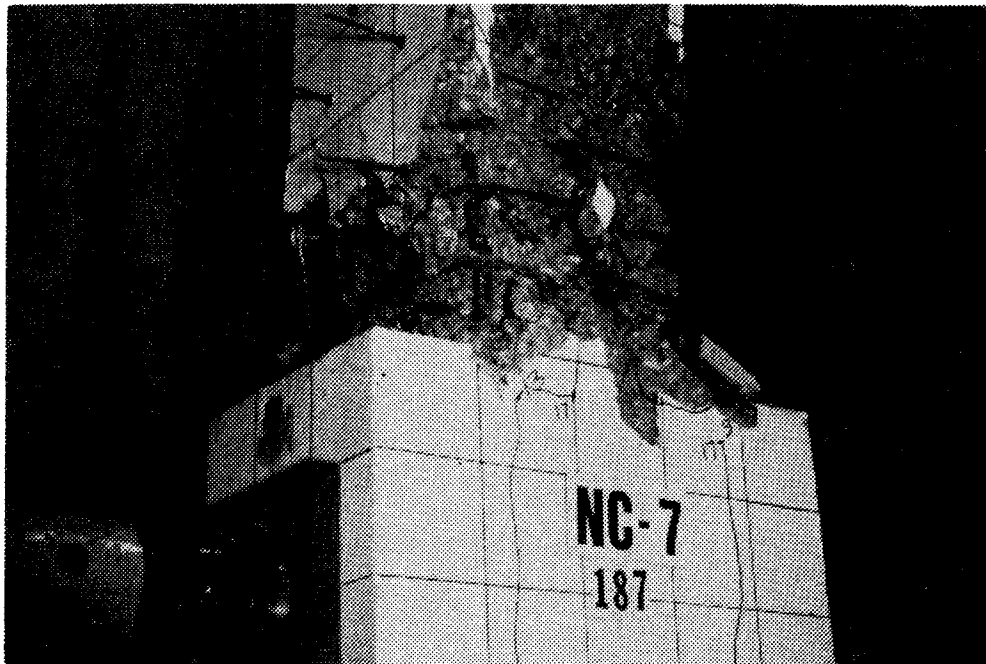
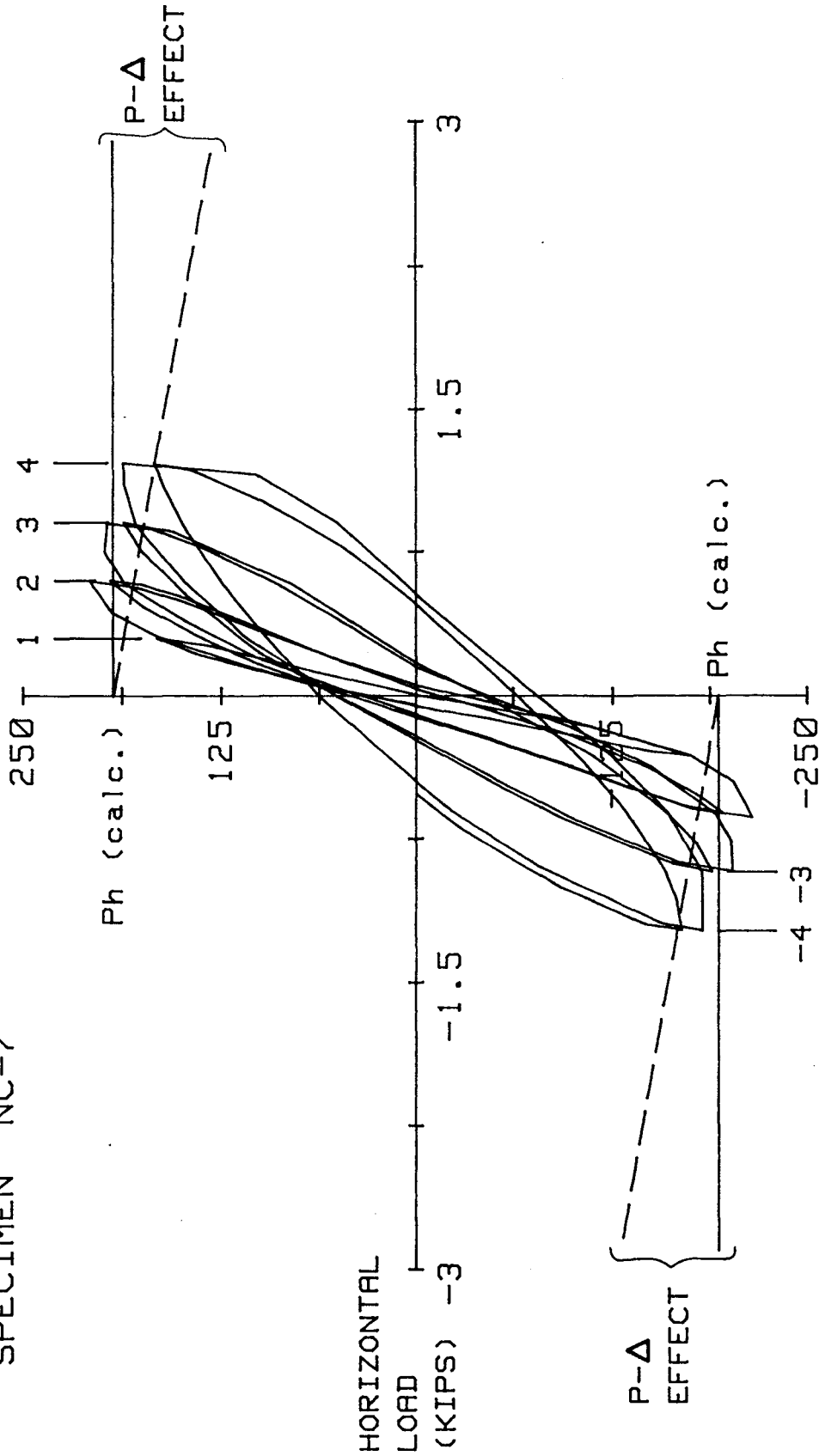


FIG. A-159 TEST SPECIMEN NC-7 AFTER TEST CONCLUSION

DISPLACEMENT DUCTILITY

SPECIMEN NC-7



Metric Equivalents

- 1 in. = 25.4 mm
- 1 kip = 4.45 KN

HORIZONTAL DISPLACEMENT (IN.)

FIG. A-160 HORIZONTAL LOAD VERSUS DISPLACEMENT, SPECIMEN NC-7

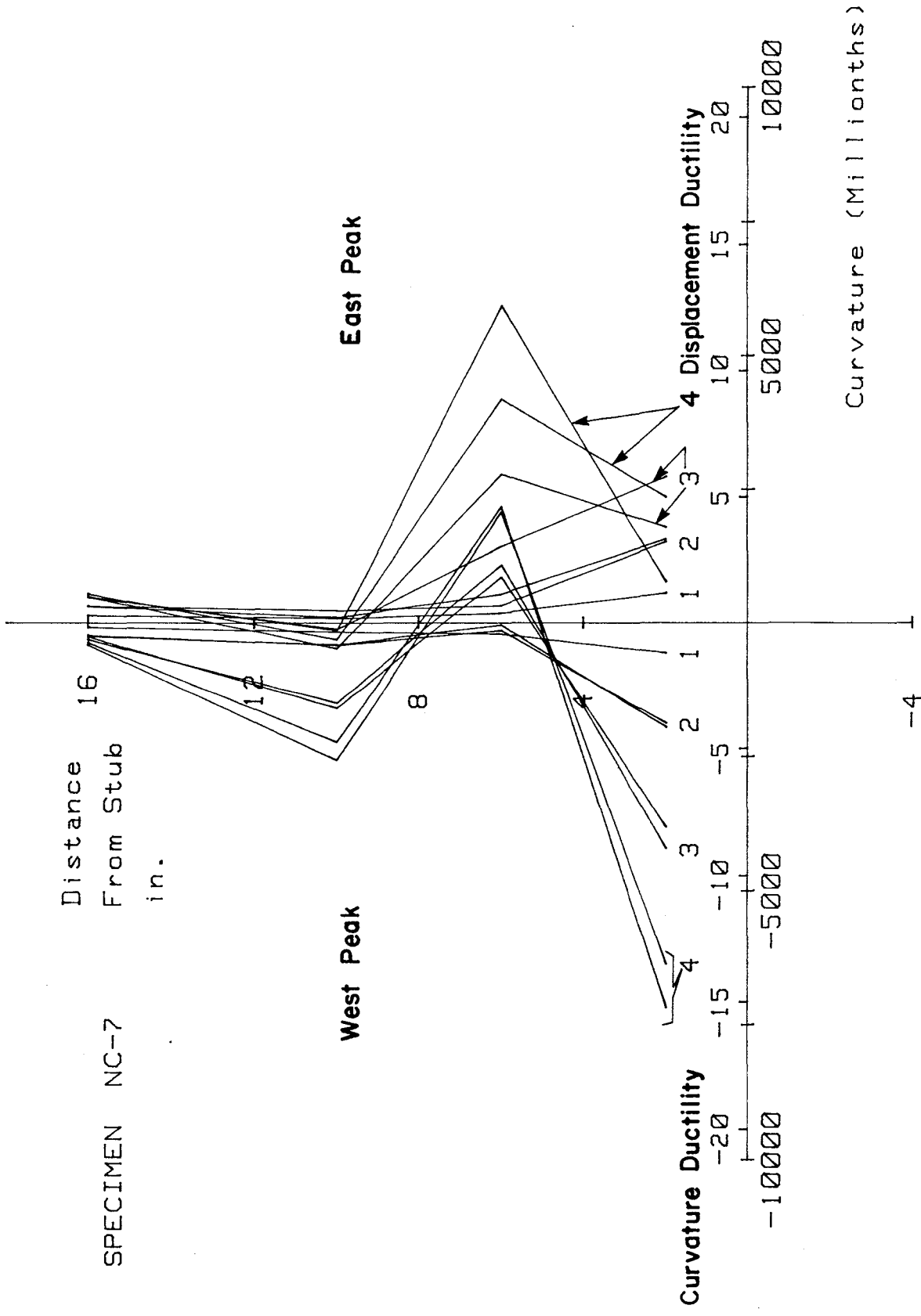


FIG. A-161 CURVATURE DISTRIBUTION ALONG UPPER COLUMN, SPECIMEN NC-7

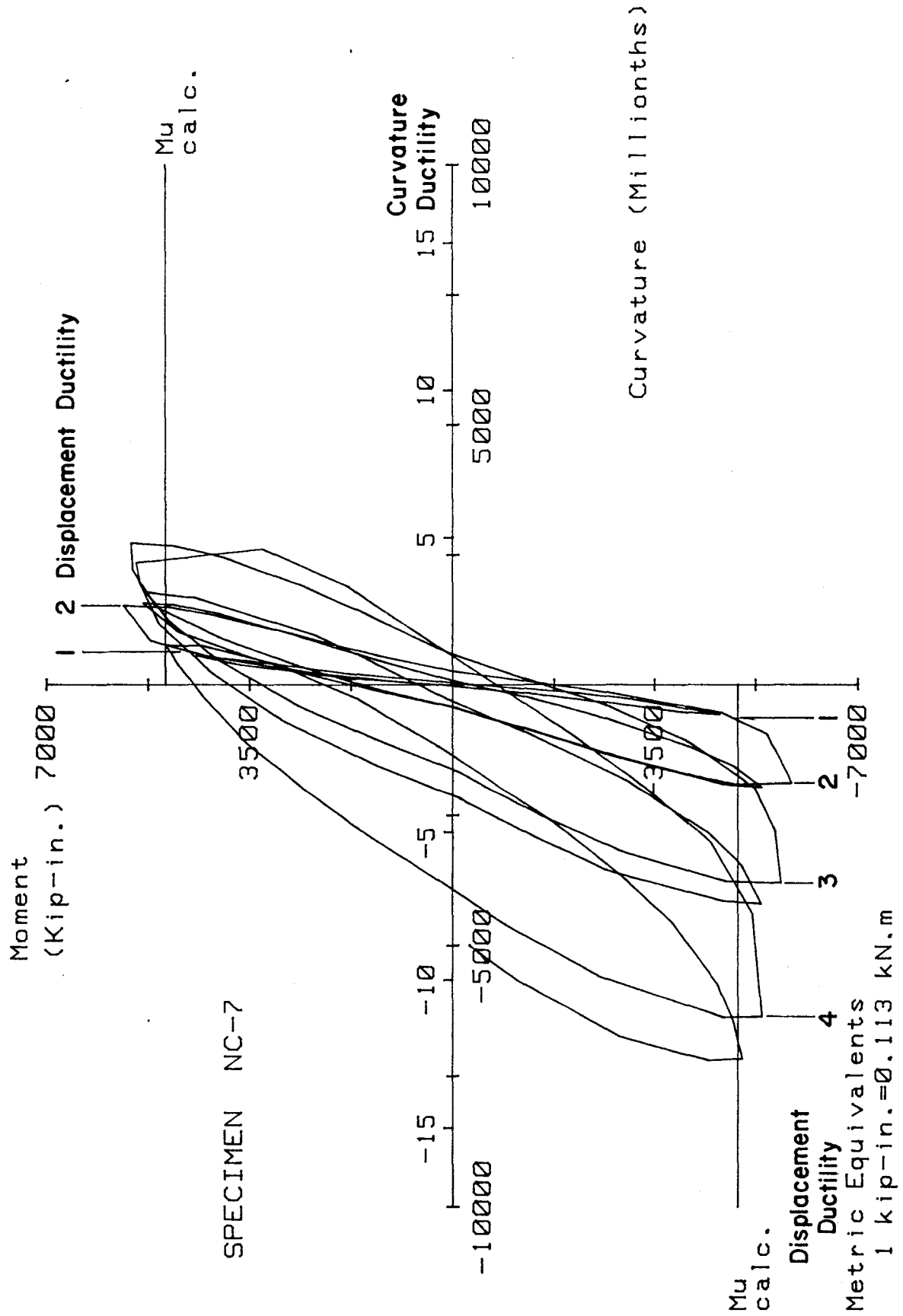


FIG. A-162 MOMENT VERSUS CURVATURE FOR SPECIMEN NC-7

Transverse Reinforcement Strain

Twelve strain gages were attached to the transverse reinforcement. Figure 4-12 shows the location of these strain gages while Figs. A-163 through A-169 show the results obtained.

Strains remained small through cycle #5, with maximum strain at approximately 60% of the yield strain. In general, the peripheral hoops located 2 in. above the stub experienced the least strain through cycle #5.

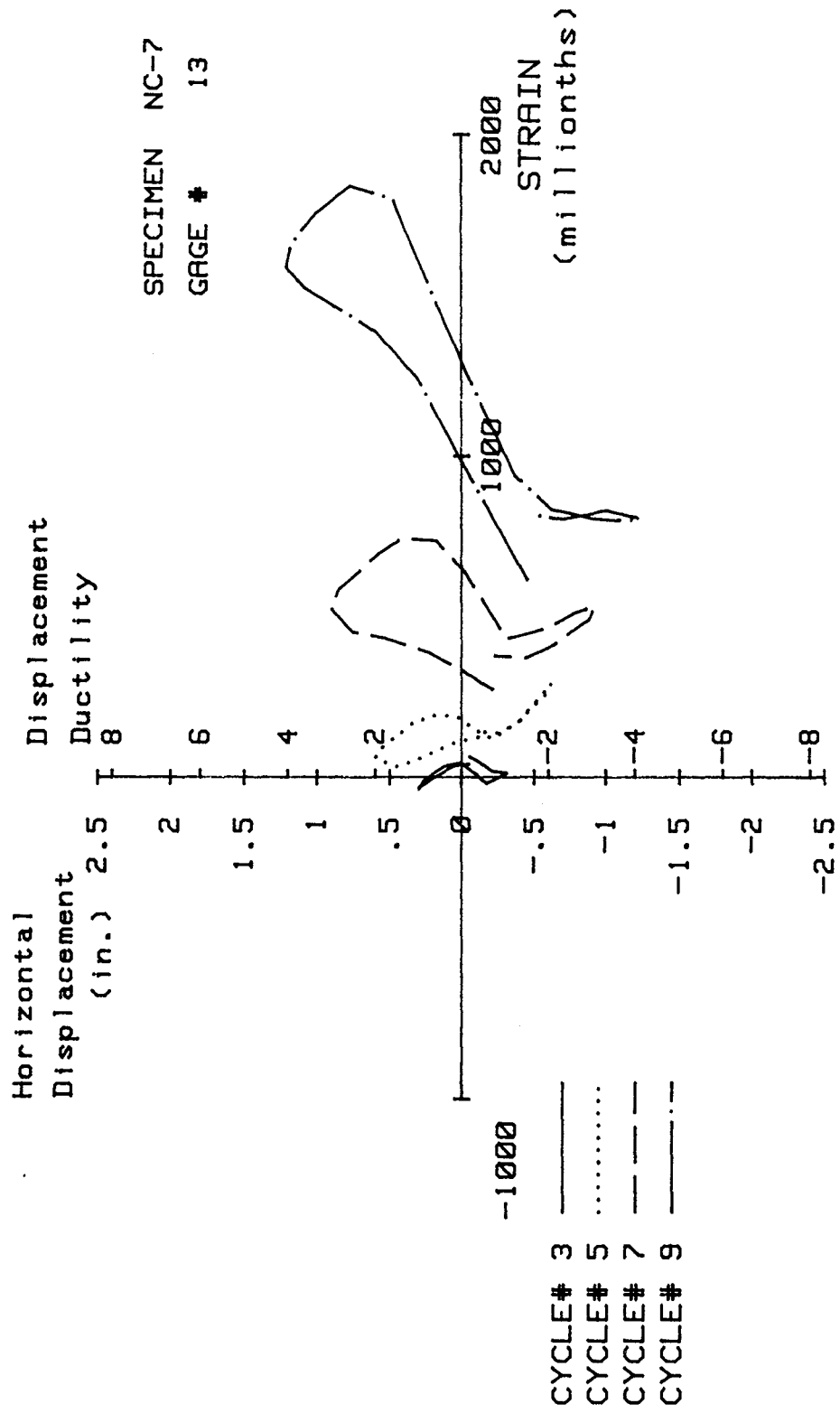


FIG. A-163 MEASURED STRAIN, GAGE #13, SPECIMEN NC-7

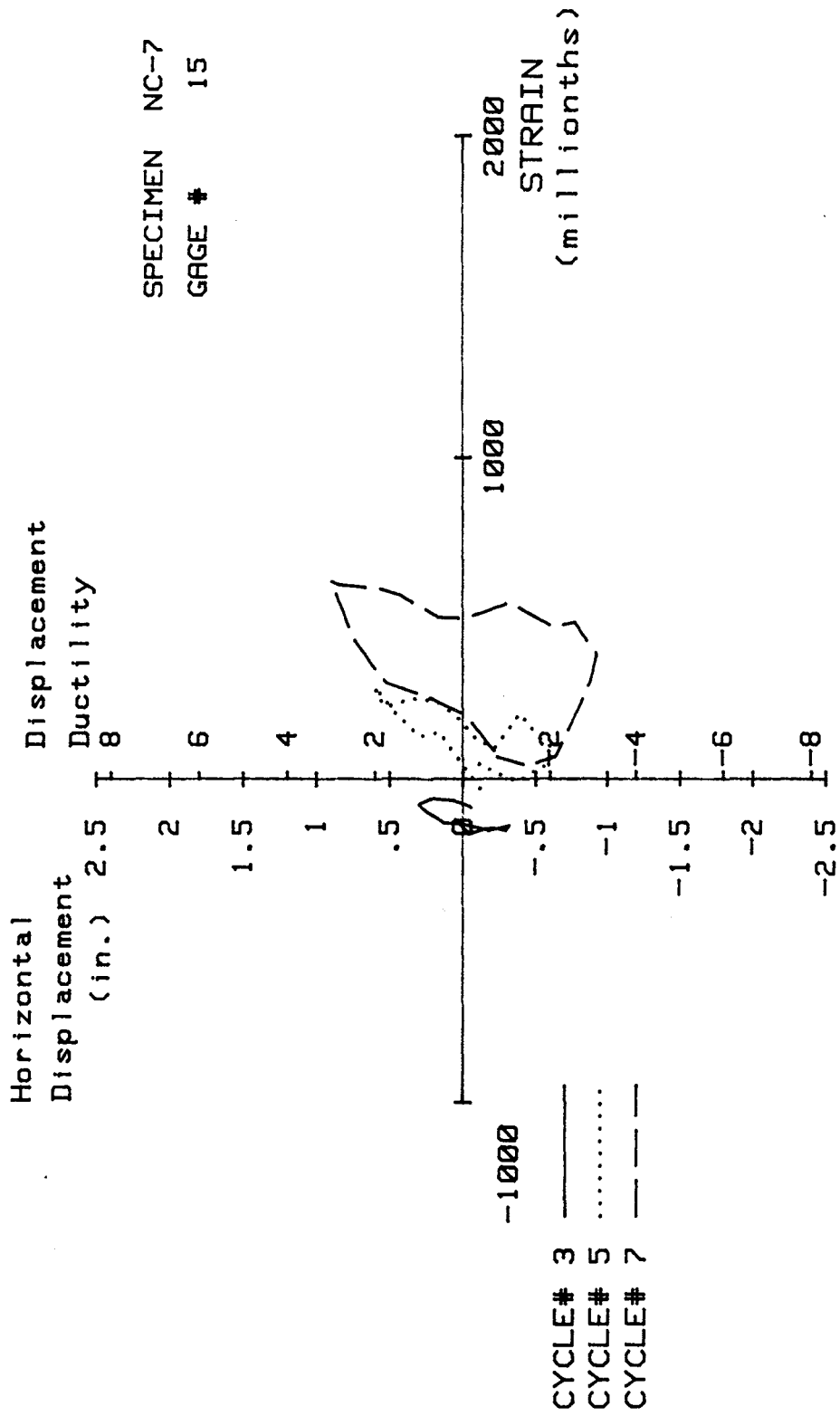


FIG. A-164 MEASURED STRAIN, GAGE #15, SPECIMEN NC-7

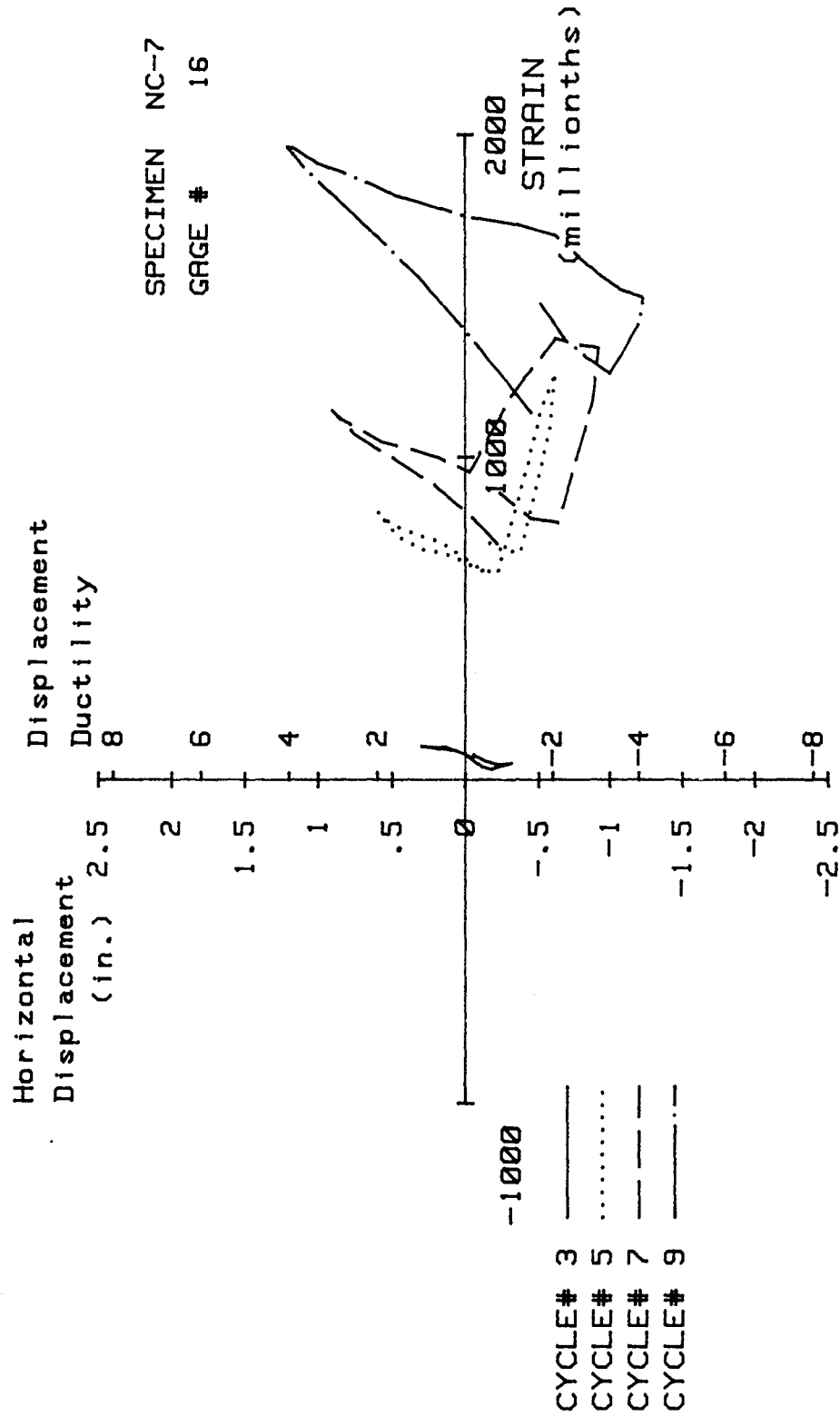


FIG. A-165 MEASURED STRAIN, GAGE #16, SPECIMEN NC-7

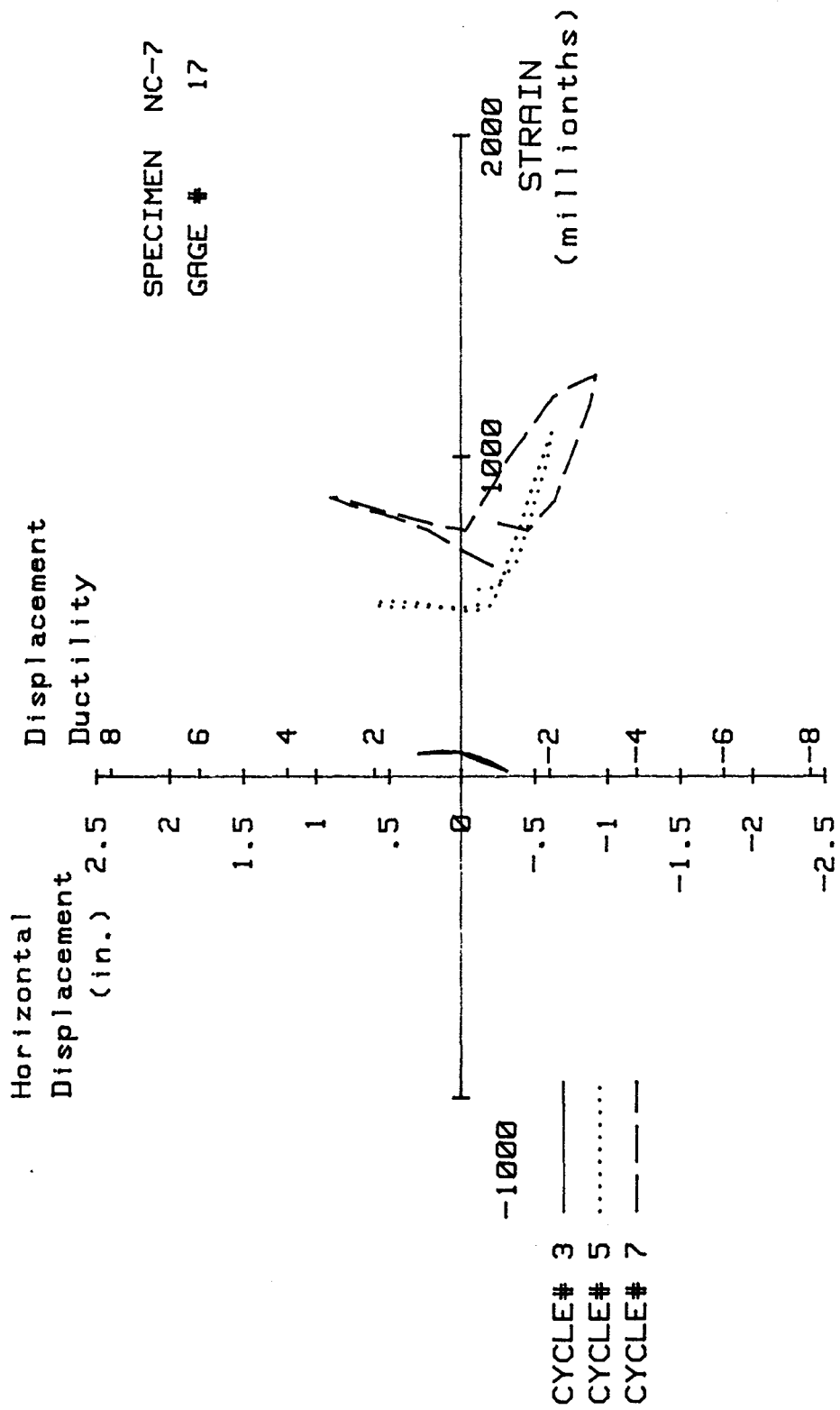


FIG. A-166 MEASURED STRAIN, GAGE #17, SPECIMEN NC-7

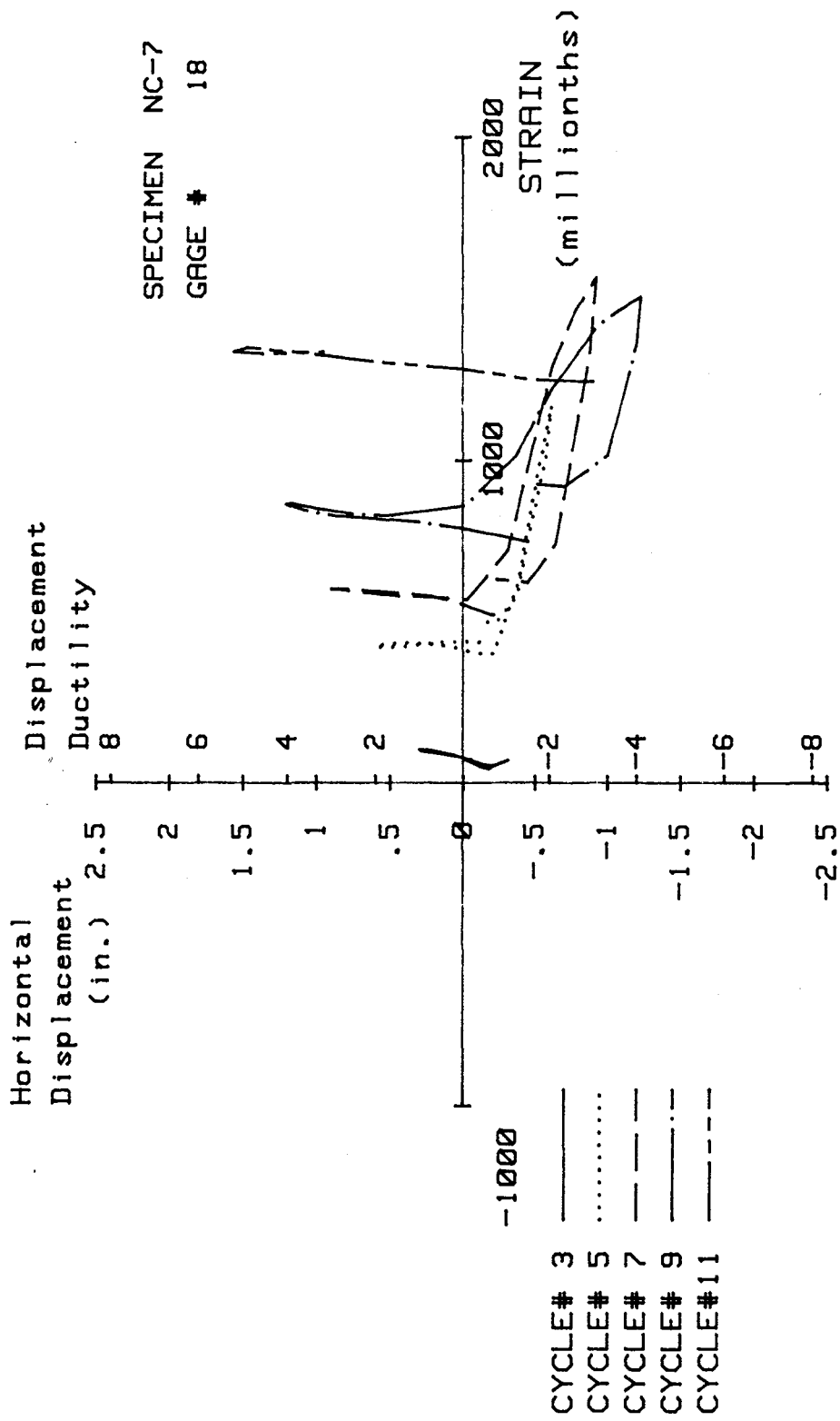


FIG. A-167 MEASURED STRAIN, GAGE #18, SPECIMEN NC-7

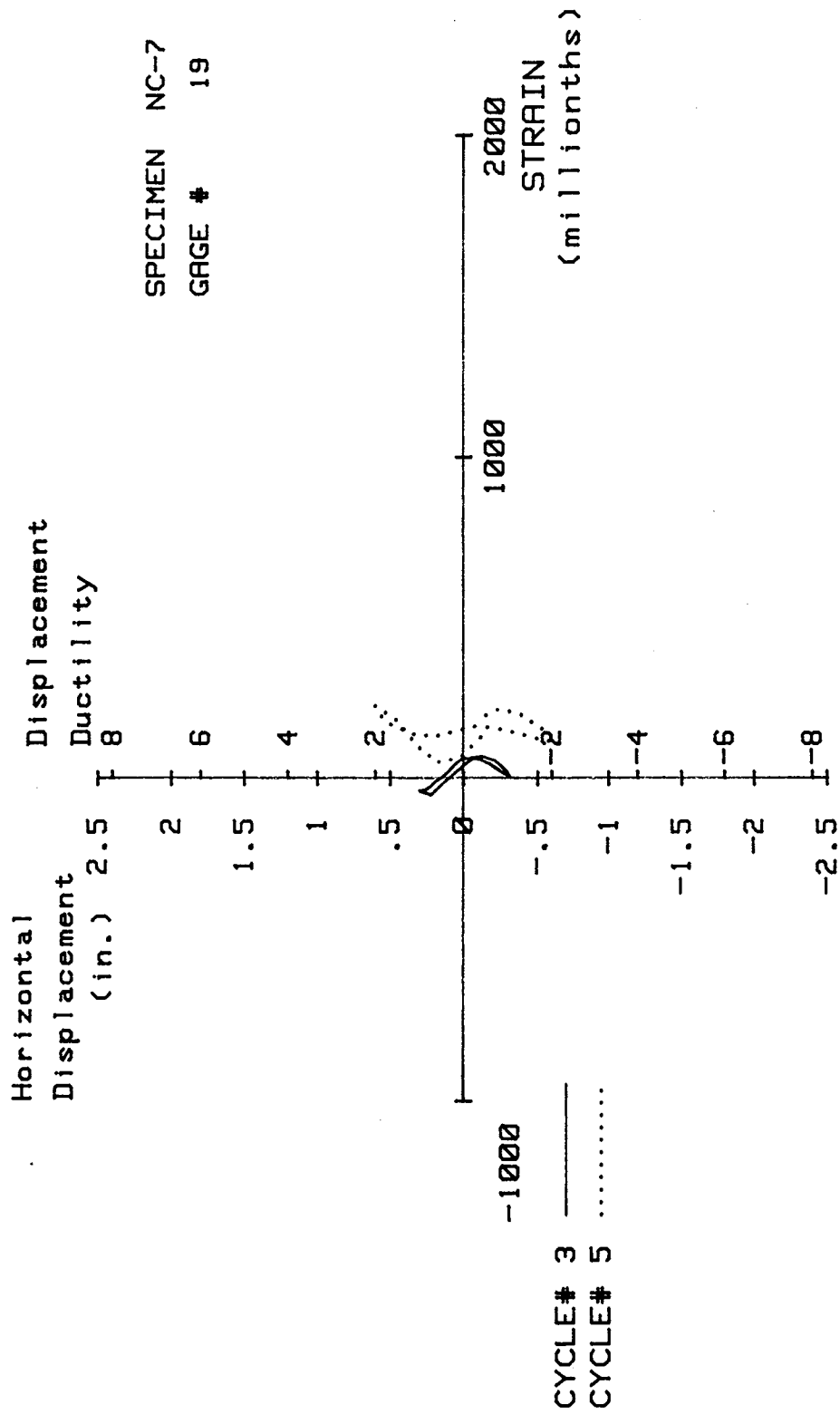


FIG. A-168 MEASURED STRAIN, GAGE #19, SPECIMEN NC-7

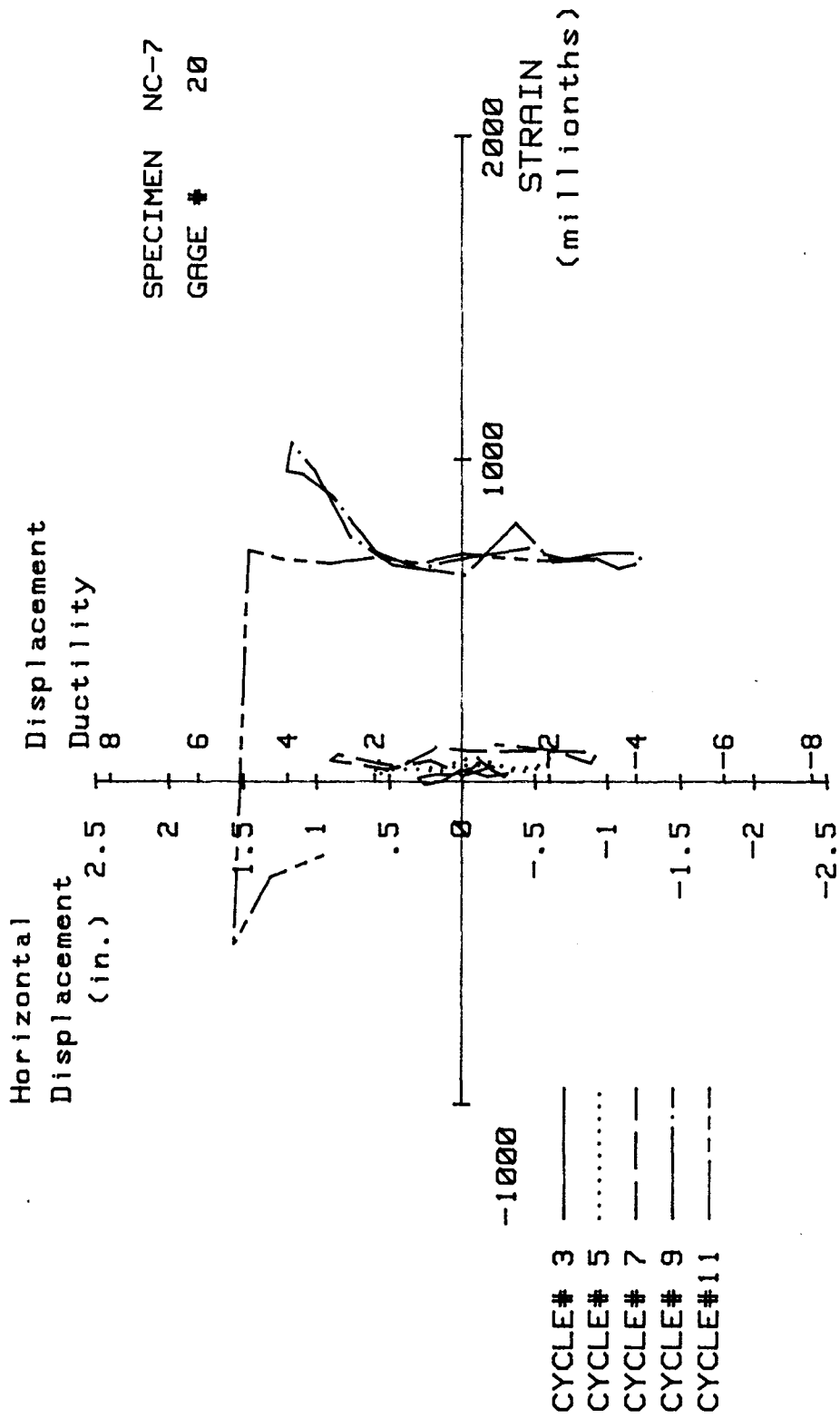


FIG. A-169 MEASURED STRAIN, GAGE #20, SPECIMEN NC-7

Specimen NC-8

Transverse Reinforcement Detail

Specimen NC-8 used an arrangement of transverse reinforcement similar to the detail shown in Fig. 4-2b, except that the inner and peripheral hoops were staggered vertically to provide a 2 in. center-to-center spacing. All crossties and peripheral hoops were made of #4 bars. The anchorages of the peripheral hoops had 135° bend and 6-bar diameter extensions while the anchorages of the inner hoops had 90° bends and 6-bar diameter extensions. The area of provided transverse reinforcement was 0.68 sq in., giving a volumetric reinforcement ratio of 2.19%. The area of the transverse reinforcement provided was 97% of the area required by ACI-318-83 Code.

This arrangement of transverse reinforcement reduces the congestion of reinforcement to some extent, as the inner and peripheral hoops are 2 in. apart.

Load History

Testing began by applying 560 kips of axial load to the specimen, which corresponds to 30% of the column's axial load capacity. The axial load was maintained constant throughout the testing. The specimen was next subjected to 15 complete cycles of horizontal loadings. During cycle #2 the first yield displacement and yield curvature were calculated to be 0.28 in. and $665 \times 10^{-6} \text{ in.}^{-1}$, respectively. Subsequently, the specimen was subjected to displacement-controlled testing consisting of one or two cycles each to a maximum displacement ductility ratio of seven. Only one cycle was applied at the displacement ductility ratio of seven; the specimen failed before completing the second cycle at this displacement level. Figure A-170 shows the history of applied horizontal loading.

Test Observations

The first hairline cracks were observed during the second cycle. These cracks were confined to a region within 18 in. from the stub. During the third cycle ($\mu=1$) some crushing of the cover concrete was observed within 5 in. of the stub.

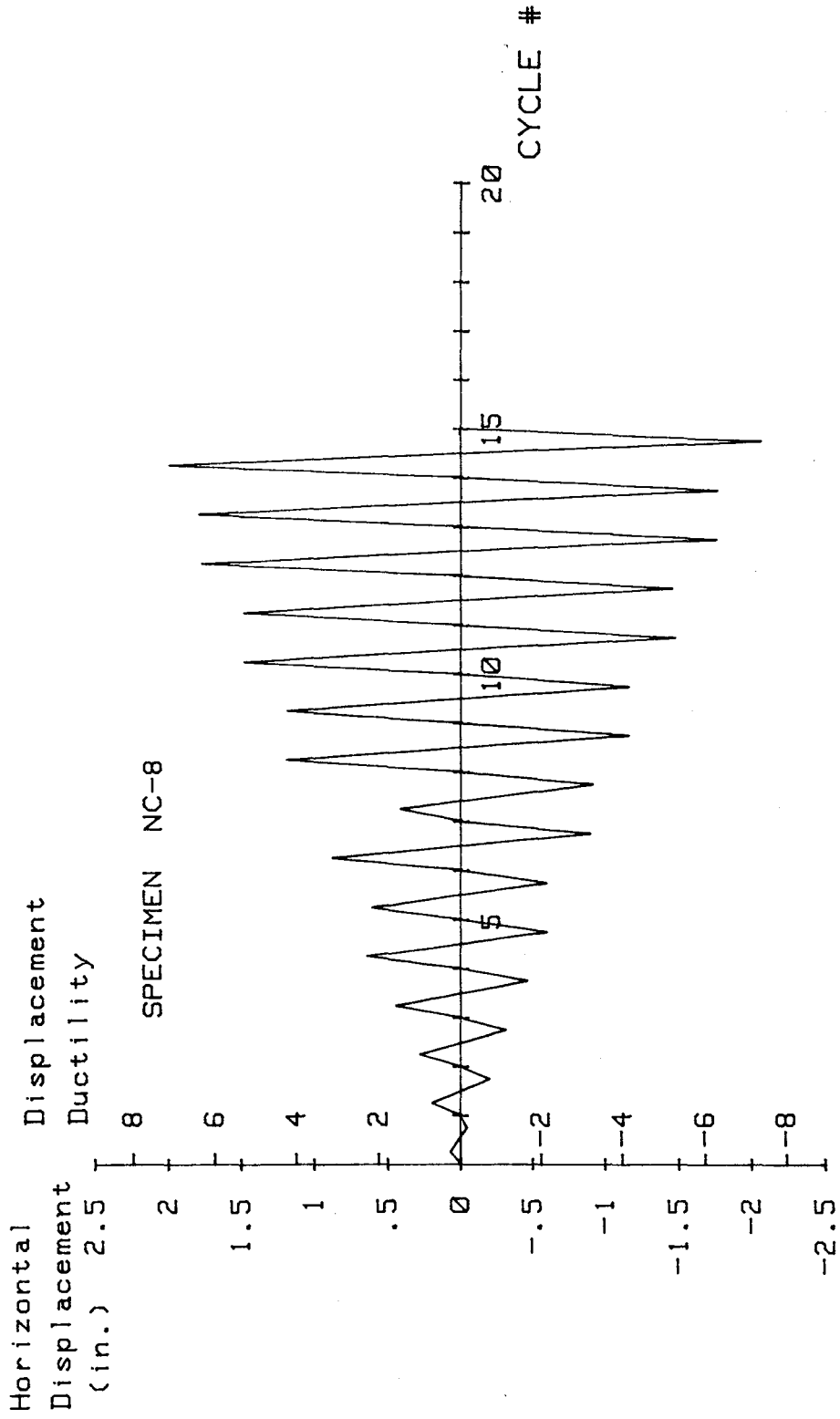


FIG. A-170 LOADING SCHEDULE, SPECIMEN NC-8

Figure A-171 shows the specimen at the end of cycle #6 ($\mu=2$). Spalling of the cover concrete on the corners extended a distance 24 in. above the stub. However, at this stage no vertical bars or transverse reinforcement were visible. Figure A-172 shows the specimen at the end of two cycles at a displacement ductility ratio of three, more cover concrete spalled off at this loading stage.

Figure A-173 shows the specimen at the end of cycle #10 ($\mu=4$) at which time extensive spalling occurred within 4 in. above the stub. However, no visible damage was detected on the vertical or transverse reinforcement. Figure A-174 shows the specimen at the end of cycle #12 ($\mu=5$). At this time vertical bars and peripheral hoops within 10 in. of the stub were visible, however, they suffered no apparent damage. The crossties were completely embedded in the concrete at this stage. During cycle #14 ($\mu=6$), some lateral bending of the corner longitudinal bars was observed but there were no signs of loss of anchorage of the peripheral hoops or crossties. As shown in Fig. A-175 at the end of the second cycle at the displacement ductility ratio of six (cycle #14), some lateral bending of the middle bars located on the east and west faces of the specimens was observed. Next, the specimen was then subjected to one complete cycle at a displacement ductility ratio of seven. At this stage some signs of anchorage loss on the peripheral hoops located 5 in. above the stub was visible. The specimen failed before completing the second cycle (see Fig. A-176) at this displacement level, at which time the anchorages of the peripheral hoops and crossties located 5 and 7 in. from the stub, respectively, were lost. The loss of the anchorages coincided with the buckling of the corner and middle longitudinal bars in compression. The remaining transverse reinforcement was intact. The length of the longitudinal bars engaged in buckling was within 3 and 9 in. from the stub.

Load Deflection and Moment-Curvature Characteristics

Figure A-177 shows the horizontal load deflection characteristics of the specimen. With the exception of the first cycle at the displacement ductility ratios of 2 and 3, the applied horizontal loads were lower than the theoretical values shown by the dashed line in Fig. A-177. The behavior

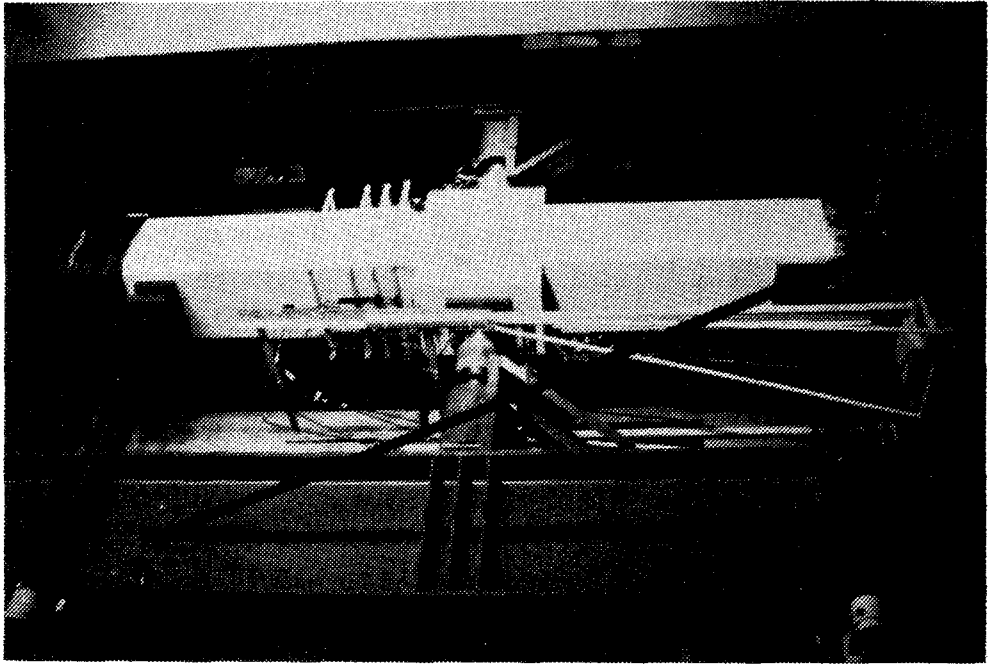


FIG. A-172 TEST SPECIMEN NC-8 AFTER CYCLE #8

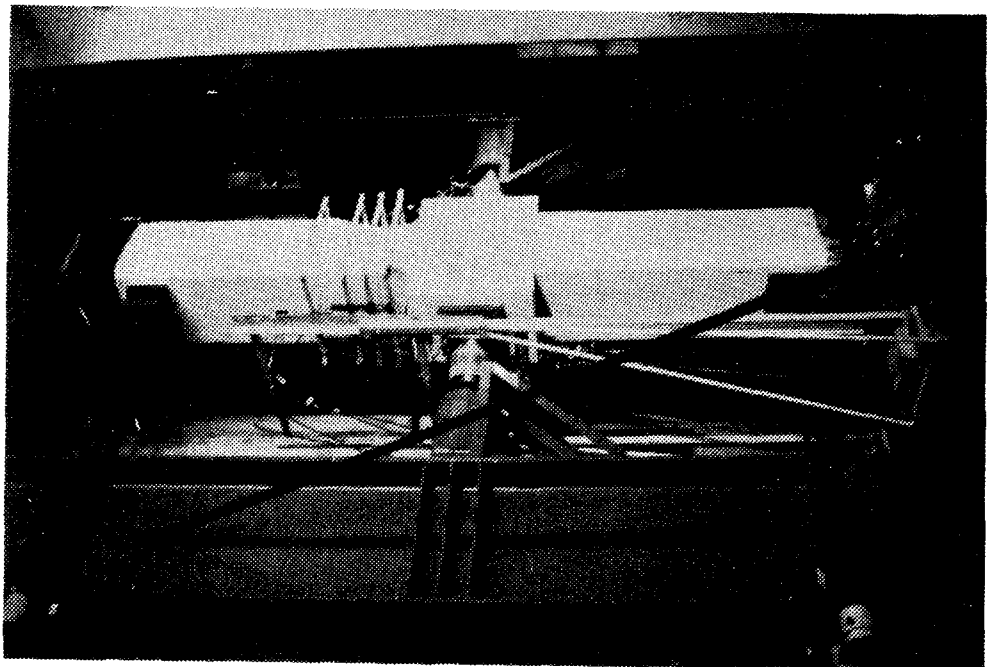


FIG. A-171 TEST SPECIMEN NC-8 AFTER CYCLE #6

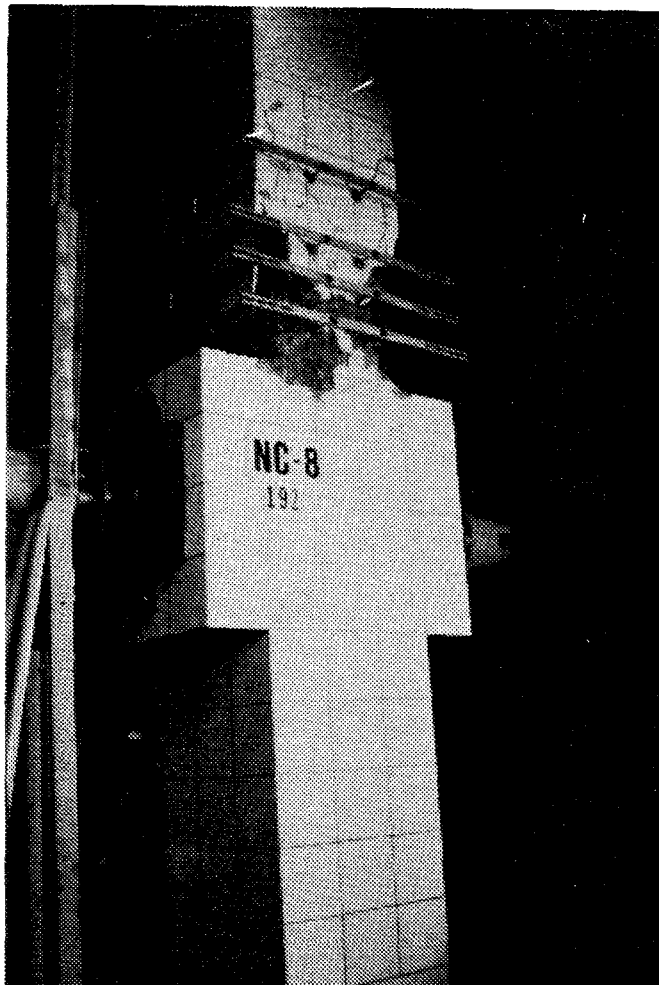


FIG. A-173 TEST SPECIMEN NC-8 AFTER CYCLE #10

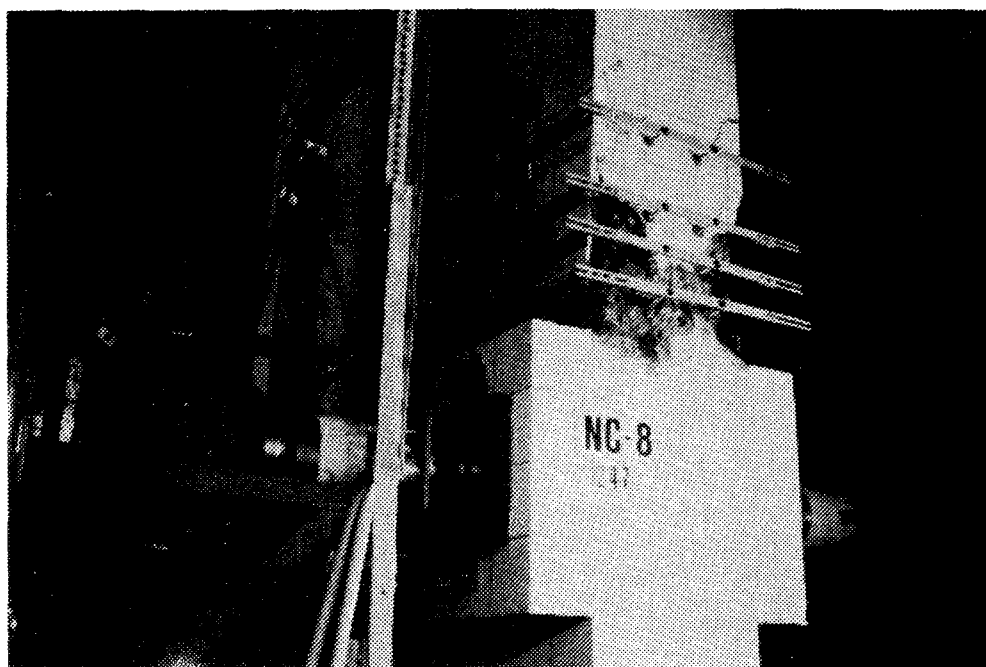


FIG. A-174 TEST SPECIMEN NC-8 AFTER CYCLE #12

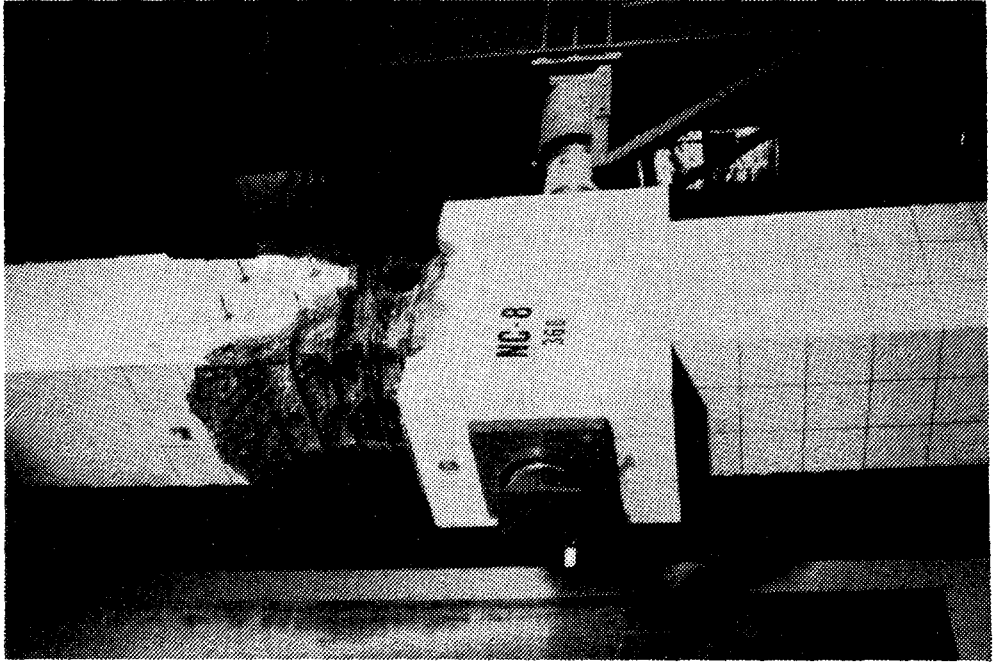


FIG. A-176 TEST SPECIMEN NC-8 AFTER TEST CONCLUSION

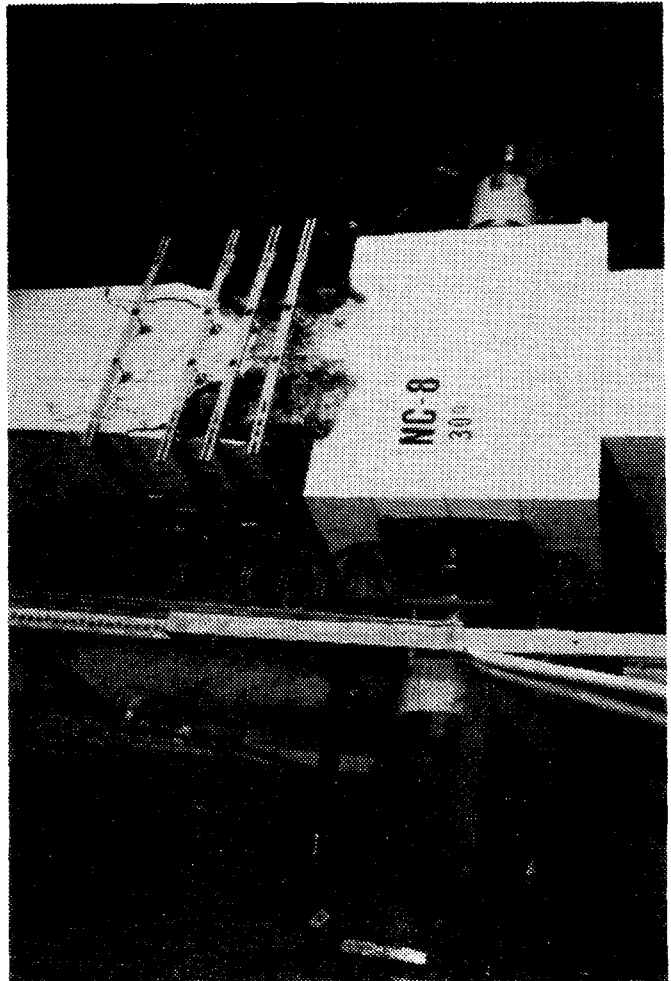
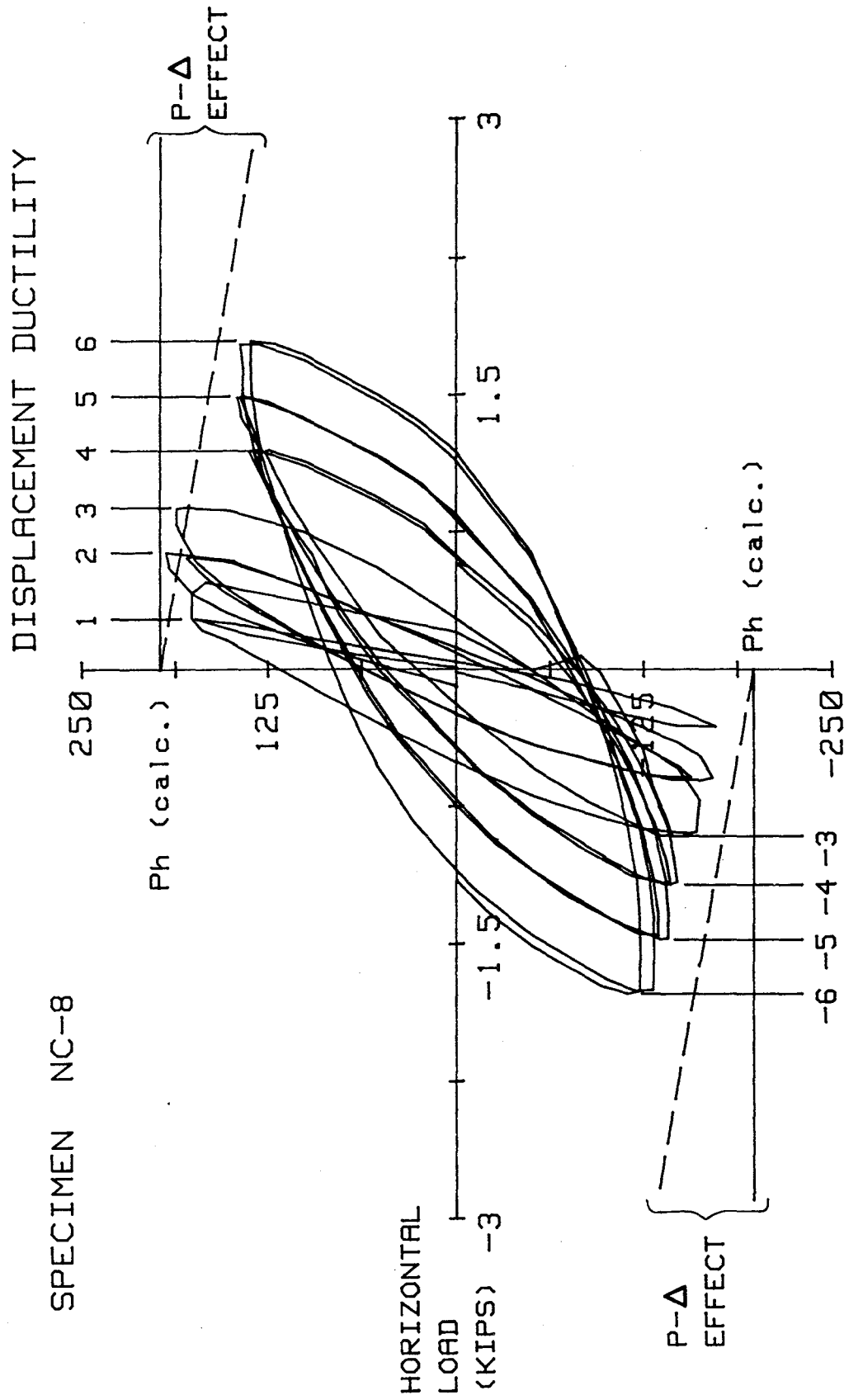


FIG. A-175 TEST SPECIMEN NC-8 AFTER CYCLE #14



Metric Equivalents
 1 in. = 25.4 mm
 1 kip = 4.45 kN

HORIZONTAL DISPLACEMENT (IN.)

FIG. A-177 HORIZONTAL LOAD VERSUS DISPLACEMENT, SPECIMEN NC-8

of Specimen NC-8 was unique with regard to the horizontal load deflection behavior. The applied horizontal load dropped from 192 kips at the displacement ductility ratio of 3 to 138 kips at cycle #9 ($\mu=4$). However, the horizontal load capacity in the forward loading direction began to increase slightly at higher displacement levels.

Figure A-178 shows the curvature distribution along the upper column to a displacement ductility ratio of six. The maximum curvature ductility ratio of 6 was approximately 11.

The ratio of curvature ductility to displacement ductility at the peak of displacement ductility ratios of 2, 4, 5, and 6 were 2.6, 1.7, 1.9, and 1.9, respectively.

Figure A-179 shows the moment curvature characteristic of the column cross-section at the upper column-stub interface. The applied total moment, except during the first cycles at displacement ductility ratios of 2 and 3, was lower than the theoretical moment capacity calculated based on the procedures outlined in Section 4.8.2. After dropping at the displacement ductility ratio of three, the moment capacity in the forward loading direction increased slightly at higher displacement levels. This behavior was unique among all test specimens.

The ratio of the peak moment at the second cycle to the peak moment at the first cycle ranged from 0.90 to 1.1 at various displacement levels.

Transverse Reinforcement Strain

A total of 24 strain gages were attached to the transverse reinforcements. Figure 4-11 shows the locations of these strain gage, except that the peripheral and inner hoops were staggered vertically. Figures A-180 through A-195 show the data obtained from these gages.

In general, the strain on the peripheral hoops was larger than the strain on the inner hoops.

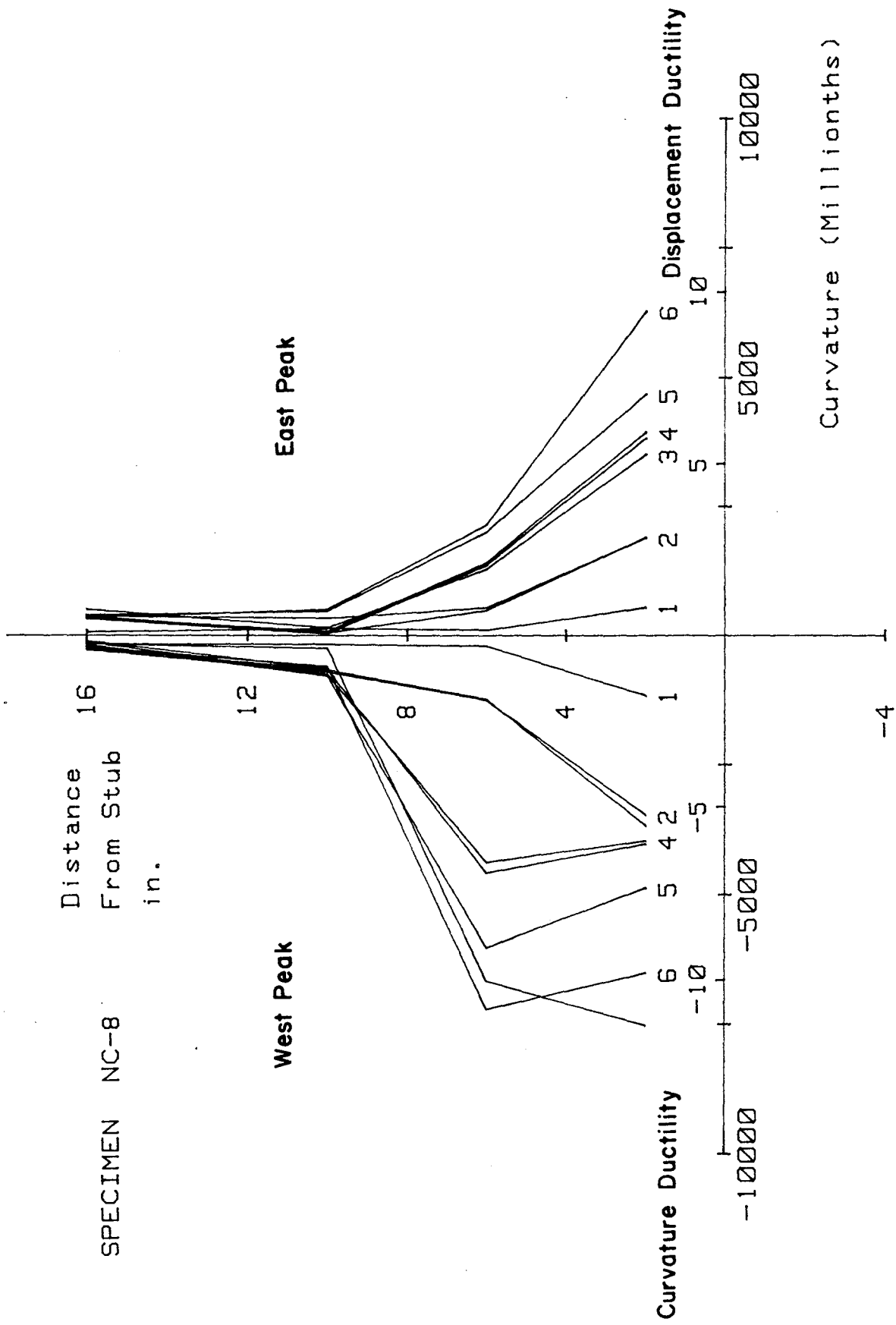


FIG. A-178 CURVATURE DISTRIBUTION ALONG UPPER COLUMN, SPECIMEN NC-8

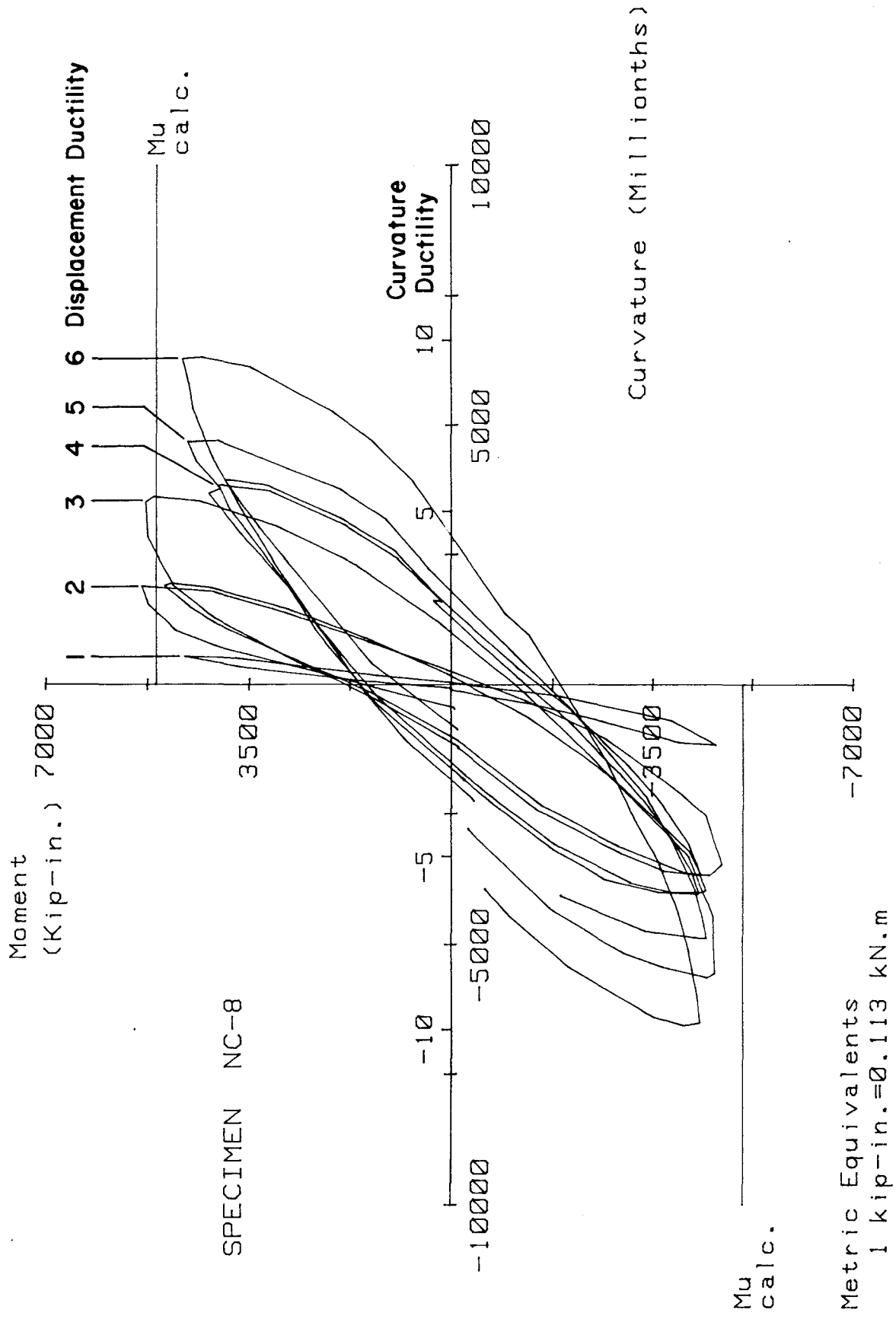


FIG. A-179 MOMENT VERSUS CURVATURE FOR SPECIMEN NC-8

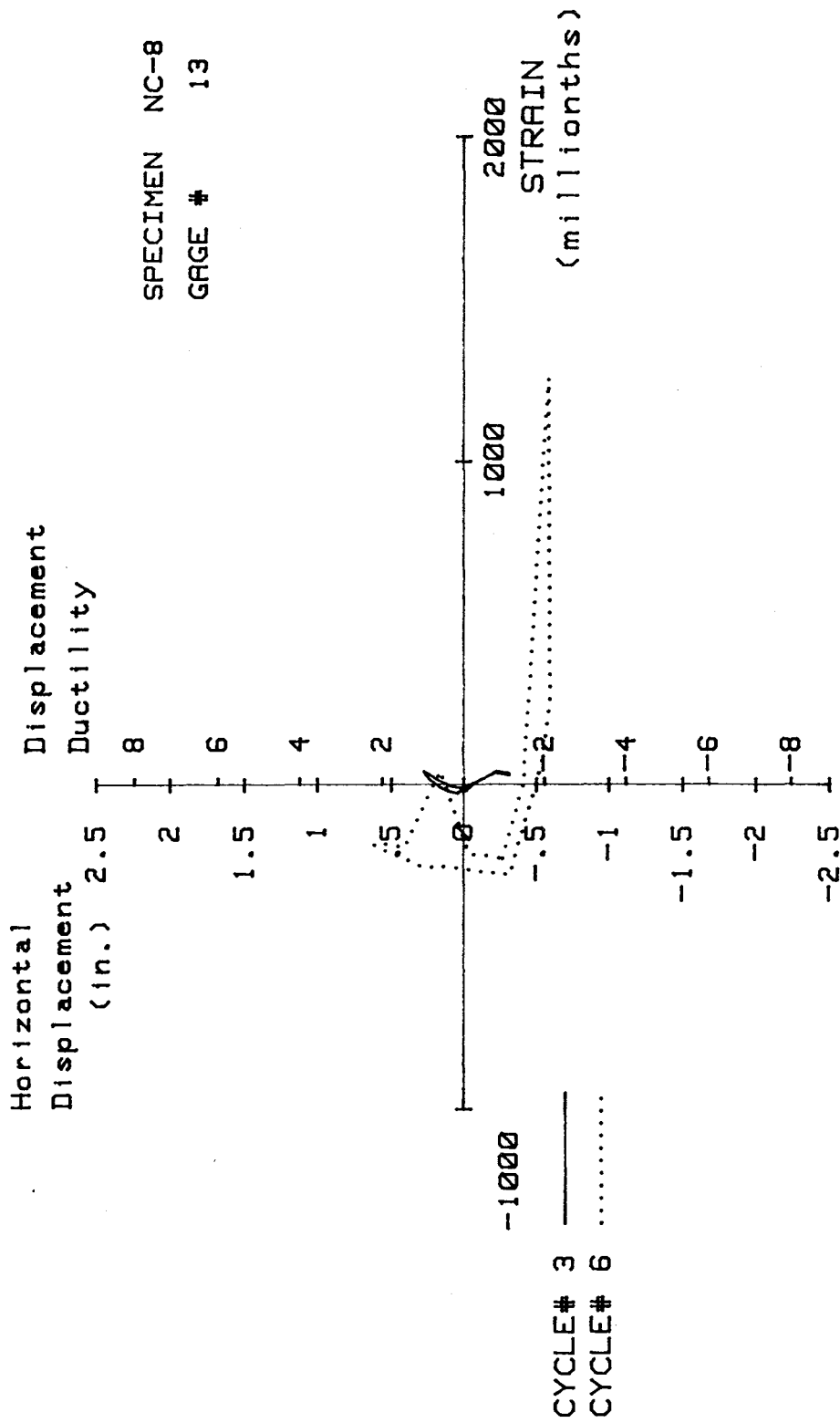


FIG. A-180 MEASURED STRAIN, GAGE #13, SPECIMEN NC-8

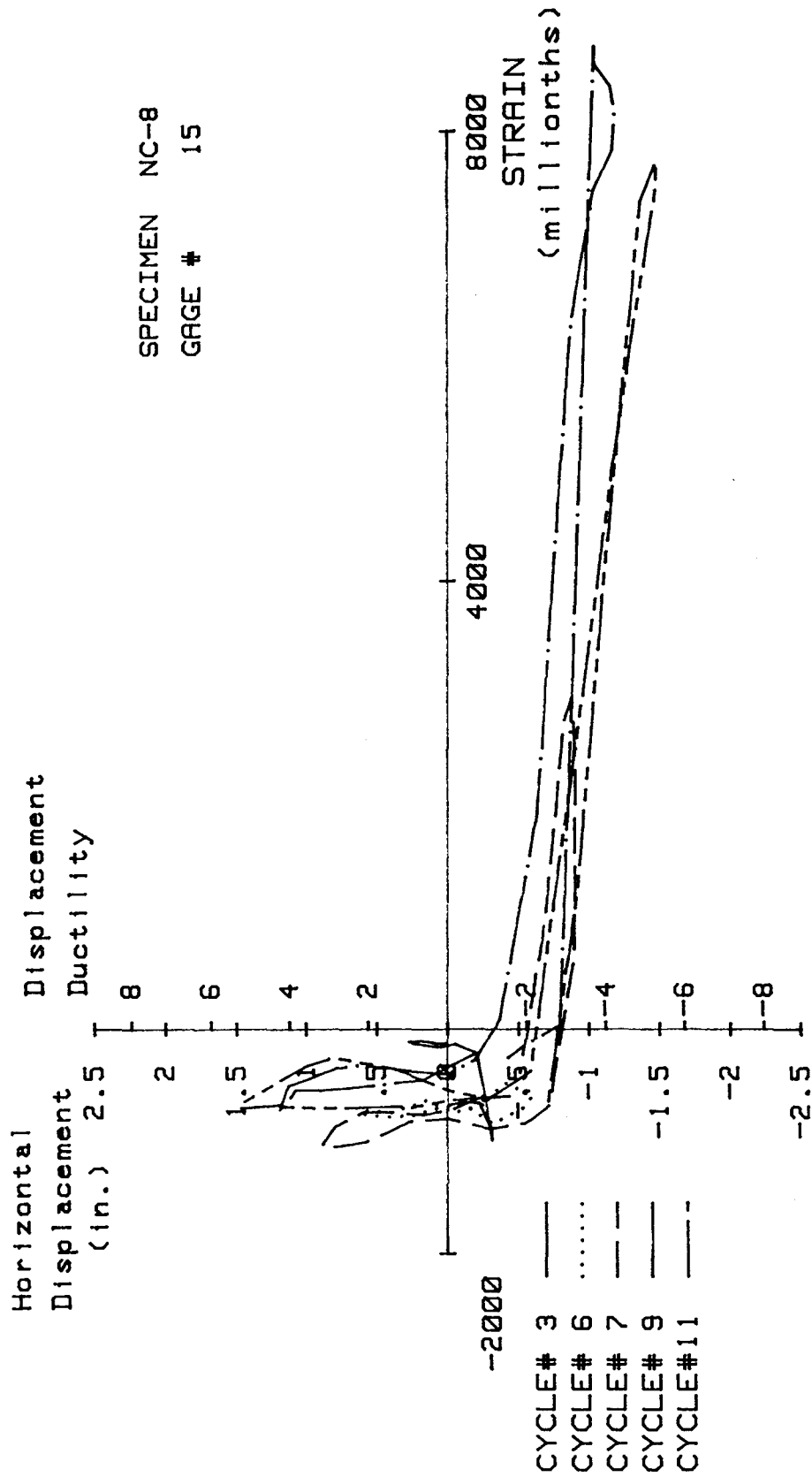


FIG. A-181 MEASURED STRAIN, GAGE #15, SPECIMEN NC-8

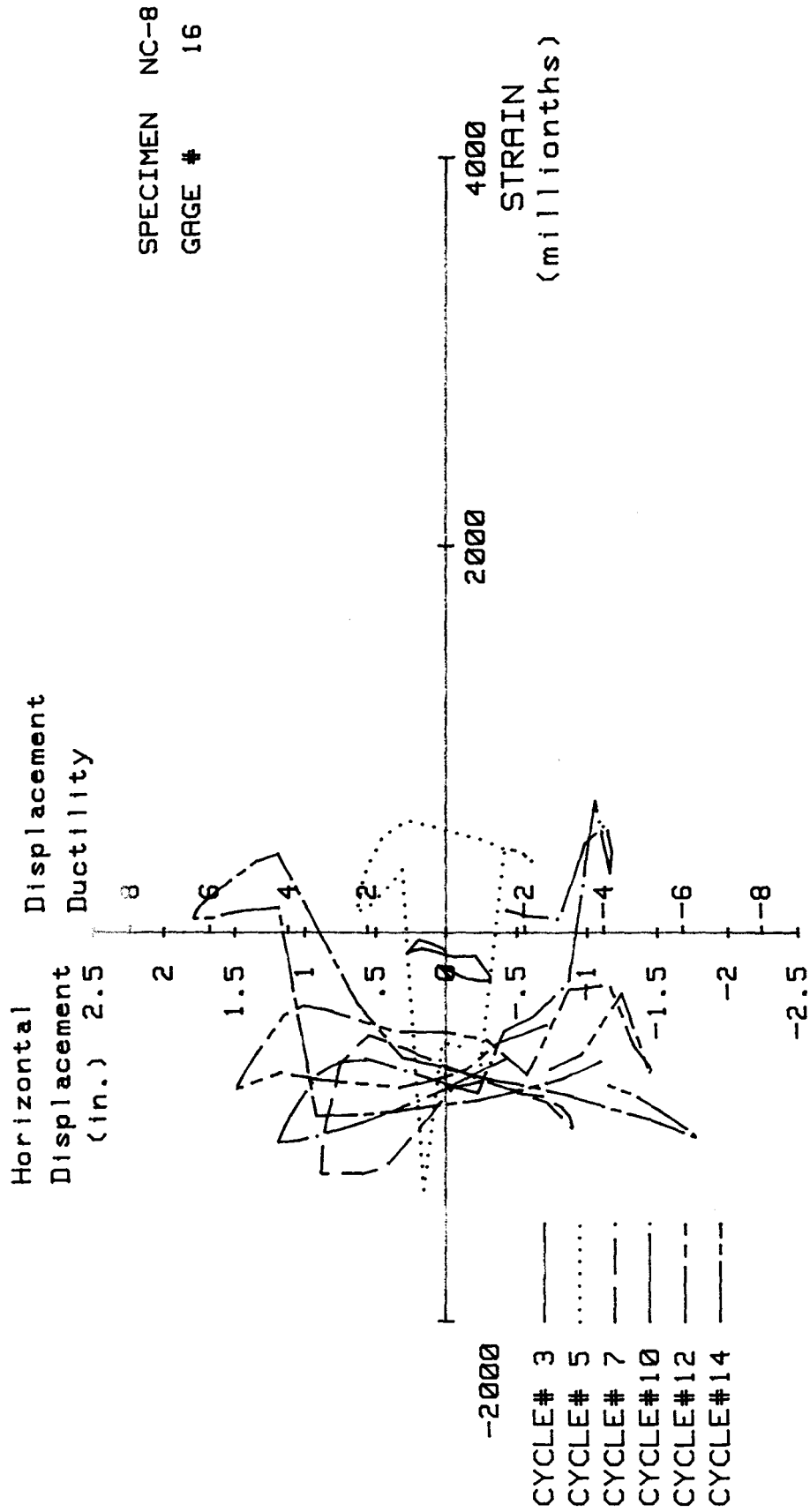


FIG. A-182 MEASURED STRAIN, GAGE #16, SPECIMEN NC-8

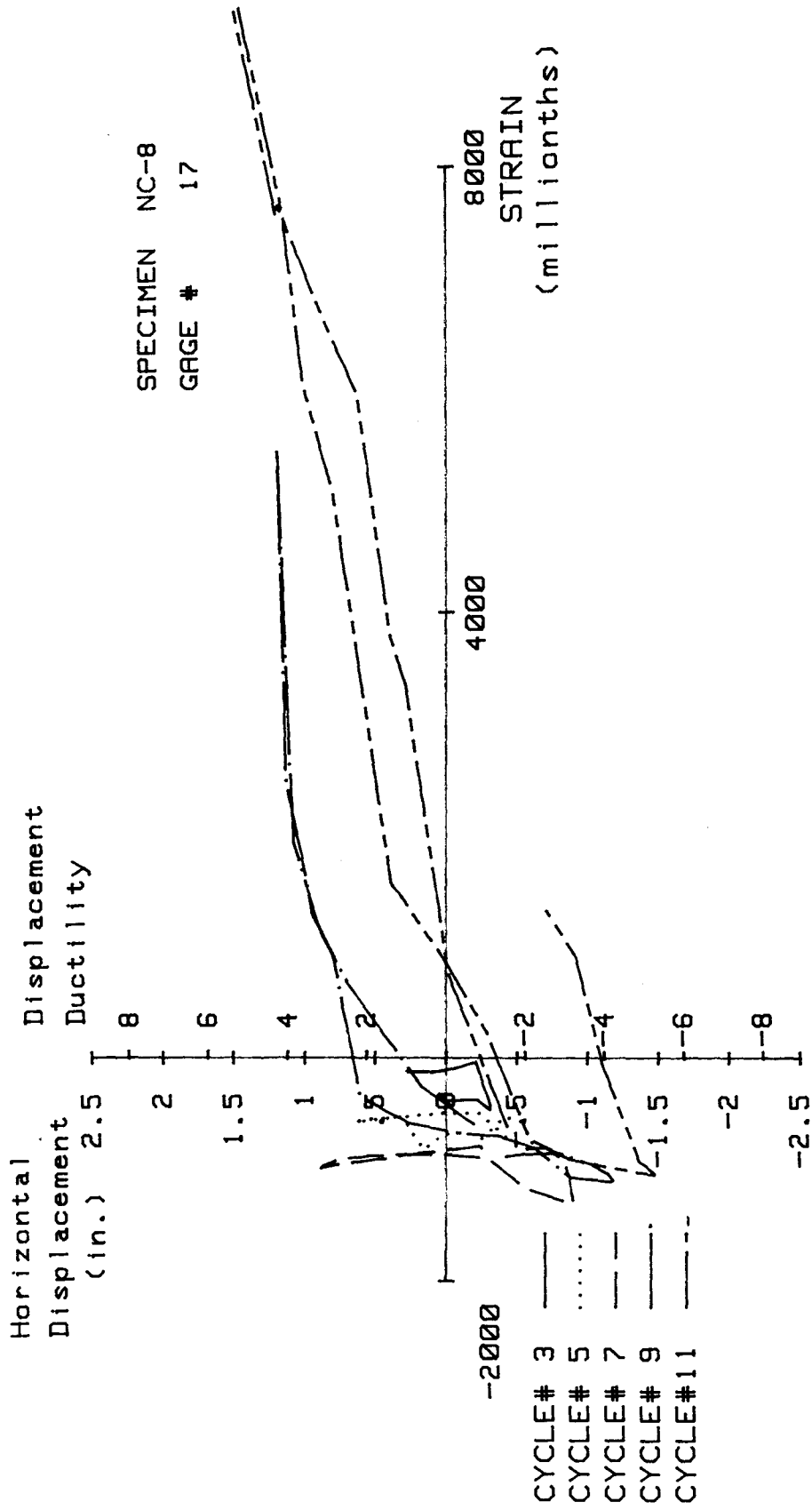


FIG. A-183 MEASURED STRAIN, GAGE #17, SPECIMEN NC-8

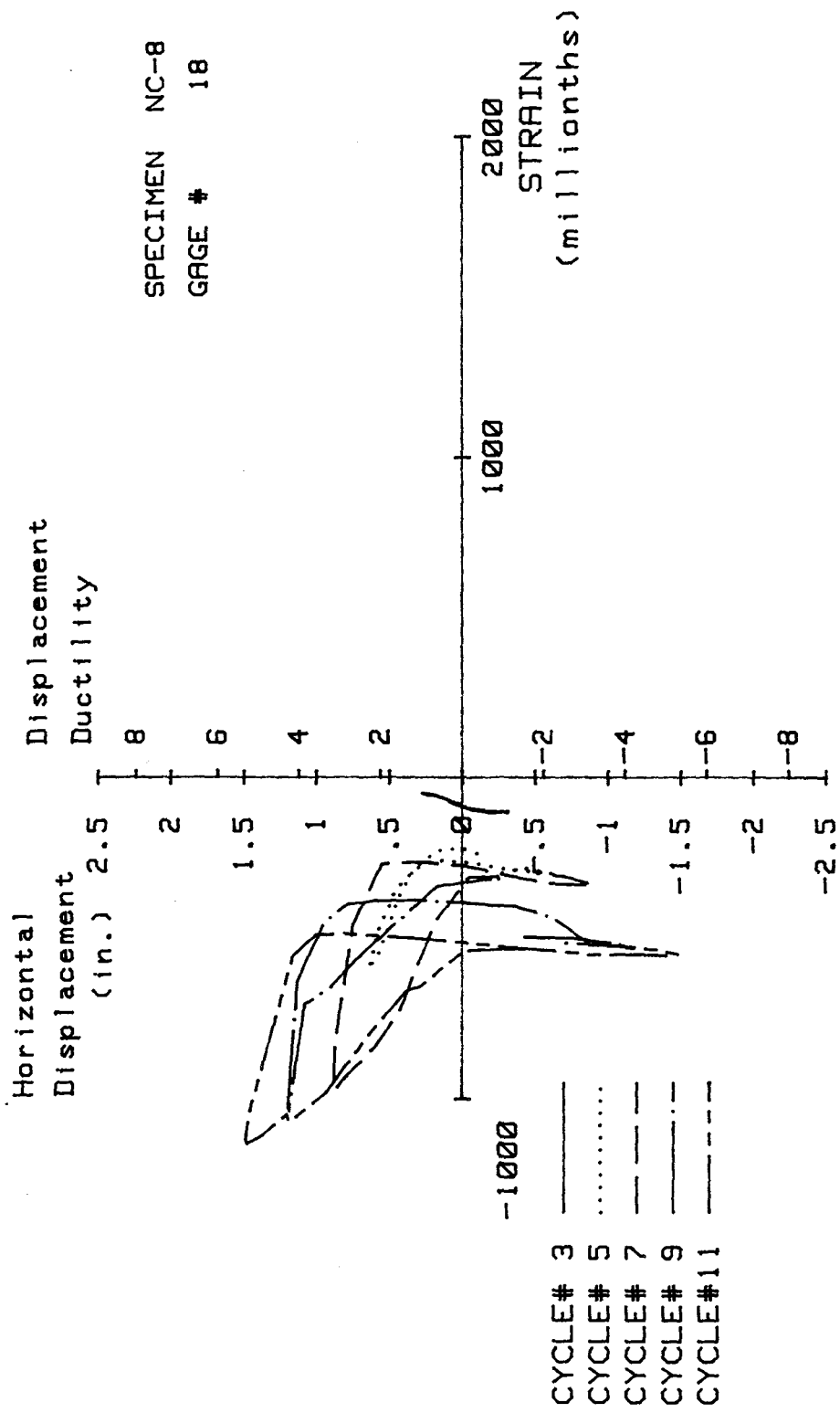


FIG. A-184 MEASURED STRAIN, GAGE #18, SPECIMEN NC-8

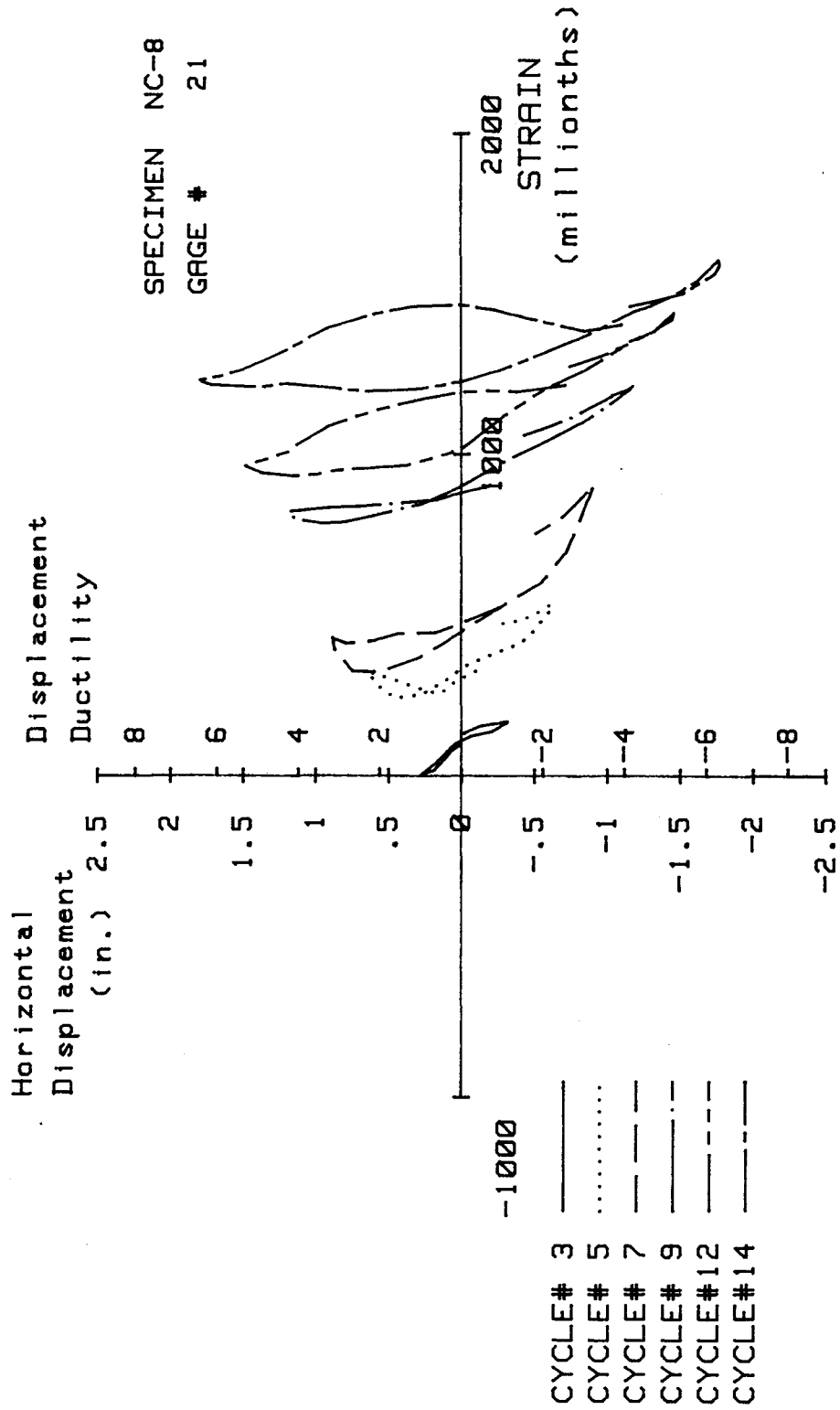


FIG. A-185 MEASURED STRAIN, GAGE #21, SPECIMEN NC-8

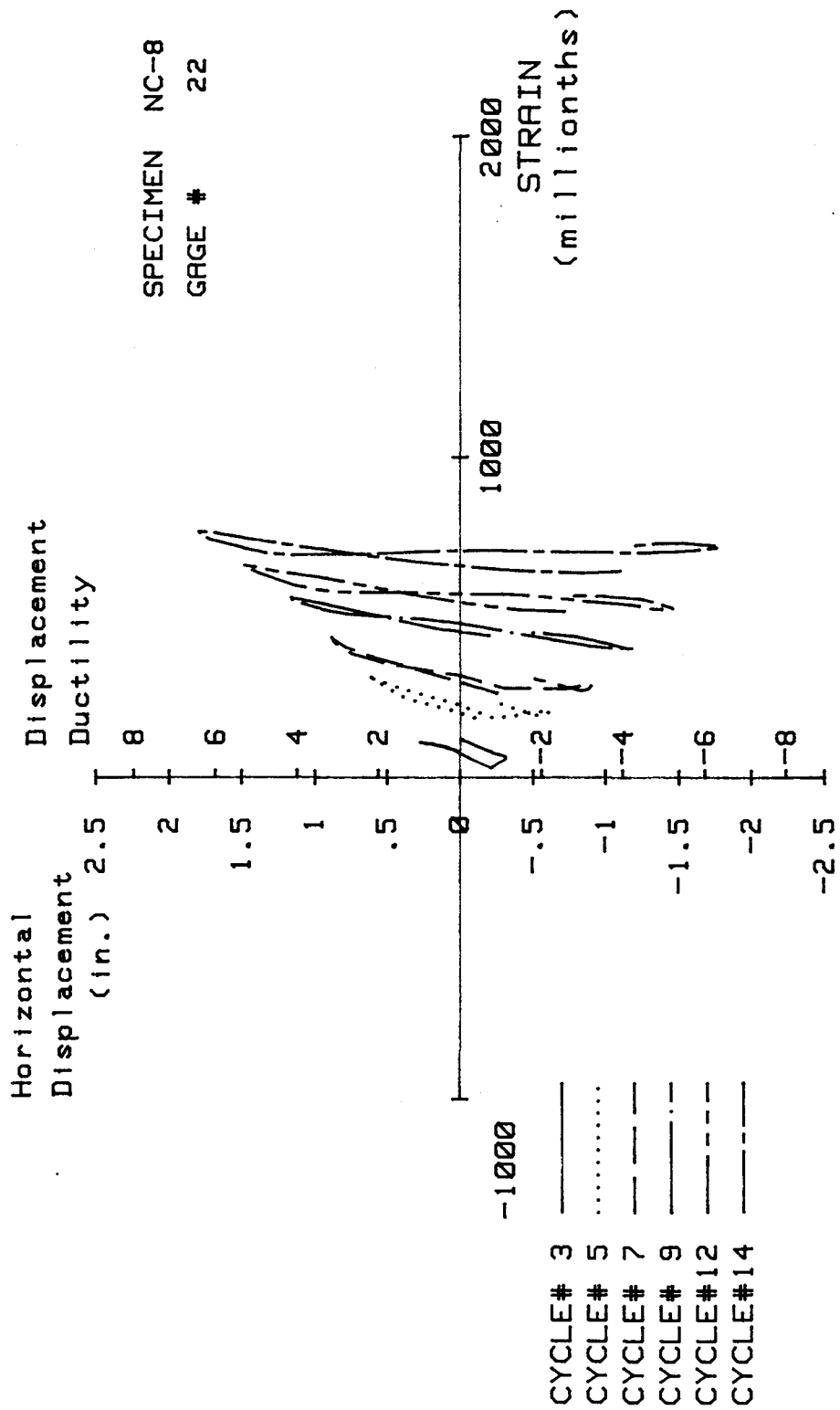


FIG. A-186 MEASURED STRAIN, GAGE #22, SPECIMEN NC-8

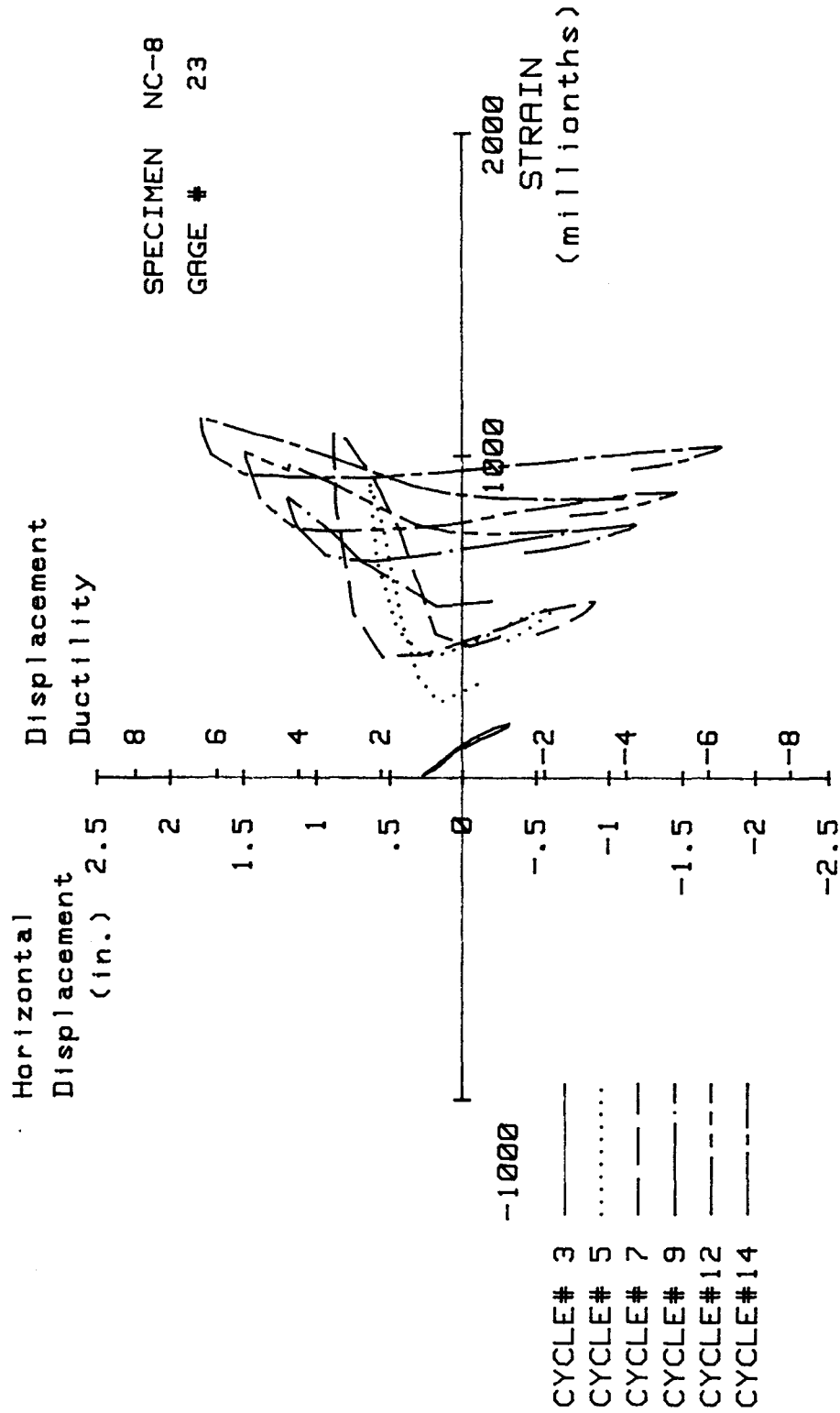


FIG. A-187 MEASURED STRAIN, GAGE #23, SPECIMEN NC-8

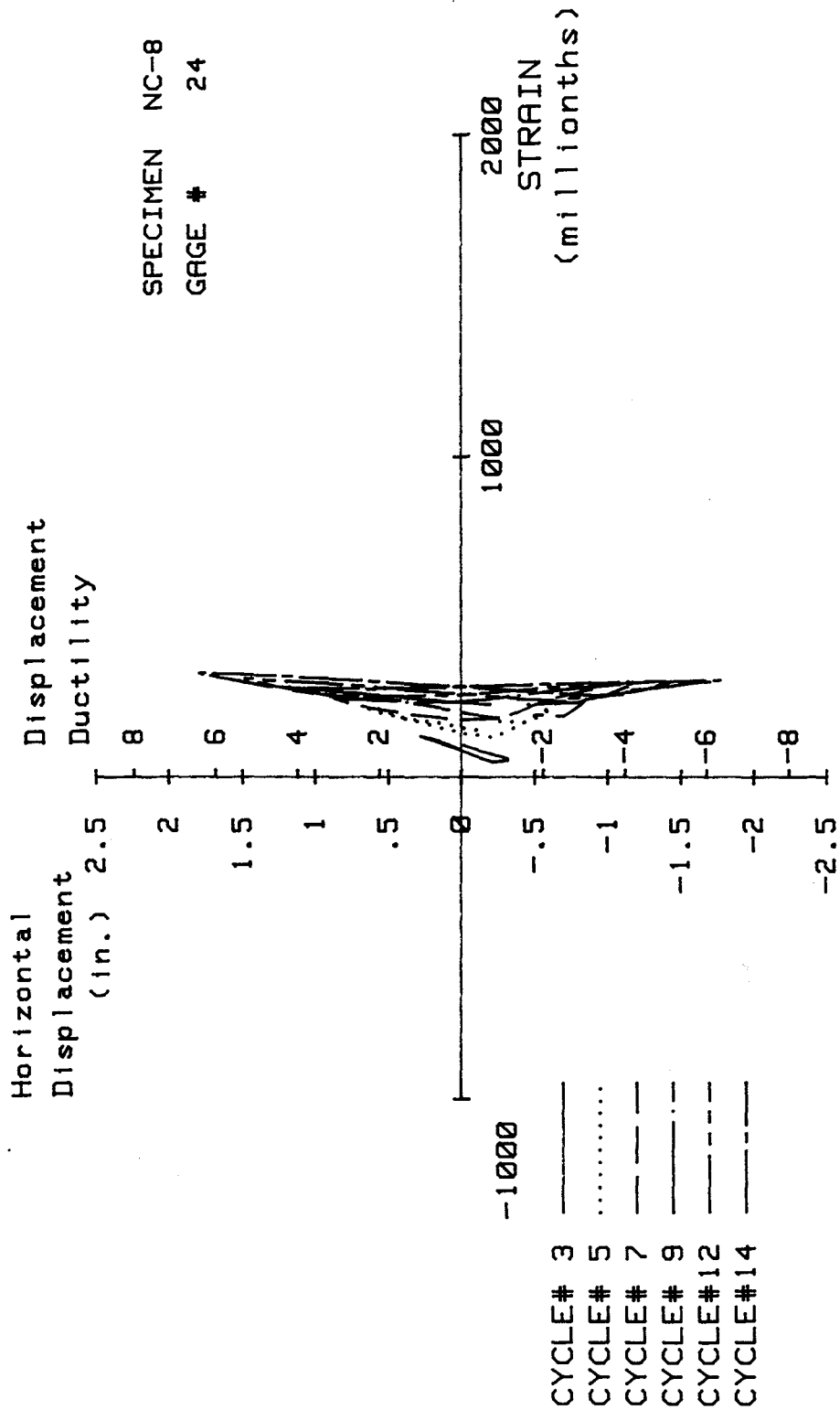


FIG. A-188 MEASURED STRAIN, GAGE #24, SPECIMEN NC-8

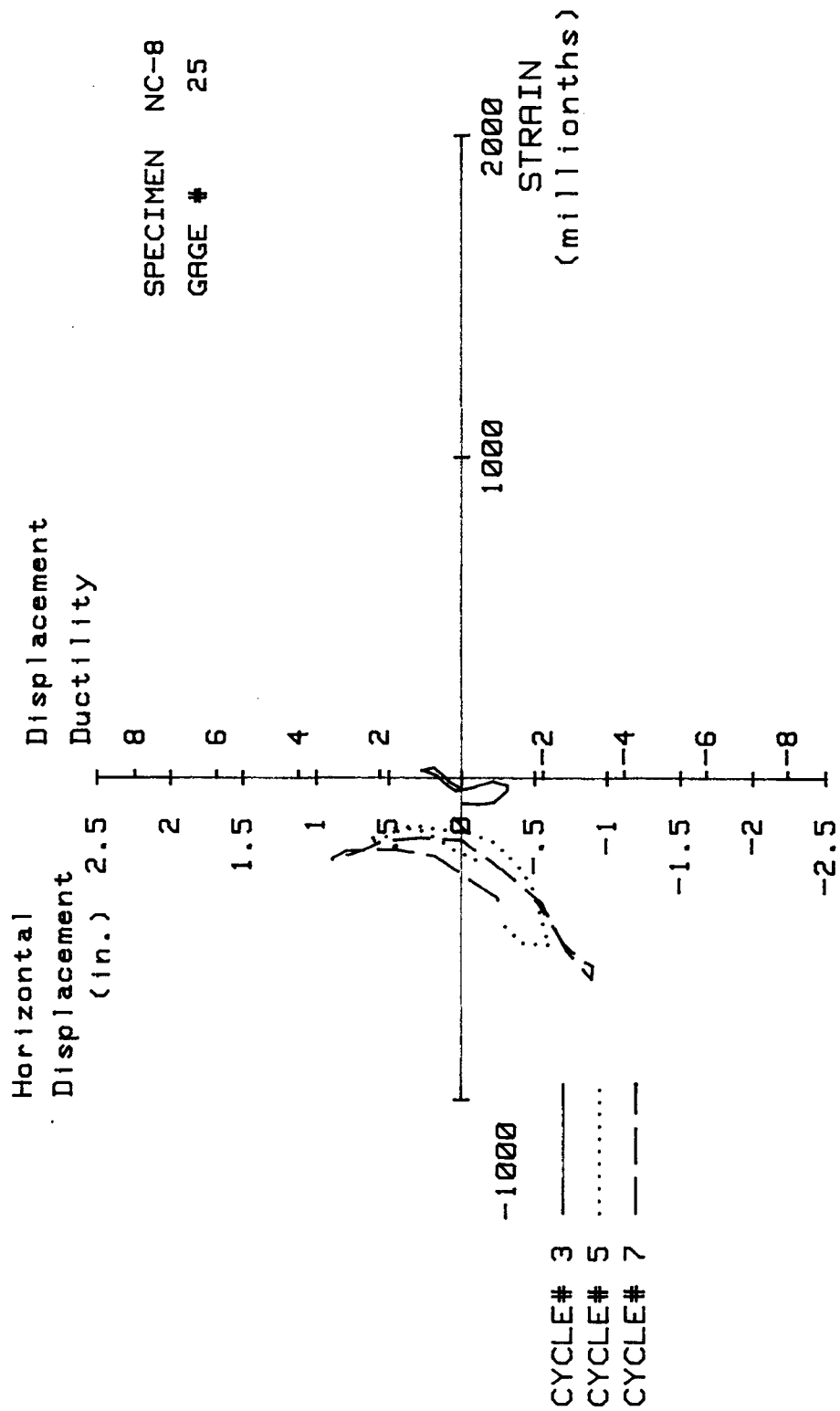


FIG. A-189 MEASURED STRAIN, GAGE #25, SPECIMEN NC-8

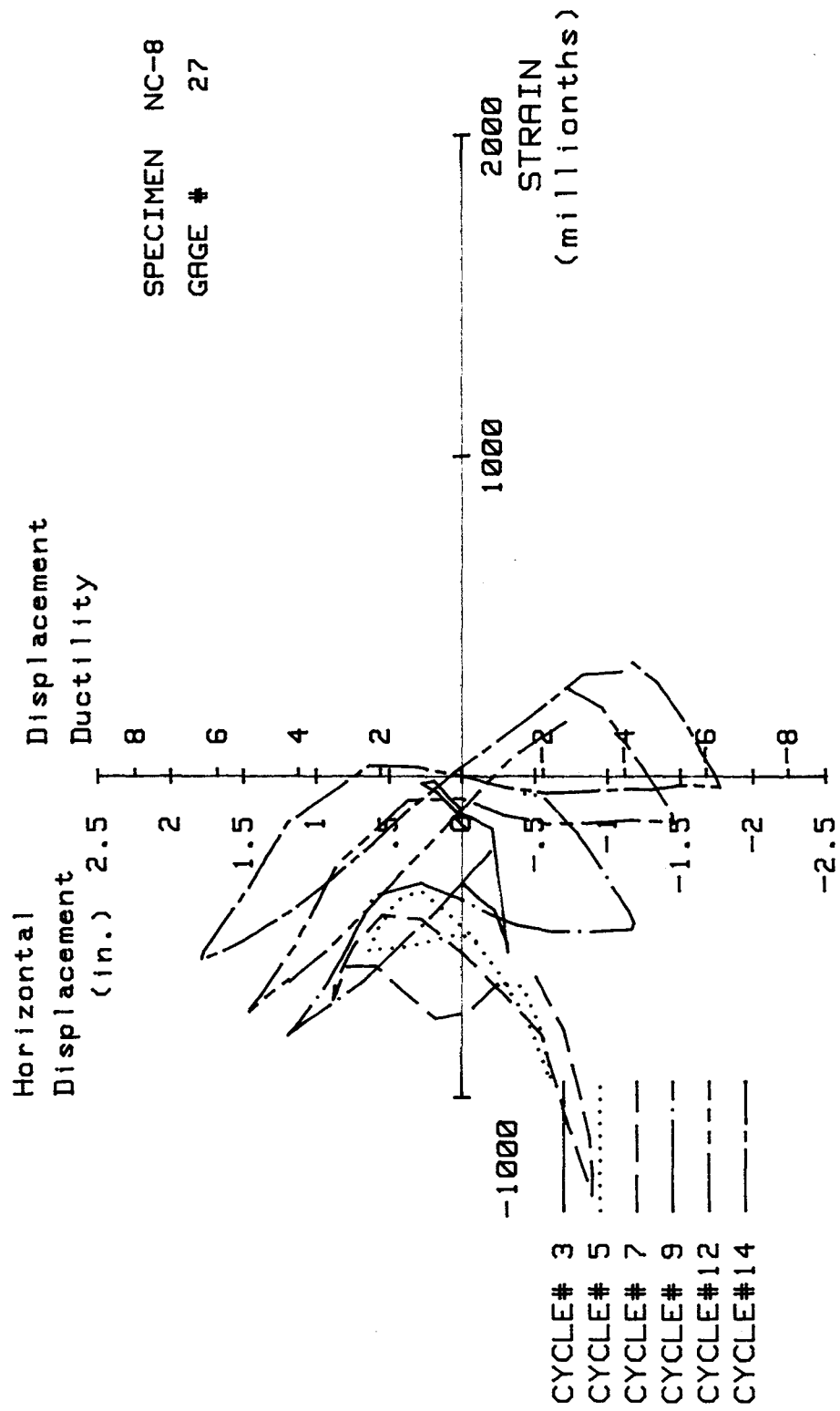


FIG. A-190 MEASURED STRAIN, GAGE #27, SPECIMEN NC-8

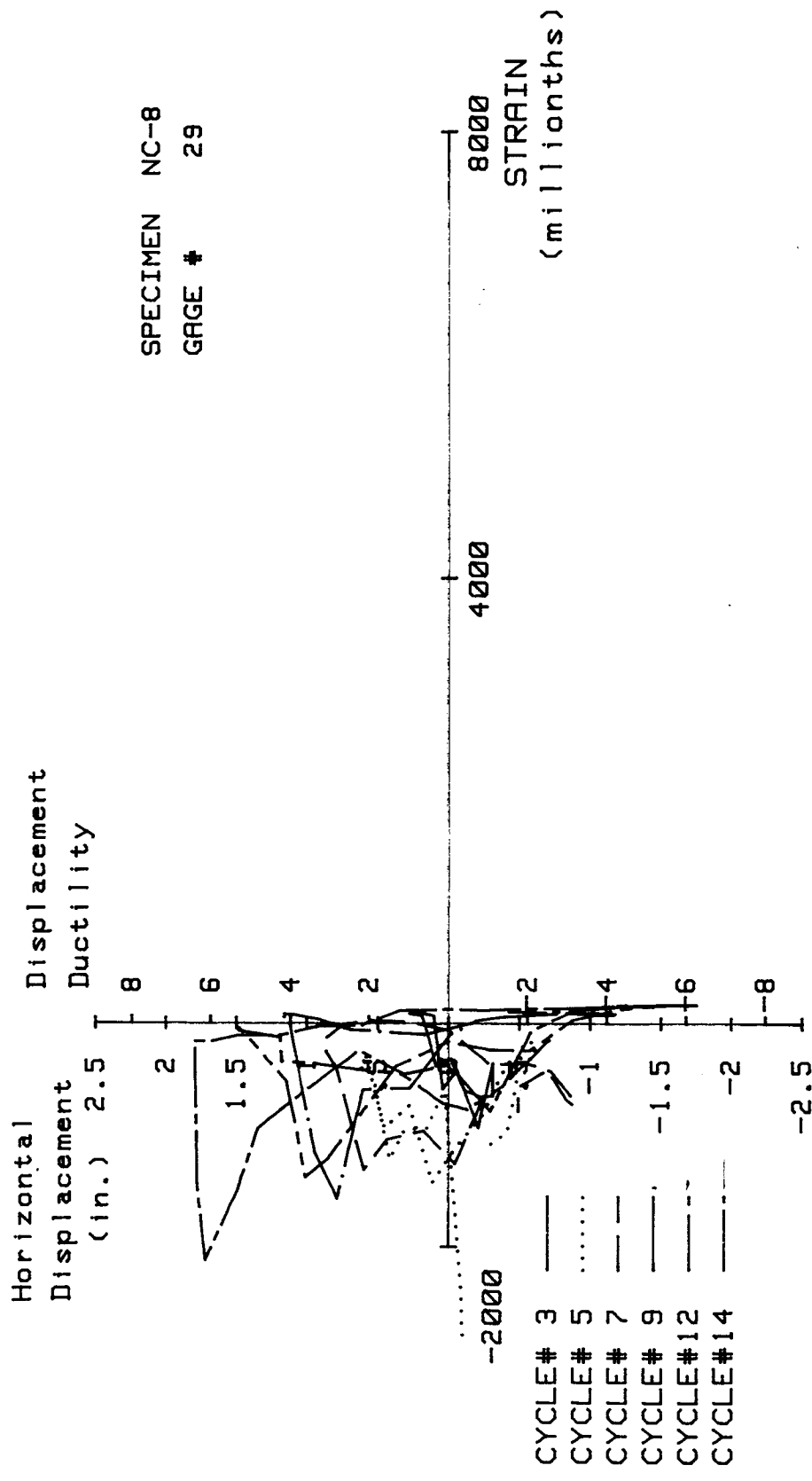


FIG. A-191 MEASURED STRAIN, GAGE #29, SPECIMEN NC-8

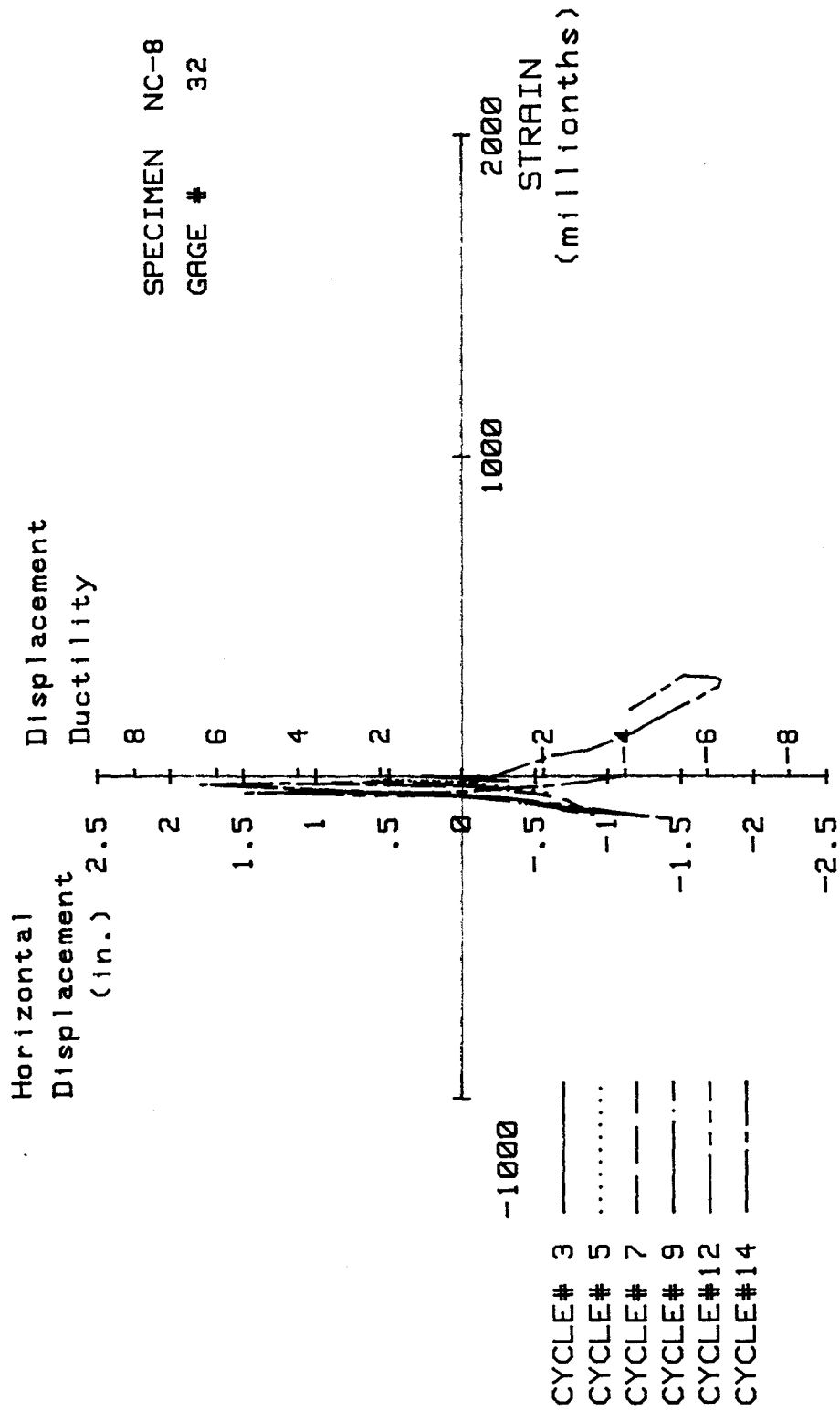


FIG. A-192 MEASURED STRAIN, GAGE #32, SPECIMEN NC-8

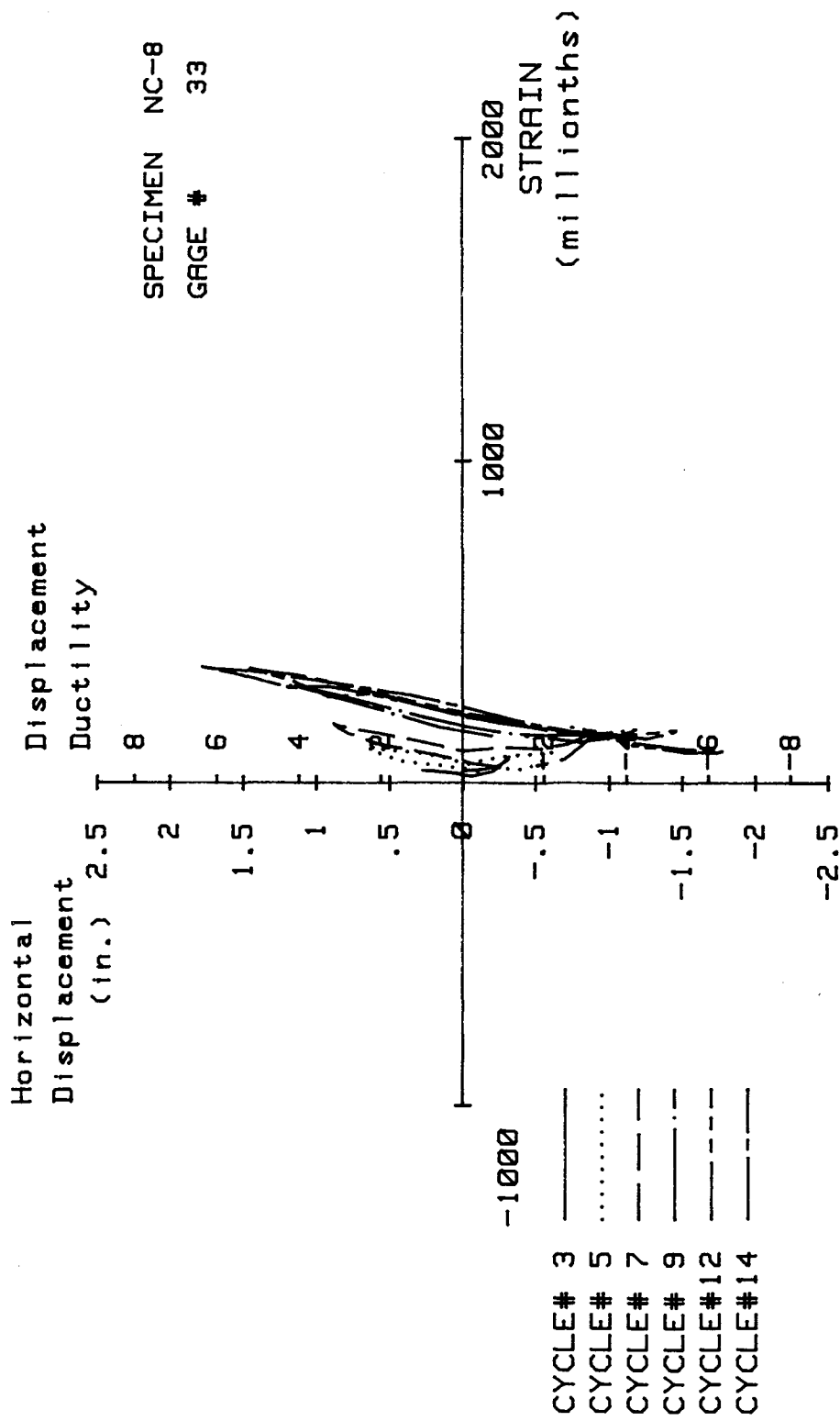


FIG. A-193 MEASURED STRAIN, GAGE #33, SPECIMEN NC-8

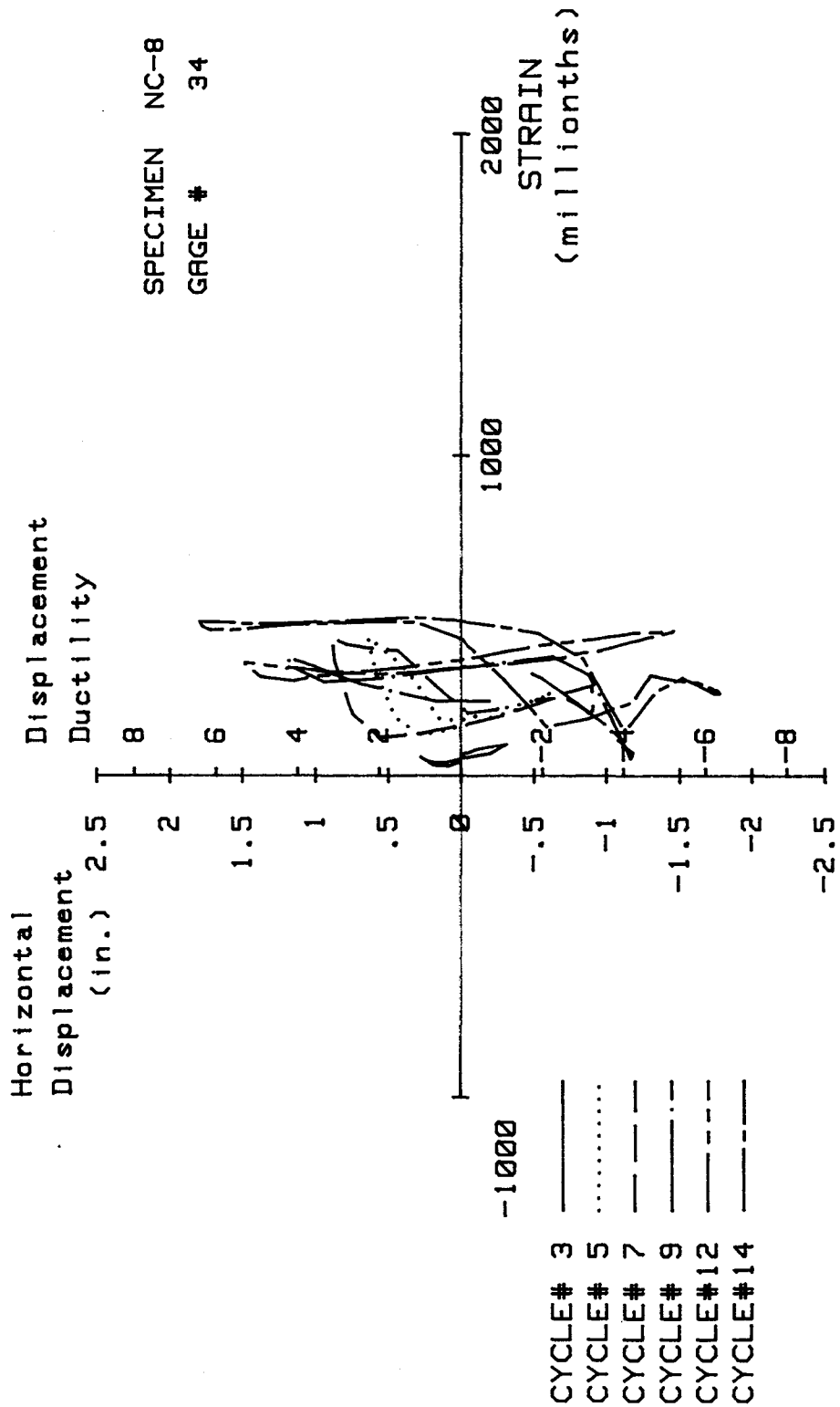


FIG. A-194 MEASURED STRAIN, GAGE #34, SPECIMEN NC-8

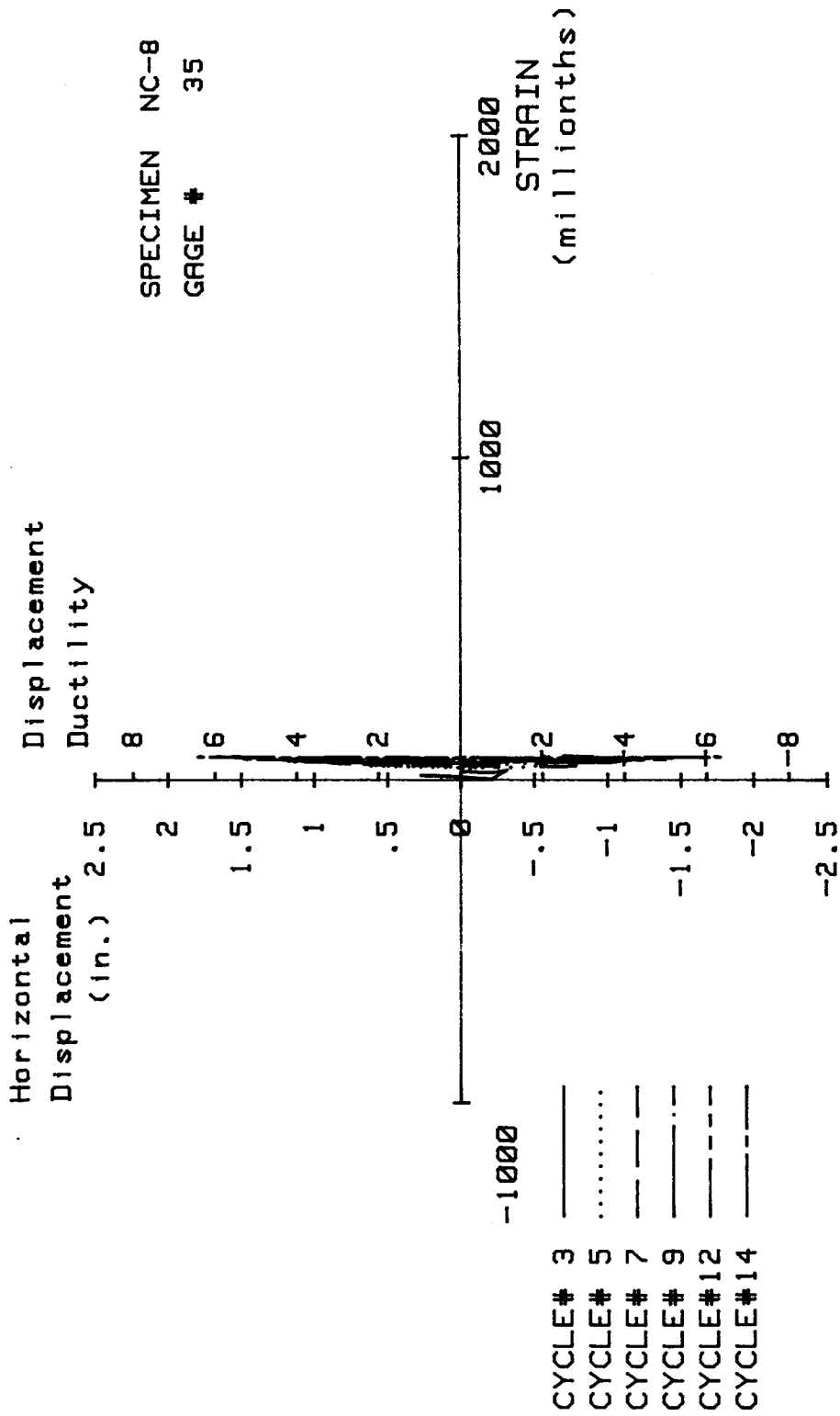


FIG. A-195 MEASURED STRAIN, GAGE #35, SPECIMEN NC-8

Specimen NC-9

Transverse Reinforcement Detail

Transverse reinforcement for Specimen NC-9 consisted of a No. 4 continuous square helix at a 4-in. pitch.

The entire transverse reinforcement for the critical region (the first 22 in. above the stub) was first constructed in one piece and dropped from the top of the cage. Next, the layers of the square helix were adjusted by placing spacers to achieve 4-in. spacing. Finally, it was tied to the longitudinal bars and the spacers were removed.

The area of the transverse reinforcement, A_{sh} , and the reinforcement ratio, ρ , were 0.4 in.^2 and 1.29%, respectively. The area of the transverse reinforcement provided was 63% of the area required by ACI-318-83 Code.

Load History

The applied axial load was 530 kips, corresponding to 30% of the column's axial load capacity. While maintaining the axial load constant the specimen was subjected to 13 cycles of horizontal loading.

Figure A-196 shows the history of the applied horizontal loading. During cycle #2 the first yield displacement and yield curvature were calculated to be 0.28 in. and $354 \times 10^{-6} \text{ in.}^{-1}$, respectively. Subsequently, horizontal loading consisted of one or two cycles each to a maximum displacement ductility ratio of five. Completing cycles 12 ($\mu=5$) and 13 ($\mu=5$), the horizontal displacement was increased to achieve a displacement ductility ratio of six. However, the specimen failed before completing the first cycle at this displacement level.

Test Observations

The first hairline cracks were observed during cycle #2. Cracks formed primarily within 6 in. above the stub. Figure A-197 shows the specimen at the end of cycle #7 ($\mu=2$), at which point some crushing of the cover concrete at the stub-upper column interface was observed. Cracking extended to within 30 in. above the stub. At the end of cycle #9 ($\mu=3$), spalling of the cover concrete had extended to 18 in. above the stub as shown in Fig. A-198. Some of the corner bars were slightly visible.

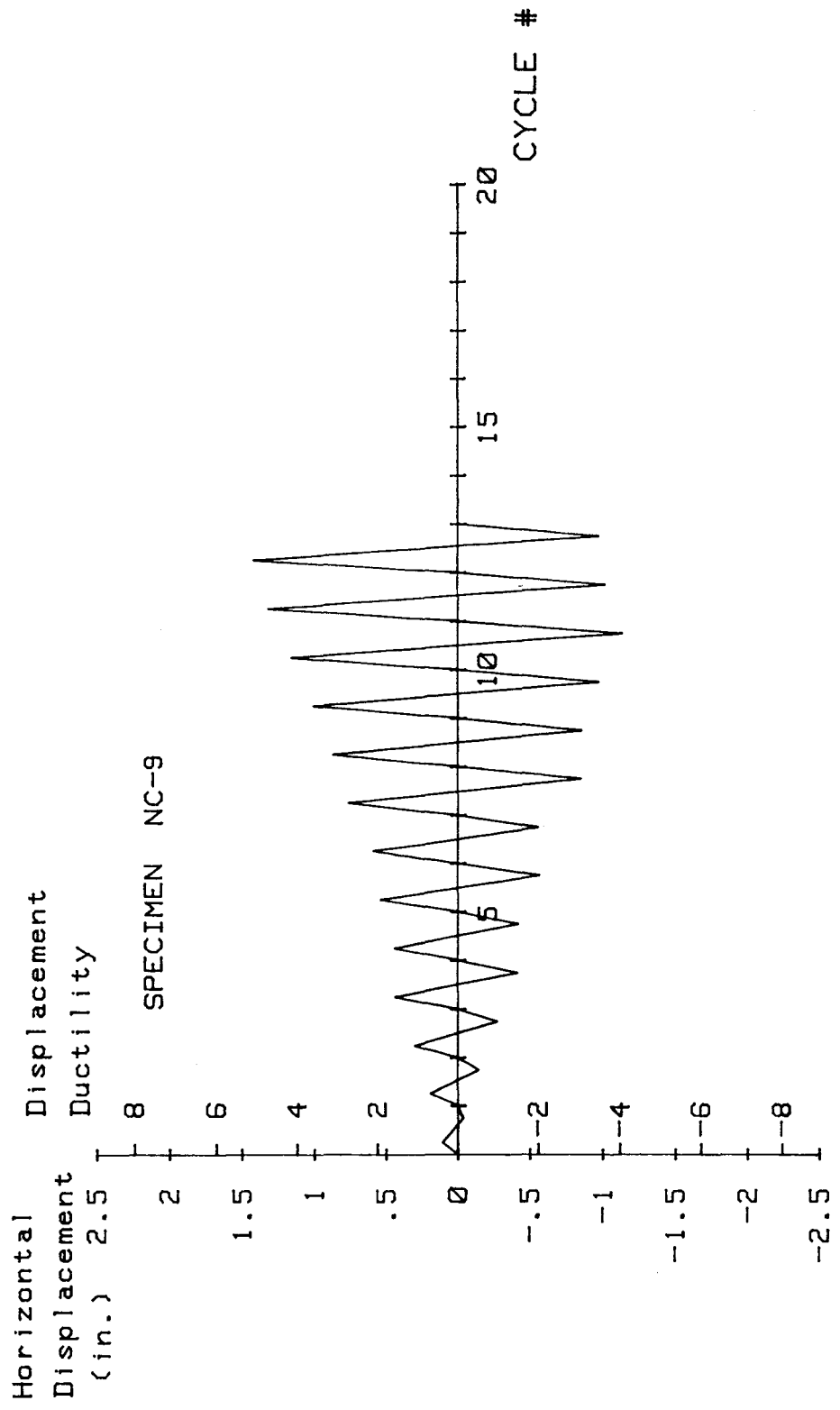


FIG. A-196 LOADING SCHEDULE, SPECIMEN NC-9

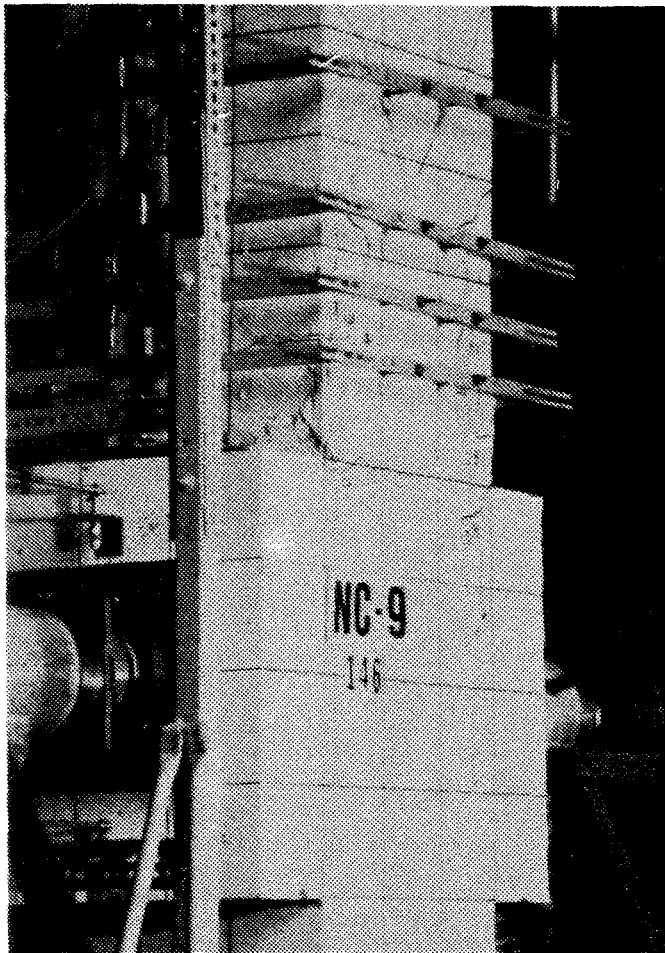


FIG. A-197 TEST SPECIMEN NC-9 AFTER CYCLE #7

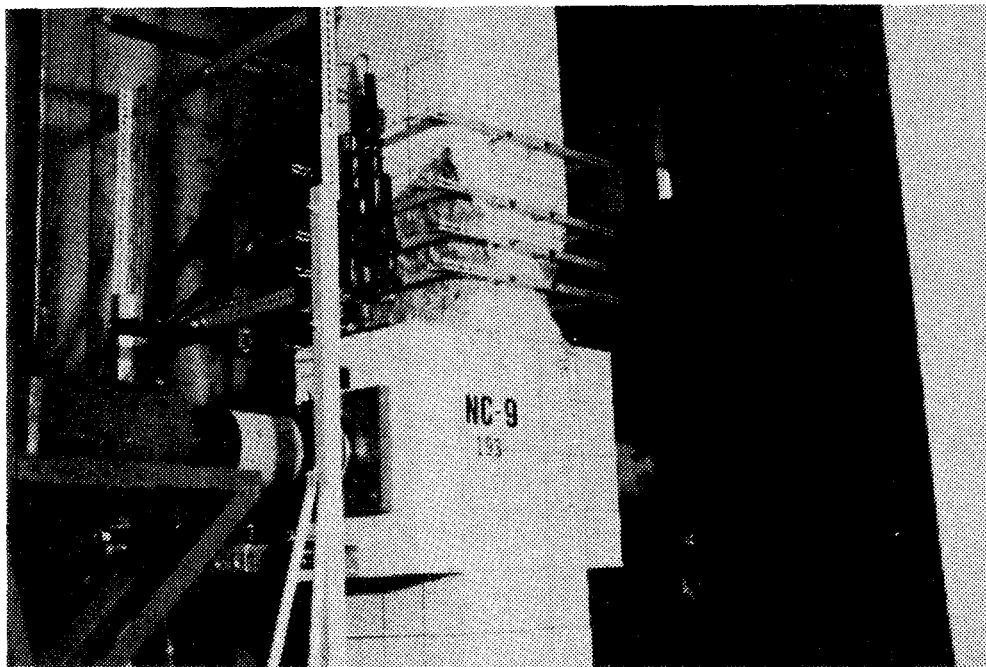


FIG. A-198 TEST SPECIMEN NC-9 AFTER CYCLE #9

The extent of cover concrete spalling did not increase with application of two more cycles at a displacement ductility ratio of four; however, the active portion of the plastic hinge was now more distinct and located approximately 8 in. above the stub. No visible damage was inflicted to either the longitudinal or transverse reinforcement. Figure A-199 shows the specimen at the end of cycle #11 ($\mu=4$).

During cycle #12 ($\mu=5$), initiation of buckling of the middle bars on the east and west faces of the specimen was observed. The maximum lateral bending of the middle bars was observed at approximately 8 in. above the stub. Figure A-200 shows the specimen at the end of cycle #13 ($\mu=5$). Spalling of the cover concrete had extended to 24 in. above the stub. The specimen failed by sudden buckling of the middle longitudinal bars before completion of the first cycle at a displacement ductility ratio of six. The layer of transverse reinforcement parallel to the east and west faces of the column and located approximately 10 in. above the stub elongated significantly due to buckling of the middle bars; however, no fracture or cracking of the transverse reinforcement were observed. Figure A-201 shows the specimen at test conclusion.

Load Deflection and Moment-Curvature Characteristics

Figure A-202 shows the horizontal load displacement behavior of the specimen. Maximum applied horizontal load was 215 kips, during the forward loading of the first cycle at displacement ductility ratio of two.

Figure A-203 shows curvature distribution along the upper column. Maximum curvature ductilities at displacement ductility ratios of 3 and 5 were approximately 6 and 21, respectively.

Figure A-204 shows the moment curvature behavior of the column cross-section at the upper column-stub level. Using the procedures outlined in Section 4.8.2, the ultimate moment capacity was calculated to be 4810 in-kips, while the maximum applied moment was 5591 in-kips. The maximum applied moments during displacement ductility ratios of 3, 4, and 5 were 5309, 4926, and 4509 in-kips respectively.

The maximum degradation in moment capacity during cycle #13 ($\mu=5$) was 21% of the theoretical moment capacity. The ratio of the peak moment at the second cycle to the peak moment at the first cycle ranged from 0.86 to 0.96 at various displacement levels.

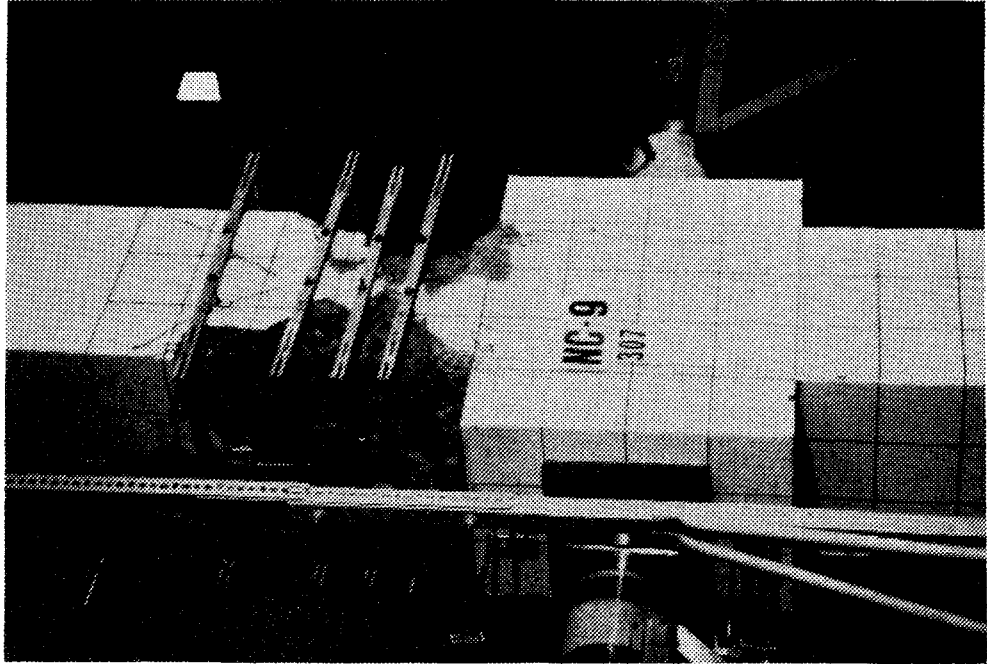


FIG. A-200 TEST SPECIMEN NC-9 AFTER CYCLE #13

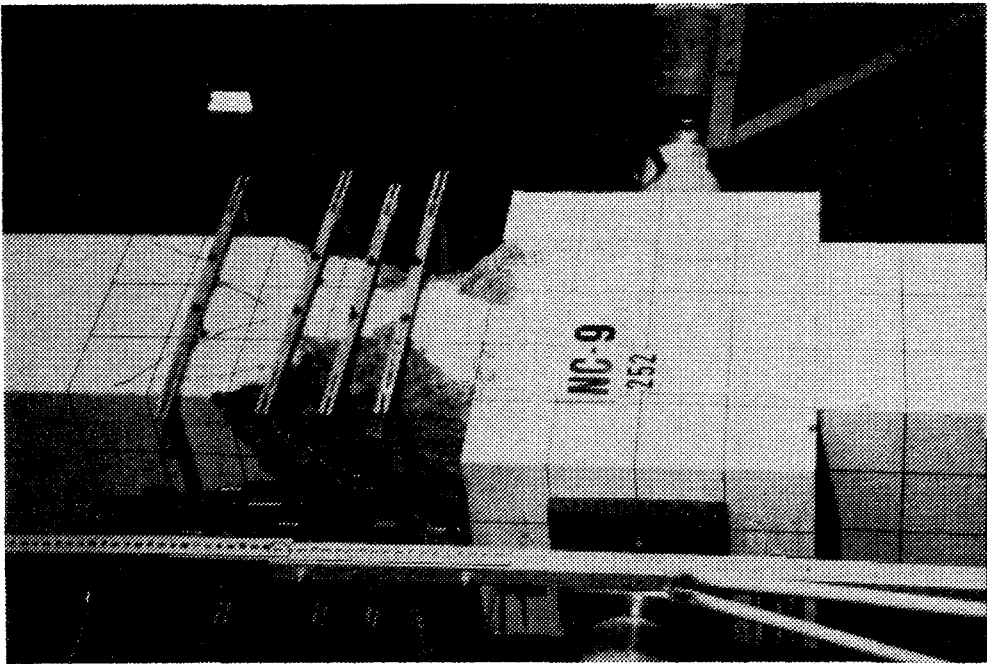


FIG. A-199 TEST SPECIMEN NC-9 AFTER CYCLE #11

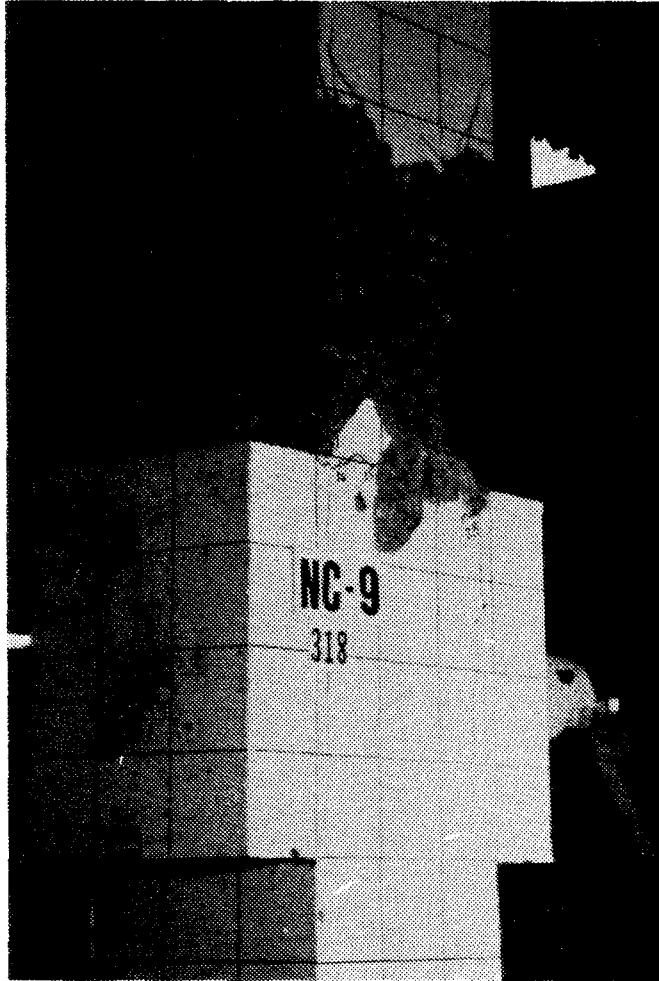
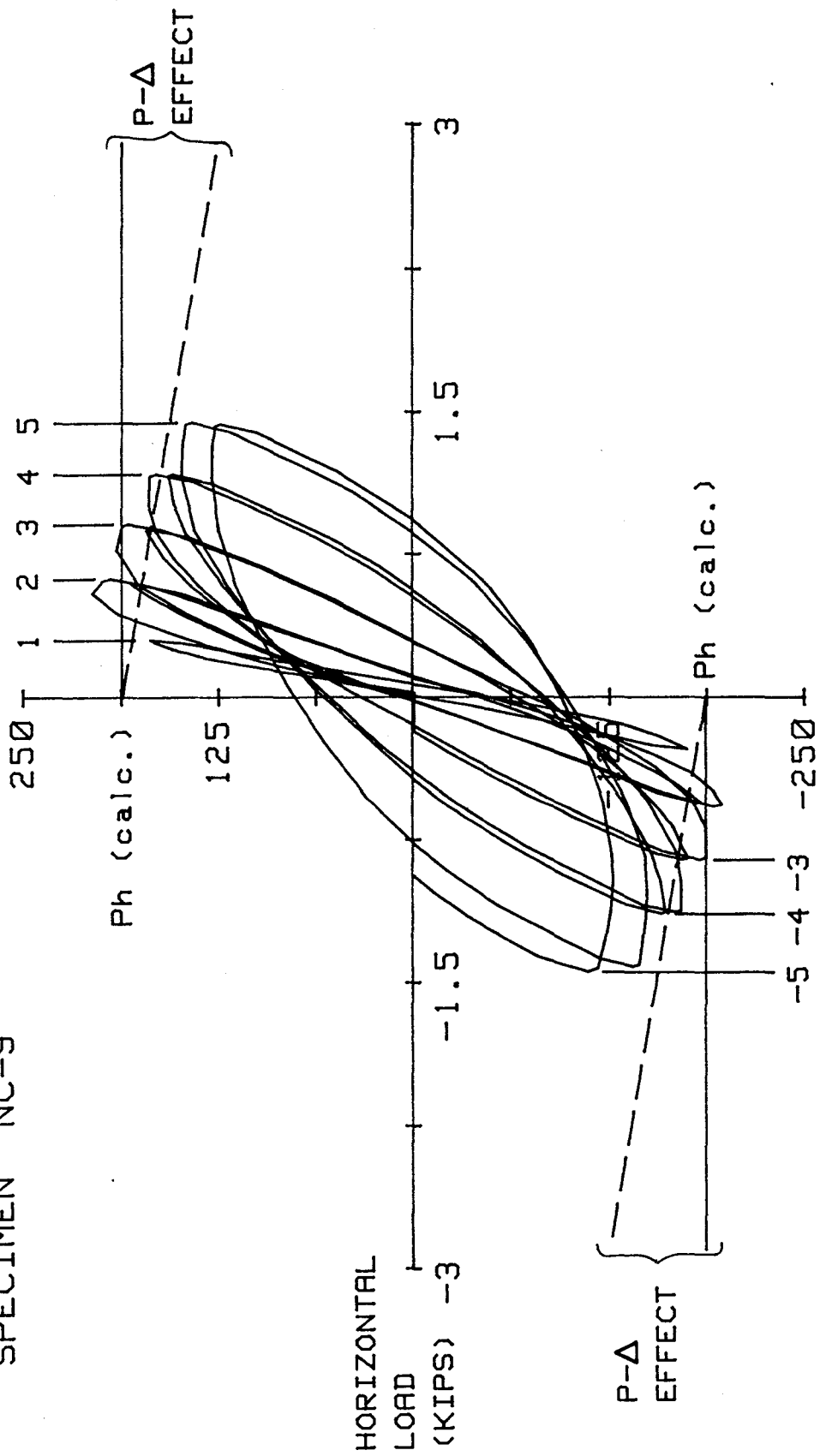


FIG. A-201 TEST SPECIMEN NC-9 AFTER TEST CONCLUSION

DISPLACEMENT DUCTILITY

SPECIMEN NC-9



Metric Equivalents
1 in. = 25.4 mm
1 kip = 4.45 KN

HORIZONTAL DISPLACEMENT (IN.)

FIG. A-202 HORIZONTAL LOAD VERSUS DISPLACEMENT, SPECIMEN NC-9

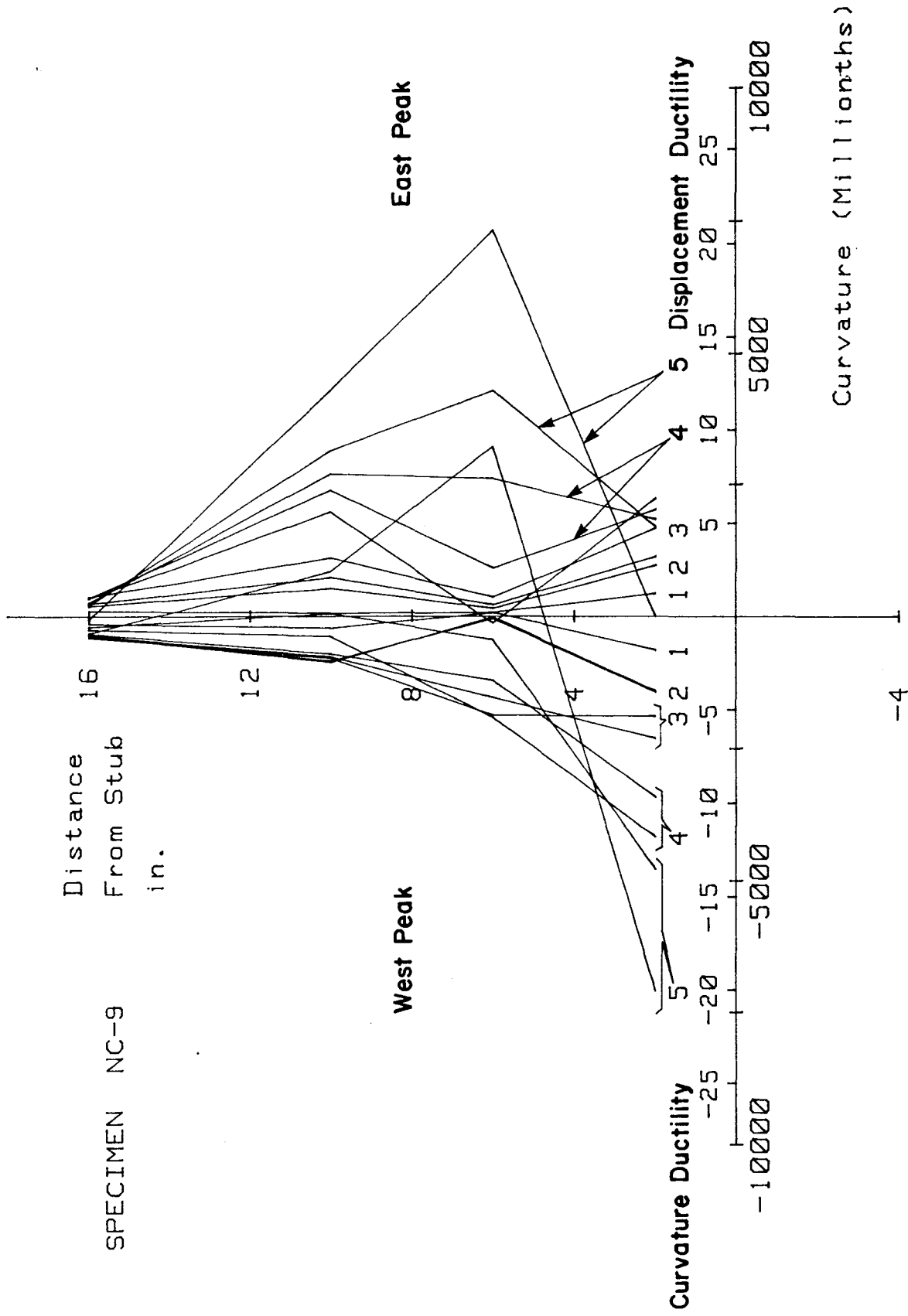


FIG. A-203 CURVATURE DISTRIBUTION ALONG UPPER COLUMN SPECIMEN NC-9

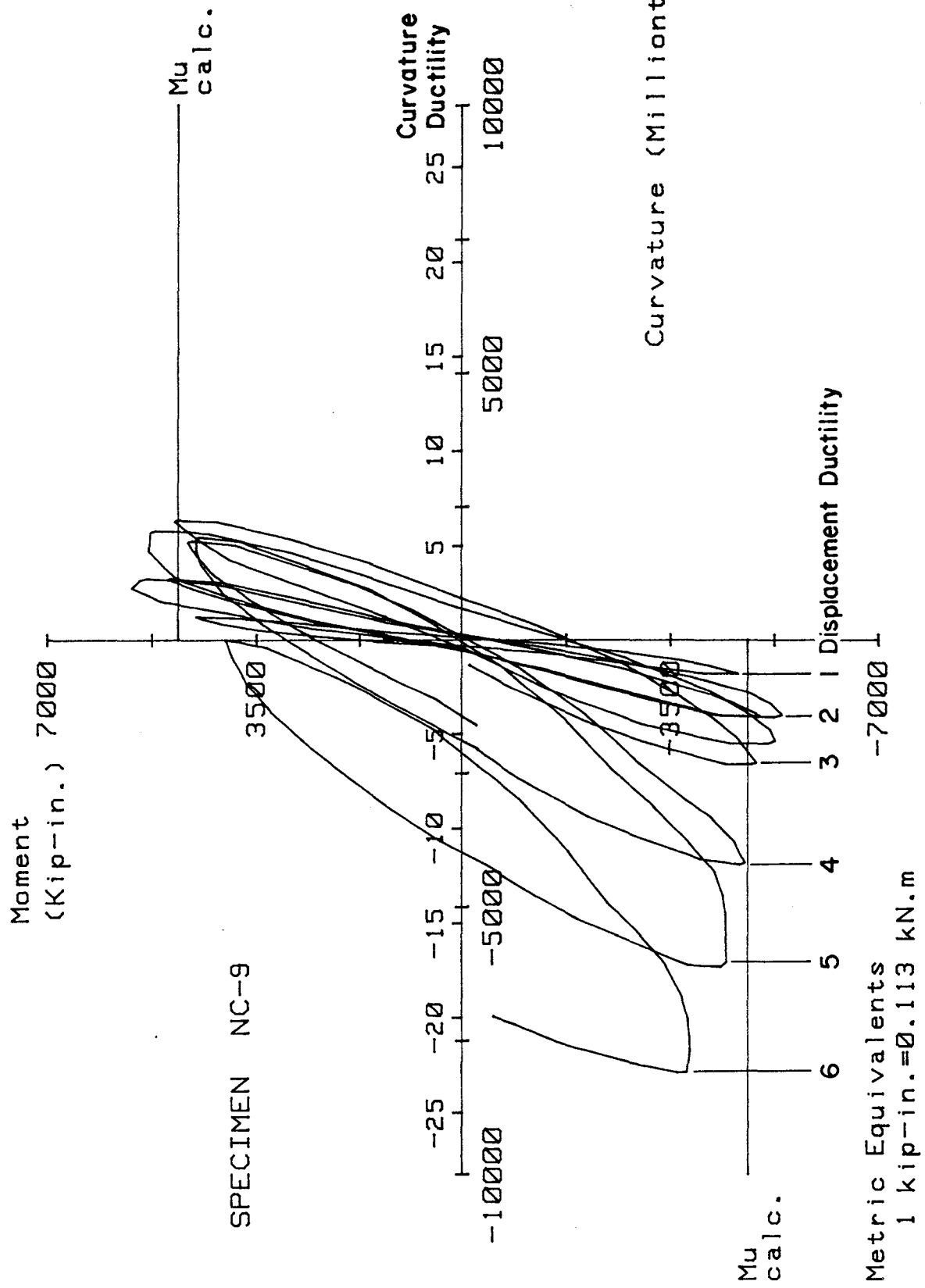


FIG. A-204 MOMENT VERSUS CURVATURE FOR SPECIMEN NC-9

Transverse Reinforcement Strain

A total of 12 strain gages were attached to the #4 continuous helix transverse reinforcement. Strain gages #13 through #18 and #19 through #24 were attached to transverse reinforcement at approximately 2, 6, 10, 14, 18, and 22 in. above the stub, respectively. Figures A-205 through A-215 show the results obtained from these gages. During cycle #6 ($\mu=2$), a sudden increase in strains at all levels was observed. This increase is more pronounced at strain gages located more than 10 in. from the stub. The maximum strain through cycle #8 ($\mu=3$) was 78% of the specified minimum yield strain of the transverse reinforcement material.

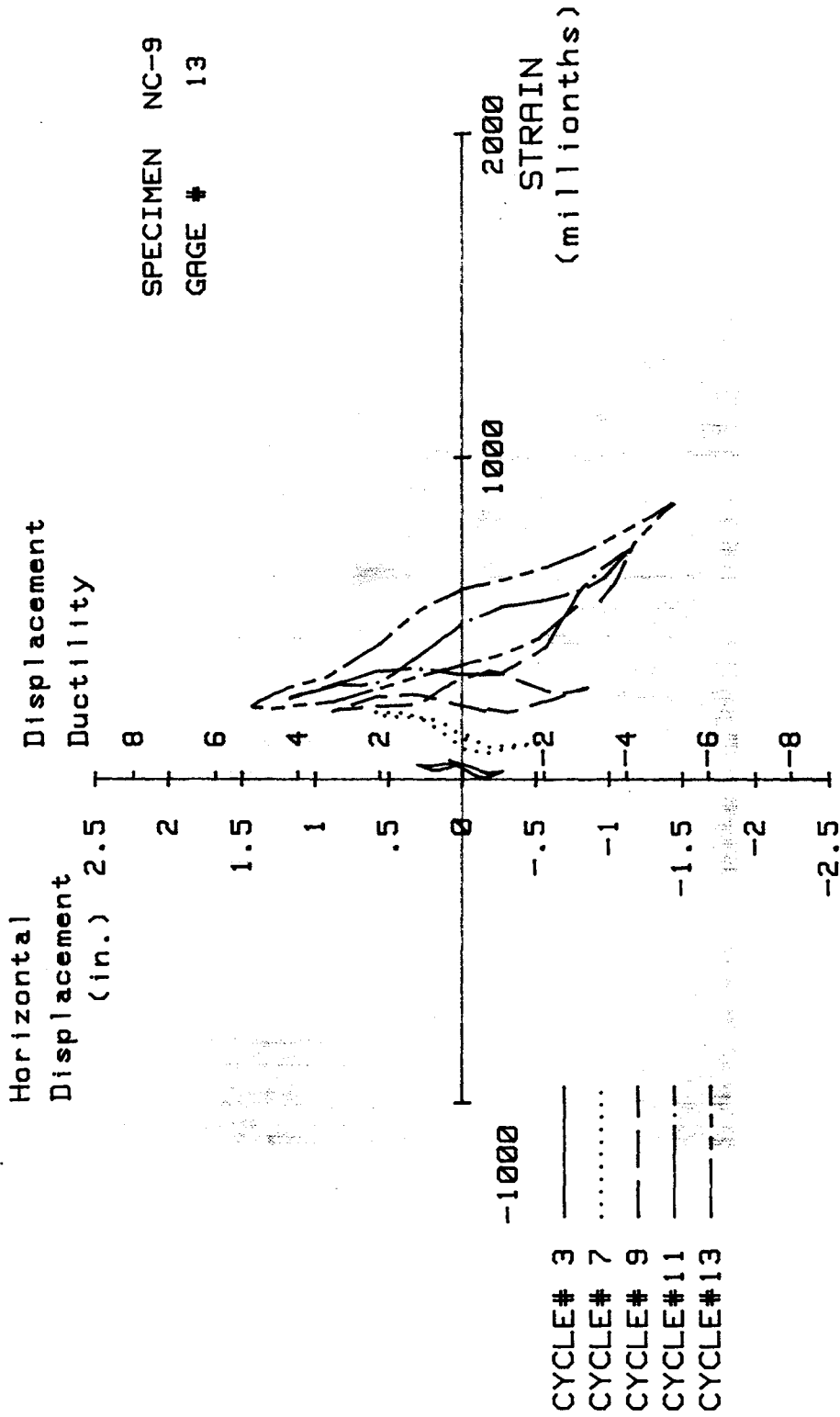


FIG. A-205 MEASURED STRAIN, GAGE #13, SPECIMEN NC-9

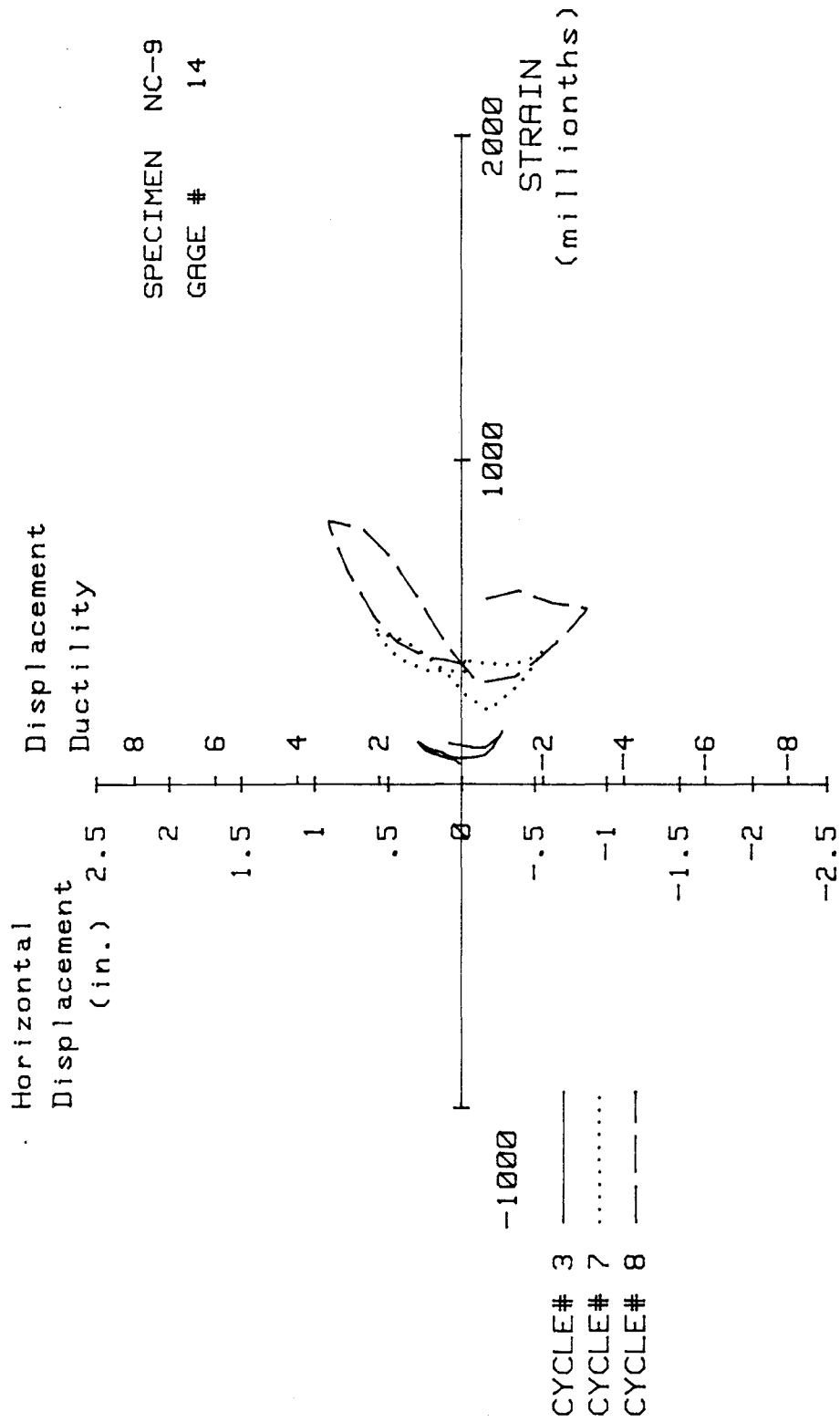


FIG. A-206 MEASURED STRAIN, GAGE #14, SPECIMEN NC-9

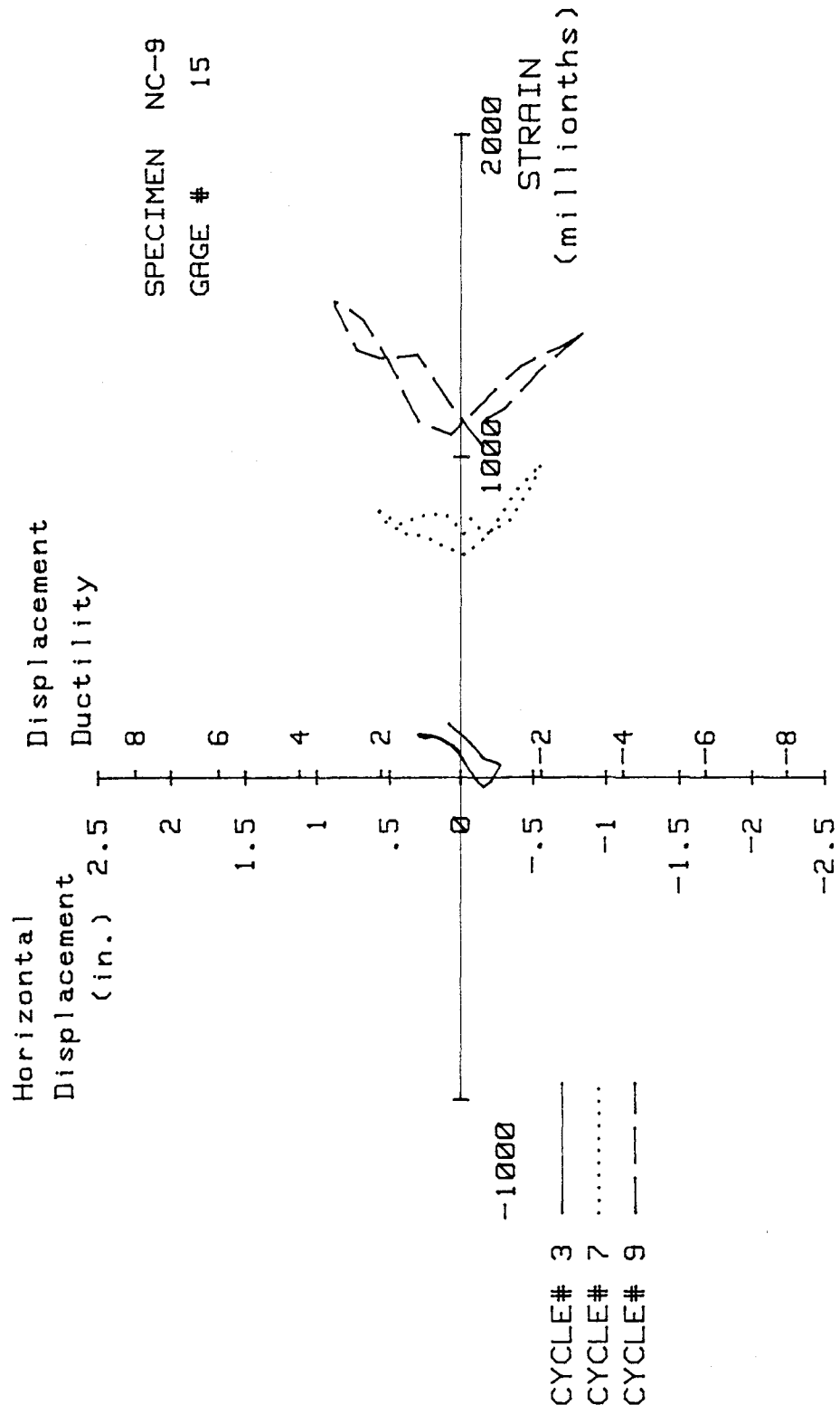


FIG. A-207 MEASURED STRAIN, GAGE #15, SPECIMEN NC-9

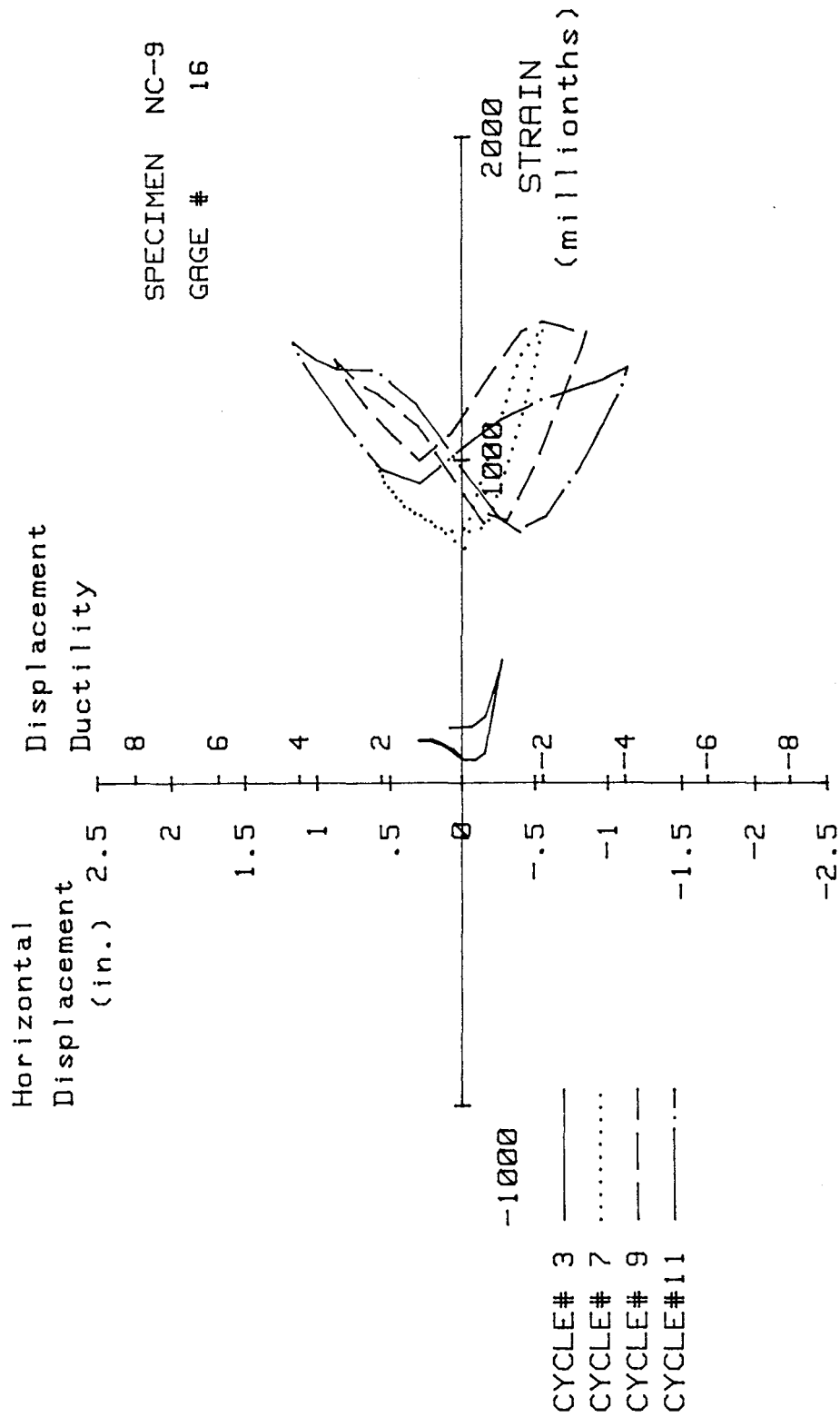


FIG. A-208 MEASURED STRAIN, GAGE #16, SPECIMEN NC-9

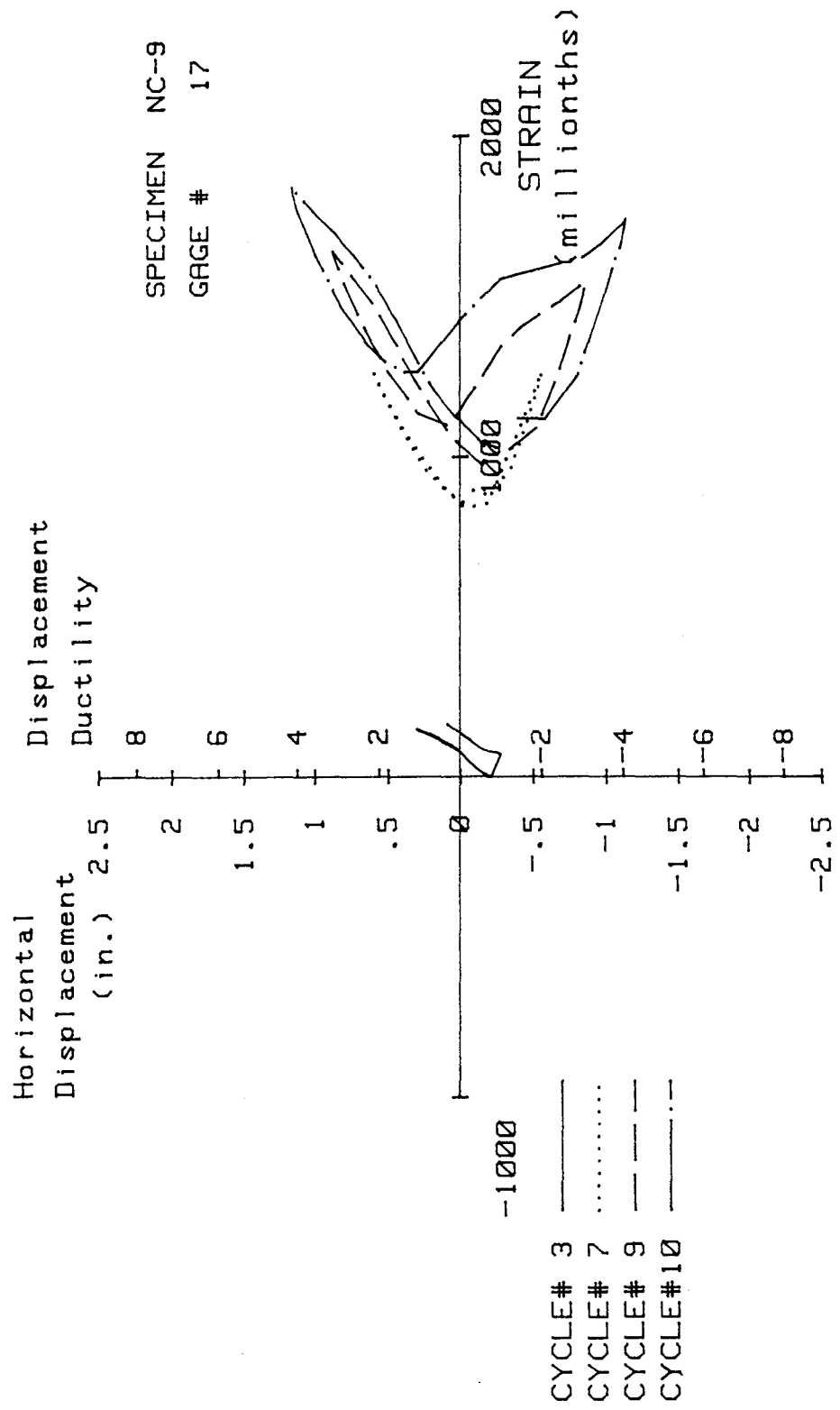


FIG. A-209 MEASURED STRAIN, GAGE #17, SPECIMEN NC-9

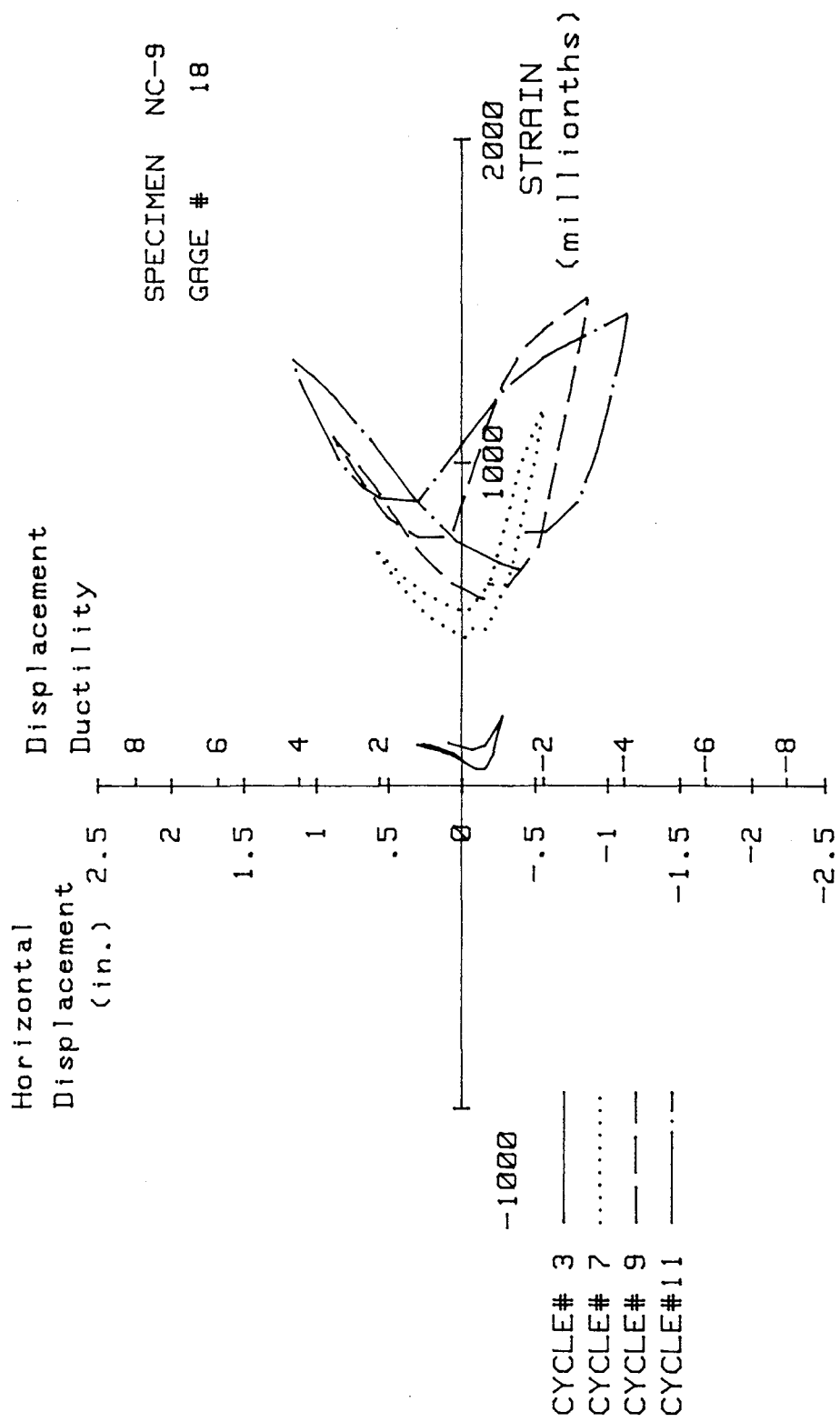


FIG. A-210 MEASURED STRAIN, GAGE #18, SPECIMEN NC-9

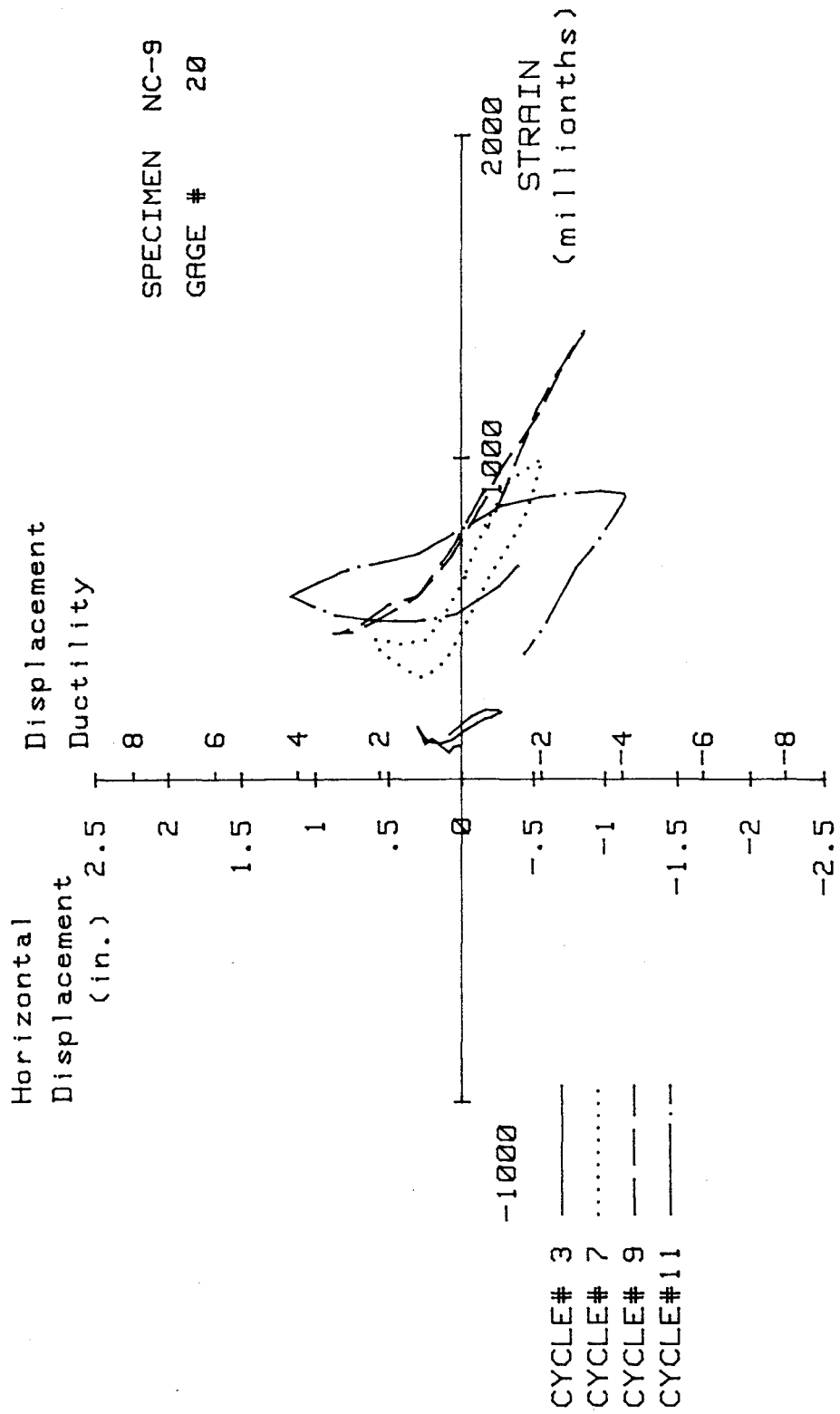


FIG. A-211 MEASURED STRAIN, GAGE #20, SPECIMEN NC-9

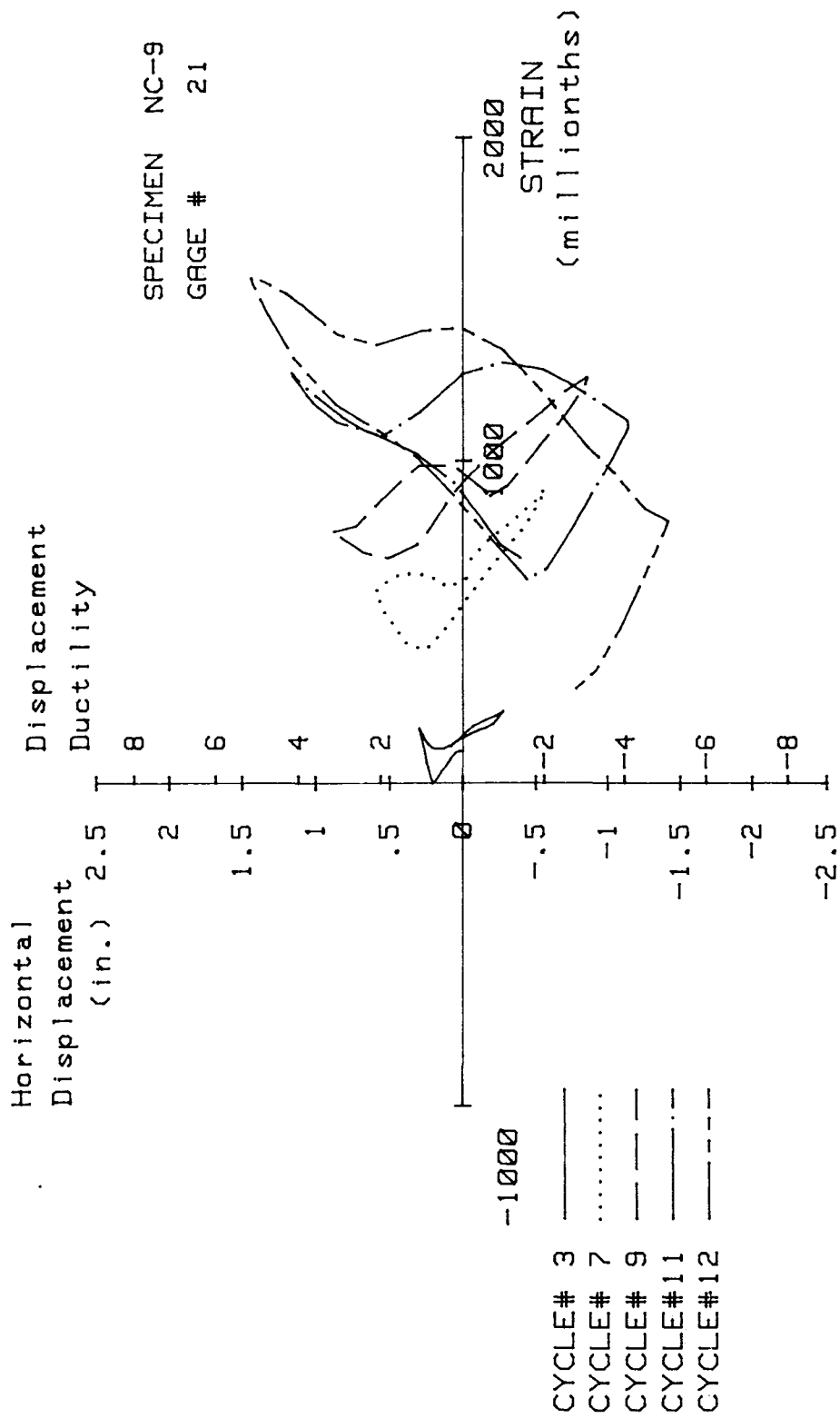


FIG. A-212 MEASURED STRAIN, GAGE #21, SPECIMEN NC-9

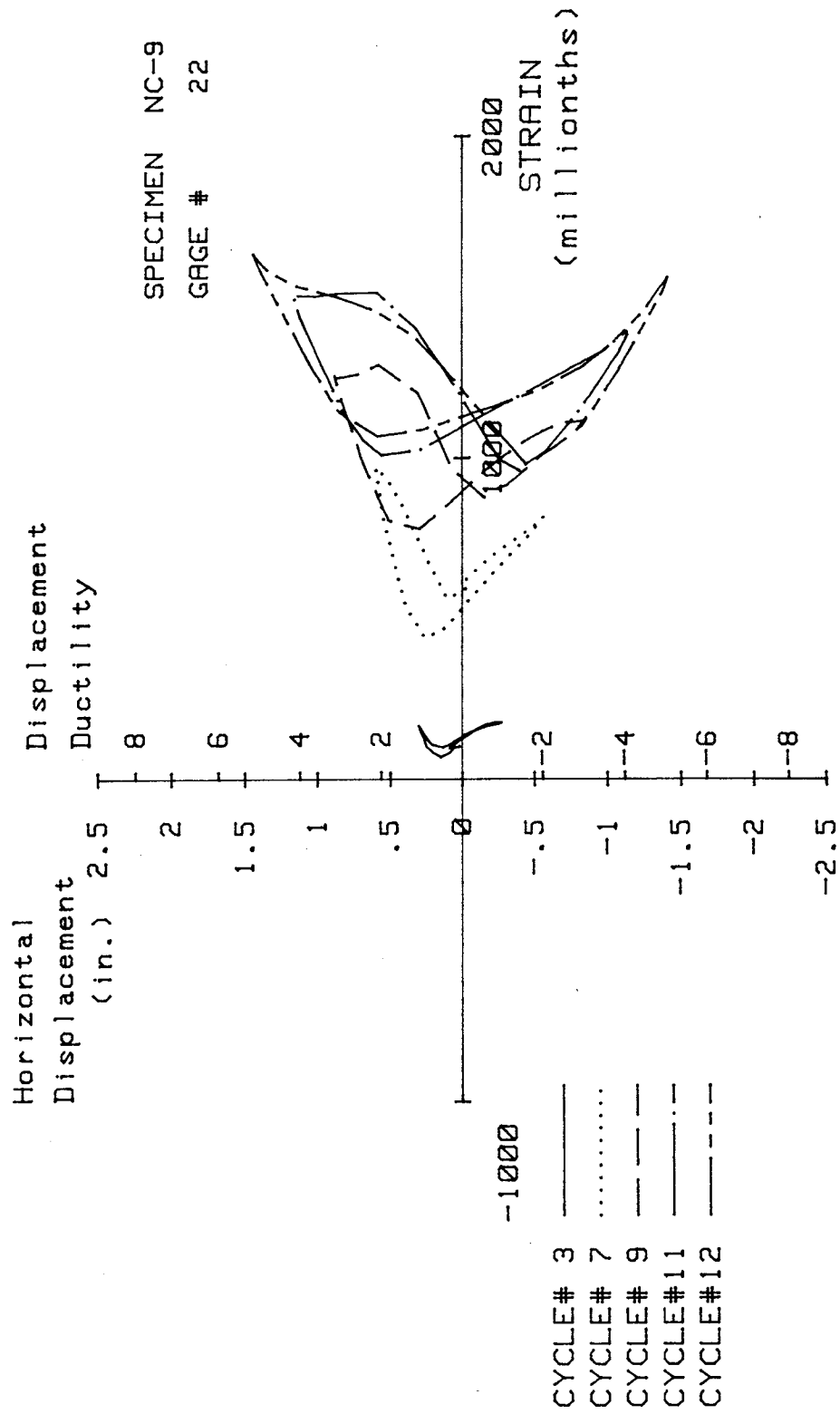


FIG. A-213 MEASURED STRAIN, GAGE #22, SPECIMEN NC-9

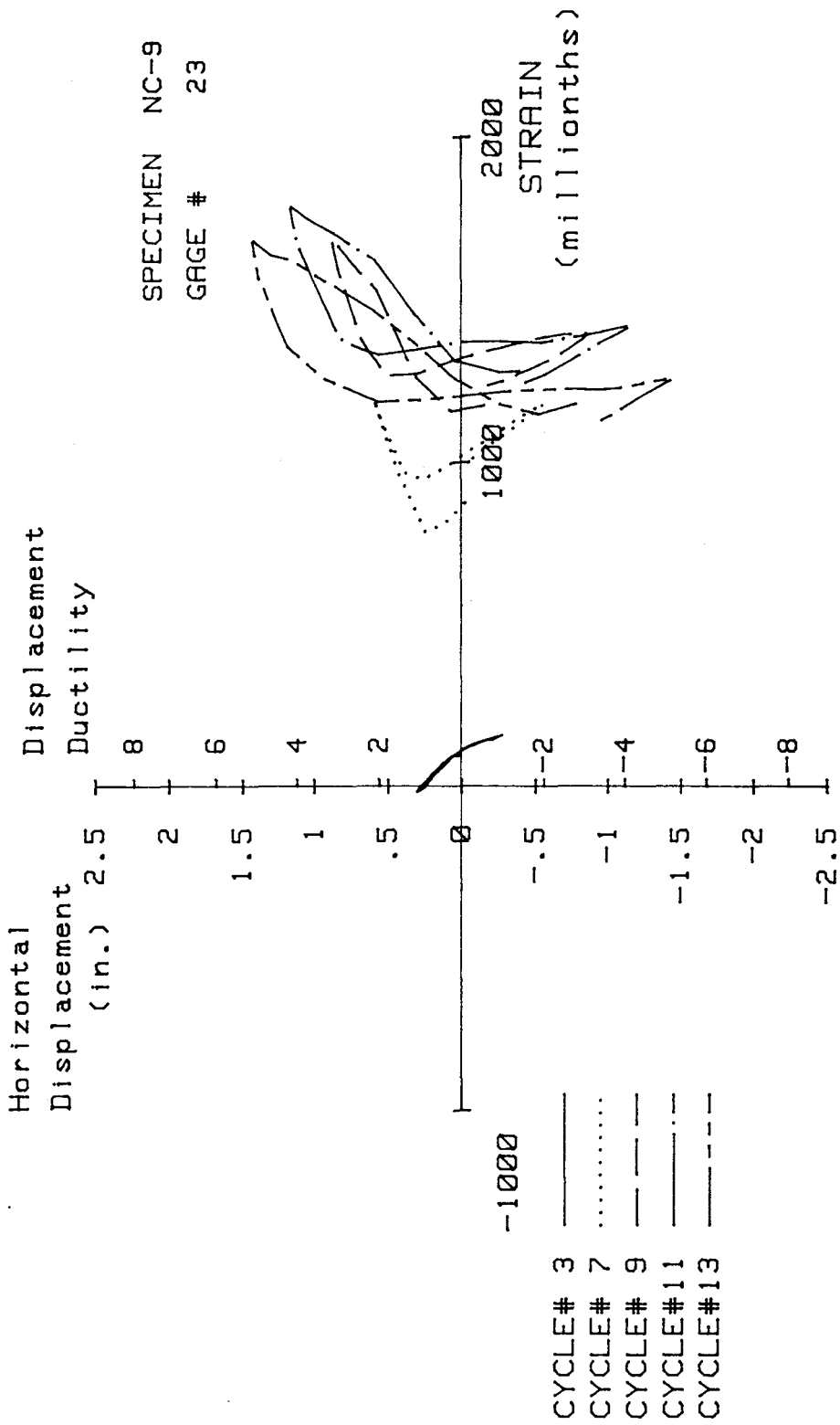


FIG. A-214 MEASURED STRAIN, GAGE #23, SPECIMEN NC-9

Specimen NC-10

Transverse Reinforcement Detail

Transverse reinforcement detail, within 22 in. above the stub, consisted of a #3 continuous square helix at a 2-1/4-in. pitch. The area of transverse reinforcement and the reinforcement ratio were .22 in.² and 1.29%, respectively. The area of the transverse reinforcement provided was 52% of the area required by ACI-318-83 Code.

Load History

Testing began with the application of an axial load of 550 kips, corresponding to 30% of the column's axial load capacity. Maintaining the axial load constant, a total of 13 complete cycles of horizontal loading were then applied. The first two cycles were load-controlled while the remaining cycles were displacement-controlled. During cycle #2, the first yield displacement and the yield curvature were calculated to be 0.28 in. and 395×10^{-6} in.⁻¹, respectively. Subsequently, loading was displacement-controlled and consisted of one or two cycles of cyclic horizontal loading to a maximum displacement ductility ratio of six. After subjecting the specimen to two cycles at the displacement ductility ratio of five, one complete cycle at the displacement ductility ratio of six was applied. However, the specimen failed prior to completion of the second cycle at the same displacement level. Figure A-216 shows the history of applied cyclic horizontal loading.

Test Observations

The first hairline cracks were observed during cycle #2 when cracks formed at the interface of the stub-upper column and approximately 6 in. above the stub. Some crushing of cover concrete was observed during cycle #5 ($\mu=2$). Limited spalling of the cover concrete at the corners extending to 6 in. above the stub was observed at the end of cycle #6 ($\mu=2$).

Figure A-217 shows the specimen at the end of cycle #8 ($\mu=3$). Cracking extended to 36 in. above the stub. Partial spalling of the cover concrete at the column corners extended to 10 in. above the stub. Figure A-218 shows the specimen at the end of cycle #10 ($\mu=4$). The active region of the plastic hinge was located approximately 9 in. above the stub. During

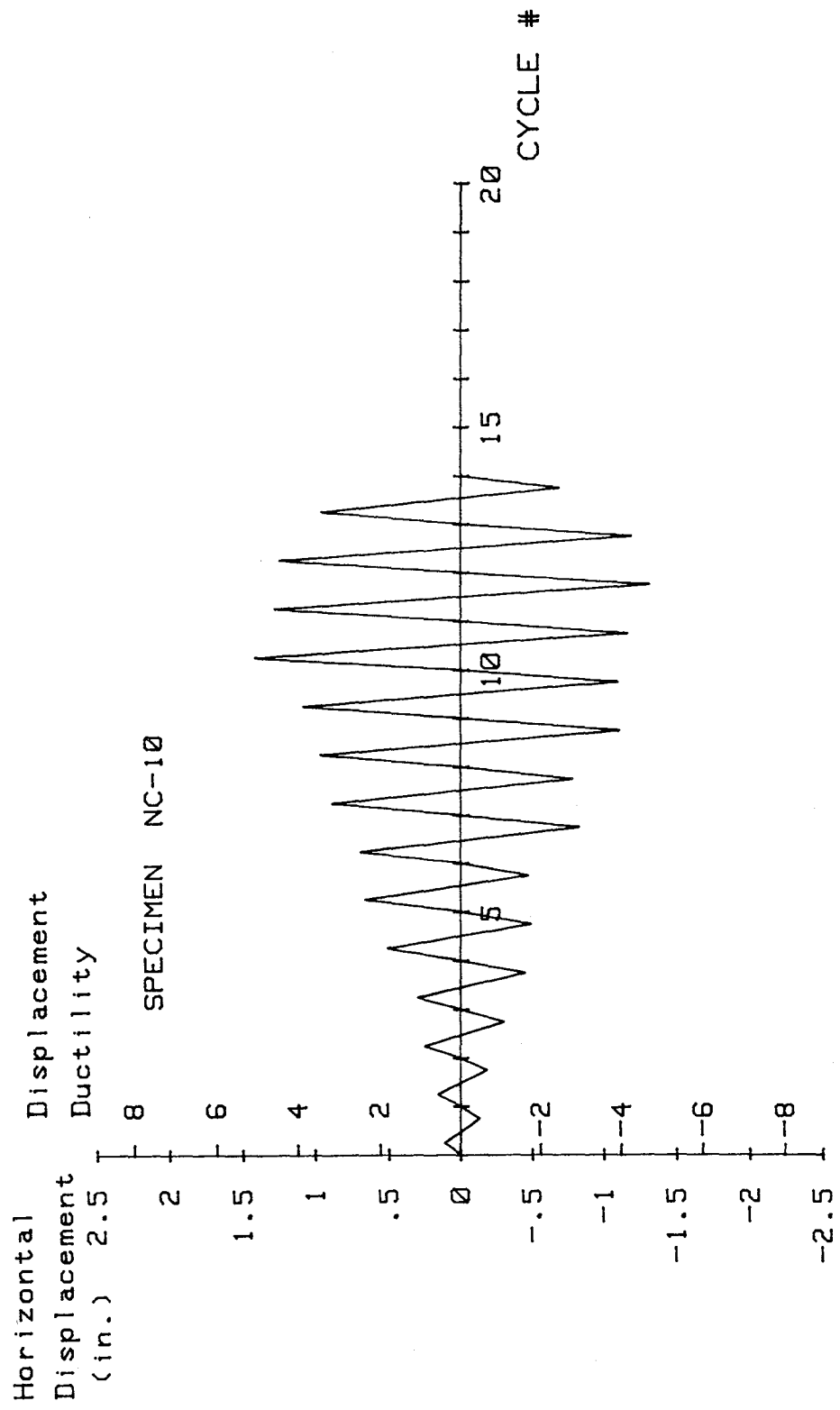


FIG. A-216 LOADING SCHEDULE, SPECIMEN NC-10

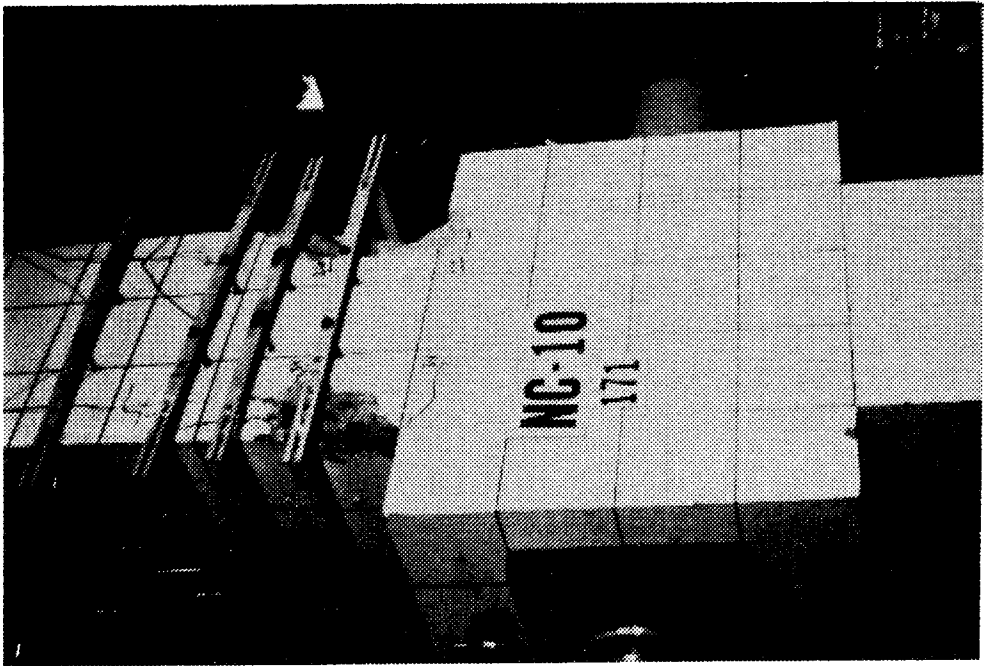


FIG. A-217 TEST SPECIMEN NC-10 AFTER CYCLE #8

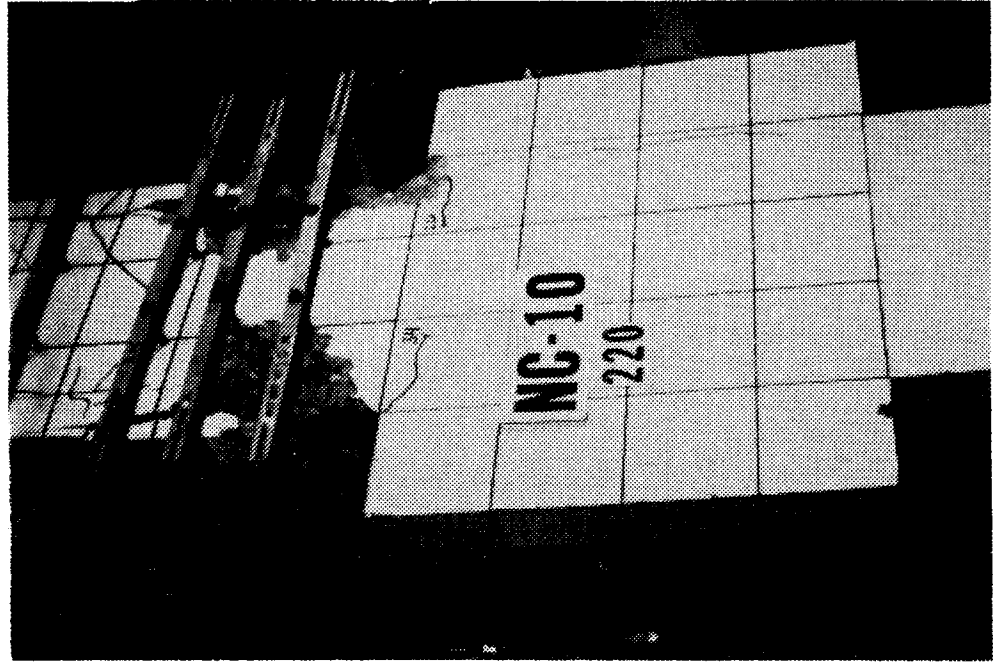


FIG. A-218 TEST SPECIMEN NC-10 AFTER CYCLE #10

cycle #12 ($\mu=5$) some lateral bending of the middle longitudinal bars located on the west face of the column was observed; however, the specimen was subjected to two complete cycles at the displacement ductility ratio of five without significant degradation in load-carrying capacity. Figure A-219 shows the specimen at the end of cycle #12 ($\mu=5$). Subsequently, the specimen was subjected to one complete cycle of horizontal loading at a displacement ductility ratio of six. As seen in Fig. A-220, spalling of cover concrete extended beyond 30 in. above the stub. The specimen failed by buckling of all four middle bars before completing the reverse loading of the second cycle at this displacement level ($\mu=6$). The maximum lateral bending of the four buckled longitudinal bars was located approximately 11 in. above the stub. Buckling of the middle bars resulted in extensive deformation of a layer of the transverse reinforcement in these locations. However, no visible cracks or fracture of the transverse reinforcement was observed. Figure A-221 shows the specimen at test conclusion. Spalling of cover concrete extended as high as 40 in. above the stub. At test conclusion the transverse reinforcement located within 3 in. above the stub was still covered by concrete to a large extent.

Load Deflection and Moment-Curvature Characteristics

Figure A-222 shows the horizontal load-deflection behavior of the specimen. The maximum applied horizontal loads during forward and reverse loading of cycle #5 ($\mu=2$) were 210 and 188 kips, respectively. Though not shown in Fig. A-222, the maximum horizontal loads applied during the first cycle at the displacement ductility ratio of six (cycle #13) were 145 and 125 kips, respectively.

Figure A-223 shows the distribution of curvature along the upper column. As is evident, during early loading stages there are two regions of relatively high curvature, one extending to 4 in. above the stub and the other extending from 8 to 12 in. above the stub. The maximum curvature ductility ratio during cycle #12 ($\mu=5$) was approximately 17 and was located 8 to 12 in. above the stub.

Figure A-224 shows the moment curvature behavior of the column cross-section just above the stub through cycle #12. The theoretical moment capacity, calculated using the procedures outlined in Section 4.8.2, was

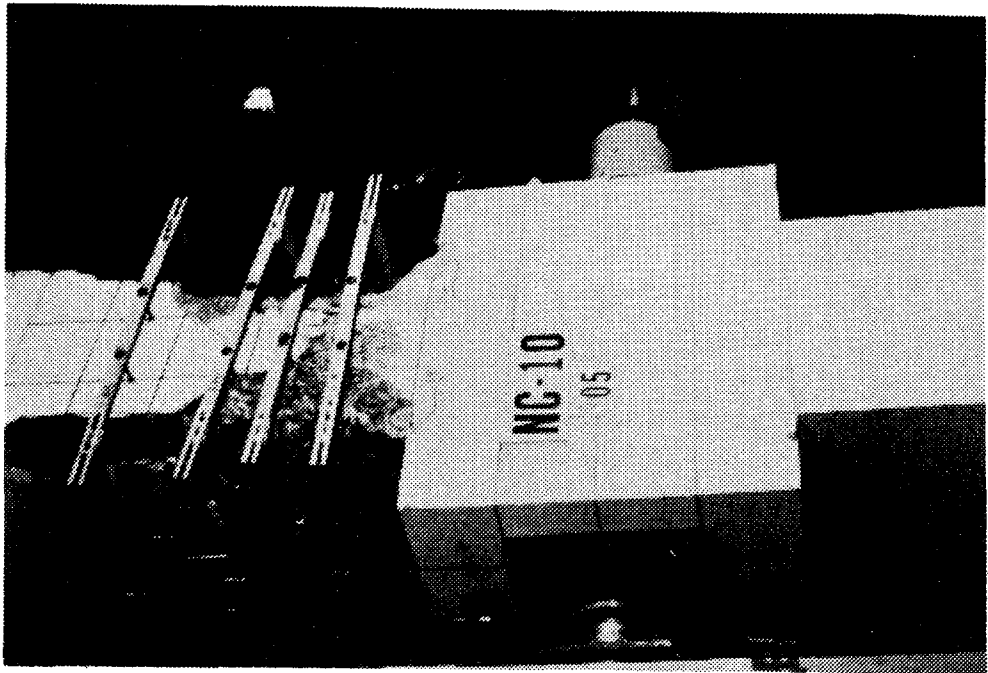


FIG. A-220 TEST SPECIMEN NC-10 AFTER CYCLE #13

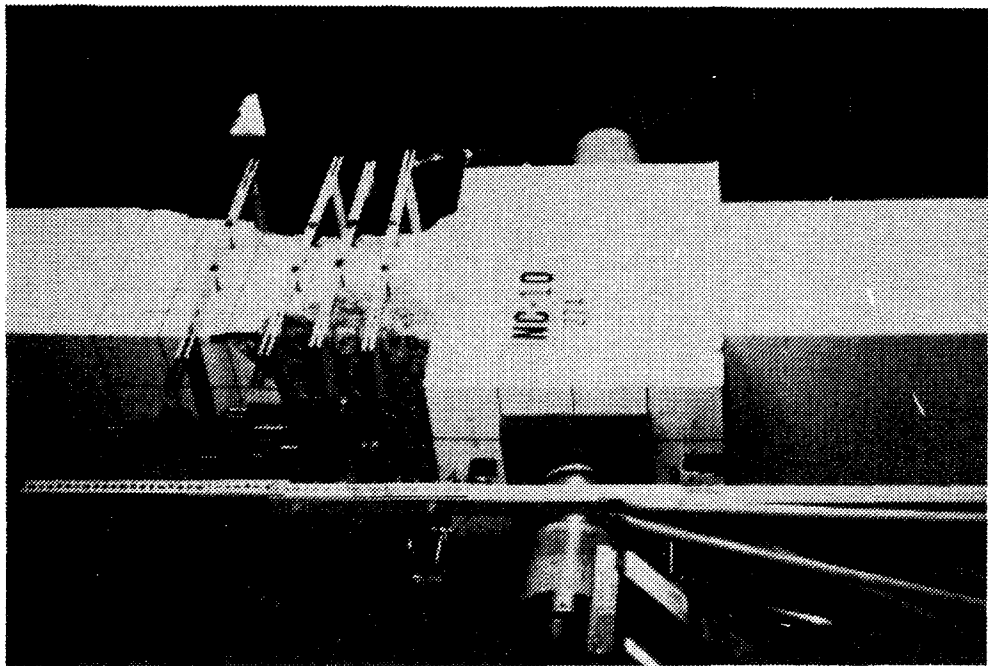


FIG. A-219 TEST SPECIMEN NC-10 AFTER CYCLE #12

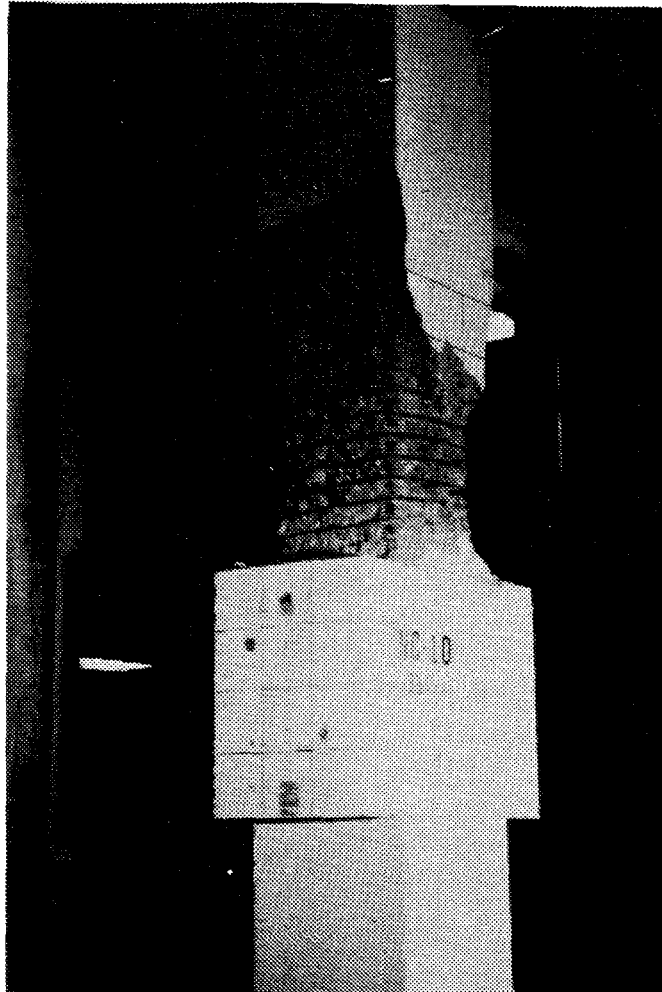
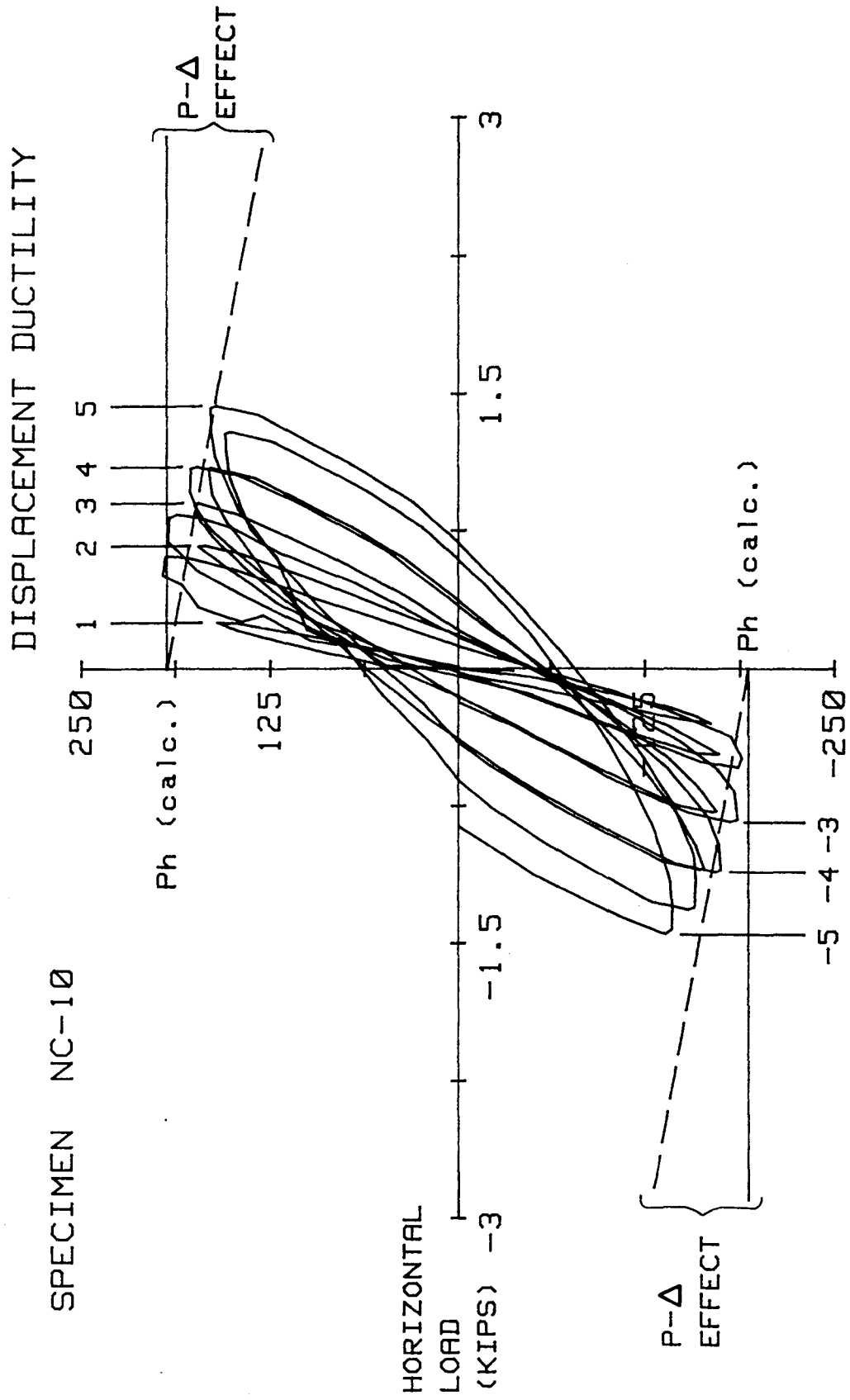


FIG. A-221 TEST SPECIMEN NC-10 AFTER TEST CONCLUSION



Metric Equivalents
 1 in.=25.4 mm
 1 kip=4.45 KN

HORIZONTAL DISPLACEMENT (IN.)

FIG. A-222 HORIZONTAL LOAD VERSUS DISPLACEMENT, SPECIMEN NC-10

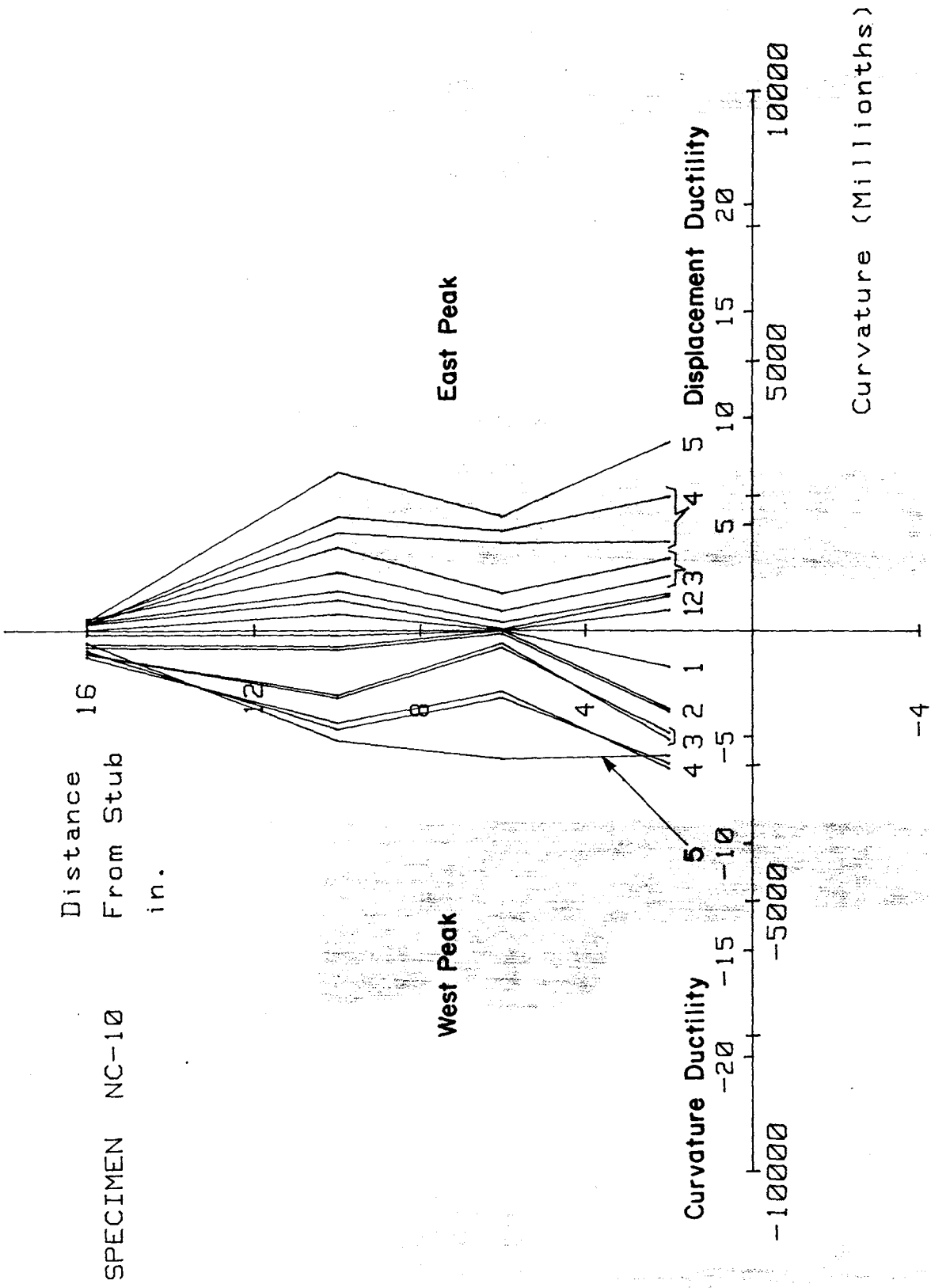


FIG. A-223 CURVATURE DISTRIBUTION ALONG UPPER COLUMN SPECIMEN NC-10

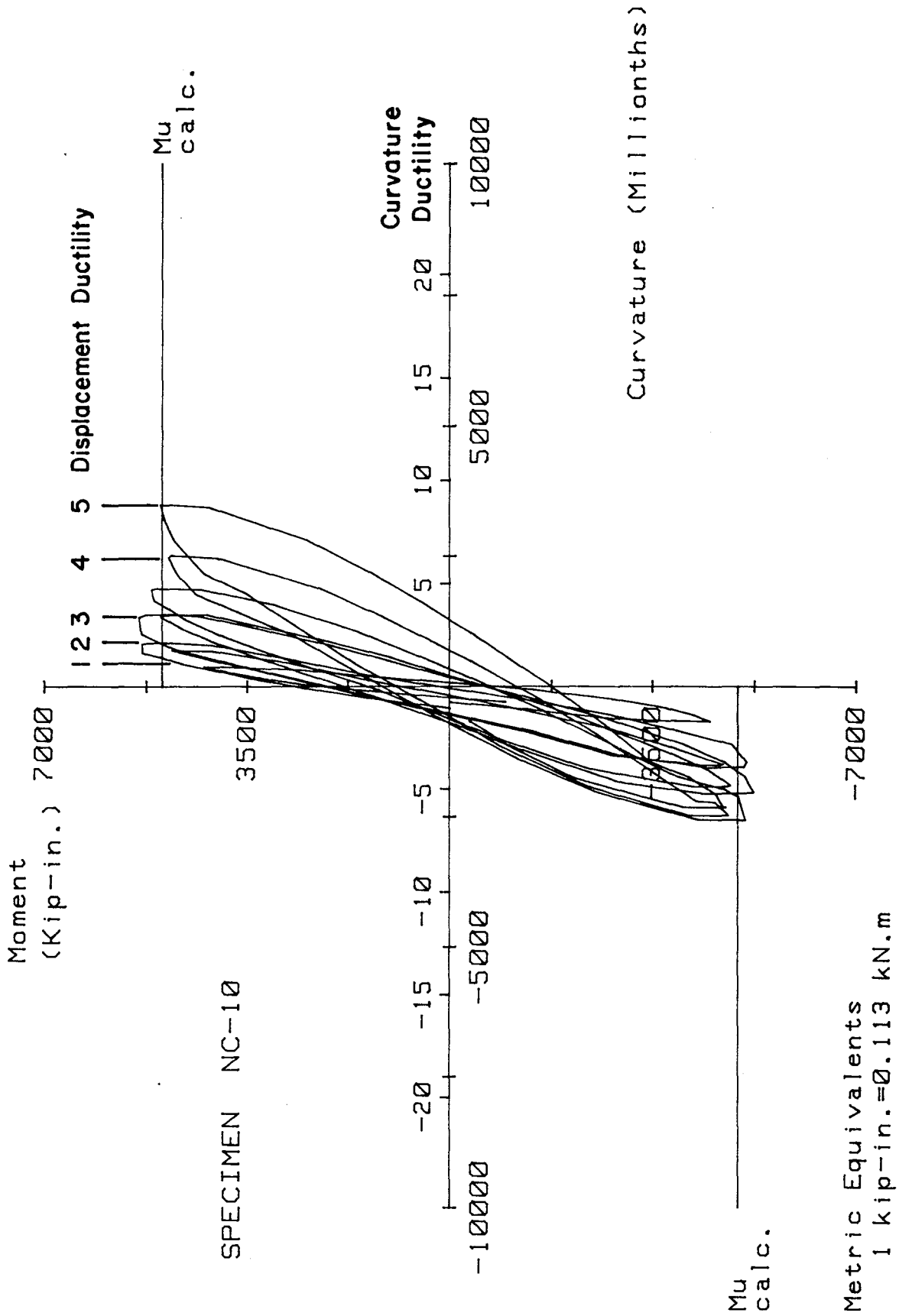


FIG. A-224 MOMENT VERSUS CURVATURE FOR SPECIMEN NC-10

4970 in-kips, while the maximum applied moment was 5379 in-kips. The maximum applied moments during displacement ductility ratios of 4 and 5 were 5168 and 5004 in-kips respectively. The ratio of the peak moment at the second cycle to the peak moment at the first cycle at various displacement levels ranged from 0.90 to 0.95.

Transverse Reinforcement Strain

A total of 10 strain gages were attached to the #3 continuous helix transverse reinforcement. Strain gages #13 through #17 were attached to the legs of the continuous helix, parallel to the horizontal loading direction on the south face, at distances of approximately 4.5, 9, 13.5, 18, and 20.5 in. above the stub. Gages #18 through #22 were attached to the legs of the continuous helix, parallel to the horizontal loading direction on the north side, at distances of approximately 2.5, 7, 11.5, 16, and 20.5 in. above the stub. Figures A-225 through A-233 show the results obtained from these strain gages. Strain gages #15, #16, #17, and #18 function through cycle #12 ($\mu=5$). The minimum specified yield strain of the transverse reinforcing material was 2070 micro-strain. The maximum strains recorded from these strain gages were 1858, 1318, 1675, and 1044 micro-strain, respectively, all recorded during cycle #12 ($\mu=5$).

In general, there was a relatively large increase in strain at all levels during cycle #5 ($\mu=2$). This increase was more pronounced on gages #15 and #20.

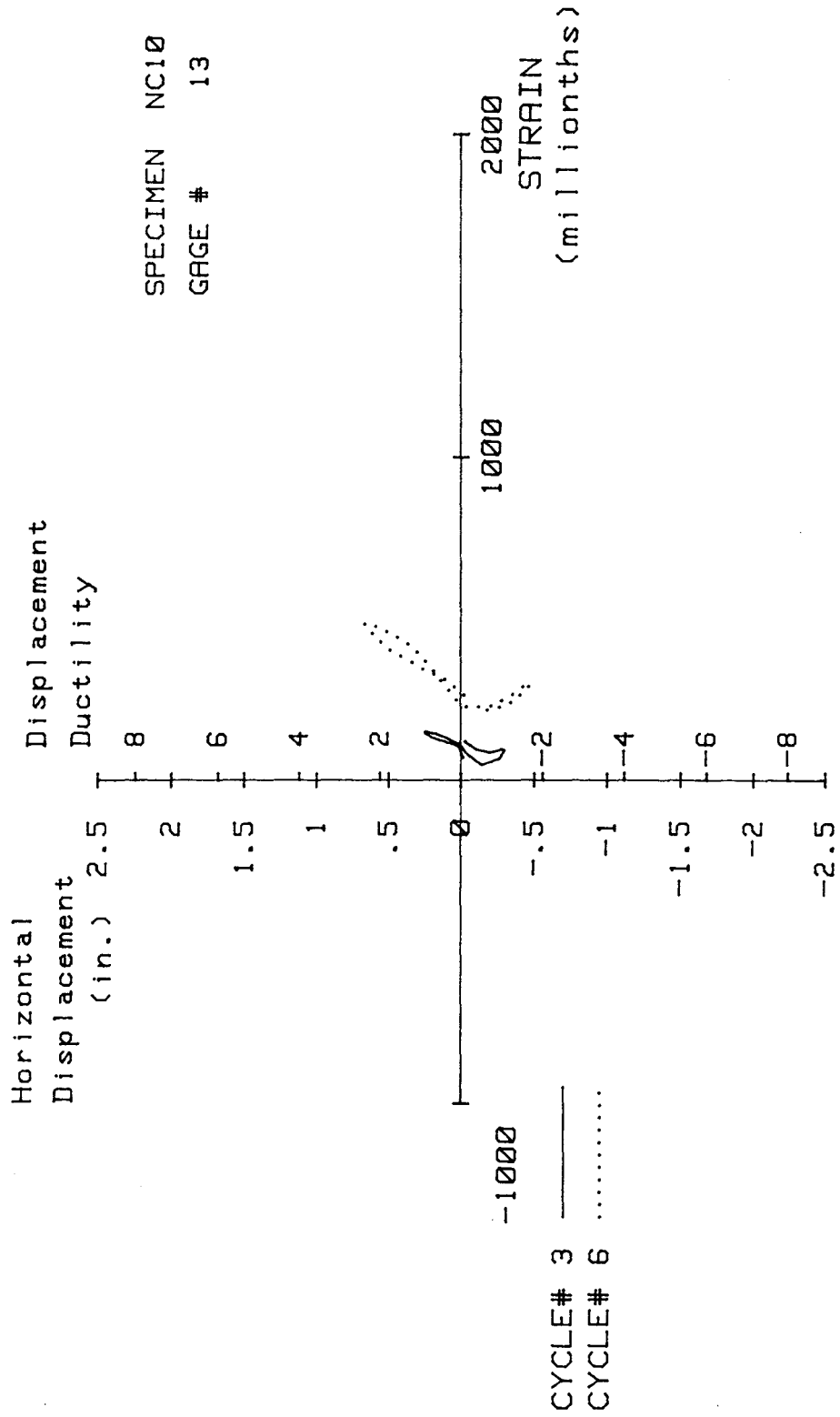


FIG. A-225 MEASURED STRAIN, GAGE #13, SPECIMEN NC-10

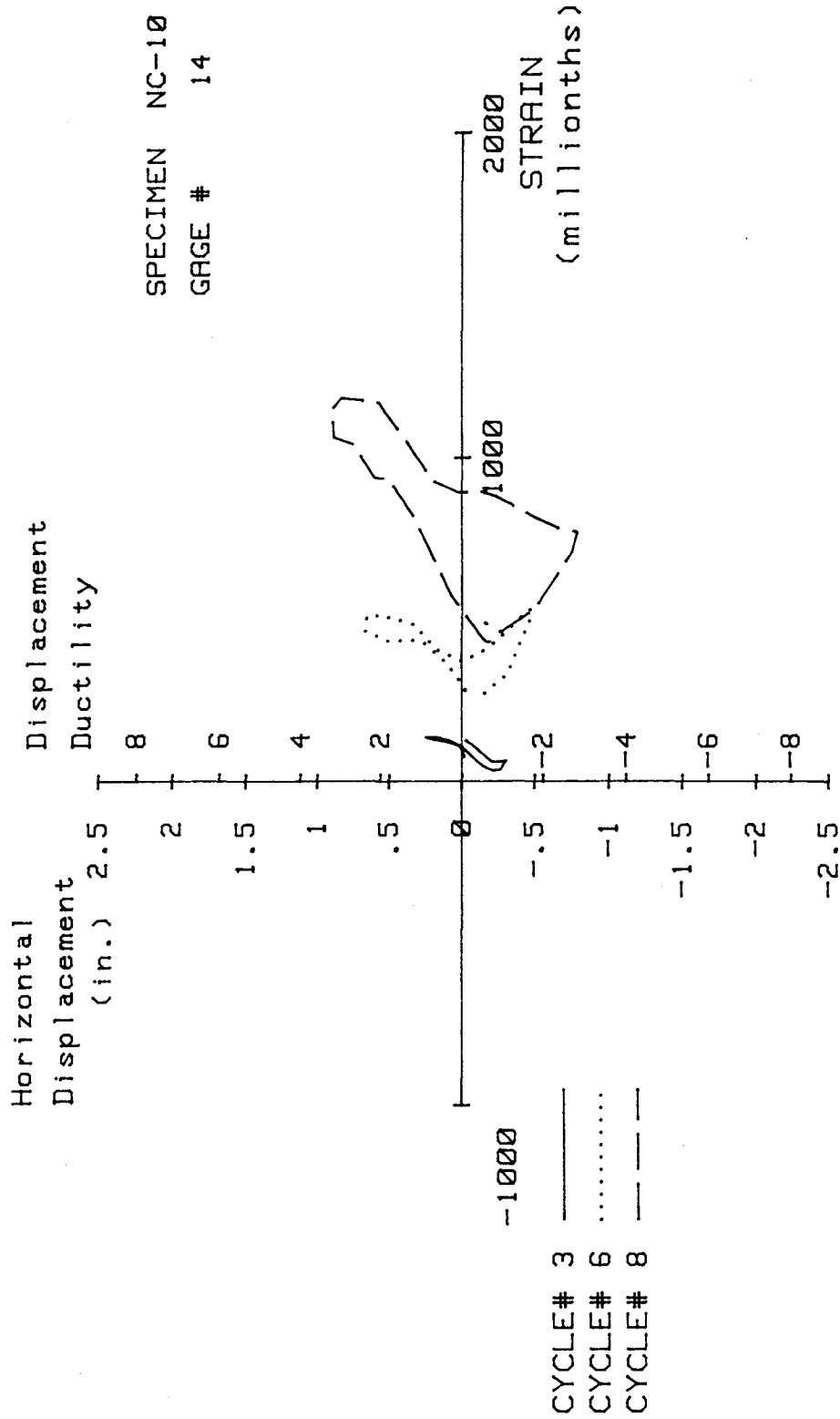


FIG. A-226 MEASURED STRAIN, GAGE #14, SPECIMEN NC-10

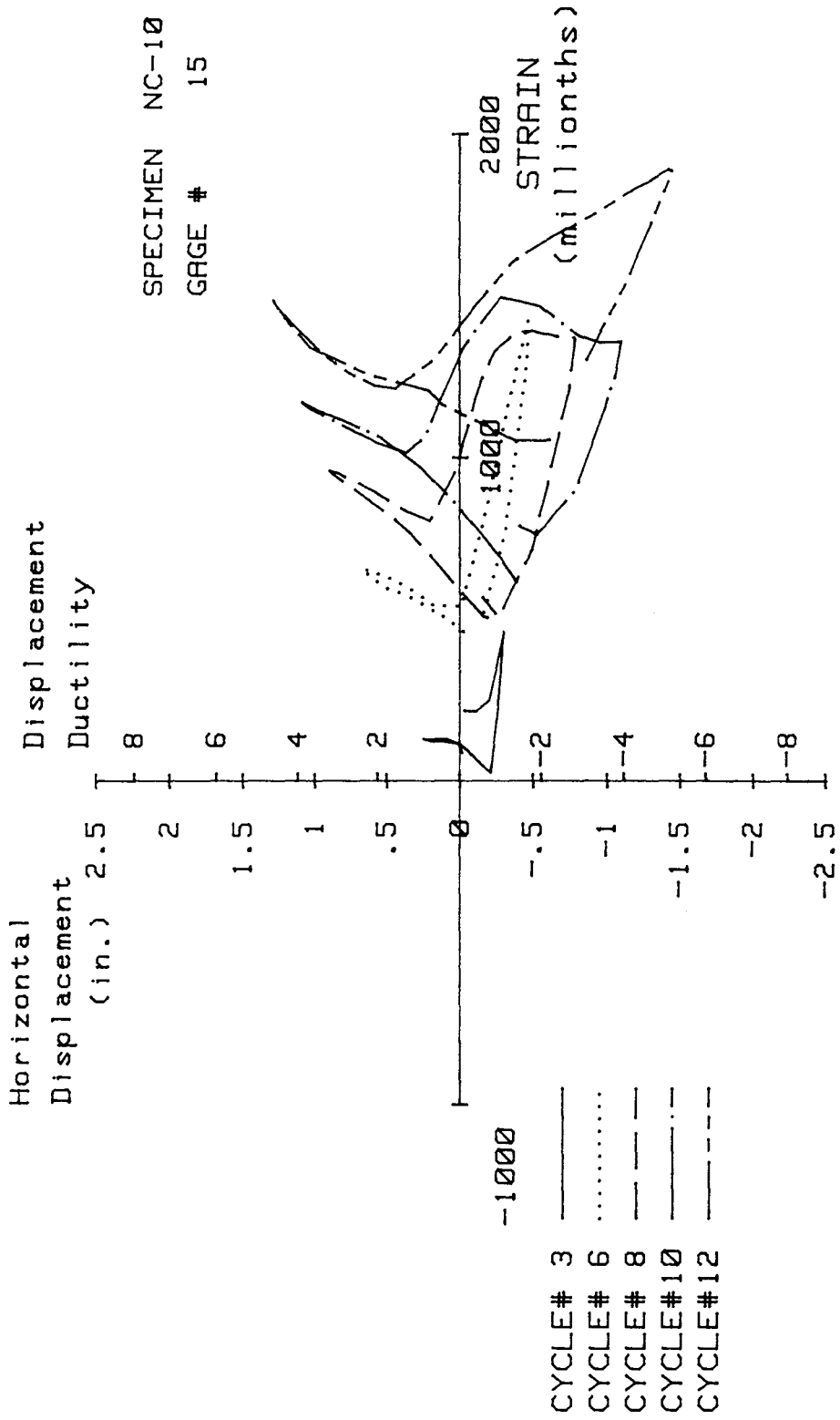


FIG. A-227 MEASURED STRAIN, GAGE #15, SPECIMEN NC-10

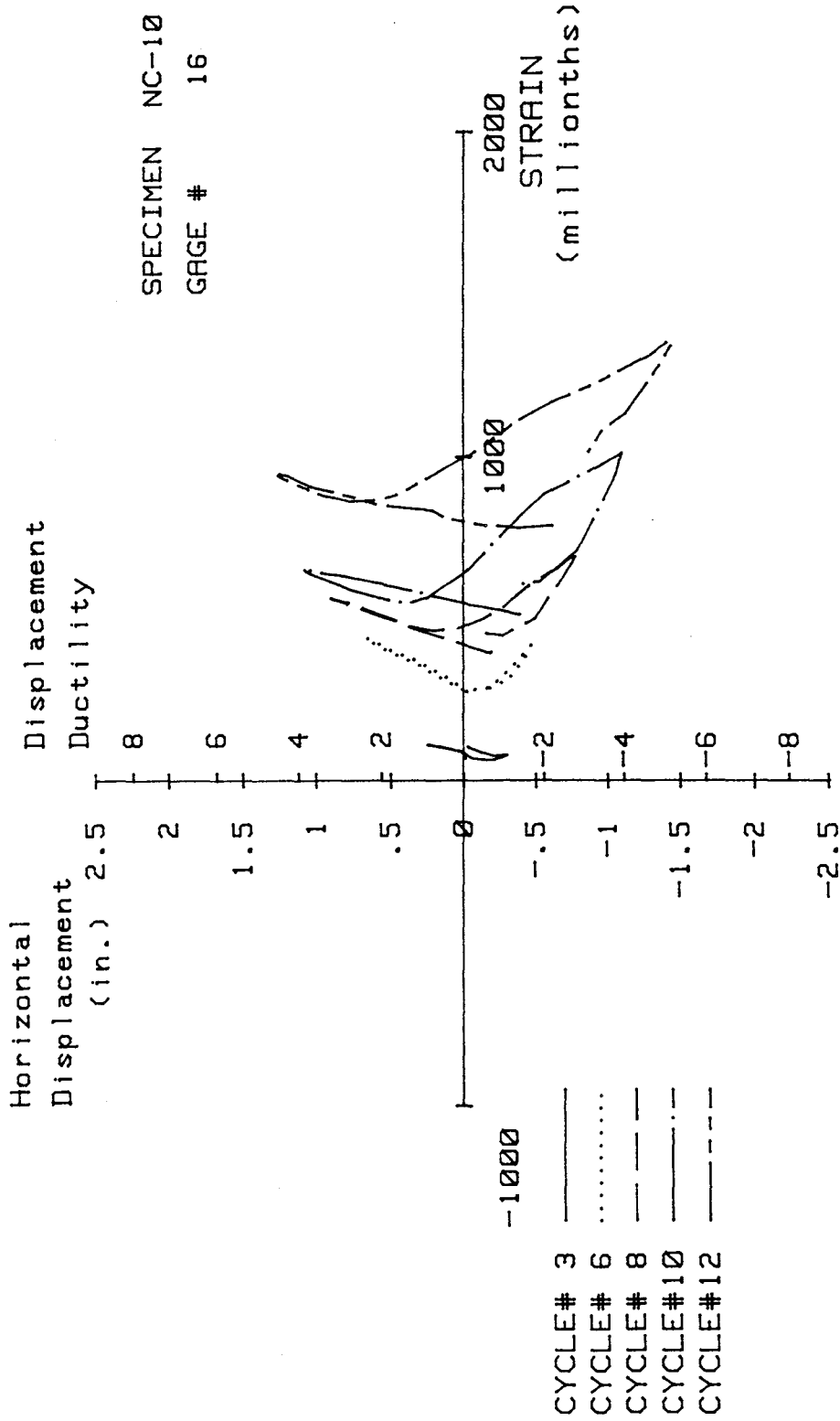


FIG. A-228 MEASURED STRAIN, GAGE #16, SPECIMEN NC-10

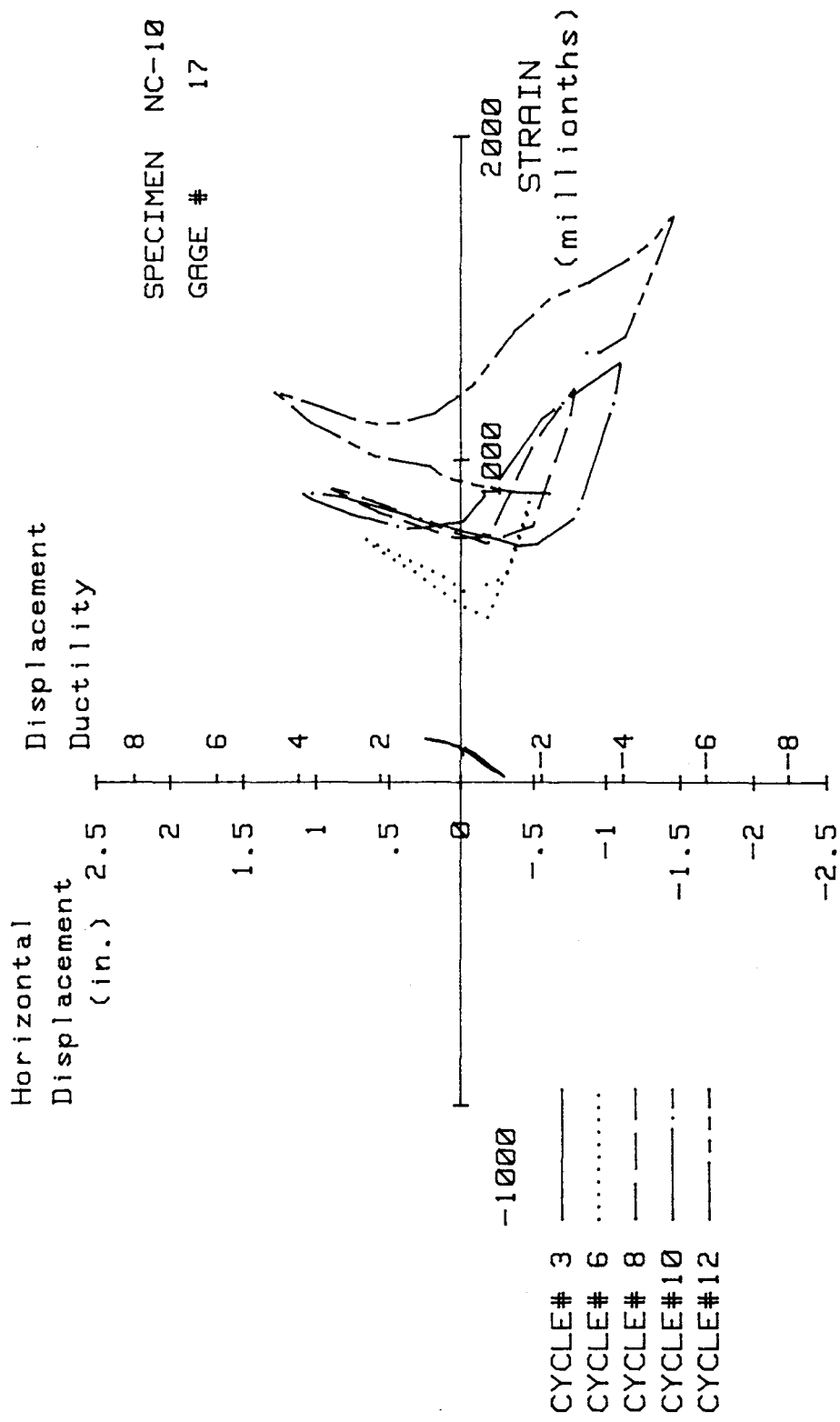


FIG. A-229 MEASURED STRAIN, GAGE #17, SPECIMEN NC-10

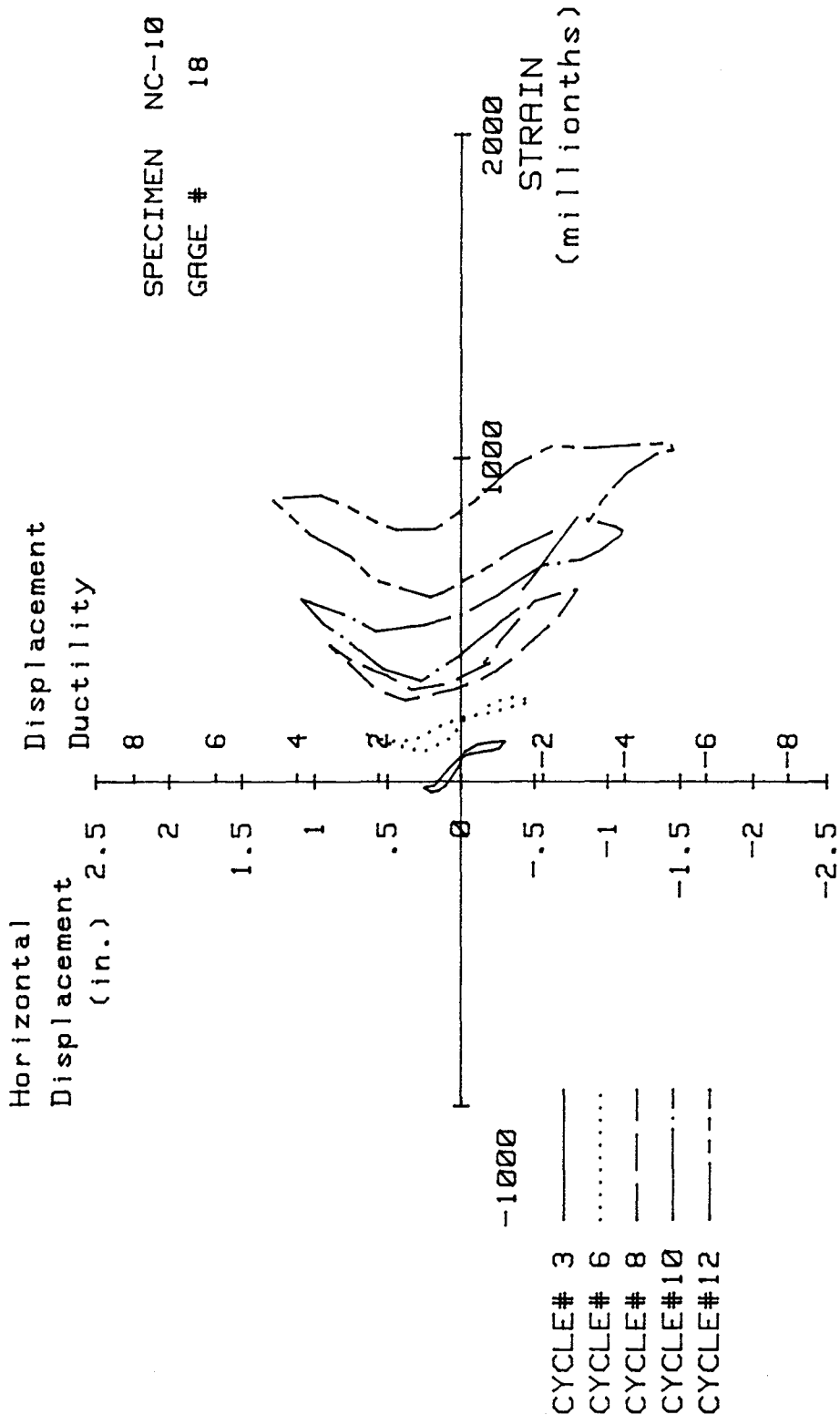


FIG. A-230 MEASURED STRAIN, GAGE #18, SPECIMEN NC-10

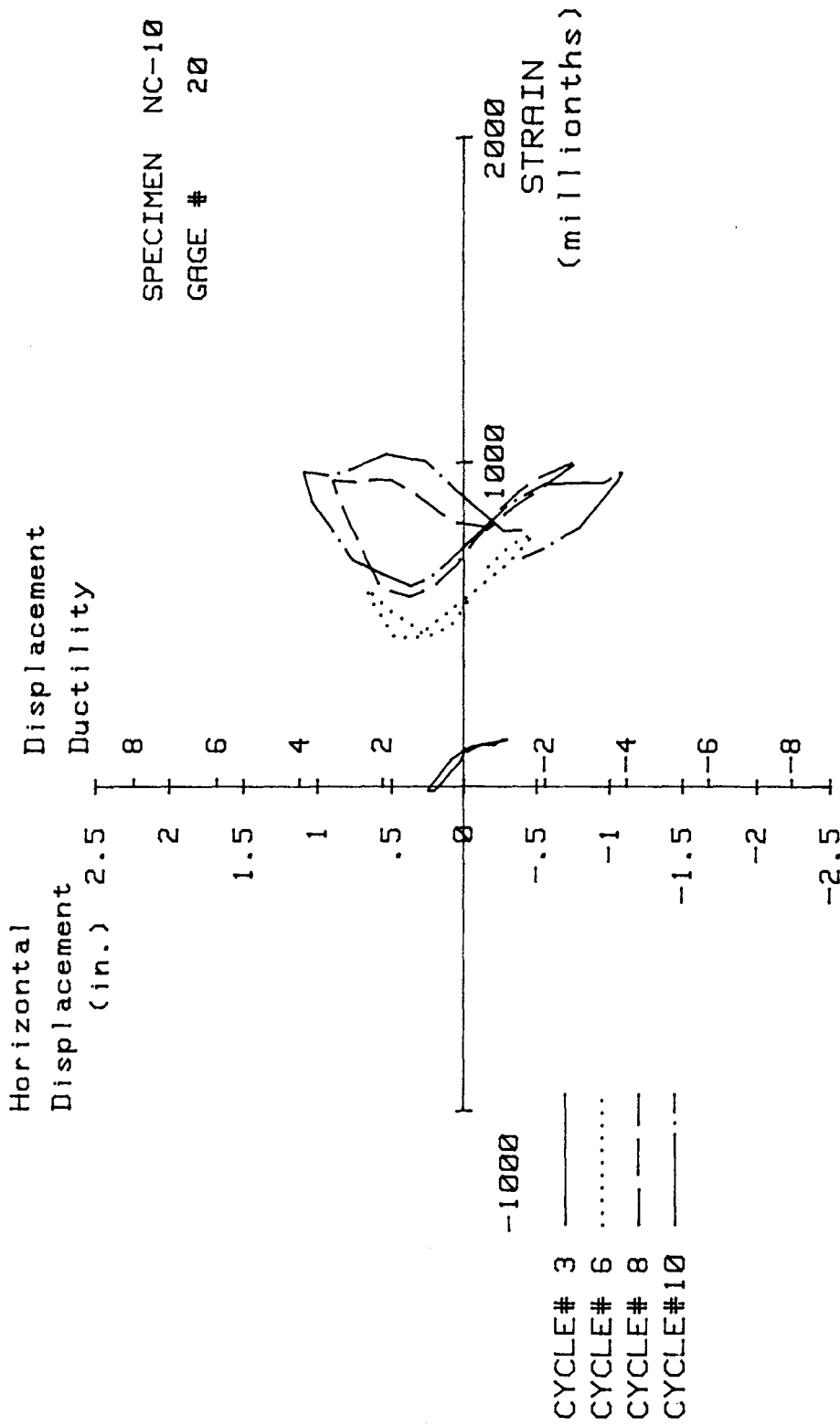


FIG. A-231 MEASURED STRAIN, GAGE #20, SPECIMEN NC-10

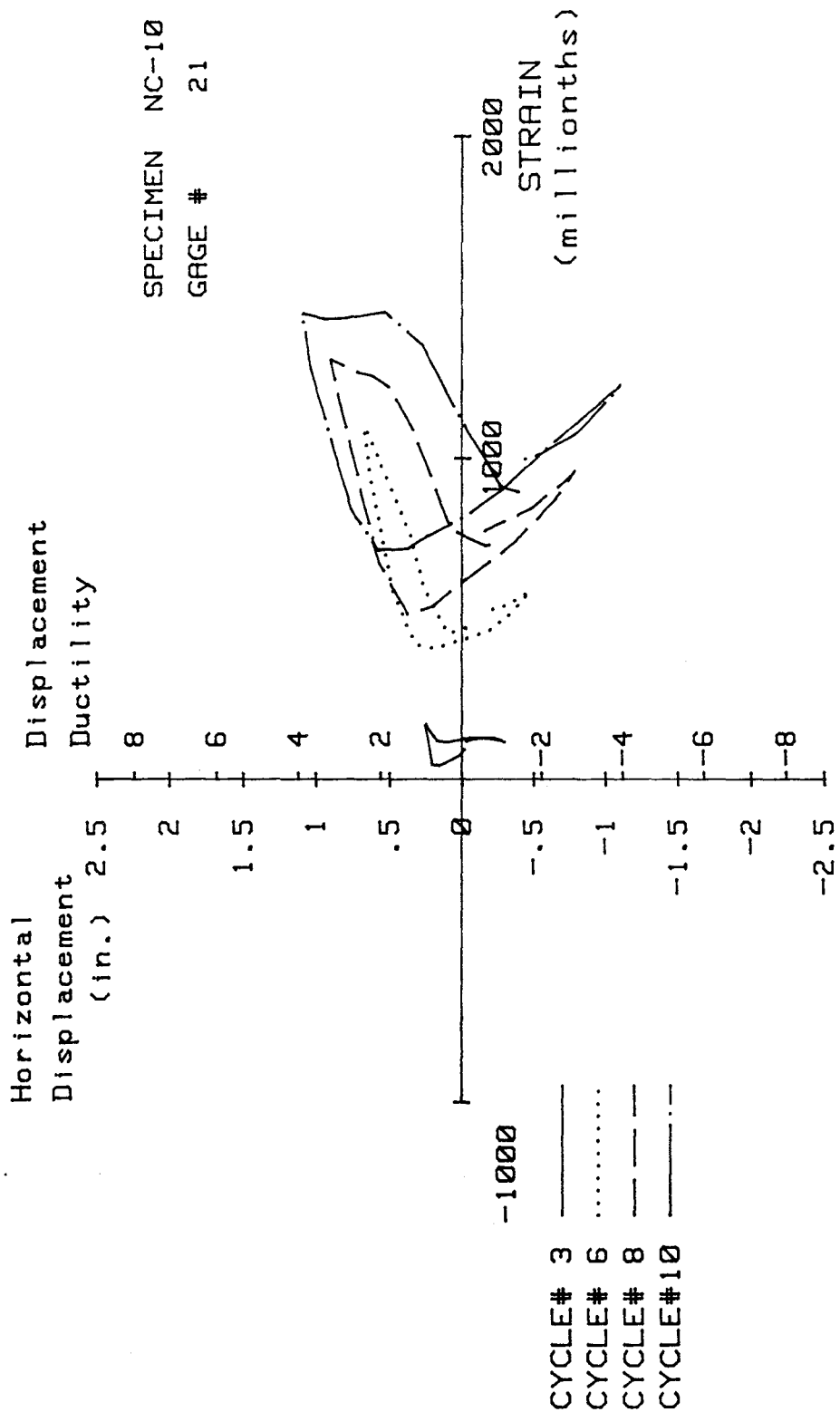


FIG. A-232 MEASURED STRAIN, GAGE #21, SPECIMEN NC-10

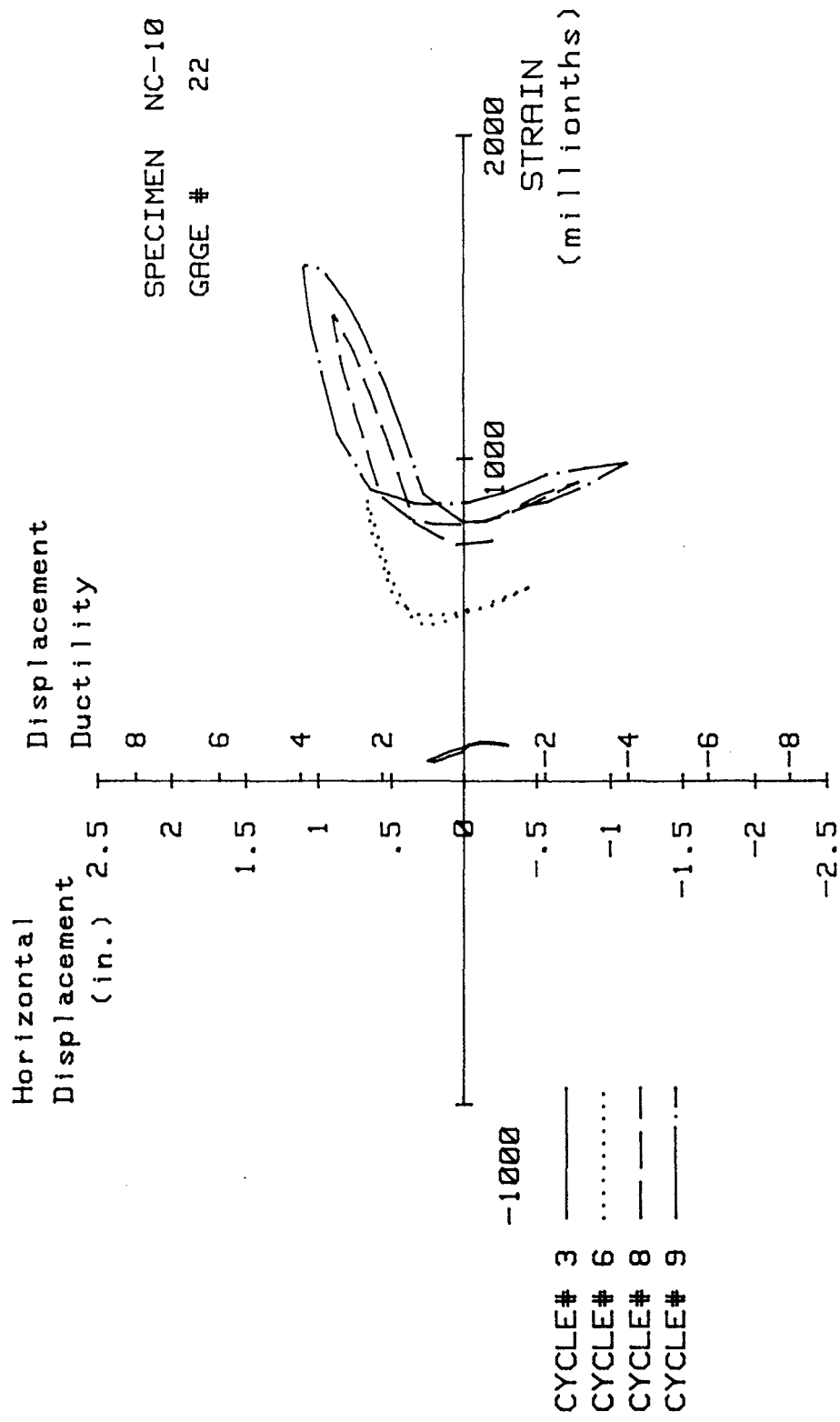


FIG. A-233 MEASURED STRAIN, GAGE #22, SPECIMEN NC-10

Specimen NC-11

Transverse Reinforcement Detail

Specimen NC-11 was similar to the other specimens studied in this investigation, except that the upper column's cross-section was circular. Figure 4-4 shows the overall dimensions of the specimen and the upper column's cross-section.

Longitudinal reinforcement of the upper column consisted of 8-#8 Grade 60 bars, arranged as shown in Fig. 4-4.

Transverse Reinforcement Detail

The transverse reinforcement for the upper column of Specimen NC-11 consisted of 3/8 in. diameter continuous spiral reinforcement at a pitch of 2-1/4 in. from the stub to 34 in. above the stub. This provided a reinforcement ratio, ρ , of 1.29%. According to ACI-318-38, the required reinforcement ratio for this region is 2.05%.

Load History

The applied axial load was 460 kips which corresponds to 30% of the column's axial load capacity. Maintaining the axial load constant, the specimen was subjected to 20 complete cycles of horizontal loading. During cycle #2 the first yield displacement and yield curvature were calculated as 0.28 in. and $623 \times 10^{-6} \text{ in.}^{-1}$, respectively, using the procedure outlined in Section 4.8.2. Subsequently, testing was displacement-controlled and consisted of one or two cycles of cyclic horizontal loading to a maximum displacement ductility ratio of nine. The specimen failed before completing the first cycle at the displacement ductility ratio of 10. Figure A-234 show the history of applied cyclic horizontal loading.

Test Observations

The first hairline cracks were observed during cycle #2, at the interface of the upper column and the stub. Figure A-235 shows the specimen at the end of cycle #6 ($\mu=2$). At this stage some crushing of the cover concrete at the junction of the upper column and the stub was observed. Cracking extended to 21 in. above the stub.

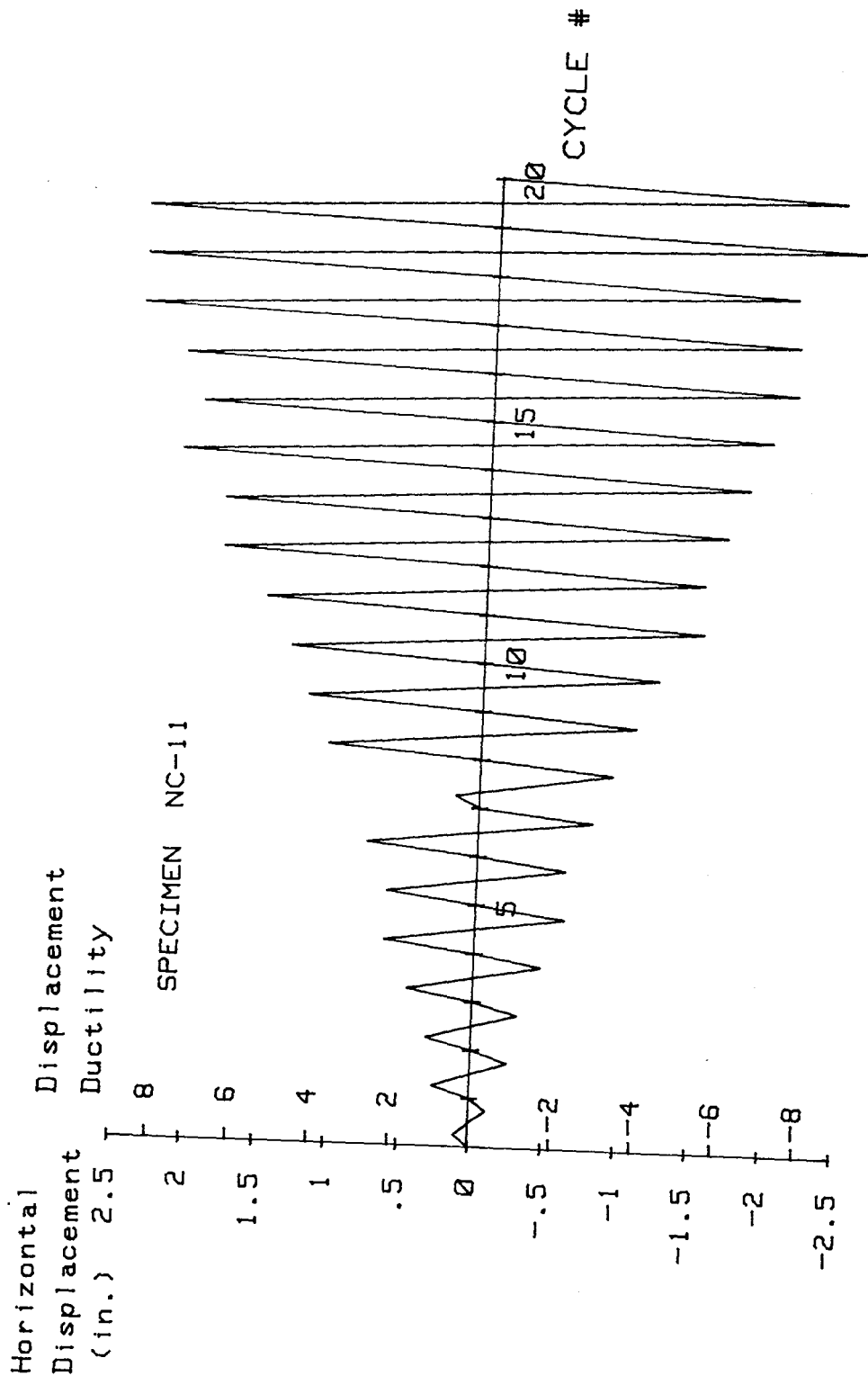


FIG. A-234 LOADING SCHEDULE, SPECIMEN NC-11

Reproduced from
best available copy.

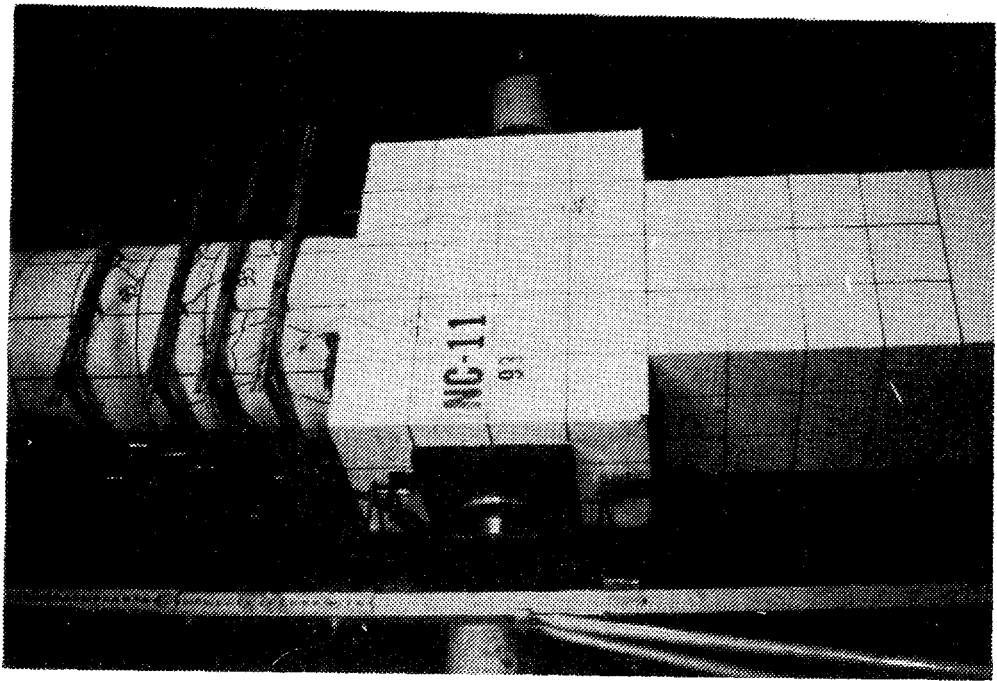


FIG. A-235 TEST SPECIMEN NC-11 AFTER CYCLE #6

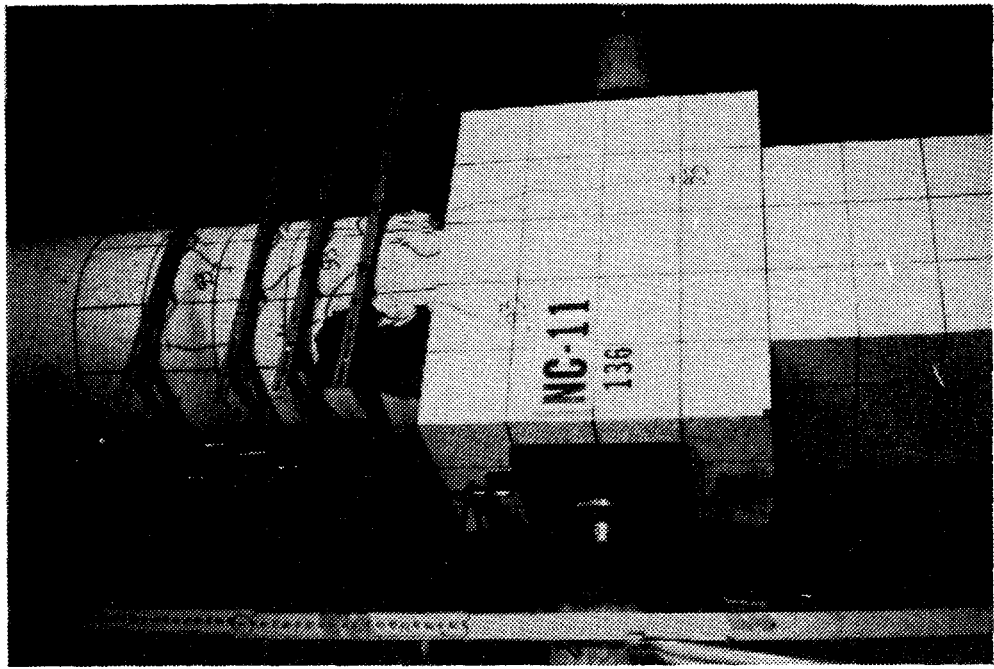


FIG. A-236 TEST SPECIMEN NC-11 AFTER CYCLE #8

Figure A-236 shows the specimen at the end of cycle #8 ($\mu=3$), at which point spalling of the cover concrete extended to approximately 12 in. above the stub. As is evident from Fig. A-237, application of two more cycles at the displacement ductility ratio of four did not alter the extent of visible damage to the specimen.

As shown in Fig. A-238, at the end of cycle #12 ($\mu=5$), the cover concrete spalled off to a distance of approximately 12 in. above the stub. No visible damage was inflicted to the transverse or longitudinal reinforcement at this stage.

At the end of cycle #17 ($\mu=8$), some lateral bending of the longitudinal bars on the east and west side was observed approximately 8 in. above the stub. Lateral bending of the longitudinal bars at this location caused elongation of the spiral reinforcement. The specimen was able to sustain horizontal displacement up to the displacement ductility ratio of nine. Buckling of the longitudinal bars approximately 9 in. above the stub occurred before completing the first cycle at displacement ductility ratio of 10.

Figure A-239 shows the specimen at test conclusion. Spalling of the cover concrete has extended to 20 in. above the stub. Buckling of the longitudinal bars resulted in elongation of the spiral reinforcement at those locations; however, no visible cracking or fracture of the spiral reinforcement was observed.

Load Deflection and Moment-Curvature Characteristics

Figure A-240 shows the horizontal load displacement characteristic of the specimen. The maximum applied horizontal load was 165 kips, which occurred during forward loading of cycle #5 ($\mu=2$). In addition to good strength characteristics, the specimen exhibited good energy dissipation characteristics.

Figure A-241 shows the curvature distribution along the upper column. As is evident, the maximum curvature during the forward and reverse loading cycles at displacement ductility ratios greater than three were located 4 to 8 in. above the stub and within 4 in. of the stub, respectively. The maximum curvature ductility ratio was achieved during the forward loading cycle #20 ($\mu=9$) and was approximately 26.

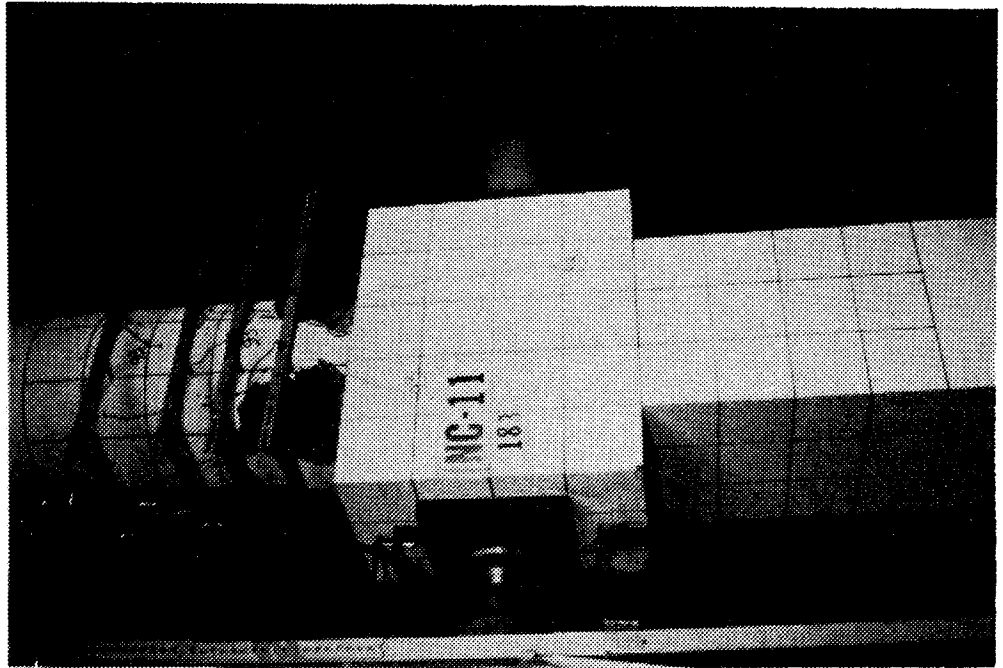


FIG. A-237 TEST SPECIMEN NC-11 AFTER CYCLE #10

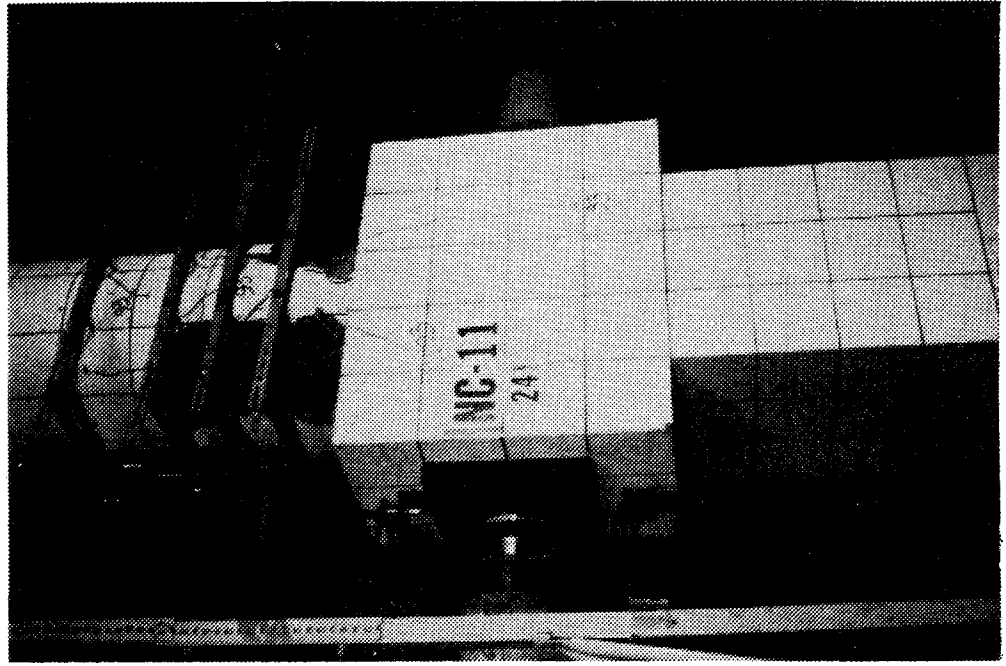


FIG. A-238 TEST SPECIMEN NC-11 AFTER CYCLE #12

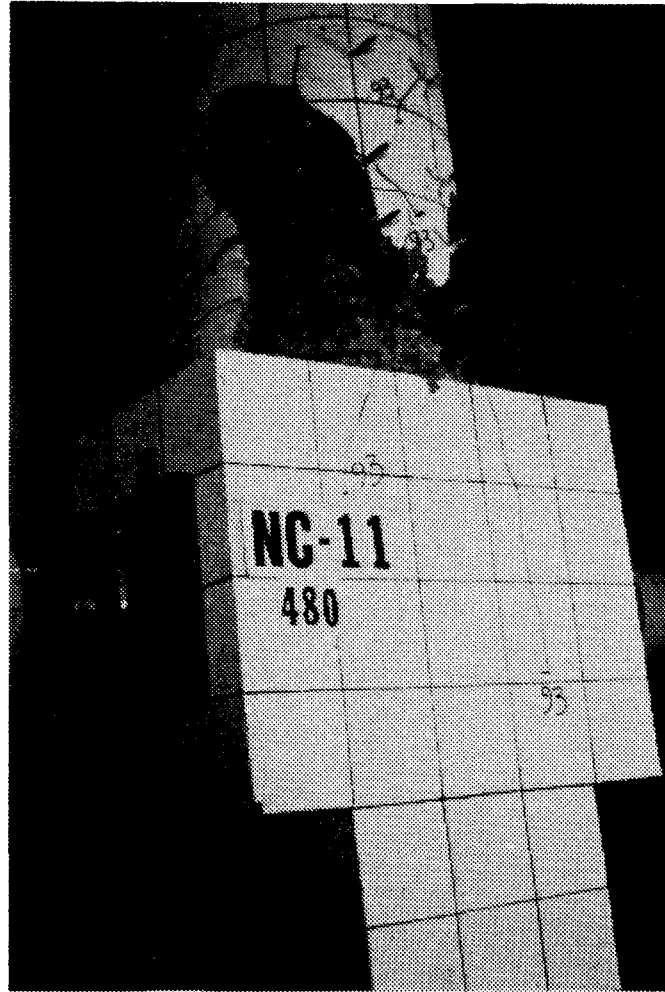
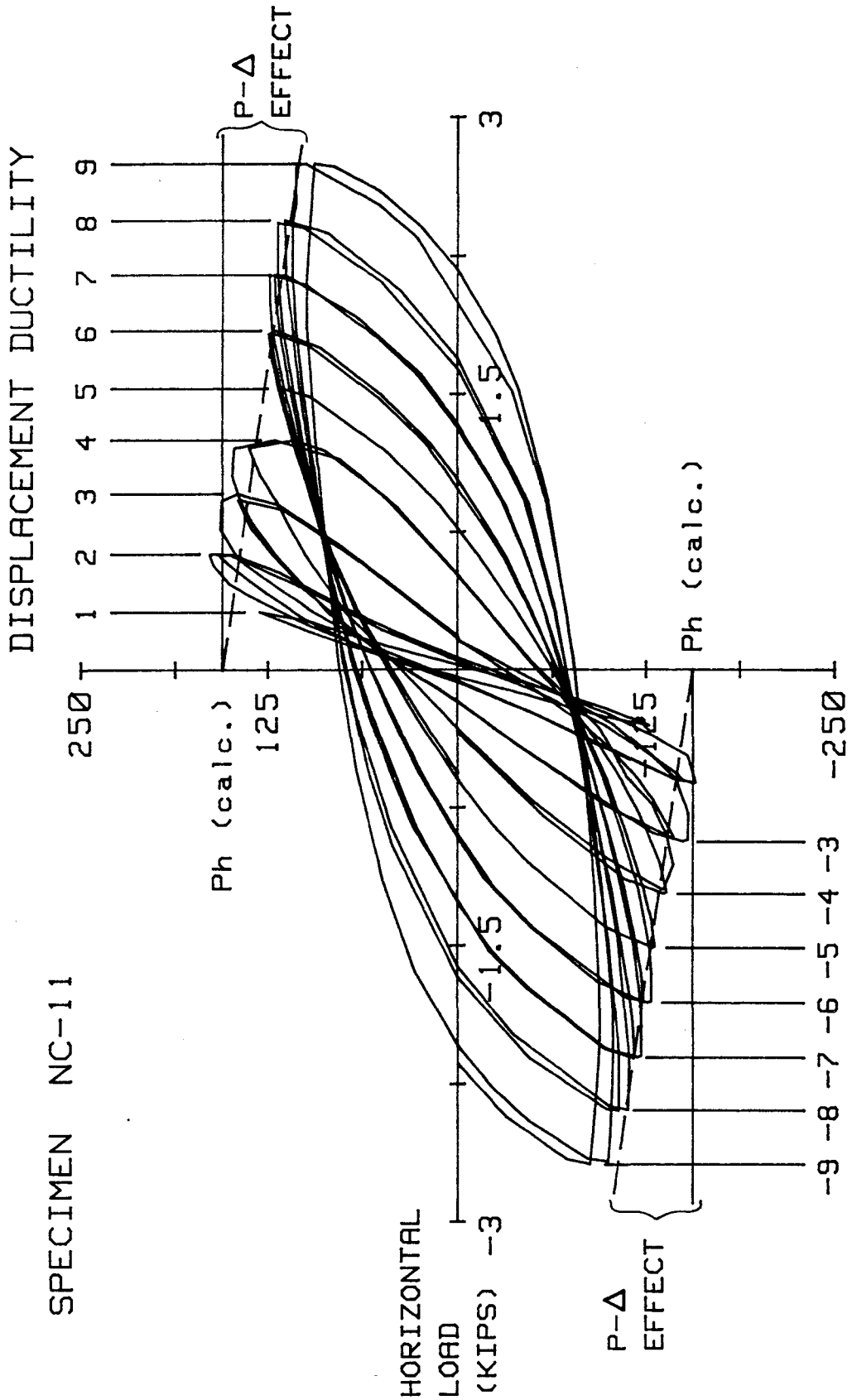


FIG. A-239 TEST SPECIMEN NC-11 AFTER TEST CONCLUSION



SPECIMEN NC-11

Metric Equivalents
 1 in. = 25.4 mm
 1 kip = 4.45 kN

HORIZONTAL DISPLACEMENT (IN.)

FIG. A-240 HORIZONTAL LOAD VERSUS DISPLACEMENT, SPECIMEN NC-11

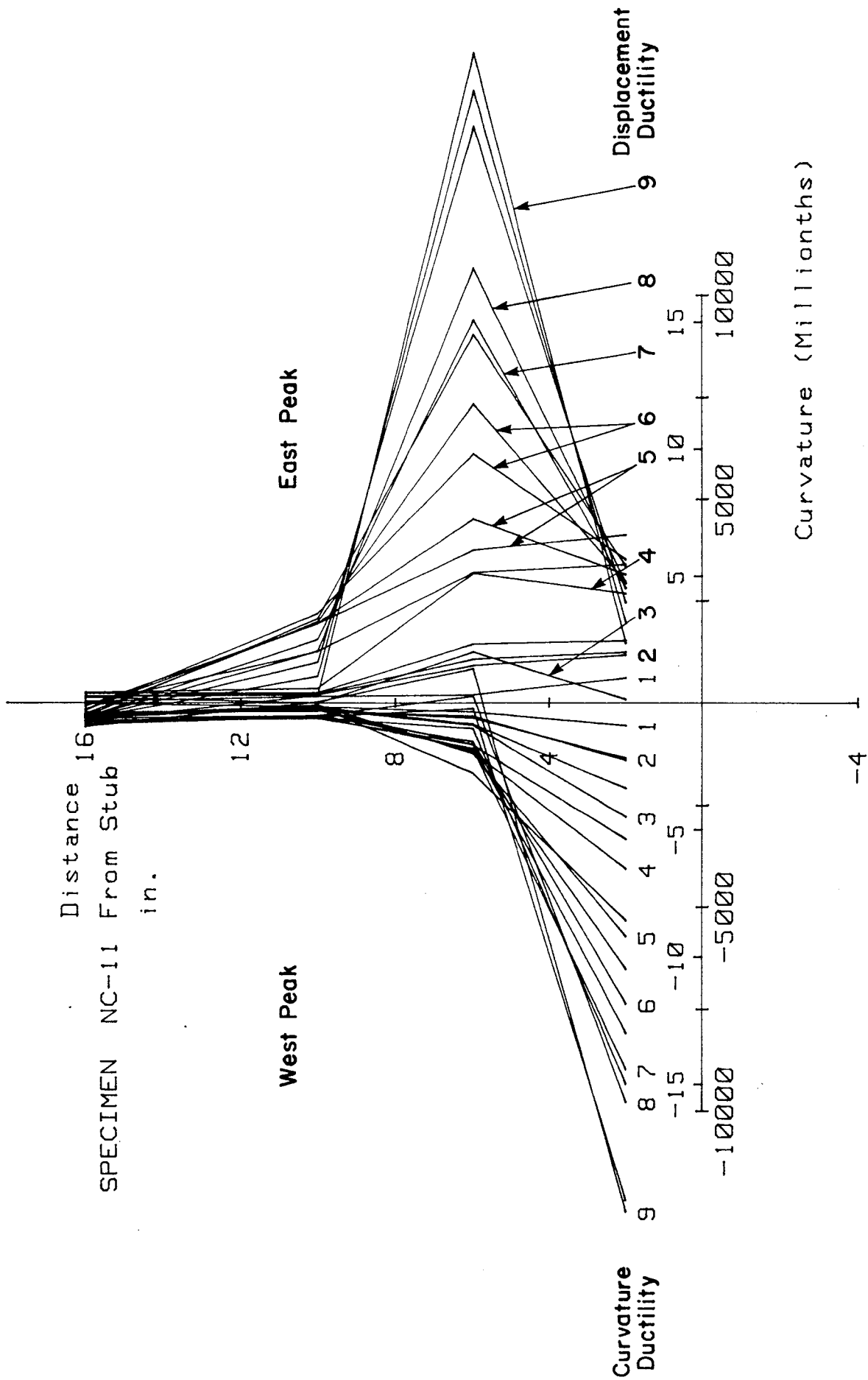


FIG. A-241 CURVATURE DISTRIBUTION ALONG UPPER COLUMN SPECIMEN NC-11

The maximum ratio of curvature ductility to displacement ductility at the peak of displacement ductility ratios of 1 through 9 were 1, 1.2, 1.5, 1.7, 1.8, 2.0, 2.2, 2.8, and 2.9, respectively.

Figure A-242 shows the moment curvature characteristics of the column cross-section at the interface of the upper column-stub. The theoretical moment capacity of the section considered was calculated to be 4000 in-kips, using the procedures outlined in Section 4.8.2. The maximum applied moment was 4543 in-kips. As shown in Fig. A-242, degradation in moment capacity at various displacement levels was small. The ratio of the peak moment at the second cycle to the peak moment at the first cycle ranged from 0.89 to 1.01 at various displacement levels.

Transverse Reinforcement Strain

A total of six strain gages were attached to the spiral transverse reinforcement of the upper column. Figures A-243 through A-248 show the results obtained from these strain gages. Strain gages #13, #14, and #15 were attached on the north side 90° from the loading axis at distances approximately 4.5, 9, and 13.5 in above the stub. Strain gages #16, #17, and #18 were attached on the south side 90° from the loading axis at distances approximately 3.5, 8, and 12.5 in. above the stub.

The minimum specified yield strain of the material used for the spiral reinforcement was 2070 micro-strain. At the peak of forward loading during cycle #5 ($\mu=2$), strain gages #13 and #16 showed a sudden increase in strain. At this stage, strain on gages #13 through #18 were 955, 227, 23, 1544, 326, and 9 micro-strain, respectively. Beyond this point, gages #14, #15, #17, and #18 gained strain at a faster rate than they did during cycle #11 ($\mu=5$), the strains in gages #13 through #18 were 1389, 2392, 3385, 2085, 1754, and 3401 micro-strain, respectively. Gage #16 showed the first strain reading beyond the yield strain at the peak of the forward loading cycle #10 ($\mu=4$), recording a strain of 2072 micro-strain.

Some of the strain gages ceased to function long before test conclusion. Gages #16, #17, and #18 functioned through cycles #20, #18, and #15, respectively. Maximum strains recorded from these three gages were 3665, 4395, and 10,429 micro-strain, respectively.

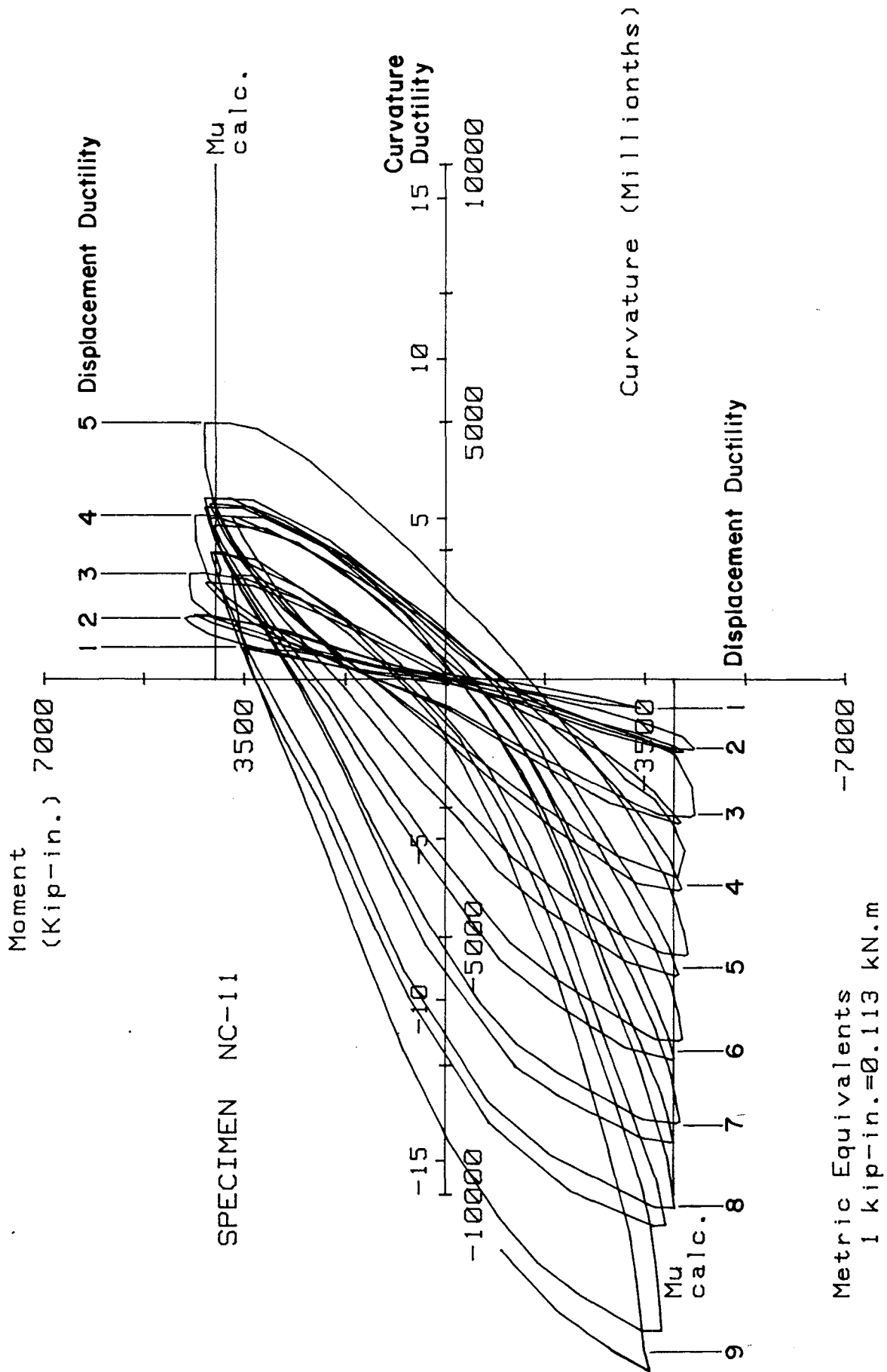


FIG. A-242 MOMENT VERSUS CURVATURE FOR SPECIMEN NC-11

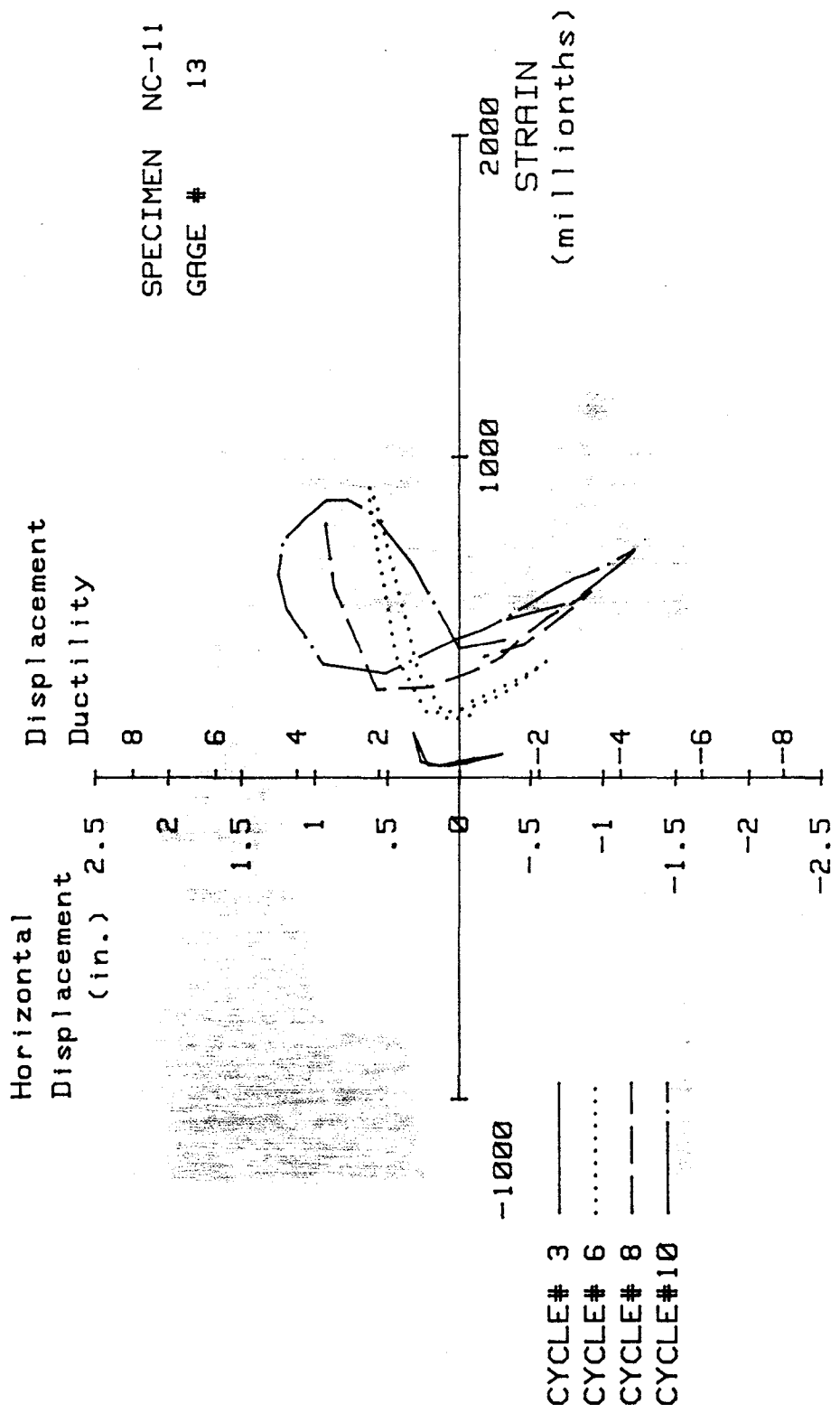


FIG. A-243 MEASURED STRAIN, GAGE #13, SPECIMEN NC-11

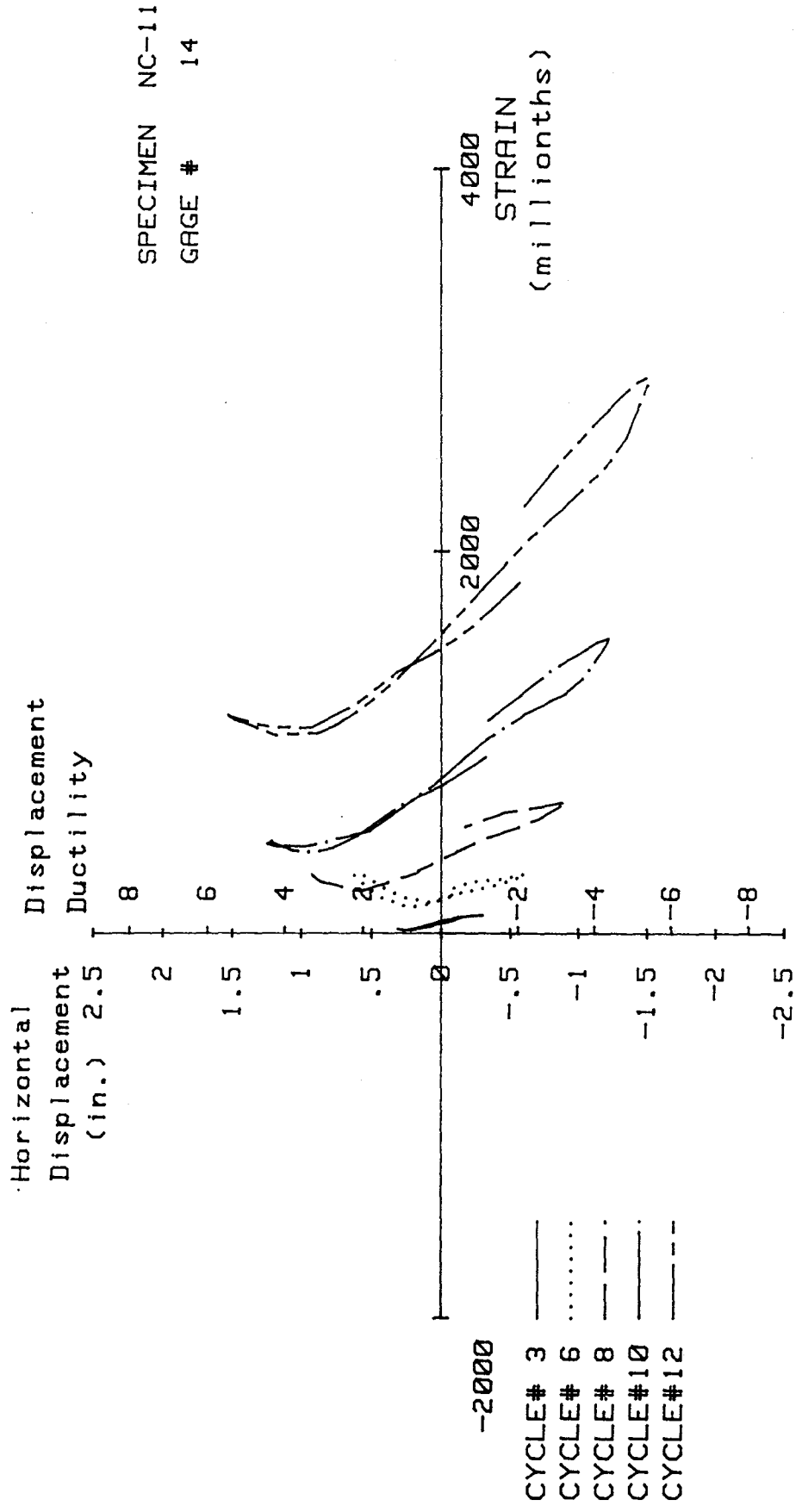


FIG. A-244 MEASURED STRAIN, GAGE #14, SPECIMEN NC-11

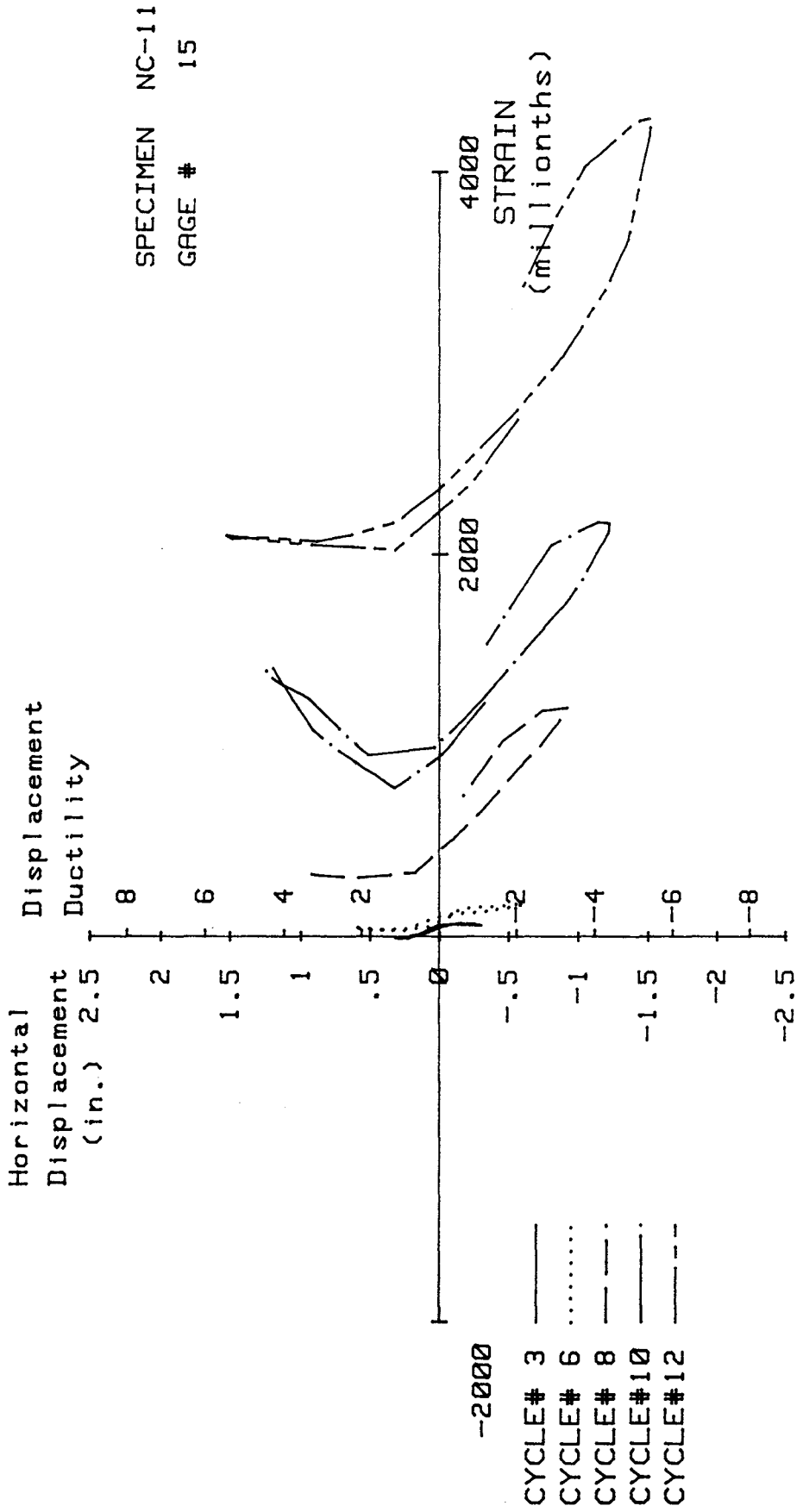


FIG. A-245 MEASURED STRAIN, GAGE #15, SPECIMEN NC-11

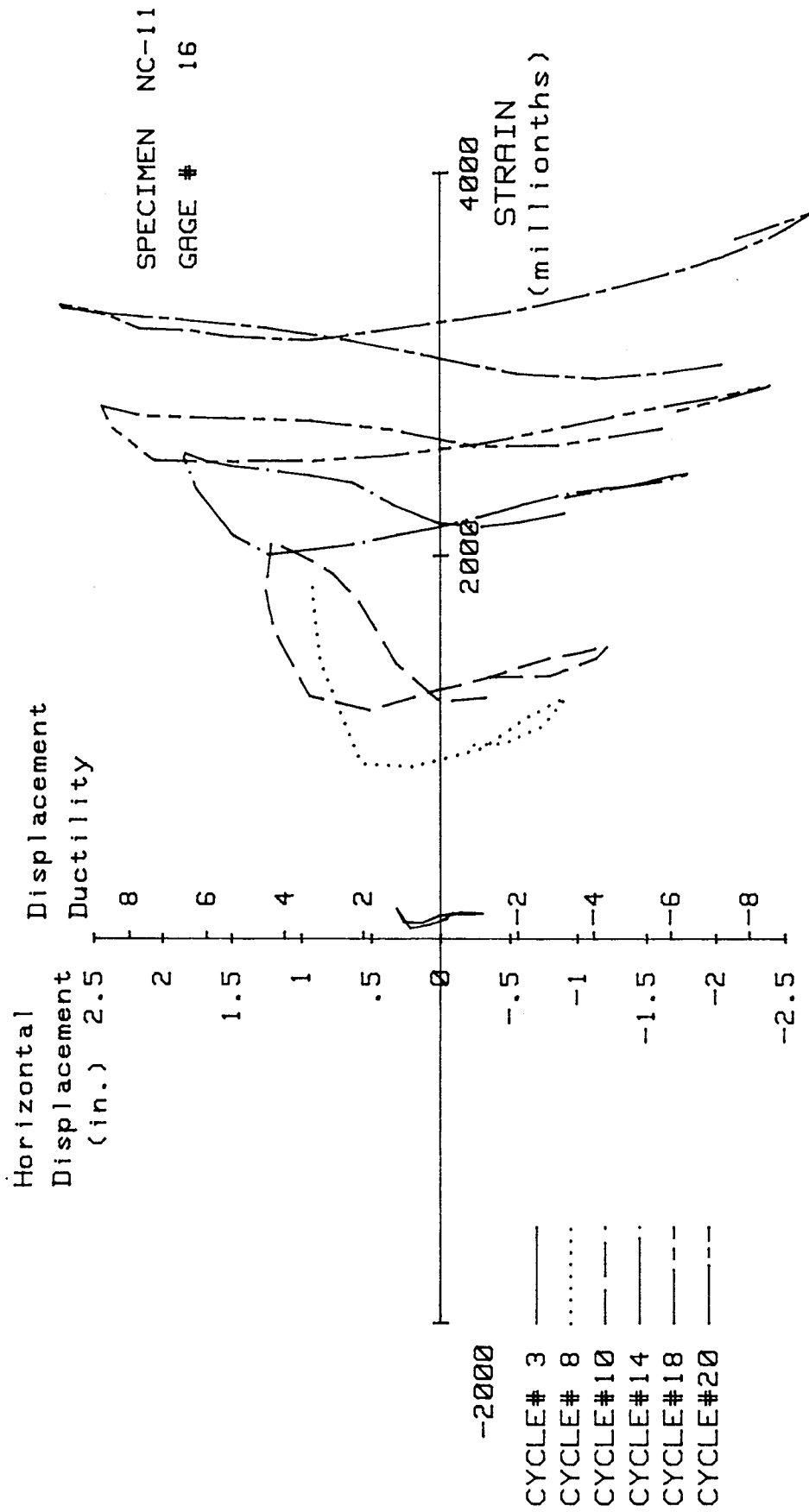


FIG. A-246 MEASURED STRAIN, GAGE #16, SPECIMEN NC-11

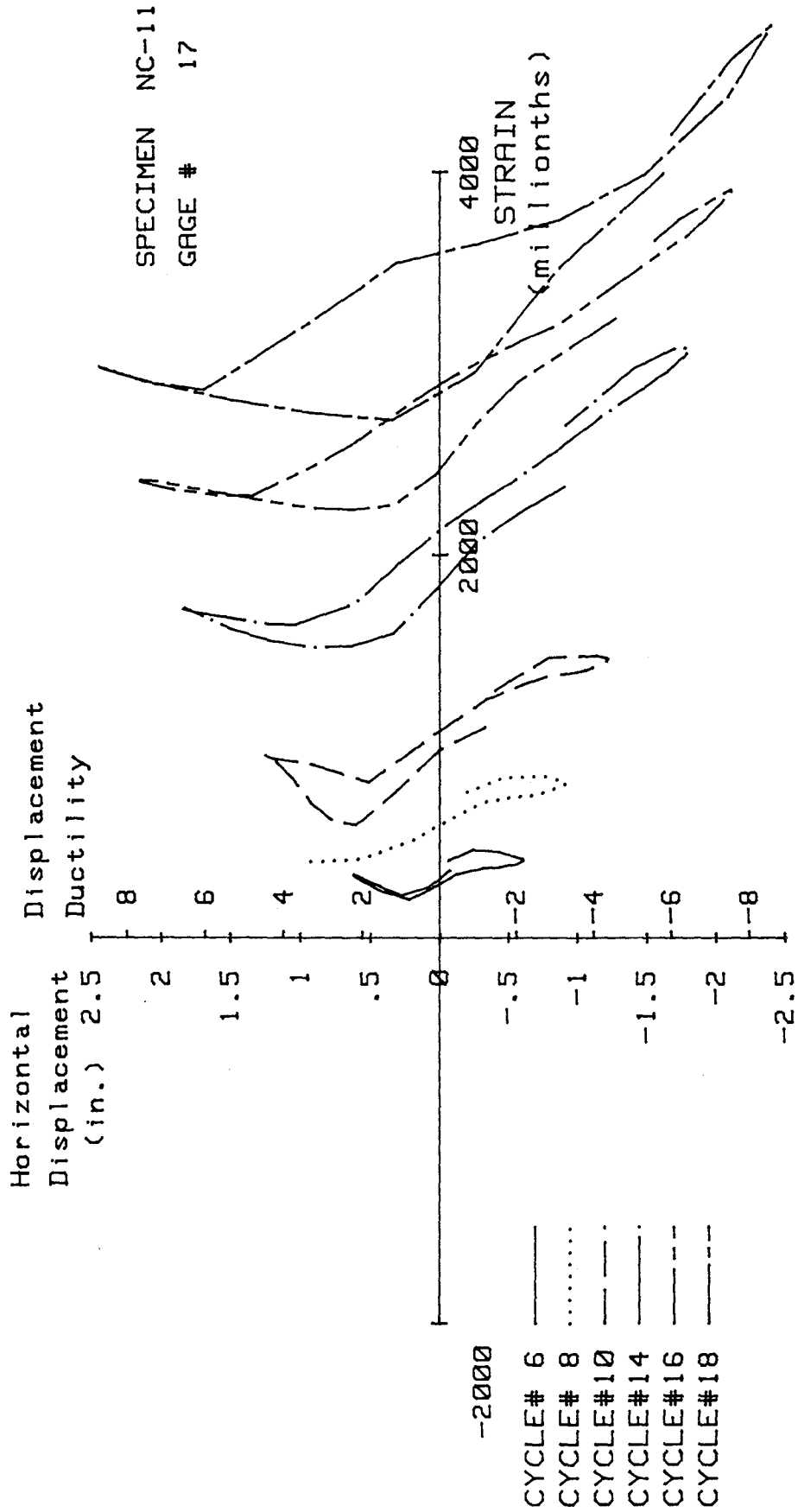


FIG. A-247 MEASURED STRAIN, GAGE #17, SPECIMEN NC-11

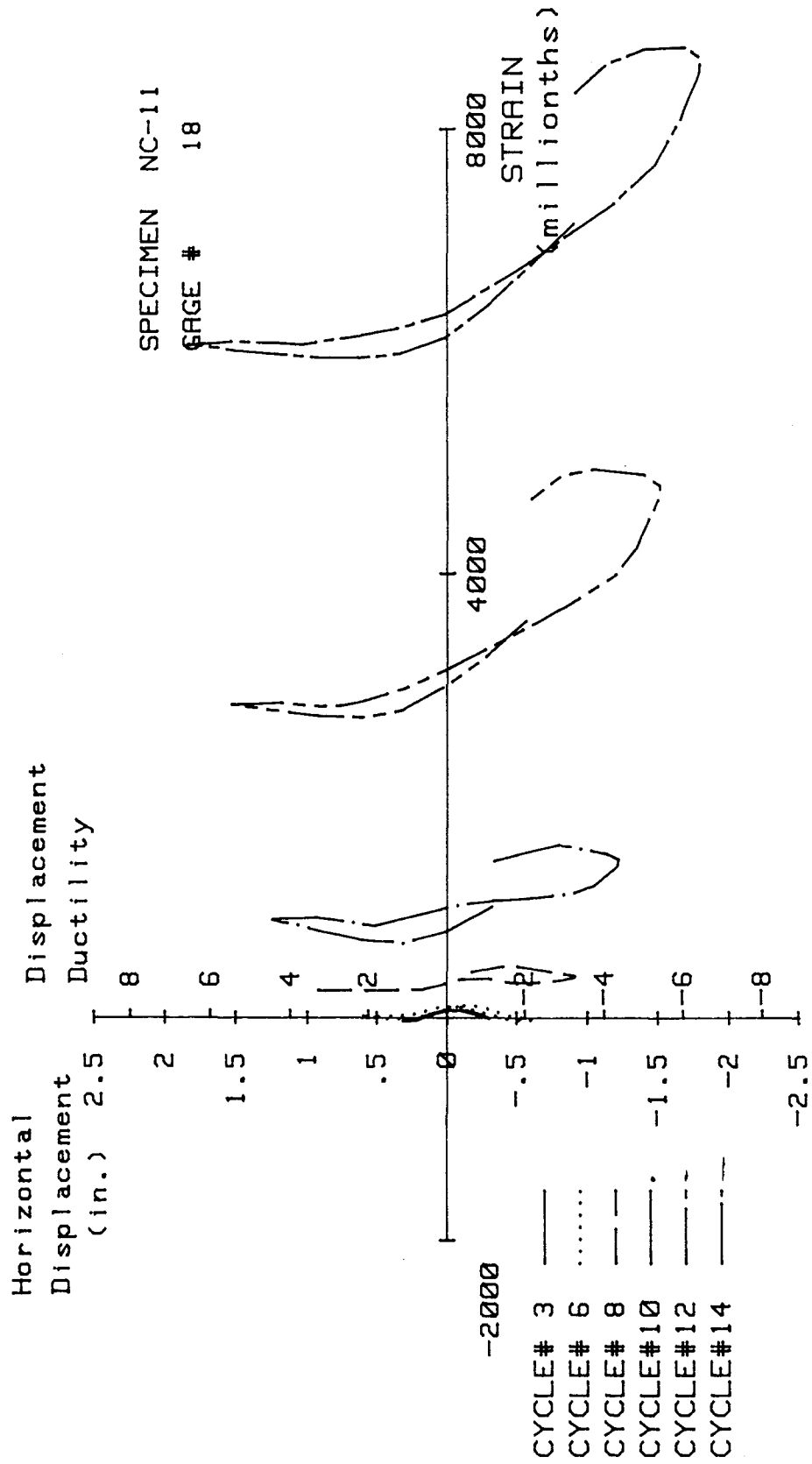


FIG. A-248 MEASURED STRAIN, GAGE #18, SPECIMEN NC-11

Specimen NC-12

Transverse Reinforcement Detail

Figures 4-2f and A-249 show transverse reinforcement detail 22 in. above the stub for Specimen NC-12. Transverse reinforcement consisted of No. 3 deformed bar continuous square helix at 3-1/2 in. pitch and No. 3 crossties at 3-1/2 in. on center. The reinforcement ratio was 1.29%, equivalent to the transverse reinforcement ratio used in Specimens NC-9 and NC-10. The area of the transverse reinforcement provided was 46% of the area required by ACI-318-83 Code. Crossties were added to provide additional support for the middle longitudinal bars.

Load History

The applied axial load was 544 kips which corresponds to 30% of the column's axial load capacity. Maintaining the axial load constant, the specimen was subjected to 12 complete cycles of horizontal loading. During cycle #2 the first yield displacement and yield curvature were established as 0.28 in. and $117 \times 10^{-6} \text{ in.}^{-1}$, respectively. Subsequently, cyclic horizontal loading was displacement-controlled and consisted of two cycles at each displacement level to a maximum displacement ductility ratio of five. The specimen failed before completing the first cycle at the displacement ductility ratio of six. Figure A-250 shows the history of applied horizontal loading.

Test Observations

The first hairline cracks formed during cycle #2 as shown in Fig. A-251. The cracks formed at the interface of the stub and upper column and were within 15 in. above the stub. Figure A-252 shows the specimen during cycle #5 ($\mu=2$). Crushing of the cover concrete at the stub level is visible, as well as large cracks extending to 15 in. above the stub. Simultaneous to the formation of these large cracks, the horizontal load-carrying capacity of the specimen dropped from 210 kips to approximately 180 kips. Figure A-253 shows the specimen during cycle #7 ($\mu=3$). At this stage cracks had extended as high as 36 in. above the stub. Additionally, the cover concrete spalled off to 15 in. above the stub; however, no

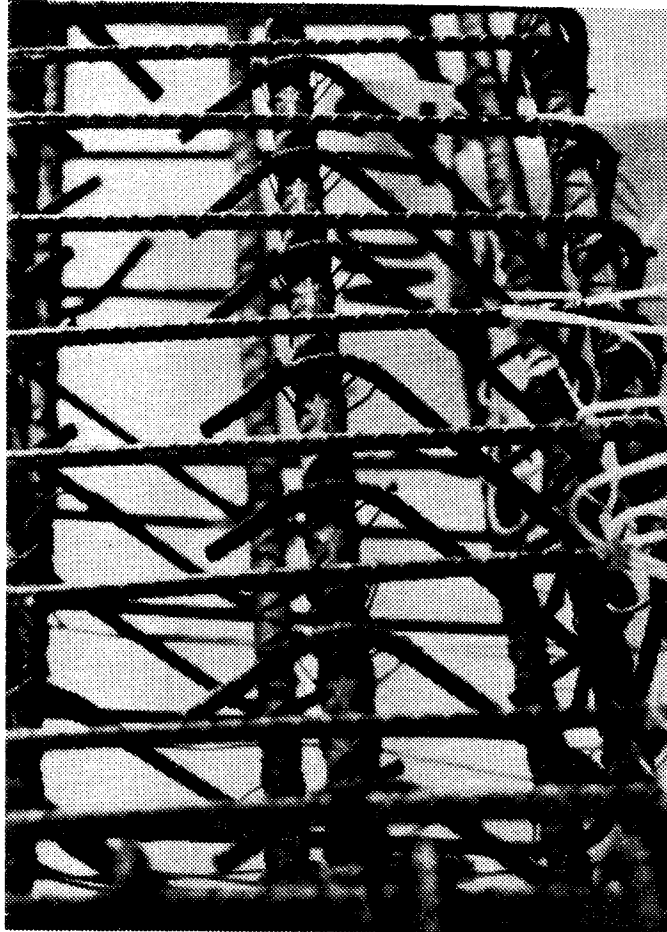


FIG. A-249 TRANSVERSE REINFORCEMENT DETAIL USED WITHIN
22 IN. ABOVE THE STUB, SPECIMEN NC-12

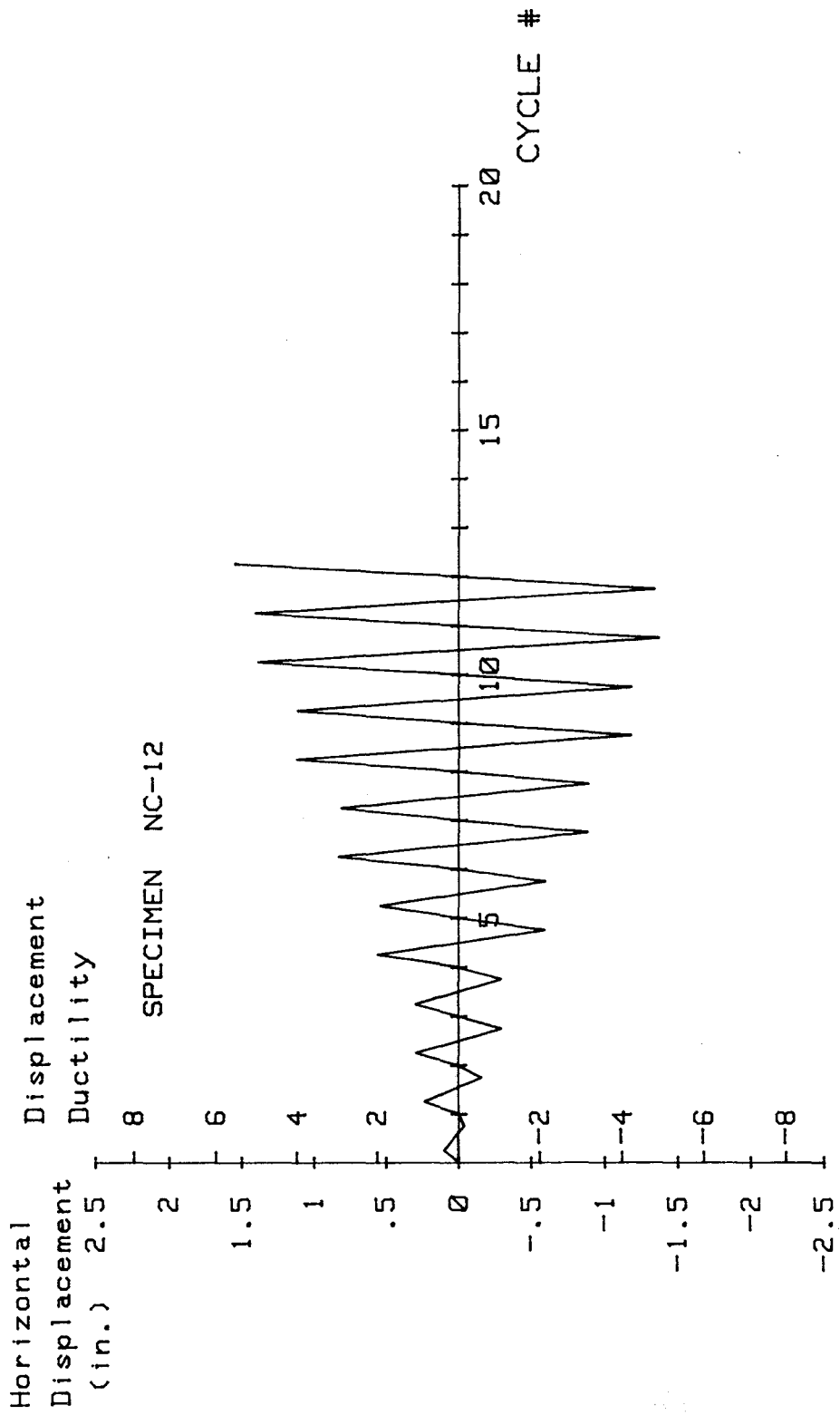


FIG. A-250 LOADING SCHEDULE, SPECIMEN NC-12

Reproduced from
best available copy.

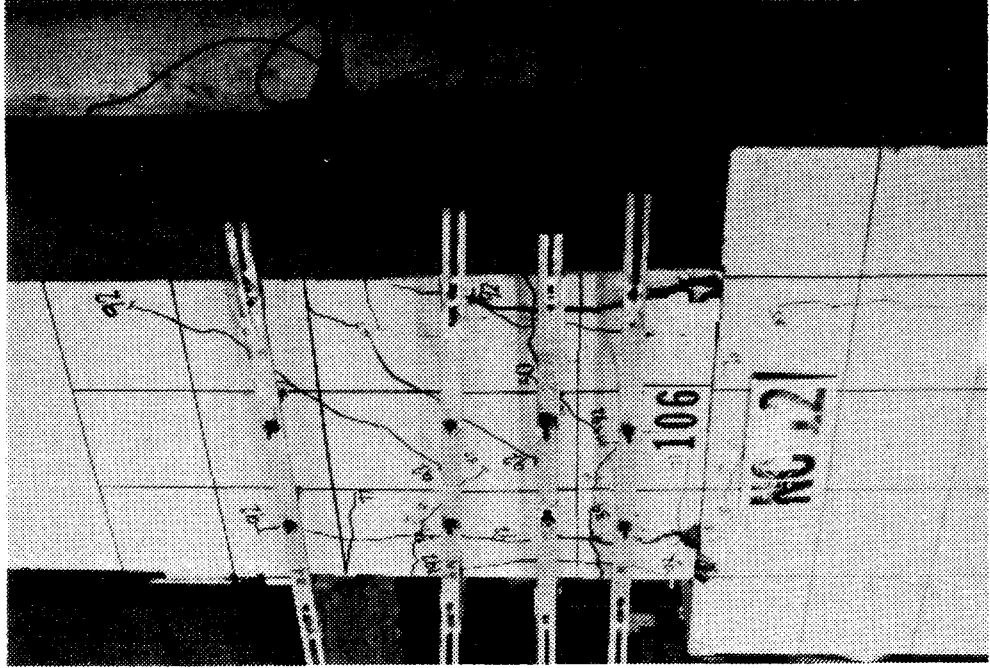


FIG. A-252 TEST SPECIMEN NC-12 DURING CYCLE #5

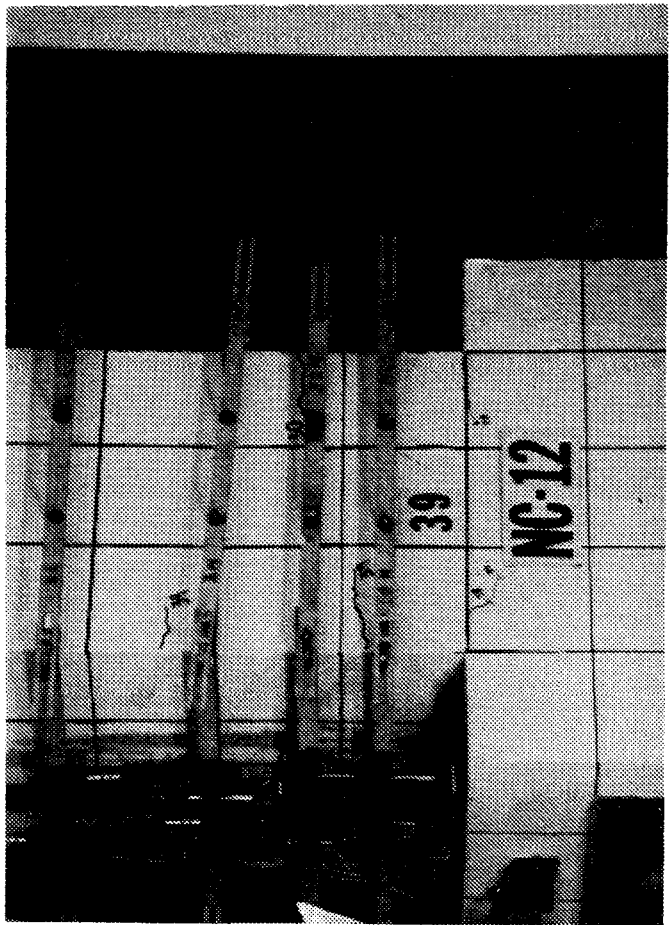


FIG. A-251 TEST SPECIMEN NC-12 AFTER CYCLE #2

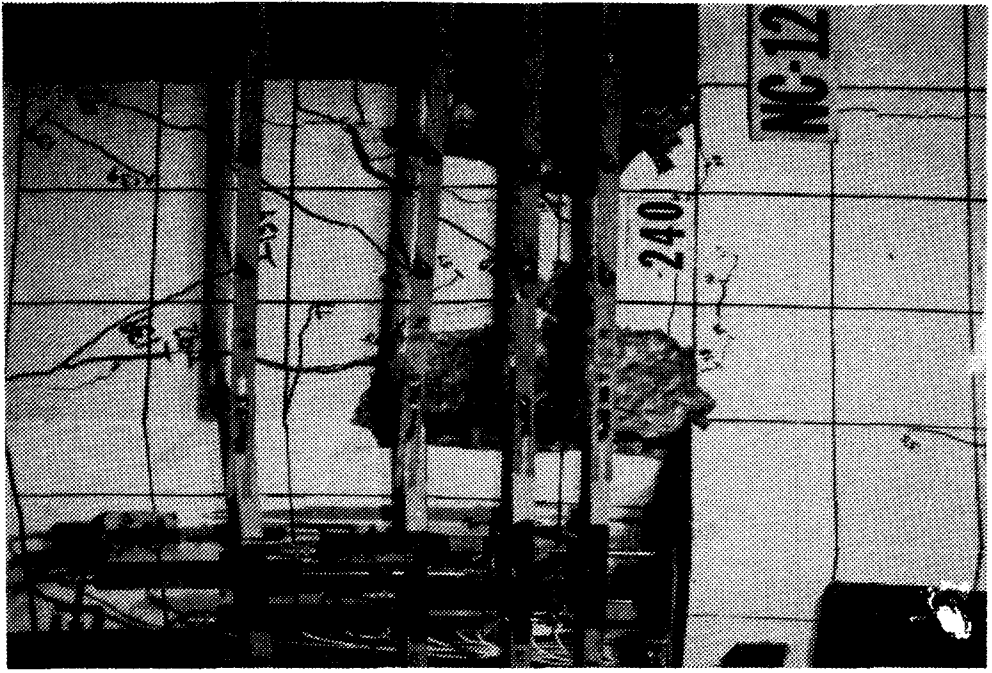


FIG. A-254 TEST SPECIMEN NC-12 AFTER CYCLE #11

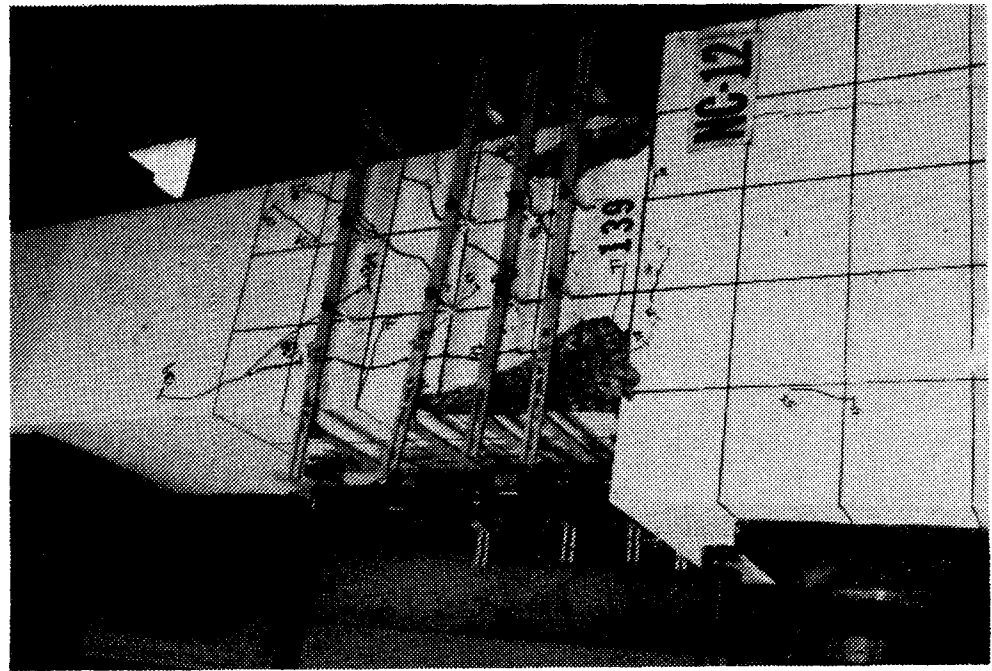


FIG. A-253 TEST SPECIMEN NC-12 DURING CYCLE #7

longitudinal or transverse steel were yet visible. Subjecting the specimen to two cycles each at displacement ductility ratios of 4 and 5 did not alter the height within which the cover concrete spalled off. However, as shown in Fig. A-254, some transverse reinforcement was visible at cycle #11 ($\mu=5$).

The specimen failed prior to completion of the reverse loading of the first cycle at the displacement ductility ratio of six, at which time the corner and middle longitudinal bars on the west side suddenly buckled. The length of the longitudinal bars engaged in buckling extended from approximately 4.5 in. above the stub to 15 in. above the stub. Transverse reinforcement experienced significant elongation, however, no visible cracks or fracture of the transverse reinforcement were observed at these locations.

Inspection of the specimen after test conclusion revealed no visible damage to anchorages of the crossties. The 90° bend on the crossties remained intact and the extensions beyond the bends were still embedded in concrete. Figures A-255 and A-256 show the specimen at test conclusion. The transverse reinforcement within approximately 4 in. above the stub was still covered with concrete at the end of testing (see Fig. A-256).

Load Deflection and Moment-Curvature Characteristics

Figure A-257 shows the horizontal load displacement behavior of the specimen. The maximum applied horizontal load was approximately 210 kips, which occurred during forward loading of cycle #5 ($\mu=2$). Maximum horizontal load at this time suddenly dropped to approximately 180 kips due to crushing and cracking of cover concrete. However, during the forward loading cycle #7 ($\mu=3$), the maximum applied horizontal load was approximately 195 kips.

Figure A-258 shows the curvature distribution along the upper column. The location of the maximum curvature was generally located within 4 to 8 in. above the stub. This can be attributed to the fact that transverse reinforcement 4 in. above the stub was still covered with cover concrete at test conclusion, thereby providing good confinement at this region. Consequently, the plastic hinge and the region of high curvature were forced upward.

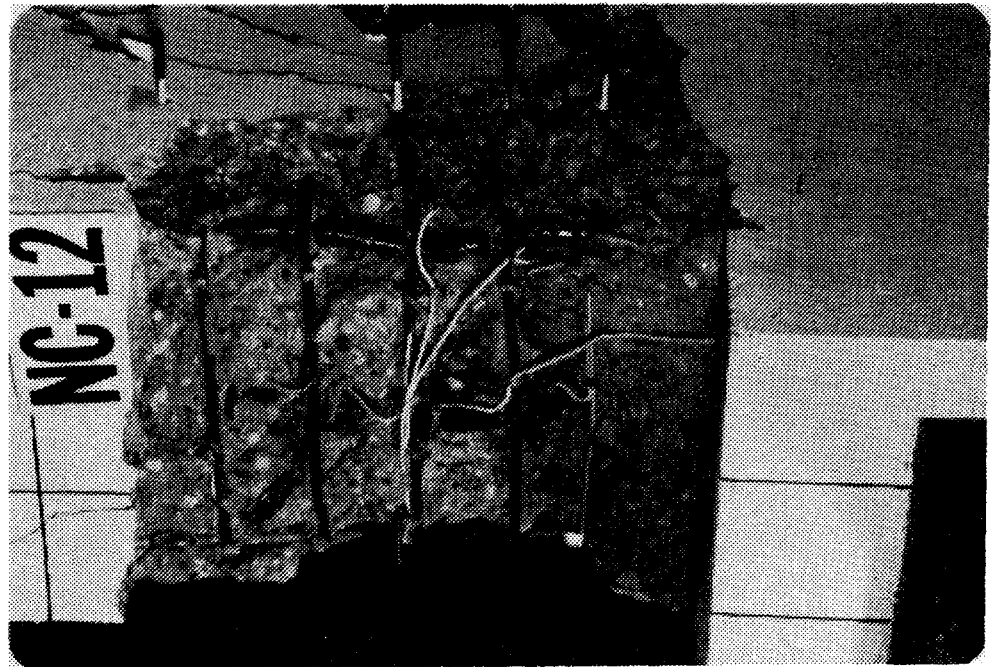


FIG. A-255 TEST SPECIMEN NC-12 AFTER TEST CONCLUSION

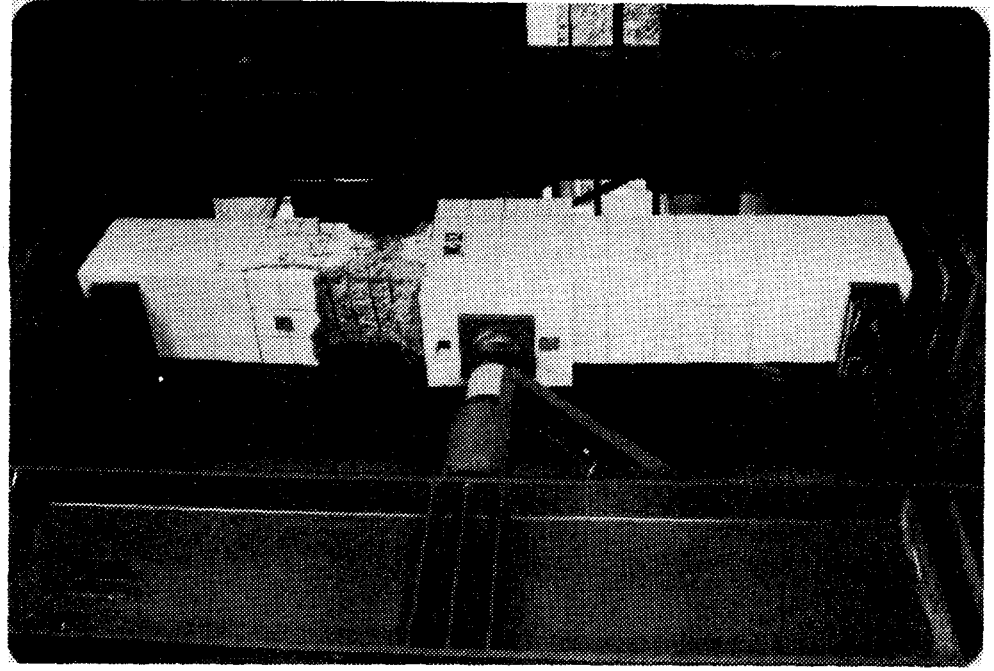
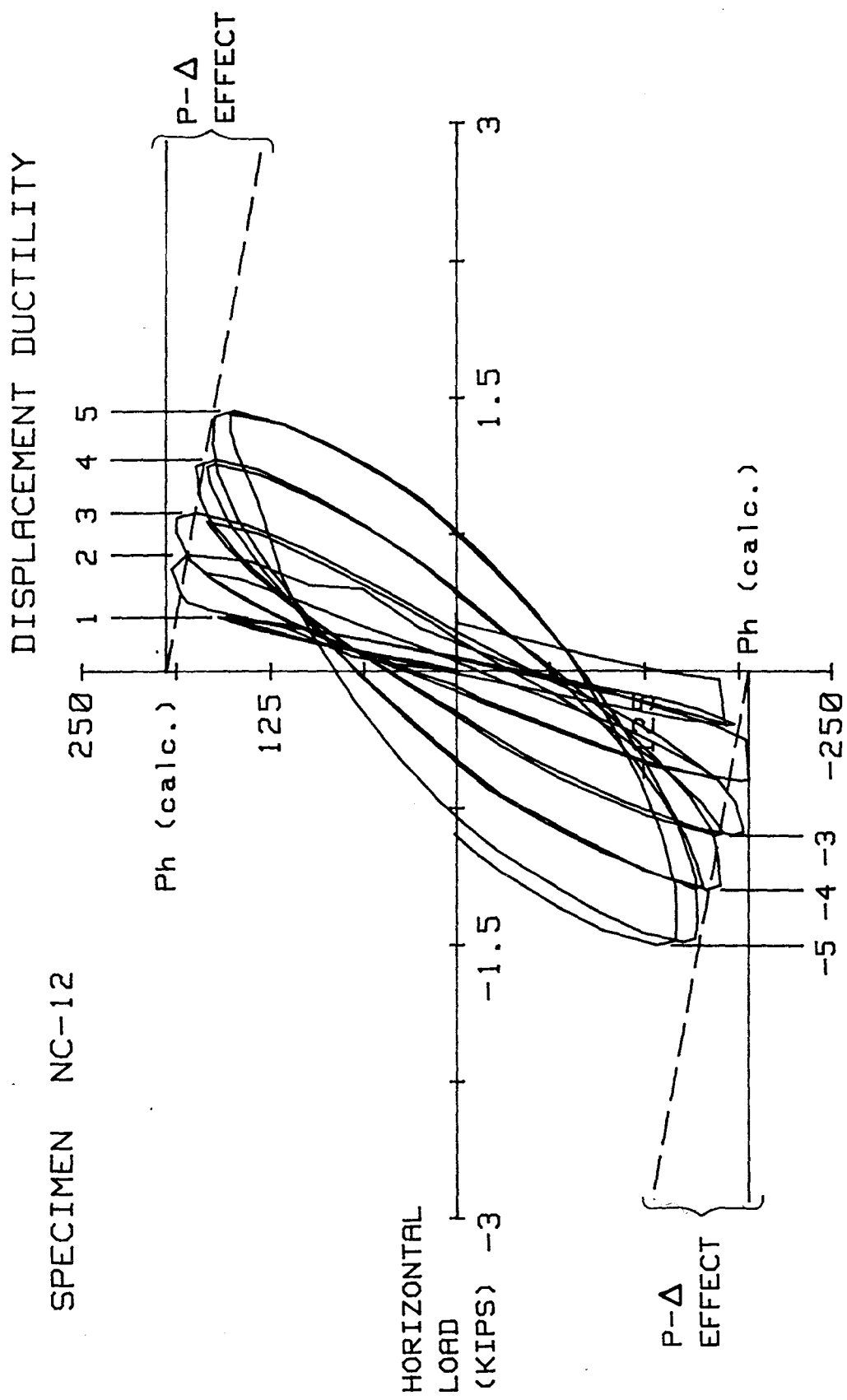


FIG. A-256 TEST SPECIMEN NC-12 AFTER TEST CONCLUSION



SPECIMEN NC-12

Metric Equivalents
 1 in. = 25.4 mm
 1 kip = 4.45 kN

HORIZONTAL LOAD VERSUS DISPLACEMENT, SPECIMEN NC-12

FIG. A-257 HORIZONTAL LOAD VERSUS DISPLACEMENT, SPECIMEN NC-12

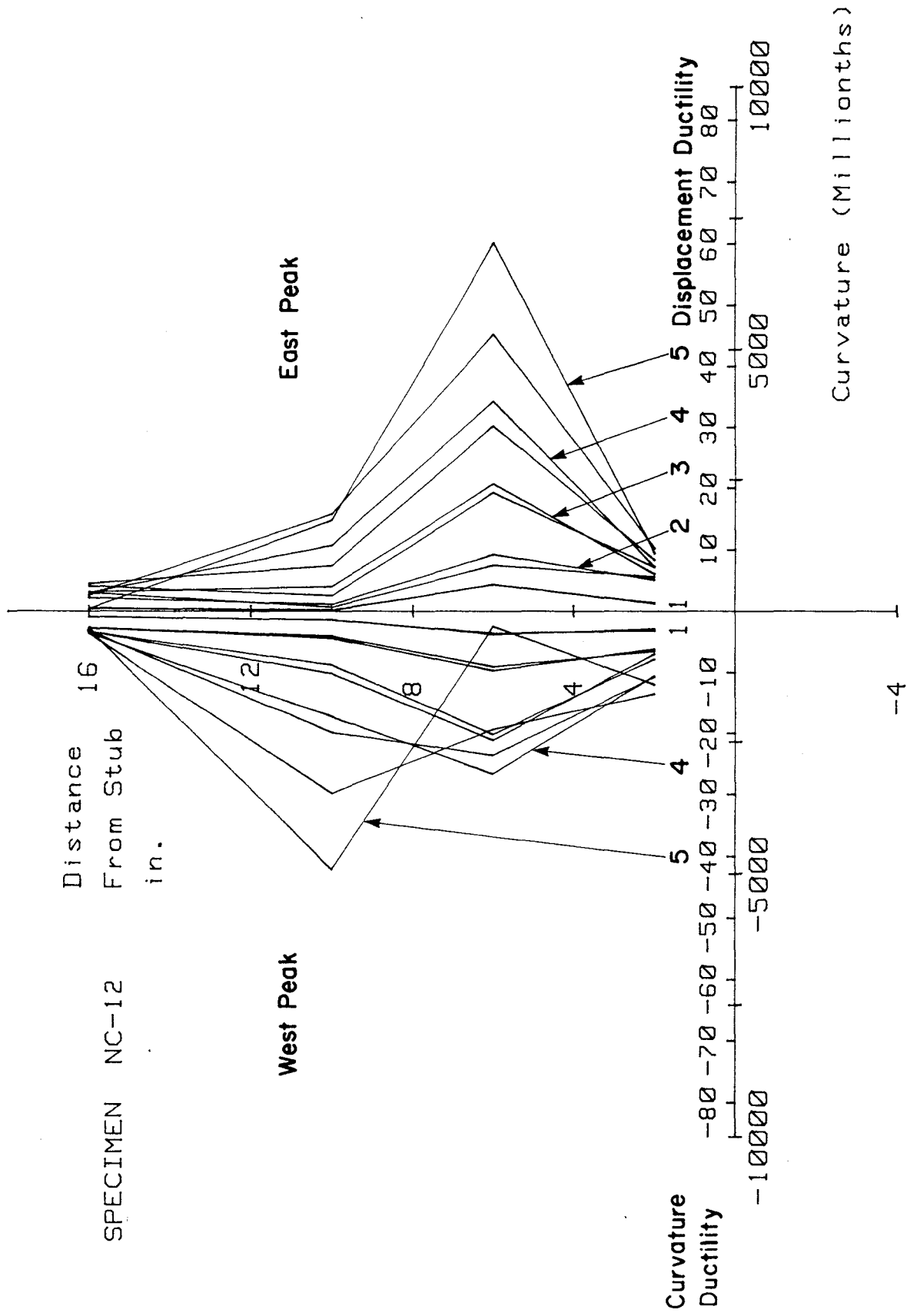


FIG. A-258 CURVATURE DISTRIBUTION ALONG UPPER COLUMN SPECIMEN NC-12

Figure A-258 shows that the maximum curvature ductility at the displacement ductility ratio of 5 within 4 to 8 in. of the stub is approximately 60. However, it should be noted that the curvature ductility ratios shown in Fig. A-258 are based on the first yield curvature of $117 \times 10^{-6} \text{ in.}^{-1}$, calculated using the peak curvature observed during cycle #2 at 4 in. above the stub. The first yield curvature at cycle #2, based on the peak curvature within 4 to 8 in. above the stub is $419 \times 10^{-6} \text{ in.}^{-1}$. Based on this later value of the first yield curvature, the maximum curvature ductility ratio during the displacement ductility ratio of 5 would be 16.8 rather than 60, which is representative of the available curvature ductility for Specimen NC-12.

Figure A-259 shows the moment curvature characteristics of the specimen at the stub-upper column interface. The area under each hysteresis loop is small, a direct consequence of the curvature distribution along the upper column. The maximum applied moment was 5389 in-kips which occurred at the peak of the reverse loading cycle #7 ($\mu=3$). The maximum applied moment during the displacement ductility ratios of 4 and 5 were 5149 and 4930 in-kips, respectively. The theoretical moment capacity of the column cross-section was calculated as 5000 in-kips, using the procedures outlined in Section 4.8.2. The ratios of the peak moment at the second cycle to the peak moment at the first cycle at various displacement levels varied between 0.9, and 0.97.

Figure A-260 shows the moment-curvature characteristic of the column cross-section located 6 in. above the stub. Maximum moment at this location during the displacement ductility ratios of 1, 2, 3, 4, and 5 were 4356, 4684, 4725, 4496, and 4240 in-kips, respectively. The maximum curvature ductility ratio, based on the first yield curvature of $419 \times 10^{-6} \text{ in.}^{-1}$ at this location at displacement ductility ratios of 2 through 5 were 2.7, 5.9, 9.6, and 16.8, respectively.

Transverse Reinforcement Strain

Figures A-261 through A-272 show the data obtained from the strain gages attached to the transverse reinforcement. Gages #13, #14, and #15 were attached to the continuous square helix reinforcement at distances of 3.5, 10.5, and 17.5 in. above the stub, respectively, on the north face. Gages

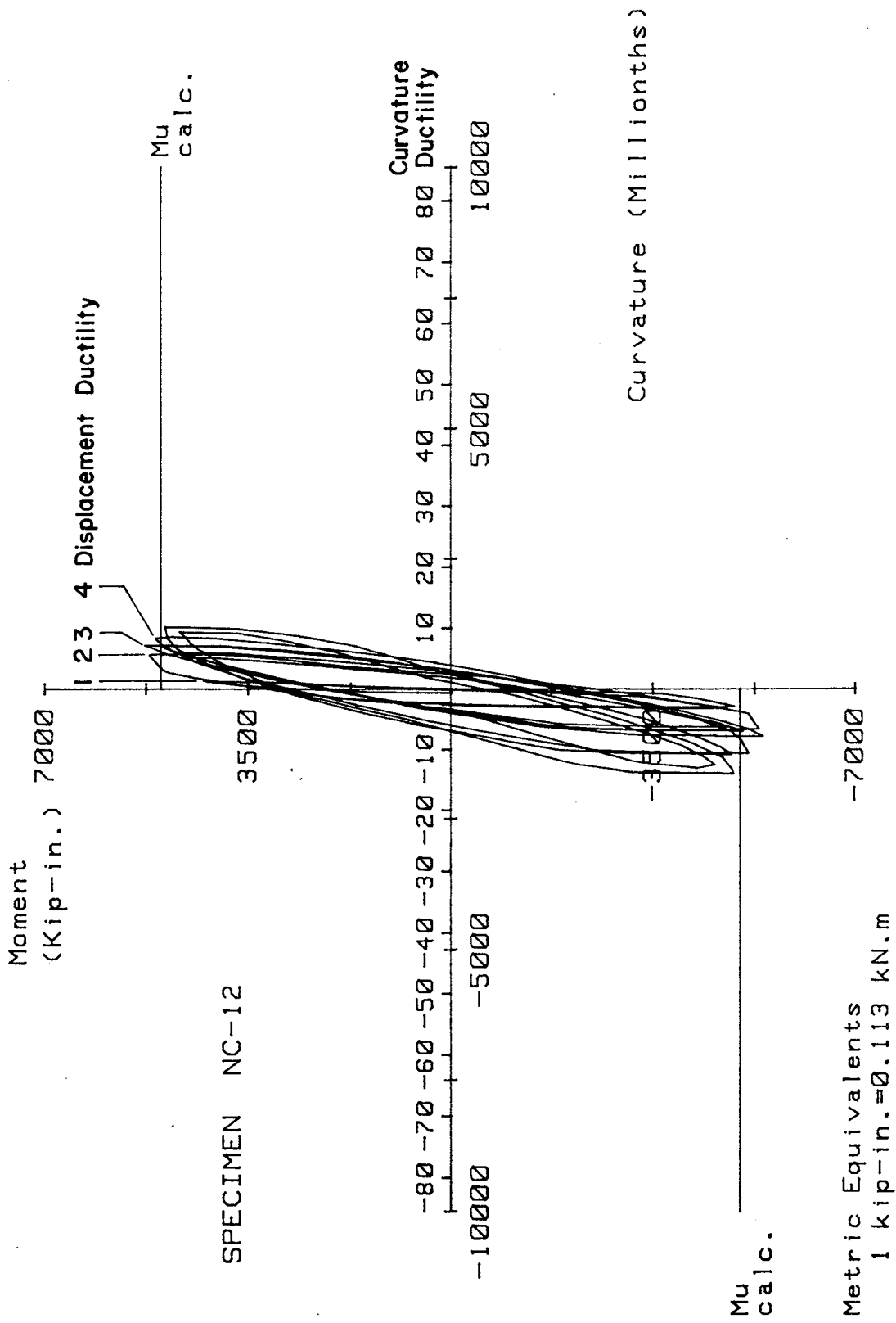


FIG. A-259 MOMENT VERSUS CURVATURE FOR SPECIMEN NC-12

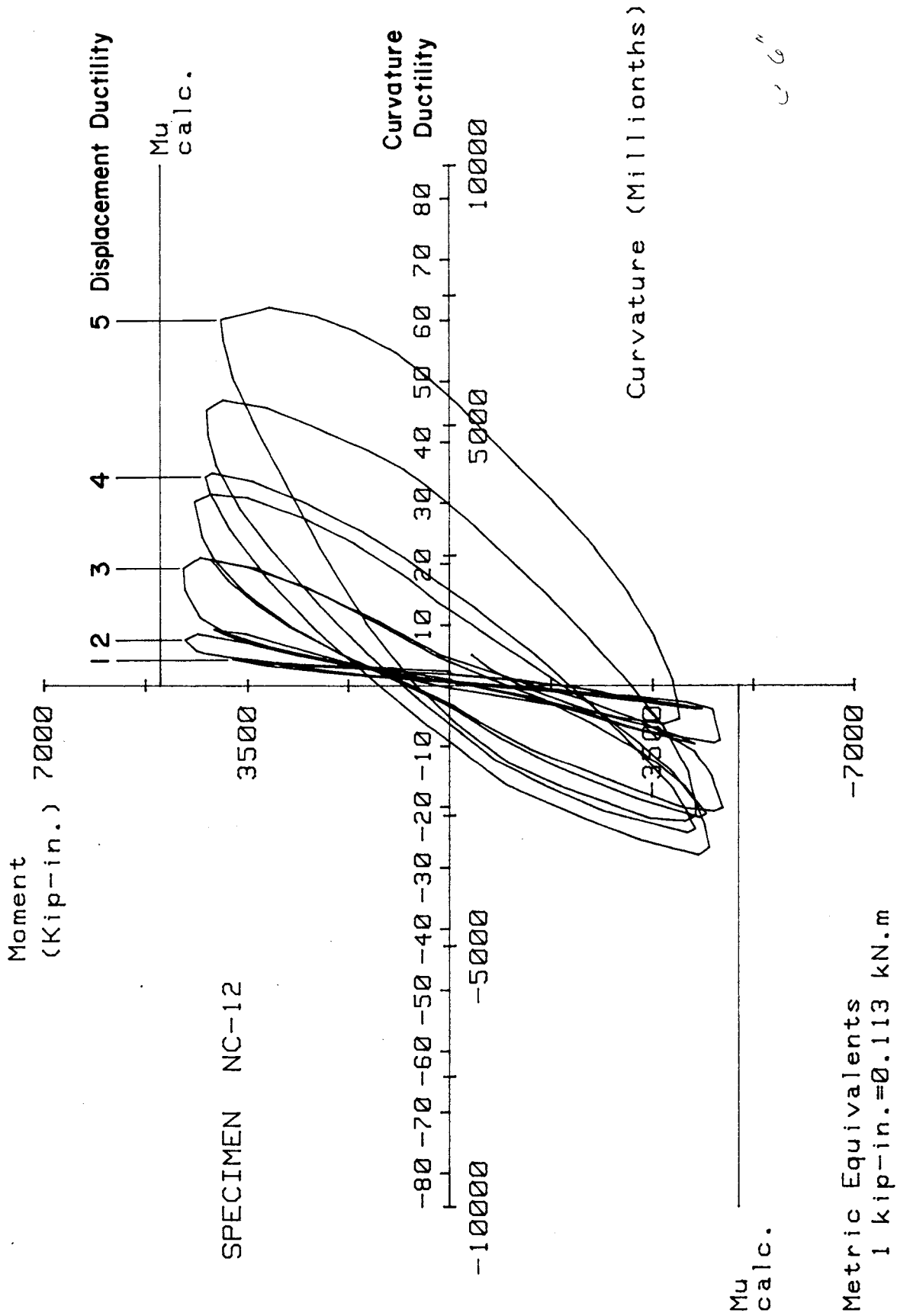


FIG. A-260 MOMENT VERSUS CURVATURE FOR SPECIMEN NC-12, 6 IN. ABOVE THE STUB

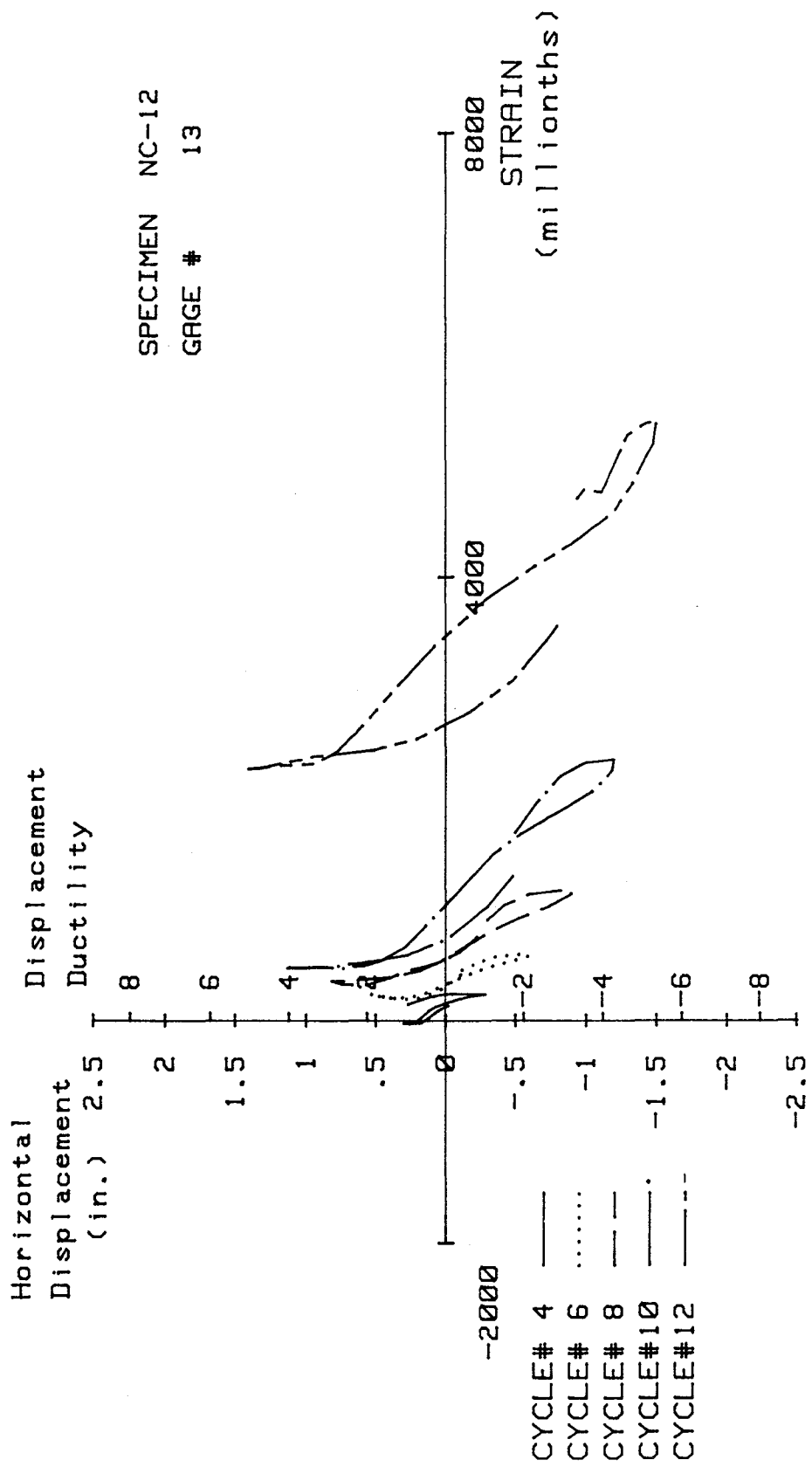


FIG. A-261 MEASURED STRAIN, GAGE #13, SPECIMEN NC-12

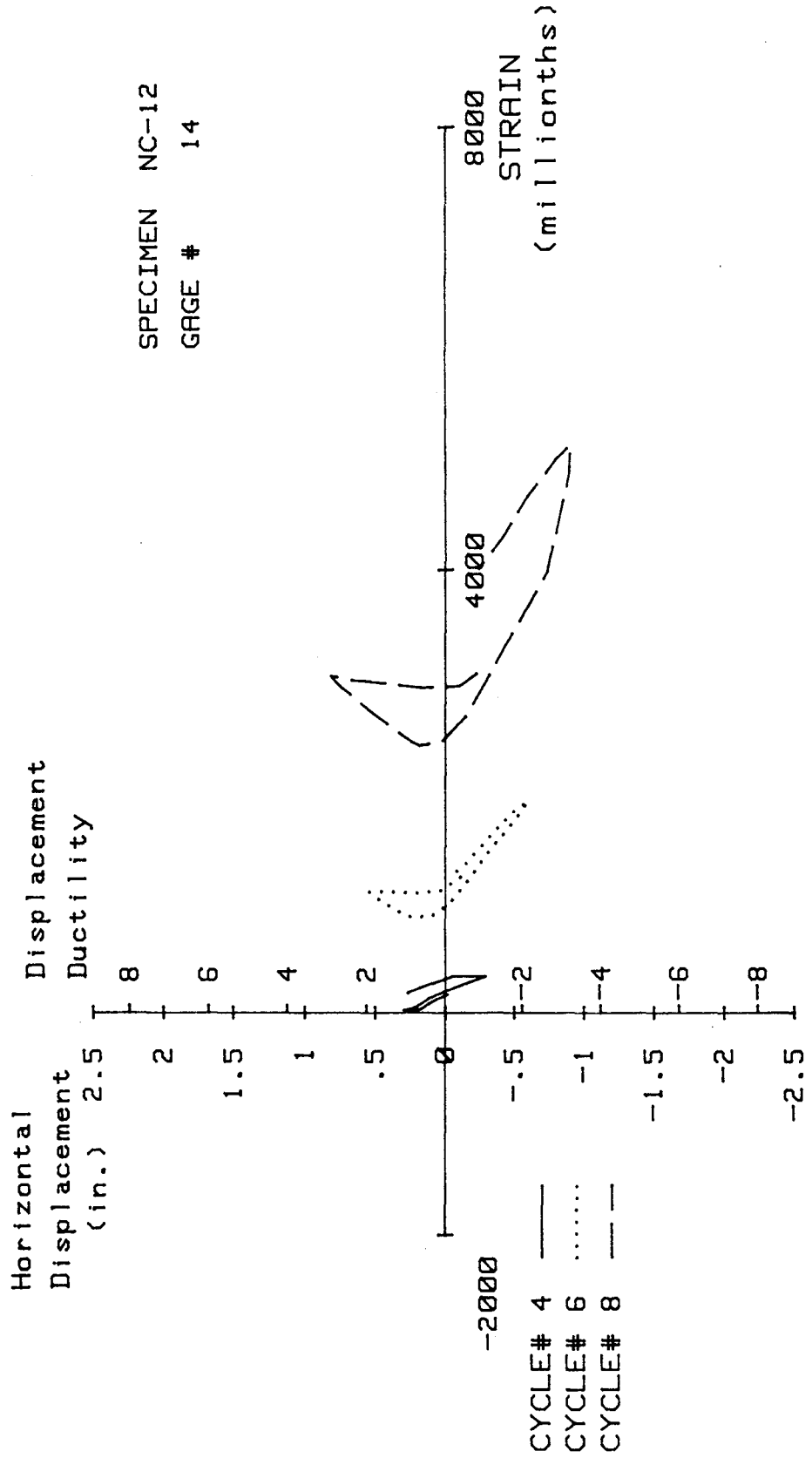


FIG. A-262 MEASURED STRAIN, GAGE #14, SPECIMEN NC-12

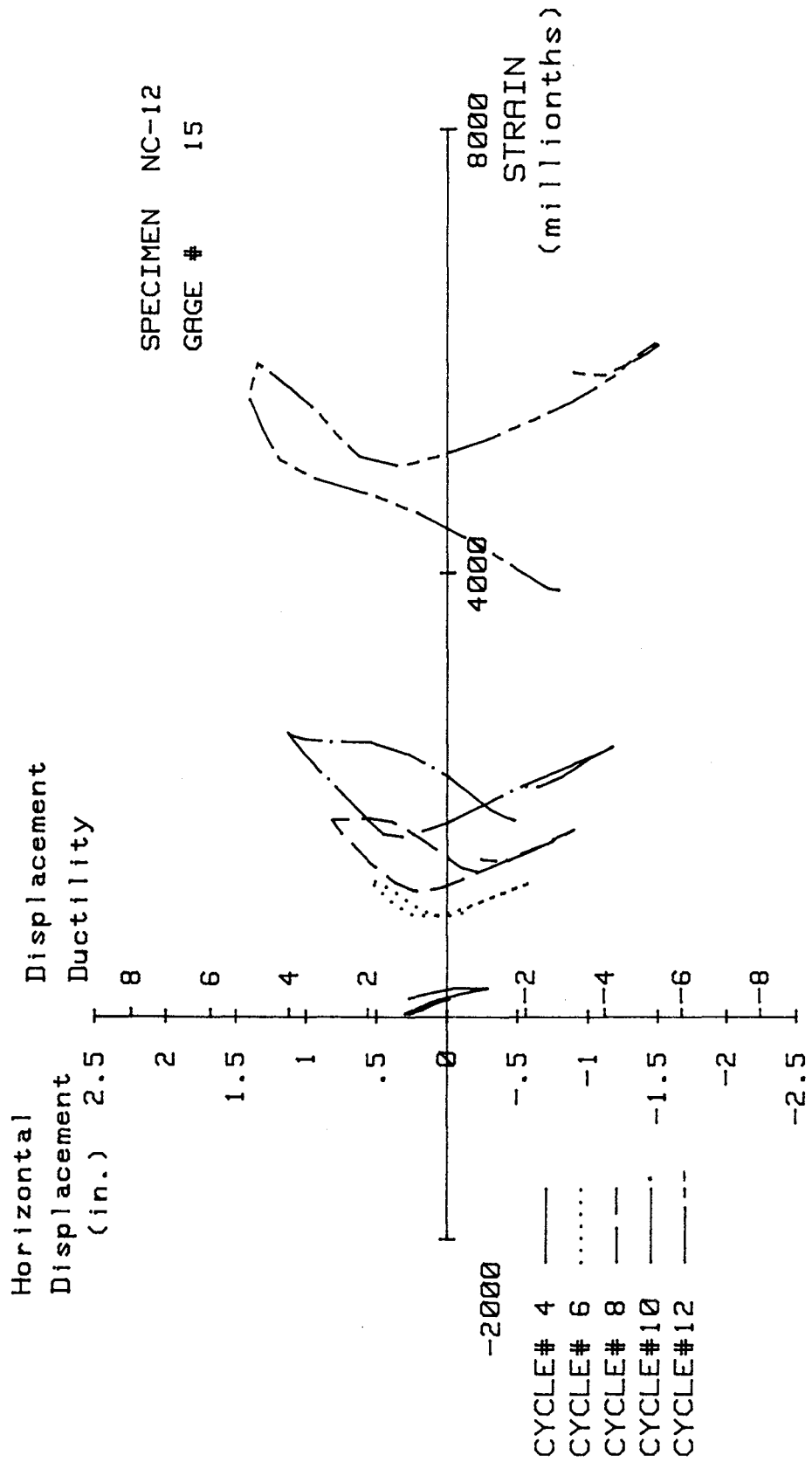


FIG. A-263 MEASURED STRAIN, GAGE #15, SPECIMEN NC-12

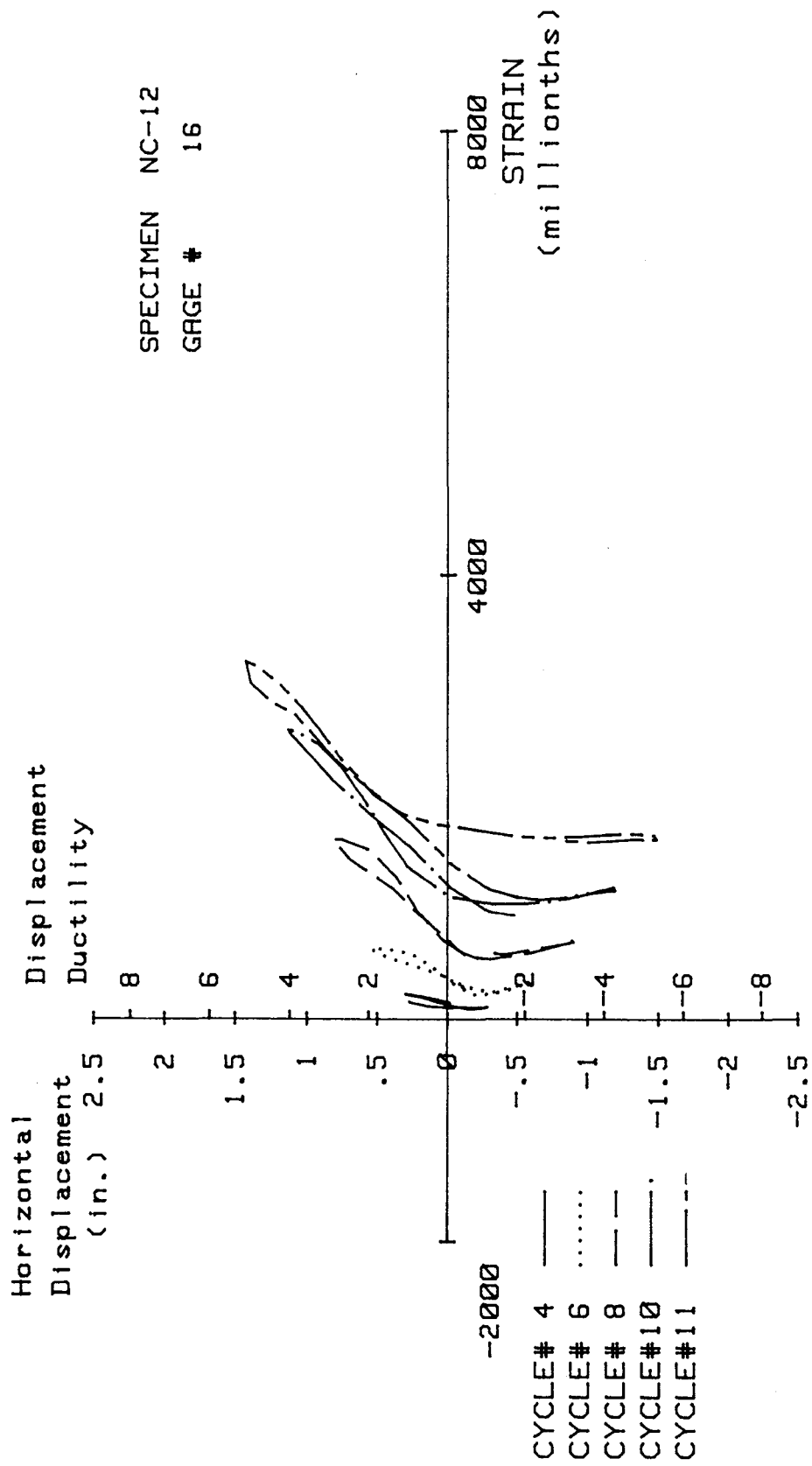


FIG. A-264 MEASURED STRAIN, GAGE #16, SPECIMEN NC-12

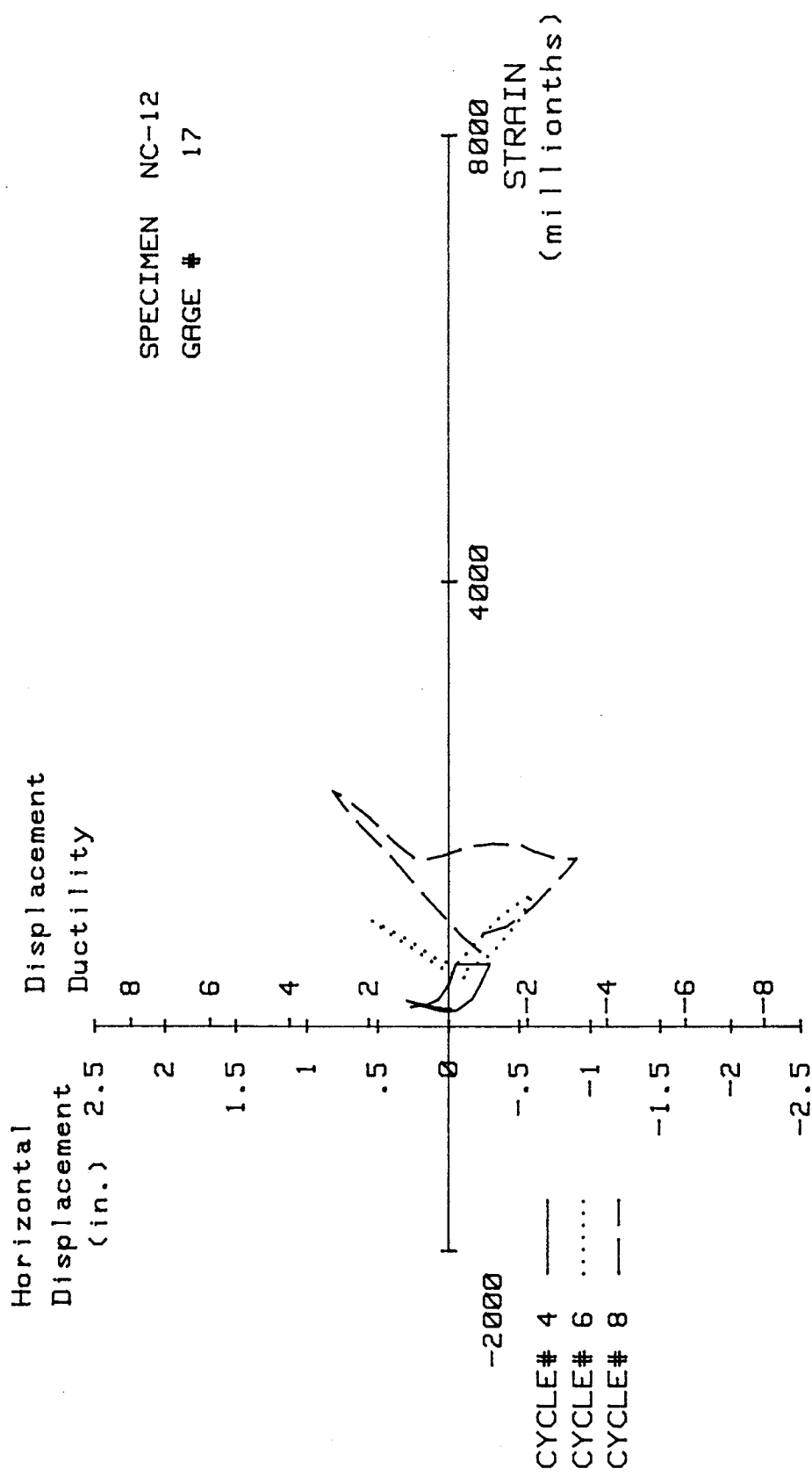


FIG. A-265 MEASURED STRAIN, GAGE #17, SPECIMEN NC-12

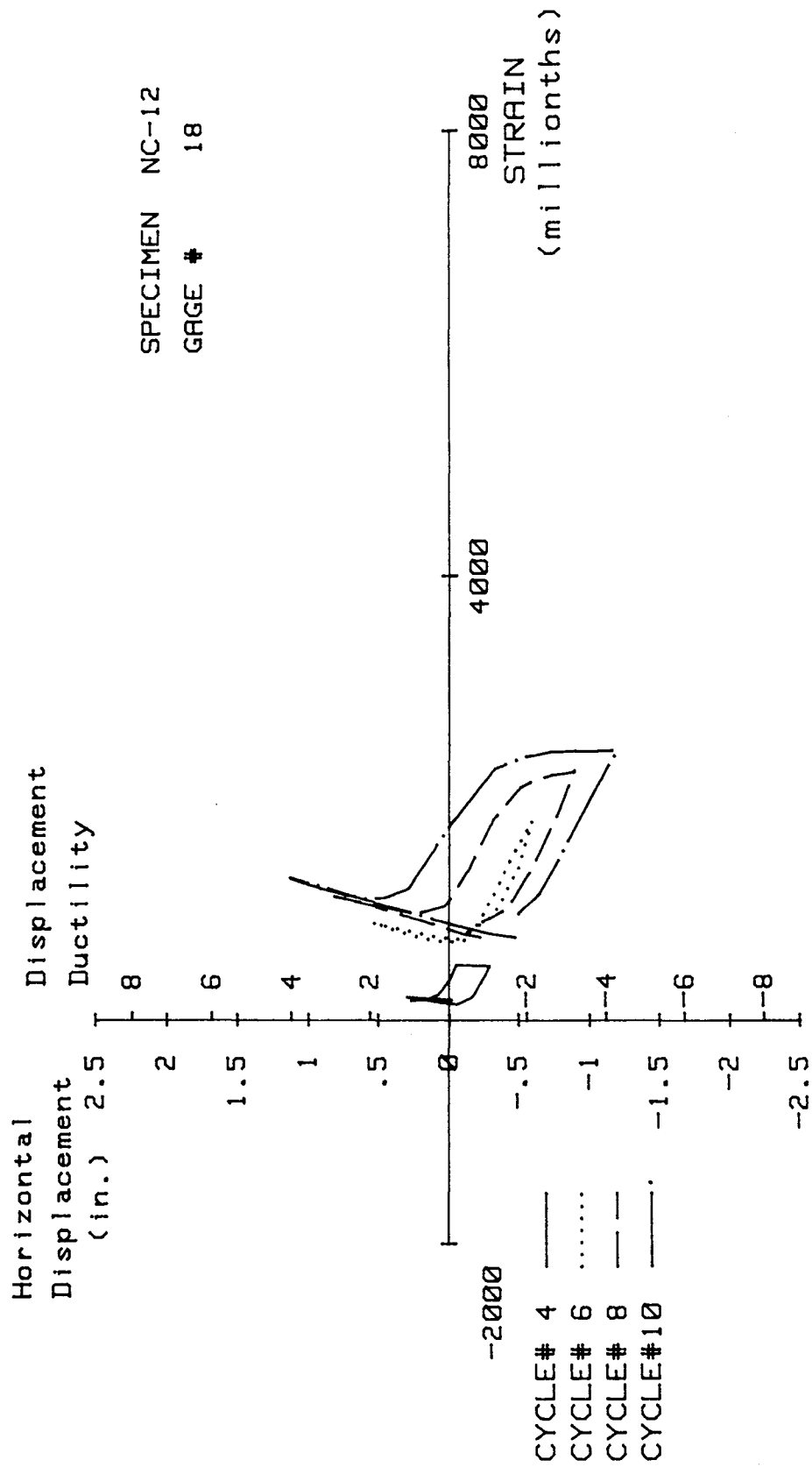


FIG. A-266 MEASURED STRAIN, GAGE #18, SPECIMEN NC-12

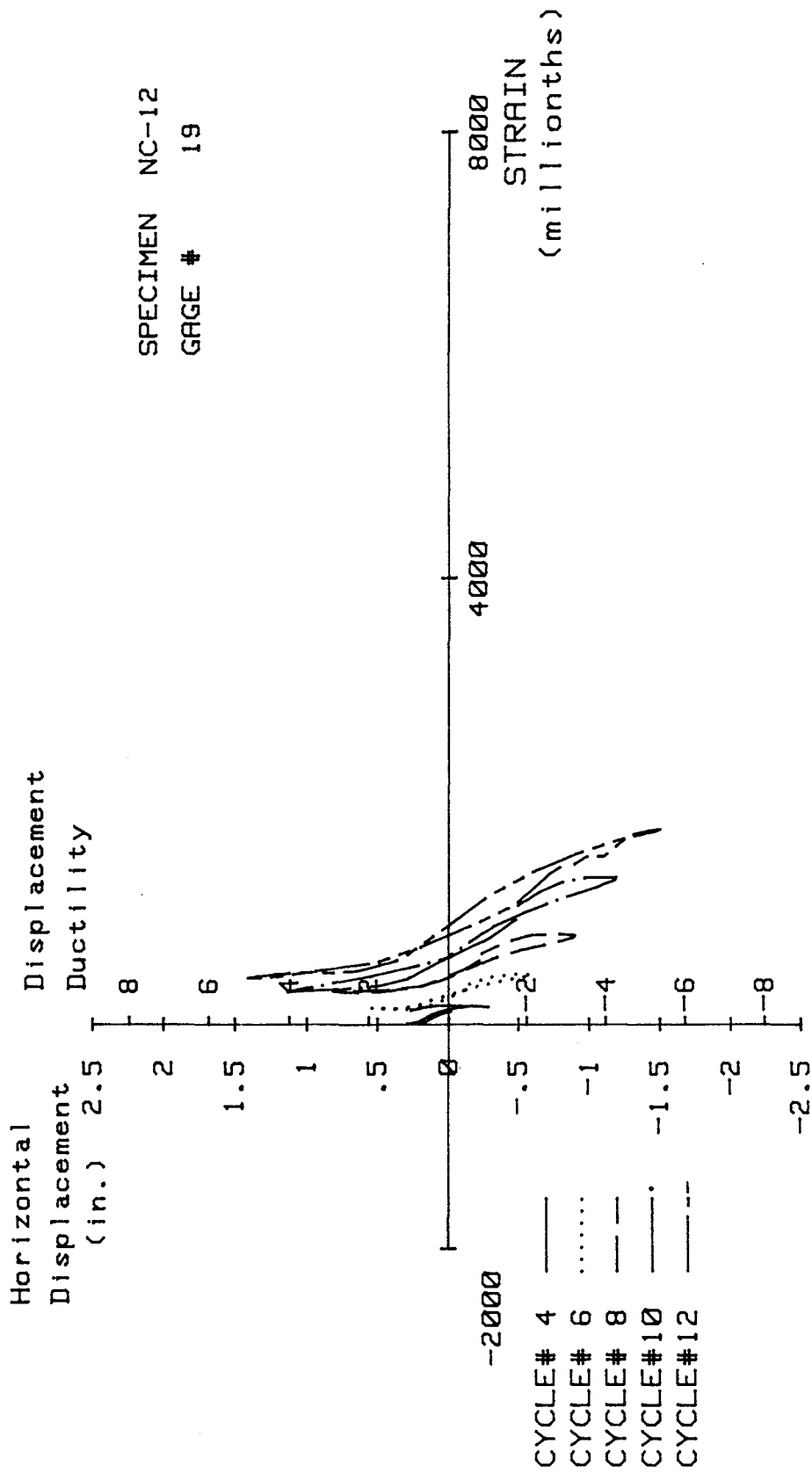


FIG. A-267 MEASURED STRAIN, GAGE #19, SPECIMEN NC-12

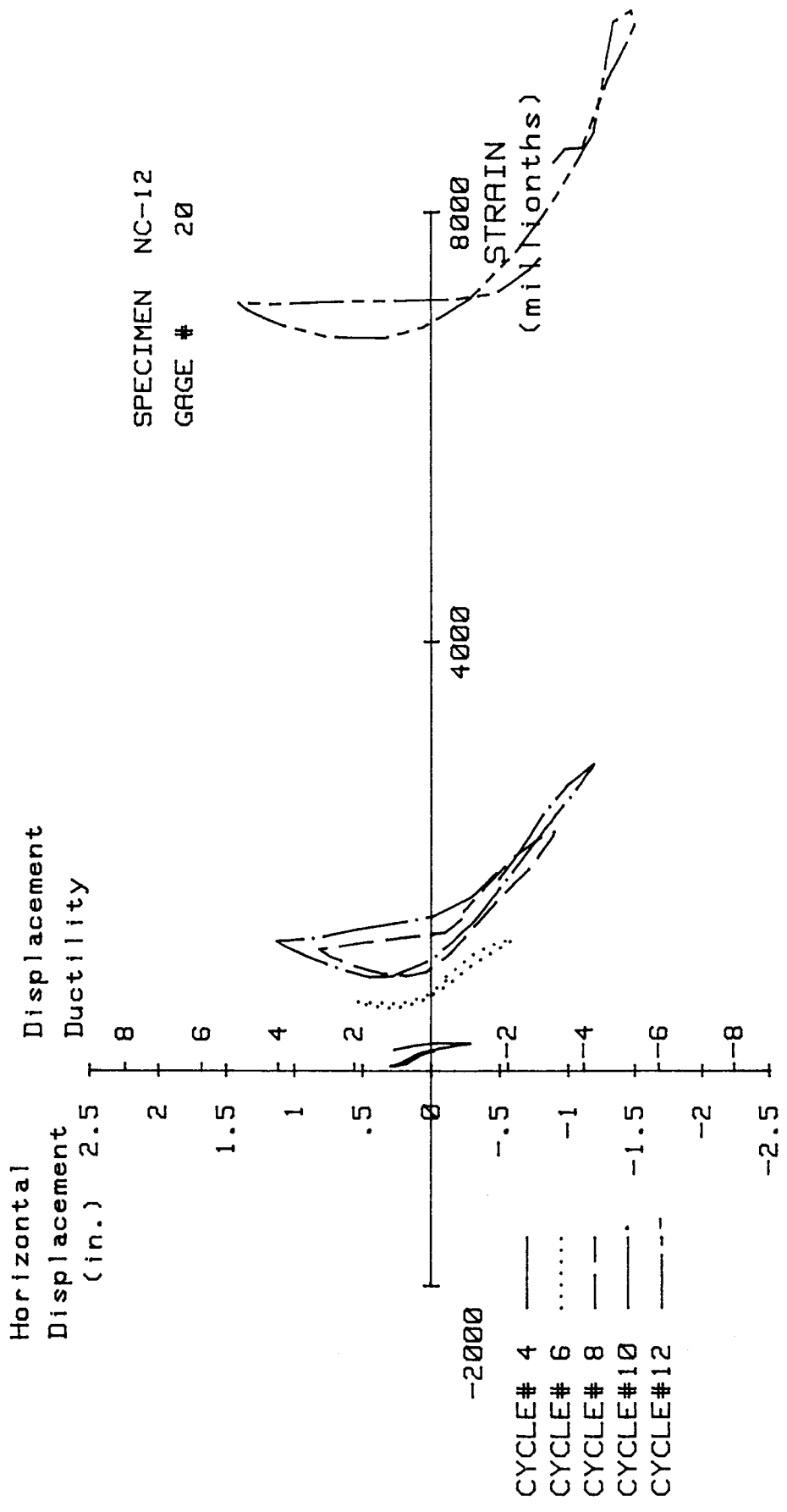


FIG. A-268 MEASURED STRAIN, GAGE #20, SPECIMEN NC-12

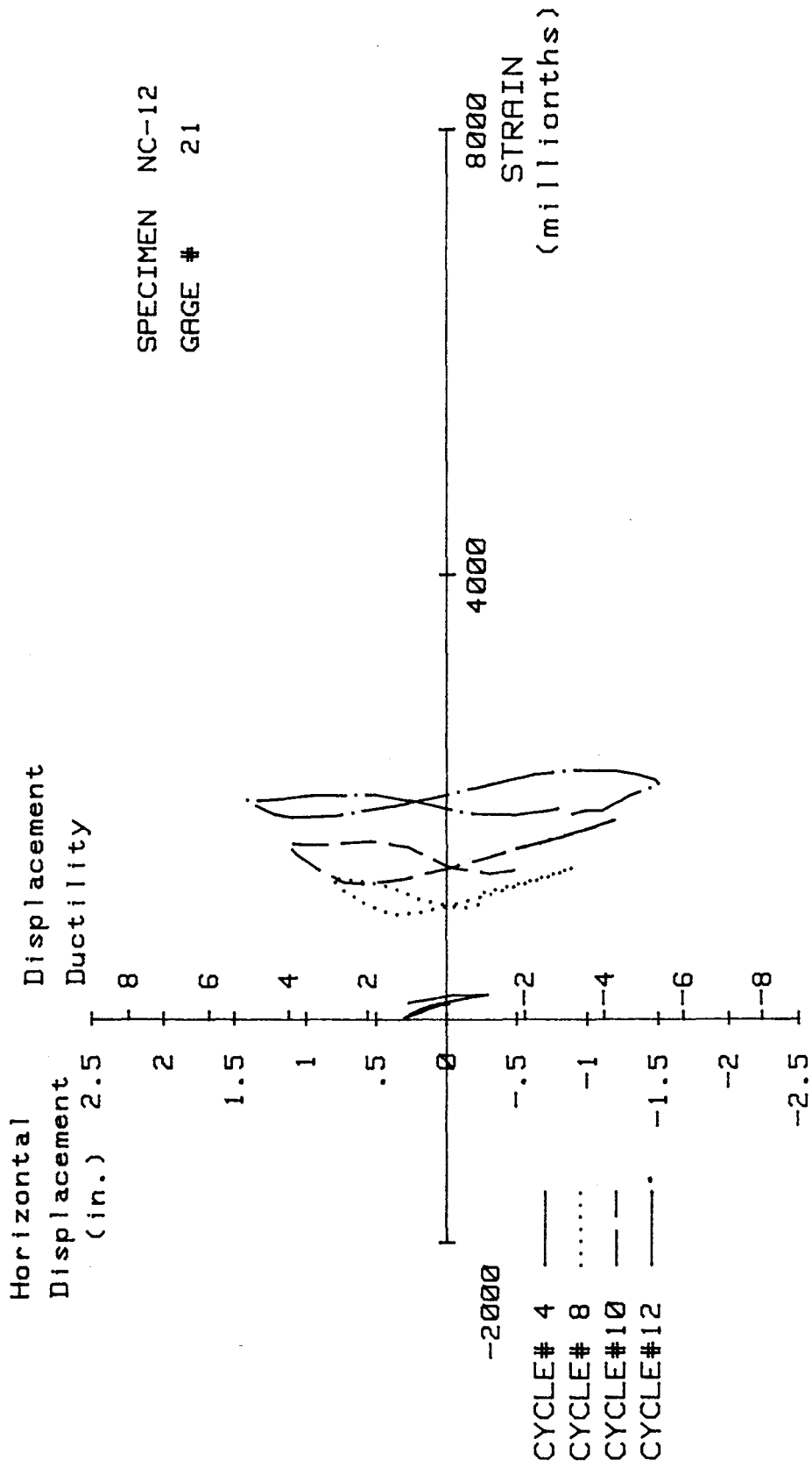


FIG. A-269 MEASURED STRAIN, GAGE #21, SPECIMEN NC-12

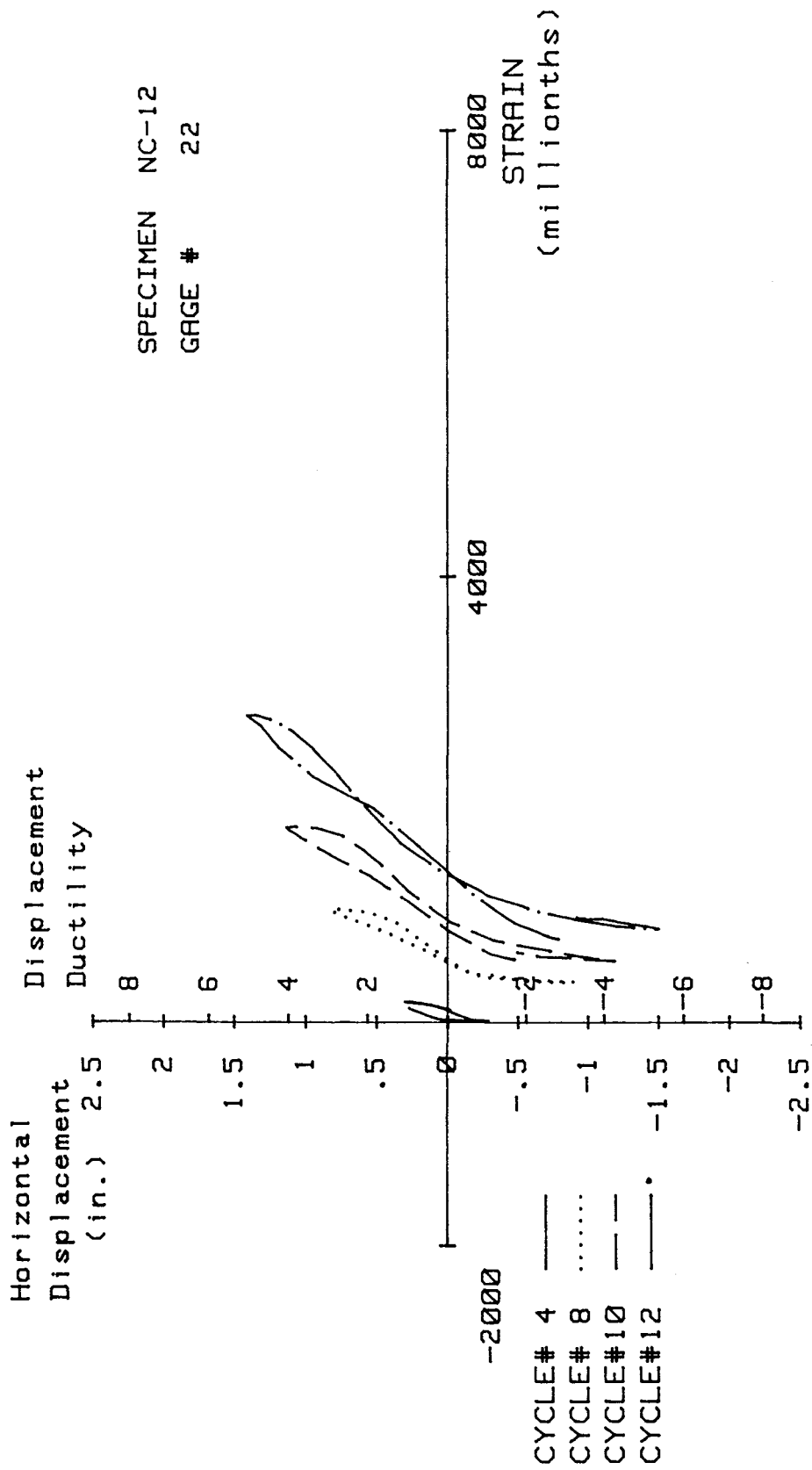


FIG. A-270 MEASURED STRAIN, GAGE #22, SPECIMEN NC-12

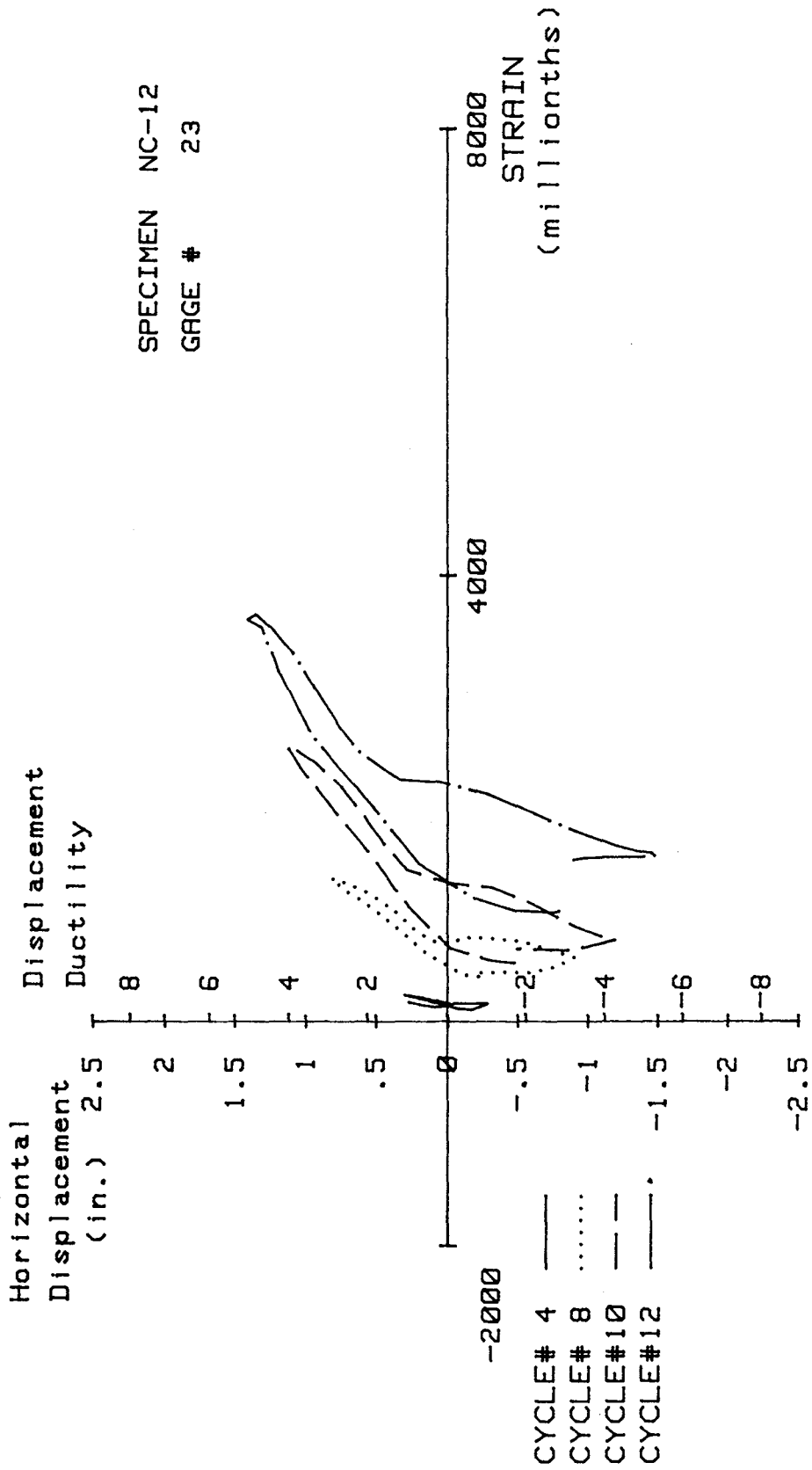


FIG. A-271 MEASURED STRAIN, GAGE #23, SPECIMEN NC-12

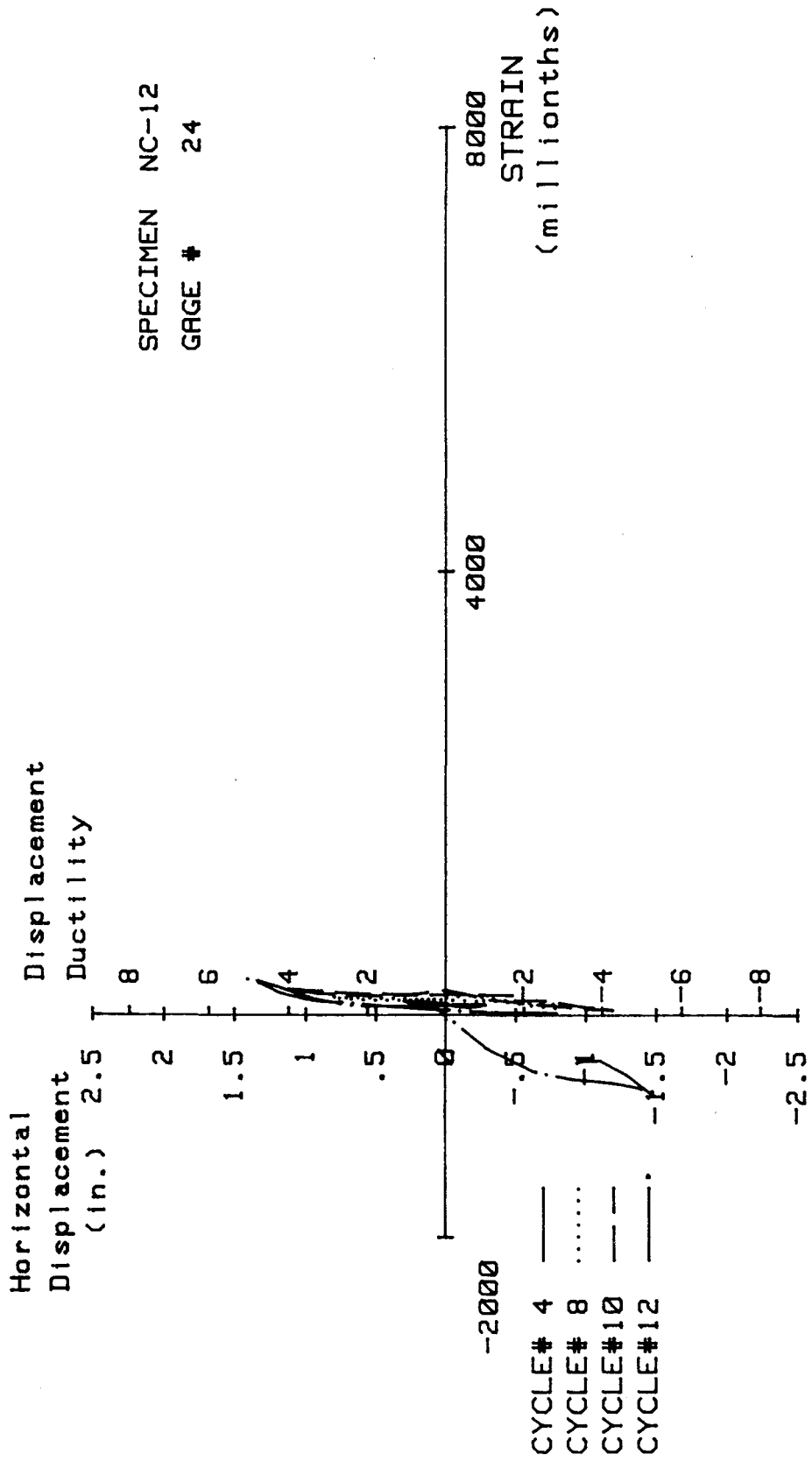


FIG. A-272 MEASURED STRAIN, GAGE #24, SPECIMEN NC-12

#16, #17, and #18 were attached to the south face at 5.3, 12.3, and 19.3 in. from the stub, respectively. Gages #19 through #24 were attached to the crossties located at distances of 3.5, 10.5, 17.5, 3.5, 10.5, and 17.5 in. from the stub, respectively.

The minimum specified yield strength of the transverse reinforcement material was 2070 micro-strain. The first yield strain was observed from strain gage #14 during cycle #7 ($\mu=3$).

In general, the strain on the crossties was smaller than the strain on the square helix reinforcement at approximately the same level.

